Archaeological Chemistry VIII

Archaeological Chemistry VIII

Ruth Ann Armitage, Editor
Eastern Michigan University
Ypsilanti, Michigan

James H. Burton, Editor
University of Wisconsin-Madison
Madison, Wisconsin

Sponsored by the
ACS Division of History of Chemistry

Foreword

The ACS Symposium Series was first published in 1974 to provide a mechanism for publishing symposia quickly in book form. The purpose of the series is to publish timely, comprehensive books developed from the ACS sponsored symposia based on current scientific research. Occasionally, books are developed from symposia sponsored by other organizations when the topic is of keen interest to the chemistry audience.

Before agreeing to publish a book, the proposed table of contents is reviewed for appropriate and comprehensive coverage and for interest to the audience. Some papers may be excluded to better focus the book; others may be added to provide comprehensiveness. When appropriate, overview or introductory chapters are added. Drafts of chapters are peer-reviewed prior to final acceptance or rejection, and manuscripts are prepared in camera-ready format.

As a rule, only original research papers and original review papers are included in the volumes. Verbatim reproductions of previous published papers are not accepted.

ACS Books Department

Preface

The 12th Archaeological Chemistry Symposium was held as part of the Spring ACS National Meeting in New Orleans, Louisiana, April 7–11, 2013. This volume is a compilation of presentations from the Symposium, the latest in a long tradition that began at the ACS National Meeting in Philadelphia in 1950. The numbering of the symposia is, however, somewhat in question. According to Brill (*1*), "…memories of only the First and Third Symposia remained clear [at the 4th Symposium]… We leave it (with a blush) to the historians…to decide upon the reality of the Second Symposium…"

The symposium consisted of four half-day symposia, an evening poster session, and a keynote address by Dr. A. Mark Pollard, Edward Hall Professor of Archaeological Science and Director of the Research Laboratory for Archaeology and the History of Art at the University of Oxford. We choose four broad categories for the symposia: Pigments, Residues and Material Analysis, X-Ray Fluorescence Spectroscopy, and Isotopes in Archaeology. These categories are by no means comprehensive. Rather, they serve as a snapshot perspective of archaeological chemistry today and are necessarily biased toward our areas of expertise and those of the participants in a chemistry meeting. Notably, studies of ancient DNA and other advances in biomolecular archaeology are underrepresented in this volume.

The papers herein show that archaeological chemistry today is more than the usual studies of trace elements in pottery and lithics, which continue to contribute to our understanding of human behavior in the past. New areas of research include more focus on portability to analyze pigments in situ and artifacts in museums, nascent developments in non- and minimally destructive chemical characterization, new applications of isotopic analyses, and an increasing interest in archaeological biomolecules.

This volume is divided into sections that roughly follow those of the Symposium. The first section, Pigments and Dyes, begins with a review of manuscript pigments by Dr. Mary Virginia Orna, the organizer of the 9th Archaeological Chemistry Symposium and Editor of *Archaeological Chemistry: Organic, Inorganic, and Biochemical Analysis* (*2*). Each of the following sections begins with a review paper from one of our invited speakers. Dr. Valerie Steele, now at the University of Bradford in the Department of Archaeological Science, provides an overview of the state — for better and for worse — of analyses of archaeological residues. Portable X-ray fluorescence instruments are becoming extremely common in archaeological chemistry investigations; Dr. Aaron Shugar of Buffalo State University provides in his chapter some perspectives and warnings against the indiscriminate use of this technology. Finally, Dr. Matthew

Sponheimer gives an overview of the contributions of stable carbon isotope and trace metal studies in understanding early hominin diets.

The final chapter of the book provides a perspective on the earliest work in archaeological chemistry in the 18th century and brings us up to today's challenges. We find ourselves in Dr. Pollard's text, carrying out our own research "on a wing and a prayer, " as both the solitary chemist supported by her institution in part for the accessible public interest aspect of her research and a scientist within an anthropology department, fighting for funding in this era of sequestration and downsizing. We hope that this volume contributes toward the "open, respectful, meaningful and iterative dialogue across the many disciplinary boundaries" encountered in archaeological chemistry (*3*).

References

1. Brill, R. H. In *Science and Archaeology*; Brill, R. H., Ed.; MIT Press: Cambridge, MA, 1968, p x−xi.
2. *Archaeological Chemistry: Organic, Inorganic, and Biochemical Analysis*; Orna, M. V., Ed.; ACS Symposium Series 625; American Chemical Society: Washington, DC, 1996.
3. Pollard, A. M. In *Archaeological Chemistry VIII*; Armitage, R. A., Burton J. H., Eds.; ACS Symposium Series 1147; American Chemical Society: Washington, DC, 2013.

Ruth Ann Armitage
Professor, Department of Chemistry, Eastern Michigan University
Ypsilanti, Michigan 48197
734-487-0290 (telephone)
rarmitage@emich.edu (e-mail)

James H. Burton
Director, Laboratory for Archaeological Chemistry, Department of Anthropology
1180 Observatory Drive, University of Wisconsin-Madison
Madison, Wisconsin 53706
608-262-4505 (telephone)
jhburton@wisc.edu (e-mail)

Editors' Biographies

Ruth Ann Armitage

Ruth Ann Armitage, Professor of Chemistry at Eastern Michigan University, earned a B.A. in Chemistry from Thiel College in 1993. She completed a Ph.D. in Analytical Chemistry at Texas A&M University with Dr. Marvin Rowe in 1998 on radiocarbon dating of charcoal-pigmented rock paintings. Her research is focused on characterizing and dating archaeological and cultural heritage materials. She has written and presented extensively her collaborative work with archaeologists and museum conservation scientists on analyses of rock paintings, residues, and colorants in textiles and manuscripts. In her 12 years at EMU, she has mentored more than 25 research students.

James H. Burton

Dr. Burton, Director of the T. Douglas Price Laboratory for Archaeological Chemistry, received a B.S. in Chemistry from the University of Virginia in 1979 and a Ph.D. in Geology from Arizona State University in 1986. His research interests include the development of new archaeometric methods, particularly the use of chemical and isotopic methods for provenience studies, not only for traditional materials but also for humans who relocated. Current projects include exploration of alkaline-earth elements and various isotopic systems in the study of human mobility and the development of non-destructive methods to characterize historical materials.

Chapter 1

Artists' Pigments in Illuminated Medieval Manuscripts: Tracing Artistic Influences and Connections—A Review

Mary Virginia Orna*

Department of Chemistry, The College of New Rochelle, New Rochelle, New York 10805, U.S.A.
*E-mail: mvorna@cnr.edu

For the art historian, chemical analysis of pigments serves two main purposes. It can confirm or deny the alleged attribution or dating of a painting based on comparison with the known painting practices of the artist or period. In addition, the analysis of pigments can have a broader, and perhaps a more profound, importance to the historian as a tool for understanding more about the artistic process itself. This paper reviews the collaborative building of a pigment database, tracing lines of influence and interconnection between medieval centers of manuscript production, clarifying periods of known usage of several important artists' pigments, the difference in pigment usage between Armenian and Byzantine artists, the problems involved with handling manuscripts directly, and anachronistic pigment usage. The technical future of chemical analysis of medieval manuscripts is also discussed.

Introduction

"Color is the most visual, pervasive example of the importance of chemistry to our lives" (*1*). Though medieval artists could not have realized nor expressed this observation since the formal discipline of chemistry would not exist for centuries yet to come, color, for them, was the most visual and pervasive reality in their pursuit of crafting the manuscripts they handed on to us as precious treasures of their era. This paper will review the scientific identification of artists' colors used in manuscripts between the 10th and 16th centuries for the following purposes:

- To determine or confirm place of origin and date;
- To trace lines of influence between and among painting schools and cultures;
- To recommend conservation & handling practice based on the content;
- To uncover forgeries (de-authentication);
- To specify attributions among different painters in a manuscript.

In addition to these objectives, Robert Feller (2) lists two additional ones: objective description of method, and restoration. Although the identification method used and described here consisted of extracting minute samples for analysis by means of X-ray diffraction, infrared spectroscopy and measurement of refractive index, this approach is now questionable in light of the availability of newer, non-invasive techniques that allow the analyst access to the manuscript in situ. The value of these methods will be discussed later in this paper.

The manuscripts described and analyzed in this work came from a variety of Armenian and Byzantine workshops; the dates of their creation range from the early 10th century to the late 16th century.

Pilot Project: The Gladzor (Glajor) Gospel Book of UCLA

The Gladzor Gospel Book (Armenian MS 1, UCLA) has been the subject of very extensive study. Analysis of its palette by X-ray diffraction, Fourier transform infrared spectroscopy and refractive index measurements yielded some rather startling information: virtually all of the pigments used in its manufacture were of mineral origin with the exception of red (madder) lake, which was employed by all five of the artists who worked on the manuscript, and of gamboge, used by the three "apprentice" artists who worked in an atelier other than that of the two master painters (3, 4). A summary of pigment usage by atelier is given in Table I; examples of two of the pigments is shown below in Figure 1.

Madder was derived from the roots of the *Rubia tinctorum* and other members of the *Rubiaceae* family. It has been known from ancient times, having been described by Strabo, Pliny the Elder, Dioscorides and the Talmud. Though most often used as a dye, it could also be used as a pigment if precipitated on a solid substrate such as aluminum hydroxide (5). Gamboge was another plant-derived colorant taken from the sap or ooze of trees of the genus *Garcinia*. It, too, was used extensively from ancient times (6). Since neither of these organic pigments was used extensively in the manuscript, one could safely say that shielding the work from light would not be a principal concern since mineral pigments are virtually lightfast over indefinite periods of time. Such analyses are enormously helpful to curators and conservators who must control the handling of such precious documents.

Analysis of the Gladzor (Glajor is an alternative spelling) Gospel Book not only yielded helpful information regarding conservation, but also was helpful in specifying attributions among different painters in the manuscript. Differences in the employment of the blue pigments indicated the involvement of two different workshops: one used azurite (basic copper(II) carbonate) and high quality natural

ultramine, while the other used lesser quality natural ultramarine. The second workshop also used a purple pigment that consisted of a mixture of red lake and ultramarine; this occurred nowhere in the miniatures attributed to the first workshop. Likewise, gamboge, used in the second workshop was not found among the pigments of the first workshop (*4*).

Table I. Pigments Listed by Atelier as Used in the Gladzor Gospel Book (*3*, *4*)

| Hue	"Master Painter" Atelier	"Apprentice" Atelier
Black	Charcoal black	Charcoal black
Blue	Azurite; Ultramarine	Ultramarine + Ultramarine Ash
Brown	Vermilion mixed with orpiment, gypsum and charcoal black	Vermilion mixed variously with orpiment, gypsum, charcoal black, whiting and hydrated iron oxide
Flesh	Orpiment mixed with realgar	Orpiment mixed with realgar, gamboge, gypsum and anhydrite
Gold	Gold	Gold
Green	Orpiment mixed with azurite or with ultramarine	Orpiment mixed with gamboge or ultramarine plus anhydrite and a trace of vermilion
Magenta	Red lake or red lake mixed with white lead	Red lake
Olive		Gamboge
Orange		Minium or orpiment mixed with minium
Purple		Ultramarine mixed with red lake
Red	Vermilion	Vermilion
White	Calcined bone mixed with quartz	White lead
Yellow	Orpiment	Gamboge, or orpiment mixed with massicot, or realgar mixed with orpiment, gamboge and massicot
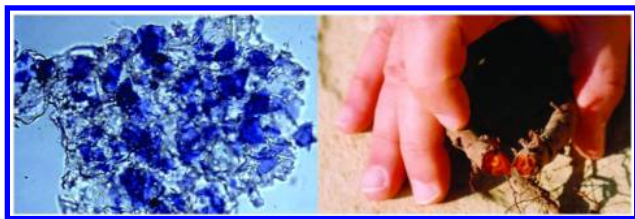
Figure 1. Two pigments found throughout the pages of the Gladzor Gospel Book. Left: A photo-micrograph (130X magnification) of natural ultramarine. (Photograph by M. V. Orna); Right: A broken-open sample of a madder root, Rubia tinctorum (Photograph courtesy of Zvi C. Koren).

Additional Analyses of Armenian and Byzantine Manuscripts

Such a wealth of information was gathered from this pilot project that it was deemed important to try to gather as much information from other Armenian manuscripts to determine if there was indeed a traditional Armenian palette, and also to compare this palette with manuscripts of different origins, such as Byzantine, Persian, Iranian, etc. origins. Hence, the second phase of the study comprised the analysis of the pigments of manuscripts in the United States and Israel representing four distinct developments in the history of Armenian art: A) manuscripts of Greater Armenia and Melitene in the 10th and 11th centuries; B) manuscripts in the vicinity of Lake Sevan in the 12th to 14th centuries (northeastern Greater Armenia); C) manuscripts in the vicinity of Lake Van in the 14th and 15th centuries (central Armenia) (*7*, *8*) and D) manuscripts of the Armenian Kingdom of Cilicia in the 13th and 14th centuries (*9*). Table II is a summary table of all twenty-four of the Armenian manuscripts analyzed by the Cabelli-Orna-Mathews group (*10*). Figure 2 is an illustration from one of these manuscripts, the monumental Trebizond Gospel, so-named from its find spot, but likely to have been produced in the area of Tsamandos (*11*) in eastern Turkey (*12*). In the pages following the summary, the results of the analyses are given and are compared to Byzantine manuscripts at the University of Chicago (Table III lists the ten manuscripts analyzed by Orna and Mathews (*13*, *14*), nineteen Iranian and eleven Indian manuscripts from the Vever Collection in the Arthur M. Sackler Collection of the Smithsonian Institution (*15*), and eight Persian and three Turkish manuscripts from the Spencer Collection of the New York City Public Library (*16*).

Needless to say, it would be impossible to include the volume of data obtained from these manuscripts in this paper, but some observations on the occurrence of certain common pigments present in them will allow us to draw some conclusions about pigment usage in the greater Middle East during the time period in question. We must realize, of course, that this is a very small sampling of the entire corpus of extant manuscripts of these genres, so any generalizations must be tentative. With these caveats in mind, we have selected certain pigments of each observed

hue and listed in Table IV their occurrence on a percentage basis in each of the types of manuscripts described above. Figure 3 is a bar graph of Table IV which affords a basis for visual comparison.

Figure 2. Detail of the Evangelist Luke. Trebizond Gospel, San Lazzaro, Venice 1400/108 and 1925, fol. 299v. Courtesy of the Director, Mekhitarist Monastery of San Lazzaro; photo credit: johndeanphoto.com.

Table II. Armenian Manuscripts

MS No.	Name	Date	Origin
SL 1144/86	Queen Ml'ke Gospel	908-921	Lake Van (east)
W. 537	Gospels of the Priest	966	
St. James 2555†	"Second Ējmiatsin" Gospels	ca. 1000	
SL 887/116	Adrianople Gospel	ca. 1007	Thrace (Greece)

Continued on next page.

Table II. (Continued). Armenian Manuscripts

MS No.	Name	Date	Origin
SL 1400/108 1925	Trebizond Gospel	mid-11th century	Trebizond
St. James 2556	Gospels of King Gagik-Abas	ca. 1050	
FGA 33.5, 47.2-4	Gospels fragment	1050	Melitene group
St. James 1924	Shukhr Khandara Gospels	1064-66	Melitene group
SL 888/159	Karapet Gospel	ca. 1200	Urfa, Cilicia
Chi MS 949	Red Gospels	ca. 1237	Northern Armenia
FGA 32.18	Baron Vasik Gospel	1250	Hromkla, Cilicia (T'oros Roslin)
FGA 44.17	Gospel of Hohannes	1253	Hromkla; Cilicia
W. 539	Gospel on vellum	1262	Hromkla, Cilicia (T'oros Roslin)
PML 789	Gospels fragment	1296	Eastern Armenia
PML 622	Menologium	1348	Sis, Cilicia; (Sargis Pitsak)
St. James 365	Isaiah Commentary	ca. 1305	Eastern Armenia
UCLA Arm MS 1	Gladzor Gospel Book	ca. 1305	Gladzor, eastern Armenia
MMA 38.171.2	John Incipit Leaf	1300-1310	Eastern Armenia
St. James 2360	Gospels of T'oros Tarōnets'i	ca. 1321	Eastern Armenia
St. James 1794	Khach'en MS by the Monk T'uma	ca. 1327	Eastern Armenia
St. James 1941	Sultaniya Gospels by Awag	1334-1336	Eastern Armenia
W. 543	Khizan Gospels by Khach'atur	1455	Lake Van, Armenia
W. 540	Gospels	1475	Lake Van, Armenia
St. James 135	Hymnal of Martiros Khizants'i	1575	Lake Van, Armenia

FGA = Freer Gallery of Art, Washington, D.C.   MMA = Metropolitan Museum of Art, New York, NY.   St. James = Monastery of Saint James, Jerusalem.   SL = Monastery of San Lazzaro, Venice.   PML = Pierpont Morgan Library, New York, NY.   W = Walters Art Gallery, Baltimore, MD.   UCLA = University of California, Los Angeles: University Research Library, Special Collections.   Chi = University of Chicago, Chicago, IL.

Table III. University of Chicago Special Collections Byzantine Manuscripts Analyzed by FT-IR

| MS No.	Name	Date
46	Haskell Gospels	Late 13th Century
129	Nicolaus Gospels	1133
131	Chrysanthus Gospels	Late 12th Century
232	Greek (Phillipps) Gospels	12th Century
727	Georgius Gospels	Late 13th Century
879	Lectionary of Constantine the Reader	Late 12th Century
948	Lectionary of Saint Menas the Wonderworker	Late 12th Century
965	Rockefeller – McCormick New Testament	Late 12th Century
972	Archaic Mark	Mid-12th Century?
1054	Elfleda Bond Goodspeed Gospels	10th Century
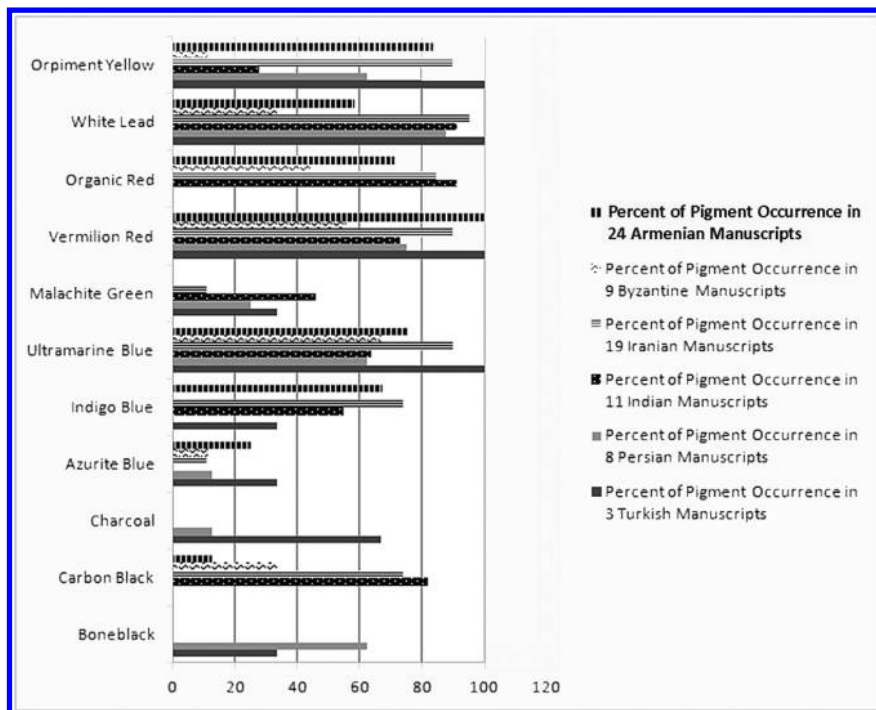
Figure 3. Graphical Representation of the Data in Table IV.

Table IV. Percent of Pigment Occurrence in Medieval Manuscripts of 6 Different Origins

Pigment	Armenian (24)	Byzantine (9)*	Iranian (19)	Indian (11)	Persian (8)	Turkish (3)
Bone-black	0	0	0	0	62.5	33.3
Carbon Black	12.5	33.3	73.7	81.8	0	0
Charcoal	0	0	0	0	12.5	66.8
Azurite Blue	25.0	11.1	10.5	0	12.5	33.3
Indigo Blue	66.8	0	73.7	54.5	0	33.3
Ultrama-rine Blue	75.0	66.7	89.5	63.6	62.5	100
Malachite Green	0	0	10.5	45.5	25.0	33.3
Vermilion Red	100	55.6	89.5	72.7	75.0	100
Organic Red	70.8	44.4	84.2	90.9	0	0
White Lead	58.3	33.3	94.7	90.9	87.5	100
Orpiment Yellow	83.3	11.1	89.5	27.3	62.5	100

* Only nine of the ten Byzantine manuscripts list in Table III are included in this analysis. Chicago MS 972 is discussed separately.

Results and Discussion

At first glance, there seem to be some very clear dividing lines with respect to pigment usage for certain areas. Taking each of the pigments in Table IV, and comparing their usage with alternatives, yields some interesting conclusions.

Carbon Black: Use of this pigment in Armenian and Byzantine manuscripts is moderate, in Iranian and Indian manuscripts, it is the predominant black, and it is totally absent from Persian and Turkish manuscripts. Since both boneblack and charcoal are also entirely absent in the Armenian and Byzantine manuscripts, we can conclude that black was not a very important pigment. Since boneblack is present in the majority of Persian manuscripts, and both charcoal and boneblack are present in the Turkish manuscripts, we conclude that painters in those areas preferred the use of these blacks as opposed to carbon black, possibly because of greater availability of wood and bone in these areas.

Azurite: Azurite, basic copper(II) carbonate, is a blue pigment with a greenish tinge. Its chemical formula is $2CuCO_3 \cdot Cu(OH)_2$. It finds its greatest usage in Armenian and Turkish manuscripts, with moderate usage in Byzantine, Iranian, and Persian manuscripts, whereas it is totally absent from the Indian manuscripts in the cohort. Again, availability may be a factor since azurite deposits throughout Europe have been known since ancient times, but would more than likely have to be imported into the Middle East and beyond. In addition, usage of indigo as a viable alternative blue pigment is very prevalent in almost all of the Armenian, Iranian, and Indian manuscripts.

Ultramarine Blue: Table IV conveys the fact that this blue pigment, obtained from the semiprecious stone lapis lazuli, was almost universally used in the manuscripts examined. While ultramarine, a clathrate compound of polysulfide ions in a silicate cage structure, was highly prized in Europe and cost more than gold, its major deposit was in Afghanistan, a location on the silk road trade route. This can possibly explain its prevalence in Middle Eastern manuscripts since it would not have been an import subject to price hikes of middlemen along the way.

Malachite Green: Malachite, the gemstone as opposed to the organic dye of the same name, is another basic copper(II) carbonate variant with the formula $CuCO_3 \cdot 2Cu(OH)_2$. Curiously, it is totally absent from the Armenian and Byzantine manuscripts examined, but finds moderate usage in the other types of manuscripts. The nearest deposits would have been the Timna Valley, Israel, and the Russian Urals.

Vermilion Red: Evidence of this pigment's almost universal usage is found in Table IV. It is often the most prevalent red pigment in any ancient or medieval sample. Known from ancient times as its natural ore, cinnabar, mercury(II) sulfide, HgS, was also synthesized by heating elemental mercury and elemental sufur together. Large deposits of cinnabar were, and are, found in China and in Almaden, Spain. While it was highly prized as a pigment, its great cost led to the use of lesser red pigments along with it: many of the manuscripts we examined also contain organic red pigments like madder (alizarin) and cochineal (carminic acid) (*14*). The latter has its origin in the "Old World" in the form of a colorant derived from the egg sacs of scale insects of the genus *Kermes*, whereas its "New World" source was the scale insect of the genus *Dactylopius* (*18*).

White Lead: Basic lead(II) carbonate, $2PbCO_3 \cdot Pb(OH)_2$, is another highly prized pigment used from ancient times. It was manufactured by corroding elemental lead with vinegar in the presence of carbon dioxide (often produced by the fermentation of hot horse dung). In the manuscripts we examined, we see its prevalence increase the farther east we go, the Turkish manuscripts being an exception. The Iranian, Indian, and Persian manuscripts examined used only white lead, while silicates are present in the Armenian and Byzantine manuscripts.

Orpiment: This yellow mineral pigment, As_2S_3, enjoyed great usage in Armenian, Iranian, Persian, and Turkish manuscripts, but moderate to little usage in Indian and Byzantine manuscripts. Due to availability, the Indian manuscript painters preferred to employ Indian Yellow, while Byzantine artists preferred to use organic yellow pigments derived from plants. Realgar, As_4S_4, is a red arsenic sulfide often found associated with orpiment in mineral deposits.

Gypsum is calcium sulfate dihydrate, $CaSO_4 \cdot 2H_2O$. Anhydrite is its anhydrous form.

Massicot is the yellowish to reddish-yellow orthorhombic form of lead(II) oxide, PbO. The tetragonal form of PbO is called litharge.

Although these analyses have not yielded information enabling the determination or confirmation of the place of origin and date of these manuscripts, we can say at least that the pigments used correspond to the accepted known usage periods, with one exception, as we will see in the next section. However, the analyses have allowed us to take tentative steps toward tracing lines of influence between and among painting schools and cultures; to recommend conservation and handling practice based on the content, and in one instance, that of the Gladzor Gospel Book, to specify attributions among different painters in a manuscript. So, we have shown that virtually all the purposes associated with the scientific identification of the colors used in manuscripts have been fulfilled with one exception: uncovering forgeries. For this, we must return to an anomalous manuscript grouped with the Byzantine manuscripts in Table III.

The "Archaic Mark," Chicago MS 972 (Gregory-Aland MS 2427)

We have deliberately omitted this manuscript from the above analysis because of the occurrence of an anachronistic pigment on many pages of this manuscript. Figure 4 shows two infrared spectra. The bottom spectrum was obtained from a blue pigment from MS 972 (2427); the top spectrum is a reference spectrum of Prussian blue. The band corresponding to the C≡N of ferric ferrocyanide is common to both spectra. Replicate spectra of blue pigments removed from different locations in MS 972 (2427) indicate that the average frequency of this band is 2083 ± 6 cm^{-1}. The ubiquitousness of an iron blue in this manuscript raises doubts about its authenticity. Figure 5 is a detail from folio 34v, the location of the Prussian blue sample from which the spectrum in Figure 4 was derived.

The iron blues are the first of the artificial pigments with a known history and an established date of first preparation. The color was made by the Berlin color makers Johann Jacob Diesbach and Johann Konrad Dippel (1673-1734) in or around 1706 (*17*). Moreover, the material is so complex in composition and method of manufacture that there is practically no possibility that it was invented independently in other times and places (*18*, *19*). This fact, in addition to the evidence indicating that both MS 972 (2427) and a Gospel fragment from the Hermitage Museum, St. Petersburg (*20*), were copies of a late 12th century gospel book in the National Library of Greece, codex 93 (*21*), suggests that these manuscripts originated some time much later than their purported 12th century fabrication. Furthermore, neither of these manuscripts has a geneaology that can be traced prior to 1930, a fact suggesting that their origin very well may be during the flurry of Athenian forgeries that came to the market in the 1920s (*13*).
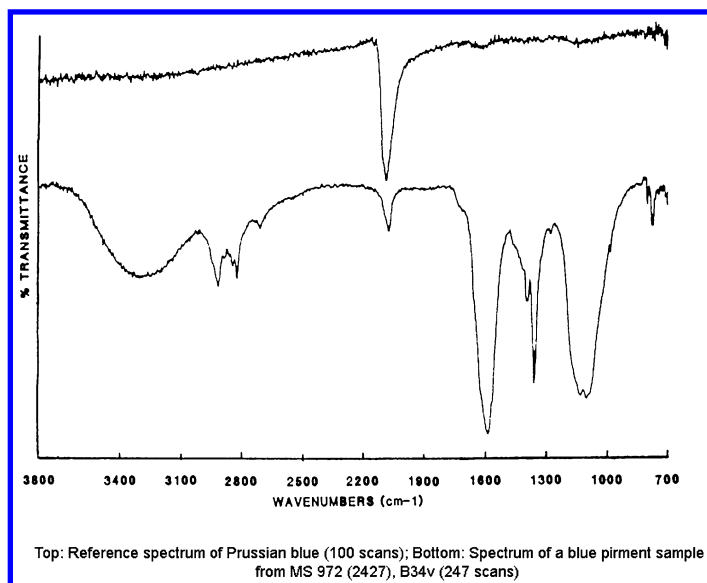
Top: Reference spectrum of Prussian blue (100 scans); Bottom: Spectrum of a blue pirment sample from MS 972 (2427), B34v (247 scans)

Figure 4. Fourier-Transform Infrared Spectrum of folio 34v, Ms. 972 (2427), the "Archaic Mark.", and Archaeological Chemistry, IV. Reproduced with permission from reference Orna, M. V.; Lang, P. L.; Katon, J. F.; Mathews, T. F.; Nelson, R. S. Applications of infrared microspectroscopy to art historical questions about medieval manuscripts. In Allen, R.O., Ed. Archaeological Chemistry, IV (Advances in Chemistry Series, 220). American Chemical Society: Washington, D.C., 1989; pp. 265-288. Copyright 1989, American Chemical Society (13).

In 2006, the University of Chicago Library and the University of Chicago Divinity School moved to lay to rest once and for all the questions that arose from our study and from some later studies done by Abigail B. Quandt of the Walters Art Gallery by calling for further research (*22*). Thanks to funding provided by an anonymous donor, McCrone Associates, Inc. of Westmont, Illinois, was charged with taking samples of the manuscript, specifically from the parchment, the ink, and a range of paints in the manuscript illuminations, and for all the spectrographic analysis carried out on them. The determined goal was, for the first time, to make a comprehensive chemical examination of all components of the codex (parchment, ink, paints and coatings), utilizing the most current technologies available (*23*).

The McCrone report (*24*) unambiguously reconfirmed our initial finding of Prussian blue, an invention of the early 18th century, in the manuscript. Furthermore, the report documented the presence of additional materials that were incongruent with a 12th date, namely, zinc white (ZnO), not used as a pigment until about 1780, and blanc fixe, a synthetic form of barium sulfate introduced in the 1820s. The report also said that the combination of zinc white and blanc fixe suggested the presence of lithopone, or Orr's white, which was not invented until 1874. These findings alone placed the manuscript, at its earliest, at the latter

part of the 19th century. Furthermore, infrared spectroscopy also indicated the presence of cellulose nitrate most likely used as a binding medium; it was only in 1920 that this material became widely available. Finally, almost three months later, the report on the radiocarbon dating of the manuscript parchment gave a calibrated (95% confidence) date range of 1461-1640 (*25*), indicating that the forger(s) used old parchment, but apparently, not old enough!

Figure 5. Folio 34v, Chicago Ms 972 (2427), the "Archaic Mark." The blue pigment in this miniature was analyzed by FT-IR (spectrum above) and found to be Prussian blue. Courtesy Special Collections Research Center, University of Chicago Library.

In a video produced by the University of Chicago and broadcast on 26 October 2009 (*26*), Dr. Margaret M. Mitchell, one of the principal investigators on the Archaic Mark project, announced the results of the investigation. She first stated the importance of the discovery because of all the New Testament manuscripts extant, the Archaic Mark had the highest degree of correspondence with Codex Vaticanus, the oldest complete text of the Gospel of Mark (4th century). She then announced that the manuscript, purchased by the university in 1941, is a modern production that was fabricated between 1874 and the first decades of the 20th century, and would no longer be included in critical editions of the Greek New Testament. However, she also pointed out the value of the data collected insofar as it will help ongoing scholarly investigations into and detection of manuscripts forged in the modern period.

The Future of Illuminated Manuscript Analysis

All of the examples cited above, including the very recent re-analysis of the "Archaic Mark," were done by extraction of minute particles from the manuscripts, and then subsequent small particle analysis by a variety of means, including X-ray crystallography, Fourier transform infrared microspectroscopy, polarized light microscopy, chemical microscopy, scanning electron microscopy with X-ray fluorescence analyzer and X-ray fluorescence. These methods, though highly sophisticated, are almost universally available to the analytical chemist.

A very promising method that until about a decade or so ago has not been universally available is micro Raman spectroscopy, or Raman microscopy (RM), a method capable of delivering unambiguous results without the necessity of removing small particles from the manuscript, and therefore a method most dear to the heart of any curator of precious manuscripts. Furthermore, according to the doyen of RM, Robin J. H. Clark (*27*), the method can identify mixtures of pigments at high spatial ($\leq$ 1 μm) resolution and down to even picogram quantities, is non-destructive, largely immune to interference, and able to be applied to manuscripts in situ, and even to identifying the reaction products of inorganic pigments that have degraded on the manuscript page (*28*). Difficulties arise when organic pigments are present as they are both prone to photochemical degradation and to fluorescence. A typical RM instrument is shown in Figure 6.

Figure 6. A typical RM Spectrometer (Horiba LabRAM) equipped with EDGE filters, 10, 50 and 100X objectives and telecamera. Courtesy of the University of Modena and Reggio Emilia, Italy. Photograph: M. V. Orna.

Another difficulty to overcome initially was the lack of a comprehensive guide to the pigments used in antiquity and a library of their Raman spectra for the sake of comparison. By dint of hard work over a period spanning more than six years, Clark and his co-workers succeeded in assembling pigment databases (*29*, *30*) that have become among the most cited papers in art conservation science. From their first major success in identifying the pigments in a 13th century Paris bible (*31*), the Clark team has gone on to identify and characterize yellow pigments in manuscripts (*32*), examine spectroscopically almost 200 manuscript cuttings and miniatures from a variety of Italian schools (*33*), and establish the palette of 16th and 17th century Persian manuscripts (*34*), among many other projects summarized in a *Chemistry in New Zealand* review article (*35*). Using RM, another team based at Trinity College, Dublin, succeeded in confirming the pigment analysis work done on the famed Book of Kells over the course of the past 60 years (*36*). New data on RM analysis of Armenian manuscripts from Yerevan, Armenia, is being developed by an Italian team headed by Pietro Baraldi anYeghis Keheyan (*37*). It is to be hoped that their data can be profitably added to the database discussed in this paper.

In addition to the spectral databases cited above, a cooperative database of IR (in the mid-infrared range) and Raman spectra pertinent to cultural heritage materials has been developed by the Infrared and Raman Users' Group (IRUG) and is available online at www.irug.org. Its most recent peer-reviewed edition contains over 2000 peer-reviewed spectra.

Another analytical tool, terahertz time-domain spectroscopic imaging (THz-TDSI), is becoming quite popular in the area of evaluation and conservation of works of art. The availability of the technique is growing rapidly, as is evidenced by the recent multi-session symposium held on the topic at the 245th American Chemical Society National Meeting at New Orleans, Louisiana during the week of April 7-11, 2013. And this one technique seems to be able to fulfill all of the requirements for examination of historical artifacts – to be non-destructive, non-invasive, spatially precise, and applicable in situ (*38*). While these are attributes of RM as well, THz-TDSI has another that is fast making it indispensable, i.e., imaging that includes THz tomography which can give non-invasive cross section images of works of art (*39*). Furthermore, as in the mid-infrared region, THz frequency spectra exhibit fingerprint-like absorption bands of substances of cultural heritage interest.

The frequency of the THz range is from 0.1 to 10 THz ($3 - 300$ cm^{-1}, i.e., between the far infrared and radar regions of the spectrum). Its use as an analytical tool was limited in the past by the lack of stable THz sources as well as by the necessity of custom building the necessary apparatus. Although these technical difficulties have largely been solved and there are several commercial instruments now on the market, an ongoing problem for THz users in art conservation was the lack of a suitable database comparable to the IRUG database. This problem is also in the process of being solved by the establishment of an online spectral database of artists' materials (www.thzdb.org) which, as of the writing of this paper, contained over 1500 spectra obtained by FT-THz in transmission and reflection modes, and by THz-TDSI in transmission mode (*40*). It seems that THz-TDSI is rapidly

catching up with RM and that the two together will form a formidable partnership in the future analysis of cultural heritage artifacts.

References

1. Freemantle, M. *C&EN*, February 26, 2001, p 50.
2. Feller, R. L., Ed.; *Artists' Pigments: A Handbook of their History and Characteristics*; National Gallery of Art: Washington, DC, 1986; Vol. I.
3. Orna, M. V.; Mathews, T. F. *Stud. Conserv.* **1981**, *26*, 57–72.
4. Mathews, T. F.; Sanjian, A. K. *Armenian Gospel Iconography: The tradition of the Glajor Gospel, with contributions by Mary Virginia Orna, OSU, and James R. Russell*; Dumbarton Oaks Research Library and Collection: Washington, DC, 1991; pp 48−51 and 227−230.
5. Schweppe, H.; Winter, J. Madder and Alizarin. In *Artists' Pigments: A Handbook of their History and Characteristics*; FitzHugh, E. W., Ed.; Oxford University Press: New York; Vol. 3, pp 47−79.
6. Hanelt, P., Ed.; *Mansfield's Encyclopedia of Agricultural and Horticultural Crops (except Ornamentals)*; Springer: Heidelberg, Germany, 2011; pp 1352 ff.
7. Cabelli, D. E.; Mathews, T. F. *J. Walters Art Gallery* **1982**, *XL*, 37–40.
8. Cabelli, D. E.; Mathews, T. F. *Revue des études arméniennes, n.s.* **1984**, *XVIII*, 33–47.
9. Cabelli, D. E.; Orna, M. V.; Mathews, T. F. Analysis of Medieval Pigments from Cilician Armenia. In *Archaeological Chemistry, III*; Lambert, J. B., Ed.; Advances in Chemistry Series 205; American Chemical Society: Washington, DC, 1984; pp 243−254.
10. Mathews, T. F.; Wieck, R. S. *Treasures in Heaven: Armenian Illuminated Manuscripts*; The Pierpont Morgan Library: New York and The Princeton University Press: Princeton, NJ, 1994; p 136.
11. Bell, G. *Amurath to Amurath: A Journey along the Banks of the Euphrates*, 1st ed.; W. Heinemann: London, 1911; p 345.
12. Mathews, T. F. *The Kars-Tsamandos Group of Armenian Illuminated Manuscripts of the Eleventh Century. Philopation: Studies in Honor of Arne Effenberger*; Romisch-Germanisches Zentralmuseum: Mainz, Germany, 2013.
13. Orna, M. V.; Lang, P. L.; Katon, J. F.; Mathews, T. F.; Nelson, R. S. Applications of Infrared Microspectroscopy to Art Historical Questions about Medieval Manuscripts. In *Archaeological Chemistry, IV*; Allen, R. O., Ed.; Advances in Chemistry Series 220; American Chemical Society: Washington, DC, 1989; pp 265−288.
14. Lang, P. L.; Orna, M. V.; Richwine, L. J.; Mathews, T. F.; Nelson, R. S. *Microchem. J.* **1992**, *46*, 234–248.
15. FitzHugh, E. W. Study of Pigments on Selected Paintings from the Vever Collection. In *An Annotated and Illustrated Checklist of the Vever Collection*; Lowry, G. D., Beach, M. C., Eds.; Arthur M. Sackler Gallery, Smithsonian Institution: Washington, DC, 1988; p 426.

16. Data supplied by Barbara Schmitz.

17. Kraft, A. *Bull. Hist. Chem.* **2008**, *33* (2), 61–67.

18. Orna, M. V. *The Chemical History of Color*; Springer: Heidelberg, Germany, 2013; p 57.

19. Gettens, R. J.; Stout, G. L. *Painting Materials: A Short Encyclopedia*; Dover Publications: Garden City, NY, 1966; pp 20−21.

20. Treu, K. *Die griechischen Handschriften des neuen Testaments in der USSR*; Akademie-Verlag: Berlin, Germany, 1966; pp 229−230.

21. Marava-Chatzinicolaou, A.; Toufexi-Paschou, C. *Catalogue of the Illuminated Byzantine Manuscripts of the National Library of Greece*; Publications Bureau of the Academy of Athens: Athens, 1978; Vol. 1, pp 224−243.

22. Mitchell, M. M.; Duncan, P. A. *Novum Testamentum* **2006**, *48*, 1–35.

23. Mitchell, M. M.; Barabe, J. G.; Quandt, A. B. *Novum Testamentum* **2010**, *52*, 101–33.

24. Private communication to Patricia A. Gibbons (University of Chicago) from Joseph G. Barabe (McCrone Associates), dated July 21, 2008; 61 pp.

25. Private communication to Joseph G. Barabe (McCrone Associates) from A. J. T. Jull (NSF Arizona AMS Laboratory), dated October 9,2008.

26. Mitchell, M. M. University of Chicago Video broadcast on October 26, 2009. http://mindonline.uchicago.edu/media/communications/news/archaic_mark_10262009_512k.mov (accessed on February 5, 2013).

27. Everts, S. *C&EN*, December 17, 2012, p 36.

28. Clark, R. J. H. *Chem. Soc. Rev.* **1995**, 187–196, DOI: 10.1039/cs9952400187.

29. Bell, I. M.; Clark, R. J. H.; Gibbs, P. J. *Spectrochim. Acta, Part A* **1997**, *53*, 2159.

30. Burgio, L.; Clark, R. J. H. *Spectrochim. Acta, Part A* **2001**, *57*, 1491.

31. Best, S.; Clark, R.; Daniels, M.; Withnall, R. *Chem. Br.* **1993** February, 118–122.

32. Clark, R. J. H.; Cridland, L.; Kariuki, B. M.; Harris, K. D. M.; Withnall, R. *J. Chem. Soc. Dalton Trans.* **1995**, 2577–82.

33. Burgio, L.; Clark, R. J. H.; Hark, R. R. *Proc. Nat. Acad. Sci. U.S.A.* **2010**, *107* (13), 5726−5731. www.pnas.org/cgi/doi/10.1073/pnas.0914797107.

34. Muralha, V. S. F.; Burgio, L.; Clark, R. J. H. *Spectrochim. Acta, Part A* **2012**, *92*, 21–28.

35. Clark, R. J. H.*Chem. N. Z.*, January 2011, pp 13−21.

36. Bioletti, S.; Leahy, R.; Fields, J.; Meehan, B.; Blau, W. *J. Raman Spectrosc.* **2009**, *40*, 1043−1049.

37. Baraldi, P.; Eliazian, G.; Keheyan, Y. *A Study on the Polychromy and Technique ofSome Armenian Illuminated Manuscripts by Raman Microscopy*, 2013, in press and private communication.

38. Jackson, J. B.; Mourou, M.; Whitaker, J. F.; Duling, I. N., III; Williamson, S. L.; Menu, M.; Mourou, G. M. *Opt. Commun.* **2008**, *281*, 527–532.

39. See for example, Adam, A. J. L.; Planken, P. C. M.; Meloni, S.; Dik, J. *Opt. Express* **2009**, *17*, 3407.

40. Fukunaga, K.; Picollo, M. *Appl. Phys. A* **2010**, *100*, 591–597.

Chapter 2

Investigation of Ancient Roman Pigments by Portable X-ray Fluorescence Spectroscopy and Polarized Light Microscopy

Ruth F. Beeston*,[1] and Hilary Becker[2]

[1]Department of Chemistry, Davidson College, Davidson, North Carolina 28035
[2]Department of Classics, University of Mississippi, University, Mississippi 38677
***E-mail: rubeeston@davidson.edu**

The subject of this study is a collection of raw pigments from a second to early fourth century C.E. pigment shop located in the Area Sacra di S. Omobono, in the Forum Boarium in Rome. The shop was excavated in 1974, yielding a total of more than two kilograms of blue, light blue, green, yellow, orange, red, pink, and white pigments. An ongoing project to re-examine materials from this excavation resulted in an opportunity to study this remarkable pigment collection. A Bruker Tracer III-SD portable X-ray fluorescence spectro-meter was used to determine major, minor and trace elements present in representative samples of each pigment. On this basis, the types of pigments available for trade in this ancient marketplace were identified as Egyptian blue (two prep-arations), green earth, at least five distinct iron earth pigments (red, yellow, and orange ochres) and lime white (calcium carbonate). Additional characterization of select pigment samples was conducted using polarized light microscopy.   Particle characteristics observed under transmitted and reflected light and between crossed-polars were compared to those observed for reference samples of historical pigments.

Background

The scientific examination of colorants used in antiquity has a long history, beginning with the characterization of pigment samples from Rome and Pompeii by Jean-Antoine Chaptal and Sir Humphry Davy in the early 19th century (*1*). Pigment studies have been motivated by the desire to understand more fully the materials and methods of ancient artists, to attribute objects to particular time periods more accurately, to re-imagine the original appearance of painted objects, and to determine appropriate treatments for the conservation of painted surfaces. A great deal is now known about the availability and origins of natural and synthetic pigments in antiquity and the techniques used to apply them to wall paintings, sculpture, architecture, and pottery.

Much of what we know about pigment use by the Greeks and Romans comes from ancient literary sources, including *De Lapidibus* by Theophrastus, *De Architectura* by Vitruvius, and *Historia Naturalis* by Pliny the Elder. Other information relating to the procurement of colorants has been gathered through experimental archaeology, including efforts to recreate processes for the production of manufactured pigments such as Egyptian blue (*2*, *3*) and the extraction of Tyrian purple from murex snails (*4*).

Most studies involving the scientific analysis of ancient pigments require the examination of samples removed from painted surfaces or *in situ* analysis using non-destructive techniques. Because painting methods involve incorporating the pigments into the surface layer of lime mortar applied to a wall or other support (*fresco* technique), or mixing powdered pigments with an organic binder such as wax, egg, gum, or oil (*secco* techniques), pigment analyses are usually complicated by the presence of mixtures of materials. The application of pigment to a surface typically results in a complex, multi-layered structure that requires careful sampling and interpretation. Further complications can be introduced by surface weathering, deterioration due to the burial environment, discoloration reactions, improper cleaning of painted objects, and modern restorations. Despite these complications, many successful studies involving the analysis of pigments found in Roman wall paintings have been conducted (*e.g.* (*5–8*)).

In more unusual instances, deposits of raw, unadulterated pigments ready for use by ancient artists have been uncovered and studied. These finds present archaeologists with unique glimpses into the practice of painting through the observation of the pure raw materials available to artists. Commercial spaces, such as workshops and shops for production and sale of colorants, a number of which were uncovered in Pompeii, offer the opportunity to study not just pigment composition but also the economics of the pigment industry in antiquity (*9*, *10*). There is even a house that was in the process of being painted on the day of the eruption of Mt. Vesuvius, the "House of the Painters at Work" (*Casa dei pittori al lavoro* (IX, 12, 9)) in Pompeii. The excavation of this house revealed pigments in their pure form (contained in roughly 50 ceramic vessels), containers of lime plaster, artists' tools, along with frescoes that were only partially finished at the time of the fateful eruption (*10*, *11*).

Pigments were an important commodity for the production of frescoes and the decoration of architectural elements as well as for use in cosmetics and medicinal

preparations. The economic values of pigments varied based on availability, the intensity of the hue, the distance from the source to the place of sale, and the difficulty in manufacturing or processing the colorant. Pliny (*HN* 35.30) describes a distinction between "florid" pigments (*floridi colores*), those that are rare and highly valuable, such as cinnabar and purple, and "austere" pigments (*austeri*), those that are common, abundant, and less brilliant, including the earth pigments. One of the motivations for this study was to understand better the trade in colorants in the Roman world during the first through fourth centuries C.E.: What pigments could one easily purchase in a marketplace? Were they mined or manufactured locally? How do they compare to the colorants described in literary sources?

The Pigment Shop at Area Sacra di S. Omobono

The pigment samples that are the subject of this study originate from a pigment shop dating to the second to early fourth centuries C.E. located in the Forum Boarium in Rome. The pigment shop was excavated in 1974, and the function of the shop was immediately apparent to those excavating (*12*). It was one of several shops built on the podium of twin temples dedicated to Fortuna and Mater Matuta in the Forum Boarium, located adjacent to the Tiber River. The pigment shop consisted of two rooms, but pigments were found only in the front room that faced a street. The pigments were found along with occasional sherds of commonware pottery mixed in with earth of the two occupation layers of this store. Significantly, this pigment shop is, to date, the only extant pigment shop from ancient Rome and so provides a fascinating opportunity to see the supply-side of an important commodity in ancient Rome.

An initial report of chemical analysis of some of the pigments was published by Maria M. Capasso in the contemporary excavation report in 1978. Selected pigment samples were examined by Marisa Laurenzi Tabasso at the Istituto Centrale del Restauro in Rome using microchemical testing and non-dispersive x-ray fluorescence; a limited number of elements (Ca, Cu, Fe, Sn, and Pb) were detected and reported (*13*). The pigments were rediscovered in 2009 as part of a systematic effort to re-examine the stratigraphy and material remains revealed by past excavations of the site. The scientific examination of the pigments was initiated in 2011.

Techniques for Pigment Characterization

Numerous analytical techniques have been applied to the identification and characterization of ancient pigments. Noninvasive methods applied to painted surfaces include infrared and ultraviolet photography, portable x-ray fluorescence spectrometry, and, more recently, Raman scattering. Where sampling is an option, the examination of pigment particles via polarized light microscopy, scanning electron microscopy with energy dispersive x-ray analysis, and microchemical testing can give valuable information about particle properties and elements present in the sample. X-ray diffraction and IR and Raman spectroscopy provide more detailed information about the specific compounds and polymorphs present in a pigment sample.

For this study, portable x-ray fluorescence spectroscopy (pXRF) was conducted on-site, allowing the determination of characteristic elements present in each sample. In this method, the sample (lump of raw pigment or powdered material) is excited by a beam of x-rays from an x-ray tube, causing the ejection of core electrons from the atoms at the surface of the sample. As higher energy electrons fall to fill these vacancies, characteristic x-rays are emitted by the atoms. The x-rays are detected and a plot of intensity (number of photons) versus energy of the transition (keV) is displayed. The elements present give rise to characteristic peaks in the spectrum, enabling the user to identify major, minor, and trace elements in the sample. Disadvantages of the method include the fact that elements lighter than magnesium are not detected, and the spectrum cannot be relied upon for quantitative information without very careful analysis of standards that are closely related to the samples under study. An excellent source of information about applications and limitations of pXRF as a tool for examination of archaeological samples can be found in a recent book edited by Shugar and Moss (*14*).

In addition to characterization by pXRF, the technique of polarized light microscopy (PLM) was utilized to examine selected pigment samples from S. Omobono. This technique allows the determination (and comparison to reference samples) of particle properties such as color, transparency, size distribution, refractive index, behavior under crossed polars, and purity. The presence of combinations of particles can provide evidence for particular types of pigments or for the mixing of pigments to produce various hues.

Materials and Methods

Samples for analysis were selected from over 15 containers each holding up to 450 g of raw pigments in lump or pellet form, sorted by color and kept in storage since their discovery during the 1974 excavation season. Sample labels used here include the pigment color and *sacchetta* number previously assigned to each container.

Most samples were analyzed without disturbing the surface, but in some cases the surface was scraped with a porcelain spatula to reveal a fresh layer, and in other cases powdered samples were produced by crushing a portion of a lump or pellet in a porcelain crucible. Historical pigment samples used for comparison purposes were obtained from Kremer Pigments, Inc. (New York) and Zecchi (Florence).

XRF spectra were collected using a Bruker Corporation Tracer III-SD portable XRF spectrometer. Samples were placed on a 2.5 inch diameter disc of 40μm gauge polypropylene film (Premier Lab Supply) placed directly over the x-ray window on the stage. The instrument was operated with S1PXRF software with a timed run time of 240 seconds. Two sets of conditions were used for each sample. For detection of low mass elements (Al, Si, P, Cl, S, K, Ca, C, Cr, and Fe), the "Blue" filter (0.001" Ti) was installed and the portable vacuum pump was turned on. Voltage was set to 15 keV with a current setting of 22.8 μA. To optimize detection of higher mass elements, the "Green" filter (0.003" Cu, 0.001" Ti, 0.012" Al) was installed, as recommended by the manufacturer for analysis of silicate and

ceramic materials as well as colorants. No vacuum was applied, and the instrument was set to 40 keV and 14 μA.

pXRF spectra were processed and analyzed using ARTAX software. The broad signal centered at 19 keV (Compton backscatter peak) and peaks for Rh (Kα, 20.22 keV; Kβ, 22.72) and Pd (Kα, 21.18 keV; Kβ, 23.82 keV) arise from the x-ray target and detector collimator, and are ignored in the spectra, since these are unrelated to the sample. Most spectra revealed a small peak at 25.27 keV, characteristic of Sn. However this peak may also be attributable to a Pb sum peak (*14*). The presence of Sn is only noted in the results presented here when both Kα and Kβ peaks can be discerned. It should also be pointed out that trace signals for other elements (Fe, Ni, Cu, Zn) may also arise from the instrument rather than the sample, depending on instrument parameters and sample density. Finally, large peaks for certain elements may mask the presence of trace peaks for other element.

Selected pigment pieces were packaged into vials, and with appropriate permission, delivered to our laboratory at Davidson College for further analysis by polarized light microcopy. An Olympus BX-40 Polarizing Microscope was utilized at 400X magnification. Slides were prepared as dispersion samples using Meltmount from Cargille Labs (refractive index 1.662). Refractive index determinations were made using the Becke line method. Photographic images were obtained with an Infinity 1-2c Camera and Infinity Analyzer software. A reference set of paint pigment slides was obtained from McCrone Microscopes and Accessories.

Results and Discussion

It is not known if the various pigment colors were found completely intermingled within the shop or were discovered in concentrated clusters of particular colors. Also unclear is the method by which the pigments were sorted by the original excavation team prior to storage. When rediscovered in 2009, the pigments were organized by color in numbered plastic containers. Figure 1 shows photos of the individual pigments in their storage containers.

In the following sections, we discuss the pigments known to be available to ancient Roman painters, and we present our findings regarding the elemental composition and particle properties of each type of pigment represented at S. Omobono.

Blue and Light Blue

It is the vivid blue pigments that are the most noticeable during a first glance at the array of Roman pigments from S. Omobono. These are also the most abundant of the samples, with a total mass of 1100 g and colors ranging from deep blue to sky blue.

Blue pigments known to be used during this time period include azurite, a ground copper mineral ($2CuCO_3 \cdot Cu(OH)_2$); indigo, an organic colorant from plant leaves that was used as both a dye and a pigment ($C_{16}H_{10}N_2O_2$); and Egyptian blue, the first manufactured pigment, dating to the third millenium B.C.E. The chemical

composition of Egyptian blue is that of the mineral, cuprorivaite ($CaCuSi_4O_{10}$). As its name suggests, the pigment we call Egyptian blue originated in Egypt but came to be used by culture groups elsewhere in the Mediterranean region. Vitruvius (*De arch.* 7.11.1) describes the process of its manufacture at Pozzuoli, a town in the bay of Naples:

"Sand is ground with flower of natron so finely that it becomes almost like flour. Copper, broken by coarse files until it is like sawdust, is sprinkled with this sand until it clings together. Then it is formed into balls by rolling it between the hands and bound together to dry. Once dry, the balls are put into a ceramic pitcher, and the pitchers are put into a kiln. In this way the copper and the sand, boiling with the energy of the fire, bond together, and exchanging their sweat between them they leave off their original properties; with their natures merged they produce a blue color" (*15*)

Figure 1. S. Omobono Pigments: a. (left to right): Blue S4, Blue S20, Blue S8 b. Blue S11.4 c. Green S12 d. Yellow S13 e. Peach S2 f. Red S5 g. Red S7 h. White S10. (see color insert)

Another ingredient necessary for the production of Egyptian blue is calcium carbonate or lime; it is thought that the local sand available at Pozzuoli was already rich in calcium (*16*), explaining the omission of this ingredient by Vitruvius. Copper, the source of the blue color, was introduced either as metallic copper, copper ore, or bronze.

There are three visually distinguishable blues at S. Omobono. The first type fills two containers, Blue S4 (212 g) and Blue S20 (423 g), and consists of small spherical pellets (and some irregular shaped pieces) of rough textured, gritty, bright blue material. These have the expected appearance of Egyptian blue, based on the description of the process and on photos of experimental batches of Egyptian blue produced by Kakoulli (*2*). These samples are very hard and not easily ground to a powder, but when pulverized produced a lighter blue color.

The pXRF spectra of representative pieces of Blue S4 and Blue S20 are shown in Figure 2. As expected, copper is found to be the major element in these samples. Significant peaks for Ca, Fe, Pb, and Sn are also present. A small peak for Si, an important component of Egyptian blue, is observed (this element is harder to detect due to the low energy of x-ray emission). Trace elements noted include K, Sr, Zr, and in some samples, Mn, Ti, and Sb. The presence of tin in these samples is very interesting. Capasso also noted traces of tin (along with copper and calcium), referring to it as an impurity (*13*). It is likely, however, that the tin in these samples originates from the use of bronze in place of copper metal in the manufacture of the Egyptian blue pigment being sold at S. Omobono, a practice that has been noted previously (*17*). Almost all of the pigment samples from S. Omobono showed a peak for lead; in Egyptian blue, lead may originate from bronze or from lead glass in the formulation, but it is also possible that the lead is introduced into these samples from the burial environment. The sample of S20 that was pulverized showed much smaller lead peaks, indicating that perhaps the lead is concentrated on the surface of the pigment pellets. However, relative lead peak sizes may also arise due to other factors related to sample size, thickness, and orientation, and cannot be relied on as quantitative indications of lead levels.

The second type of blue pigment consists of powdery, light blue lumps of variable size and shape, Blue S8 (446 g). Despite the difference in appearance and texture, the pXRF spectrum of Blue S8 (Figure 3) is very similar to those of Blue S4 and S20, although the relative peak sizes for Sn and Pb vary considerably from sample to sample. pXRF again shows the presence of a dominant Cu peak, with Ca, Fe, Pb, Sn as minor elements, and small peaks for Si, K, Ti, Sr, and Zr. The third type of blue pigment, Blue S11.4 (30 g) is chalky, pale blue, uniform in color and very soft and powdery. The pXRF spectrum of Blue S11.4 is indistinguishable from that of Blue S8 shown in Figure 3. Based on the similarities in the elemental profiles of the darker and lighter blue pigments, it appears likely that the pale blues are more highly processed samples of Egyptian blue, ground to smaller particle sizes and perhaps purified by washing, screening or other processes.

The same conclusion was reached based on examination of samples of Blue S20, Blue S8, and Blue S11.4 with polarized light microscopy. Dispersion samples of each of these pigments showed a heterogeneous mixture of particle types, including clear, bright blue particles mixed with colorless, very transparent particles of varying shapes and sizes. Blue S20 and Blue S8 additionally show

In Archaeological Chemistry VIII; Armitage, R., et al.;
ACS Symposium Series; American Chemical Society: Washington, DC, 2013.

brown, red, and tan impurities. The blue and colorless particles are anisotropic and have a refractive index below 1.662. Particle characteristics are similar to those observed for a modern sample of Egyptian blue obtained from Kremer pigments. The presence of multiple particle phases, including blue $CaCuSi_4O_{10}$, and colorless glass or quartz particles is also evident in photomicrographs of Egyptian blue presented by Kakoulli (*18*).

As shown in the photomicrographs provided in Figure 12a (Blue S20) and 12b (Blue S8), the particles are smaller and more uniform in size for the paler blue sample. This observation is consistent with the idea that these pigments are more finely ground versions of the Egyptian blue pellets.
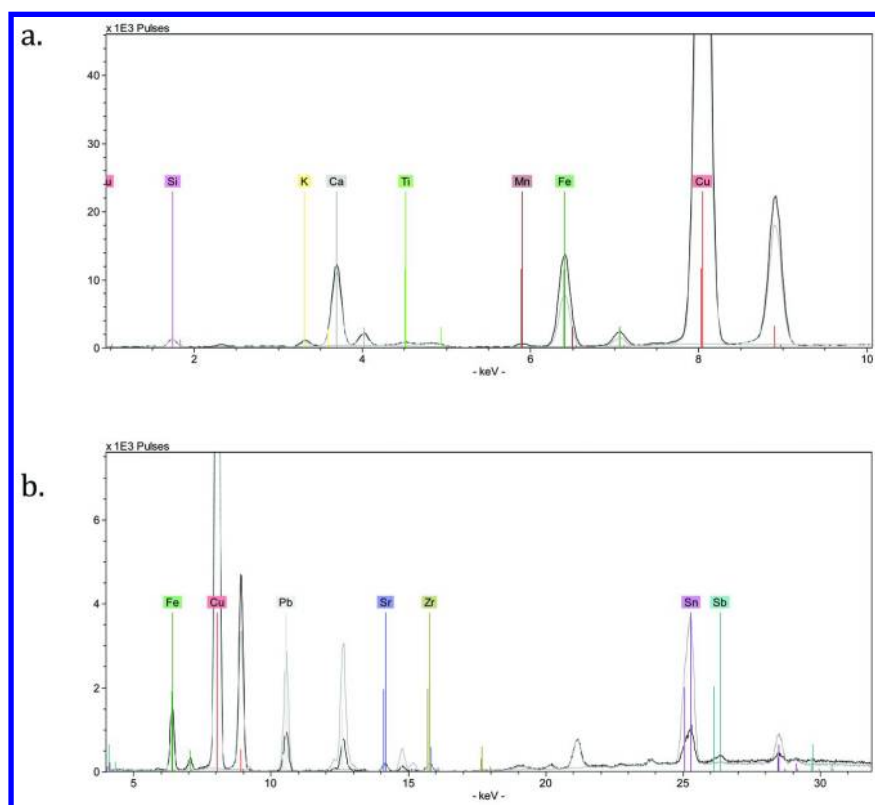
Figure 2. pXRF Spectra of Pigments Blue S4 (black line) and Blue S20 (gray line); a. Low mass elements b. High mass element.
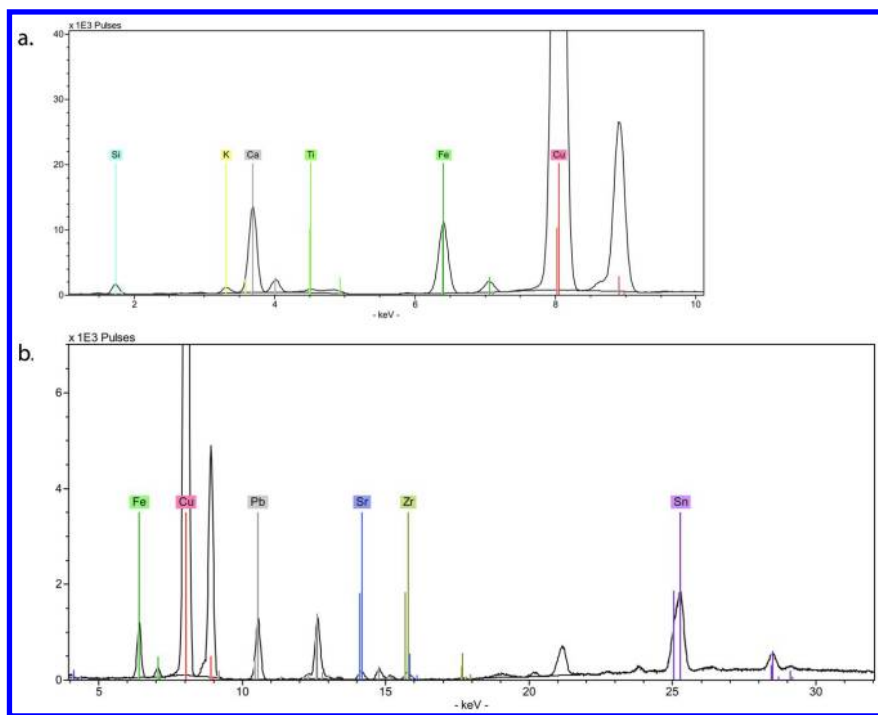
Figure 3. pXRF Spectra of Pigment Blue S8 a. Low mass elements b. High mass elements.

Green Pigment

Green pigments known in antiquity include malachite, a ground copper ore $(CuCo_3 \cdot Cu(OH)_2)$; verdigris, a synthetic pigment produced by the corrosion of copper with vinegar or wine $(Cu(C_2H_3O_2)_2 \cdot 2Cu(OH)_2)$; and green earth, a class of iron aluminosilicate minerals that includes, most commonly, glauconite and celadonite. Vitruvius mentions "green chalk" from Smyrna (*De arch.* 7.7.4) and Pliny refers to a pigment known as *appianum*, an inexpensive imitation of malachite (*HN* 35.48). The chemical formula of green earth is variable: $(K,Na)(Mg,Fe)(Fe,Al)Si_4O_{10}(OH)_2$.

The green pigments from the shop at S. Omobono are found in two containers and are referred to as Green S12 (135 g) and Green S3 (90 g). Both consist of soft lumps of blue-green (aqua) material and there is no obvious visual difference between the contents of the two containers. Two pieces of green pigment had been analyzed previously and were found to contain Fe and Ca (*13*). These results suggest that this pigment is green earth. However, the hue is more similar to the bluish-green of ground malachite than the duller, more earthy hue of many green earths.

Both the pXRF spectra (Figure 4) and the microscopic examination of Green S12 and Green S3 samples confirm that these are, indeed, green earth. It is not possible to identify the specific mineral by these methods, but it is clear that Fe is the major element, with smaller peaks observed for other elements known to be present in green earth, including K, Al, and Si. Peaks for Ti, Mn, Cu, Zn, Pb, Rb, and Sr are also observed. Although Capasso reports the presence of calcium in this pigment (*13*), no Ca peaks were observed in the XRF spectra of samples tested in this study.

A dispersion sample of Green S3 was examined by polarized light microscopy, revealing pale, transparent rounded particles that appear flattened and fragmented (Figure 12c). While the individual particles vary somewhat in hue from aqua to yellow-green in transmitted light, there is no evidence for mixing with Egyptian blue in order to create the blue green color (mixing could explain the copper peak observed by pXRF). The particles have a refractive index below 1.662, low contrast, and are anisotropic, appearing blue between crossed polars. When compared to reference slides of green earth, a good match between particle characteristics is observed.
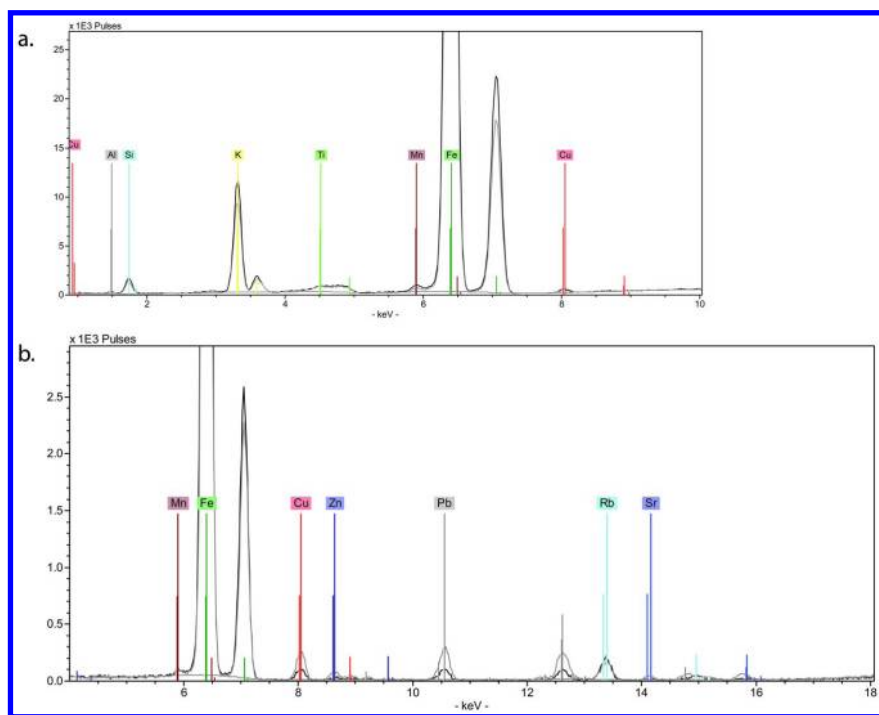

Figure 4. pXRF Spectra of Pigments Green S3 (black line) and Green S12 (gray line); a. Low mass elements b. High mass elements.

Yellow and Orange Pigments

The most widely used and readily available yellow pigment in antiquity is yellow ochre, a class of earth pigments that owe their color to minerals containing FeO(OH)·nH₂O (goethite and limonite). Vitruvius (*De arch.* 7.7.1) mentions the superior quality of a yellow ochre obtained from silver mines in Athens and also indicates that ochre is found in many other locations. Less common, but also mentioned by Vitruvius (*De arch.* 7.7.5) are the arsenic containing minerals, orpiment (yellow As_2S_3) and realgar (orange-red As_4S_4).

Among the finds from the S. Omobono pigment shop are two distinct pigments with a yellowish hue. One is a yellow-gold color, present in large soft lumps that are easily powdered (Yellow S13, 430 g), the other consisting of powdery pastel orange/peach lumps (Peach S2, 80 g). In the 1978 study, three pieces described as *giallo* (yellow) were analyzed; only Fe and Ca were detected, and the samples were identified as yellow ochre (*13*).

The pXRF spectra of a sample of Yellow S13 (shown in Figure 5) are dominated by a very large iron peak; other smaller peaks include Ca, Ti, V, Mn, Cu, Zn, Pb, As, Sr, and Zr.
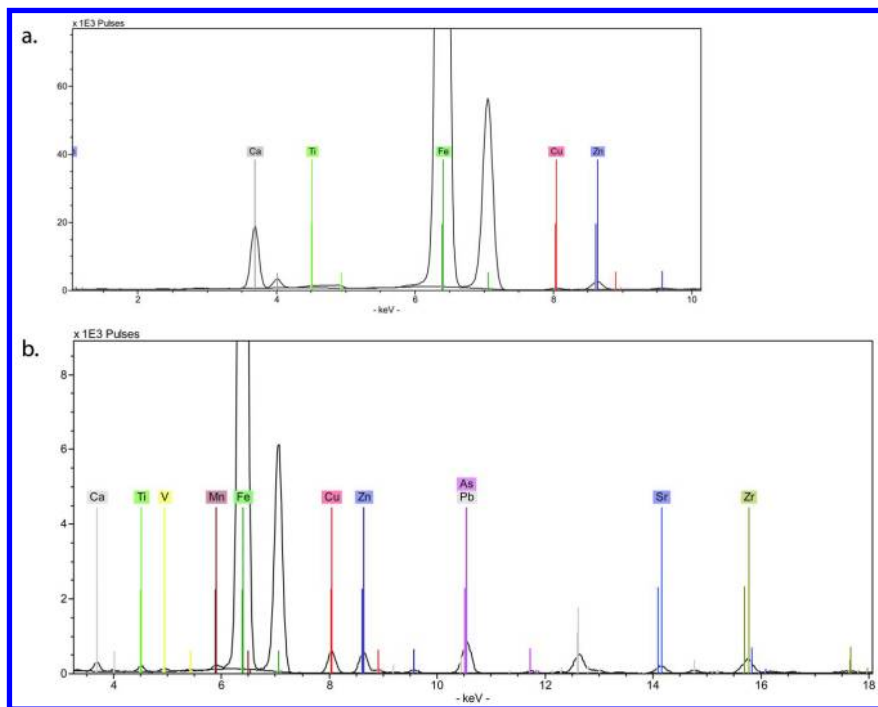

Figure 5. pXRF Spectra of Pigment, Yellow S13; a. Low mass elements b. High mass elements.

The pXRF spectra of the paler Peach S2 pigment reveal a significantly different element profile (Figure 6). Although iron is still the major element, the Fe peaks are lower in intensity than in the spectra of the yellow sample. Although both Yellow S13 and Peach S2 samples show peaks for Ca, Ti, Mn, Cu, Zn, Pb, Sr, and Zr, the Peach S2 sample additionally shows prominent peaks for K, Rb, and Y as well as traces of Al, Si, Ni, Nb, and Sn.

Polarized light microscopy confirms the identification of Yellow S13 as yellow ochre (Figure 12d). The very small, somewhat elongated particles have varied particle size and opacity, with hue ranging from yellow to brown. In reflected light, the particles appear yellow-orange. The transparent yellow particles are anistropic with a refractive index greater than 1.662. Comparison of Yellow S13 to reference samples of yellow ochre reveals many similarities.

In contrast, the dispersion sample of Peach S2 does not resemble reference slides of yellow ochre. In this slide (Figure 12e), a heterogeneous mixture of colorless, transparent flakes of various sizes and irregular shapes and very small yellow-orange, anisotropic particles is observed. The colorless particles have a refractive index less than 1.662, while the yellow particles have a high refractive index. It is possible that this more heterogeneous sample represents a mixture of yellow ochre from a different source, mixed with clay or another white powder to produce a pale "flesh-tone" for painting figures. Peach S2 does not react with hydrochloric acid, so the colorless particles are not likely to be chalk or limestone.
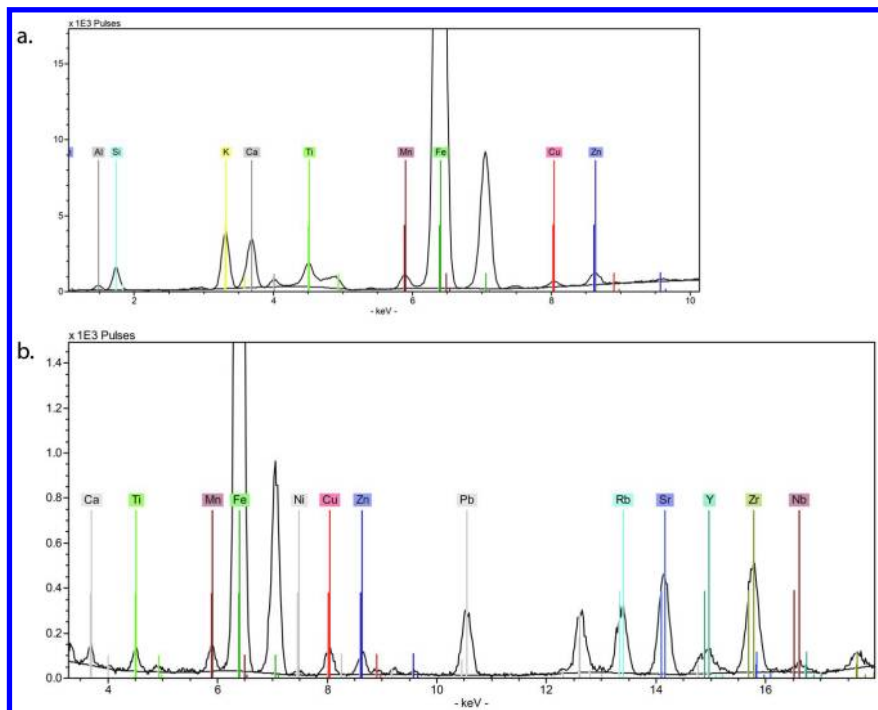

Figure 6. pXRF Spectra of Pigment, Peach S2; a. Low mass elements b. High mass elements.

Red Pigments

Red pigments known to the ancient Romans include red ochres ($Fe_2O_3 \cdot nH_2O$), either naturally occurring or produced by heating of yellow ochre, red lead (Pb_3O_4), realgar (As_2S_2) and cinnabar (HgS). Of these, cinnabar, a vivid red isolated from the mineral, was the most highly valued. Vitruvius (*De arch.* 7.7-7.8) devotes two chapters to the extraction, processing, and use of cinnabar as a pigment.

The red pigments at S. Omobono exhibit a diversity of appearance, texture, and hue. Four separate samples were analyzed previously, and all contain iron as the principal component. Capasso reports the detection of calcium in two of the samples, and concluded that all were iron oxide-containing materials combined with varying amounts of silica and clay (*13*). These red pigments were organized into three containers, referred to here as Red S5, Red S7, and Red S9. As expected for red ochre, all of these samples showed a dominant iron peak in the XRF spectrum, but individual results for minor and trace elements varied considerably. It is likely that red ochre pigments originating from a variety of sources were available at S. Omobono.

The pigment Red S5 (165 g) consisted of large and small lumps of dark red, friable pigment with varying brightness. Two pieces were analyzed (Red S5 Bright and Red S5 Dull) and the pXRF spectra are shown in Figure 7. The duller red piece shows large peaks for Pb, significant peaks for As, and traces of Mn and Sn. Both pieces show traces of Al, Si, Ca, Ti, Cu, Zn, Rb, Sr, Zr, and Sb. Red S5 Bright also contains K and has a much smaller Pb peak with no evidence of As. The variations in these spectra may indicate two different sources, or may arise from different degrees of surface contamination.

The sample of Red S5 that was examined by polarized light microscopy was very similar to reference slides of red ochre. Microscopic examination of Red S5 revealed very fine rounded particles and agglomerates that appear red-brown with transmitted light, orange in reflected light, and dull red between crossed polars. The refractive index of these particles is greater than 1.662.

The pigment referred to as Red S7 (50 g) has different visual characteristics as well as a different elemental profile. As seen in the pXRF spectrum (Figure 8), in addition to the major peak for Fe, minor peaks are observed for Ca, Ti, Cu, Pb, As, Sr, Sb, and Ba (Red S7 is the only pigment at S. Omobono to show the presence of Ba). Red S7 consists of flat, hard "scales" of a more purplish (maroon) hue. It does not easily break apart or crumble; unlike the other reds, Red S7 requires effort to grind to powder. Microscopically, a powdered sample of Red S7 (Figure 12f) shows very uniform, tiny, round particles that are dark red in transmitted light and red-orange in reflected light. Between crossed polars, the particles appear bright red. The refractive index of these particles, like the other reds, is greater than 1.662.

Red S9 (8 g) has a similar texture to Red S5, but the color is lighter and more red-orange. The pXRF spectrum of Red S9 (also given in Figure 9) shows small peaks for Si, K, Ca, Ti, Cu, Pb, Rb, Sr, and Zr, an element profile that is most similar to Red S5 Bright (Figure 8). When examined by polarized light microscopy, Red S9 reveals the same characteristics observed for Red S5 particles.

However, some larger angular particles that are a clear, pale yellow color are also present. These larger particles have a refractive index <1.662 and are anisotropic.
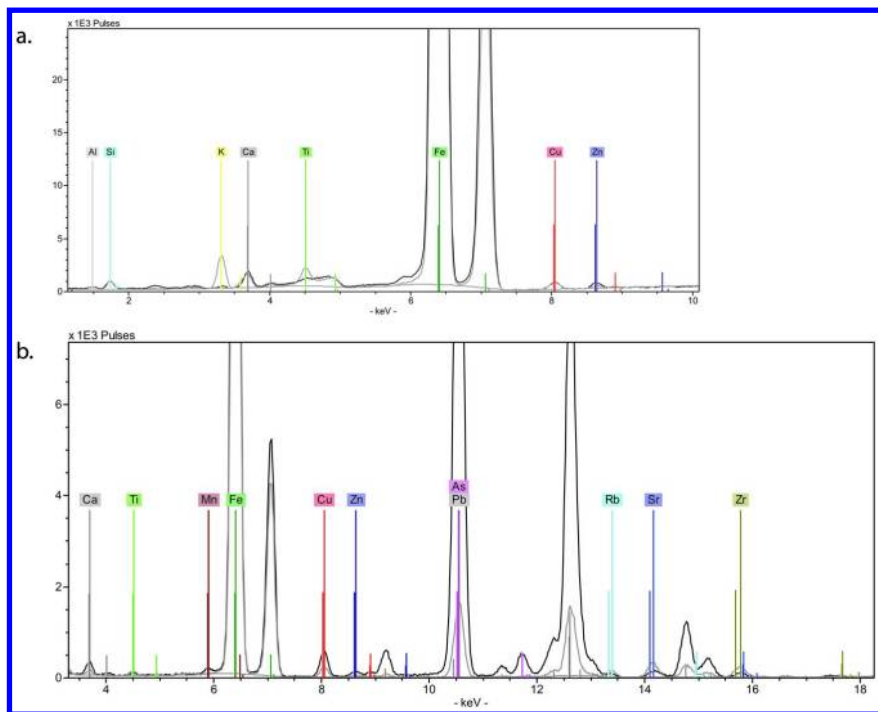

Figure 7. pXRF Spectra of two pieces of Pigment Red S5: Red S5 Bright (gray line) and Red S5 Dull (black line); a. Low mass elements; b. High mass elements.

Pink Pigments

Small amounts of two unusual pigments, one a bright salmon pink color and the other a pale pink were also found in the materials from the pigment shop. Both were discovered in a tray of soil (*cassetta* 179) saved from excavation of the pigment shop. This soil is strewn with colored powders and lumps of colors that were not previously removed and sorted.

The salmon pink pigment stood out among the other reddish pigments examined based on its color and pXRF spectrum, shown in Figure 9. In this spectrum, Pb and Fe are the major elements present. Smaller peaks for Cu and As are observed, along with traces of Zn, Sr, and Zr. The dominant lead peak suggests that red lead or lead white may be present, along with red ochre. However, the PLM observations lead to a different conclusion. This sample consists of a mixture of red ochre (small dark red-brown particles similar to those observed for the red pigments) and large, colorless, transparent, particles that are anisotropic (Figure 12g). Microchemical testing with hydrochloric acid produced vigorous effervescence, suggesting that the colorless particles are a

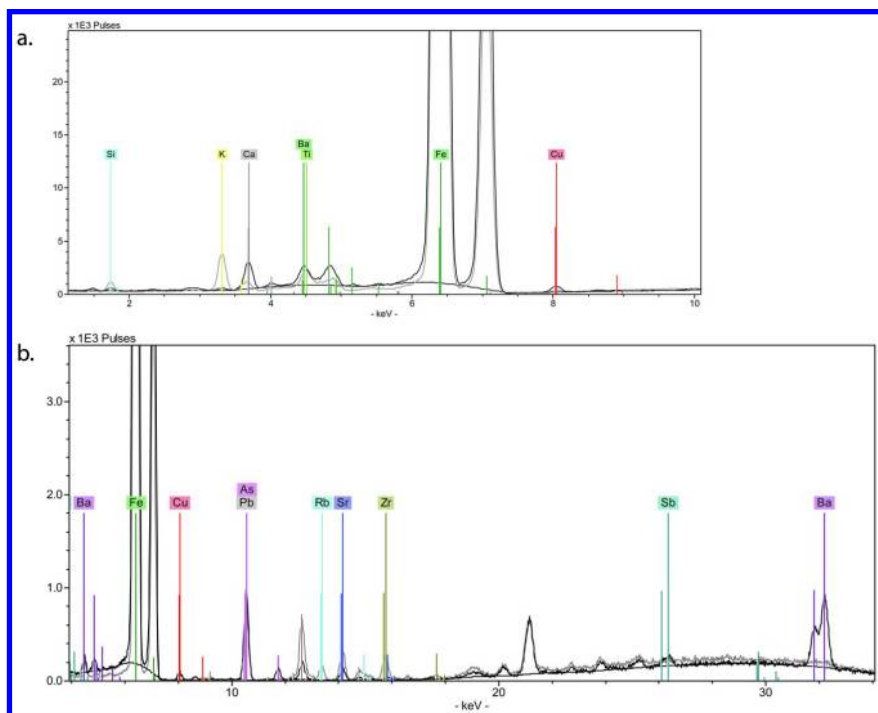form of calcium carbonate or lead white, but the latter is not consistent with the particle properties.

Figure 8. pXRF Spectra of Pigments Red S7 (black line) and Red S9 (gray line); a. Low mass elements b. High mass elements.

One piece of light pink pigment was previously analyzed; Capasso reported the presence of Fe, Ca, Pb, and Cu in the sample but did not identify the pigment (*13*). We analyzed a powdered sample of pink pigment that was carefully removed from the surrounding soil in *cassetta* 179. The pXRF spectrum, shown in Figure 10, is similar to that of the salmon pink pigment, but the Pb peaks are much less intense in this sample. The pale pink powder shows additional peaks for Ca, Ni, and Re. Microchemical testing of this sample with hydrochloric acid did not produce a reaction.

Surprisingly, this sample is not a mixture of red ochre and white pigments. Colorless anisotropic particles mixed with isotropic, transparent pink particles are observed (Figure 12h). Particle properties best matched those of a reference slide of rose madder. It is possible that madder lake was available in the shop at S. Omobono; both Pliny (*HN* 19.17) and Vitruvius (*De arch.* 7.14.1) mention *Rubia tinctorum* (madder); the alizarin-rich dye extracted from madder was adhered to a white powder for use as a pigment. However, further investigation of this pink pigment is needed before a conclusive identity can be established.
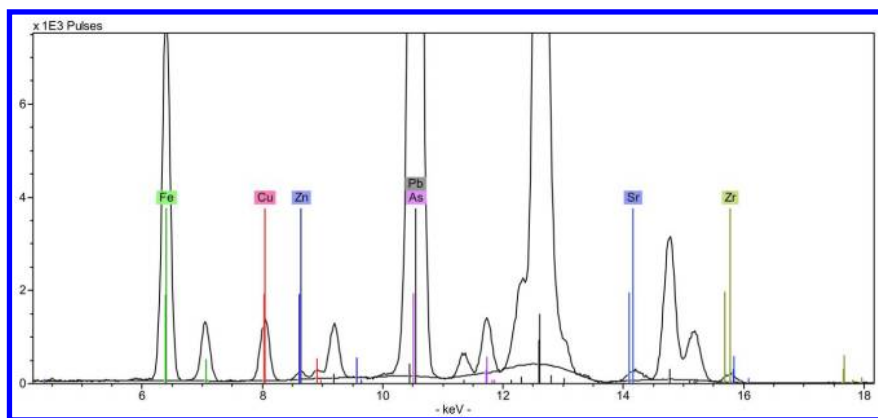
Figure 9. pXRF Spectrum of lump of salmon pink pigment, from cassetta C179 (soil and mixed pigments).
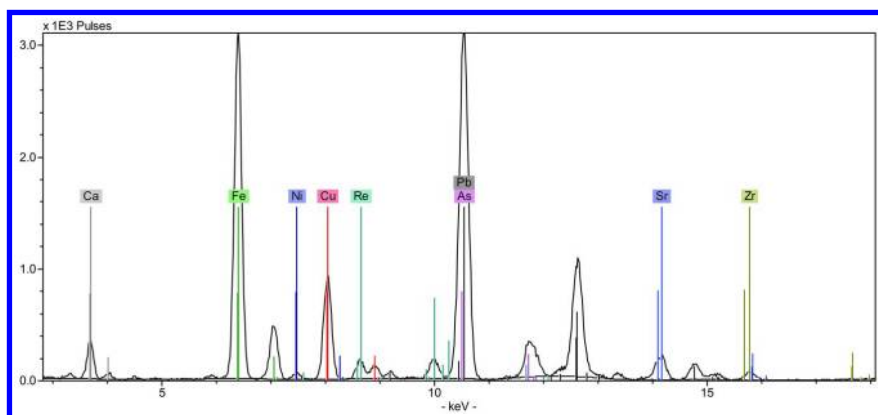
Figure 10. pXRF Spectrum of powdered sample of unidentified pink pigment, obtained from cassetta 179 (soil and mixed pigments).

White Pigments

White pigments used by the Romans include various forms of lime white ($CaCO_3$ from chalk, limestone, shells, or marble), clay minerals such as kaolinite, and the manufactured pigment, lead white ($PbCO_3 \cdot Pb(OH)_2$). The preparation of lead white by the corrosion of lead metal with vinegar is described by Vitruvius (*De arch.* 7.12.1).

Two containers from the pigment shop at S. Omobono hold masses of powdery white pigment that have regions of grayish or light brown powder mixed with white. These samples are labeled White S10 and White S11.3, with a total mass of 240 g.

The pXRF spectra obtained from a lump of White S10 are shown in Figure 11. This sample was scraped lightly to produce a flat surface showing distinct white

and gray regions that were analyzed separately. This material is obviously quite heterogeneous, with very different results observed for the two regions within one sample. The white region is rich in Ca and Sr, with small peaks for Fe, Cu, and Pb. Analysis of the darker, gray area reveals larger peaks for Fe, Cu, and Pb, much smaller peaks for Ca and Sr, and traces of Si, K, Ti, Mn, Zn, and Sn that are not present in the white region. Additionally, this spectrum shows peaks for Hg, not observed in any other pigment samples.
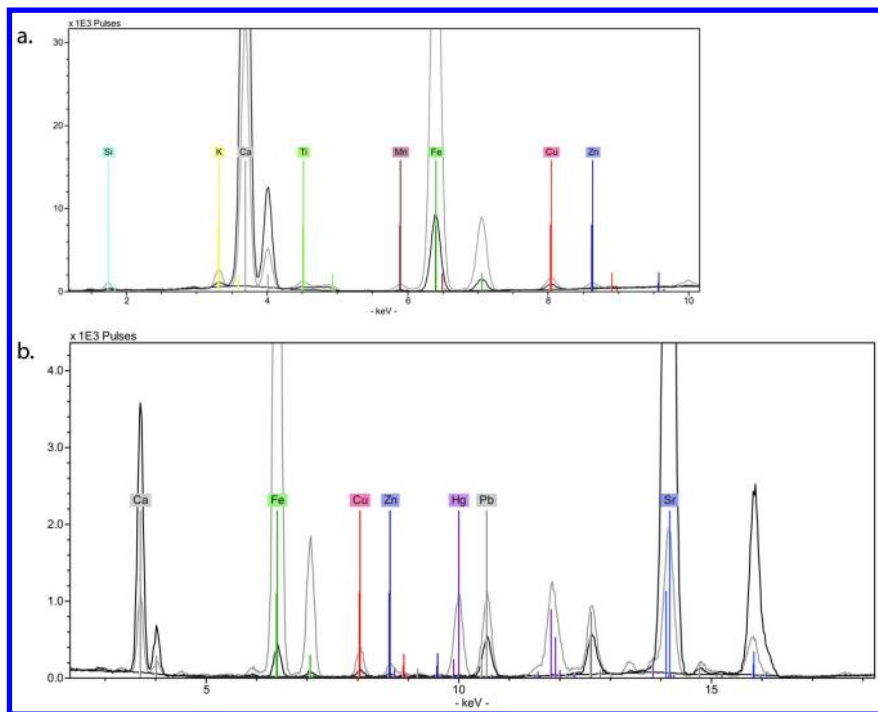
Figure 11. pXRF Spectra of Pigment White S10 (black trace shows white region; gray trace shows gray region; a. Low mass elements b. High mass elements.

White S10 is clearly a calcium-based pigment rather than lead white; pXRF results for this and other white samples are consistent with chalk or other form of $CaCO_3$. The presence of carbonate (expected for both lime white or lead white) was confirmed by microchemical testing with 3 M hydrochloric acid. Vigorous effervescence was observed. Particle properties observed by PLM for were consistent with an identification of lime white based on comparison to reference slides. Very small, colorless, highly anisotropic particles, as well as large agglomerates of those particles with a pale tan color, are observed (Figure 12i).

In Archaeological Chemistry VIII; Armitage, R., et al.;
ACS Symposium Series; American Chemical Society: Washington, DC, 2013.
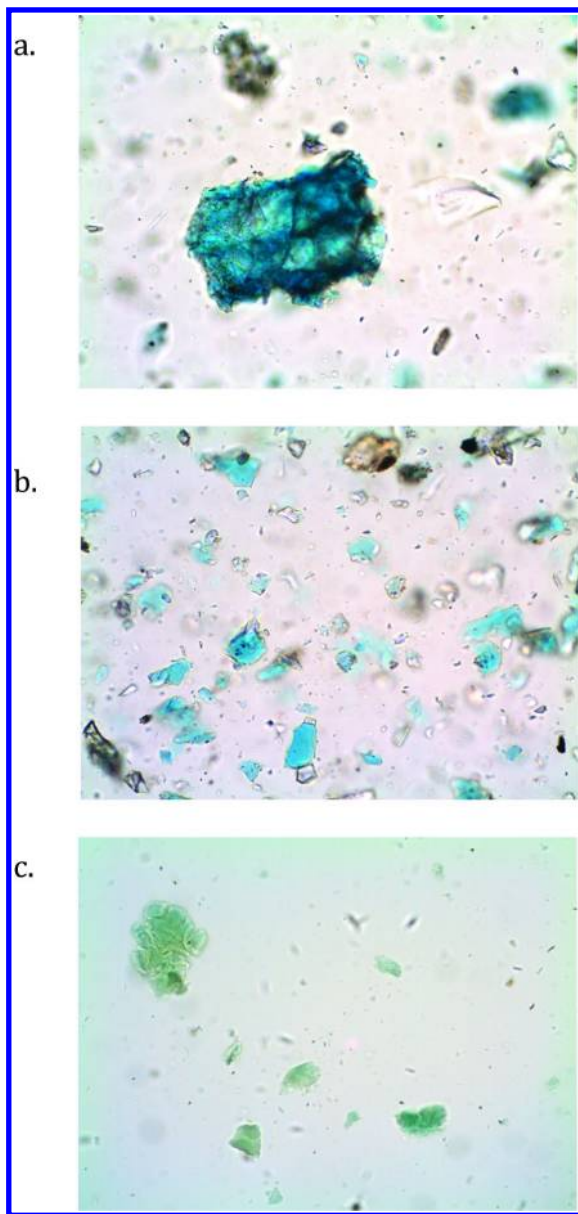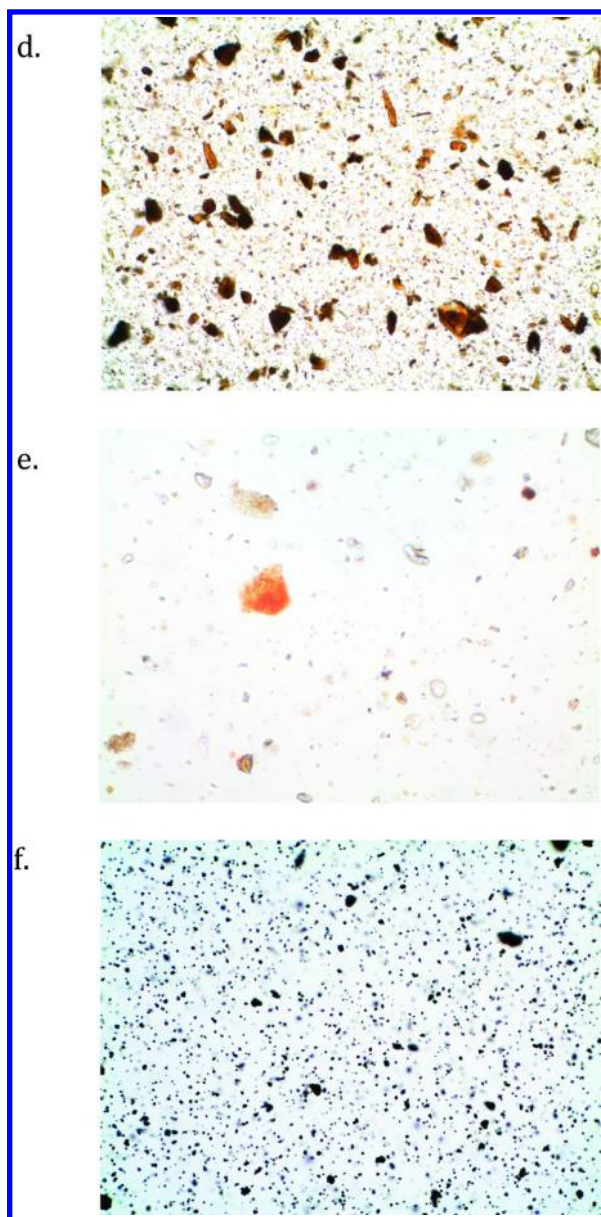
Figure 12. Photomicrographs of S. Omobono Pigments, 400X, transmitted light;
a. Blue S20 b. Blue S8 c. Green S3 d. Yellow S13 e. Peach S2 f. Red S7 g.
Salmon Pink h. Pale Pink i. White S10. (see color insert)

Conclusions

A summary of pXRF results and pigment identifications is provided in Table I. From this study it is evident that the pigment shop at S. Omobono housed an important assemblage of raw colors that all belong to the class of "austere" pigments described by Plin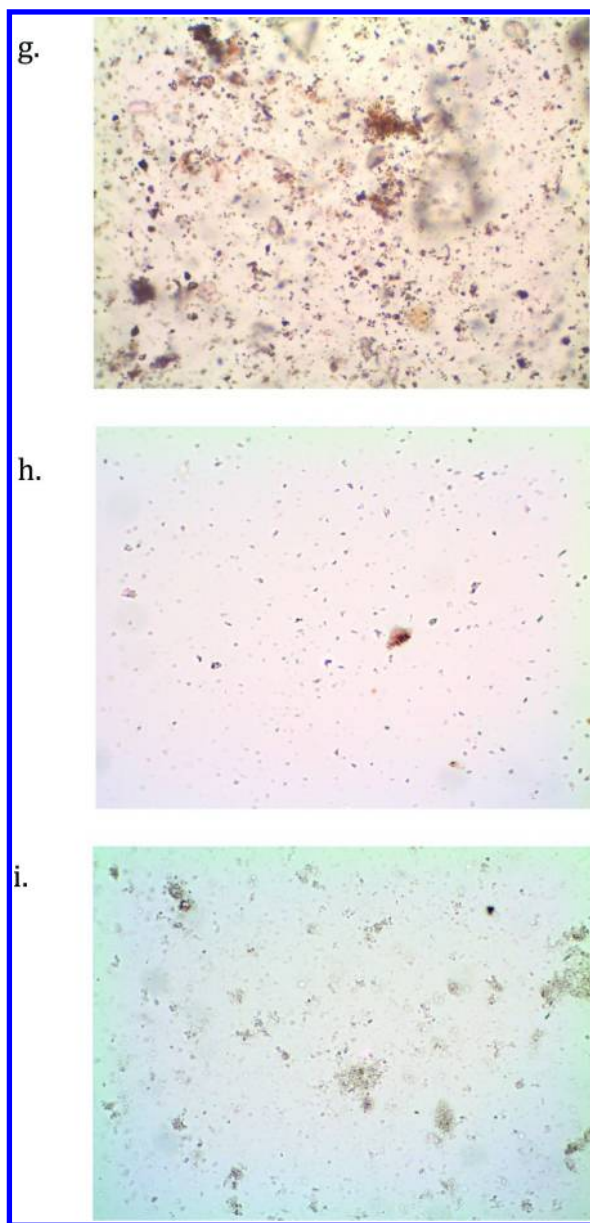y; These are the pigments that are readily available for purchase in the marketplace; the more expensive and rare "florid" pigments, such as azurite and cinnabar, are notably absent. The pigments identified at S. Omobono have also been identified through scientific analyses of numerous Roman wall paintings (*6*). Included are Egyptian blues manufactured with bronze, green earth, yellow and red ochres, lime white, as well as other samples that may represent the mixing/processing of pigments for specific end uses.

Analyses by pXRF and PLM enabled us to characterize the types of pigments present, investigate the variability in composition of the samples that may ultimately suggest different sources, and add significant information to the results of previous examination of these samples. However, since these methods do not provide quantitative elemental compositions or definitive identifications of minerals present, we have not been able to identify specific sources of the pigments being sold at S. Omobono or to address the question of whether they were mined or manufactured locally.

The pXRF and PLM study reported here represents an important first step in bringing these forgotten samples to light. It is our hope that future studies involving more in-depth microscopical examination, IR and Raman spectroscopy, XRD, and other techniques will continue to inform our understanding of the manufacture, trade, and use of pigments in ancient Rome.

Table I. Summary of Pigment Results

Sample Number	Color	Major Element	Minor and Trace Elements	Figure Number	Identification
Blue S4, S20	bright blue	Cu	Si, K, Ca, Ti, Mn, Fe, Pb, Sr, Zr, Sn, Sb	Figs 2, 12a	Egyptian blue
Blue S8, 11.4	light blue	Cu	Si, K, Ca, Ti, Fe, Pb, Sr, Zr, Sn	Figs 3, 12b	Egyptian blue
Green S12, S3	blue-green	Fe	K, Al, Si, Ti, Mn, Cu, Zn, Pb, Rb, Sr	Figs 4, 12c	green earth
Yellow S13	yellow-gold	Fe	Ca, Ti, V, Mn, Cu, Zn, Pb, As, Sr, Zr	Figs 5, 12d	yellow ochre
Peach S2	pale orange	Fe	Al, Si, K, Ca, Ti, Mn, Ni, Cu, Zn, Pb, Rb, Sr, Y, Zr, Nb, Sn	Figs 6, 12e	orange ochre possible mix
Red S5 dull	red	Fe, Pb	Al, Si, Ca, Ti, Mn, Cu, Zn, As, Rb, Sr, Zr, Sn, Sb	Fig 7	red ochre

Table I. (Continued). Summary of Pigment Results

Sample Number	Color	Major Element	Minor and Trace Elements	Figure Number	Identification
Red S5 bright	bright red	Fe	Al, Si, K, Ca, Ti, Cu, Zn, Pb, Rb, Sr, Zr, Sb	Fig 7	red ochre
Red S7	maroon	Fe	Ca, Ti, Cu, Pb, As, Sr, Sb, Ba	Figs 8, 12f	red ochre
Red S9	red-orange	Fe	Si, K, Ca, Ti, Cu, Pb, Rb, Sr, Zr	Fig 8	red ochre
Salmon pink C179	salmon pink	Fe, Pb	Cu, Zn, As, Sr, Zr	Figs 9, 12g	red ochre possible mix
Pink C179 powder	light pink	Fe, Pb	Ca, Ni, Cu, Re, As, Sr, Zr	Figs 10, 12h	unknown
White S10	white area	Ca, Sr	Fe, Cu, Pb	Figs 11, 12i	calcium carbonate
White S10	gray area	Fe, Ca	Si, K, Ti, Mn, Cu, Zn, Hg, Pb, Sr, Sn	Fig 11	mixture

Acknowledgments

References

1. Rees-Jones, S. G. *Stud. Conserv.* **1990**, *35*, 93–101.
2. Kakoulli, I. *Greek Painting Techniques and Materials from the Fourth to the First Century BC*; Archetype: London, 2009; pp 61−66.
3. Pages-Camagna, S.; Colinart, S. *Archaeometry* **2003**, *45*, 637–58.
4. Koren, Z. C. *Dyes Hist. Archaeol.* **2005**, *20*, 136–149.
5. Bearat, H.; Fuchs, M.; Maggetti, M.; Paunier, D., Eds.; *Roman Wall Painting: Materials, Techniques, Analyses, and Conservation, Proceedings*

of the International Workshop, Fribourg 7−9 March 1996; Fribourg University, 1997.

6. Siddall, R. *Infocus Magazine R. Microsc. Soc.* **2006**, June, 19–31.

7. Walsh, V.; Eastaugh, N. *Infocus Magazine R. Microsc. Soc.* **2006**, June, 38–57.

8. Kakoulli, I. *Greek Painting Techniques and Materials from the Fourth to the First Century BC*; Archetype: London, 2009; pp 37−60.

9. Augusti, S. *I Colori Pompeiani*; De Luca: Rome, 1967.

10. Tuffreau-Libre, M; Barbet, A. "Les pots a couleurs dans l'antiquité romaine. *Actes du Congrès du Mans, 8-11 mai 1997*; Société française d'étude de la céramique antique en Gaule: Marseille, France, 1997; pp 399−405.

11. Varone, A. Pompei. Attiviatà dell'Ufficio Scavi: 1990. *Rivista di studi pompeiani* **1990**, *4*, 201–11.

12. Colini, A. M.; Virgili, P.; Capasso, M. M. Area sacra di S. Omobono in Roma. Ricerca stratigrafica 1974−76. In *Un decennio di ricerche archeologiche*, Volume 2; Consiglio nazionale delle ricerche: Rome, 1978; pp 422−424.

13. Colini, A. M.; Virgili, P.; Capasso, M. M. Area sacra di S. Omobono in Roma. Ricerca stratigrafica 1974−76. In *Un decennio di ricerche archeologiche*, Volume 2; Consiglio nazionale delle ricerche: Rome, 1978; pp 431−433.

14. Shugar, A. N.; Mass, J. L., Eds.; *Handheld XRF for Art and Archaeology*; Leuven University Press: Leuven, Belgium, 2012; pp 7−36.

15. Rowland, I. D.; Howe, T., trans. Vitruvius. In *Ten Books on Architecture*; Cambridge University Press: New York, 1999, p 94.

16. Kakoulli, I. *Greek Painting Techniques and Materials from the Fourth to the First Century BC*; Archetype: London, 2009; p 62.

17. Jaksch, H.; Seipel, W.; Weiner, K. L.; El Goresy, A. *Die Naturwissenschaften* **1983**, *70*, 525–535.

18. Kakoulli, I. *Greek Painting Techniques and Materials from the Fourth to the First Century BC*; Archetype: London, 2009; pp 38−39.

Chapter 3

New Chemical Insights into the Ancient Molluskan Purple Dyeing Process

**Zvi C. Koren*

**The Edelstein Center for the Analysis of Ancient Artifacts,
Department of Chemical Engineering,
Shenkar College of Engineering and Design, Ramat-Gan 52526, Israel
*E-mail: zvi@shenkar.ac.il**

Archaeological and chemical evidence associated with ancient dye vats used for purple dyeings have provided new scientific perceptions regarding the various stages of the process of dyeing with the pigments extracted from *Muricidae* sea snails. These steps were described two millennia ago by Pliny the Elder in his encyclopedic treatise on the natural history known during the Roman Period, and also in a concise description of the dyeing of the related biblical blue-purple *Tekhelet* dye noted three centuries later by the Talmud. A critical re-analysis of Pliny's and the Talmud's writings, combined with the archaeological record and with modern laboratory experiments on all-natural dyeings, have provided new insights into the basic principles of chemistry associated with this craft. The major findings from this current investigation follow: (a) The *"salem"* (Latin for salt) that was mentioned, but not identified, by Pliny as the only external auxiliary reagent needed for purple dyeing must have been an alkaline salt (such as natron, lime, or limestone), which was necessary for the reductive dissolution of the purple pigment. (b) Similarly, the Talmud's mention of *"samanin"* (Aramaic-Hebrew for substances) as an ancillary agent in the *Tekhelet* dyeing process must have also been of an alkaline nature, as in the case of Pliny's salt. (c) Since alkaline conditions were required in the dye bath, seawater, which is naturally slightly alkaline, and not fresh water, could have been used for the initial preparation of the dye bath, with more basic salt added for the necessary higher pH values. (d) A typical

archaeological vat containing 100 L of dye solution would have contained the meaty flesh of 10,000 *Hexaplex trunculus* sea snails and would produce up to a kilogram and a half of dyed wool – enough for one to two all-purple cloaks or mantles, depending on the depth of color desired. (e) The other two Mediterranean snail species, *Bolinus brandaris* and *Stramonita haemastoma*, produce much less purple pigment than *H. trunculus* and, thus, tens of thousands of these mollusks would have been needed in such a vat; hence these snails would not have been used alone, but rather, when needed, as additions to a *H. trunculus* vat of that size. (f) In order to maintain anaerobic conditions for the slow bacterial reduction of the indigoid pigments to their soluble leuco form, the dye bath would have needed to be covered throughout the process (except for the brief periods of gently stirring the contents of the dye bath), and hence, no significant photo-debromination of the brominated dyes would have occurred as a result of the action of the sun. (g) Consequently, the final general color of the dyeing was dependent on the original color of the raw pigment, whether it was reddish-purple or bluish-purple (violet). (h) Thus, in order to produce the Tyrian or Biblical-*Argaman* red-purple dyeings, a DBI-rich *H. trunculus* species was used alone or with some *B. brandaris* and/or *S. haemastoma* added for even redder dyeings; for the blue-purple dyeings, as in the Biblical-*Tekhelet*, an IND-rich *H. trunculus* was used alone. (i) The direct chemical evidence to date indicates that the production of the molluskan purple colorant solely as a pigment for painting was originated by the Minoans in the Aegean approximately four millennia ago; however, the transformation of the purple pigment into a dye for the dyeing of textiles originated with the Levantine Phoenicians a half millennium later.

Introduction

History and archaeology have recorded that the colors of the garments and palatial furnishings of royalty, military generals, and high priests were various shades of purple. These include red-purples similar to the common names of bordeaux, maroon, burgundy, etc., as well as blue-purple or violet colors. In antiquity, these purple dyeings were performed along the Mediterranean basin on cleansed woolen fleeces by using the pigments extracted from various sea snails, *Muricidae* mollusks, primarily from the *Hexaplex trunculus* (also known as *Murex trunculus*) species, *Bolinus brandaris*, and *Stramonita haemastoma* species (*1*), as depicted in Figure 1. It has been established that the latter two species can only produce red-purple dyeings, whereas there are two chromatic varieties of *H. trunculus* species, perhaps even zoological sub-species; one that can produce the red-purple dyeings similar to that produced from *B. brandaris*

and *S. haemastoma* snails, and the other that produces blue-purple or violet dyeings (*2, 3*). A review of the history and chemistry of these molluskan dyes (*4, 5*), and the analytical methods developed for multi-component identifications of *Muricidae* pigments via liquid chromatography have been previously published (*2, 6*). The main components of molluskan pigments are the indigoids, but they could also contain minor contributions from isatinoids and indirubinoids, and these have all been discussed at length elsewhere (*2, 3, 6*).
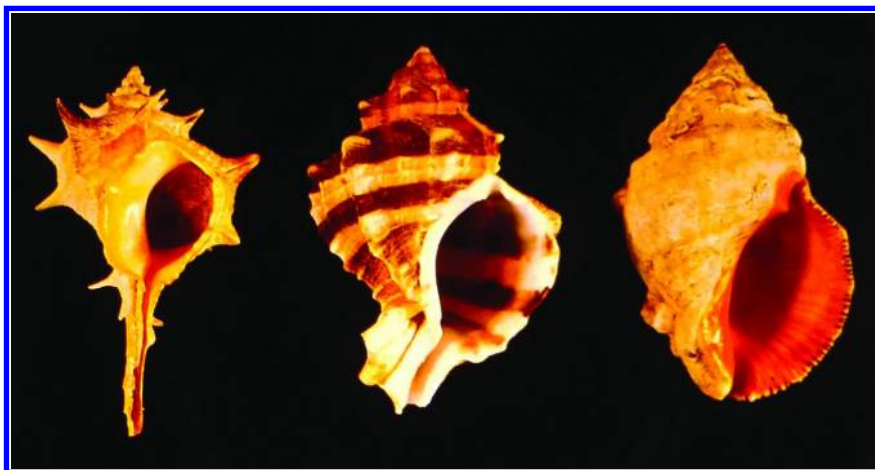
Figure 1. The three most common purple-producing Muricidae sea snails inhabiting the Mediterranean (from left to right): Bolinus brandaris, Hexaplex trunculus (also commonly known as Murex trunculus), and Stramonita haemastoma. (Courtesy of the Eretz-Israel Museum, Tel-Aviv.)

The most detailed ancient account of the various steps associated with purple dyeing from molluskan snails was provided by the 1st century CE Roman historian, Pliny the Elder (Gaius Plinius Secundus), in his epic work titled *Naturalis Historia* – Natural History (*7*). The excerpts from Pliny's work given in the sections below are based on the Latin version and English translation given by Rackham, with certain etymological emendations offered by this author. There have been various English translations of Pliny's work and these have shown differences in textual styles as well as sometimes ambiguous renditions of the Latin weight and volume measures, and hence the excerpts below do not include these quantities. However, though these translational differences exist, nevertheless, the overall renditions of Pliny's descriptions are all similar.

The main questions that have perturbed historians of Pliny's writings are whether his descriptions of various technologies, and specifically, of the processes associated with purple dyeing, are incomplete or even incorrect, and whether Pliny actually observed the purple dyeing process (*8*). As far as Pliny's working method is concerned, in the Preface of his 37-volume Natural History treatise dedicated to his friend Titus Vespasian Caesar, Pliny specifically states that he

was occupied with many official tasks, but yet his work includes 20,000 topics garnered from 2,000 books of 100 authors (*9*). His nephew, Pliny the Younger, concurs and writes in his letter to Baebius Macer (*10*, *11*) how extremely busy his uncle was, but he still found the time to write multi-volume works. Thus, there is no doubt that probably most of what Pliny wrote about was gleaned from other sources. However, Pliny also clearly states that he introduces new ideas not written anywhere (*9*).

> "… and to these I have made considerable additions of things, which were either not known to my predecessors, or which have been lately discovered."

Hence, not every topic that he discusses in his Natural History is one that has been copied or re-written from other sources. For some of his descriptions of chemical processes, he probably was an eyewitness. The author (or authors) of the relevant Wikipedia articles indicate that Pliny's description in Book 33 of the gold mining process is so detailed that it was probably written as an eyewitness account, and based on the proximity of where Pliny was stationed he could have certainly have visited the mine sites (*12*, *13*). So, it may have been possible that he also witnessed the purple dyeing process.

However, the question of whether Pliny actually saw the technology first-hand or was told about it or read it from other sources available to him at the time is an irrelevant matter. The ultimate point is: was Pliny's account correct?

From the various experiments conducted by this author on purple pigments over the last two decades, certain insights into the dyeing process practiced in antiquity have now been gained. These investigations include optimizations of all-natural purple dyeings produced from the *H. trunculus* molluskan pigments (*14*). These studies have shown that Pliny's descriptions parallel that of modern laboratory experiments performed in reconstructing natural dyeing with molluskan purple pigments.

The Preliminary Stages: From Snail Collection to Pigment Production

Collecting Live Snails

According to Pliny:

> People strive to catch this shellfish alive, because it discharges this juice with its life.

Personal experience has shown that *Muricidae* sea snails, especially *H. trunculus* species, can be found in relatively shallow waters (ca. 1 m) in rocky shore areas full of seaweed vegetation, such as depicted in Figure 2. These snails are usually partly concealed as they are found burrowed in the sandy seabed with only a small hump from their shell visible. They must be collected live – and kept alive until the pre-dyeing stage is begun – in order to be effectively exploited for

the production of the purple pigment. This is due to the necessity of avoiding the premature ejection of the purple pigment from the dying animal. As the snail expires, it expels the purple pigment, and if these snails are still in the water, then the pigment will be lost as it is dispersed in the sea.

Figure 2. The coastline of the beach at Akhziv in modern northern Israel where Muricidae sea snails inhabit the seabed of this rocky and flora-filled seascape.

Cracking the Shell To Expose the Chromogenic Gland

Pliny writes:

> The murex … has the famous 'flower of purple', sought after for dyeing robes, in the middle of its throat: here there is a white 'vein' of very scanty fluid from which that precious dye, suffused with a dark rose color, is drained, but the rest of the body produces nothing.

The exposed hypobranchial glands of two *H. trunculus* snails are shown in Figure 3, and in one snail the gland (Pliny's "vein", the "flower of purple") is indeed white, and in the other snail it is gray-colored, and yet in others it could be beige. The gland contains the colorless brominated and unbrominated indoxyl precursors in its fluid (*4*, *5*). As long as the snail is alive, only these colorless precursors exist, and no purple pigment is yet present or produced in the gland. In order to initiate the production of the purple pigment from these precursors, which can be straightforwardly accomplished, the snail shell is strategically cracked so

that the sharp broken shell pieces will deliberately rupture the gland. This piercing would then allow the purpurase enzyme, which is naturally present in the gland but physically separated from the precursors, to come in contact with the chromogens. This interaction initiates the necessary spontaneous enzymatic hydrolysis steps on the precursors and a series of natural photochemical air-oxidation steps follow. This procedure is performed without heating in order not to destroy the required enzyme. In a matter of a few days, the "dark rose color" of the pigment is produced (also see below). In modern times, *Muricidae* snails are sold as seafood, *fruits de mer* and escargot, at various markets in Mediterranean countries and cooking them in boiling water destroys the enzyme and thus the purple pigment is not produced.
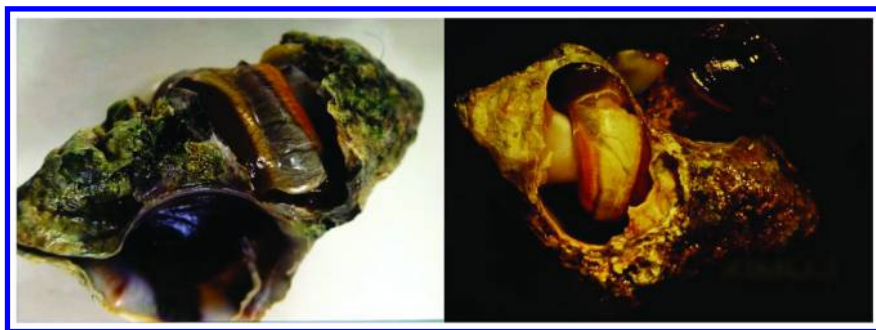
Figure 3. Two Hexaplex trunculus mollusks with their shells cracked open to expose their hypobranchial glands: (left) gray vein, (right) off-white vein.

Separating the Meaty Snail from the Shell

According to Pliny:

From the larger purples they get the juice by stripping off the shell, but they crush the smaller ones alive with the shell, as that is the only way to make them disgorge the juice.

Once the shell has been cracked and the gland exposed or has been punctured, then the snail meat with the developing pigment can be forcibly separated from the shell. The shell is discarded as it will occupy too much space in the vat and the entire snail meat – with the developing pigment adhering to it – is placed in a vat. This snail meat is a necessary nutrient for the reductive bacteria also present in the snail (as described below). With smaller snails, the act of stripping off the snail meat from its shell is more difficult and unnecessary; the simple act of crushing the snail shells insures that the gland has been punctured and that the development of the purple pigment has begun. The crushed smaller snails are added to the vat containing the flesh of the larger snails.

Further Pigment Development

From Pliny's treatise:

Subsequently the vein of which we spoke is removed, to this, salt [*"salem"* in Pliny's Latin] has to be added …; three days is the proper time for it to be steeped, as certainly the fresher it [the extract] is the much stronger it is.

Experiments have indeed shown (*14*) that the visceral mass of snail flesh with the pigment adhering to it needs to be left undisturbed for a total of about 3 days from the time it was initially produced by the rupturing of the gland until the purple or violet pigment is spontaneously fully developed.

Fermentative Anaerobic Bacterial Reduction

A necessary step for any dyeing – natural or synthetic – is that the dye be solubilized and thus can form strong chemical and physical bonds to the textile fibers on a molecular level. Since the main indigoid components of the molluskan purple pigment are relatively insoluble in aqueous solutions, they must first be converted to a soluble form. This water-soluble state is the reduced indigoid molecule, which is yellow and thus much less-colored or "whiter" than the original highly colored indigoid, and hence this reduced form is known as the "leuco" state. Figure 4 shows the schematics of the reduction of an indigoid to its leuco, moderately soluble non-ionic acid form, and further ionization.

Though 2,000 years ago Pliny obviously never identified the biochemical mechanism or the reducing agent necessary to solubilize the indigoids, in antiquity the reducing agent for such a process must have been the bacteria present in the snail meat. Bacteria found in various plant fermentation vats were successful in the reduction and dissolution of the indigo pigment from plant sources. For example, an anaerobic moderate thermophilic bacterium, named *Clostridium isatidis*, capable of reducing indigo was extracted from a fermented medieval woad (*Isatis tinctoria* L.) vat (*15–17*). It was found that growth occurred at pH 5.9 – 9.9 (initial pH) with an optimum at 50 °C of pH 7.2 ± 0.2 (constant pH). Further, at pH 7.8, the temperature range for growth was 30 – 55 °C with the optimum at 49 – 52 °C.

The mechanism by which the bacterium *C. isatidis* reduces indigo was not initially understood. However, it is believed to be a direct interaction between the bacteria and indigo and not as a result of the metabolic products, though H_2 gas has been detected as a product of the fermentation; CO_2 gas and acidic products have also been identified (*18*, *19*). Electrochemical measurements showed that the mechanism of the bacterial reduction of indigo appears to be due to two features: the bacteria produce extracellular factors that decrease indigo particle size, and they also generate a negative potential of sufficient magnitude. The solid state bacterial-driven reduction for indigo dyeing in the absence of a redox mediator requires direct contact between bacteria and the solid indigo and

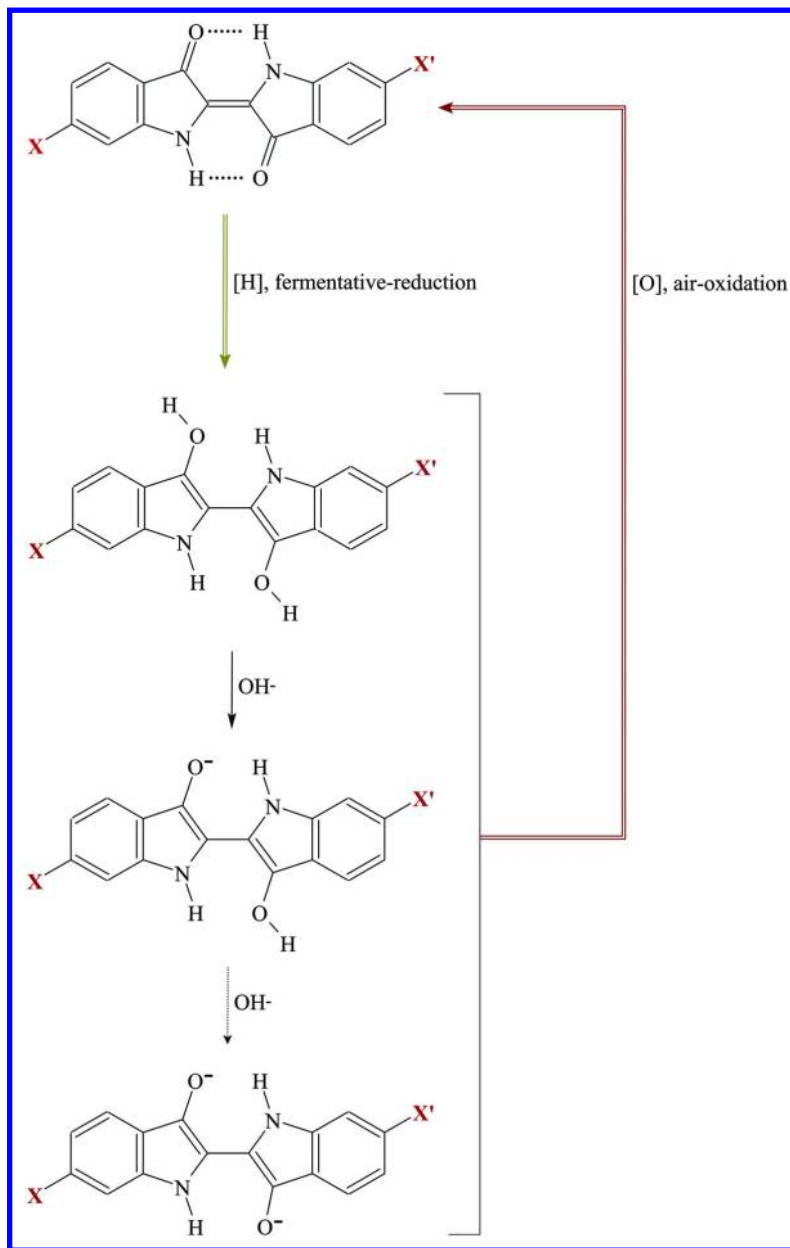transfers an electron from the bacterial cell interior to a solid external electron acceptor (indigo).

Figure 4. Schematic of the reduction of the indigoid components from the purple pigment and re-oxidation to the original pigment: indigo (IND) for X = X' = H; 6-bromoindigo (also known as monobromoindigo, MBI) for X = Br, X' = H; 6,6'-dibromoindigo (DBI) for X = X' = Br.

Other bacterial strains, different from *C. isatidis*, able to reduce indigo have also been found in other fermentation vats, as for example from the Asian indigo-producing *Polygonum tinctorium* plant species (*20*).

Thus, in the case of the molluskan purple pigment, in which the main constituents are indigoids – indigo and its brominated derivatives – similar anaerobic moderately thermophilic bacteria must also be responsible for the reductive dissolution of these pigments, though these strains have not yet been identified. Successful fermentation vats have been produced for all-natural dyeings with molluskan pigments in the United Kingdom, France, and Israel (*14*). In modern times, there are strong synthetic reducing agents, such as sodium dithionite (also known as sodium hydrosulfite), $Na_2S_2O_4$, that can nearly instantly reduce any indigoid. However, in antiquity, since the molluskan pigment was naturally reduced by the anaerobic bacterium acting as a mild reducing agent, the time necessary for the full reduction was a matter of days.

The anaerobic nature of the bacteria can be deduced from the archaeological evidence associated with molluskan purple dyeing. Figure 5 shows a potsherd from a 7th century BCE clay vat used for purple dyeing and excavated from a Phoenician site in Tel Kabri in modern northern Israel. The residual purple pigment is still clearly visible after more than 2,500 years as a result of the undesired oxidation – and precipitation – of the dissolved purple. This pigment has been previously analyzed and shown to contain the three indigoids, which indicates that it is from a molluskan source (*21*). Since this fragment has a curved finished top it is clearly from the uppermost part of the vessel. Thus, the location of this pigment at the very top of the interior of the vat indicates that the liquid contained in the vessel reached nearly the top of the vat. A similar potsherd with residual purple pigmentation at the top was also found at the 8th – 9th centuries Tel Shikmona site near Haifa in modern northern Israel. In order to reduce the amount of atmospheric oxygen from entering the bath – and thus to prevent the unwanted oxidation of the reduced indigoids – the vat would have also been covered with either a slab of stone or wood. Thus, only a small amount of space would have existed between the top of the liquid and the vat's cover. With the various gases produced from the fermentation process, only a small quantity of air would have been present in the head space above the liquid. This would aid the anaerobic nature of the bacterial action. The lid of the vat would have been opened for very brief periods in order to stir and mix the contents of the liquid very gently so as not to introduce much air into the dye bath, but, except for these very short interludes, the cover would have stayed in place to prevent the entrance of air into the dye liquid. This preventative measure has filtered down through the ages so that already two centuries ago, historic dyeing books directed dyers to fill an indigo vat nearly to the top and to keep it covered (*22*).

The necessity of keeping the dye bath covered would also have prevented sunlight from entering the dye solution. Hence, no significant photo-debromination of the brominated indigoids would have occurred, and the compositions of the dyes in the woolen dyeing would have reflected the constitution of the original pigment. Different dyes have different affinities to textile fiber materials and since the purple pigment consists of a number of colorants, the compositions of the dyes in the dyed fibers will, in general, be

different from their compositions in the original pigment. Nevertheless, the overall color of the dyeing is reflected by and dependent on the original color of the raw pigment, whether it is reddish-purple or bluish-purple (violet). Only the *H. trunculus* sea snail species produces the violet singly-brominated MBI dye in significant quantities. This snail's pigments also contain the other two indigoids – the doubly-brominated DBI dye and the unbrominated indigo (IND) dye – in varying quantities. The *H. trunculus* mollusks consist of two chromatic varieties: one produces red-purple pigments owing to its relatively large quantity of DBI, whereas the other produces bluer, violet, pigments due to its relatively abundant IND dye (*2*, *3*). Thus, in order to produce the Tyrian or Biblical-*Argaman* red-purple dyeings, a DBI-rich *H. trunculus* species was used alone or with some *B. brandaris* and/or *S. haemastoma* added for even redder dyeings; for the blue-purple dyeings, as in the Biblical-*Tekhelet*, an IND-rich *H. trunculus* was used alone.

Figure 5. The interior of a purple-stained potsherd, part of the upper mouth of a dye vat, excavated at 7ᵗʰ century BCE Tel Kabri in northern Israel. (Courtesy of the Tel Kabri Expedition, Tel-Aviv University.)

In order not to destroy this moderately thermophilic micro-organism, the dye bath was not boiled, but raised to a moderately hot temperature. This is in accordance with Pliny's statement whereby he describes the heating from a heat source that is not directly in contact with the dye bath, as follows:

> It [the snail flesh with the adhering pigment] should be heated … with … water … and kept at a uniform and moderate temperature by a pipe brought from a furnace some way off. This will cause it gradually to deposit the portions of flesh that are bound to have adhered to the veins.

Pliny's lyrical description of the application of indirect heat to the dye bath can be evident from the presence of the charred areas, visible even today, on the

exterior of the more than 2,500 year-old potsherd (Figure 6), which is the reverse side of the fragment from Figure 5. This marking would be the result of heating the vat to moderate temperatures by means of, for example, hot charcoal. The scenario could have been that the vat would have been placed in a pit in order to maintain relatively constant warm to hot temperatures while placing smoldering wood pieces all around the vat. These chunks could have easily been removed as they cooled down and replaced by fresh hot charcoals as needed. A comparable practice to this ancient method of heating can be seen two centuries ago by the placement of hot embers around the vat (*23*).

Figure 6. The exterior of the potsherd from Figure 5 with visible charred stains. (Courtesy of the Tel Kabri Expedition, Tel-Aviv University.)

Pliny's Salt

Pliny indicated that a salt (*"salem"*) was a necessary auxiliary agent in the purple dyeing process. The misconception of many interpreters of this statement was that Pliny referred to ordinary salt, i. e., sodium chloride (NaCl). However, experiments have shown that this neutral salt has no effect on the necessary dissolution of the indigoids and plays no part in the reduction. However, from the general chemistry topic of acids and bases, students are taught that there are acidic and basic salts too. It is then obvious that while Pliny was not of course discussing the chemistry principles associated with the reductive dissolution of the indigoids, his mention of a salt must have alluded to a basic salt for the reasons discussed below.

The solubility of a reduced leuco-indigoid increases with increasing pH. Figure 4 shows that an increase in alkalinity generates the soluble mono-anionic leuco from the moderately soluble non-ionic acid, and a further increase in the pH would then produce the soluble di-anion. The relative amounts of these leuco-species were studied for indigo with the following results (*24*): At pH 8,

about 80% exists as the acid and 20% as the mono-anion; At pH 9, about 60% is the acid, almost 40% mono-anion, and less than 5% di-anion.

The mono-anion reaches a maximum of about 70% at a pH of about 11, with nearly equal amounts of the acid and di-anion also present. However, since wool was to be dyed, the pH must be less than 9 in order not to cause damage to the proteinic textile.

Though that work was produced for indigo itself, it may be assumed that similar results would be obtained for brominated indigoids – MBI and DBI (see Figure 4) – originating from molluskan pigments. Hence, dissolution of the indigoids in their reduced leuco state would be increased in an alkaline environment; however, in the limiting pH needed for dyeing wool, the majority of the reduced leuco-indigoids would be in their nonionic form with some mono-anion also present. Such an alkaline system can be naturally produced by various means and are hereby discussed.

Stale Urine

The use of stale urine, which contains ammonia from the decomposition of urea caused by bacterial contamination, can produce moderately alkaline solutions of about pH 8 (*25*, *26*). Stale urine was a popular reagent in Europe in the 18th and 19th centuries for the dyeing of indigo (*27*).

However, during the fermentation process acidic compounds are generated and reduce the initial pH of the dye mixture to acidic levels and will decrease the solubilities of the brominated leuco indigoids. Thus, the alkalinity of the dye bath would have needed to be monitored in antiquity, not a simple process unless the dyer was willing to use the sense of taste and/or touch on a portion of the bath in order to determine its pH. With this lowering of the pH of the dye bath, it was necessary to add more of the base on a regular basis until fermentation ceases. If stale urine was to be used as the alkaline medium, then a considerable quantity of it would be necessary in order to raise the pH of the dye bath to the desired degree of basicity, an action that will considerably dilute the dye bath to an unacceptable level as it would produce inferior purple dyeings. Hence, most probably stale urine solutions were not used for producing an alkaline dye bath with the molluskan purple pigment. In addition, of course, this liquid reagent could not have been Pliny's salt.

Soluble Carbonates: Natron or Soda Ash and Potash

A soluble carbonate, such as sodium carbonate (Na_2CO_3) or potassium carbonate (K_2CO_3), can produce strongly alkaline aqueous solutions. Sodium carbonate can be naturally obtained from the raw mineral natron, which also contains some of the moderately alkaline sodium bicarbonate ($NaHCO_3$), or from the ashes of certain plants ("soda ash"), and similarly potassium carbonate is present in wood ash ("potash"). The benefits of these soluble carbonates is that they can be added as solids and thus not dilute the original dye bath, although the level of alkalinity was still needed to be monitored and the carbonate added as needed throughout the reduction process.

Lime

Quicklime, burnt lime, or more simply lime is calcium oxide (CaO), which can be produced from limestone, calcium carbonate (CaCO$_3$), by heating, and when added to the aqueous dye solution generates the alkaline limewater (also known as slaked lime), aqueous calcium hydroxide, Ca(OH)$_2$*(aq)*. The pH values that can be attained are higher than 11 (*28*). Here too, the lime is added as a solid to the dye bath, and, as in the case of the soluble carbonates, will also not dilute the dye bath when added to increase the pH of the dye solution as needed throughout the reduction.

Lime + Soluble Carbonate

A strongly alkaline solution can be produced from the combination of lime with a soluble carbonate, such as the ones described above. For example, with potash, this mixture in water will produce the strong base, potassium hydroxide, according to the following reaction:

$$\text{CaO}(s) + \text{K}_2\text{CO}_3(s) + \text{H}_2\text{O}(l) \;\;\rightarrow\;\; \text{CaCO}_3(s) + 2\,\text{KOH}(aq)$$
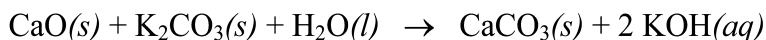
The disadvantages of this alkaline combination is that, as with the other salts mentioned above, it could produce pH values that are much higher than 9. Thus, its pH would have also been needed to be monitored as in the above cases.

Limestone

In Pliny's account the only missing ingredient from the process is an alkaline reagent, and any of the above-mentioned salts – natron or soda ash, potash, lime with or without ash – could be possible candidates for Pliny's salt. However, these solids all possess practical disadvantages in this process. These soluble salts can initially produce relatively high pH values, but since acidic products are formed during the fermentation process, the pH of the solution is drastically reduced. For example, in recent natural dyeing experiments (*14*), an initial pH of 9 was produced in the dye bath by means of sodium carbonate just prior to fermentation, and in less than a day, the pH was reduced to an acidic pH of 6.7. In order to solubilize as many leuco-indigoid species as possible (see Figure 4), the pH was then re-adjusted to 9 by the addition of more salt. This repeated cycle of checking the pH and the subsequent addition of more salt lasted for about three days, until the fermentation ceased and no more acidic products were produced, and thus the pH did not change.

A much simpler method was possible in antiquity for maintaining moderate alkalinity with an eye towards the final dyeing step in this time-consuming multi-stage procedure, and it could have been the one used by the ancient dyer. This step invokes the basic principles of general chemistry, even as taught at the freshman university level, and it pertains to the equilibrium constant associated with relatively insoluble salts, the solubility product constant K$_{sp}$. Thus, use was made of the widely available mineral limestone or chalk (a softer form), either the calcite or aragonite crystalline forms, which is essentially calcium carbonate (CaCO$_3$). This choice of salt was deliberately made due to the fact that unlike

the other salts mentioned-above, limestone is only a sparingly soluble salt. Its reported literature value for its solubility product constant (K_{sp}) at 25 °C shows a range of values, from 1 x 10^{-8} (*28*), 3.36 x 10^{-9} (*29*), 3.8 x 10^{-9} (*30*), 4.95 x 10^{-9} (*31*), and 8.7 x 10^{-9} (*32*).

Similarly, variable values are given in the literature for the solubility of this salt. For example, from the 66th edition of the CRC Handbook (*31*), the solubilities of the two crystalline forms of calcium carbonate in 100 cc of water are given as follows. Aragonite: 1.53 mg at 25 °C, 1.90 mg at 75 °C; Calcite: 1.4 mg at 25 °C, 1.8 mg at 75 °C.

However, from the 93rd edition of the 2013 online edition of CRC (*29*), the solubilities at 20 °C of these crystalline forms are equal at 0.66 mg per 100 g water. Further, in 100 cc of water, Wikipedia (*32*) reports a solubility of 4.7 mg, and additionally a value of 1.3 mg has been reported (*33*).

In order to evaluate the expected pH of saturated $CaCO_3$ solutions, various aqueous equilibria associated with $CaCO_3$, HCO_3^-, CO_3^{2-}, and the partial pressure $CO_2(g)$ above the solution and dissolved in the dye bath (Henry's Law) need to be considered. Some of the pH values reported in the literature for saturated aqueous solutions of calcium carbonate at 25 °C are 8.6 (*34*), 9.95 in CO_2-free water and 8.31 for the normal 0.03 % contribution of CO_2 in atmospheric air (*35*), and 8.27 (*32*). Hence, these values are all in relative agreement that for an aqueous saturated calcium carbonate solution at room temperature and at the normal atmospheric contribution of CO_2, the pH is about 8.3.

The ancients could have then used an excess of this very sparingly soluble salt, with the added value that there would be no need to replenish it during the overall dyeing process, which is not the case with all of the above-mentioned solids. An excess quantity of limestone in general chemistry terms would cause the acids produced in the fermentation process to be the limiting reagents and thus as there would always exist a saturated solution of calcium carbonate, its concentration would be constant even as it neutralizes the produced acids. Even as the action of an acid on the calcium carbonate produces its soluble calcium bicarbonate conjugate, the latter is still alkaline and a buffer system of carbonate/bicarbonate would be established to maintain the necessary alkalinity of the solution. Thus, a constant alkaline environment would be maintained throughout the fermentation and would aid in the solubility of the leuco species, especially the mono-anion, while, at the same time insuring that the pH would be less than 9 so as not to damage the proteinic wool during the later dyeing process. This dual action of the limestone is a double advantage over the other salts.

Archaeological evidence also supports the supposition that limestone may have been used as the salt mentioned in Pliny's description. Small pebble-sized stone pieces were found in a 6th century BCE Phoenician purple dyeing installation at Tel Dor in modern north-central Israel. One of these is portrayed in Figure 7, and it is stained with a soiled dark residue. The original color of this pigment was not visually discerned with the naked eye, but a spectrophotometric analysis of a DMF extract of this residue showed it to be from a molluskan pigment source (*36*). The highly magnified picture now seen in Figure 7 does show that the residue is purple in color. These stone pieces were analyzed by this author in order to determine whether they are, in fact, essentially limestone ($CaCO_3$), or of a different material,

as for example lime (CaO). The simplest chemical examination towards this end is to treat the stone sample with a drop of dilute hydrochloric acid, HCl(*aq*). This drop caused an immediate acid-base reaction with frothing, which is clearly a result of the production of gaseous carbon dioxide (CO_2) from a carbonate. This limestone sample, with some of the purple pigment still adhering to it after 2,500 years, may have been used for the production of an alkaline environment at the Tel Dor dyeing site. Though it has been previously conjectured that the role of these limestone pieces was to provide the necessary alkalinity (*36*), the reasons why this compound was specifically chosen over other possibilities has never been clearly explained.
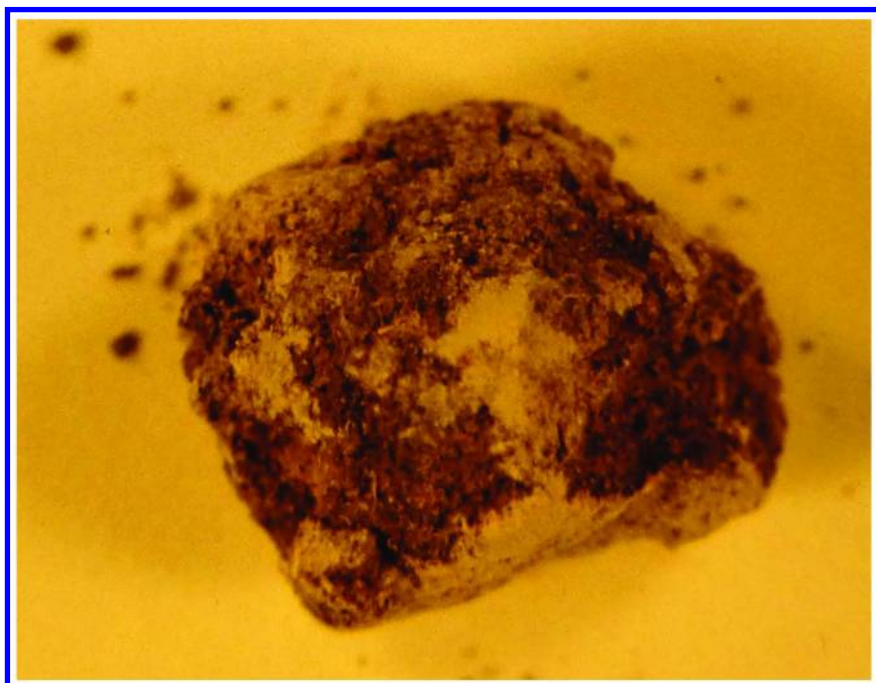
Figure 7. A dark soiled residue on a small piece of limestone found in the channel between two pits at a Phoenician site dated to the 6th century BCE at Tel Dor, in north-central Israel.

The realization that the quantity of the limestone introduced at the beginning of the process decreases throughout the reduction would have been apparent to the ancient dyers as they inspected the vat after the dye bath was emptied. These ancient empirical chemists must have been cognizant of the fact that certain compounds – today we call them acids – can react with the limestone. In fact, legend records that this elementary chemistry principle was already known several centuries before Pliny. The Roman historian, Titus Livius Patavinus,

known simply as Livy in English, living 2,000 years ago wrote an epic history of Rome called *Ab Urbe Condita Libri* ("Books from the Foundation of the City"), which covered the periods from the 8th century BCE until his present time. Livy recounts (*37*) how the famous Hannibal, the Punic Carthagian military commander, crossed the Alps in his march into northern Italy in the latter part of the 3rd century BCE. The only way for Hannibal's army to advance was across the rock face. In order to build a more manageable track for the baggage animals and war elephants to navigate down the mountainous slope, the soldiers needed to soften the limestone rocks so that it would then be easier to break them. According to Livy, this softening reaction was accomplished by pouring sour wine vinegar – a weak acid – into the cracks of the limestone.

Though the shells of sea snails are mostly calcium carbonate, they cannot be used to produce the necessary alkaline environment in the dye bath. A molluskan shell is a natural composite biomaterial with superior mechanical properties (*38*). Its complex organo-mineral structure is composed of an organic matrix, which consists of a mixture of glycoproteins and polysaccharides, bound to a mineral phase. This close association produces the resistance of shells not only to fracture but also provides for the resistance of the calcium carbonate to dissolution in water. Thus, shells that are thousands of years old have survived.

Source and Quantity of Water and Mollusks Used for the Dye Bath

Most archaeological dyeing installations for purple dyeing have been found near the coast as this was obviously a normal strategic location for processing the collected sea snails from the nearby waters. Hence, the question that is posed is whether seawater was used to prepare the purple dye bath in antiquity or whether use was made of fresh waters from lakes, streams, wells, etc.

The normal present day seawaters are mildly alkaline with a typical range of pH values of 7.5 – 8.5 (*39, 40*). At these values, the HCO_3^- ion predominates. When CO_2 from the atmosphere reacts with seawater, it immediately forms carbonic acid (H_2CO_3), which in itself is unstable. This further dissociates to form bicarbonate and carbonate ions. These ions are responsible for the buffering capacity of seawater, and thus seawaters can resist drastic pH changes even after the addition of weak bases and acids. Thus, since an alkaline environment was needed anyway for the dye vat, the ancients definitely could have initially used seawater – and would not have needed to use fresh water – before adding more of the alkaline substance to the bath in order to raise it to the proper alkalinity.

The quantity of liquid needed to fill a purple dye vat can be inferred, for example, from Figure 8, a partially reconstructed dye vat using the original potsherds. Amazingly, this 11th century BCE vat from Tel Keisan in modern northern Israel still shows residual purple stains that have survived 3,000 years (Figure 9). This type of vat would have contained a liquid volume on the order of about 100 L (or more). Previous natural dyeings have shown (*14*) that good depth of color was obtained by dyeing a woolen fleece according to the following ratio: 1 g wool : 7 medium *H. trunculus* snails : 70 mL dye solution

Figure 8. A partially reconstructed dye vat from an 11th century BCE Phoenician site at Tel Keisan in northern Israel.

Figure 9. Partial view of the interior of the potsherd from Figure 8 showing spots with purple pigment.

Thus, for a vat containing 100 L of liquid, the flesh of ten thousand *H. trunculus* snails would be needed, and such a vat could dye about a kilogram and a half of wool, which may be enough to produce one or two all-purple royal cloaks or mantles, depending on the depth of color desired.

The other two sea snail species that have been associated with purple dyeing, *B. brandaris* and *S. haemastoma*, produce much less pigment than even the small quantities extracted from the *H. trunculus* snail. Hence, it is a staggering thought to propose that whole dyeings would have occurred in such dye vats with either *B. brandaris* or *S. haemastoma* alone, since many more than 10,000 snails would be needed, which is already an astounding figure. As mentioned above, some *H. trunculus* snails can produce red-purple dyeings while others blue-purple, whereas *B. brandaris* and *S. haemastoma* only yield red-purple dyeings. Thus, pigments from these latter two species were probably added to a *H. trunculus* bath when needed to produce even redder purples than the *H. trunculus* snails alone can provide. An interesting example that has recently been observed of this possibility is the red-purple fibers in a Late Roman-Period textile whereby these fibers were mostly dyed with *H. trunculus* pigments with an additional contribution from one of the other two snail species (*3*).

Archaeological evidence also exemplifies the preponderance of the usage of *H. trunculus* over that of *B. brandaris* and *S. haemastoma*. In both Aegean and Levantine sites, many more *H. trunculus* shells are usually found than the other two species (*41*, *42*). In addition, all the archaeological purple paint pigments discovered as well as the archaeological and historical textiles that have been chemically analyzed via a full chromatographic analysis have all shown the presence of all three indigoids, with some minor components (*2*, *3*, *6*, *43*). Koren already established that the significant presence of MBI is a chromatic biomarker for the use of the *H. trunculus* species, alone or with some minor additions of one or more of the redder producing snails. Since, as explained above, no significant photo-debromination would have occurred during the anaerobic pre-dyeing stage of the bacterial reductive dissolution of the pigment, any MBI present in a sample, and certainly any IND, would not be as a result of the photo-debromination of the DBI, which is the main colorant in *B. brandaris* and *S. haemastoma*. Hence, all archaeological molluskan purple colorants – pigments and dyes – found to date are a result of the use of *H. trunculus*, alone or with some addition.

Textile Dyeing

The dyeing process commences when the indigoids are properly reduced after all the above-mentioned steps have been followed. The typical color of the naturally reduced solution is greenish due to the combination of the yellowish reduced and dissolved indigoids together with the dispersed undissolved blue indigo particles; hence blue and yellow will produce a greenish coloration.

Dyeing of the textile actually consists of two steps: textile immersion into the vat containing the reduced leuco indigoid dyes followed by air-oxidation of these reduced dyes to their original relatively insoluble state (see also Figure 4).

Immersion of the Textile

Pliny describes the dyeing as such:

After about nine days the cauldron is strained and a fleece that has been washed clean is dipped for a trial, and the liquid is heated up until fair confidence is achieved. A ruddy color is inferior to a blackish one. The fleece is allowed to soak for five hours and after it has been carded is dipped again, until it soaks up all the juice.

Though Pliny indicates that a total of about 9 days is needed for the dye vat to be ready for the actual dyeing, as a consequence of the reductive dissolution of the indigoids, in all-natural dyeing experiments (*14*) it was shown that the indigoids were in their dissolved leuco state after about 6 days from the start of this whole process, which began with the cracking of the snail's shell as described above.

Air-Oxidation

The last step is the simplest: the textile is removed from the reduced bath and its greenish color immediately begins to turn to its purple color while undergoing air-oxidation to its original insoluble pigment. In any chemical dyeing, the uptake of the dye by a textile is never 100%. In order to exhaust the expensive dye bath as fully as possible, after the textile was dyed and the dissolved reduced leuco-dye re-oxidized in air to its original oxidized state, the textile is then re-inserted into the dye bath in order to obtain a richer and darker color. This is in accordance with the latter part of the afore-mentioned excerpt from Pliny:

The fleece is allowed to soak for five hours and after it has been carded is dipped again, until it soaks up all the juice.

Talmudic Parallels to Pliny

Pliny the Elder wrote a detailed accounting of the practice of Tyrian Purple or Imperial Purple as practiced in the Roman Period. A much more succinct, but parallel recounting of the method by which *Tekhelet* – the "Biblical Blue-Purple" dye – was produced is noted in a Jewish source, specifically in the Babylonian Talmud (*44*). This woolen dye and another biblical dye, the red-purple *Argaman*, were both produced from sea snails. The passage is dated to the early 4th century CE, just a few centuries after Pliny's work, with parenthetical explanations given by the author in square brackets:

Abbayei said to Rabbi Samuel son of Rabbi Judah: 'That Tekhelet, how do you dye it?' He said to him: We bring sea snail 'blood' [the red-purple pigment] and substances ['*samanin*' in Aramaic-Hebrew] and put them into a vat (and we heat [literally '*boil*'] the mixture). We then take out a little [of the liquid] into an egg-shell and test [the liquid] with a fleece of

wool. We then throw away that egg-shell and burn the [trial sample of dyed] wool.

The word *'samanin'* as used throughout the Talmud has referred to various substances. These materials have included the following: dyes, dyestuffs, and pigments; drugs, medicines, medicinal ingredients, and wound ointments; and as cleansing and laundering substances. In the latter case, seven substances are itemized for the purpose of removal of a blood stain on a cloth in order to differentiate it from a dyed area – the dye will not be removed. The substances included are alkaline materials, including *neter*, which is synonymous with natron (sodium carbonate).

From this current investigation of Pliny's description, it is then obvious that the Talmud's mention of "substances" (*samanin*) in the context of a dyeing auxiliary for *Tekhelet* and Pliny's salt (*salem*) are equivalent and perhaps even identical. Besides water, all the ingredients, except one, are contained within the snail as implied by both Pliny's and the Talmud's descriptions of the molluskan dyeing practice. These include the extracted purple pigment, the bacteria and their meaty nutrients. The only external reagent needed to produce a successful reduced dye bath was Pliny's *salem* or the Talmud's *samanin*, which in both instances, was an alkaline substance, such as one of the salts mentioned above.

The Origin of Purple Dyeing

There has been much discussion as to where and when did the processing of the molluskan purple pigment begin (*41*, *45*). The more recent trend is to assign the origin of this biotechnological industry to the ancient Minoans and related peoples from the Aegean area or from Italy (*41*) from perhaps as far back as four millennia ago. In the not-so distant past, the previous popular notion was that the Levantine Phoenicians were the ones who developed the methods by which this purple pigment can be utilized. Based on that latter assignation, the famous term "Tyrian Purple" was coined after Tyre, one of the important ancient Phoenician cities where purple was produced.

Those who credit the inhabitants of the Aegean area indicate that there is evidence for "purple dye production" that pre-dates that from the Levantine coast. The claim is that there is "direct evidence" for the production of the purple "dye" from the various broken or crushed *Muricidae* snails that have been found at various sites in the Aegean. The scientific problem with this assertion is that this is not "direct" evidence that can be upheld in a court of scientific law, but rather indirect evidence alluding to the fact that these shells may have been used for the production of the purple pigment.

Various authors have misused the word "dye" to indicate any colorant. It is therefore imperative that those who write about the origin of purple dyeing understand the difference between "pigment" and "dye". While they can be both generically referred to as "colorants", a "pigment" is a substance that is essentially insoluble in water, whereas a "dye" is water-soluble. In order to perform a true dyeing of a textile – and not just to paint its surface – the colorant must be dissolved

in an aqueous solution so that the individual dye molecules can penetrate into the interior of the textile fibers and then form strong physico-chemical bonds with the fibers. In this way, the dye will be fast, i.e., will be stable and will not wash out of the textile when laundered. When the colorant is a pigment, it cannot be used in dyeing unless it is converted to a soluble form, and then that pigment becomes a dye. For example, in the current study, indigo and its brominated derivatives that constitute the molluskan purple pigment, if they were to be used as true dyes, must be solubilized by reducing them to their soluble reduced leuco-form, as mentioned above, and in that state they function as "dyes" for the dyeing of textiles. On the other hand, if a pigment is left as such in its water-insoluble state without further processing, it cannot be used for the dyeing of textiles – an internal phenomenon – but only in the painting of objects – an external, surface treatment. Examples of the latter are wall paintings or frescoes, painting of vessels, and perhaps even in the painting of textiles that are to be used as burial shrouds, where they will not of course be washed and thus without the possibility that the colorant will wash off the substrate.

Hence, the molluskan purple colorant of this study could have been used as a pigment for the surface coloration of objects, or, if further processed to a soluble form, could have been used as a dye for the dyeing of textiles. In archaeological sites whereby deliberately broken or crushed *Muricidae* sea snails have been found, it is a safe conjecture to state that these snails were probably not destined to be used as sea food, as the broken shells would have gotten attached to the meaty flesh of the snail, which would have made eating them difficult (*46*). However, finding broken shells does not automatically imply that these snails were processed for dyeing of textiles. Broken shells can simply mean that most probably these snails were used to produce the purple pigment. What will then happen to that pigment is a different story: it could be used as a paint pigment, once cleaned from the snail meat to which it adheres, or, if the intention is there, to be further processed and reductively dissolved into a dye form for the dyeing of textiles. Hence, finding broken shells is not "direct evidence" of purple dyeing; it is simply circumstantial evidence that, most probably, a pigment was produced.

The only direct evidence that the relevant sea snails were processed at a certain site for textile dyeing is from physical and chemical evidence of the presence of a purple residue whose source is molluskan. After dyeing of a textile was performed, the remaining dye in the bath eventually becomes oxidized to the solid pigment, which will adhere to the interior walls of the vessel. As mentioned above, the indigoid pigments are so water-insoluble that after more than three millennia visibly noticeable residual staining can still be seen. In a number of Phoenician sites along the Levantine coast of the Eastern Mediterranean, various purple-stained potsherds, fragments from vats, have indeed been found, as can be seen for example from Figures 5 and 9. Chemical analyses of these purple residues have determined that the source of that purple pigment is indeed molluskan. The oldest such purple-stained potsherds date from about the 14th century BCE (*41*). This then constitutes "direct evidence" that at this site, purple dyeing of textiles was practiced. The chemical requirement that a full multi-component chromatographic analysis of that pigment be performed is essential for the determination if "purple dye production" was performed.

In spite of the fact that numerous sites in the Aegean have shown the presence of Muricidae shells, to the knowledge of this author, to date, not a single example of a purple residue has been found at any of these sites. This is most unusual as due to the insolubility of the pigment, if a clay fragment from a true dye vat was found then part of the vat would most certainly show some residual purple stains. The fact that no such example has been found is very telling, and thus there is no chemical evidence, to date, that dyeing of textiles did take place in the Aegean.

The question that then arises is what was the function or purpose of these sea snails whose shells have been found in the Aegean if not for dyeing, and not for food? There is another purpose for these snails other than to produce a dye. They may be used for producing the colorant to be used as a pigment for painting. In fact, there are five archaeological examples of the purple pigment found at various sites in the Aegean where chemical evidence has definitively shown the presence of molluskan purple as a paint pigment, either as already used in the painting or pigment ready to be used (*43*). These samples are the earliest direct chemical evidence and date from the Late Bronze Age (17th century BCE or earlier). They were found in the following Aegean sites: Akrotiri and Raos – both located in the island of Santorini (Thera) – and from Trianda on the island of Rhodes. All of these purple specimens are pigments and not dyes.

The scientific conclusions are that the only bona fide chemical evidence, so far, for the use of purple from the Aegean is as a paint pigment and not as a dye. Hence, researchers who discuss the findings of *Muricidae* shells in the Aegean should not refer to that find as "proof" of "purple dye production". The more correct terminology is to refer to that indirect evidence of finding broken shells as probable indication for "purple pigment production". To date, that is the only find from the Aegean.

The major conclusion of the above discussion is extremely important. Archaeologists have already determined that Aegean sites associated with the Muricidae snails may date from as far back as four millennia and pre-date those sites from the Levantine coast by a few centuries, where textile dyeing has been chemically proven to have occurred. Until chemical evidence points to the contrary – i. e., if a purple-stained potsherd from a vat will been found in the Aegean whereby chemical analyses prove that the source of the purple pigment is molluskan – only the following conclusion can be scientifically drawn: The extraction of the purple pigment from sea snails to be used as a paint pigment probably originated in the Aegean; however, the transformation of that purple pigment to a dye for the dyeing of textiles probably originated later by the Levantine Phoenicians.

Conclusions

Archaeological artifacts that have survived the ravages of thousands of years of hoary history have borne witness to the multiple stages associated with the overall dyeing process using molluskan purple pigments. This critical study has found that the detailed description of these procedures given by Pliny the Elder is relatively complete and correct, which vindicates Pliny's veracity on the subject,

2,000 years after he documented them. Understanding the complexity of this dyeing process lies in its simplicity: all the steps involved can be explained by invoking the elementary principles of chemistry.

Acknowledgments

References

1. Spanier, E.; Karmon, N. In *The Royal Purple and the Biblical Blue: Argaman and Tekhelet. The Study of Chief Rabbi Dr. Isaac Herzog on the Dye Industries in Ancient Israel and Recent Scientific Contributions*; Spanier, E. Ed.; Keter: Jerusalem, Israel, 1987; pp 179−192.
2. Koren, Z. C. *Microchim. Acta* **2008**, *162*, 381–392.
3. Koren, Z. C.; Verhecken-Lammens, C. *e-Preserv. Sci.* **2013**, *10*, 27–34, and references therein.
4. Cooksey, C. J. *Molecules* **2001**, *6*, 736–769.
5. Cooksey, C. *Sci. Prog.* **2013**, *96*, 171–186, and references therein.
6. Koren, Z. C. In *Cultural Heritage and Archaeological Issues in Materials Science*; Sil, J. L. R., Trujeque, J. R., Castro, A. V., Pesqueira, M. E., Eds.; Materials Research Society Symposium Proceedings; Cambridge University Press: New York, 2012; Vol. 1374, pp 29–48, and references therein.
7. Pliny, *Natural History*; Rackham, H., Transl.; The Loeb Classical Library; Harvard University Press: Cambridge, MA, 1940; Vol. 3, Book 9.
8. Vykukal, R. L. Master's Thesis, University of Tennessee, Knoxville, TN, 2011. http://trace.tennessee.edu/utk_gradthes/1034.
9. *Pliny the Elder. The Natural History*. Bostock, J.; Riley, H. T. Transls.; Taylor and Francis: London, 1855. http://www.perseus.tufts.edu/hopper/text?doc=Perseus:text:1999.02.0137.
10. *Pliny the Younger. Letters. XXVII. To Baebius Macer*; The Harvard Classics, 1909–14. http://www.bartleby.com/9/4/1027.html.
11. *Pliny the Younger. Letters. XXVII. To Baebius Macer*. The Project Gutenberg EBook of Letters of Pliny. http://www.gutenberg.org/files/2811/2811-h/2811-h.htm#link2H_4_0028.
12. Pliny the Elder. *Wikipedia*. http://en.wikipedia.org/wiki/Pliny_the_Elder.
13. Natural History (Pliny). *Wikipedia*. http://en.wikipedia.org/wiki/Natural_History_(Pliny)
14. Koren, Z. C. *Dyes Hist. Archaeol.* **2005**, *20*, 136–149, and references therein.
15. Padden, A. N.; Dillon, V. M.; John, P.; Edmonds, J.; Collins, M. D.; Alvarez, N. *Nature (London)* **1998**, *396*, 225.
16. Padden, A. N.; Dillon, V. M.; Edmonds, J.; Collins, M. D.; Alvarez, N.; John, P. *Int. J. Syst. Bacteriol.* **1999**, *49*, 1025–1031.
17. John, P.; Arghyros, S.; Nicholson, S. *Dyes Hist. Archaeol.* **2008**, *21*, 45–50.
18. Nicholson, S. K.; John, P. *Appl. Microbiol. Biotechnol.* **2005**, *68*, 117–123.

19. Compton, R. G.; Perkin, S. J.; Gamblin, D. P.; Davis, J.; Marken, F.; Padden, A. N.; John, P. *New J. Chem.* **2000**, *24*, 179–181.

20. Park, S.; Ryu, J.-Y.; Seo, J.; Hur, H.-G. *J. Korean Soc. Appl. Biol. Chem.* **2012**, *55*, 83–88.

21. Koren, Z. C. *Isr. J. Chem.* **1995**, *35*, 117–124.

22. Haigh, J. *The Dier's Assistant in the Art of Dying Wool and Woollen Goods. Extracted from the Philosophical and Chymical Works of Those Most Eminent Authors Ferguson, Dufay, Hellot, Geoffery, Colbert; and That Reputable French Dier Mons. de Julienne. Translated from the French. With Additions and Practical Experiments*. James Humphrey's: Philadelphia, PA, 1810; p 31.

23. Haigh, J. *The Dier's Assistant in the Art of Dying Wool and Woollen Goods. Extracted from the Philosophical and Chymical Works of Those Most Eminent Authors Ferguson, Dufay, Hellot, Geoffery, Colbert; and That Reputable French Dier Mons. de Julienne. Translated from the French. With Additions and Practical Experiments*. James Humphrey's: Philadelphia, PA, 1810; pp 54, 55.

24. Baig, G. A. *AUTEX Res. J.* **2010**, *10*, 21–25.

25. McConnell, T. H. *The Nature of Disease: Pathology for the Health Professions*; Lippincott Williams & Wilkins: Baltimore, MD, 2007; p 490.

26. Alcamo, I. E.; Krumhardt, B. *Barron's Anatomy and Physiology the Easy Way*, 2nd ed.; Barron's Educational Series: Hauppauge, NY, 2004; p 442.

27. Sandberg, G. *Indigo Textiles: Technique and History*; A & C Black: London, 1989; pp 171, 172.

28. Dillard, C. R.; Goldberg, D. E. *Chemistry Reactions, Structure, and Properties*, 2nd ed.; Macmillan: New York, 1978; p 203.

29. Haynes, W. M., Ed.; *CRC Handbook of Chemistry and Physics*, 93rd ed. (Internet Version 2013); CRC Press/Taylor and Francis: Boca Raton, FL, 2013; pp 5−196.

30. Kotz, J. C.; Treichel, P., Jr. *Chemistry & Chemical Reactivity*, 4th ed.; Saunders College Publishing: Fort Worth, TX, 1999; p A−28.

31. Weast, R. C., Ed.; *CRC Handbook of Chemistry and Physics*, 66th ed.; CRC Press: Boca Raton, FL, 1985−1986; pp B-82, B-222.

32. Calcium carbonate. *Wikipedia*. http://en.wikipedia.org/wiki/Calcium_carbonate.

33. Geyssant, J. In *Calcium Carbonate: From the Cretaceous Period into the 21st Century*; Tegethoff, F. W., Rohleder, J., Kroker, E., Eds.; Birkhäuser Verlag: Basel, Switzerland, 2001; pp 1–52.

34. Naydowski, C. In *Calcium Carbonate: From the Cretaceous Period into the 21st Century*; Tegethoff, F. W., Rohleder, J., Kroker, E., Eds.; Birkhäuser Verlag: Basel, Switzerland, 2001; pp 197–237.

35. Yaalon, D. H. *Plant Soil* **1957**, *8*, 275–288.

36. Koren, Z. C. *Dyes Hist. Archaeol.* **1993**, *11*, 25–33.

37. Livy. Book 21, Chs. 30-38, Secs. 30.1, 37.2, 37.3. http://www.johndclare.net/AncientHistory/Hannibal_Sources3.html.

38. Marin, F.; Luquet, G. *Mater. Sci. Eng. C* **2005**, *25*, 105−111.

39. Marion, G. M.; Millero, F. J.; Camões, M. F.; Spitzer, P.; Feistel, R.; Chen, C.-T. A. *Mar. Chem.* **2011**, *126*, 89–96.
40. Garrison, T. *Oceanography: An Invitation to Marine Science*, 7th ed.; Brooks/Cole, Cengage Learning: Belmont, CA, 2010: pp 195–196.
41. Reese, D. S. *Mediterranean Archaeol. Archaeom.* **2010**, *10*, 113–141.
42. Reese, D. S. In *Kommos IV. The Greek Sanctuary, Part 1*; Shaw, J. W., Shaw, M. C., Eds.; Princeton University: Princeton, NJ, 2000; pp 643−645.
43. Karapanagiotis, I.; Mantzouris, D.; Cooksey, C.; Mubarak, M. S.; Tsiamyrtzis, P. *Microchem. J.* **2013**, *110*, 70–80.
44. Babylonian Talmud, Tractate *Menahot*, p 42b.
45. Stieglitz, R. R. *Biblical Archaeol.* **1994**, *57*, 46–54.
46. Çakırlar, C.; Becks, R. *Studia Troica* **2009**, *18*, 87−103.

Chapter 4

Developing Direct Analysis in Real Time Time-of-Flight Mass Spectrometric Methods for Identification of Organic Dyes in Historic Wool Textiles

Calvin J. Day,[1] Cathy Selvius DeRoo,[2] and Ruth Ann Armitage*,[1]

[1]Department of Chemistry, Eastern Michigan University, Ypsilanti, Michigan 48197
[2]Conservation Department, Detroit Institute of Arts, Detroit, Michigan 48202
***E-mail: rarmitage@emich.edu**

Identifying organic dye compounds in textiles is a significant challenge in conservation science. Existing methods, such as liquid chromatography, require lengthy sample preparation procedures that can induce structural changes in the extracted colorants. Direct analysis in real time mass spectrometry is a simple method for identifying a number of classes of dye compounds in single fibers. Blue and red fibers from historic tapestries from the Detroit Institute of Arts collections yielded clear spectra for indigotin and several anthraquinones including alizarin and purpurin, indicating the use of indigo and madder as sources of the colorants. Flavonoid dyes that impart yellow colors are generally considered more difficult to identify, as many of the colorant compounds are structural isomers.

Introduction

Identification of organic dye sources in historic textiles is a significant problem in archaeological and conservation sciences. Derived from a wide array of plant, animal, lichen, and insect sources, organic dyes are identified not just

by the presence of a single colorant molecule, but generally by the ratios in which multiple colorant compounds are present relative to one another. Typically, samples must be extracted with acid to separate the colorants from the fiber matrix prior to analysis with chromatographic methods. Extraction protocols are well known to induce hydrolysis in many of the colorant compounds (*1*, *2*). High performance liquid chromatography is the most commonly applied technique, usually using either photodiode array UV-visible spectroscopic or electrospray ionization mass spectrometric detection (*3–6*). The destructive nature of these sample preparation methods, the complexity of the separation protocols, and the length of time required for chromatographic analyses suggest that there is need for simple and rapid methods for identification of organic dye sources in cultural heritage materials. Surface-enhanced resonance Raman spectroscopy is one possible alternative to HPLC for this application (*7*, *8*). The necessity of preparing the nanoparticle substrates, however, is a significant limitation.

For the past three years, the collaborative efforts of scientists at the DIA and Eastern Michigan University have led to new methods for direct analysis in real time ionization coupled to high-resolution time-of-flight mass spectrometry (DART-MS) for characterization of organic colorants directly from textile fibers. DART ionization (*9*) is ideal for direct identification of small (<1000 Da) molecules, and can be used in either positive or negative ion mode. The method has been embraced by the forensic and pharmaceutical analysis communities for its speed and ease of use (*10–18*). Few examples of its application in conservation or archaeological sciences have been published to date. Of note is Adams' work with paper at the Library of Congress (*19*). Previous studies of dyed cotton samples from *Traité des Matiéres Colorantes du Blanchiment et de la Teinture du Coton,* a 19th-century treatise on dyes and dyeing practices in the DIA research library, provided initial study materials to evaluate the efficacy of DART-MS for identifying colorants in textiles (*20*). Anthraquinones, indigoids, homoisoflavonoids, curcuminoids, and flavonoids have been readily identified without sample preparation by direct analysis of the fibers (*21*). Such compounds are also of forensic and food/pharmaceutical interest, and DART-MS has proven a useful technique in detecting and identifying them in other materials as well (*13*, *22–24*)

Previous DART-MS studies of dyes on textiles focused solely on cotton fibers, though proteinaceous fibers are arguably more common in historic European textiles than are cellulosic fibers. In the spring of 2012, several tapestries from the DIA collections were removed from storage for photographic documentation and presented a concomitant opportunity to acquire fiber samples. This opportunity was provided in support of this research and in recognition of the fact that establishing the efficacy of a new analytical technique requires not only successfully analyzing reference materials, but, most critically, the ability to detect the dye moities present in historic textiles. An analytical technique employed in the analysis of dyed fibers must possess the requisite sensitivity to detect organic dye constituents, which yield very high tinting strength at very low concentrations. The fiber samples from these tapestries enabled us to continue our studies of the applicability of DART-MS to identification of organic dyes in textiles of cultural heritage importance.

Methods and Materials

Historic Samples

A number of tapestries belonging to the Detroit Institute of Arts were removed from storage for photography and documentation for the museum's database. The tapestries (Table I), dating from the 17th to18th centuries and French or Flemish in origin, all demonstrate fading /color loss to some degree. Given that synthetic dye development did not begin until the mid-19th century, presumably the dyes employed in these tapestries are natural dyes derived from plant material. At the time that these tapestries were produced the primary natural dyes would have included madder (red), weld (yellow), and either woad or indigo. It is likely, given the dates of attribution of the tapestries used in this study, that woad had been supplanted as the primary source of indigotin in Western Europe by the massive importation of indigo from Asia and later from the Caribbean and Central America (*25*). Throughout Europe, weld remained the primary source of the yellow flavonoid luteolin with dyer's madder the predominant source of the anthraquinone red dye

Table I. Tapestries from the Detroit Institute of Arts sampled for analysis

DIA no.	Title	Origin	Date
14.6	*Honeymoon*	Aubusson, French	Late 18th century
T79.1145	unaccessioned	Unknown	Unknown
27.186	*Verdure*	Flanders/Belgium	c. 1700
43.52	*Scene from Roman History: The Tribute*	Flanders/Belgium Michel Wauters weaver's mark	17th century
52.311	*Game of Bowls*	Lille, France	Late 17th/early 18th century
68.346	*Allegorical Landscape*	Flanders/Belgium	Late 17th/early 18th century

Permission was granted to remove (~ 1 cm long) samples from the numerous loose ends left by the weaver on the backs of the tapestries. Wool fibers were removed from the tapestries listed in Table I. Samples of each relevant color were collected, including reds, blues, greens, and yellows or golds. These tapestries provided an opportunity to refine previous studies and further develop the DART-MS technique for identification of organic colorants in historic textiles.

Figure 1 shows some of the tapestries sampled for this study. Many of the colors are quite faded, especially DIA no.14.6. Because natural yellow dyes are known to be fugitive, many of the greens – trees and foliage – now appear blue, as the yellow has faded. Reds and blues are well preserved. Knowing that light

degradation has taken place in these materials, we also had the opportunity to evaluate the ability of DART-MS to identify degradation products directly in dyed textile fibers.
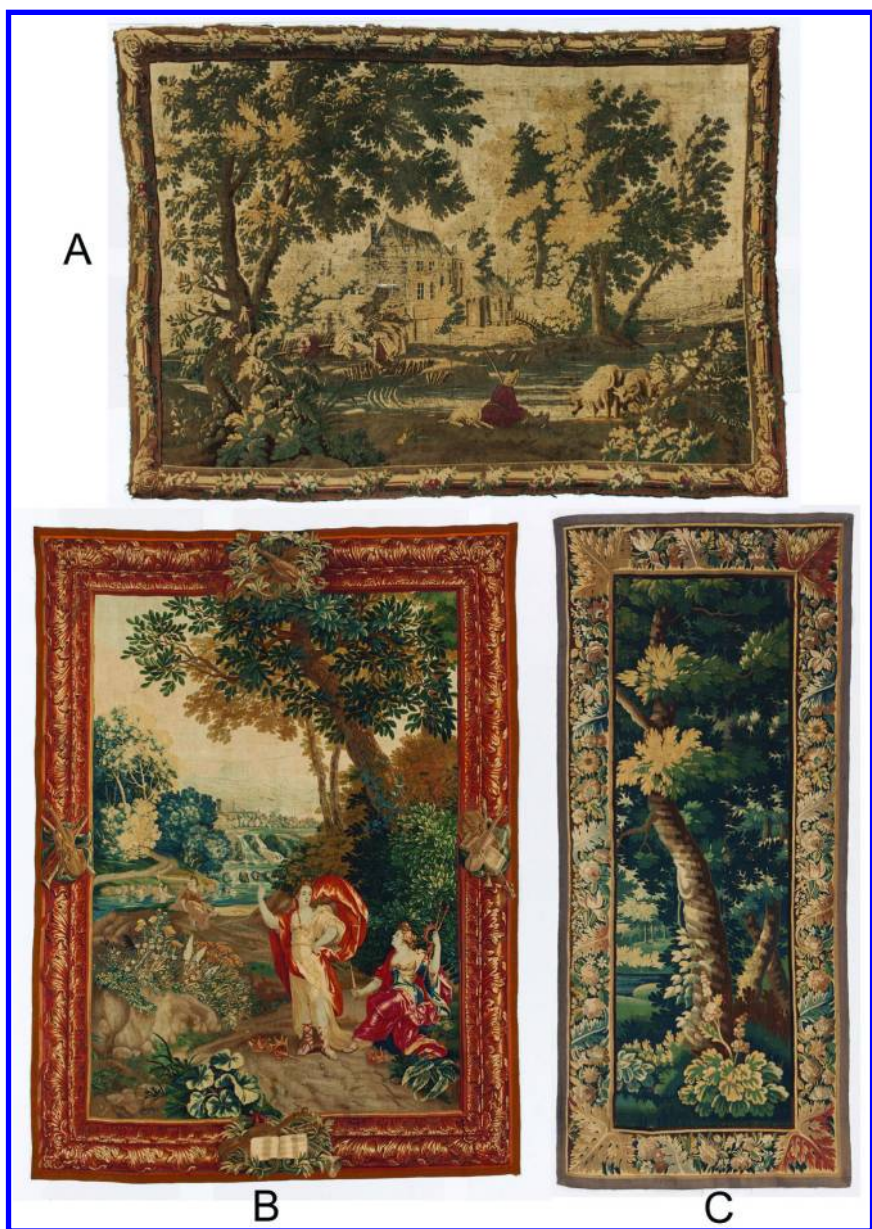

Figure 1. Some of the tapestries from the Detroit Institute of Arts that were sampled for this study. A: DIA no. 14.6. B. DIA no. 68.346. C. DIA no. 27.186. Images courtesy of the DIA.

Reference Materials

Wool skeins (TestFabrics, West Pittstown, PA) were either directly dyed or dyed after being mordanted with alum using appropriate recipes (*26–28*) prepared from the plant and insect materials listed in Table II. Green wool samples were prepared by first dyeing skeins yellow in each of the four yellow dyestuffs, then over-dyeing the yellow with the indigo vat to yield a green color. Proteinaceous fibers (rabbit hair yarn) dyed with lady's bedstraw were provided by Kathryn Jakes, Ohio State University.

Table II. Dyes used to prepare comparative materials

Dye source	Botanical name	Commercial source	Primary colorant(s) (25)	Other colorants (25, 29)
Madder root	*Rubia tinctoria*	Kremer[1]	Alizarin, purpurin	Rubiadin, lucidin
Lac	*Laccifer lacca*	Maiwa[2]	Laccaic acids A-D	Erythrolaccin, deoxyerythrolaccin
Cochineal	*Dactylopius coccus*	Kremer	Carminic acid	
Broom	*Genista tinctoria*	Kremer	Genistein	Luteolin, apigenin, luteolin methyl ether
Weld	*Reseda luteola*	Kremer	Luteolin	Apigenin, luteolin methyl ether
Young fustic	*Cotinius coggyria*	Kremer	Fisetin	Sulfuretin,quercetin
Green buckthorn (Avignon) berries	*Rhamnus saxitilis* and others	Kremer	Rhamnetin	Emodin, quercetin, kaempferol, rhamnazin, rhamnocitrin, isorhamnetin
Indigo	*Indigofera* sp.	Maiwa	Indigotin	

[1] Kremer Pigments, New York, NY, USA.   [2] Maiwa Dyes, Vancouver, BC, Canada.

Sample Analysis

Forceps were used to retrieve ***single fibers*** where possible from the collected tapestry material. The fiber or small clump of fibers (a few mm long, of mass too small to weigh reliably on an analytical balance) was then simply held in the gap between Orifice 1 of the AccuToF mass spectrometer (JEOL USA, Peabody MA) and the DART ionization source (IonSense, Saugus, MA). The DART was used in both positive and negative ionization modes with helium at two temperatures : 350°C and 500°C. Orifice 1 was set to 30V to minimize fragmentation of the colorant compounds and 120°C; Orifice 2 was held at 5V, and the ring lens

voltage at 5V. The DART grid voltage was kept at the default values of +240V and -530V. The mass spectrometer RF ion guide ("peaks voltage") was set to 1500V to maximize sensitivity in the intermediate mass range. Mass calibration was carried out using PEG-600 in methanol during each acquisition. The mass resolving power was approximately 6000 (calculated as m/Δm) over the mass range of interest.

Results and Discussion

Method Development

Under the conditions employed, many of the dye colorant compounds in Table II are observed in positive ion mode as protonated MH$^+$ ions without fragmentation within a few seconds of exposure in the DART source. In negative ion mode, which gives better sensitivity, particularly for acidic compounds, the primary peak for each compound generally occurs as the M-H$^-$ ion, except as noted below.

Temperature

The temperature of the DART ionization gas greatly affects what ions are observed in the mass spectrum. At 350°C, most of the dye colorant compounds – indigotin from indigo, alizarin and purpurin from madder, and some of the yellow dye compounds – can be easily identified above the background in the resulting spectrum. This temperature had little effect on the fibers. However, carminic and laccaic acids from the insect dyes cochineal and lac do not readily ionize at this "low" temperature. Only at 500°C in negative ion mode does carminic acid become detectable in the background from the pyrolysis products of the wool fiber. Carminic acid was observed as the aglycone under these conditions, which is consistent with the observation of JEOL mass spectrometry applications specialists (*30*). Wool dyed with lac showed the presence of deoxyerythrolaccin, but none of the laccaic acids, even at 500°C.

At 500°C, the wool fibers are completely charred during the analysis. Under most circumstances, particularly with historic materials, this is less than ideal. Further work is necessary to determine the optimal balance between observed signal and preservation of the fibers.

Ionization Mode

While positive ion mode proved to be sufficient for many of the colorants in the reference materials, significantly higher intensity signals were obtained for all of the colorants except indigotin in negative ion mode. For all reference materials containing indigo, two peaks were observed for indigotin in negative ion mode: the base peak, corresponding to the M$^-$ ion was observed at m/z 262.074 (± 0.015 Da) and a second peak corresponded to the M-H$^-$ ion at *m/z* 261.066, as expected in negative ion mode (Figure 2). Ribechini et al. (*31*) observed similar discrepancies

in negative-ion laser desorption/ionization MS studies of indigoids. A similar pattern was observed in very dark blue wool fibers in positive ion mode: the MH+ ion at m/z 263.082 dominated in this case, with the M+ ion (*m/z* 262.077) at about half the abundance. While proton transfer is generally the lowest energy ionization pathway, if the ionization energy of the molecule is lower than the energy required to transfer the proton to or from the molecule, then direct Penning ionization can occur.
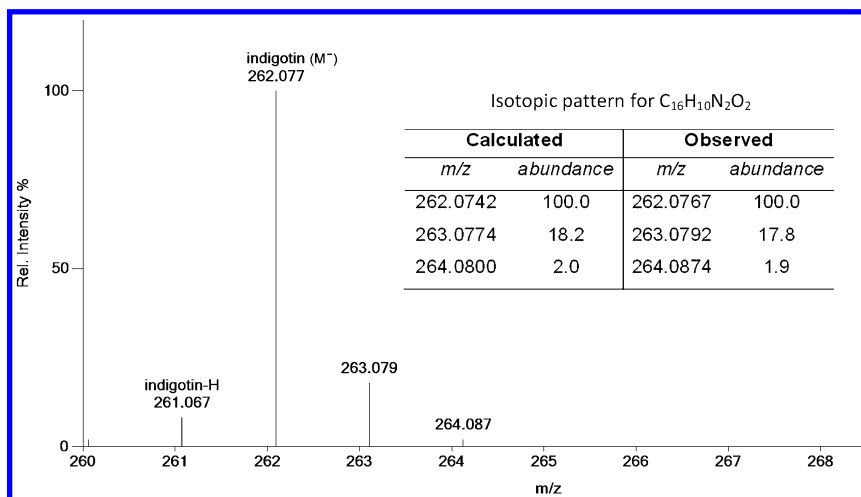

	Isotopic pattern for $C_{16}H_{10}N_2O_2$			
	Calculated		Observed	
	m/z	*abundance*	*m/z*	*abundance*
	262.0742	100.0	262.0767	100.0
	263.0774	18.2	263.0792	17.8
	264.0800	2.0	264.0874	1.9

Figure 2. Negative ion DART mass spectrum for indigo on wool reference sample, showing expected isotopic pattern for indigotin.

Red Dyes

Anthraquinones in Red Dye Reference Materials

Mordanted wool fibers dyed with madder, lac, and cochineal insects as well as rabbit hair yarn dyed with lady's bedstraw (*Galium verum*) were examined in negative ion mode at 500°C as described above. Four anthraquinones dominated the spectra for madder and bedstraw: alizarin, purpurin, rubiadin, and lucidin (Table III). The ratios of these anthraquinones relative to each other generally followed the expected patterns, with alizarin dominating in madder-dyed wool and rubiadin dominating in bedstraw. The presence of alizarin and purpurin are typically considered indicative of madder as the dye source, as bedstraw contains little or no alizarin. The relatively low intensity for purpurin in the madder-dyed wool prepared for this study may be due to the dye bath temperature, mordant concentration, or other conditions of sample preparation. Xanthopurpurin (isomeric with alizarin) and anthrogallol (isomeric with purpurin), which will not be directly identified by this method, are other minor anthraquinone colorants from madder and bedstraw.

Table III. Absolute intensities for the relevant ions for the anthraquinone colorants from madder root and bedstraw reference materials. Data is for negative ion mode at 500 °C. Relative intensities in parentheses are calculated based on these four ions only.

Exact mass (M-H⁻ ion)	Compound	Madder	Bedstraw
239.034	Alizarin	158335 (**100**)	13899 (**6**)
255.029	Purpurin	44271 (**28**)	126708 (**53**)
253.050	Rubiadin	72656 (**46**)	238604 (**100**)
269.045	Lucidin	14551 (**9**)	75726 (**32**)

Carminic acid aglycone (M-H⁻, m/z 329.026) was the primary characteristic colorant in cochineal-dyed wool at 500°C in negative ion mode. Deoxyerythrolaccin was observed in both cochineal and lac reference samples. Wetting the lac- and cochineal-dyed wool with a few microliters of 88% formic acid prior to exposure to the DART source hydrolyzed the dye and extracted it from the fibers, resulting in significantly improved signal. After treatment with formic acid, several characteristic colorants for lac were observed in negative ion mode at 500°C, including laccaic acid A (as M-H_2O^-, m/z 519.070), laccaic acid B (as M-H_2O^- at m/z 478.058), laccaic acid C (as M-H_2O^- at m/z 521.053), and laccaic acid D (also called flavokermesic acid, as M-H⁻, m/z 313.034).

Red Tapestry Fibers

In positive ion mode at 350°C, only some of the red fibers from the six tapestries showed the presence of alizarin and purpurin, the primary anthraquinones present in madder (*Rubia tinctoria*). Negative ion mode at 500°C yielded much stronger signals for the anthraquinones, and enabled the identification of the less abundant compounds rubiadin and lucidin as well. The anthraquinone composition of the red fiber samples is summarized in Table IV. None of the red dye compounds were observed in DIA no. 27.186, even at 500°C in negative ion mode. Upon closer inspection, it was determined that the "red" fibers from DIA no. 27.186 were more brown than red; this sample is not included in Table VI. DIA no. 68.346 provided two different colors of red fibers: a light reddish-pink color and a dark burgundy (Figure 3). Because of the deep red color, we suspected that the burgundy sample might contain carminic acid, so a second sample was analyzed using the 88% formic acid treatment described above. Carminic acid aglycone – as was observed in the cochineal wool reference materials – was present in the acid hydrolyzed sample. None of the other red fibers showed evidence of carminic acid under these conditions.

Previous studies have attempted to establish a relationship between the abundance of the anthraquinones and the *Rubia* species used as the original dyestuff (*32*). Wouters has further suggested that a higher percentage of purpurin relative to alizarin may be indicative of *Rubia peregrina*, or wild madder (*33*). Further studies, using different extraction conditions and HPLC, indicate that the identification of *Rubia* species may be possible if other compounds are taken into account (*34*). As previous studies have focused on the extracts from textiles, it is difficult to draw comparisons to direct mass spectral analysis. We have found significant differences between the relative amounts of alizarin and pupurin in madder root depending on whether it is analyzed fresh or dried. Regardless, it seems reasonable to conclude that all of the true red fibers from the DIA tapestries were likely dyed with madder root. Only the burgundy sample from DIA no. 68.346 showed evidence of cochineal dye. Because rubiadin was not present in large quantities in any of the tapestry samples, it is unlikely that bedstraw was used as a dye source.

Table IV. Absolute intensities for the relevant ions for the anthraquinone colorants from the red DIA tapestry samples

Anthraquinone colorants	14.6	T79.1145	43.52	52.311	68.346 light	68.346 dark + FA
Alizarin	34674	4198	281377	336126	16719	2138
Purpurin	26744	6807	70573	156827	17094	1418
Rubiadin	3490	1646	35536	80932	0	634
Lucidin	3989	0	19730	10027	0	1039
Carminic acid aglycone	0	0	0	0	0	1928

Ahn and Obendorf (*35*) report that the primary photo-oxidative degradation products of alizarin are phthalic acid, dimethyl phthalate, phthalic anhydride, di-t-butylphenol, and benzoic acid. Phthalates are ubiquitous environmental contaminants and may be false positives when considered as degradation products of alizarin in archaeological or art materials that may have come in contact with plastic at some point in the past. Pure alizarin on alum-tartaric acid-mordanted wool showed a small amount of benzoic acid, but no phthalates after two years of storage under laboratory conditions. DIA no. 14.6 was a faded red color and showed phthalic acid, dimethyl phthalate, and benzoic acid present. DIA no. T179.1145, a dark red, showed only a trace of phthalic anhydride. DIA no. 43.52, also a dark red color, showed a trace of benzoic acid. Significant quantities of both phthalic acid and dimethyl phthalate were observed in the light red sample from DIA no. 68.346. In comparison, only a small amount of dimethyl phthalate was found in the dark red sample of DIA no. 68.346. No degradation products of alizarin were observed in red fibers from DIA no. 52.311.
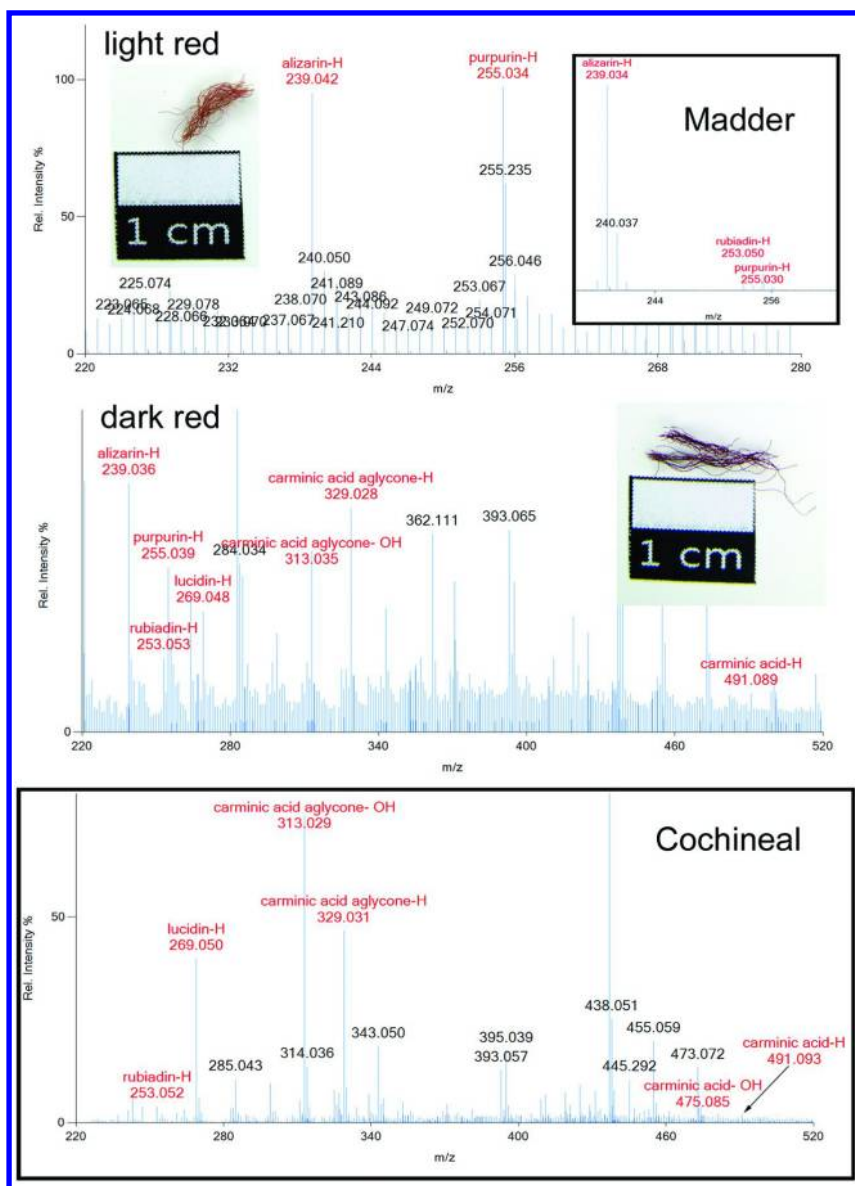
Figure 3. Negative ion DART mass spectra for red fibers from DIA no. 68.346. Spectra for madder root and cochineal on wool reference materials (boxes) provided for comparison.

Yellow Dyes

Flavonoids in Yellow Dye Reference Materials

The identification and differentiation of yellow dyes in historic textiles is particularly challenging. In part, this is due to the structural similarities of the colorants; merely identifying the presence of a single colorant is insufficient to clearly identify the source. The relative amounts of the different colorants are routinely used to draw conclusions about the source of yellow dyes. The most common method for determining these relative quantities is high performance liquid chromatography, coupled to either diode array UV-visible spectroscopy or electrospray ionization mass spectrometry. One drawback of the DART-MS method is that structural isomers yield the same molecular ion. Thus a peak at m/z 269.045 could equally correspond to apigenin from weld, emodin from buckthorn, genistein from broom, or sulfuretin from young fustic (Table V). However, the relative amounts of each of the possible flavonoids can be estimated by comparing the absolute intensities of the relevant peaks. Because the wool fibers pyrolyze during analysis, many ions are formed that are not relevant to the dye composition. Therefore, the overall relative intensities cannot be used reliably, as the base peak may differ from run to run. Table VI shows the intensities of the relevant ions observed in the negative ion DART mass spectra of the freshly dyed wool reference samples. at 500°C. Broom and green buckthorn berries can be differentiated based on their most abundant flavonoid compounds, genistein (and apigenin, both as M-H-, m/z 269.045) and quercetin (M-H-, m/z 301.050). Rhamnetin was expected to be the primary colorant in green buckthorn berries, based on literature reports for hydrolyzed textiles (*36*). Weld and young fustic both have the same "base flavonoid" at m/z 285.050, but differ in that young fustic has a much higher proportion of m/z 269.050 than weld. The young fustic reference material prepared for this study also contained a significant quantity of m/z 301.050. This does not correspond to the presence of ellagic acid, which would have an exact mass of 302.006 Da, resulting in an M-H- ion at m/z 300.998. A mass resolution (calculated as m/Δm) of 5800 would be necessary to resolve these two ions. The AccuTOF mass spectrometer provided resolution greater than this (6000) in this mass range.

Green and Yellow/Gold Tapestry Fibers: Flavonoids

Flavonoid compounds were observed in four of the six green fibers, as shown in Table VII. Green fibers from DIA no. 14.6 contained only m/z 269.050, which may be indicative of the presence of genistein from broom, though luteolin methyl ether should also be present. DIA nos. 43.52 and 52.311 green fibers both showed primarily m/z 285.050 and 269.045, possibly corresponding to fisetin and sulfuretin from young fustic. Only DIA no. 43.52 also contained m/z 301.050, likely corresponding to quercetin. The yellow present in green fibers from DIA no. 27.186 might be a mixture of broom and weld, but the pattern does not match that of any of the reference material samples. The absence of any flavonoids in

In Archaeological Chemistry VIII; Armitage, R., et al.;
ACS Symposium Series; American Chemical Society: Washington, DC, 2013.

both the green and yellow fibers from DIA no. 68.346 is consistent with the poor preservation state of the tapestry.

Table V. Flavonoids in yellow dyes and expected ions by negative ion DART-MS

Molecular formula	Exact mass (M-H⁻ ion)	Compounds
$C_{15}H_{10}O_5$	269.045	Apigenin, emodin, genistein, sulfuretin
$C_{15}H_{10}O_6$	285.040	Kaempferol, luteolin, fisetin
$C_{15}H_{10}O_7$	301.033	Quercetin, morin
$C_{16}H_{12}O_6$	299.063	Rhamnocitrin, luteolin methyl ether
$C_{16}H_{12}O_7$	315.050	Rhamnetin, isorhamnetin
$C_{17}H_{14}O_7$	329.070	Rhamnazin

The five other yellow or gold fibers all contained flavonoid compounds. DIA no. T79.1145 was the only sample that contained m/z 315.050, indicating the presence of rhamnetin which is characteristic of green buckthorn berries (*Rhamnus saxitilis*). DIA no. 52.311 showed significant signals at m/z 285, 269 and 299 in decreasing order of abundance, which may indicate a mixture of dye sources, possibly weld and broom. The remaining samples shared a pattern of flavonoid compounds, with m/z 269, 285, and 299 occurring in decreasing order of abundance. The differences in abundance may be indicative of different combinations of dye sources, different mordants, or variations in dye plants and bath preparation.

Blue and Green Fibers: Indigoids

Six blue fibers were collected from five of the DIA tapestries. No blue material was collected from DIA no. 14.6. In positive ion mode, all of the blue fibers examined by DART-MS showed a large peak at m/z 263.082, corresponding to the MH⁺ ion for indigotin ($C_{16}H_{10}N_2O_2$). Both dark and light blue fibers were collected from tapestry T79.1154, and both showed the characteristic peak, though at different intensities (Figure 4).

All of the green tapestry fibers were run in both positive and negative ion modes. As was observed for the blue fibers, in positive ion mode all of the green fibers showed the MH⁺ at m/z 263.082 of indigotin; in only one case (DIA no. 68.346) was this not the base peak of the observed mass spectrum. In negative ion mode, both the M⁻ and M-H⁻ ions for indigotin (m/z 262.074 and 261.067, respectively) were observed, as was the case with the lab prepared green wool samples.

In addition to the primary colorant, three degradation products of indigotin – isatin, isatoic anhydride, and aminobenzoic acid (*37*) – were detected in the blue and green tapestry samples. Isatin was detected in positive ion mode for all but the light blue fiber from DIA no. T79.1145 and the green fiber from DIA no. 52.311. Green fibers from DIA no. 27.186 showed significant quantities of all three degradation products in positive ion mode. However, it is important to note that we also observed isatin by DART-MS in wool that had been dyed with indigo approximately two hours prior to analysis, indicating that this "degradation product" may exist in the vat as well.

Table VI. Absolute intensities for the relevant ions for the flavonoid colorants from four common yellow dyes, as observed in reference materials. Data is for negative ion mode at 500 °C. Relative intensities in parentheses are calculated based on these six ions only.

Exact mass (M-H⁻ ion)	Broom	Weld	Green buckthorn berries	Young fustic
269.045	17980 (**100**) Genistein+ Apigenin	6867 (**6**) Apigenin	62043 (**27**) Emodin	4310 (**64**) Sulfuretin
285.040	2566 (**14**) Luteolin	106382 (**100**) Luteolin	7018 (**3**) Kaempferol	6728 (**100**) Sufuretin
299.063	14921 (**83**) Luteolin methyl ether	5994 (**6**) Luteolin methyl ether	3185 (**1**) Rhamnocitrin	nd (**0**)
301.033	nd (**0**)	nd (**0**)	232368 (**100**) Quercetin	5267 (**78**)
315.050	nd (**0**)	nd (**0**)	146085 (**63**) Rhamnetin + isorhamnetin	nd (**0**)
329.070	nd (**0**)	nd (**0**)	9937 (**4**) Rhamnazin	nd (**0**)

nd, not detected.

Indigoids are the easiest of the organic colorants to identify by DART-MS. Within a few seconds of exposure to the ion source, the primary ion for indigotin is observed in real time without sample preparation or separation required. While there are some differences in the dye precursors found in the various botanical sources, the vat process yields primarily indigotin. DART-MS may have potential for identifying other compounds in blue dyes that are from the various *Indigofera, Isatis,* and *Polygonum* species, thereby providing a rapid way of differentiating these sources.

Table VII. Absolute intensities for the relevant ions for the flavonoid colorants from the DIA tapestry samples. Relative intensities in parentheses are calculated based on these six ions only.

Exact mass (M-H⁻ ion)	14.6	T79.1145	27.186	43.52	52.311	68.346
Green fibers						
269.045	4294 (**100**)	nd (**0**)	1088 (**100**)	349 (**71**)	4595 (**69**)	nd (**0**)
285.040	nd (**0**)	nd (**0**)	1019 (**94**)	492 (**100**)	6679 (**100**)	nd (**0**)
301.033	nd (**0**)	nd (**0**)	nd (**0**)	287 (**58**)	nd (**0**)	nd (**0**)
299.063	nd (**0**)	nd (**0**)	nd (**0**)	78 (**16**)	nd (**0**)	nd (**0**)
315.050	nd (**0**)	nd (**0**)	nd (**0**)	nd (**0**)	nd (**0**)	nd (**0**)
329.070	nd (**0**)	nd (**0**)	nd (**0**)	nd (**0**)	nd (**0**)	nd (**0**)
Yellow fibers						
269.045	4774 (**100**)	3484 (**24**)	6448 (**100**)	150 (**100**)	35807 (**45**)	nd (**0**)
285.040	2527 (**53**)	14784 (**100**)	6011 (**93**)	114 (**76**)	79163 (**100**)	nd (**0**)
299.063	1592 (**33**)	2299 (**16**)	nd (**0**)	287 (**69**)	19862 (**25**)	nd (**0**)
301.033	nd (**0**)	1238 (**8**)	nd (**0**)	nd (**0**)	nd (**0**)	nd (**0**)
315.050	nd (**0**)	1074 (**7**)	nd (**0**)	nd (**0**)	nd (**0**)	nd (**0**)
329.070	nd (**0**)	nd (**0**)	nd (**0**)	nd (**0**)	nd (**0**)	nd (**0**)

Flavonoid dye colorants are well known to undergo both photo and oxidative degradation. Ferreira et al. (*2*) describe the mechanisms by which 3,4-dihydroxybenzoic acid and 2,4,6-trihydroxybenzoic acids form via photo-oxidation of quercetin. However, Degano et al. (*31*) caution that di- and trihydroxybenzoic acids cannot be reliably used to indicate degraded flavonoid dyes. In this study, alum mordanted wool dyed with weld showed the presence of both di- and trihydroxybenzoic acids at m/z 153.019 and 169.014. The positional isomers of these compounds cannot be differentiated based on mass, so it is impossible to say specifically which of them was present. 4-Hydroxybenzoic acid is considered a more reliable indicator of degradation of flavonoids. The green fibers from DIA no. T79.1145 showed no indication of the presence of any of the flavonoid dye compounds, and no evidence of hydroxybenzoic acid degradation products, indicating that the green fibers are not likely colored with

flavonoid dyes. DIA no. 68.346 showed none of the flavonoids in either the green or yellow fibers, though hydroxybenzoic acid was observed in both. All the rest of the yellow and green fibers contained a combination of mono-, di-, and trihydroxybenzoic acids, consistent with the determination that all were dyed with some combination of weld and broom, or other flavonoid-containing dye plants.
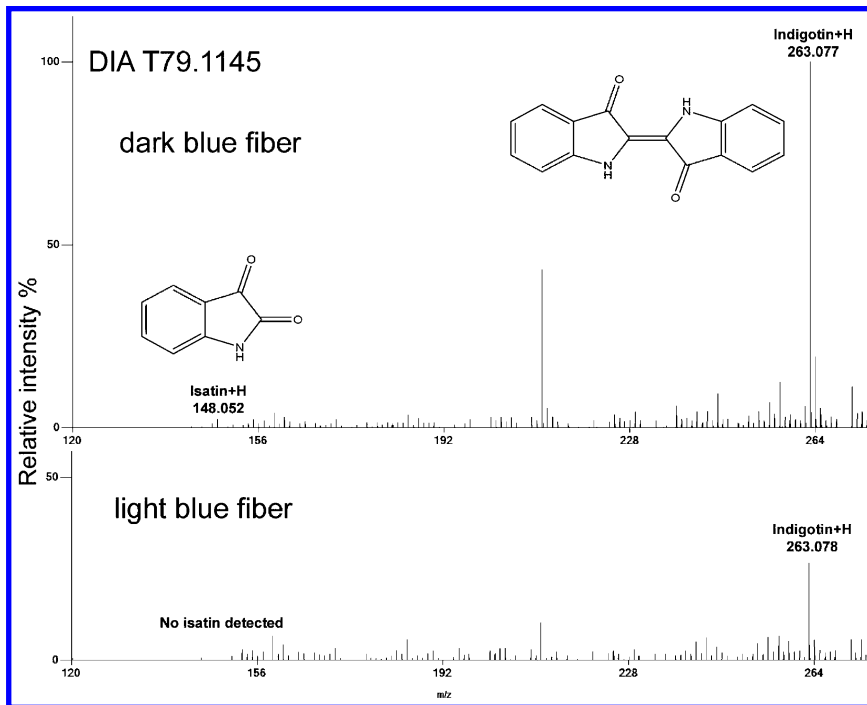

Figure 4. Positive ion DART mass spectra for two blue fibers from DIA no. T79.1145.

Conclusions

DART-MS has successfully been applied to identify dyes in wool fibers from historic tapestries from the collections of the Detroit Institute of Arts. The method is fast, taking only a few seconds per sample for analysis, and can be done with single fibers without separation or extraction. The samples acquired are only minutely destructive to the tapestries, and were collected from the back, resulting in no aesthetic impact. The acid hydrolysis and extraction process required for chromatographic separations induces undesireable chemical changes in many of the colorant and degradation product compounds, which are avoided with this direct mass spectrometric method. Indigoids and the characteristic anthraquinones of madder in particular were readily identified directly in wool fibers. In-source hydrolysis using formic acid made it possible to identify carminic and laccaic acids from the insect dyes cochineal and lac on wool. Differentiating specific isomeric flavonoid colorants is not possible with mass spectrometry alone, but

the relative ratios of different compounds observed provide an indication of the botanical sources of the yellow dyes. Degradation products of all three classes of color compounds were directly detected in the tapestry fibers as well as the primary colorants. The flexibility of the ion source – ionization mode, temperature – and the high resolution of the time-of-flight mass spectrometer make this a rapid, simple method for characterizing organic colorants in textile fibers.

Direct analysis in real time mass spectrometry may not be able to answer every question regarding the dye sources in historic materials, but it provides significant information about general classes of colorants in small samples within a short amount of time and without significant sample preparation. The limitations of the DART-MS method – the inability to differentiate structural isomers of the same mass, the difficulties of identifying mixtures (especially of flavonoid dyes), etc. – clearly show that it will never supplant extraction and traditional HPLC analysis for a complete characterization of the colorants in historic textiles. In pursuing answers to most conservation questions, however, an exhaustive study of the colorants is not warranted: a fast, simple overview of the composition of the materials is sufficient.

Acknowledgments

References

1. Zhang, X.; Laursen, R. A. *Anal. Chem.* **2005**, *77*, 2022–2025.
2. Ferreira, E. S. B.; Quye, A.; McNab, H.; Hulme, A. N. *Dyes Hist. Archaeol.* **2002**, *18*, 63–70.
3. Degano, I.; Ribechini, E.; Modugno, F.; Colombini, M. P. *Appl. Spectrosc. Rev.* **2009**, *44*, 363–410.
4. Ferreira, E. S. B.; Hulme, A. N.; McNab, H.; Quye, A. *Chem. Soc. Rev.* **2004**, *33*, 329–336.
5. Wouters, J.; Grzywacz, C. M.; Claro, A. *Stud. Conserv.* **2011**, *56*, 231–249.
6. Zhang, X.; Laursen, R. *Int. J. Mass Spectrom.* **2009**, *284*, 108–114.
7. Casadio, F.; Leona, M.; Lombardi, J. R.; Van Duyne, R. *Acc. Chem. Res.* **2010**, *43*, 782–791.
8. Leona, M. *Proc. Natl. Acad. Sci. U.S.A.* **2009**, *106*, 14757–14762.
9. Cody, R. B.; Laramee, J. A.; Durst, H. D. *Anal. Chem.* **2005**, *77*, 2297–2302.
10. Musah, R. A.; Domin, M. A.; Cody, R. B.; Lesiak, A. D.; Dane, A. J.; Shepard, J. R. E. *Rapid Comm. Mass Spectrom.* **2012**, *26*, 2335–2342.
11. Green, F. M.; Salter, T. L.; Stokes, P.; Gilmore, I. S.; O'Connor, G. *Surf. Interface Anal.* **2010**, *42*, 347–357.
12. Bennett, M. J.; Steiner, R. R. *J. Forensic Sci.* **2009**, *54*, 370–375.

13. Pfaff, A. M.; Steiner, R. R. *Forensic Sci. Int.* **2011**, *206*, 62–70.
14. Rowell, F.; Seviour, J.; Lim, A. Y.; Elumbaring-Salazar, C. G.; Loke, J.; Ma, J. *Forensic Sci. Int.* **2012**, *221*, 84–91.
15. Higuchi, M.; Saito, K. *Bunseki Kagaku* **2012**, *61*, 705–711.
16. Musah, R. A.; Cody, R. B.; Dane, A. J.; Vuong, A. L.; Shepard, J. R. E. *Rapid Commun. Mass Spectrom.* **2012**, *26*, 1039–1046.
17. Grange, A. H.; Sovocool, G. W. *Rapid Commun. Mass Spectrom.* **2011**, *25*, 1271–1281.
18. Chernetsova, E. S.; Morlock, G. E. *Mass Spectrom. Rev.* **2011**, *30*, 875–883.
19. Adams, J. *Int. J. Mass Spectrom.* **2011**, *301*, 109.
20. Selvius Deroo, C.; Armitage, R. A. *Anal. Chem.* **2011**, *83*, 6924–6928.
21. Geiger, J.; Armitage, R. A.; Selvius DeRoo, C. In *Collaborative Endeavors in the Chemical Analysis of Art and Cultural Heritage Materials*; Lang, P. L., Armitage, R. A., Eds.; ACS Symposium Series 1103; American Chemical Society: Washington, DC, 2012; pp 123−129.
22. Kim, H. J.; Jang, Y. P. *Phytochem. Anal.* **2009**, *20*, 372–377.
23. Lojza, J.; Cajka, T.; Schulzova, V.; Riddellova, K.; Hajslova, J. *J. Sep. Sci.* **2012**, *35*, 476–481.
24. Chernetsova, E. S.; Crawford, E. A.; Shikov, A. N.; Pozharitskaya, O. N.; Makarov, V. G.; Morlock, G. E. *Rapid Comm. Mass Spectrom.*, *26*, 1329–1337.
25. Cardon, D. *Natural Dyes: Sources, Tradition, Technology and Science*; Archetype: London, 2007.
26. Cannon, J.; Cannon, M. *Dye Plants and Dyeing*; Timber: Portland, 1994.
27. Adrosko, R. J. *Natural Dyes and Home Dyeing*; Dover: Mineola, NY, 1971.
28. Schweppe, H. *Practical Hints on Dyeing with Natural Dyes: Production of Comparative Dyeings for the Identification of Dyes on Historic Textiles*; Smithsonian Institution: Washington, DC, 1986.
29. Perry, J. J.; Brown, L.; Jurneczko, E.; Ludkin, E.; Singer, B. W. *Archaeometry* **2011**, *53*, 164–177.
30. JEOL USA AccuTOF DART Molecule of the Week. http://www.jeolusa.com/Portals/2/MOTW/carminic-acid.gif (accessed March 5, 2013).
31. Ribechini, E.; Pérez-Arantegui, J.; Colombini, M. P. *J. Mass Spectrom.* **2013**, *48*, 384–391.
32. Mouri, C.; Laursen, R. *Microchim. Acta* **2012**, *179*, 105–113.
33. Wouters, J. *Stud. Conserv.* **1985**, *30*, 119–128.
34. Wouters, J. *Dyes Hist. Archaeol.* **2001**, *16/17*, 145–157.
35. Ahn, C.; Obendorf, S. K. *Textile Res. J.* **2004**, *74*, 949–954.
36. Degano, I.; Biesaga, M.; Colombini, M. P.; Trojanowicz, M. *J. Chromatogr., A* **2011**, *1218*, 5837–5847.
37. Poulin, J. *J. Can. Assoc. Conserv.* **2007**, *32*, 48–56.

Chapter 5

Organic Residues in Archaeology: The Highs and Lows of Recent Research

Val Steele*,[1,2]

[1]Department of Conservation and Scientific Research, The British Museum, Great Russell Street, London, United Kingdom WC1B 3DG
[2]Current address: Department of Archaeological Science, University of Bradford, Richmond Road, Bradford, United Kingdon BD7 1DP
***E-mail: v.j.steele1@bradford.ac.uk**

The analysis of organic residues from archaeological materials has become increasingly important to our understanding of ancient diet, trade and technology. Residues from diverse contexts have been retrieved and analysed from the remains of food, medicine and cosmetics to hafting material on stone arrowheads, pitch and tar from shipwrecks, and ancient manure from soils. Research has brought many advances in our understanding of archaeological, organic residues over the past two decades. Some have enabled very specific and detailed interpretations of materials preserved in the archaeological record. However there are still areas where we know very little, like the mechanisms at work during the formation and preservation of residues, and areas where each advance produces more questions rather than answers, as in the identification of degraded fats. This chapter will discuss some of the significant achievements in the field over the past decade and the ongoing challenges for research in this area.

Introduction

This chapter represents a personal view from the perspective of ten years' involvement in the field of organic residue research in archaeology and as such is not intended to be an exhaustive review article. Comprehensive reviews of the field are available in the literature and present a more detailed view of the research published in the last 10 years (*1–5*). In particular this chapter does not address advances in the field of ancient DNA research as applied to archaeological residues as this is a separate field outside the scope of this review (*1*). It will deal with some of the challenges facing research, including questions which are fundamental to our understanding of how organic residues behave in an archaeological context and others which arise directly from current and previous research.

It will then summarize some of the significant research carried out in recent years and, looking forward, the many possibilities which are opening up through the application of new analytical techniques from other areas of research. This 'cross-fertilization' between science and archaeology has been, and will continue to be, key to advancing the field of organic residue research and to applying the results from laboratory analysis in ways which are truly relevant to archaeology in the field.

What Are Organic Residues in an Archaeological Context?

Organic residues encompass a vast range of amorphous materials from diverse natural sources and associated with a wide variety of artefacts. They include residues of foods and other materials in pottery, residues left on stone tools during use, substances used in mummification, residues left in plaster floors by human activities, pastes and glues used in the construction of artworks and other artefacts, binders used to apply colour to paintings and statues, organic colourants used on textiles, organic material preserved in the mineral matrix of bone, and even the remains of ancient manures found in soils (*3*). Their analysis can inform us about trade, technology, diet, medicine, cosmetics, arts, crafts, farming practices, how people organized their houses and how they prepared their dead for burial (*3, 6–8*).

For organic material to survive over archaeological time it must be relatively resistant to degradation or burial conditions must be exceptionally favourable to its preservation. Lipids (fatty and waxy materials, bituminous substances, resins etc) are the most commonly occurring materials in archaeological residues as they are relatively insoluble in water and resistant to degradation (*3, 9*). In the past it was considered that proteins, starches and sugars would not survive over archaeological time (*9*). However more recent research has found that, in some circumstances, these too can survive hundreds, perhaps thousands, of years (*10–13*).

Wet chemistry methods were the only analytical tools available to early analysts of archaeological residues (*14–16*). These require very large samples and in many cases are not sufficiently diagnostic to fully characterize the types of degraded samples found in archaeological contexts. From the 1970s onwards instrumental methods of analysis became increasingly available (*17*), and today instrumental chromatography (gas or liquid), more recently combined with mass

spectrometry, has been the most widely used method. Other methods used to characterize ancient organic residues include various spectroscopies (infrared (FT-IR), Raman, nuclear magnetic resonance (NMR), ultraviolet (UV) etc.), scanning electron microscopy (SEM) for imaging and elemental analysis by energy dispersive X-ray spectroscopy (EDX), X-ray diffraction (XRD), X-ray fluorescence (XRF), and high magnification light microscopy. Since the discovery that the fractionation of stable isotopes can provide a new dimension to residue research, isotope ratio mass spectrometry (IRMS) has also become part of the residue analysts tool kit (*18*). Over the past 15 years the use of chromatography (gas or liquid) combined with combustion-isotope ratio mass spectrometry (eg GC-C-IRMS) to measure the carbon isotopic signatures of individual fatty acids and amino acids has also become relatively routine (*3*, *11*, *19*).

Challenges Facing Organic Residue Research

There are many questions and challenges in the field of organic residue research. Some of these are outlined below with the object of highlighting some of the more interesting and relevant questions and encouraging debate about and research into some of these issues.

Residue Formation and Preservation

Some fundamental questions about how residues form and how they survive over archaeological time remain unanswered. For example absorbed residues in ceramics are present within the voids or pores in the ceramic fabric and this provides at least partial protection from degradation and dissolution (*3*, *4*, *6*, *8*, *9*). In soils organic compounds are adsorbed onto the surfaces of clay particles (*20*, *21*) and it is not unreasonable to theorize that a similar process may take place between organic materials and ceramic fabrics (*3*, *4*, *6*, *22*). Similar processes may be at work in partially-carbonized visible residues found in cooking pots where residues are encapsulated in a protective, organic matrix (*3*, *6*). However little work has been done in this area and very little is known about the effect of different ceramic fabrics on the formation and preservation of residues. It is probable that the chemistry of a pottery fabric, including the presence of metal ions such as iron and copper within the clay, will affect the formation and preservation of residues. There is evidence for this in the formation of ketones in heated fats when metal oxides are present in the ceramic fabric (*23*, *24*). Formation and preservation of residues may also be affected by the physical nature of the ceramic (coarseness, degree of firing etc). Evidence from soil science suggests that the size of the voids in ceramics may affect the preservation of residues by limiting the size of microorganisms that can access material within the pores (*20*).

Similarly there is much to be learned about how residues accumulate in ceramics. Is the residue which remains in a ceramic vessel indicative of the first use of that vessel, the last use of the vessel or an accumulation over the whole lifetime of the vessel, and how much organic material can a particular ceramic

accumulate? Some experimental work has been done (*4*), but the answer to this question is still unclear. This is in part because it is very difficult to replicate the sustained use of a cooking pot, for example, over many years. Analysis of ethnographic pottery, where an accurate use-history is available for each vessel, could provide insights into some of these questions but such studies are rare and often remain unpublished (*4*, *25*).

The effects of degradation on the chemical composition of organic materials during their use and subsequent burial is reasonably well understood (*3*, *4*, *6*, *8*, *26–30*). However, the increasing importance of isotopic analysis of various types of materials raises the question of whether isotopic values are stable under burial conditions. Two studies in the late 1990s measuring the carbon isotopic values ($\delta^{13}C$) of stearic and palmitic acids before and after simulated burial in oxic and anoxic environments showed that, under these conditions, isotopic values remained robust (*4*, *7*, *31*). It has also been shown that the changes in hydrogen isotopic values (δD) of individual fatty acids caused by cooking followed by burial for 16 months are significantly less than the natural variation in δD of fatty acids from a range of animal fats (*32*). However analysis of experimental cooking residues produced by boiling a range of foods in replica vessels, found that the bulk nitrogen and carbon isotopic values were not preserved during burial (*33*). More investigation would help to provide a better understanding of the processes affecting isotopic values of materials over archaeological time.

Another area where more research would be advantageous concerns conditions at archaeological sites and how these affect the preservation of organic residues. Organic materials, including amorphous organic residues, are well preserved in water-logged burial environments and at some, but not all, very dry sites (*3*, *4*, *26*, *34–43*). By contrast organic material is very poorly preserved at sites where the water table is constantly rising and falling creating cycles of wet and dry conditions (*3*). Exactly how site conditions affect the preservation of organic residues has yet to be investigated in detail. It is a potentially important question as the ability to assess whether food residues are likely to be preserved in pottery vessels from a particular site, in advance of a project, would allow decisions about the feasibility of residue analysis to be made at an early stage. However, soils are very variable in their chemistry, water content, and texture, all of which may affect the survival of organic residues buried in them. Local climatic conditions, in particular temperature, may also play a part in the destruction or survival of organic residues. It is rare to be offered soil samples from a site when analysing organic residues but the availability of soil would allow basic measurements of texture and pH to be recorded. The state of water-logging at sites is generally published in site reports and is often available for interrogation. A compilation of information from published residue analysis projects could begin to provide a basic understanding of some of these issues. The incorporation of research into future projects could also build up a significant amount of data on this question which would enhance the understanding of how organic residues behave under different burial conditions.

Contamination

In seeking to characterize organic material from the past analysts are faced with the problem of trying to identify traces of significant compounds within an environment full of similar compounds of modern origin. Despite this little has been published about contamination and organic residues.

Over the lifetime of an organic residue there are several possible sources of contamination. The most obvious is the burial environment but it can prove extremely difficult to quantify exactly what soil or groundwater has contributed to an organic residue. In the one published study, Heron et al. (*44*) analysed pottery residues and organic material from adjacent soil and concluded that differences in type, distribution and abundances of organic compounds in the soil and the pottery were too significant for the soil to be the source of the residue in vessels.

By contrast, a recent pilot project on unwashed sherds from a north African site which had been cyclically wet and dry since its abandonment about 4,500 years ago, discovered no residues of archaeological interest in the pottery (*45*). Instead, organic compounds which are typical of modern, urban waste water were identified (*45–48*). It is possible that, in this case, the degradation and dissolution of any original residues in the pottery by the constant wet and dry cycles in the burial environmnent allowed the ingress of organic material from the ground water during the wetter cycles.

During post-excavation handling and storage the possibilities for contamination multiply rapidly and are even less well understood. However, there have been no published studies designed to measure how much material might be absorbed by ceramics, for example, during handling, washing and storage. Compounds from sun screens and insect repellants as well as insecticides have been identified in pottery residues (*49*, *50*). When these are recently synthesized or isolated compounds, they can quickly be identified as modern and excluded from consideration but, when they are compounds which might have been present in the ancient world, distinguishing the modern from the archaeological can be challenging.

Plasticizers from plastic storage materials are easily identified as they are very distinctive and have no ancient equivalent (*6*, *51*). However plastics contain a wide range of compounds which have the potential to migrate into material stored in close proximity, some of which are also found in ancient materials (*52–54*). Some plastics exude fatty acids (*53*, *55*) which are the biomarker compounds for degraded fats (*3*, *6*, *8*) but fatty acids are also shed from the surface of human skin and will be deposited on any artifact which is handled (*6*, *56*). Human skin lipids and other animal fats also contain the sterol cholesterol, used as an indicator of animal origin in degraded fats, which can sometimes be deposited on surfaces by contact with hands (*6*, *56*, *57*). Skin also excretes the compound squalene which degrades rapidly (*57*) and it is usually considered that, if cholesterol and squalene occur together, any lipid residues present may be due to handling (*6*). However squalene is also present in olive and other plant oils, sometimes in large abundances (*58*), and is not always present in skin (*57*). Skin lipids in fact appear to be very variable (*59*) and skin may also carry compounds from food, cosmetics, topical medicines and any other materials handled (*57*)

As a result, fatty material present at very low abundances may not be archaeological, and could be background contamination. In addition background levels of many contaminants are present in dust and air (*60*, *61*) and may be a source of contamination in the laboratory. One study found low, but quantifiable, abundances of fatty acids in previously Soxhlet extracted pottery (*62*), suggesting that background levels of fatty acids are between 3 and 13 µg/g, and Evershed (*4*) suggests that levels of residues below 5 µg/g should be considered as background.

The preparation and analysis of method blanks can identify and quantify contamination introduced in the laboratory, while the analysis of soil samples, when available, can provide a picture of potential contamination from the burial environment. In the case of pottery residues, drilling samples from both sides of a pottery sherd can provide an assessment of any contamination present as residues of archaeological interest will usually be present on only one surface of a sherd (most often the interior), while contamination will accumulate on both surfaces. An awareness of the problem of distinguishing contamination from residues of archaeological interest, and a basic knowledge of potential contaminants, is also advantageous when seeking to interpret the results of residue analysis.

Identification of Fatty Material

One of the most challenging questions facing organic residue researchers at the present time is the secure identification of fatty material from the past. Fat residues include the remains of meat, oily fish, dairy products and vegetable oils, and their identification is particularly relevant to questions relating to diet and food culture but also to trade, technology, arts and crafts, and the use of specific features within ancient structures. They are found primarily in pottery but can also be present in hearths, floors, plaster surfaces, on stone tools, in works of art etc.

Degraded fats are usually composed primarily of palmitic ($C_{16:0}$) and stearic ($C_{18:0}$) acids regardless of the original source of the fat. This is due to the processes of degradation and dissolution that occur during burial and, in some cases, alteration of the fats during the lifetime of the vessel, for example during cooking. These processes tend to deplete diagnostic biomarker compounds that are characteristic of particular fats (*3–5*, *63–67*) preventing the unique identification of degraded fatty material.

Work by Evershed's group in Bristol during the 1990s established that it was possible to distinguish different degraded fats by measuring the carbon stable isotope ratios, expressed as $\delta^{13}C$ values, of $C_{16:0}$ and $C_{18:0}$ (*3*, *32*, *64*, *66*). Modern reference fats fall within well-defined areas on a scatter plot of $\delta^{13}C_{18:0}$ against $\delta^{13}C_{16:0}$, reflecting the different metabolic processes by which different organisms synthesize these two acids (*5*, *32*, *68*). Results can also be plotted as $\Delta^{13}C$ vs $\delta^{13}C_{16:0}$ (where $\Delta^{13}C = \delta^{13}C_{18:0} - \delta^{13}C_{16:0}$), a method which eliminates minor local variations in isotopic values by using $\Delta^{13}C$, while still incorporating the variations in $\delta^{13}C_{16:0}$ produced by the presence of marine fats or C_4 plants (*67*). Isotopic analysis has proved to be a very powerful tool for identifying individual fats, in particular dairy fats, even within mixtures. However, as more archaeological residues and modern reference fats are analysed, it is becoming clear that this may not be a universal solution to the question of identifying fats. Analysis of modern,

reference horse fats from Kazakhstan showed almost complete overlap in carbon isotopic values between dairy and adipose fats (*32*, *69*). Measurements of C$_3$ plant oil isotopic signatures show them to lie either on the mixing line between ruminant and non-ruminant adipose fats (*70*) or in the same range as cattle adipose fats (*68*). This is not typically a problem in pre-historic northern Europe, where the presence of plant oils is unlikely, but will be significant in the interpretation of results from the Mediterranean. There is also some evidence that occasionally deer adipose fat shows carbon isotopic signatures where $\Delta^{13}C$ is lower than -3.3 ‰ (*5*, *71*), an offset value generally used to define milk fats. The effect of cooking on the carbon isotopic values of individual fatty acids in milk was also considered by Spangenberg et al. (*68*) who measured variations of up to 4‰ between heated and unheated milk, an effect which varied with species.

Continuing research in this area is steadily increasing understanding of the strengths and weaknesses of compound specific carbon stable isotope analysis and providing solutions to some of the problems encountered (*5*, *32*). The measurement of hydrogen isotopic values, while technically challenging, may provide a new level of discrimination in the identification of archaeological fats, already showing success in distinguishing horse milk and adipose fats (*5*, *32*). Nevertheless, the interpretation of isotopic data from residues should always be carried out with full reference to the results of molecular analysis and to faunal and other evidence from the site. It is unlikely that it will ever be sufficient to examine isotopic data alone for the identification of fats.

Detecting Alcoholic Drinks

The question of how to detect alcoholic drinks in archaeological residues continues to be one of the most debated areas in organic residue analysis (*3*, *72*). There is no consensus among researchers on what unique biomarker compounds might survive over archaeological time to indicate the presence of a fermented beverage. The difficulty arises because alcoholic drinks consist mostly of water and water-soluble compounds such as sugars and alcohols which either leave no trace or disappear very rapidly in the burial environment. The main question then becomes which of the minor components of wine or beer might survive over archaeological time and be unique to only one type of fermented drink.

Tartaric and syringic acid have been suggested as suitable biomarker compounds for wine in archaeological residues (*73–77*). Syringic acid is derived from malvidin and is only found in significant abundances in red wine, increasing with the age of the wine – no other plant contains significant amounts (*72*, *76*). Syringic acid can polymerize and this may contribute to its survival in archaeological residues (*72*). Tartaric acid is abundant in all grapes, and is strongly adsorbed onto silicates in pottery by hydrogen bonding, facilitating its survival (*72*). Tartaric acid itself is water soluble but its salts are far less soluble and may survive over archaeological time (*72*, *76*). Both tartaric acid and syringic acid have been identified in visible and absorbed organic residues from pottery using high performance liquid chromatography with tandem mass spectrometry (HPLC-MS-MS) (*73*, *78*, *79*) and in modern pottery soaked in wine (*72*). However tartaric acid is present in other plant species, sometimes at

much higher abundances than in grapes (*80*), although in many cases these other plants would not have been used in the same contexts as wine. In addition the presence of tartaric acid would only indicate the presence of grapes and does not provide any information about fermentation (*77, 80*). These problems have led researchers to question its use as a biomarker for wine. More recently analysis of modern wine and archaeological residues using GC-MS has identified not just tartaric acid, but a range of other organic acids including succinic, malic, fumaric and citric which may together provide a better indication of the presence of wine in organic residues (*81*).

Other approaches for detecting the presence of wine in organic residues are also being explored. Garnier et al. (*82*) used in situ tetramethylammonium hydroxide treatment followed by thermal hydrolysis and methylation-gas chromatography-mass spectrometry (THM-GC-MS) to look for phenolic compounds in modern wines, archaeological grape pips and two samples of Roman wine present as visible residues within amphorae. Phenolic compounds were detected in the ancient wines but some of the same compounds are also present in lignin and more research will be needed to determine whether any of the phenolic compounds identified prove to be unique biomarkers for wine. Polyphenols were identified in absorbed residues by Romanus et al. (*83*) using the Folin-Ciocalteu colorimetric reaction. This method has the disadvantage of requiring 1g of drilled sample from a sherd (a large sample for this type of analysis) and there is potential for false positives due to a reaction with reduced iron. This method detects the presence or absence of polyphenols but does not provide a detailed analysis of the compounds present.

Much of the analysis of wine residues has been carried out on exceptionally well preserved residues that were already known to be derived from wine, and these methods remain untested on more typical archaeological residues.

Beer and other fermented beverages present similar problems. Beer forms a deposit known as "beerstone" on standing which is primarily composed of calcium oxalate (*77*). Calcium oxalate has been identified in beer containers using a Fiegl spot test but it is also abundant in some plants, notably rhubarb and spinach (*77*). More recent work by Issakson et al. (*84*) has suggested that ergosterol might be used as a biomarker for fermentation as it is produced in large quantities by fungi including yeasts causing fermentation. This would only identify the use of a vessel or feature for fermentation and it is impossible to determine whether this happened in the course of bread-making or beer brewing as yeast would be active in both cases (*84*). The fact that fungi are present everywhere in the environment, including soil, raises some questions about the unique identification of fermentation using ergosterol as the sole biomarker (*84*). In addition the use of ergosterol in many modern skin preparations should be noted, particularly in the light of the contamination issues raised above (*84*). Microscopic analysis of visible beer residues has also been used to identify the cereals used to produce beer, and also identified malting and fermentation from the morphology of starch grains within the residue (*85*).

Experimental work incorporating the use of traditional brewing and fermentation procedures, the use of modern reconstructed ceramic vessels and simulated burial and/or degradation experiments would be invaluable in

attempting to detect the remains of fermented beverages in organic residues. In addition, continuing work on the analysis of DNA for identifying wine or grape residues and yeasts (*86*, *87*) may also provide answers questions about detecting ancient fermented beverages.

New Developments in Organic Residue Analysis

An increasing number of new methods and approaches are being tested which will shape the field of organic residue analysis in the future and may provide answers to the some of the questions posed above.

New Methods in the Analysis of Organic Residues

There are a number of techniques in use in other areas of science which show great promise as tools for the analysis of organic residues. In particular, advances in the fields of proteomics and lipidomics have potential applications to the analysis of archaeological organic materials.

New Mass Spectrometric Techniques

Several new techniques which involve the introduction of samples directly into a mass spectrometer are proving fruitful in the analysis of some organic materials from the past. The application of direct analysis in real time-mass spectrometry (DART-MS) to the fast screening of samples for organic residues is discussed in detail elsewhere in this volume. As a method involving no/minimal sample preparation and allowing non-destructive analysis of suitable samples, it is clear that there are many potential applications in archaeological and cultural heritage situations (*88–90*). It may become invaluable for the screening of large numbers of samples, allowing more time to be spent on the preparation and analysis of those which contain organic material. Ionisation of the organics within the sample without the need for a vacuum presents the possibility of a whole new set of applications for direct mass spectrometry. Within the wider scientific community DART-MS is already being combined with separation techniques such as thin layer chromatography (TLC), gas chromatography (GC), HPLC and tandem mass spectroscopy (*91–95*) and these techniques all have the potential to find applications in the analysis of archaeological organic residues.

The use of matrix-assisted laser desorption ionization-mass spectrometry (MALDI-MS) or more specifically MALDI-time of flight mass spectrometry (MALDI-TOF) has become routine in the analysis of large molecules such as lipids, proteins, carbohydrates and nucleic acids (*96–101*). It has been applied more recently to the analysis of proteins in ancient bones (*102*, *103*) and eggshells (*104*), where it allows the identification of species, and has been used to analyse proteinaceous and lipid binders in works of art and wall plasters (*105–108*). It has been used to analyze proteinaceous glue from a wooden building (*109*), to study the photo-degradation of terpenoid varnishes (*110*), and to assess the condition

97

In *Archaeological Chemistry VIII*; Armitage, R., et al.;
ACS Symposium Series; American Chemical Society: Washington, DC, 2013.

and penetration of polyethylene glycol in preserved ships (*111*). There are also potential applications to pottery residues (*112*) and in the analysis of proteins from dental enamel (*113*, *114*). A variation of MALDI-TOF, graphite-assisted laser desorption ionisation mass spectrometry (GALDI-TOF) has also been tested in the analysis of aged triterpenoid resins in varnishes (*115*). It seems probable that more applications will be published over the next few years.

Desorption electrospray ionization-mass spectrometry (DESI-MS) has also been used to analyse proteins from experimental residues applied to stone tools and archaeological pottery with a view to applying it to archaeological residues (*116*). DESI-MS, like DART-MS, allows the analysis of organic material with little or no sample preparation at ambient conditions (*116*). It has the capacity to detect and identify large molecules and, apart from proteins, has the potential to analyse triacylglycerols in fatty material, allowing the identification of fats without the need for isotopic analysis.

The development of gas chromatography-thermal conversion-isotope ratio mass spectrometry (GC-TC-IRMS) for the compound specific analysis of hydrogen isotopes has been cited above in connection with the discrimination of animal fats (p8). It appears likely that other applications of hydrogen compound specific isotope analysis will be forthcoming.

New Chromatographic Techniques

Although GC-MS is probably the technique most often associated with the analysis of ancient organic residues, the potential of liquid chromatography (LC) and HPLC with mass spectrometry or tandem mass spectrometry should not be overlooked. LC and HPLC have been used to identify caffeine and theobromine from chocolate residues (*117–120*), organic colourants on fabrics (*121–126*) and in Cretan icons (*127*), and used to examine the degradation of dyed and natural wool and silk fibres by measuring the concentrations of their degradation products (*128*). It is the method of choice for examining organic colourants which are often not suitable for GC-MS analysis. As described above, HPLC-MS-MS has successfully been used to detect tartaric and syringic acids in the search for wine residues, and this particular application highlights the use of tandem mass spectrometric techniques to isolate particular target compounds from a complex sample. However the use of tandem mass spectrometric techniques seems limited for the present, possibly due to the difficulties of method development.

In the wider scientific community there has also been a rapid growth in the use of multiple tandem techniques, for example combining GC with HPLC and MS, and the use of two dimensional GC-GC-MS. These can also be combined with methods such as FT-IR or Raman spectroscopy. Few applications in organic residue research have been seen so far but may in future provide yet more powerful methodologies for interrogating archaeological residues.

Application of Established Methods to New Situations

The application of established methods to new types of residue and the use of multiple techniques to characterize a single residue both offer exciting new possibilities.

Plant Microfossils

The extraction and analysis of starch grains and phytoliths from organic residues is not new. These plant microfossils have been used extensively to examine residues from stone tools (*129–133*), shell tools (*134*), sediments (*135–137*), grinding stones (*138*), and dental calculus (*139, 140*). The presence of starch grains and phytoliths has also been used to identify maize and beans in pottery residues from North America (*141, 142*) and of a range of plant foods in residues from ceramic and stone artefacts from Bolivia (*143*). However the full potential of this type of analysis when applied to visible residues from pottery is only just beginning to be explored and presents a unique opportunity to identify the past culinary use of specific plants.

This approach has rarely been applied to cooking residues in northern Europe (*144*). Phytoliths form at a much reduced rate in plants growing in temperate conditions compared with those grown in tropical or arid regions, and until recently it was unclear whether phytoliths would still be present in residues from northern Europe (*145*). However, a recent study found both starch grains and phytoliths in carbonized residues from Late Mesolithic Ertebølle and Early Neolithic Funnel Beaker pottery from Neustadt in northern Germany (*145*). The analysis of starch grains revealed very few cereals, even in the Neolithic samples, supporting the archaeological evidence that the introduction of cereal crops was slow in this area (*145*). Wild resources continued to be exploited across the transition to agriculture, predominantly acorns but also sweet flag, sedge, meadowsweet, reeds, hazelnuts and bracken (*145*). Phytolith analysis revealed other plant material usually considered invisible in organic residues, including plants which would have been used as flavourings (*146*).

Residues from Unexpected Sources

Over the past decade residues have been detected on and in artefacts where their survival was unexpected. The retrieval of residues from stone tools, originally regarded with some skepticism, is now well established as legitimate research (*147–157*). Residues of archaeological interest have also been extracted from pottery assemblages after long-term storage in museums (*50*), and pottery which has been washed (*50*).

Since 2009 two separate and independent studies on material from different countries have identified both absorbed and visible residues from soft stone cooking pots (*158, 159*). The study of 5th to 13th century chlorite vessels from Merv in Turkmenistan also used modern, chlorite cooking pots to investigate

the structure of the stone itself, how it behaves when heated and how this could facilitate the preservation of absorbed residues (*158*).

The detection of partially carbonized residues from the hoard of Iron Age copper alloy and iron cauldrons found in a field near Chiseldon, Wiltshire, U.K. was unexpected (*160–162*). The fact that the cauldrons had been lifted in blocks and micro-excavated in the Conservation Department at the British Museum allowed areas different to the surrounding soil or metal corrosion products to be identified by the exavators (*160–162*). These turned out to be remarkably well-preserved, partially carbonized food residues, probably owing their good preservation to an interaction with the iron and copper corrosion products formed on the metal surfaces (*20, 163*).

Use of Multiple Techniques in Residue Research

There are an increasing number of papers illustrating the application of multiple techniques to a single question. Sometimes these projects employ the use of a screening method followed by more detailed analysis of selected samples. Others use multiple methods to provide a fuller picture of the nature of the residue(s) under examination, particularly where the residue has inorganic components.

In food residues the use of GC-MS followed by isotopic analysis is routine (*3, 32*), sometimes combined with phytolith and starch grain analysis of visible food residues (*145, 164*). The use of different chromatographic methods to analyse the same material is also becoming more routine, particularly in the area of dyes and paints where organic colourants may be mixed with different binding materials (*165, 166*). Where inorganic colourants are also present, a combination of chromatographic and other techniques such as XRF, XRD, SEM, SEM-EDX, Raman and FT-IR can provide a complete characterization of the paints, dyes or other materials being analysed (*28, 122, 167–169*). This approach has also proved successful in the analysis of vessel contents suspected of being paints, inks, medicines or cosmetics (*168, 170, 171*). For a round robin analysis of a 17th century ointment, recreated to an authentic recipe, 11 laboratories used 10 different methods to analyse a sample of the ointment (*172*). The methods used included FT-IR, Raman and micro-Raman spectroscopies, surface enhanced Raman scattering (SERS), GC-MS, pyrolysis-GC-MS, solid phase micro extraction-GC-MS (SPME-GC-MS), HPLC-MS and XRF. No laboratory employed all of these methods and no laboratory completely characterized the ointment, although many identified the majority of components. This illustrates the importance of considering multiple techniques when analyzing very complex residues from the past.

Future of Organic Residue Analysis

The application of new techniques and the discovery that organic residues have the capacity to survive in unexpected circumstances are opening up increased opportunities for residue analysis. However to take full advantage of these new opportunities carefully planned, rigorously executed research is necessary that combines best practice from both science and archaeology.

All new research projects should be designed to answer one or more questions of archaeological or scientific significance. These questions will determine how the material is sampled, what methods will be used and what data is collected to give the answers required. Much time, effort and money can be wasted by not establishing the aims and objectives of a project at the planning stage.

Careful consideration should be given to how the material is sampled. The sampling strategy should be designed to answer the archaeological or scientific question and should also aim to be statistically significant (*173*, *174*). Sampling is always a compromise between what is ideal and what is possible but careful use of the samples available can maximize the relevance of the data obtained.

Analytical methods should be appropriate to the types of samples and the information expected from the analysis. All methods have strengths and limitations and it is important to know what these are in order to decide which methodologies will provide the best results. It is also useful to know the limitations of the data produced by any analytical method so that complementary analysis can be included in the project design if necessary. Data analysis should be carried out either by, or in close collaboration with, an analyst with experience in the techniques being used.

Data intepretation must always be carried out with due reference to historical and geographical context. Some knowledge of contamination issues, including possible modern contaminants and their sources, is essential in data interpretation. This will avoid obvious mistakes in identifying a residue as a material which was not available in the historical period and/or geographical area where the residue originated. Other data from the same or similar archaeological sites, such as faunal analyses, environmental data etc., is also helpful when interpreting residue analysis data.

In designing new projects which incorporate these features, close collaboration is necessary between archaeologists and scientists. This collaboration will be the key to excellent research in the future. Ideally organic residue research should involve archaeologists who have some knowledge of science and scientific method and scientists who have a basic understanding of archaeology. With increasingly complex analytical techniques finding applications in the study of organic residues more communication will be required between scientist and archaeologist in the future.

So much is still unknown about how our ancestors lived, worked, sourced and cooked their food and buried their dead that there is ample scope for more research for many years to come. Well designed, well executed organic residue analysis projects, incorporating the best from archeology and science, have an important part to play in this quest to understand the past.

References

1. Brown, T.; Brown, K. *Biomolecular Archaeology: An Introduction*; Wiley-Blackwell: Chichester, U.K., 2011.
2. Colombini, M. P., Modugno, F., Eds. *Organic Mass Spectrometry in Art and Archaeology*; Wiley: Chichester, U.K., 2009.
3. Evershed, R. P. *Archaeometry* **2008**, *50*, 895–924.
4. Evershed, R. P. *World Archaeol.* **2008**, *40*, 26–47.
5. Regert, M. *Mass Spectrom. Rev.* **2011**, *30*, 177–220.
6. Evershed, R. P. *World Archaeol.* **1993**, *25*, 74–93.
7. Evershed, R. P.; Dudd, S. N.; Charters, S.; Mottram, H. R.; Stott, A. W.; Raven, A.; van Bergen, P. F.; Bland, H. A. *Philos. Trans. R. Soc., B.* **1999**, *354*, 19–31.
8. Heron, C.; Evershed, R. P. In *Archaeological Method and Theory*; Schiffer, M., Ed.; University of Arizona Press: Tuscon, AZ, 1993; pp 247−284.
9. Eglinton, G.; Logan, G. A. *Philos. Trans. R. Soc., B.* **1991**, *333*, 315–328.
10. Brecoulaki, H.; Andreotti, A.; Bonaduce, I.; Colombini, M. P.; Lluveras, A. *J. Archaeol. Sci.* **2012**, *39*, 2866–2876.
11. Corr, L.; Richards, M.; Grier, C.; Mackie, A.; Beattie, O.; Evershed, R. P. *J. Archaeol. Sci.* **2009**, *36*, 12–18.
12. Högberg, A.; Puseman, K.; Yost, C. *J. Archaeol. Sci.* **2009**, *36*, 1735–1737.
13. Yohe, R. M., II; Bamforth, D. B. *J. Archaeol. Sci.* **2013**, 2337–2343.
14. Åström, P. *Bull. Medelhavsmuseet.* **1969**, *5*, 16–21.
15. Mathiassen, T. *Acta Archaeol.* **1935**, *VI*, 139–152.
16. Pollard, A. M.; Batt, C.; Stern, B.; Young, M. M. *Analytical Chemistry in Archaeology*; Cambridge University Press: Cambridge, U.K., 2007.
17. Condamin, J.; Formenti, F.; Metais, M. O.; Michel, M.; Blond, P. *Archaeometry* **1976**, *18*, 195–201.
18. Vogel, J. C.; van de Merwe, N. J. *Am. Antiq.* **1977**, *42*, 238–242.
19. Evershed, R. P.; Arnot, K. I.; Collister, J.; Eglinton, G.; Charters, S. *Analyst (Cambridge, U.K.)* **1994**, *119*, 909–914.
20. Mayer, L. M. *Chem. Geol.* **1994**, *114*, 347–363.
21. Ashman, M. R.; Puri, G. *Essential Soil Science*; Blackwell Publishing: Oxford, U.K., 2002.
22. Craig, O. E.; Collins, M. *J. Immunol. Methods* **2000**, *236*, 89–97.
23. Evershed, R. P.; Stott, A. W.; Raven, A.; Dudd, S. N.; Charters, S.; Leyden, A. *Tetrahedron Lett.* **1995**, *36*, 8875–8878.
24. Raven, A. M.; van Bergen, P. F.; Stott, A. W.; Dudd, S. N.; Evershed, R. P. *J. Anal. Appl. Pyrolysis* **1997**, *40-41*, 267–285.
25. Heron, C. University of Bradford, U.K., unpublished.
26. Regert, M.; Bland, H. A.; Dudd, S. N.; van Bergen, P. F.; Evershed, R. P. *Proc. R. Soc., B.* **1998**, *265*, 2027–2032.
27. Regert, M.; Colinart, S.; Degrand, L.; Decavallas, O. *Archaeometry* **2001**, *43*, 549–569.
28. Colombini, M. P.; Giachi, G.; Modugno, F.; Pallecchi, P.; Ribechini, E. *Archaeometry* **2003**, *45*, 659–674.

29. Colombini, M. P.; Modugno, F.; Ribechini, E. *J. Mass Spectrom.* **2005**, *40*, 675–687.

30. Egenberg, I. M.; Aasen, J. A. B.; Holtekjølen, A. K.; Lundanes, E. *J. Anal. Appl. Pyrolysis* **2002**, *62*, 143–155.

31. Evershed, R. P.; Dudd, S. N.; Lockheart, M. J.; Jim, S. In *Handbook of Archaeological Sciences*; Brothwell, D. R., Pollard, A. M., Eds.; Wiley: Chichester, U.K., 2001; pp 331−349.

32. Evershed, R. P. In *Organic Mass Spectrometry in Art and Archaeology*; Colombini, M. P., Modugno, F., Eds.; Wiley: Chichester, U.K., 2009; pp 391−432.

33. Heron, C.; Hancock, H. University of Bradford, U.K., unpublished.

34. Buckley, S. A.; Clark, K. A.; Evershed, R. P. *Nature (London, U.K.)* **2004**, *413*, 294–298.

35. Buckley, S. A.; Evershed, R. P. *Nature (London, U.K.)* **2001**, *413*, 837–841.

36. Copley, M. S.; Bland, H. A.; Rose, P.; Horton, M.; Evershed, R. P. *Analyst (Cambridge, U.K.)* **2005**, *130*, 860–871.

37. Copley, M. S.; Rose, P. J.; Clapham, A.; Edwards, D. N.; Horton, M. C.; Evershed, R. P. *Antiquity* **2001**, *75*, 538–542.

38. van Bergen, P. F.; Bland, H. A.; Horton, M. C.; Evershed, R. P. *Geochim. Cosmochim. Acta* **1997**, *61*, 1919–1930.

39. van Bergen, P. F.; Peakman, T. M.; Leigh-Firbank, E. C.; Evershed, R. P. *Tetrahedron Lett.* **1997**, *38*, 8409–8412.

40. Berstan, R.; Dudd, S. N.; Copley, M. S.; Morgan, D. M.; Quye, A.; Evershed, R. P. *Analyst (Cambridge, U.K.)* **2004**, *129*, 270–275.

41. Evershed, R. P. *Archaeometry* **1990**, *32*, 139–153.

42. Evershed, R. P. *Archaeometry* **1992**, *34*, 253–265.

43. O'Donoghue, K.; Clapham, A.; Evershed, R. P.; Brown, T. A. *Proc. R. Soc., B.* **1996**, *263*, 541–547.

44. Heron, C.; Evershed, R. P.; Goad, L. J. *J. Archaeol. Sci.* **1991**, *18*, 641–659.

45. Steele, V. J. University of Bradford, U.K., unpublished.

46. Eriksson, E.; Auffarth, K.; Henze, M.; Ledin, A. *Urban Water* **2002**, *4*, 85–104.

47. Diskowitzky, L.; Schwarzbauer, J.; Kronimus, A.; Littke, R. *Chemosphere* **2004**, *57*, 1275–1288.

48. Grigoriadou, A.; Schwarzbauer, J.; Georgakopoulos, A. *Environ. Pollut. (Oxford, U.K.)* **2008**, *151*, 231–242.

49. Stacey, R.; Steele, V. J. The British Museum, London, U.K., 2002, 2013, unpublished results.

50. Steele, V. J. Ph.D., University of Bradford, Bradford, U.K., 2009

51. Shen, H.-Y. *Talanta* **2005**, *66*, 734–739.

52. Garrido-López, Á.; Esquiu, V.; Tena, M. T. *J. Chromatogr., A.* **2007**, *1150*, 178–182.

53. Haider, N.; Karlsson, S. *J. Appl. Polym. Sci.* **2002**, *85*, 974–988.

54. Huber, M.; Franz, R. *J. High Resolut. Chromatogr.* **1997**, *20*, 427–430.

55. Bradley, E.; Coulier, L. *An Investigation into the Reaction and Breakdown Products from Starting Substances Used to Produce Food Contact Plastics*;

FD07/01; Central Research Laboratory, Food Standards Agency: York, U.K., 2007.

56. Grenacher, S.; Guerin, P. M. *J. Chem. Ecol.* **1994**, *20*, 3017–3025.

57. Archer, N. E.; Charles, Y.; Elliott, J. A.; Jickells, S. *Forensic Sci. Int.* **2005**, *154*, 224–239.

58. Gunstone, F. D. *The Chemistry of Oils and Fats: Sources, Composition, Properties and Uses*; Blackwells: Oxford, U.K., 2004.

59. Ramasastry, P.; Downing, D. T.; Pochi, P. E.; Strauss, J. S. *J. Invest. Dermatol.* **1970**, *54*, 139–144.

60. Clausen, P. A.; Wilkins, K.; Wolkoff, P. *J. Chromatogr., A.* **1998**, *814*, 161–170.

61. Mandalakis, M.; Tsapakis, M.; Tsoga, A.; Stephanou, E. G. *Atmos. Environ.* **2002**, *36*, 4023–4035.

62. Stern, B.; Heron, C.; Serpico, M.; Bourriau, J. *Archaeometry* **2000**, *42*, 399–414.

63. Dudd, S. N.; Regert, M.; Evershed, R. P. *Org. Geochem.* **1998**, *29*, 1345–1354.

64. Evershed, R. P.; Mottram, H. R.; Dudd, S. N.; Charters, S.; Stott, A. W.; Lawrence, G. J.; Gibson, A.; Conner, A.; Blinkhorn, P. W.; Reeves, V. *Naturwissenschaften* **1997**, *84*, 402–406.

65. Mottram, H. R.; Dudd, S. N.; Lawrence, G. J.; Stott, A. W.; Evershed, R. P. *J. Chromatogr., A.* **1999**, *833*, 209–221.

66. Evershed, R. P.; Dudd, S. N.; Copley, M. S.; Berstan, R.; Stott, A. W.; Mottram, H. R.; Buckley, S. A.; Crossman, Z. *Acc. Chem. Res.* **2002**, *35*, 660–668.

67. Copley, M. S.; Berstan, R.; Dudd, S. N.; Straker, V.; Payne, S.; Evershed, R. P. *J. Archaeol. Sci.* **2005**, *32*, 485–503.

68. Spangenberg, J. E.; Jacomet, S.; Schibler, J. *J. Archaeol. Sci.* **2006**, *33*, 1–13.

69. Outram, A. K.; Stear, N. A.; Bendry, R.; Olsen, S.; Kasparov, A.; Zaibert, V.; Thorpe, N.; Evershed, R. P. *Science (Washington, DC, U.S.)* **2009**, *323*, 1332–1335.

70. Steele, V. J.; Stern, B.; Stott, A. W. *Rapid Commun. Mass Spectrom.* **2010**, *24*, 3478–3484.

71. Craig, O. E.; Allen, R. B.; Thompson, A.; Stevens, R. E.; Steele, V. J.; Heron, C. *Rapid Commun. Mass Spectrom.* **2012**, *26*, 2359–2364.

72. Stern, B.; Heron, C.; Tellefsen, T.; Serpico, M. *J. Archaeol. Sci.* **2008**, *35*, 2188–2203.

73. Guasch-Jané, M. R.; Ibern-Gómez, M.; Andrés-Lacueva, C.; Jáuregi, O.; Lamuela-Ravantós, R. M. *Anal. Chem.* **2004**, *76*, 1672–1677.

74. McGovern, P. E. *J. Egypt. Archaeol.* **1997**, *83*, 69–108.

75. McGovern, P. E.; Glusker, D. L.; Exner, L. J.; Voigt, M. M. *Nature (London, U.K.)* **1996**, *381*, 480–481.

76. Singleton, V. L. In *The Origins and Ancient History of Wine*; McGovern, P. E., Fleming, S. J., Katz, S. H., Eds.; Gordon and Breach: Luxembourg, 1996; pp 67−77.

77. Michel, H. V.; McGovern, P. E.; Badler, V. R. *Anal. Chem.* **1993**, *65*, 408–413.

78. Guasch-Jané, M. R.; Andrés-Lacueva, C.; Jáuragui, O.; Lamuela-Ravantós, R. M. *J. Archaeol. Sci.* **2006**, *33*, 1075–1080.

79. Guasch-Jané, M. R.; Andrés-Lacueva, C.; Jáuregui, O.; Lamuela-Ravantós, R. M. *J. Archaeol. Sci.* **2006**, *33*, 98–101.

80. Barnard, H.; Dooley, A. N.; Areshian, G.; Gasparyan, B.; Faull, K. F. *J. Archaeol. Sci.* **2011**, *38*, 977–984.

81. Pecci, A.; Giorgi, G.; Salvini, L.; Ontiveros, M.Á. C. *J. Archaeol. Sci.* **2013**, *40*, 109–115.

82. Garnier, N.; Richardin, P.; Cheynier, V.; Regert, M. *Anal. Chim. Acta.* **2003**, *493*, 137–157.

83. Romanus, K.; Baeten, J.; Poblome, J.; Accardo, S.; Degryse, P.; Jacobs, P.; De Vos, D.; Waelkens, M. *J. Archaeol. Sci.* **2009**, *36*, 900–909.

84. Isaksson, S.; Karlsson, C.; Eriksson, T. *J. Archaeol. Sci.* **2010**, *37*, 3263–3268.

85. Samuel, D. *J. Am. Soc. Brew. Chem.* **1996**, *54*, 3–12.

86. Foley, B. P.; Hansson, M. C.; Kourkoumelis, P.; Theodoulou, T. A. *J. Archaeol. Sci.* **2012**, *39*, 389–398.

87. Cavalieri, D.; McGovern, P. E.; Hartl, D. L.; Mortimer, R.; Polsinelli, M. *J. Mol. Evol.* **2003**, *57*, S226–S232.

88. DeRoo, C. S.; Armitage, R. A. *Anal. Chem.* **2011**, *83*, 6924–6928.

89. Fraser, D.; DeRoo, C. S.; Cody, R. B.; Armitage, R. A. *Analyst (Cambridge, U.K.)* **2013**, in press.

90. Adams, J. *Int. J. Mass Spectrom.* **2011**, *301*, 109–126.

91. Beißmann, S.; Buchberger, W.; Hertsens, R.; Klampfl, C. W. *J. Chromatogr., A.* **2011**, *1218*, 5180–5186.

92. Eberherr, W.; Buchberger, W.; Hertsens, R.; Klampfl, C. W. *Anal. Chem.* **2010**, 5792–5796.

93. Cody, R. B. *Anal. Chem.* **2009**, *81*, 1101–1107.

94. Kim, H. J.; Jang, Y. P. *Phytochem. Anal.* **2009**, *20*, 372–377.

95. Hajslova, J.; Cajka, T.; Vaclavik, L. *TrAC, Trends Anal. Chem.* **2011**, *30*, 204–218.

96. Bonk, T.; Humeny, A. *Neuroscientist* **2001**, *7*, 6–12.

97. Fuchs, B.; Schiller, J. *Eur. J. Lipid Sci. Technol.* **2009**, *111*, 83–98.

98. Fuchs, B.; Süß, R.; Schiller, J. *Prog. Lipid Res.* **2010**, *49*, 450–475.

99. Gut, I. G. *Hum. Mutat.* **2004**, *23*, 437–441.

100. Schiller, J.; Arnhold, J.; Benard, S.; Müller, M.; Reichl, S.; Arnold, K. *Anal. Biochem.* **1999**, *267*, 46–56.

101. Schiller, J.; Süß, R.; Arnhold, J.; Fuchs, B.; Leßig, J.; Müller, M.; Petković, M.; Spalteholz, H.; Zschörnig, O.; Arnold, K. *Prog. Lipid Res.* **2004**, *43*, 449–488.

102. Buckley, M.; Kansa, S. W.; Howard, S.; Campbell, S.; Thomas-Oats, J.; Collins, M. *J. Archaeol. Sci.* **2010**, *37*, 13–20.

103. Richter, K. K.; Wilson, J.; Jones, A. K. G.; Buckley, M.; van Doorn, N.; Collins, M. *J. Archaeol. Sci.* **2011**, *38*, 1502–1510.

104. Stewart, J. R. M.; Allen, R. B.; Jones, A. K. G.; Penkman, K. E. H.; Collins, M. J. *J. Archaeol. Sci.* **2013**, *40*, 1797–1804.

105. Calvano, C. D.; van der Werf, D.; Palmisano, F.; Sabbatini, L. *Anal. Bioanal. Chem.* **2011**, *400*, 2229–2240.

106. Kuckova, S.; Crhova, M.; Vankova, L.; Hnizda, A.; Hynek, R.; Kodicek, M. *Int. J. Mass Spectrom.* **2009**, *284*, 42–46.

107. Kuckova, S.; Hynek, R.; Kodicek, M. *J. Cult. Heritage* **2009**, *10*, 244–247.

108. Kuckova, S.; Sandu, I. C. A.; Crhova, M.; Hynek, R.; Fogas, I.; Schafer, S. *J. Cult. Heritage* **2013**, *14*, 31–37.

109. Chamberlain, P.; Drewello, R.; Korn, L.; Bauer, W.; Gough, T.; Al-Fouzan, A.; Collins, M.; van Dorn, N.; Craig, O.; Heron, C. *Archaeometry* **2011**, *53*, 830–841.

110. Scalarone, D.; Duursma, M. C.; Boon, J. J.; Chiantore, O. *J. Mass Spectrom.* **2005**, *40*, 1527–1535.

111. Mortensen, M. N.; Egsgaard, H.; Hvilsted, S.; Shashoua, Y.; Glastrup, J. *J. Archaeol. Sci.* **2007**, *34*, 1211–1218.

112. Solazzo, C.; Erhardt, D. In *Theory and Practice of Archaeological Residue Analysis*; Barnard, H., Eerkens, J., Eds.; Archaeopress: Oxford, U.K., 2007; pp 161−178.

113. Nielsen-Marsh, C. M.; Stegenann, C.; Hoffmann, R.; Smith, T.; Feeney, R.; Toussaint, M.; Harvati, K.; Panagopoulou, E. *J. Archaeol. Sci.* **2009**, *36*, 1758–1763.

114. Porto, I. M.; Laure, H. J.; Barbosa de Sousa, F.; Rosa, J. C.; Gerlach, R. F. *J. Archaeol. Sci.* **2011**, *38*, 3596–3604.

115. Dietemann, P.; Herm, C. In *Organic Mass Spectrometry in Art and Archaeology*; Colombini, M. P., Modugno, F., Eds.; Wiley: Chichester, U.K., 2009; pp 131−163.

116. Heaton, K.; Solazzo, C.; Collins, M.; Thomas-Oats, J.; Bergström, E. T. *J. Archaeol. Sci.* **2009**, *36*, 2145–2154.

117. Hurst, W. J.; Tarka, S. M., Jr.; Powis, T. G.; Valdez, F., Jr.; Hester, T. R. *Nature (London, U.K.)* **2002**, *418*, 289–290.

118. Washburn, D. K.; Washburn, W. N.; Shipkova, P. A. *J. Archaeol. Sci.* **2011**, *38*, 1634–1640.

119. Washburn, D. K.; Washburn, W. N.; Shipkova, P. A. *J. Archaeol. Sci.* **2013**, *40*, 2007–2013.

120. Henderson, J. S.; Joyce, R. A.; Hall, G. R.; Hurst, W. J.; McGovern, P. E. *Proc. Natl. Acad. Sci. U.S.A.* **2007**, *104*, 18937–18940.

121. James, M. A.; Reifarth, N.; Mukherjee, A. J.; Crump, M. P.; Gates, P. J.; Sandor, P.; Robertson, F.; Pfälzner, P.; Evershed, R. P. *Antiquity* **2009**, *83*, 1109–1118.

122. Karapanagiotis, I.; Mantzouris, D.; Kamaterou, P.; Lampakis, D.; Pnayiotou, C. *J. Archaeol. Sci.* **2011**, *28*, 3127–3232.

123. Karapanagiotis, I.; Theologou, J.; Lakka, A.; Ozoline, A.; Panayiotou, C. *Archaeometry* **2011**, *53*, 587–599.

124. Petroviciu, I.; Albu, F.; Medvedovici, A. *Microchem. J.* **2010**, *95*, 247–254.

125. Wouters, J.; Rosario-Chirinos, N. *J. Am. Inst. Conserv.* **1992**, *31*, 237–255.

126. Liu, J.; Guo, D.; Zhou, Y.; Wu, Z.; Li, W.; Zhao, F.; Zheng, X. *J. Archaeol. Sci.* **2011**, *38*, 1763–1770.

127. Karapanagiotis, I.; Lampakis, D.; Konstanta, A.; Farmakalidis, H. *J. Archaeol. Sci.* **2013**, *40*, 1471–1478.

128. Degano, I.; Biesaga, M.; Colombini, M. P.; Trojanowicz, M. *J. Chromatogr., A.* **2011**, *1218*, 5837–5847.

129. Kealhofer, L.; Torrence, R.; Fullager, R. *J. Archaeol. Sci.* **1999**, *26*, 527–546.

130. Pearsall, D. M.; Chandler-Ezell, K.; Zeidler, J. A. *J. Archaeol. Sci.* **2004**, *31*, 423–442.

131. Piperno, D. R.; Ranere, A. J.; Holst, I.; Hansell, P. *Nature (London, U.K.)* **2000**, *407*, 894–897.

132. Piperno, D. R.; Weiss, E.; Holst, I.; Nadel, D. *Nature (London, U.K.)* **2004**, *430*, 670–673.

133. Li, M.; Yang, X.; Ge, Q.; Ren, X.; Wan, Z. *J. Archaeol. Sci.* **2013**, *40*, 1667–1672.

134. Allen, M. S.; Ussher, E. *J. Archaeol. Sci.* **2013**, *40*, 2799–2812.

135. Perry, L.; Sandweiss, D. H.; Piperno, D. R.; Rademaker, K.; Malpass, M. A.; Umire, A.; de la Vera, P. *Nature (London, U.K.)* **2006**, *440*, 76–79.

136. Sullivan, K. A.; Kealhofer, L. *J. Archaeol. Sci.* **2004**, *31*, 1659–1673.

137. Albert, R. M.; Weiner, S.; Bar-Yosef, O.; Meignen, L. *J. Archaeol. Sci.* **2000**, *27*, 931–947.

138. Tao, D.; Wu, Y.; Guo, Z.; Hill, D. V.; Wang, C. *J. Archaeol. Sci.* **2011**, *38*, 3577–3583.

139. Hardy, K.; Blakeney, T.; Copeland, L.; Kirkham, J.; Wrangham, R.; Collins, M. *J. Archaeol. Sci.* **2009**, *36*, 248–255.

140. Henry, A. G.; Piperno, D. R. *J. Archaeol. Sci.* **2008**, *35*, 1943–1950.

141. Boyd, R.; Surette, C.; Nicholson, B. A. *J. Archaeol. Sci.* **2006**, *33*, 1129–1140.

142. Boyd, M.; Varney, T.; Surette, C.; Surette, J. *J. Archaeol. Sci.* **2008**, *35*, 2545–2556.

143. Dickau, R.; Bruno, M. C.; Iriarte, J.; Prümers, H.; Betancourt, C. J.; Holst, I.; Mayle, F. E. *J. Archaeol. Sci.* **2012**, *39*, 357–370.

144. Pető, Á.; Gyulai, F.; Pópity, D.; Kenéz, Á. *J. Archaeol. Sci.* **2013**, *40*, 58–71.

145. Saul, H.; Wilson, J.; Heron, C. P.; Glykou, A.; Hartz, S.; Craig, O. E. *J. Archaeol. Sci.* **2012**, *39*, 3483–3492.

146. Saul, H.; Fischer, A.; Glykou, A.; Hartz, S.; Madella, M.; Craig, O. *Phytoliths in Pottery Reveal Prehistoric Hunter-Gatherers' Taste for Spice*; Department of Archaeology, University of York, U.K.; Danish National Heritage Agency, Copenhagen, Denmark; Institute of Prehistoric and Protohistoric Archaeology, University of Kiel, Germany; Stiftung Schleswig-Holsteinische Landesmuseen, Schleswig, Germany; Department of Archaeology and Anthropology, Spanish Council for Scientific Research, Barcelona, Spain, unpublished.

147. Langejans, G. H. J. *J. Archaeol. Sci.* **2010**, *37*, 971–985.

148. Loy, T. H. *World Archaeol.* **1993**, *25*, 44–63.

149. Shanks, O. C.; Bonnichsen, R.; Vella, A. T.; Ream, W. *J. Archaeol. Sci.* **2001**, *28*, 965–872.

150. Wadley, L.; Lombard, M. *J. Archaeol. Sci.* **2007**, *34*, 1001–1010.

151. Lombard, M.; Wadley, L. *J. Archaeol. Sci.* **2007**, *34*, 155–165.

152. Anderson, P. C. *World Archaeol.* **1980**, *12*, 181–194.

153. Bruier, F. L. *Am. Antiq.* **1976**, *41*, 478–484.
154. Downs, E. F. *J. Archaeol. Sci.* **1995**, *22*, 11–16.
155. Haslam, M. *J. Archaeol. Sci.* **2006**, *33*, 114–121.
156. Smith, P. R.; Wilson, M. T. *J. Archaeol. Sci.* **1992**, *19*, 237–241.
157. Odell, G. H. *J. Archaeol. Res.* **2001**, *9*, 45–100.
158. Namdar, D.; Stacey, R.; Simpson, S. J. *J. Archaeol. Sci.* **2009**, *36*, 2507–2516.
159. Steele, V. J.; Turner, V. *The Analysis of Visible and Absorbed Residues in Viking Age Steatite Vessels From Shetland*; University of Bradford, U.K.; Shetland Amenity Trust, Lerwick, Shetland, U.K., unpublished.
160. Winterburn, J. *Curr. Archaeol.* **2008**, *214*, 25–32.
161. Joy, J.; Baldwin, A.; Hood, J.; Fitzpatrick, A. *Chiseldon Cauldrons*; The British Museum, Research Projects pages. http://www.thebritishmuseum.org/research/research_projects/all_current_projects/chiseldon_cauldrons.aspx (accessed May 25, 2013).
162. Baldwin, A.; Crummy, S.; Hood, J.; Joy, J.; Wang, Q. *Chiseldon Cauldrons* The British Museum, Chiseldon Cauldrons Blog. http://blog.britishmuseum.org/category/archaeology/chiseldon-cauldrons/ (accessed May 25, 2013).
163. Steele, V. J.; Baldwin, A.; Hood, J.; Joy, J. *Analysis of Organic Residues From the Chiseldon Cauldrons*; The British Museum, London, U.K., unpublished.
164. Craig, O. E.; Steele, V. J.; Fischer, A.; Hartz, S.; Andersen, S. H.; Donohoe, P.; Glykou, A.; Saul, H.; Jones, D. M.; Koch, E.; Heron, C. *Proc. Natl. Acad. Sci. U.S.A.* **2011**, *108*, 17910–17915.
165. Valianou, L.; Wei, S.; Mubarak, M. S.; Farmakalidis, H.; Rosenberg, E.; Stassinopoulos, S.; Karapanagiotis, I. *J. Archaeol. Sci.* **2011**, *38*, 246–254.
166. Scott, D. A.; Warmlander, S.; Mazurek, J.; Quirke, S. *J. Archaeol. Sci.* **2009**, *36*, 923–932.
167. Degano, I.; Colombini, M. P. *J. Archaeol. Sci.* **2009**, *36*, 1783–1790.
168. Pérez-Arantegui, J.; Ribechini, E.; Colombini, M. P.; Escudero, F. *J. Archaeol. Sci.* **2011**, *38*, 3350–3357.
169. Scott, D. A.; Swartz Dodd, L.; Furihata, J.; Tanimoto, S.; Keeney, J.; Schilling, M. R.; Cowan, E. *Stud. Conserv.* **2004**, *49*, 177–192.
170. Canevali, C.; Gentile, P.; Orlandi, M.; Modugno, F.; Lucejko, J. J.; Colombini, M. P.; Brambilla, L.; Goidanich, S.; Riedo, C.; Chiantore, O.; Baraldi, P.; Baraldi, C.; Gamberini, M. C. *Anal. Bioanal. Chem.* **2011**, *401*, 1801–1814.
171. Stacey, R. *Anal. Bioanal. Chem.* **2011**, *401*, 1749–1759.
172. Colombini, M. P.; Modugno, F.; Gamberini, M. C.; Rocchi, M.; Baraldi, C.; Deviese, T.; Stacey, R.; Orlandi, M.; Saliu, F.; Riedo, C.; Chiantore, O.; Sciutto, G.; Catelli, E.; Brambilla, L.; Toniolo, L.; Miliani, C.; Rocchi, P.; Bleton, J.; Baumer, U.; Dietemann, P.; Pojana, G.; Marras, S. *Anal. Bioanal. Chem.* **2011**, *401*, 1847–1860.
173. Orton, C. *Sampling in Archaeology*; Cambridge University Press: Cambridge, U.K., 2000; pp 177−209.
174. Shennan, S. *Quantifying Archaeology*, 2nd ed.; University of Iowa Press: Iowa City, IA, 1997; pp 361−400.

Chapter 6

18th-Century Glue Recipes: Towards Identifying Glue Residues from Ferry Farm, George Washington's Boyhood Home

Daniel Fraser,[*,1] **Mara Kaktins,**[2] **and Ruth Ann Armitage**[3]

[1]Department of Chemistry and Physical Sciences, Lourdes University, Sylvania, Ohio 43560
[2]George Washington Foundation, Fredericksburg, Virginia 22405
[3]Department of Chemistry, Eastern Michigan University, Ypsilanti, Michigan 48197
[*]E-mail: dfraser@lourdes.edu

Archaeological investigations at Ferry Farm, home to the Washington family from 1738−1772, have yielded numerous ceramic artifacts associated with Mary Washington, George Washington's mother. Several of these bear residues of historic mending. The nature of the glues, and the relationship between these various artifacts, remains poorly understood. We are using direct analysis in real time mass spectrometry to investigate the composition of three classes of replica historic glues made from hide, resin, and milk/cheese. Based on these results, we sought to characterize the historic glue residues to provide insight into the practice of china mending in the 18th century.

Introduction

Ferry Farm, located across the Rappahannock River from Fredericksburg, Virginia, was the boyhood home of George Washington. The Washington family lived at the Farm from 1738-1772, occupying the second of five houses to be built at the site. The house was reportedly damaged by fire on Christmas Eve, 1740. It was repaired and occupied by the Washington family until 1772, at which point Mary Washington moved to Fredericksburg. Presumably the house was in decline by the end of the 18th/early 19th century. By 1833 artist John Gadsby Chapman painted the landscape of Washington's boyhood, depicting only a ruin where the

house once stood. This foundation was further damaged by Union soldiers during the Civil War who denuded the landscape and put a trench through the foundation of the Washington house (*1*)

Intensive archaeological investigations at Ferry Farm have been ongoing since 2001. More than 500,000 artifacts have been excavated during this time, and the location of the original Washington house has been identified. Amongst the large collection of excavated materials were several ceramic sherds from Mary Washington's collection of tea and tablewares.

Examination of one of Mary Washington's more elaborate tablewares, a creamware punch bowl with an enameled floral motif accented with cherries (Figure 1), revealed the presence of eighteenth century glue residues. Sherds from this punch bowl were recovered from the Washington house cellar. The hand-painted designs and distinct vertical crazing is similar to vessels attributed to the Cockpit Hill potters of Derby, England (*2*). It would initially appear as though the bowl was broken into at least four different fragments and subsequently glued together before a presumed second breakage episode and eventual discard. The glue residue can be seen as a light brown substance adhering to the broken edges of the vessel and aligning along "seams" where the bowl was broken previously. Figure 2 illustrates a cross-section of the bowl's interior with glue extending across multiple adjacent sherds along the entire base. It should be noted that prior to our recognition of these residues, the historic glue was durable enough to survive washing by lab technicians unaware of the adhesives present. Microscopic examination confirms that the residues are not simply organic deposits which often accumulate on archaeological ceramics, although deposits of this nature are not common in materials excavated at Ferry Farm.

Figure 1. Mary Washington's enameled creamware punchbowl with floral and cherry motif. Courtesy of George Washington Foundation.
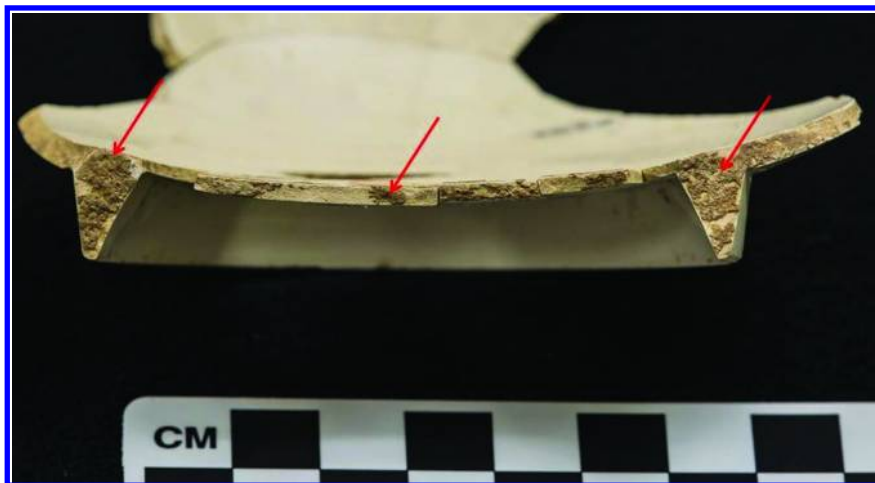
Figure 2. Glue residue adhering to the base of the punchbowl. Courtesy of George Washington Foundation.

To date, at least four additional vessels associated with the Washington family have been found to also exhibit glue residues along the broken edges. These include a creamware platter and plate, both with Royal Pattern rims, an enameled creamware lid, probably from a teapot, and a fragment of a porcelain hollowware with Imari palette. Additionally, two wig curlers recovered from the site also feature an adhering substance that bears some resemblance to the glue residues on the tablewares. Each has a seemingly identical application which runs the length of the curler on one side only, as though they were glued to another object, or possibly each other. While repairing broken ceramics is a practice that continues to this day, an explanation for why glue would be present on wig curlers has thus far eluded us.

The discovery of these residues has prompted several questions: Are the same glues present on all of the sherds? What are the compositions of the glues? Were the mended vessels functional after their repair or used only for display? Was the mending done professionally or by a resident on the property? These questions led to undertaking some experimental archaeology to replicate and test the efficacy of 18th- and 19th-century home glue recipes and to the chemical analysis reported here.

Glues and adhesives are found on archaeological materials as early as the Paleolithic period, where bitumen (*3*, *4*) and birch bark tars (*5*) were used in hafting stone points. Birch bark tar was widely used in Europe, as a hafting material in Mesolithic Britain (*6*), and has been used to repair ceramics across Europe since the Neolithic (*7*, *8*) and in Roman Britain (*9*). Some of these birch bark tar glues also contained beeswax (*7*). Others have observed mixtures of pine resins or birch bark tar and beeswax or animal fat in archaeological adhesives (*10–13*). Pine resins, possibly processed into a glue for hafting or repairs, have been identified on a ceramic sherd from the Western Great Basin (*14*). Proteinaceous glues are water

soluble, and thus are unlikely to survive for long in the archaeological record. Two exceptions worth noting are the use of a proteinaceous animal glue in the construction of a terracotta horse from Qingzhou, China (*15*) and of an Egyptian cartonnage mummy case from the 22nd Dynasty (*16*). Most evidence for such glues is found in artists' materials, where they are well preserved and appear as both adhesives and binding media in paints.

Identification of characteristic compounds in glues – steranes, terpenes, waxes, amino acids – by mass spectrometry provides more specificity in analysis than does spectroscopic analysis (e.g., FT-IR). Gas chromatography-mass spectrometry (GC-MS) is the primary method for identifying di- and triterpenoids, lipids, and waxes in archaeological glues (e.g., 7-9). Extraction and derivatization is necessary for GC-MS studies, except when sufficiently volatile components can be collected from the headspace of a glue or whole artifact using solid-phase microextraction (*17*). For proteinaceous glues, hydrolysis – for up to 24 hr – is necessary to reduce the protein to amino acids, and derivatization must also be carried out for GC-MS (*18*). Identification of species-specific peptides may also be undertaken by mass spectrometry, though this area of research remains somewhat in its infancy (*19*, *20*). Pyrolysis GC-MS, with or without on-line hydrolysis/methylation, eliminates the need for lengthy sample preparations, though separation still requires significant amounts of time. Direct inlet mass spectrometry of archaeological glues (*21*, *22*) has been reported as a fast, simple identification method, though the extensive fragmentation and overlap of ions makes interpretation of the complex spectra a significant undertaking.

Such an analysis without fragmentation that is able to clearly differentiate between sources of glues without sample preparation would be ideal. Ambient ionization methods like desorption electrospray ionization (DESI) and direct analysis in real time (DART) are capable of rapid, simple mass spectrometric analysis of intact proteins and small molecules alike (*23*, *24*). Such applications have great potential for archaeological materials (*25*, *26*). We report here on applying DART with high resolution time-of-flight mass spectrometry to characterizing the glue residues from Ferry Farm, and comparing their composition to replica glues based on period recipes.

Methods and Materials

Experimental Archaeology

One of us (MK) and Melanie Marquis, Archaeological Laboratory Supervisor, replicated three basic glue types from period literature that may have been used at Ferry Farm in the 18th century: resin glues, hide glues, and cheese glues (*27–29*). Because it seemed unlikely that the wig curlers had been repaired, we replicated an 18th-century recipe for a pomade that would have been used to set wigs on such curlers. The ingredients in the replica glues and pomade are provided in Table I. A sample of pitch obtained by heating birch bark in an oxygen-free environment was also prepared for comparison to the historic glues.

To determine how well the glues performed, each of the replica glues was used to repair modern ceramic objects with pastes similar to those of 18th-century

In Archaeological Chemistry VIII; Armitage, R., et al.;
ACS Symposium Series; American Chemical Society: Washington, DC, 2013.

wares. The glues were evaluated for their ease of application, adhesive properties, and post-depositional change. Hide glue was simple to apply thinly with a brush and made nearly imperceptible repairs, but it decomposed almost completely during six months of burial on site. The cheese and resin glues were both difficult to apply and the repairs were not suitable for either future use or display. The resin glue was significantly altered by burial, darkening perceptibly and becoming brittle and flaky. The cheese glues appeared to survive best, bonding tightly to the ceramic paste and changing color slightly. These glues appear to be the most likely of the three replica glues to survive archaeologically.

Table I. Replica 18th- and 19th-century glues prepared for this study

Glue name	Ingredients
Hide glue 1	Hide/sinew glue, isinglass, brandy, pickling lime
Hide glue 2	Hide/sinew glue, white vinegar, garlic, ox gall, pine resin, turpentine, sandarac, gum mastic, brandy
Cheese glues 1 and 2	White vinegar, whole milk, pickling lime, egg white
Cheese glue 2A	Grated cheese, pickling lime, egg white
Resin glue	Pine tar resin, beeswax, pickling lime
Birch bark pitch	Pitch prepared from heating birch bark in the absence of air
Pomatum	Beef bone marrow, hazelnut oil, lemon oil

Table II. Authentic 18th-century glue samples submitted for analysis

Ferry Farm ID number	Description
FF-12-100-161 (a)	Punchbowl footring
FF-12-100-161 (b)	Creamware plate bottom w/ Marley
FF-10-273-22	Imari
FF-12-411-2	Creamware tea lid
FF-12-100-161	Creamware platter
FF-10-273-17	Wig curler 1 (broken)
FF-10-254-2	Wig curler 2 (complete)

In Archaeological Chemistry VIII; Armitage, R., et al.;
ACS Symposium Series; American Chemical Society: Washington, DC, 2013.

Samples for Analysis

Samples of the replica glues described in Table I were sent to EMU for characterization by direct analysis in real time time-of-flight mass spectrometry. Fragments of glues from Mary Washington's ceramics and the residues from the wig curlers were removed using scalpels, placed into clean glass vials and sent to EMU for analysis as well (Table II). Additional samples of the cheese and resin glues after six months of burial were also analyzed, along with samples of the soil from both the reproduction burials and the Washington house cellar from which the authentic ceramics were excavated.

The glue samples – both replica and authentic – were analyzed both as received and as hydrolysates by direct analysis in real time time-of-flight mass spectrometry. Hydrolysis was carried out to determine the amino acid content of the glues, which would differentiate hide glues from the other recipes based on the high concentration of hydroxyproline relative to other amino acids from collagen. A few micrograms of each sample and 20 μL of BOC-bromophenylalanine as internal standard (0.2 mg/mL) was placed into a reaction vial with 40 μL 6 M hydrochloric acid, purged with nitrogen, sealed with a teflon septum and cap, and heated to 120 °C for 60 min in a heating block. A control sample with only internal standard and HCl was prepared in the same manner. After cooling, the resulting solution was subjected to DART-MS analysis on the closed end of a melting point capillary tube.

DART-MS Analysis

The hydrolysate solution, glue powder or fragment was simply held in the gap between Orifice 1 of the AccuToF mass spectrometer (JEOL USA, Peabody MA) and the DART ionization source (IonSense, Saugus, MA). The DART was used in both positive and negative ionization modes with helium at 350°C. Orifice 1 was set to 30V to minimize fragmentation and 120°C; Orifice 2 was held at 5V, and the ring lens voltage at 5V. The DART grid voltage was kept at the default values of +240V and -530V. The mass spectrometer RF ion guide ("peaks voltage") was set to 700V to maximize sensitivity in the low mass range to include all of the amino acids. Mass calibration was carried out using PEG-600 in methanol during each acquisition. The mass resolving power was approximately 6000 (as calculated by $m/\Delta m$).

Results and Discussion

Replica Glues: Hydrolysis

While amino acids can be detected using DART-MS in either positive ion mode (as MH^+ ions) or in negative ion mode (usually as $M-H^-$ ions), negative ion mode has better sensitivity. This was confirmed in our analyses when the internal standard could not be detected at all in positive ion mode in some of the samples, yet was readily observed in negative ion mode. The results for amino acids and fatty acids are reported here for negative ion mode. The control hydrolysate sample

In Archaeological Chemistry VIII; Armitage, R., et al.;
ACS Symposium Series; American Chemical Society: Washington, DC, 2013.

contained no significant quantities of amino acids, though traces of asparagine (Asn), glutamine (Gln), and glutamic acid (Glu) were observed.

High resolution mass spectra of the hydrolysates of the replica glues showed that the three general types of glues differed greatly in amino acid content. Hydroxyproline (Hpro) ($C_5H_9NO_3$, M-H⁻ m/z 130.050) was readily distinguishable from leucine/isoleucine (Leu/Ile) ($C_6H_{13}NO_2$, M-H⁻ m/z 130.087) at high resolution, eliminating the need to chromatographically separate the amino acids for analysis. Hide glues 1 and 2 contained significant quantities of hydroxyproline, as expected. The cheese glues surprisingly contained few or no amino acids; however, it was also observed that little of the internal standard was recovered from the cheese glue samples. The high proportions of pickling lime in the cheese glues may have neutralized a significant amount of the acid, leading to a lower yield of amino acids in the hydrolysate. Two saturated fatty acids – palmitic (hexadecanoic) acid and stearic (octadecanoic) acid – and their monounsaturated counterparts were present in significant quantities. These fatty acids are the dominant lipids used as evidence of dairy products in archaeological materials, though their presence can be attributed to numerous fat-containing substances as well. The resin glue contained a tiny amount of both Asn and Gln, but no other amino or fatty acids. The mass spectrum for the hydrolysate of the resin glue was dominated by a peak at m/z 299.195, indicating the presence of significant quantities of dehydroabietic acid ($C_{20}H_{28}O_2$, Figure 3). Abietic acid ($C_{20}H_{30}O_2$), a marker compound for pine resin, was also present at m/z 301.210, as were numerous other oxidation products (15-hydroxy-7-oxodehydroabietic acid, 3,15-dihydroxydehydroabietic acid, etc.). The replica pomatum contained small amounts of all of the amino acids except cysteine (Cys), HPro, Glu, methionine (Met), histidine (His), and tyrosine (Tyr). The spectrum for the pomatum hydrolysate was dominated by the saturated fatty acids. The birch bark pitch was not hydrolyzed for this study.

Replica Glues: Direct Analysis

Direct analysis of the replica glues required no sample preparation: subsamples of the material were simply held in the ion source. This was useful in that it revealed the presence of a large number of different compounds. For simplicity sake, we focus here on two groups of compounds that differentiated the glue recipes for which amino acids were unhelpful. For the cheese glues, this meant looking at the fatty acid composition, while for the resin glue and birch bark pitch, we considered characteristic marker compounds including abietic acid and lupenone. Birch bark pitch has been well characterized in archaeological contexts, as discussed in the Introduction. While there are many characteristic compounds in birch bark pitch besides lupenone and betulinic acid (Figure 3), only those compounds were readily identified in positive ion mode for the birch bark pitch prepared for this study.

The even-chain fatty acids observed by positive ion direct mass spectrometry of the replica glues are summarized in Table III. Hide glue #1 may have been contaminated, as palmitic and stearic acids were both observed along with the monounsaturated C16:1 and C18:1 fatty acids. Hide glue #2 showed no evidence

of fatty acids. The cheese glues contained butanoic acid, and palmitic acid, as well as other fatty acids. The resin glue was devoid of fatty acids. As expected, the mass spectrum of the pomatum was dominated by fatty acids.

Abietic acid

$C_{20}H_{30}O_2$
Exact Mass: 302.2246

Dehydroabietic acid

$C_{20}H_{28}O_2$
Exact Mass: 300.2089

15-Hydroxy-7-oxodehydroabietic acid

$C_{20}H_{26}O_4$
Exact Mass: 330.1831

Betulinic acid

$C_{30}H_{48}O_3$
Exact Mass: 456.3603

Lupenone

$C_{30}H_{48}O$
Exact Mass: 424.3705
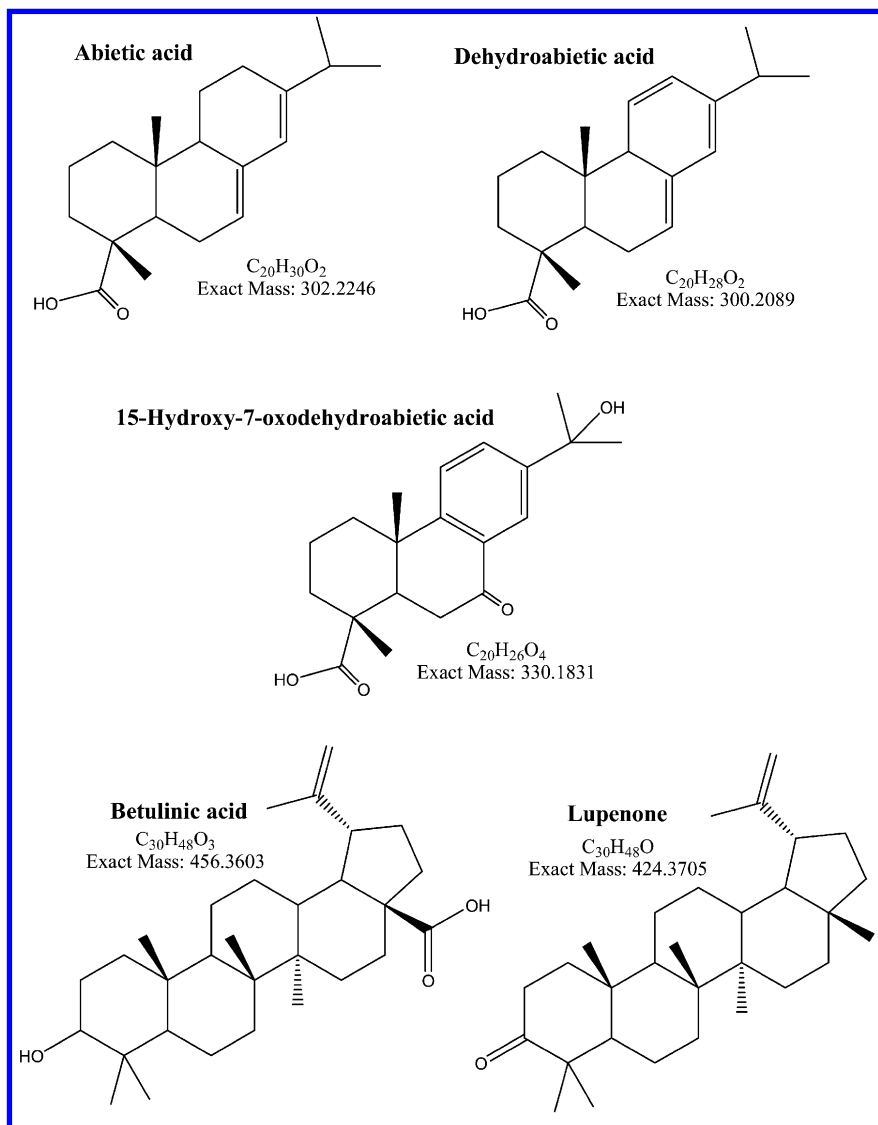
Figure 3. Structures for some of the compounds observed in pine resin and birch bark pitch.

Table III. Saturated and monounsaturated fatty acid composition of replica glues. Number denotes the length of the carbon chain in the saturated and degrees of unsaturation (where applicable).

Replica glue	4	6	8	10	10:1	12	14	16	16:1	18	18:1
Hide glue (recipe 1)								x	x	x	x
Hide glue (recipe 2)											
Cheese glue (recipe 1)	x	x							x		
Cheese glue (recipe 2)	x	x	x	x		x		x	x		x
Cheese glue (recipe 2a)	x							x			x
Resin glue					x						
Pomatum				x			x	x	x	x	x

Hide glue #2 contained both pine resin and mastic in the recipe, which contributed abietic acid and oxidation products as well as several of the acids from mastic (oleanonic/moronic/masticadienoic/isomasticadienoic acids, all $C_{30}H_{46}O_3$). The resin glue mass spectrum was dominated by abietic and dehydroabietic acid and other oxidation products. The birch bark pitch was complex, containing the mastic acid and pine resin compounds in addition to the expected betulinic acid and lupenone. The reason for the presence of these other compounds remains unclear. No resin compounds were observed in any of the other glue recipes or the pomatum.

Replica Glues After Burial

Because the replica hide glues decomposed almost completely within the six months during which it was buried, no sample was available for analysis. Samples of the cheese glues and resin glue after six months buried on site were examined using DART-MS. Only the direct analysis of the buried glues has been completed so far. Even after six months, the fatty acid composition of the cheese glue remained unchanged. The resin glue did not acquire any fatty acids from the burial environment, as its composition was also unchanged. The cheese glues did not contain any resin compounds after burial. Resin glue after burial also contained abietic and dehydroabietic acids, as well as 7-oxodehydroabietic acid. For comparison, samples of soil from the context in which the replica glues were buried were also examined with DART-MS. This soil showed no evidence of resin compounds and only traces of a few of the fatty acids ($C_{4:0}$, $C_{10:1}$, $C_{16:0}$, and $C_{18:1}$).

Authentic 18th-Century Glue Residues

Hydrolysates from the authentic glue samples described in Table II showed little evidence of amino acids. Only the glue from the footring of the punchbowl showed small amounts of serine (Ser), threonine (Thr), and tryptophan (Trp). Asn and Gln were both observed in nearly all of the samples, including the control hydrolysate, indicating some contamination in the sample preparation process. No hydroxyproline was observed in any of the hydrolysates of the authentic glues. Considering that the replica hide glues prepared from contemporary recipes did not survive even six months of burial, it appears unlikely that the authentic glues were prepared primarily from hide.

Direct analysis of the authentic glue residues revealed the presence of phthalates in some of the samples, and dominated the spectrum of the glue from the Imari porcelain. All of the glue residues contained both $C_{4:0}$ and $C_{10:1}$, as well as other small even-chain fatty acids in the range from C_4-C_{14}. None of the authentic residues contained palmitic or stearic acids. Three of the authentic glue residues – the creamware plate bottom and teapot lid and the Imari porcelain – showed the presence of abietic acid. The broken wig curler showed the presence of dehydroabietic acid. If pine resin were truly present in these samples from their original repairs, we would expect oxidation products to be present. Direct analysis of the soil from the cellar from which the authentic ceramics were excavated showed the presence of both abietic and dehydroxyabietic acids, indicating that the presence of these compounds in the glue residues are likely due to environmental contamination. The context soil also contained short even-chain fatty acids.

The Mass Mountaineer (R. B. Cody, Peabody, MA) software provided for DART-MS data analysis provides a mechanism for comparing and matching spectra. Figure 4 shows a head-to-tail comparison between the 17th-c.glue from the punchbowl and the buried cheese glue. The search algorithm looks for significant similarities in both the ions present in the spectra and their intensities to make a match. The ions in the spectra that led to the buried cheese glue being considered a good match for the authentic glues do not correspond to any known compounds. This pattern was consistent across all of the authentic glue residues. We believe this is a consequence of similarities in burial context, and not related to similarities in the composition of the replica and authentic glues. A head-to-tail comparison of another of the authentic glue residues and soil from the Ferry Farm burial context is shown in Figure 5. Except for the ion at m/z 107.066, the strongest signals from the teapot lid glue residue correspond to those in the soil sample.
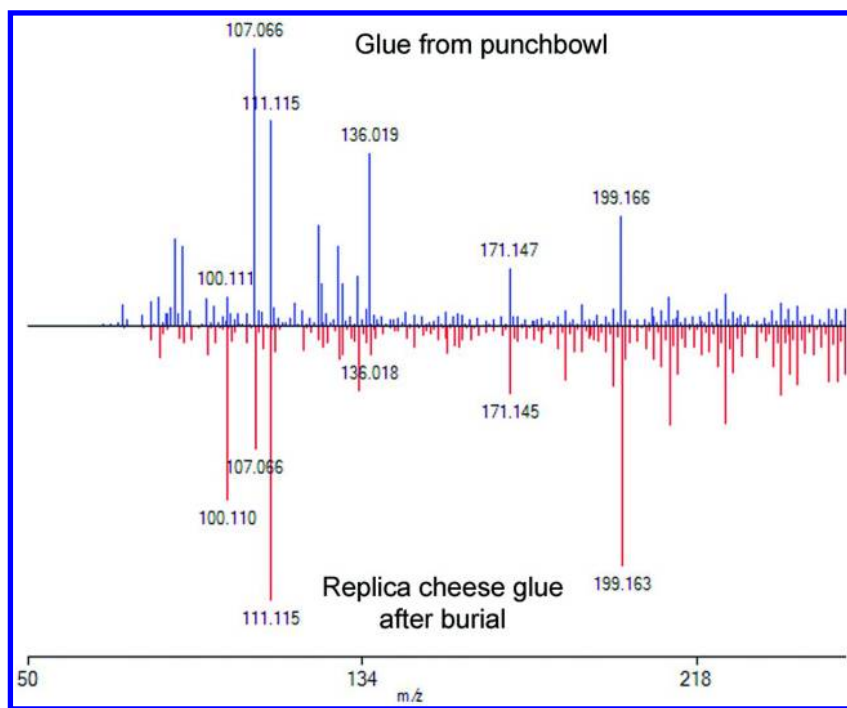
Figure 4. Head-to-tail comparison of authentic glue and replica cheese glue after 6 months of burial.
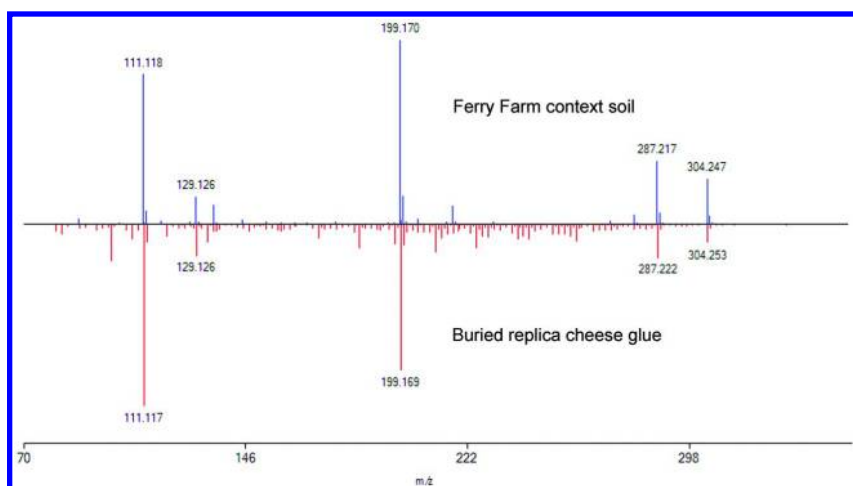
Figure 5. Head-to-tail comparison between DART mass spectra of soil (top) and buried replica cheese glue.

Conclusions

Based on these results, we can draw two primary conclusions. DART-MS can differentiate between the replica glues without sample preparation, and a short hydrolysis step makes identification of collagenous glues possible without derivatization or chromatography. We were unable to identify the nature of the authentic glue residues on the ceramics excavated at Ferry Farm. This may be due to decomposition of the organic components of the glues, or contamination from the burial environment. The samples provided were too small to reliably weigh on the equipment available at EMU. As the bulk of these samples appears to have been carbonate, even good preservation of the organic content may not have provided detectable amounts of diagnostic compounds. Further studies are ongoing, with larger samples where more material was available for study. Quantitative analysis of the hydrolysates using both transmission DART and GC-MS will, we hope, shed further light on the nature of these unique residues.

Acknowledgments

References

1. Muraca, D.; Nasca, P.; Levy, P. *Report on the Excavation of the Washington Farm: The 2004-2005 Field Seasons*; George Washington Foundation: Fredericksburg, VA, 2011.
2. Towner, D. *Creamware*; Faber and Faber: London, Boston, 1978.
3. Boëda, E.; Connan, J.; Dessort, D.; Muhesen, S.; N., M.; Valladas, H.; Tisnerat, N. *Nature* **1996**, *380*, 336–338.
4. Carciumaru, M.; Ion, R. M.; Nitu, E. C.; Stefanescu, R. *J. Archaeol. Sci.* **2012**, *39*, 1942–1950.
5. Mazza, P. P. A.; Martini, F.; Sala, B.; Magi, M.; Colombini, M. P.; Giachi, G.; Landucci, F.; Lemorini, C.; Modugno, F.; Ribechini, E. *J. Archaeol. Sci.* **2006**, *33*, 1310.
6. Aveling, E. M.; Heron, C. *Ancient Biomol.* **1998**, *2*, 69–80.
7. Regert, M. *J. Sep. Sci.* **2004**, *27*, 244–254.
8. Mitkidou, S.; Dimitrakoudi, E.; Urem-Kotsou, D.; Papadopoulou, D.; Kotsakis, K.; Stratis, J. A.; Stephanidou-Stephanatou, I. *Microchim. Acta* **2008**, *160*, 493–498.
9. Charters, S.; Evershed, R. P.; Goad, L. J.; Heron, C.; Blinkhorn, P. *Archaeometry* **1993**, *35*, 91–101.
10. Ribechini, E.; Bacchiocchi, M.; Deviese, T.; Colombini, M. P. *J. Anal. Appl. Pyrolysis* **2012**, *91*, 219–223.

11. Ribechini, E.; Orsini, S.; Silvano, F.; Colombini, M. P. *Anal. Chim. Acta* **2009**, *638*, 79–87.
12. d'Errico, F.; Backwell, L.; Villa, P.; Degano, I.; Lucejko, J. J.; Bamford, M. K.; Higham, T. F. G.; Colombini, M. P.; Beaumont, P. B. *Proc. Natl. Acad. Sci. U.S.A.* **2012**, *109*, 13214–13219.
13. Dudd, S. N.; Evershed, R. P. *Tetrahedron Lett.* **1999**, *40*, 359–362.
14. Eerkins, J. *Archaeometry* **2002**, *44*, 95–105.
15. Wei, S. Y.; Ma, Q. L.; Schreiner, M. *J. Archaeol. Sci.* **2012**, *39*, 1628–1633.
16. Farrell, E. F.; Snow, C.; Vinogradskaya, N. *J. Am. Inst. Conserv.* **2006**, *45*, 1–15.
17. Regert, A.; Alexandre, V.; Thomas, N.; Lattuati-Derieux, A. *J. Chromatogr., A* **2006**, *1101*, 245–253.
18. Schilling, M. R.; Khanjian, H. P.; Souza, L. A. C. *J. Am. Inst. Conserv.* **1996**, *35*, 45–59.
19. Kuckova, S.; Sandu, I. C. A.; Crhova, M.; Hynek, R.; Fogas, I.; Schafer, S. *J. Cult. Heritage* **2013**, *14*, 31–37.
20. Dallongeville, S.; Koperska, M.; Garnier, N.; Reille-Tailefert, G.; Rolando, C.; Tokarski, C. *Anal. Chem.* **2011**, *83*, 9431–9437.
21. Regert, M.; Rolando, C. *Anal. Chem.* **2002**, *74*, 965–975.
22. Modugno, F.; Ribechini, E.; Colombini, M. P. *Rapid Commun. Mass Spectrom.* **2006**, *20*, 1787–1800.
23. Takats, Z.; Wiseman, J. M.; Gologan, B.; Cooks, R. G. *Science* **2004**, *306*, 471–473.
24. Cody, R. B.; Laramee, J. A.; Durst, H. D. *Anal. Chem.* **2005**, *77*, 2297–2302.
25. Heaton, K.; Solazzo, C.; Collins, M. J.; Thomas-Oates, J.; Bergstrom, E. T. *J. Archaeol. Sci.* **2009**, *36*, 2145–2154.
26. Hopkins, J.; Armitage, R. A. In *Collaborative Endeavors in the Chemical Analysis of Art and Cultural Heritage Materials*; Lang, P. L., Armitage, R. A., Eds.; ACS Symposium Series 1103; American Chemical Society: Washington, DC, 2012; pp 131−142.
27. Dossie, R. *Handmaid to the Arts*; 2nd ed.; J. Nourse: London, 1764.
28. Cements. In *The Encyclopaedia Britannica: A Dictionary of Arts, Sciences, and General Literature*, 9th ed.; Baynes, T. S., Ed.; H. G. Allen: New York, 1833; Vol. 5, p 328.
29. Cements. In *Cooley's Cyclopaedia of Practical Receipts and Collateral Information*, 5th ed.; Cooley, A. J., Ed.; Churchill: London, 1872; pp 305−311.

Chapter 7

Physicochemical Study of Black Pigments in Prehistoric Paints from Oxtotitlán Cave, Guerrero, Mexico

Joseph McPeak,[1] Mary D. Pohl,[2] Christopher L. von Nagy,[3] Heather Hurst,[4] Marvin W. Rowe,[5] Eliseo F. Padilla Gutiérrez,[6] and Jon Russ[*],[1]

[1]Department of Chemistry, Rhodes College, Memphis, Tennessee 38112
[2]Department of Anthropology, Florida State University, Tallahassee, Florida 32306
[3]Department of Anthropology, University of Nevada, Reno, Nevada 89547
[4]Department of Anthropology, Skidmore College, Saratoga Springs, New York 12866
[5]Department of Chemistry, Texas A&M University-Qatar, Doha, Qatar and Office of Archaeological Studies and Conservation: Laboratory, Museum of New Mexico, Santa Fe, New Mexica 87507
[6]Escuela Nacional de Antropología e Historia, Mexico City 14030, Mexico
[*]E-mail: russj@rhodes.edu

This paper investigates the potential for identifying and dating black pigments in the Formative-style (800-400 B.C.E.) murals at Oxtotitlán Cave, Guerrero, Mexico, with the goal of studying prehistoric paint technology and the socio-political context of early Mesoamerican art. These murals are among the earliest in Mexico, if not the earliest, and represent the beginning of the highly influential Mexican muralism tradition that continues to this day. We employed multiple analytical techniques including pXRF, ATR-FTIR, SEM-EDS and Py-GC-MS to analyze black paints used to construct several motifs, including the depiction of a costumed, dancing lord at Oxtotitlán (Mural C-1). The

results indicate that the pigment present is a byproduct of pyrolyzed plant material, most likely a mixture of soot and charcoal. The black pigment appears to occur directly on the surface of the limestone substrate but is completely covered by a natural rock coating composed of calcium oxalate, carbonate and sulfate. The presence of charcoal and biogenic oxalate promises to allow crucial radiocarbon analysis of the rock art.

Introduction

The murals of Oxtotitlán Cave in Guerrero, Mexico (Figure 1) first came to the attention of academia in the late 1960s (*1–3*). Iconographic similarities with Gulf Coast Olmec monuments from La Venta (*4*, *5*) were immediately apparent. Nevertheless, lack of chronological dates on the cave paintings has hindered analysis of historical relationships. The Oxtotitlán rock paintings are part of a body of public and private art found in caves and on mountainsides that can be incorporated into emerging architectural traditions that define an era. This era, The Formative Period, saw the emergence of many of the cultural features that would come to define Mesoamerican life: A complex set of secular and religious calendars, impressive public art, writing, large scale government, and an increasingly dynamic international trade between what were, or would soon become, kingdoms.

Oxtotitlán Cave comprises a compact chain of several large grottos and deep caves along a limestone cliff face overlooking and marking the eastern edge of a large Formative site, Cerro Quiotepec (*6*). The caves are decorated with numerous monochrome pictographs and polychrome murals that are presumed to range in date and style from the Archaic to the Postclassic periods (< 2000 BCE to 1519 CE). The pictographs tend to be small in size and appear in clusters, often on highly inaccessible areas meters above the c ave floor. The murals are located toward the front of the cave and are more public than many of the pictographs. The murals differ from the pictographs in that they are complex polychromatic paintings that arguably function architecturally within the context of the cave. The largest mural, a composite juxtaposition of the Mexican cara-cara raptor and a bird-costumed lord and probable ruler, was painted high on the cliff face above the cave and is easily visible from the ancient town below (Figure 2). Archaeological materials at the lip of the cave, including grinding stones, suggest that the cave site may have served as a living area or may be the result of feasting or offertory rituals commonly associated with caves in Mesoamerica.

Many of the paintings are faint, eroded, and covered with a natural mineral accretion making them difficult to see. Sandra Cruz Flores of the Mexican National Institute of Anthropology and History finished selective cleaning of the Oxtotitlán paintings in 2009 as part of a conservation program, exposing new images that were previously concealed by the mineral accretion. Mural C-1 was cleaned at this time, revealing previously obscured parts of the mural that lay beneath the natural mineral coating.

Figure 1. Map showing the location of the Oxtotitlán Cave.

These developments have further highlighted similarities between the Gulf Coast Olmec monuments and Oxtotitlán Cave, and have renewed questions about the nature of their relationship. Accurate dating of pigments within these murals is essential for evaluating relationships developing throughout Mexico between 800-400 B.C.E. Breakthroughs in chemical analysis and radiocarbon dating have made this an opportune time to reevaluate the connections between caves in southwestern Mexico and early Olmec ceremonial centers on the Gulf Coast.
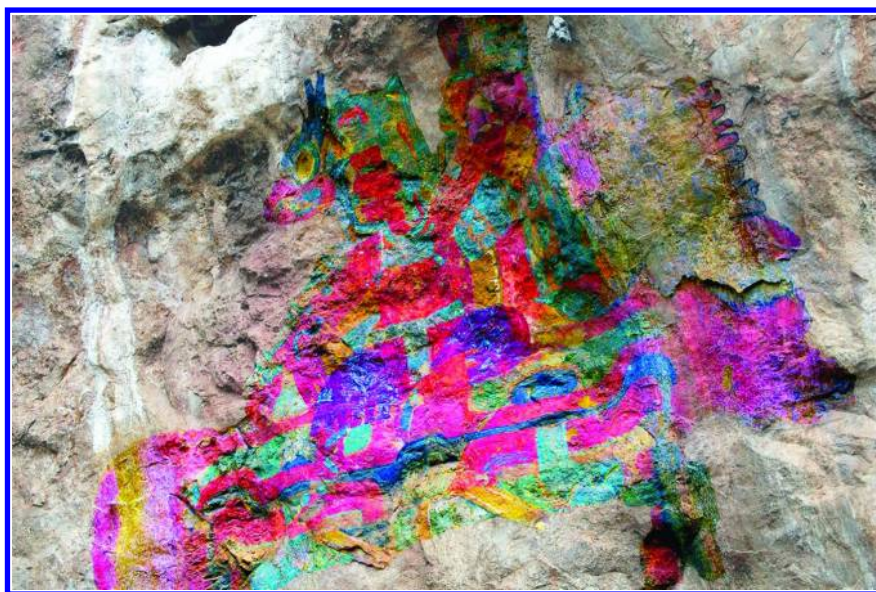
Figure 2. Digitally enhanced image of Mural C-1 at Oxtotitlán Cave. Samples of black paint were collected from this mural for this study. The mural is ~ 3 m x 3 m. (see color insert)

Experimental Methods and Results

Preliminary in Situ pXRF Analysis

One of the primary objectives of the project was to establish the age of one or more of the iconographic pictographs and murals in the Oxtotitlán Cave. The first phase of this study was to identify paints that appear to be most favorable for radiocarbon dating, either directly by ^{14}C assay of bioorganic matter in the paint, or indirectly via ^{14}C dating of the rock coating that covers the natural rock surfaces and the rock art in the site. Our strategy for identifying artifacts for direct dating was based on the assumption that black pigments at that time would have been produced from either manganese oxides or burned plant material (charcoal), both of which are used in wall painting traditions throughout Mesoamerica (*7*). Since the latter can be more reliably radiocarbon dated, black paints lacking manganese would be candidates for sampling and further study. Charcoal has been identified as a component in numerous prehistoric rock paintings worldwide, and radiocarbon assays of the material have provided absolute ages of these artifacts (*8*).

We analyzed the rock paints at the study site using a portable X-ray florescence (pXRF) spectrophotometer. This technique is non-invasive and provides semi-quantitative data on a variety of metals in the paints and natural surfaces (*9–12*). We used an Innov-X Alpha Series pXRF system that consists of a silver (Ag) anode X-ray tube source and a SiPIN diode detector. The instrument was operated in "soil mode" using 40 kV excitation energy with 30-second analysis times. Each artifact was analyzed at multiple locations, with several background analyses performed on adjacent unpainted surfaces.

The results from the pXRF analyses of black pigments (N = 43) showed that Mn was below the instrument detection limit in 35 (81%) of the measurements (Table I). For the eight analyses where Mn was detected the average concentration in the paints was 0.0139 ± 0.004 %. In the background analyses (N = 22) Mn was undetected in 18 measurements (82%); the average concentration of the four where Mn was detected was 0.0138 ± 0.003 %. As a comparison, the analysis of red paints in the site (N = 22) and the background (N = 27) resulted in an average Fe concentrations of 0.95 ± 0.83% and 0.17 ± 0.17%, respectively. The assumption that the red pigments were produced from iron based minerals, most likely iron oxides, was confirmed since the mean Fe concentration in the paints is significantly greater than the background ($p = 7.3 \times 10^{-5}$). In the case of Mn, however, the concentration of the metal in the paint is statistically indistinguishable to that in the background ($p = 0.98$). We conclude that all the black paints in the Oxtotitlán Cave that we analyzed were produced using pigments other than manganese, and thus most likely pyrolyzed carbon.

Table I. Semi-quantitative metal concentrations from the pXRF analysis of rock paints and background (∗ indicates below detection limits)

black paints	Mn (wt %)	Fe (wt %)	Cu (wt %)	As (wt %)	Sr (ppm)	Pb (ppm)	Zn (wt %)
Panel D, PET 1	0.021	0.22	2.78	0.06	67	69	*
Panel D, PET 1	*	0.23	2.89	0.07	68	52	*
alcove	*	0.12	1.29	0.05	65	363	*
alcove	*	0.31	2.26	0.06	65	101	*
alcove	*	0.13	0.41	0.01	67	38	*
alcove	*	0.26	0.63	0.03	118	66	*
C-1	*	0.23	2.37	0.05	142	*	*
C-1	0.015	0.58	0.01	0.01	220	*	0.027
C-1	*	0.59	0.01	0.01	208	*	0.035
C-1	0.012	0.21	1.80	0.01	69	*	*
Panel D, PET 1	*	0.05	0.01	*	48	*	*
Panel D, PET 1	*	0.06	*	*	68	44	*
Panel D, PET 1	*	0.66	*	0.02	53	25	
Handprints	*	0.10	0.01	*	29	*	0.010
Handprints	0.010	0.15	0.01	*	29	28	0.010
Panel C PET 3	*	0.08	*	*	72	*	*

black paints	Mn (wt %)	Fe (wt %)	Cu (wt %)	As (wt %)	Sr (ppm)	Pb (ppm)	Zn (wt %)
Panel 3, PET 2	*	0.06	*	*	55	30	0.002
Panel 3, PET 2	*	0.04	*	*	57	*	*
Panel 3, PET 2	*	0.05	*	*	57	45	0.002
Panel 3, PET 2	*	0.05	*	*	61	15	*
Panel 3, PET 2	*	0.03	*	*	65	*	*
Panel 3, PET 2	*	0.08	*	*	76	25	0.002
Jaguar man	*	0.20	0.01	*	73	39	0.006
Jaguar man	*	0.05	*	*	83	*	*
Jaguar man	*	0.05	*	*	70	16	
Jaguar man	*	0.05	*	*	73	24	0.003
Jaguar man	*	0.48	0.01	*	75	*	0.004
critters	*	0.06	*	*	49	34	0.003
critters	*	0.06	*	*	57	40	0.003
critters	0.011	0.07	*	*	62	*	0.002
Jaguar man	*	0.10	*	*	66	17	*
Jaguar man	*	0.04	*	*	76	27	0.005
C-1	*	0.30	0.06	0.02	68	*	0.003

Table I. (Continued). Semi-quantitative metal concentrations from the pXRF analysis of rock paints and background (∗ indicates below detection limits)

black paints	Mn (wt %)	Fe (wt %)	Cu (wt %)	As (wt %)	Sr (ppm)	Pb (ppm)	Zn (wt %)
C-1	*	0.18	0.42	0.02	131	*	*
alcove	0.018	1.03	0.02	0.03	120	94	0.009
shield	*	0.32	*	*	84	*	0.002
shield	0.011	0.25	*	*	28	*	0.003
shield	0.011	0.24	*	*	78	*	*
shield	*	0.19	*	0.01	75	51	0.004
shield	*	0.13	*	*	63	*	0.002
shield	*	0.03	*	*	125	*	*
Background							
Panel C PET 3	*	0.19	0.01	0.01	89	34	0.004
	*	0.08	*	*	72	*	*
	*	0.05	*	0.02	58	*	*
	0.011	0.12	0.01		37	17	0.008
Monkey	0.013	0.17	*	0.03	107	*	0.008
	*	0.17	*	0.02	77	*	0.003
	*	0.07	*		69	*	*

black paints	Mn (wt %)	Fe (wt %)	Cu (wt %)	As (wt %)	Sr (ppm)	Pb (ppm)	Zn (wt %)
Panel 3, Pet 2	*	0.05	*	*	80	*	*
	*	0.09	*	*	60	*	*
	*	0.07	*	0.01	79	95	*
jaguar man	*	0.11	*	*	71	15	0.003
	*	0.07	*	*	60	55	0.003
panel C-2	*	0.02	*	*	7	*	*
	*	0.04	*	*	53	*	0.002
shield	*	0.08	*	*	76	*	*
	*	0.20	*	0.01	85	32	*
	*	0.09	*	*	58	*	*
	*	0.04	*	*	63	*	*
left of panel 1	*	0.26	*	*	235	*	0.005
	*	0.03	*	*	125	*	*
	*	0.08	*	*	158	*	0.006
	0.014	0.44	*	*	274	25	0.003
	0.017	0.40	*	*	159	*	0.005

Based on the assumption that the black pigments were carbon based, we collected samples from three paintings including the C-1 mural (Figure 2) and an image that appears to be a warrior and shield (Figure 3). We also collected samples from unpainted surfaces adjacent to the artifacts to serve as background for the pigment analyses. Sample sizes were typically less than 1 cm² surface area and were taken directly from the shelter wall and placed immediately into Al foil for transport back to the laboratory.

Figure 3. View of the bi-chrome (black and red) warrior and shield painting (Panel 4-05) at the mouth of the north cave at Oxtotitlán. The primary lines of the painting are black with red filling the centers of the tab-like projections of the shield. The scale is 1.0 m with 10.0 cm increments.

Laboratory Analyses

We analyzed paint and unpainted (background) samples using optical microscopy, attenuated total reflectance Fourier transform infrared (ATR-FTIR) spectroscopy, environmental scanning electron microscopy with energy dispersive X-ray spectrometry (ESEM-EDS), and pyrolysis-gas chromatography–mass spectrometry (Py-GC-MS). Optical microscopy revealed that the paints were covered by a natural rock coating; however, because of the limited amount of sample available we did not construct thin-sections to discern the coating/paint/substrate stratigraphy. Instead we broke two samples manually and observed each fragment microscopically in cross-section. These observations were consistent with the black paint occurring primarily on or near the limestone substrate. Nevertheless, a considerable amount of the black pigment was dispersed within the ~0.5mm thick rock coating.

To determine the general molecular composition of the rock coating we analyzed sub-milligram aliquots of the material (scraped from the surface using a needle) using a Perkin-Elmer Spectrum 100 ATR-FTIR. The ATR crystal used was diamond/ZnSe and all spectra were background corrected. The instrument was set at 4 cm^{-1} resolution and four scans collected. We identified oxalate as the principle component of the coating based on the characteristic broad absorption band centered at 1630 cm^{-1} and the sharp peak at 1320 cm^{-1} (Figure 4). Sulfate was also present as indicated by the broad absorbance between 1080 and 1180 cm^{-1}. There was evidence of carbonate based on the broad band at 1360 cm^{-1}.
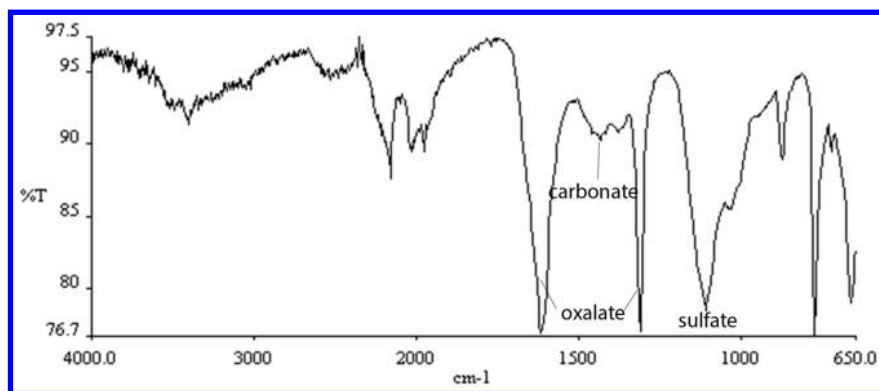
Figure 4. An ATR-FTIR spectrum of the rock coating that covers the black paint showing the presence of oxalate, sulfate and carbonate.

High magnification imaging and elemental analyses were performed using a Philips XL 30 ESEM operated at 30 keV in the "wet mode." This technique allowed us to analyze samples without adding a conductive coating, thereby leaving the samples unaltered for further study. We analyzed bulk sample surfaces, cross-sectional views of bifurcated samples, and powdered aliquots scraped from the surfaces using a needle

The ESEM/EDS analysis of the natural accretion revealed two distinctive microcrystalline forms comprising the rock coating (Figure 5). One consisted of relatively larger, platy crystals with high concentrations of Ca and S (Figure 5A). This is likely gypsum ($CaSO_4 \cdot 2H_2O$), which is prevalent on rock and stone surfaces, usually as a result of efflorescence (*13*). The second component appeared microcrystalline and was chemically consistent with calcium oxalate, either whewellite ($CaC_2O_4 \cdot H_2O$) or weddellite ($CaC_2O_4 \cdot 2H_2O$), based on the relative concentrations of Ca, C and O (Figure 5B). Oxalates are also common on rock surfaces inside dry rock shelters and under rock overhangs, i.e., surfaces not exposed to direct rain or runoff (*14*).
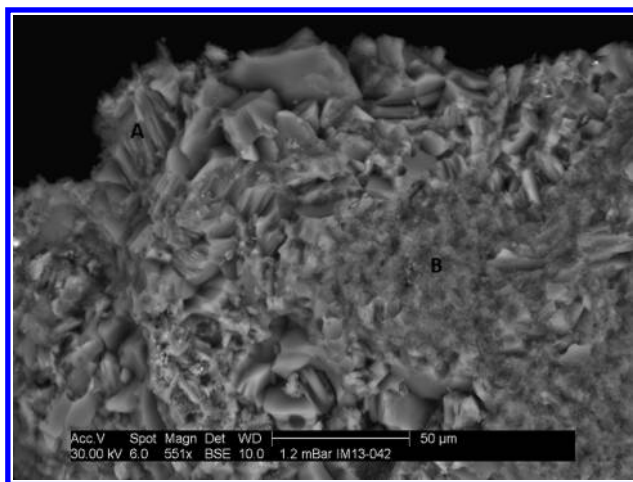
Figure 5. ESEM photomicrograph showing the rock coating in cross-sectional view. Two distinctive types of structures are observed. The EDS spectra (A) suggests that the platy material is calcium sulfate (probably gypsum), while the microcrystalline substance appears to be calcium oxalate (B).

High magnification of the paint samples using the ESEM/EDS also revealed two physically different pigment morphologies, although both pigment forms were chemically similar. One form of the paint appeared amorphous and smooth under high magnification, with small fractures occurring on the surface (Figures 6 & 7). The elemental composition of these areas was predominantly carbon (~70% C) with O/C ratios of 0.3. A second form of pigment consisted of small, black, cylindrical shaped particles, ~15 µm in height with ~3µm radii, and carbon rich, containing 70% to 80% C with O/C ratios between 0.2 – 0.3 (Figures 8 & 9).

Experiments using pyrolysis GC-MS were performed on scrapings from a black paint sample and a non-painted background sample using a CDS Pyroprobe 5200 coupled to a Varian PE Autosystem GC/MS system. The powdered samples (~10 mg) were placed in a boat that was inserted into the pyrolyzer and first heated to 250°C then to 600°C. Whereas there was no significant detection of compounds at 250°C, at 600°C there were a considerable number of organic compounds released from both the paint and background samples. Moreover, the chromatograms and mass spectra revealed essentially the same suite of compounds from both the paint and background sample, indicating that there were no unique materials released in the pyrolysis of the paint (Figure 10; Table 2). There were three groups of organic compounds released during the pyrolysis: aromatics, oxygenates and normal hydrocarbons. This result demonstrated that there is a considerable quantity of organic matter in the samples, but that these compounds were native to the oxalate-rich coating and not unique to the paint.

In Archaeological Chemistry VIII; Armitage, R., et al.;
ACS Symposium Series; American Chemical Society: Washington, DC, 2013.
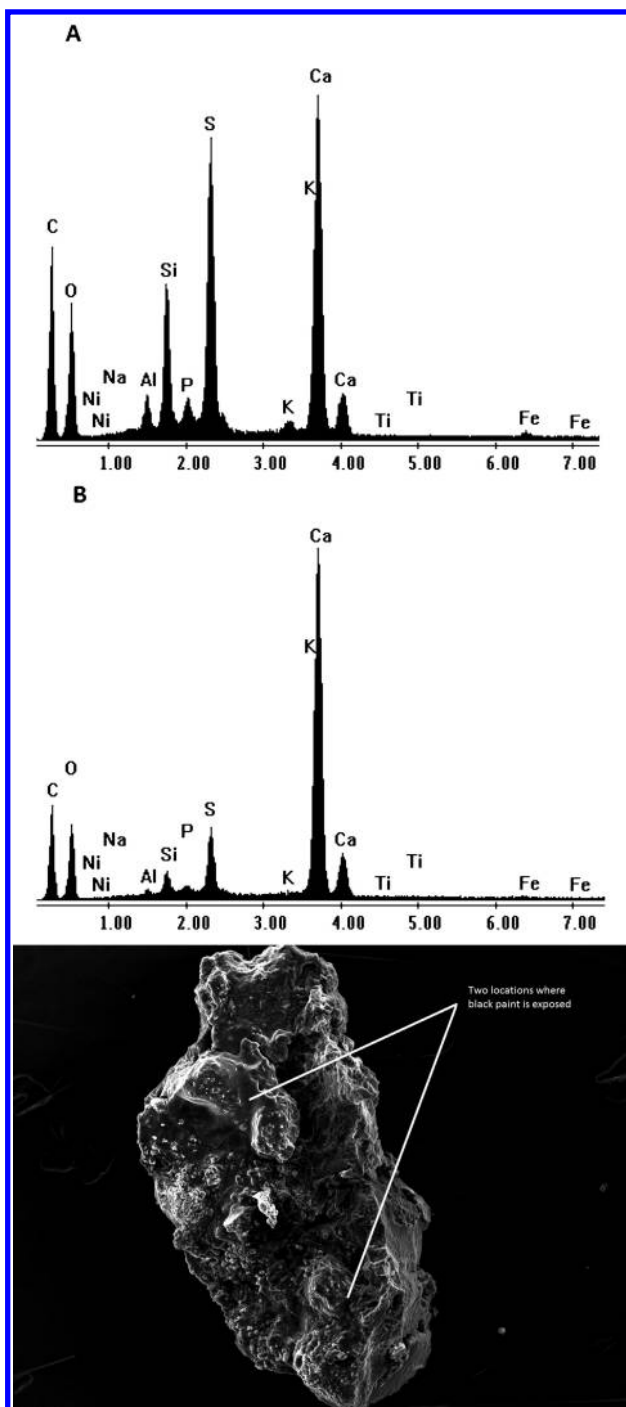
Figure 6. ESEM photomicrograph of a small fragment of the coating with exposed paint. The painted areas appear smooth and amorphous.
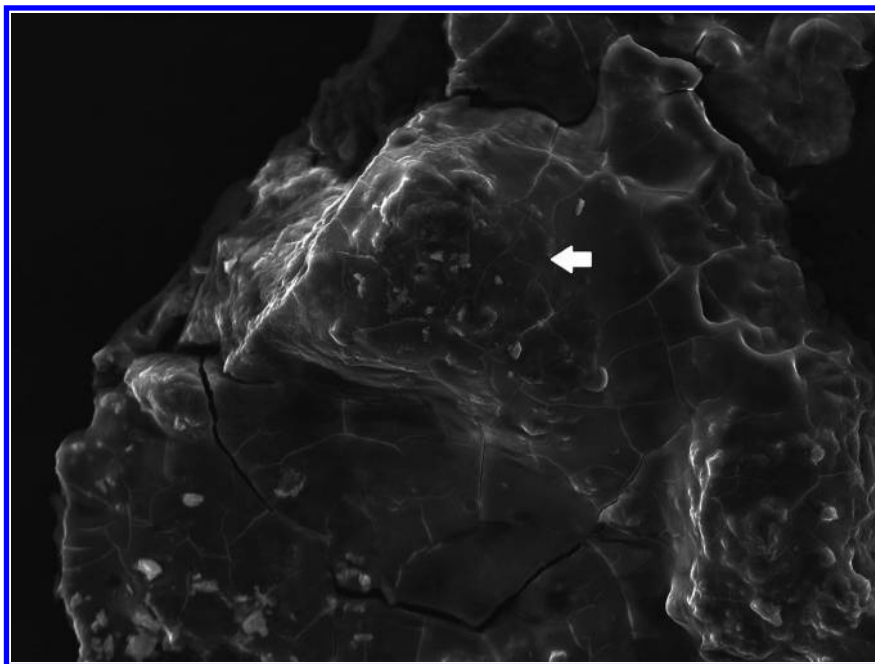
Figure 7. A highly magnified region in the top of Figure 7 showing the smooth texture of the paint. The EDS analysis (at arrow) demonstrates the paint matieral is predominately carbon.
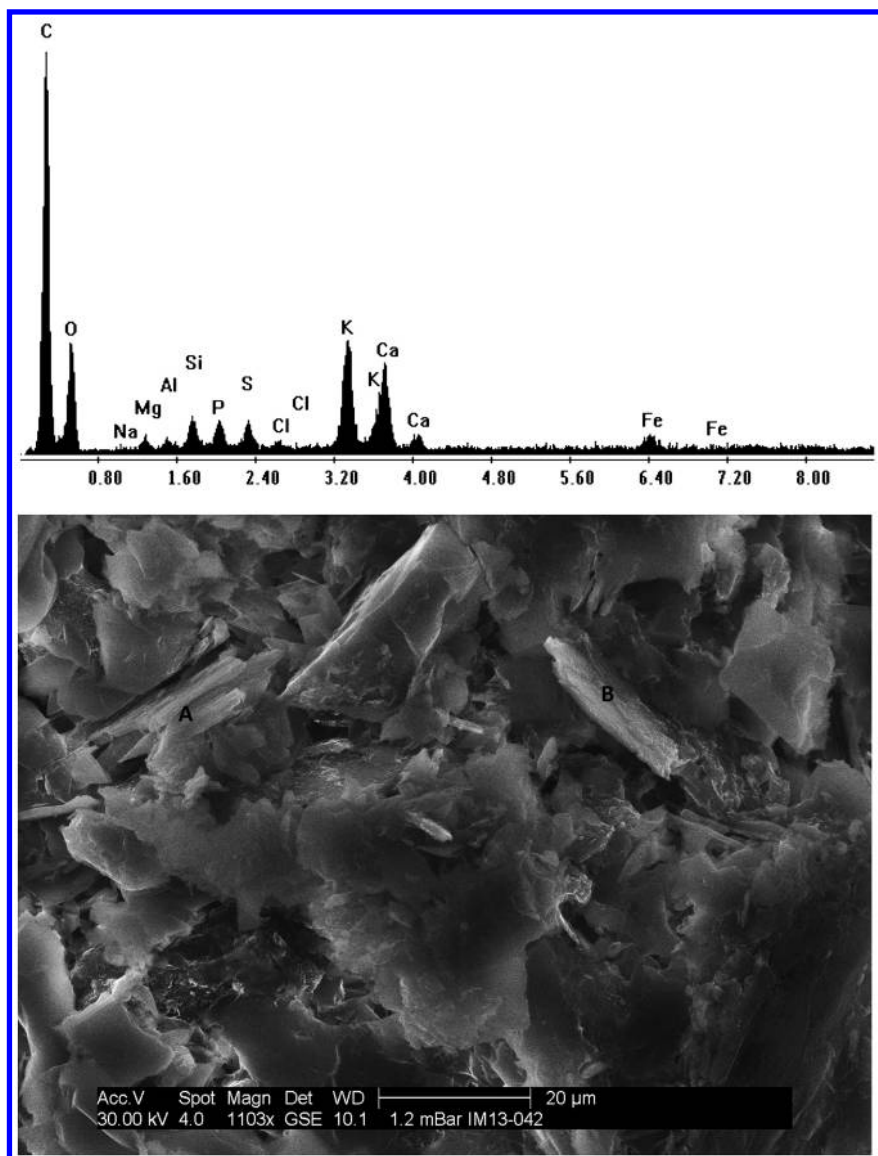
Figure 8. An ESEM photomicrograph of material scraped from the surface of a paint sample. The small particles labeled A and B are carbon rich, as shown in the EDS spectra A & B.
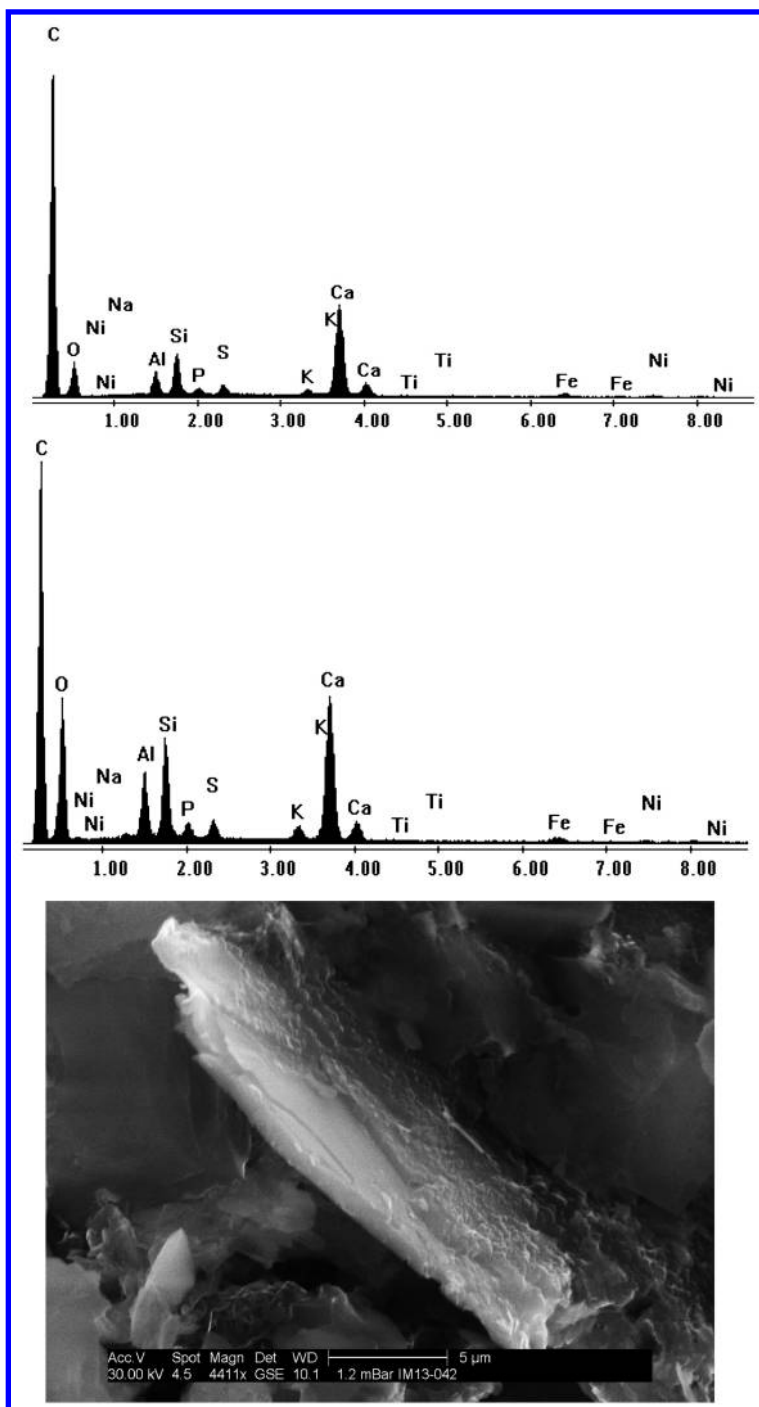
Figure 9. A high magnification ESEM photomicrograph showing what appears to be a charcoal fragment in the paint.
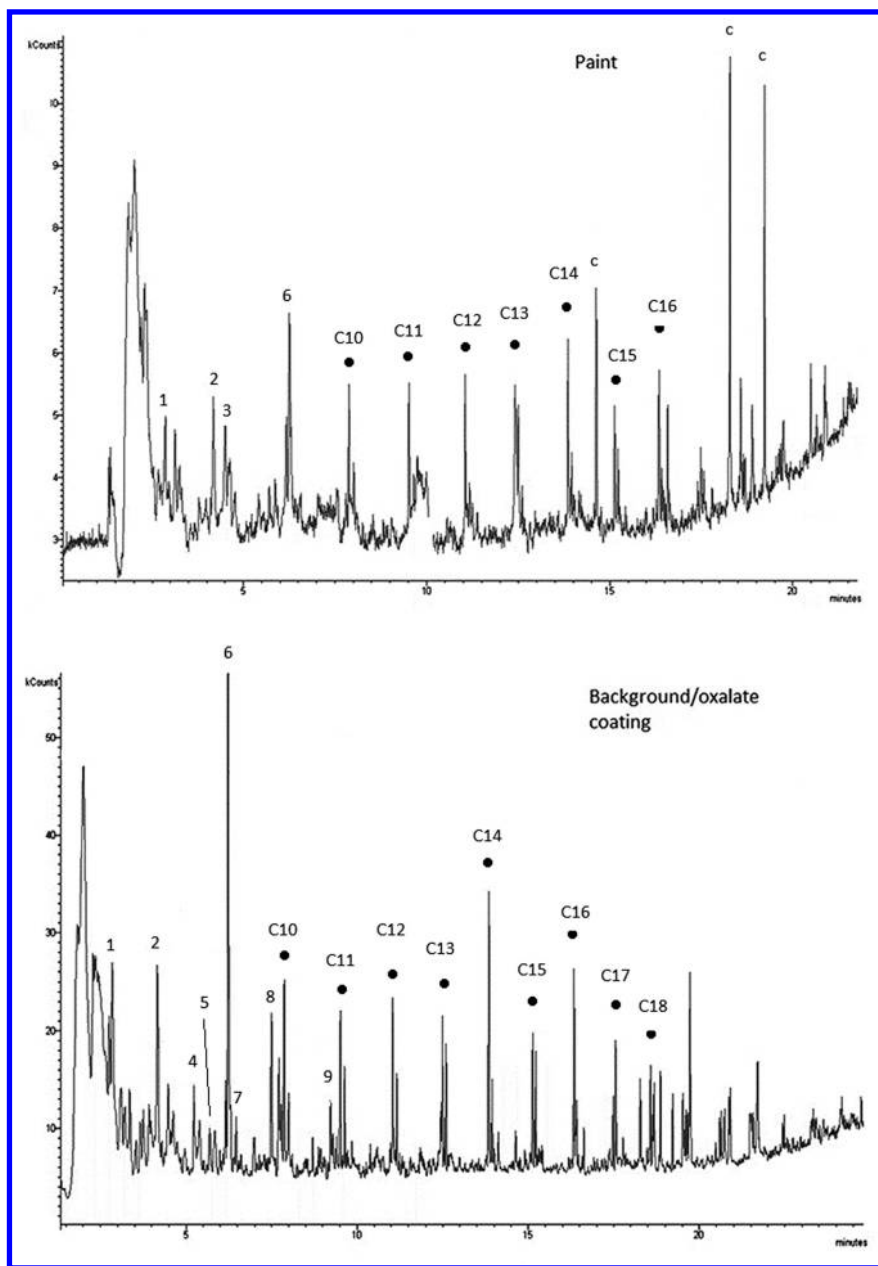
Figure 10. Pyrograms of a black paint sample from the C-1 Mural (Top) and a sample of the natural rock coating.collected adjacent to the mural (Bottom).

Table 2. Compounds identified in the pyrograms of black paint and natural rock coating

Peak number	Compound
1	Benzene
2	Methylbenzene (toluene)
3	1-Octene
4	2-Cyclopenten-1-one
5	Ethylbenzene
6	Phenylethene (styrene)
7	2-Methyl-2-Cyclopenten-1-one
8	Benzaldehyde
9	2,2-dihydroxy-1-phenylethanone
●	n-Alkane/Alkene pair
c	Contamination

Conclusions

One of the principal goals of this study was to investigate the feasibility of radiocarbon dating the rock art in the Oxtotitlán Cave. The results demonstrate that the pigments in samples of black paint from the site are most likely from pyrogenic carbon (PyC), specifically a combination of amorphous black carbon and charcoal. The incomplete combustion of plant material can produce a variety of PyC residues that have a continuum of physical and chemical properties (*15*). Depending on the extent of combustion based on factors such as temperature, chemical reformation (*16*), and oxygen availability, the combustion byproducts can take on a variety of characteristics. For example, partially charred plant materials that retain much of the original plant cellular structure are referred to as *charred biomass* (or simply *char*); when a more complete decomposition occurs but with particles > 0.2 μm^2 remaining the substance is defined as *charcoal*; and finally, higher temperatures with limited available oxygen produces *soot* (*15–17*). The amount of oxygen remaining in the PyC relative to carbon also decreases continuously with these trends, with O/C ratios of ~0.6 for char, ~0.4 for charcoal, and ~0.2 for soot (*15, 16*).

The characteristics of the black pigments, with observable carbon rich particles mixed with amorphous carbonaceous matter, both with O/C ratios between 0.2 – 0.3, suggest that the pigment material is a mixture of charcoal and soot. Because there is PyC in the paint it is therefore feasible to radiocarbon date the pigment, assuming that this material can be isolated from the oxalate-rich

coating and limestone substrate for the ^{14}C assay. Absolute dating of the paint will allow evaluation of socio-political relationships that are suggested by similarities in iconography between the sacred Oxtotitlán Cave and the capitals of early kingdoms, most especially the Olmec ceremonial center of La Venta, which was one of Mesoamerica's first cities.

A second strategy for establishing age constraints of the paintings is also feasible in the Oxtotitlán site. The samples of rock paint that we collected are covered by a Ca oxalate-rich rock coating. These coatings are the byproduct of either lichen or microbial activity (*14*, *18*, *19*) and as the oxalate is a biogenic byproduct it can be ^{14}C dated. Since the coating is superimposed over the paint, the creation of the paintings occurred prior to the formation of the oxalate. Thus, ^{14}C dating of the oxalate provides a minimum age. The strategy of using radiocarbon assays of oxalate coatings to constrain the age of rock art has been used worldwide, including Europe (*20*), Africa (*21*), Australia (*22–24*), South America (*25*, *26*), North America (*27*, *28*) and the Middle East (*29*).

Discussion

Our goal is to investigate early Mesoamerican social networks and the symbols and public representational art that developed alongside and mediated political power in the region's emerging kingdoms. The Formative period saw the emergence of multiple traditions of writing in Mesoamerica and rich iconographic systems that linked political power to history, core cultural myths, the landscape, and a tradition of performative political and religious theatre. This cave, as a portal to the world of night and death, and as a place of rebirth and transformation, is often represented as such within this cultural phenomenon. Accurate dating is essential for reconstructing how cave ritual evolved over millennia within the framework of the rise and fall of these prehistoric societies. A chronological framework allows evaluation of stylistic similarities, and underlying Formative period socio-economic relationships, between Oxtotitlán in southwestern Mexico and early ceremonial centers such as La Venta (ca. 800–400 B.C.E.) to the east on the Gulf Coast and Chalcatzingo to the northeast in Central Mexico.

The technology of prehistoric painting has the potential to contribute to this study in addition to dating. In the future we would like to characterize the composition of colors such as black and compare paint formulas used in Oxtotitlán to those identified different geographical regions and time periods. Mesoamerica has a long tradition of muralism, and the use of paints extended to decorating paper, cloth and animal hide, and the creation of painted manuscripts. The practitioners of these traditions were often highly trained individuals, and data from a variety of regions shows the emergence of schools characterized by particular stylistic and technological approaches to art and writing (*30–33*). Thus, understanding the underlying compositional formulae of early Mesoamerican muraling paints will contribute to our understanding of the evolution of technical skill and stylistic schools among Mesoamerica's artisans. The presence of murals such as C-1 from Oxtotitlán is a testament to the technical expertise of their anonymous authors.

Acknowledgments

References

1. Gay, C. *Nat. Hist.* **1967**, *4*, 28–35.
2. Grove, D. *Dumbarton Oaks, Studies in Precolumbian Art and Archaeology*; No. 6; Harvard University Press: Washington, DC, 1970.
3. *The Middle Preclassic Paintings at Oxtotitlán, Guerrero*. http://www.famsi.org/research/grove/ (accessed July 13, 2013).
4. Drucker, P.; Heizer, R. F.; Squier, J. *Bureau of American Ethnology*; Bulletin 170; Smithsonian Institution: Washington, DC, 1959.
5. González Lauck, R. *Olmec Art of Ancient Mexico*; Benson, E., de la Fuente, B., Eds.; National Gallery of Art: Washington, DC, 1996; pp 73−81.
6. Schmidt Shoenberg, P. *Thule Riv. ital. di studi americanistici* **2010**, *22*, 277–291.
7. Magaloni, D. *La pintura mural prehispánica en México: Área Maya*; de la Fuente, B., Staines Cicero, L., Eds.; Universidad Nacional Autónoma de México, Instituto de Investigaciones Estéticas: México, 2001; pp 155−198.
8. Rowe, M. W. *Rock Art Res.* **2012**, *29*, 118–131.
9. Newman, B.; Loendorf, L. L. *Plains Anthropol.* **2005**, *50*, 277–283.
10. Rowe, M. W.; Mark, R.; Berrier, M.; Billo, E.; Steelman, K. L.; Dillingham, E. *Am. Indian Rock Art* **2011**, *37*, 37–47.
11. Huntley (née Ford), J. *Austral. Archaeol.* **2012**, *75*, 78–94.
12. Beck, L.; Genty, D.; Lahlil, S.; Lebon, M.; Tereygeol, F.; Vignaud, C.; Reiche, I.; Lambert, E.; Valladas, H.; Kaltnecker, E.; Plassard, F.; Menu, M.; Paillet, P. *Radiocarbon* **2013**, *55*, in press.
13. Charola, A. E.; Pühringer, J.; Steiger, M. *Environ. Geol.* **2007**, *52*, 339–352.
14. Hofmann, B. A.; Bernasconi, S. M. *Chem. Geol.* **1998**, *149*, 127–146.
15. Preston, C. M.; Schmidt, M. W. I. *Biogeosciences* **2006**, *3*, 397–420.
16. Hedges, J. I.; Eglinton, G.; Hatcher, P. G.; Kirchman, D. L.; Arnosti, C.; Derenne, S.; Evershed, R. P.; Kögel-Knabner, I.; de Leeuw, J. W.; Littke, R.; Michaelis, W.; Rullkötter, J. *Organic Geochem.* **2000**, *31*, 945–958.
17. Thevenon, F.; Williamson, D.; Bard, E.; Anselmetti, F. S.; Beaufort, L.; Cachier, H. *Global Planet. Change* **2010**, *72*, 381–389.
18. Russ, J.; Palma, R. L.; Loyd, D. H.; Boutton, T. W. *Quaternary Res.* **1996**, *46*, 27–36.
19. Hess, D.; Coker, D. J.; Loutsch, J. M.; Russ, J. *Geoarchaeology* **2008**, *23*, 3–11.
20. Ruiz, J. F.; Hernanz, A.; Armitage, R. A.; Rowe, M. W.; Viñas, R.; Gavira-Vallejo, J. M.; Rubio, A. *J. Archaeol. Sci.* **2012**, *39*, 2655–2667.
21. Mazel, A. D.; Watchman, A. L. *South Afr. Humanit.* **2003**, *15*, 59–73.
22. Watchman, A.; O'Coonor, S.; Jones, R. *J. Archaeol. Sci.* **2005**, *32*, 369–374.

23. Smith, M. A.; Watchman, A.; Ross, J. *Geoarchaeology* **2009**, *24*, 191–203.
24. Aubert, M. *J. Archaeol. Sci.* **2012**, *39*, 573–577.
25. Hedges, R. E. M.; Ramsey, C. B.; Van Klinken, G. J.; Pettitt, P. B.; Nielsen-Marsh, C.; Etchegoyen, A.; Fernandez Niello, J. O.; Boshcin, M. T.; Llamazeres, A. M. *Radiocarbon* **1998**, *40*, 35–44.
26. Steelman, K. L.; Rickman, R.; Rowe. M. W.; Boutton, T. W.; Russ, J.; Guidon, N.; *Archaeological Chemistry*; Jakes, K. A., Ed.; ACS Symposium Series 831; American Chemical Society: Washington, DC, 2002; pp 22−35.
27. Russ, J.; Kaluarachchi, W. D.; Drummond, L.; Edwards, H. G. M. *Stud. Conserv.* **1999**, *44*, 91–103.
28. Scott, S. A.; Davis, C. M.; Steelman, K. L.; Rowe, M. W.; Guilderson, T *Plains Anthropol.* **2005**, *50*, 57–71.
29. Hassiba, R.; Cieslinski, G. B.; Chance, B.; Al-Naimi, F. A.; Pilant, M.; Rowe, M. W. *QScience Connect* **2012**, *4*. DOI: http://www.qscience.com/doi/abs/10.5339/connect.2012.4 (accessed July 11, 2013).
30. Lacadena, A. *PARI J.* **2008**, *8*, 1–22.
31. Reents-Budet, D. *Painting the Maya Universe: Royal Ceramics of the Classic Period*; Duke University Press: Durham, NC, 1994.
32. Rice, P. M. *J. Arch. Meth. Theory* **2009**, *16*, 117–156.
33. O'Grady, C. R; Hurst, H. In *ICOMM-CC 16th Triennial Preprints*; Bridgland, J., Ed.; Lisbon, Portugal, 2011; pp 869−879.

Chapter 8

Plasma Oxidation of Organic Residues on Modern Stone Tools

Karen L. Steelman* and Hayden Burger

Department of Chemistry, University of Central Arkansas, Conway, Arkansas 72035
*E-mail: ksteel@uca.edu

We utilized plasma oxidation and stable isotope mass spectrometry to study organic residues on stone tools. Corn, a C_4 plant, was processed using modern tools. Different washing techniques were explored prior to placing stone tools in an oxygen glow discharge. Remaining organic residues were oxidized to carbon dioxide for stable isotope mass spectrometry. This preliminary study explored the possibility of bulk stable isotope analysis and radiocarbon dating of organic residues on stone tools.

Introduction

Stone tools are well-preserved materials commonly found in the archaeological record. Projectile points, scrapers, choppers, knives, and other prehistoric tools provide information regarding site chronology, manufacturing strategies, material procurement, and food preparation practices. To assign age estimates for stone tool artifacts, archaeologists have relied upon indirect dating methods. Dates on charcoal from hearths or burned structures found in the same stratigraphic layers as stone tools are used to construct stone tool chronologies (*1*). Oftentimes, these associations are used across large geographical regions as well as broad archaeological time periods (e.g. Early Archaic, etc.). Differences in morphology are used to classify chronological sequences of stone tools with similar typology. Stone tools are currently dated by their anatomy and archaeological inference, rather than directly (*2*).

In 1986, Nelson et al. reported radiocarbon dates for blood residues on two stone tools from northern British Columbia, which were extracted using CHAPS

detergent, centrifugation, and filtration (*2*). That study was the first direct date for a stone tool. While results matched expected ages, further collaboration was not conducted. Recently, Yates et al. reported a pilot study for radiocarbon dating stone tool residues by processing ancient plant materials with modern stone tools (*3*).

For this current study, we used plasma oxidation to convert organic residues on modern stone tools to carbon dioxide for stable carbon isotope ratio mass spectrometry (IRMS). For ancient stone tools, extracted carbon dioxide could be radiocarbon dated using accelerator mass spectrometry (AMS) if artifacts contain organic material related to the event of interest – in our case, when stone tools were crafted and used by prehistoric cultures. Stable isotope analysis on surviving organic residues may also provide opportunities for understanding the source of residues and how prehistoric cultures utilized stone tools.

Surviving organic material on stone tools may reside on both the surface as well as in subsurface microcracks that are formed from pressure and percussion flaking (*4*). While some washing and extraction regimes remove surface residues, Shanks et al. (*5*) demonstrated that residue extraction from microcracks is only achieved through harsh cleaning. Thus, even stone tools that have been washed to remove sediment may still contain organic residues in microcracks.

Organic residue analysis in archaeology uses analytical techniques to identify organic remains associated with artifacts (*6*). For example, Evershed's research group has focused on chromatographic analysis of organic residues in pottery, including compound-specific AMS radiocarbon dating of fatty acids (*7*). On stone tools, surviving organic residues from plants and animals have been observed using microscopic visual identification as well as chemical analysis (*8–16*). To identify protein residues on stone tools, the three most common methods are counter-immunoelectrophoresis (CIEP), enzyme-linked immunosorbant assay (ELISA), and radioimmunoassay (RIA). For DNA sequencing, polymerase chain reaction (PCR) is used to amplify ancient DNA (e.g., (*17*)). Many organic residue studies have been criticized because of issues with ancient and modern contamination resulting in false positives as well as irreproducibility (*18–25*). However, if organic material on stone tools is preserved, found frequently, and in sufficient quantity, then it may be possible to determine the use and chronology of these artifacts by studying the objects themselves.

Plasma Oxidation

In this study, we used a plasma glow discharge to oxidize organic material on stone tools. Rowe and coworkers originally developed the method of plasma oxidation to extract organic carbon from ancient paint samples for radiocarbon dating (*26–29*). In addition, plasma oxidation has been used to oxidize perishable organic artifacts in a minimally destructive manner (*30, 31*). As an alternative to combustion, plasma oxidation is below the decomposition temperature of carbon-containing minerals, such as calcium carbonate and calcium oxalate (*26, 27*). Therefore, plasma oxidation is ideal for dating samples with a high mineral content such as rock art and stone tools.

Glow discharges are produced via radio frequency capacitive coupling with two external copper electrodes on either end of a glass sample chamber (Figure 1). A plasma is an electrically excited gas composed of neutral atoms, both negative and positive molecular and atomic ions, and electrons. Electrons gain kinetic energy from an oscillating electric field, while temperatures of gas components are increased by elastic collisions between electrons and the gas. Electrons are thermally isolated from gas components by their very large mass differences. Temperatures of plasma gas can remain near ambient temperatures at the same time electrons are sufficiently energetic to break molecular bonds. Active species in a glow discharge allow reactions that normally occur only at high temperatures to proceed at low temperatures. Oxygen plasmas convert organic matter to carbon dioxide, which is collected by freezing with liquid nitrogen for stable isotope analysis or AMS radiocarbon dating.
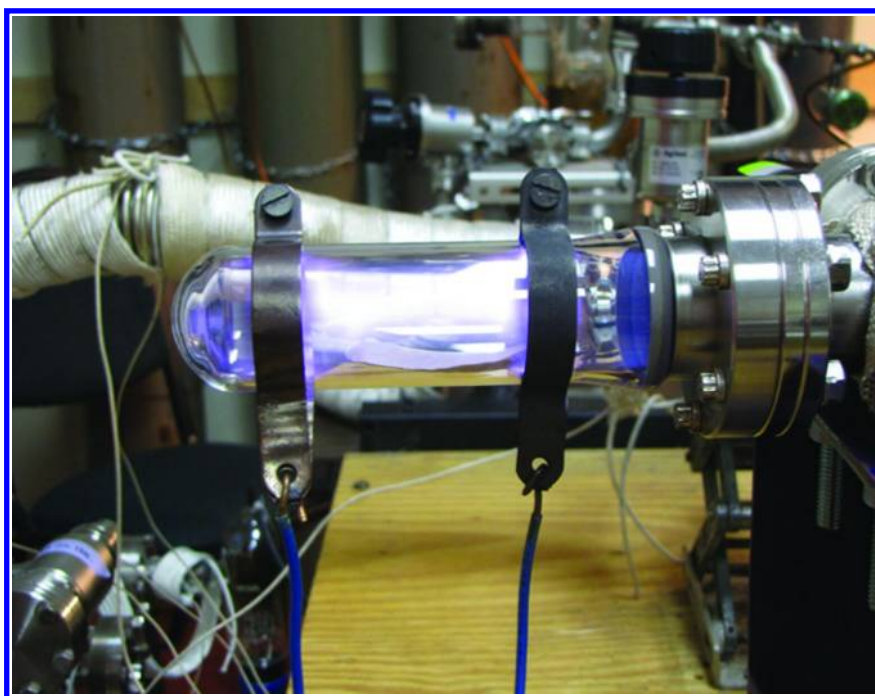
Figure 1. Stone tool in plasma sample chamber with glow discharge.

Stable Isotope Analysis
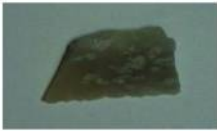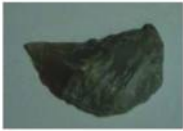
For this preliminary study, we analyzed organic carbon extracted from stone tools using stable carbon isotope analysis. Corn, a C_4 plant, was processed with modern stone tools so that we could differentiate organic residues on the stone tool from human contamination and organic material inherent in the stone of the tool – all of which have distinct $\delta^{13}C$ values. Stable isotope ratios are fingerprint values for the identification of materials, as well as assisting in paleodietary studies (*32*). A $\delta^{13}C$ value conveys the source of material being analyzed, i.e.

animal, vegetable, or mineral. Mass or isotopic fractionation occurs because lighter isotopes react more readily and at a faster rate than heavier isotopes. Natural isotopic fractionation occurs in nature through various biochemical reactions, such as C_3, C_4, and CAM photosynthesis as well as metabolism. Due to the small difference in $^{13}C/^{12}C$ ratios between all materials, isotope abundances are converted to relative ratios using the delta notation in parts per thousand or per mil.

Experimental Methods

Replica novaculite stone tools were made using percussion methods. Stone tools were labeled in groups by similar shape and surface area (A1-A5, B1-B5, etc). Table I shows the general shape, cross-sectional area, and mass of the tools. The groupings were correlated on the basis of shape and surface area rather than mass, as these properties are related to surfaces with available organic residues and ignores tool thickness.

Table I. Modern Stone Tools

Sample ID	Tool Shape	Area (mm²)	Mass (g)	Cleaning Method
A1		260	1.52	corn: water rinse
A2		250	1.44	corn: rotary shaker
A3		360	1.97	corn: soaking
A4		320	1.90	control: water rinse
A5		280	1.87	control: none
B1		400	3.79	corn: water rinse
B2		360	2.89	corn: rotary shaker
B3		380	3.38	corn: soaking
B4		420	4.01	control: water rinse
B5		390	3.89	control: none
C1		690	8.04	corn: water rinse
C2		630	5.95	corn: rotary shaker
C3		670	8.01	corn: soaking
C4		700	8.22	control: water rinse
C5		680	6.99	control: none
D1		840	9.85	corn: water rinse
D2		700	6.80	corn: rotary shaker
D3		870	11.14	corn: soaking
D4		880	10.23	control: water rinse
D5		800	8.47	control: none

Each stone tool in groups 1, 2, and 3 were used to remove corn from an entire cob. After corn processing, stone tools and their residues were dried at room temperature for 24 hours. For control experiments, stone tools in groups 4 and 5 were not used to process corn. We used different cleaning methods for the different stone tool groups (method 1 for group 1, method 2 for group 2, etc.). Methods 2 and 3 were modified from Shanks et al. (*16*).

During tool manufacture and corn processing, tools were handled without gloves. With commencement of laboratory analysis, tools were stored and handled with aluminum foil to prevent organic contamination. We also wore latex gloves. To avoid organic contamination in the laboratory, glassware was baked in a muffle furnace for 24 hours at 500°C prior to use. Water was retrieved from a Millipore Elix Advantage 5 with a Millipak 40 EPOD.

Group 1: Water Rinse

Typically, stone tools are cleaned after excavation with a dry paintbrush and immersion in water to remove soil. We modified this by using crumpled aluminum foil to physically remove visible corn residues. Stone tools were immersed in Millipore water for one minute and then rinsed before drying at room temperature for 1 day.

Group 2: Rotary Shaker

Stone tools were immersed in Millipore water for 10 minutes at 100 rpm on a rotary shaker. Then, they were scrubbed with crumpled aluminum foil for three minutes before drying at room temperature for 1 day.

Group 3: Soaking and Scrubbing

Stone tools were immersed in Millipore water for 10 minutes at room temperature. Then, they were scrubbed with crumpled aluminum foil for three minutes. Millipore water was poured over the tools to rinse surfaces before repeating the process. Soaking, scrubbing, and rinsing were repeated a total of five times before drying the stone tools at room temperature for 1 day.

Group 4: Water Rinse Control

Stone tools in group 4 were not used to process corn. However, we used method 1 to clean the stone tools. This control was to test the effectiveness of removing human contamination from handling.

Group 5: No Wash Control

Stone tools in group 5 were not used to process corn. No washing was performed on the tools prior to plasma oxidation. This control was to test for levels of human contamination from handling.

Plasma-Chemical Extraction

A custom-built plasma oxidation apparatus was used to convert organic material on stone tools to carbon dioxide. Corn kernels and human hair samples followed a parallel procedure. The apparatus, routinely kept under vacuum at a pressure of approximately 1×10^{-6} torr, utilized ultra-high purity (99.999%) oxygen and argon gases to minimize contamination. The empty sample chamber was cleaned by igniting successive oxygen plasma reactions at 1 torr oxygen gas and 100 or 150 watts radio frequency power for one hour each. These cleaning oxygen plasma reactions removed any organic material on the inside of the chamber introduced by previous samples or modern contamination from handling.

Next, we loaded a stone tool into the chamber and evacuated the system overnight using a turbomolecular pump with a scroll forepump to a pressure of $\leq 1 \times 10^{-6}$ torr. Then, successive argon plasma discharges, at 1 torr and 40 watts radio frequency power were ignited for one hour, to remove adsorbed gasses by impinging on the surface of the sample (Figure 1). Argon was used because it is an inert gas and will not chemically react with the sample.

Finally, organic residues were oxidized with oxygen plasma at a pressure of 1 torr and 100 watts radio frequency power. Stone tools experienced ambient temperatures of ~100°C. There was no observable damage to stone tools after plasma oxidation. Any organic material on the sample was converted into carbon dioxide and water during the one-hour exposure. Product carbon dioxide was flame-sealed into a glass tube cooled to liquid nitrogen temperature (-194°C), after water had been separated out using a dry ice/ethanol slurry (-58°C). Collected carbon dioxide was analyzed by IRMS at the University of Arkansas Stable Isotope Laboratory.

Stable Carbon Isotope Measurement

A multi-port on the IRMS instrument allowed automation of ten samples in a tube cracker system in which the glass fingers that were flame-sealed were scored and then cracked under a vacuum. A gas source, dual-inlet mass spectrometer with an electron impact source and a magnetic sector was used for stable carbon isotope analysis. Sample and standard gas were alternated in order to calculate the isotopic composition of the sample carbon dioxide. Three ion beams for carbon dioxide, corresponding to masses 44, 45, and 46 were measured using Faraday cup detectors. From this signal intensity data, a $\delta^{13}C$ value was determined. Instrumental precision of such measurements was typically greater than sample reproducibility.

Results and Discussion

Results for the stone tool groups are shown in Figure 2 and Table II. Tool D2 did not have sufficient carbon for measurement, due to a small crack in its CO_2 glass tube. Reported $\delta^{13}C$ values are expressed relative to V-PDB. Depending upon the size of the carbon dioxide samples, one or two significant figures were reported in the error. As samples with ≤ 10 µg extracted carbon have larger

error, their values are known with less certainty and, therefore, fewer decimal places. The data suggests three possible sources of organic carbon present on the stone tools (Figure 2): organic material inherent in the stone of the tools, human contamination from handling, and the actual corn residue. Differences in the amounts of carbon extracted per tool and stable isotope values are consistent between washing methods (1, 2, 3, 4, 5), instead of stone tool surface area and size (A, B, C, D).
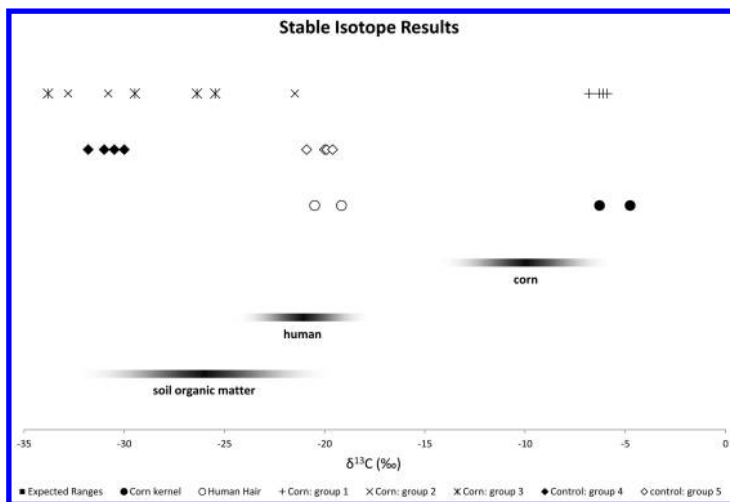
Figure 2. Stable carbon isotope values for extracted residues from stone tools. Human hair and corn kernels were measured independently. The ranges shown for soil organic matter inherent in the stone of the tool, human tissue, and corn are expected values (32, 33).

For group 1, we used a cleaning method similar to one that tools would experience after excavation to remove soil. Significantly more carbon (100-220 μg C) is present on tools in group 1, compared to groups 2 and 3. Bulk stable isotope results range from -6.80 to -5.90 ‰, agreeing with measured corn kernel $\delta^{13}C$ values of -6.28 and -4.75 ‰ as well as the expected range of corn (Figure 2). We were successfully able to extract corn residue from a modern stone tool for stable isotope analysis.

Groups 2 and 3 experienced more vigorous cleaning using methods modified from Shanks et al. (*16*). Our results are consistent with their findings. Both the rotary shaker and soaking method combined with scrubbing removed the majority of organic material. Only 9 to 30 μg C were remaining for plasma-chemical extraction and $\delta^{13}C$ values ranged from -33.8 to -21.48 ‰, consistent with soil organic matter that may be inherent in the stone. Also of interest was the large spread in the data for groups 2 and 3. An interesting linear trend was observed when the stable carbon isotope values were plotted versus the amount of carbon extracted (Figure 3). This suggests that the cleaning methods were not entirely sufficient at removing organic residues on the tools and that the measured values are a weighted average of soil organic matter and corn.

Table II. Results of stable isotope analyses

Sample	UCA ID #	μg C per tool	$\delta^{13}C$ (‰)
A1	B241	220	-6.80 ± 0.06
A2	B219	30	-21.48 ± 0.20
A3	B221	20	-25.46 ± 0.90
A4	B240	10	-30.5 ± 1.0
A5	B242	490	-20.00 ± 0.08
B1	B243	110	-6.30 ± 0.08
B2	B220	9	-32.8 ± 1.1
B3	B222	10	-33.8 ± 1.0
B4	B244	10	-30.0 ± 1.1
B5	B245	240	-19.90 ± 0.10
C1	B246	120	-5.90 ± 0.10
C2	B223	9	-30.8 ± 1.1
C3	B218	10	-29.5 ± 1.1
C4	B247	10	-31.0 ± 1.1
C5	B248	320	-19.60 ± 0.10
D1	B249	150	-6.10 ± 0.06
D2	B224	20	----
D3	B225	20	-26.37 ± 0.80
D4	B250	10	-31.8 ± 1.0
D5	B251	360	-20.90 ± 0.04
Corn	B226	80	-6.28 ± 0.06
Corn	B227	150	-4.75 ± 0.10
Hair	Hair1	40	-20.49 ± 0.10
Hair	Hair2	60	-19.16 ± 0.08

As corn is processed, not all components of the corn are equally retained by stone tools. Washing regimes using water will selectively remove water-soluble components, such as sugars and proteins, over lipids and starch. Importantly for this study, starch, the main component of corn, is insoluble in cold water. The

stable isotope value for starch would be similar to the bulk stable isotope value, which is a weighted average of the material in a corn kernel. Interestingly, lipids are consistently the most depleted biochemical relative to bulk material. However, corn lipids have $\delta^{13}C$ values ranging rom -14 to -17 ‰, a -4 to -7 ‰ shift from a bulk value (*34*) and would not explain the stable isotope values observed for groups 2 and 3.

We conducted two control experiments to test for the efficiency of removing human contamination from handling stone tools during their manufacture and use. We did not process corn with either group 4 or 5. Control group 5 was not washed prior to plasma-chemical extraction and had the largest amount of organic carbon present (240 to 490 μg C). Stable isotope values for control Group 5 ranged from -20.90 to -19.60 ‰, agreeing with measured human hair $\delta^{13}C$ values of -20.49 and -19.16 ‰ as well as the expected range for human tissue (Figure 2). This data suggests that human contamination is present on the stone tools from handling. Human fingerprint residues consist of 99% water, as well as water-soluble (salts, amino acids) and water-insoluble (lipids) trace components (*35*). To test the efficiency of removing this human contamination, we conducted another control experiment using cleaning method 1 on group 4. Only 10 μg carbon was remaining on the tools for plasma-chemical extraction and the $\delta^{13}C$ values ranged from -31.8 to -30.0 ‰, consistent with soil organic matter inherent in the stone tool. If human lipids from fingerprint residues had remained after washing, expected values would have been expected to range from -23 to -27 ‰ (shifted -4 to -7 ‰ from bulk). This suggests that cleaning method 1 is sufficient to remove human contamination from handling artifacts. Also, levels of organic material from the stone are minimal (≤10 μg C) and would not shift stable isotope or radiocarbon results if significant levels of organic residues are present (>100 μg C).
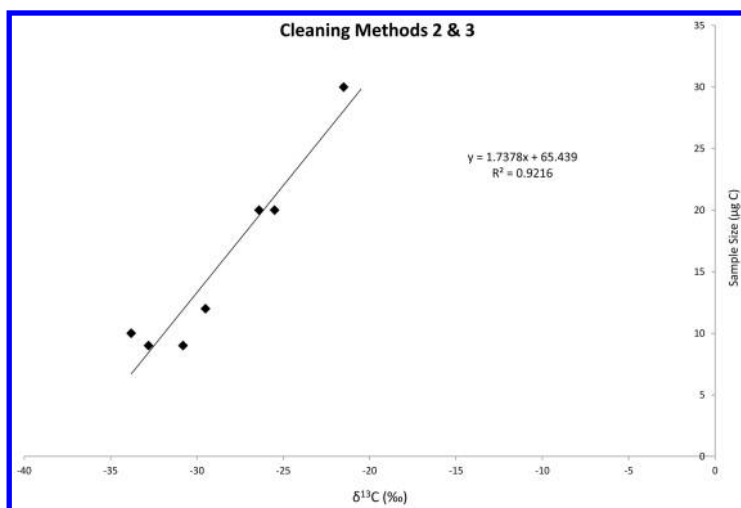
Figure 3. Linear trend showing that tools with 20 and 30 μg carbon extracted are shifted towards less negative stable isotope values.

Conclusions

The purpose of this preliminary experiment was to determine if organic residues on stone tools could be extracted using plasma oxidation for bulk stable isotope analysis or AMS radiocarbon dating. Cleaning method 1, which involved the physical removal of material from tool surfaces and rinsing with water, was sufficient to remove human contamination from handling. Corn residue was successfully extracted from modern stone tools for stable isotope analysis, with $\delta^{13}C$ values consistent with a C_4 plant.

This study highlights exciting new avenues of research for using plasma oxidation in archaeology. As residue analysis studies suffer from minimal levels of surviving material, the ability to extract a combination of proteins, starches, sugars, lipids, etc. and their degradation products remaining on a stone tool has a certain advantage. However, this advantage of plasma oxidation is also its disadvantage – we are able to directly oxidize all organic material on a stone tool, but we do not know the chemical identity of the material being collected. Bulk stable isotope analysis may provide some answers to these questions, but results would be a weighted average of organics present, especially for an ancient tool that had multiple uses.

We are seeking future archaeological studies with ancient stone tools found in well-dated contexts. Study sites with deep-time depth as well as associated organics (charcoal, plant or animal remains) found within close proximity to stone tools is needed to truly test the method. In this study, these modern stone tools were not buried. Only organic material inherent in rock itself and not the uptake of any soil organic material that might occur in a burial environment was considered. Cleaning procedures to remove contamination will be critical in future research. We hope to conduct dual-analyses: stable isotope analysis as well as accelerator mass spectrometry to directly radiocarbon date stone tools.

Acknowledgments

References

1. Geneste, J. M.; David, B.; Plisson, H.; Clarkson, C.; Delannoy, J. J.; Petchey, F.; Whear, R. *Aust. Archaeol.* **2010**, *71*, 66–69.
2. Nelson, D. E.; Loy, T. H.; Vogel, J. S.; Southon, J. R. *Radiocarbon* **1986**, *28*, 170–174.
3. Yates, A.; Smith, A. M.; Parr, J.; Scheffers, A.; Joannes-Boyau, R. *J. Archaeol. Sci.* **2013**, http://dx.doi.org/10.1016/j.jas.2013.02.016.
4. Shanks, O. C. Ph.D. dissertation, Oregon State University, Corvallis, OR, 2003.

5. Shanks, O. C.; Bonnichsen, R.; Vella, A. T.; Ream, W. *J. Archaeol. Sci.* **2001**, *28*, 965–972.

6. Evershed, R. P. *Archaeometry* **2008**, *50*, 895–924.

7. Stott, A. W.; Berstan, R.; Evershed, R. P.; Bronk-Ramsey, C.; Hedges, R. E. M.; Humm, M. J. *Anal. Chem.* **2003**, *75*, 5037–5045.

8. Haslam, M. In *Archaeological Science under a Microscope: Studies in Residue and Ancient DNA Analysis in Honour of Thomas H. Loy*; Haslam, M., Robertson, G., Crowther, A., Nugent, S., Kirkwood, L., Eds.; Terra Australis, Australian National University E Press: Canberra, Australia, 2009, Vol. 30, pp 47−79.

9. Loy, T. H. *Science* **1983**, *220*, 1269–1271.

10. Fullagar, R.; Furby, J.; Hardy, B. *Antiquity* **1996**, *70*, 740–745.

11. Newman, M. E.; Ceri, H.; Kooyman, B. *Antiquity* **1996**, *70*, 677–682.

12. Tuross, N.; Dillehay, T. D. *J. Field Archaeol.* **1995**, *22*, 95–110.

13. Hyland, D. C.; Tersak, J. M.; Adovasio, J. M.; Siegel, M. I. *Am. Antiq.* **1990**, *55*, 104–112.

14. Shanks, O. C.; Kornfeld, M.; Hawk, D. D. *J. Archaeol. Sci.* **1999**, *26*, 1183–1191.

15. Shanks, O. C.; Hodges, L.; Tilley, L.; Kornfeld, M.; Larson, M. L.; Ream, W. *J. Archaeol. Sci.* **2005**, *32*, 27–38.

16. Shanks, O. C.; Kornfeld, M.; Ream, W. *Archaeometry* **2004**, *46*, 663–672.

17. Hardy, B. L.; Raff, R. A.; Raman, V. *J. Archaeol. Sci.* **1997**, *24*, 601–611.

18. Kooyman, B. P. *Understanding Stone Tools and Archaeological Sites*; University of Calgary Press: Calgary, Canada, 2000, pp 161−164.

19. Potter, B. A.; Reuther, J. D.; Lowenstein, J. M.; Scheuenstuhl, G. *J. Archaeol. Sci.* **2010**, *37*, 910–918.

20. Lowenstein, J. M.; Reuther, J. D.; Hood, D. G.; Scheuenstuhl, G.; Craig Gerlach, S.; Ubelaker, D. H. *Forensic Sci. Int.* **2006**, *159*, 182–188.

21. Lombard, M.; Wadley, L. *J. Archaeol. Sci.* **2007**, *34*, 155–165.

22. Loy, T. H.; Jones, R.; Nelson, D. E.; Meehan, B.; Vogel, J.; Southon, J.; Cosgrove, R. *Antiquity* **1990**, *64*, 110–116.

23. Nelson, D. E. *Antiquity* **1993**, *67*, 893–895.

24. Gillespie, R. *Antiquity* **1997**, *71*, 430–437.

25. Loy, T. H. *Antiquity* **1994**, *68*, 147–148.

26. Russ, J.; Hyman, M.; Shafer, H. J.; Rowe, M. W. *Nature* **1990**, *348*, 710–711.

27. Armitage, R. A.; Brady, J. E.; Cobb, A.; Southon, J. R.; Rowe, M. W. *Am. Antiq.* **2001**, *66*, 471–480.

28. Steelman, K. L.; Ramirez, F. C.; Valcarce, R. F.; Guilderson, T. P.; Rowe, M. W. *Antiquity* **2005**, *79*, 379–389.

29. Steelman, K. L.; Rowe, M. W. In *A Companion to Rock Art*; McDonald, J., Veth P., Eds.; Blackwell Companions to Anthropology Series; Wiley-Blackwell Publishing: Oxford, U.K., 2012; pp 565−582.

30. Steelman, K. L.; Rowe, M. W. *Am. Antiq.* **2004**, *68*, 741–750.

31. Armitage, R. A.; Ellis, M. E.; Merrell, C. In *Collaborative Endeavors in the Chemical Analysis of Art and Cultural Heritage Materials*; Lang, P. L., Armitage, R. A., Eds.; ACS Symposium Series 1103; American Chemical Society: Washington, DC, 2012; pp 143−154.

32. Fry, B. *Stable Isotope Ecology*; Springer: New York, 2006, pp 1−308.
33. Stuiver, M.; Polach, H. A. *Radiocarbon* **1977**, *19*, 355–363.
34. Fagre, T.; Tieszen, L. L.; Rodriguez, S. *Proc. South Dakota Acad. Sci.* **1991**, *70*, 83–98.
35. Yamashita, B.; French, M. In *The Fingerprint Sourcebook*; McRoberts, A, Ed.; National Institute of Justice: Washington, DC, 2011; Chapter 7, pp 1−67.

Chapter 9

GC-MS Characterization of Carbohydrates in an Archaeological Use Residue: A Case Study from the Coahuila Desert

Badrinath Dhakal and Ruth Ann Armitage*

Department of Chemistry, Eastern Michigan University, Ypsilanti, Michigan 48197, U.S.A.
***E-mail: rarmitage@emich.edu**

A GC-MS method, which involves the formation of diethyldithioacetal trimethylsilyl derivatives of monosaccharides, was employed to characterize carbohydrates in a residue on a stone tool from the Coahuila Desert. The carbohydrate composition of the residue is consistent with the composition of desert food plants such as yucca, sotol, and lechuguilla. Quantitative analysis of carbohydrates in some ethnobotanically relevant standard materials was also performed to precisely understand the origin of the tool residue. The residue's composition is consistent with processing of a variety of sugar-rich desert food plants.

Introduction

Determining how an artifact was used in the past is a challenging undertaking. Bruier (*1*) describes some of the earliest work on determining the function of a stone tool based on the adhering macro- and microscopic residues. Microscopic examination of use-wear is often employed to identify markings, pollen and starch on stone tools in order to identify their original uses, with varying degrees of success (*2*, *3*). Blood and protein residues on stone tools were a controversial, even contentious area of study in the 1990s as DNA and immunological analyses became readily available (*4*–*8*). Even validated methods for identification of fresh proteins on stone tools (*9*) have proven unreliable for archaeological samples (*10*).

Rarely are macroscopic residues on stone tools preserved. While most archaeological contexts would not have preserved carbohydrate-rich gums, dry

conditions such as those in desert regions might better allow such residues to persist, as noted by Briuer (*1*). The work presented here sought to identify a use residue on a unique hafted stone tool from the Ivey Collection at the Center for Big Bend Studies. Preliminary FT-IR analysis indicated that this residue consisted primarily of carbohydrates, but more precise characterization was needed to better identify the source of that material (*11*)

Various methods for the analysis of carbohydrates in art and archaeological materials have been reported which include but are not limited to TLC (*12*), high performance liquid chromatography-mass spectrometry (HPLC-MS) (*13*), thermally assisted hydrolysis/methylation gas chromatography-mass spectrometry (THM-GC-MS) (*14–16*), pyrolysis-GC-MS (*17*, *18*), and GC-MS with derivatization (*19–25*).

Kharbade et al. (*12*) reported on the use of TLC to separate the monosaccharides present in the hydrolysate of plant gums identified in wall painting samples from India. This method is limited to only qualitative analysis of carbohydrates and a large (about 50 mg) sample is necessary for the analysis. Colombini et al. (*23*) reported on the analysis of a monosaccharide mixture by using high performance anion exchange chromatography with pulsed amperometric detection. This method requires solvents free of carbon dioxide, suffers from limited selectivity and resolution, and the high pH mobile phase leads to degradation of the carbohydrates.

With derivatization, gas chromatography-mass spectrometry (GC-MS) methods have some advantages over liquid chromatographic techniques. Fabbri et al. (*17*) reported on analysis of carbohydrates by pyrolysis-GC-MS where tetramethylammonium hydroxide (TMAH) was used as the derivatizing agent. This method is a convenient one for the qualitative study of carbohydrates. However, formation of a complex chromatogram with multiple peaks for even a single monosaccharide limits its use. Trimethylsilylation is the most common derivatization method for the GC-MS analysis of sugars but it, too, generally yields multiple peaks for a single monosaccharide. Vallance et al. (*19*) reported on the development of first GC-MS method with trimethylsilyl derivatization for the characterization of gum media in artists' materials. The chromatogram obtained from the carbohydrates was found to be complex due to the presence of up to five separate peaks for each monosaccharide, depending on the structural isomers present. However, identification of gum media was performed by comparing chromatograms of the samples with those of the standard gum materials.

To overcome the limitations of these other derivatization procedures, Pitthard and Finch proposed mercaptylation followed by trimethylsilylation, which yields only one peak for a single monosaccharide (*20*). This method was successfully employed to analyze the monosaccharides present in plant gums of interest in museum materials. The conversion of the carbonyl moiety into a diethyl dithioacetal or lactone prevents the monosaccharide from existing in different anomeric forms. This method seems to be suitable to identify as well as quantify different monosaccharides encountered in analysis of cultural heritage materials. This method has, however, been criticized as it involves the formation of some by-products during the derivatization and may result in interferences that complicate the analysis. Others (*21*, *22*, *24*) have discussed possibilities

In Archaeological Chemistry VIII; Armitage, R., et al.;
ACS Symposium Series; American Chemical Society: Washington, DC, 2013.

for the optimization of this method by sample cleaning and pretreatment but the possibility of sample loss during pretreatment precludes their application to the small samples of degraded materials that are common in this area of study. A report by Lluveras-Tenorio et al. (25) describes recent work on identifying carbohydrates in artists' materials.

Methods and Materials

Stone Tool from the Coahuila Desert, Mexico

The subject of this study is a use residue on a hafted stone tool from the Ivey Collection at the Center for Big Bend Studies (CBBS) in Texas. The tool was probably removed from a dry rockshelter near the town of Cuatro Ciénegas in Coahuila, Mexico by pothunters at some point in the past. The unifacial chert "scraper" is bound with an animal-derived string onto an approximately 70 cm long fragile sotol shaft (Figure 1). An organic substance, thought to be asphaltum or mineral pitch, secures the lithic portion within the shaft. Another substance, apparently accumulated from the use of the tool, covers the working end and lower end of the tool handle. This residue is marked with arrows in the close-up images in Figure 1. The original way in which this unusual tool was used has been questioned for many years. Other members of the Armitage and Rowe groups have undertaken several different analyses to determine the nature of this residue to determine what this object was indeed used for in the ancient past. Some possible uses suggested include collection of wild honey, harvesting of resins, processing of foodstuff plants, or scraping of hides (11).

Figure 1. Hafted stone tool from the Ivey Collection, Center for Big Bend Studies: (A) entire 70 cm artifact; (B) side view of stone tip; (C) top view of stone tip, with sampled use residue indicated by arrow.

Portions of the residue were removed by Dr. Marvin Rowe, now professor emeritus of chemistry at Texas A&M University, under the guidance of Dr. Robert Mallouf, director (now retired) of the Center for Big Bend Studies (CBBS) at Sul Ross State University, Alpine, TX. Preliminary results from analysis of extracts of the residue with GC-MS indicated the presence of carbohydrates, as did attenuated total reflectance Fourier transform infrared spectroscopy on samples of the residue (*11*). Based on these preliminary results, this sample was selected for further characterization using the more selective GC-MS method of Pitthard and Finch (*20*) specifically for carbohydrates.

Chemicals and Reagents

Monosaccharide standards D-(+)-glucose, D-(+)-galactose, L-(−)-mannose, D-(+)-xylose, L-(+)-arabinose, D-ribose, and D-fructose were obtained from Supelco (USA). D-glucuronic acid, L-(−)-rhamnose, L-(−)-fucose and mannitol (internal standard), were from Sigma-Aldrich. D-(+)-galacturonic acid monohydrate was obtained from Fluka, UK. Trifluoroacetic acid (TFA) 90% purity, anhydrous pyridine, ethanethiol (analytical grade), and hexamethyldisilazane (HMDS) were obtained from Sigma-Aldrich. Stock solutions of monosaccharide (1 mg/mL) were prepared by direct weighing of the materials and 5 µL diluted solution (100 µg/mL) of each of the monosaccharides was used for the derivatization.

Standard Materials

Powder samples of desert food plants such as lechuguilla (*Agave lechugilla*), sotol (*Dasylirion texanum*) and yucca (*Yucca torrey* or other species) were prepared by grinding the dry root, stem or leaf bases, as available. These materials were provided by Dr. Robert Mallouf from CBBS. Approximately 1-5 mg of each of the powdered materials was hydrolyzed in 400 µL 2M TFA. A 5 µL aliquot of the hydrolyzed solution was used for the derivatization.

Apparatus and Equipment Conditions

GC-MS studies were carried out using a Varian CP-3800 gas chromatograph coupled to a Varian Saturn 2000 ion trap mass spectrometer. The chromatographic separation was carried out on a 5% phenyl polydimethylsiloxane (PDMS) column (30 m long, 0.25 mm i.d. and 0.1 µm film thickness). The injector was in splitless mode at a temperature of 150 °C. Helium (99.998 % purity) was used as a carrier gas at an inlet pressure of 19.25 psi. The column oven was programmed to ramp from 165°C to 235°C at 2 °C per minute. The MS was operated in electron impact ionization (70 eV) mode, scanned over the m/z range of 40-650 using a solvent delay of 10 minutes. The total time of collection was 35 minutes. Mass spectra were recorded in total ion chromatogram (TIC) mode. Selected ion chromatograms were extracted after the analysis, using ions at m/z 319 for mannitol, m/z 249 for xylose, arabinose, rhamnose, fucose, mannose and galactose, and m/z 135 for galacturonic acid and glucuronic acid.

Sample Preparation for the GC-MS Analysis

The method described by Pitthard and Finch (*20*) was used to prepare the samples for analysis. Aliquots of the sample materials were weighed as described into individual vials, to which was added 400 µL of TFA (2M). Material was hydrolyzed at 105 °C for 5 hours. A 100 µL aliquot of hydrolyzed sample, after cooling to room temperature, was taken into another vial, mixed with 5 µL of mannitol (100 µg/mL) as internal standard and dried down with a nitrogen stream before subjecting it to mercaptalation and derivatization. A mixture (25 µL) of ethanethiol and TFA (2:1, v/v) was added to the dried sample to convert the resulting monosaccharides into diethyldithioacetals and lactones. The mercaptalation was performed at room temperature for 15 minutes. To obtain trimethylsilyl derivatives, 50 µL pyridine was added, followed by hexamethyldisilyzane (100 µL) and TFA (30 µL). The mixture was kept at room temperature for 1 hr and then concentrated to dryness under nitrogen. It was reconstituted in 200 µL of n-hexane, and 1 µL of this solution was injected into the GC-MS for the analyses. An outline of the method is shown in Figure 2. A scheme for the typical reaction that occurs during the derivatization of a monosaccharide is shown in Figure 3.
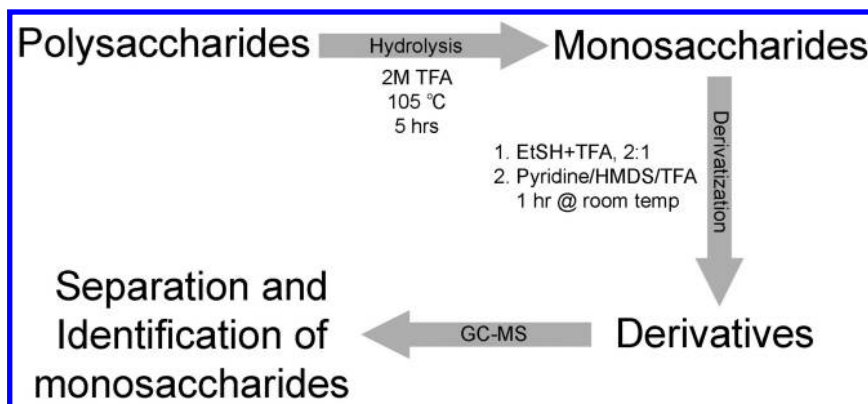
Figure 2. Outline of the method for the analysis of carbohydrates.
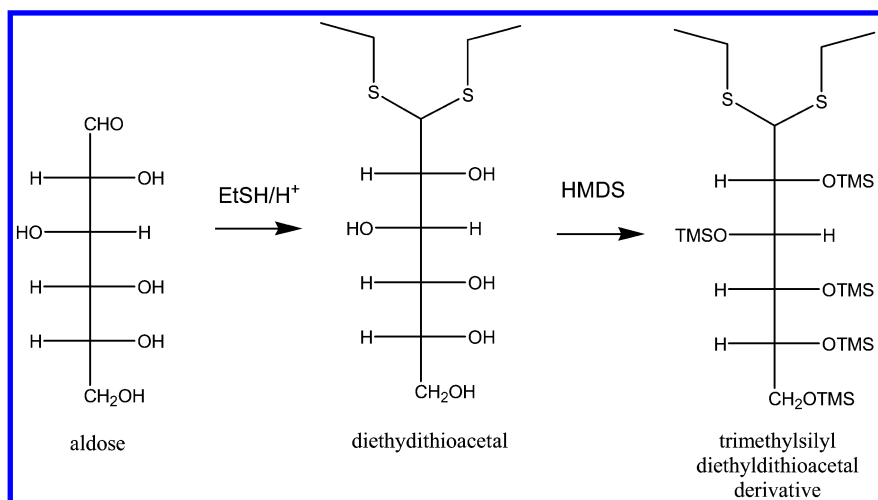
Figure 3. Typical reactions which occur during the derivatization of carbohydrates.

Results and Discussion

Qualitative Results

Analysis of Standard Monosaccharide Mixture and Reference Materials

The GC-MS method was validated by running monosaccharide standards and various reference materials. The retention time and the nature of the mass spectrum of each monosaccharide run individually and in the standard mixture as well as in the reference material were found to be consistent with the literature (*26*). Table I shows the peak numbers and abbreviations used in all the chromatogram shown. Figure 4 shows the selected ion chromatograms of the standard monosaccharide mixture.

A method blank containing only the internal standard was separately analyzed to evaluate background contamination, and found no significant levels of carbohydrates. A mass spectral user database was created for the identification of different monosaccharides in the sample. However, retention time was the primary consideration in identifying the peaks because the dominant ion fragment is the same for more than one monosaccharide. For example, both xylose and arabinose have as the base peak m/z 249, but the xylose standard eluted earlier than arabinose under the experimental conditions used herein. Similarly, galacturonic acid and glucuronic acid have the major peak at m/z 135 but the former eluted before the latter. However, identification of glucuronic acid was difficult at low concentrations because it is less susceptible to derivatization and often overlaps with galacturonic acid.

Table I. Compound identities for all chromatographic peaks

Peak #	Name of monosaccharide	Abbreviation
IS	internal standard (mannitol)	IS
1	Xylose	Xyl
2	Arabinose	Arab
3	Rhamnose	Rham
4	Fucose	Fuc
5	Galacturonic acid	GalAc
6	Glucuronic acid	GluAc
7	Glucose	Glc
8	Mannose	Man
9	Galactose	Gal
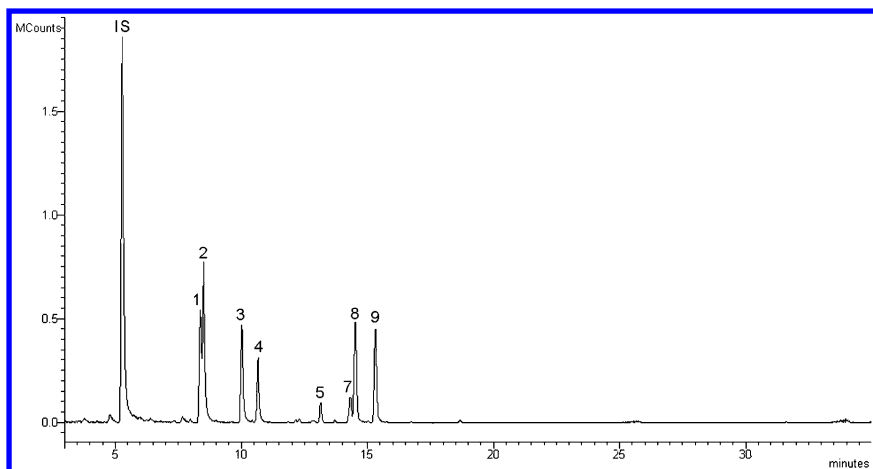
Figure 4. Selected ion chromatogram of standard monosaccharide mixture. Peak numbers refer to the compound list in Table I.

Analysis of Carbohydrates in the Stone Tool Residue and Desert Food Plants

The carbohydrate composition of the residue on the Ivey Collection's stone tool would be indicative of a certain source and its analysis could be useful in understanding the use of the tool. Attenuated total reflectance FT-IR analysis of this residue showed an intense peak for alcohol groups which might be indicative of sugars (*11*).

Most of the common monosaccharides were identified in the tool usage residue, as shown in Figure 5a, which supports the previous studies that suggested the residue consists primarily of carbohydrates. However, this information is not enough to understand what the tool was used for. The presence of sugars in the residue may indicate that the tool was used for harvesting or preparing food materials. Literature on the ethnobotany of the region where the tool was discovered, reports that ancient people used many of the desert plants as a source of food (*26*). Plants like yucca, lechuguilla, and sotol in particular have roots and leaf bases that are rich in sugars, though releasing the sugars into a digestible form requires considerable effort, including roasting the plant hearts in stone lined pits over several days. One way of understanding the source of the carbohydrates in the tool usage residue is to compare the carbohydrate composition with that in the ethnobotanically relevant plant materials. Figure 5b-d shows the carbohydrate compositions of yucca root, lechuguilla and sotol leaf bases. A close resemblance can be found in the sugar composition between the tool use residue and these desert food plants. All of these materials including the residue contain xylose, arabinose, rhamnose, galacturonic acid, glucose, mannose and galactose. Fucose is present only in sotol and the residue. This shows that the residue more closely resembles sotol (unsurprising, as some of the sotol from the handle of the tool may have been incorporated into the sample). The qualitative results imply that the tool might be used for harvesting sugar-rich food materials like yucca and lechuguilla. The residue is likely to be a complex mixture that accumulated over the time during which the tool was used. It is highly likely that the tool would have been used for whatever foods were available, not for one specific plant over another. The qualitative results of the carbohydrates in the tool usage residue and the desert food plants are included in Table II.
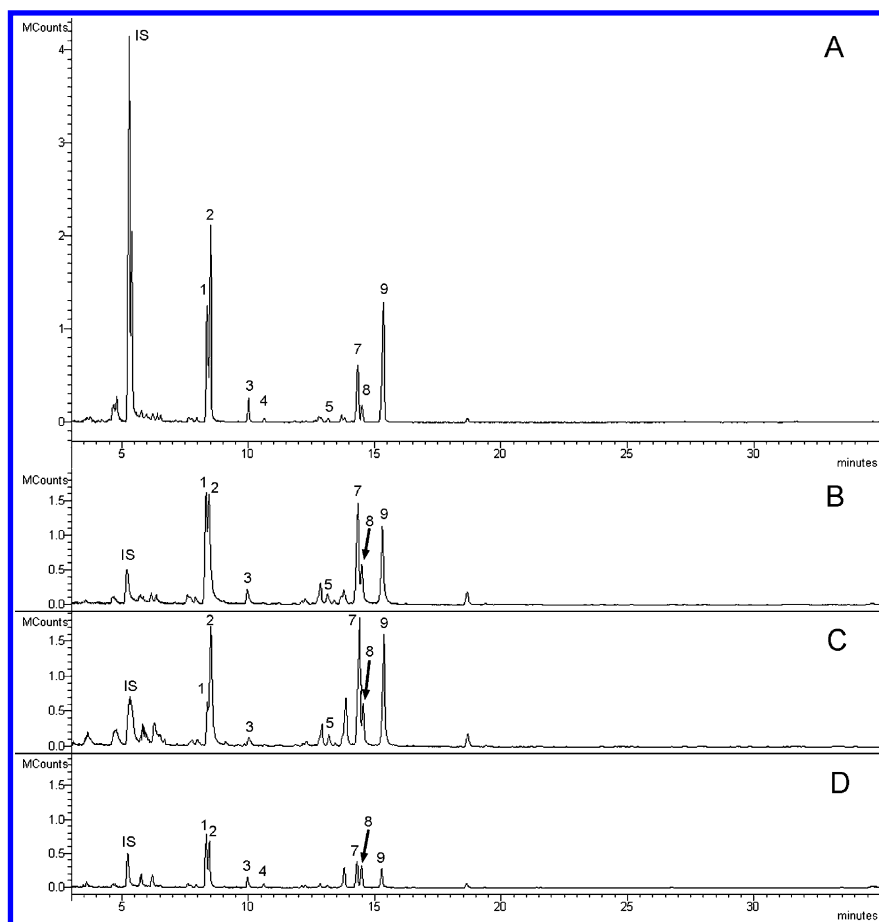
Figure 5. Selected ion chromatograms for the stone tool residue (a) and the desert food plants: yucca (b), lechuguilla (c), and sotol (d). Peak numbers refer to the compound list in Table I.

Table II. Summary of qualitative results for the carbohydrates in the stone tool residue, desert food plants and some possible known binding materials (x = present, 0 = not detected)

	Stone tool residue	Yucca	Sotol	Lechuguilla
xylose	x	x	x	x
arabinose	x	x	x	x
rhamnose	x	x	x	x
fucose	x	0	x	0
galacturonic acid	x	x	x	x
glucuronic acid	0	0	0	0
glucose	x	x	x	x
mannose	x	x	x	x
galactose	x	x	x	x

Quantitative Results

Qualitative results can provide further insight into the type of carbohydrates present in the samples. This information is not always helpful in determining the nature of an archaeological residue, as there are many sources of carbohydrates in the environment and the samples are in constant exposure to the environment over a long timespan. Quantitative analysis is necessary to understand the origin of the carbohydrates in the sample. It is generally assumed that the relative distribution of different monosaccharides in the sample is indicative of its source. While this is true for museum specimens like watercolor paintings (in which the pigment is suspended in a gum base), the decomposition and exposure of archaeological carbohydrates mean that there may be more significant variation in the observed carbohydrate composition in the ancient residue compared to modern reference materials. It might, if decomposition and contamination are minimal, be possible to identify the source of the use residue by comparing the results from the quantitative analysis of carbohydrates in the material with that of possible sources. Materials like this one from an arid environment have the best possibility of being well preserved.

Carbohydrates in the Stone Tool Residue and Desert Food Plants

The relative proportions of different monosaccharides present in the residue would be helpful in determining its origin. There should be a relationship between the nature of materials present in the residue and the use of the tool in the past. From the qualitative analysis of carbohydrates, it was found that the carbohydrate

composition of the residue resembles that in some of the desert food plants like lechuguilla, sotol, and yucca. A quantitative analysis would be helpful to find a better correlation of the tool residue with any of these food plants. Figure 6 shows the relative distribution of different monosaccharides in the tool residue as well as in the food plants.

The amount of each of the monosaccharides in micrograms present per milligram of each sample was calculated using the internal standard metho to determine if there was any unique pattern. Generally, the carbohydrate compositions look similar to each other. However, the ratio of some specific monosaccharides can be considered to find a better correlation of the tool residue with the food plants. Table III shows the ratio of masses of different monosaccharide pairs in the tool residue and the desert food plants. The ratios of different pairs of monosaccharides do not correlate the composition of the tool residue to that of any single plant, but in some cases are similar to an average of the ratios from all three plants. This may indicate that the tool was used for harvesting food materials from different plants and the residue was accumulated over time. Another possibility is that the carbohydrates in the tool residue have been degraded to some extent and hence it is now not consistent with any single material.
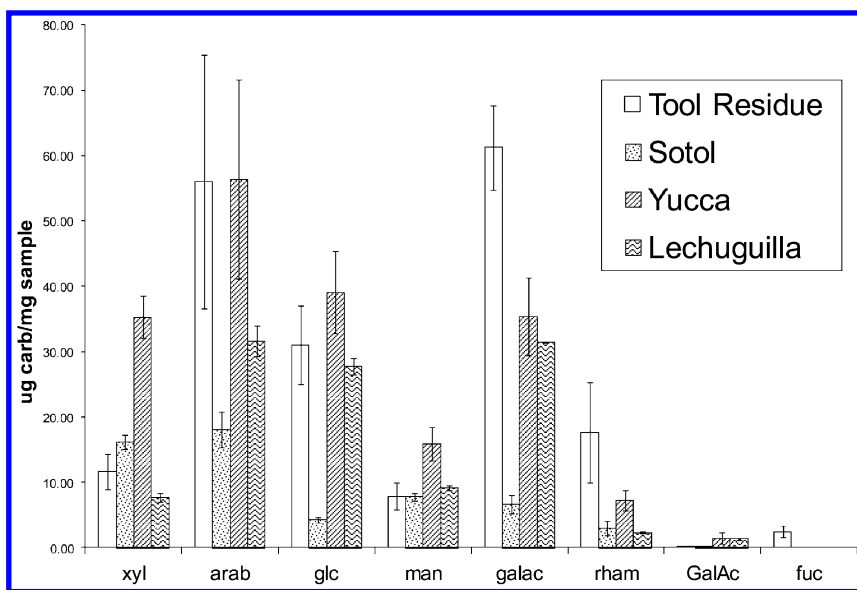
Figure 6. Quantitative comparisons of carbohydrates (in micrograms per mg of material) between the stone tool residue and three desert food plants.

Table III. Quantitative ratio of different monosaccharide pairs in the tool residue and the desert food plants

	residue	yucca	sotol	lechuguilla	Average of plants
Xyl/Arab	0.78	1.03	1.15	0.25	0.81
Glc/Man	3.65	2.97	1.22	3.45	2.55
Gal/Rham	6.09	5.11	2.17	12.88	6.72
Man/Arab	0.11	0.37	0.50	0.30	0.39
Man/Xyl	0.14	0.36	0.44	1.18	0.66
Gal/Xyl	1.08	0.81	0.42	3.42	1.55
Glc/Xyl	0.50	1.08	0.54	4.07	1.90

Conclusions

An existing GC-MS method with suitable derivatization was successfully applied to evaluate the carbohydrate composition in the tool usage residue. The qualitative as well as the quantitative analysis of carbohydrates in the tool residue indicate that the tool might have been used for harvesting food materials from desert plants such as yucca, sotol, and lechuguilla. The tool residue is likely a mixture of materials accumulated from different plants over time.

Future Work

The contamination of archaeological materials makes them difficult to characterize. Both qualitative as well as quantitative results might be altered compared to reference materials and consequently might lead to unreliable conclusions. Comparison of the carbohydrate composition of the tool usage residue with other possible reference materials is necessary to further clarify how the stone tool was actually used by the ancient people in the Coahuila Desert.

Though this GC-MS method is suitable for the characterization of carbohydrates, the mandatory derivatization step makes this method difficult and time consuming and not very sensitive. One future direction for the analysis of similar archaeological materials will be to combine direct analysis in real time mass spectrometry (DART-MS) and principle components analysis, a method that has been shown to be beneficial for differentiating wood, pharmaceuticals and food materials (27–29). DART-MS requires no sample preparation, a significant advantage over this GC-MS method that is complex and uses toxic reagents. Green methods that reduce exposure and waste should be sought out when possible. Resins, sugars, lipids, and possible biomarker compounds can all be measured at once with DART-MS, which should aid in better determining the nature of this unique residue.

Acknowledgments

References

1. Briuer, F. L. *Am. Antiq.* **1976**, *41*, 478–484.
2. Anderson, P. C. *World Archaeol.* **1980**, *12*, 181–194.
3. Monnier, G. F.; Ladwig, J. L.; Porter, S. T. *J. Archaeol. Sci.* **2012**, *39*, 3284–3300.
4. Smith, P. R.; Wilson, M. T. *J. Archaeol. Sci.* **1992**, *19*, 237–241.
5. Cattaneo, C.; Gelsthorpe, K.; Phillips, P.; Sokol, R. J. *World Archaeol.* **1993**, *25*, 29–43.
6. Tuross, N.; Dillehay, T. *J. Field Archaeol.* **1995**, *22*, 97–110.
7. Eisele, J. A.; Fowler, D. D.; Haynes, G.; Lewis, R. A. *Antiquity* **1995**, *69*, 36–46.
8. Tuross, N.; Barnes, I.; Potts, R. *J. Archaeol. Sci.* **1996**, *23*, 289–296.
9. Reuther, J. D.; Lowenstein, J. M.; Gerlach, S. C.; Hood, D.; Scheuenstuhl, G.; Ubelaker, D. H. *J. Archaeol. Sci.* **2006**, *33*, 531–537.
10. Lowenstein, J. M.; Reuther, J. D.; Hood, D. G.; Scheuenstuhl, G.; Gerlach, S. C.; Ubelaker, D. H. *Forensic Sci. Int.* **2006**, *159*, 182–188.
11. Van Gemert, J. ; Stambek, J.; Mallouf, R.; Rowe, M.; Armitage, R. A. Paper presented at the *37th International Symposium on Archaeometry*, Siena, Italy, May 2008.
12. Kharbade, B. V.; Joshi, G. P. *Stud. Conserv.* **1995**, *40*, 93–102.
13. Shen, X.; Perreault, H. *J. Chromatogr., A* **1998**, *811*, 47–59.
14. Fabbri, D.; Helleur, R. *J. Anal. Appl. Pyrolysis* **1999**, *49*, 277–293.
15. Schwarzinger, C. *J. Anal. Appl. Pyrolysis* **2004**, *71*, 501–514.
16. Li, R.; Baker, S.; DeRoo, C. S.; Armitage, R. A. In *Collaborative Endeavors in the Chemical Analysis of Art and Cultural Heritage Materials*; Lang, P. L., Armitage, R. A., Eds.; ACS Symposium Sereis 1103; American Chemical Society: Washington, DC, 2012; pp 75−89.
17. Fabbri, D.; Chiavari, G. *Anal. Chim. Act.* **2001**, *449*, 271–280.
18. Chiantore, O.; Riedo, C.; Scalarone, D. *Int. J. Mass Spectrom.* **2009**, *284*, 35–41.
19. Vallance, S. L.; Singer, B. W.; Hitchen, S. M.; Townsend, J. H. *J. Am. Inst. Conserv.* **1998**, *37* (3), 294–311.
20. Pitthard, V.; Finch, P. *Chromatographia* **2001**, *53*, S-317–321.
21. Bonaduce, I.; Brecoulaki, H.; Colombini, M.; Lluveras, A.; Restivo, V.; Ribechini, E *J. Chromatogr., A* **2007**, *1175*, 275–282.
22. Lluveras, A.; Bonaduce, I.; Andreotti, A.; Colombini, M. P. *Anal. Chem.* **2010**, *82*, 376–386.
23. Colombini, M. P.; Ceccarini, A.; Carmignani, A. *J. Chromatogr., A* **2002**, *968*, 79–88.

24. Lluveras-Tenorio, A.; Mazurek, J.; Restivo, A.; Colombini, M.; Bonaduce, I. *Chem. Cent. J.* **2012**, *6*, 1–16.
25. Lluveras-Tenorio, A.; Mazurek, J.; Restivo, A.; Colombini, M. P.; Bonaduce, I. *PLoS ONE*, *7*, e49383.
26. Ethnobotany of the Lower Pecos Canyonlands. Texas Beyond History. http://www.texasbeyondhistory.net/ethnobot/index.html (accessed March 10, 2011).
27. Kim, H. J.; Baek, W. S.; Jang, Y. P. *Food Chem.* **2011**, *129*, 1305–1310.
28. Cody, R. B.; Dane, A. J.; Dawson-Andoh, B.; Adedipe, E. O.; Nkansah, K. *J. Anal. Appl. Pyrolysis* **2012**, *95*, 134–137.
29. Zeng, S. S.; Wang, L.; Chen, T.; Wang, Y. F.; Mo, H. B.; Qu, H. B. *Anal. Chim. Acta* **2012**, *733*, 38–47.

Chapter 10

Portable X-ray Fluorescence and Archaeology: Limitations of the Instrument and Suggested Methods To Achieve Desired Results

Aaron N. Shugar*

Art Conservation Department, Buffalo State College, Rockwell Hall 230, 1300 Elmwood Ave., Buffalo, New York 14222
***E-mail: shugaran@buffalostate.edu**

This is an exciting time for archaeology. The ongoing miniaturization of analytical instrumentation has advanced to a state where traditionally lab-based analysis can now be performed in the field (i.e. XRF, Raman, FTIR etc...). In situ analysis can be enormously advantageous for archaeologists by providing on the spot identification of elements in artifacts. In addition, the resulting analyses can help guide subsequent excavation toward achieving specific goals. But what seems advantageous can also be problematic if not fully understood or properly implemented. PXRF may promote Utopian expectations for on-site elemental analysis, but what is often offered and promoted by manufacturers rarely produces viable data when used to investigate the material types encountered in archaeology. The underlying physics of XRF may limit what can be considered acceptable data, yet it is still possible to extract exceptionally useful information. Several examples will be given to highlight issues that can arise during in-situ analysis. Analytic methods will be described that will aid in proper interpretation of raw data.

Introduction

X-ray fluorescence has a long and diverse history as an analytical technique. The development and miniaturization of components (detectors, X-ray tubes etc…) has facilitated the evolution of this powerful tool into a handheld/portable device (*1*, *2*). (These instruments have been named handheld XRF, HHXRF, Portable XRF, and PXRF. For the remainder of this paper I will refer to them all as PXRF.) The range of applications for these instruments is diverse, including industries such as geology, environmental remediation, and recycling. The development of PXRF has allowed the technology to maintain its relevance in these industries. In geological analysis PXRF is used to identify precious metals and major and trace elements, to conduct geochemical surveys or for prospecting (*3–5*). It is also used for characterizations of rocks (*6–8*), ores (*9*, *10*) and soils (*11*, *12*) and it has a long history of usefulness in the mining industry. For environmental remediation handheld PXRF has been used extensively to identify and quantify lead in paint. There is currently a NIST methodology and calibration reference set (SRM 2579a) for handheld XRF identification of lead in paint. In addition, EPA method 6200 (*13*) was designed for identifying heavy metals in soils (*11*, *12*, *14*, *15*).

It is the recycling industry which has really allowed this field to blossom. The ability to rapidly complete alloy identification in scrap metal yards has helped this industry make billions of dollars. Quickly and easily differentiating between high alloy stainless steels and lower grade steels has increased business profits and this has been a driving force for promoting sales of PXRF instrumentation.

The fields of art, archaeology, industrial hygiene, and the emerging use of PXRF in forensics can best be described as minor applications for the manufacturers of handheld XRF. This is because they add a very small market share to the industry. What is most intriguing is that the fields of art and archaeology provide manufacturers with some of the most difficult samples to characterize. Most modern materials are generally homogenous, have uniform structure, and are well-characterized, whereas the materials that are investigated in art and archaeology have few or none of those features. Nevertheless, the use of PXRF has exploded in the field of archaeology based on its effectiveness, relatively cheap cost and its ease-of-use. In addition, the ability to transport instrumentation to the site and work *in situ* has enormous benefits. For these reasons, it is not surprising that there has been a relatively recent surge of publications incorporating PXRF technology.

Publications using the term handheld XRF started to appear as early as 2005. The expression PXRF had a slightly earlier introduction in the literature with articles from 1995 to 1999. Expanding the search terms to include portable XRF reveals publications as early as the 1970s. When looking at all of the data in combination, an exponential rise in publications becomes apparent (Figure 1).
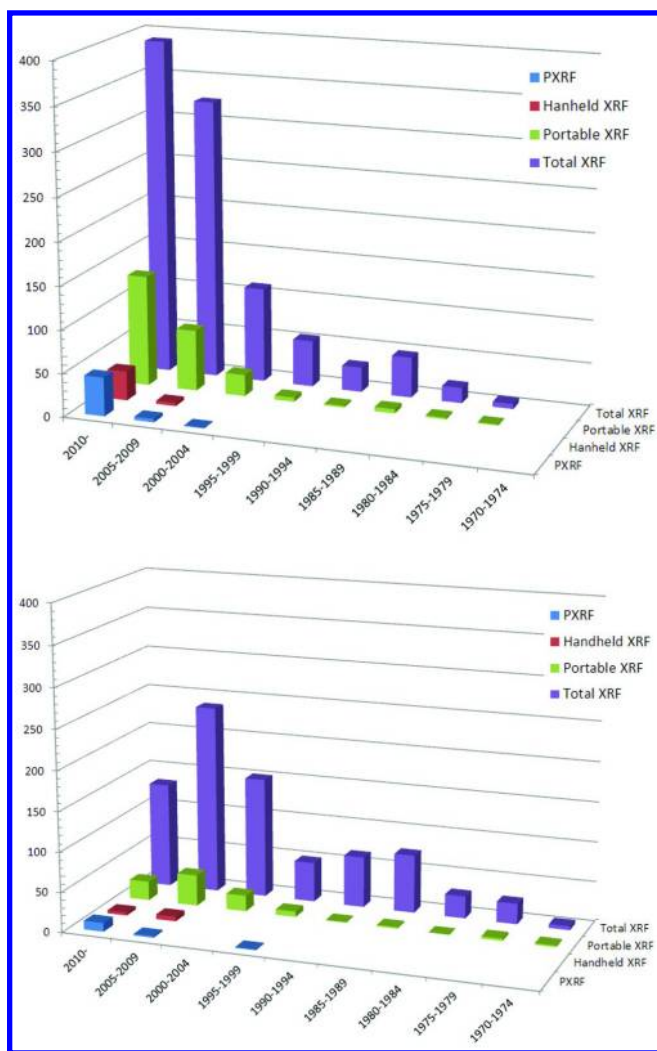
Figure 1. Publications in the last 43 years using the key search terms PXRF, Handheld XRF and Portable XRF, broken down into 5 year periods. The top graph represents the data from sciencedirect.com using the search terms in combination with archaeology. The graph on the bottom represents the data from the AATA database. The low numbers in data from 2010 on are likely due to publication reporting lag.

The ease with which people can access PXRF has increased dramatically. However, when used with the 'point and shoot' mentality often recommended by manufacturers, the end result can be analysis without scientific rigor and published data that has a high chance of not being properly vetted. This ultimately will, and has, resulted in flawed data being added to the literature. It is not the

place of this paper to single out specific articles that the author feels are lacking in their methodological approaches, or that misrepresent data, or whose data should be considered entirely incorrect. In the last few years there have been some unfortunate examples of these problems raised in the literature. Most recently, the discussion surrounding the methodology, quantification and analysis of obsidian has come to the forefront (*20–22*). Those with an interest should read these articles, which highlight many of the issues facing archaeologists who employ analytical instrumentation in their gamut of tools. As with any instrumentation, if PXRF is improperly used, or if the expectations are outside the realm of possibility, or if inappropriate analysis and interpretation are performed, the resulting data will reflect these shortcomings. The term 'garbage in, garbage out' truly applies to the range of misuse possible with PXRF.

Questions from Archaeologists

The primary question is this: What do archaeologists want to know about their materials? Archaeological scientists often get asked questions of this sort. Generally, many more questions must be asked by the scientist to determine what level of analysis is required in order to answer the initial query. These include, but are not limited to:

1. What is this material? This open ended question can be narrowed down in many if not all cases. The question of whether an object is a brass or a bronze copper alloy is a relatively easy one to answer. Typically, this question will be answered with a qualitative assessment of the material.
2. What is the composition of this artifact? This question requires a more extensive inquiry. Examples are presented throughout this chapter, but typically additional follow-up questions are necessary: What level of information are you looking for? Are you interested in the bulk chemistry or the trace chemistry or both? The answers to these questions could be found through a simple qualitative response identifying key elements present in the artifact or they may require a more extensive quantitative analysis.
3. What is the trace element concentration in this sample? I want to investigate its provenance. Can you perform comparative analysis with other datasets that have already been compiled? The answers to these questions require some level of analytical quantification and are much more difficult to obtain.

Archaeologists should think through their requirements and desires and discuss them with a scientist to determine the proper analytical technique(s) that may help provide an appropriate answer. In many cases, there will be a need for more than one analytical approach to properly answer the questions being posed. It is critical that the correct instrument be chosen if you want to answer the question being asked in a helpful and effective manner.

Materials Investigated

A quick look at the currently published literature demonstrates the wide range of archaeological materials investigated using PXRF. Within archaeology itself, there have been diverse applications of XRF technology to analyze multiple materials. These include, but are not limited to stone and obsidian tools, rock art, stone based sculpture and architectural features, glass, ceramics, soils, corroded metals, precious metals, jewelry and museum collections (Table I). Several excellent books have been published that focus on all or some of these topics and they deserve review by those who seek to use handheld XRF in archaeological applications (*16–19*).

Table I. Sciencedirect.com search for the number of articles using the terms XRF and Archaeology in conjunction with obsidian, glass, ceramics, soil, metal and stone

Search Terms	Obsidian	Glass	Ceramics	Soil	Metal	Stone
XRF and Archaeology	223	553	395	452	534	410

Archaeological materials that are presented for analysis can have specific qualities and characteristics that may be problematic for XRF analysis. In many cases, the artifacts are deemed too valuable to allow for physical sampling for more traditional analysis, and in many cases it is difficult to export artifacts, limiting the analyses that can be performed. We may be limited in how we can interact with some materials or how we can prepare them for analysis. (This will be discussed further in the chapter.)

Most archaeological artifacts tend to have one or more of the following characteristics:

- They have layered structures (a painted surface, or surface accretion).
- They have variable particle size (a coarse ceramic paste, or soil content).
- There may be variations in moisture content (as found with *in situ* soil analysis).
- They have corroded surfaces (like metal artifacts).
- They have leached components (such as glass artifacts).
- They have uneven or curved surfaces (as is true for most artifacts).
- They have variable thickness (this includes many artifacts of metal, glass, ceramics, and organic materials).
- They have variable sample size (think of glass beads or vessels, obsidian flakes or various ceramic sherds).

All such artifacts will have characteristics that are problematic or challenging when you attempt to obtain quantitative data with handheld XRF.

Quantification

To better understand the inherent problems related to quantification one should review a basic introduction to the physics behind XRF analysis. There are excellent articles and books that can be read to get a fuller understanding. Those basics are not presented here but I suggest that you read and clearly understand the principles before undertaking any analysis (*23–30*).

When data are collected with an instrument, proprietary software is typically used to provide quantification, typically as weight percent (wt. %), ppm or mg/cm^2. The resulting concentration determined for those elements is directly related to the area under peak for those elements that are pre-programmed into the software. In the case shown in Figure 2, the corresponding area under peak of copper (peak heights are a good indication of this) reflects the total concentration of copper in each sample (Table II). The green spectrum has a larger area under peak which represents 97.08 wt. % copper while the red spectrum has a smaller area under peak and represents less copper at 78.96 wt. %. Most manufactures suggest a 'Point and Shoot' methodology that is meant to serve as an over-riding solution for analysis. It is stated to provide 'accurate results' and 'on-the-spot quality data'. We shall see that for archaeological artifacts this option is rarely useful if it is even possible.
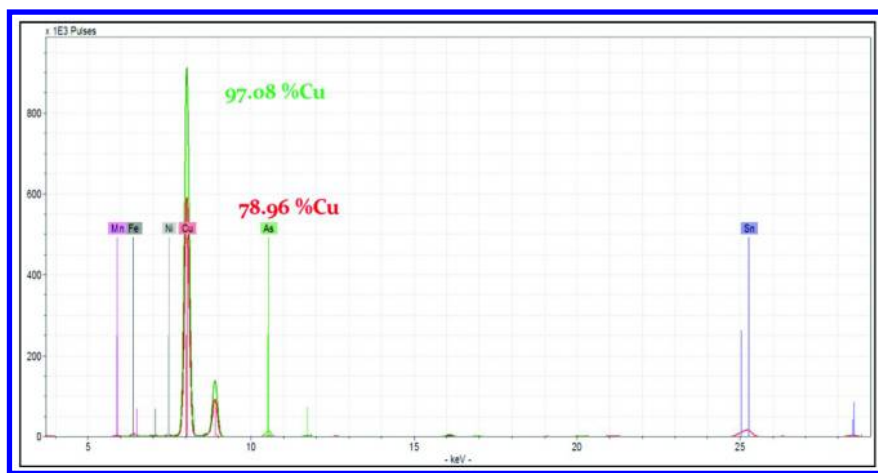
Figure 2. Two spectra of metal reference standards. Area under peak for each element directly relates to total concentration (see Table II for published data).

The goal of quantification is to determine the concentrations of the elements present. Manufacturers use one of several quantification techniques to achieve this. These techniques are well presented in the X-ray physics literature and only the basics are covered here. Further reading is available for those interested in the available methods for quantification and the issues related to them (*31–34*).

Quantification methods typically fall under two categories; a compensation method and a matrix correction method.

Table II. Published data for the two spectra in Figure 2

	Mn	Fe	Co	Ni	Cu	Zn	As	Pb	Ag	Cd	Sn	Sb
Red	0.72	1.20	0.14	0.50	78.96	0.49	0.06	0.26	0.10	0.15	16.05	0.66
Green					97.08		2.90				0.01	

Compensation Methods

For compensation methods, 'Compton scattering' is normally used. This method is well established and is used in other analytical spectroscopy techniques. Typically, sample preparation is required to achieve accurate results and only a limited number of elements – primarily those of low Z – can be quantified. This method uses an algorithm developed from known compounds that are calibrated to the inelastic scattering from the spectrum (Compton scatter). The Compton peak will change energy range, shape and intensity depending on the density and composition of the material being analyzed. Thus, the Compton peak can be used as an internal standard when materials of similar density and composition are analyzed. Ideal materials to quantify using this method include soils, glass, ceramics, textiles, and wood, to name a few. Compton scattering compensation provides concentrations in the ppm range.

Matrix Correction Methods

Matrix corrections typically use three methods for quantification of elements in archaeological materials. These are 'fundamental parameters', 'empirical coefficients', and 'theoretical coefficients'. All three methods are based on mathematical models of X-ray photon interaction within a sample due to the excitation of atoms and their response. There are many variables that can potentially alter this interaction. These models attempt to reduce the variables to make the mathematical calculations manageable. Simplifying assumptions is necessary for success and this includes such things as ensuring sample homogeneity, sample orientation and sample shape. Fundamental parameters (FP) apply some of these basic assumptions including the physical parameters of the sample and fluorescent yields to arrive at quantification. Results are typically normalized to 100% and if any elements are not represented in the calibration, they will not be recognized in the results. Thus, the remainder of elements will be normalized to 100%. Sometimes this produces extended false values.

An alternative to FP is to use empirical methods. This technique relies on a direct relationship between total photon count and known concentrations, creating a linear calibration curve. It provides one with the opportunity to choose reference materials that best represent the unknown samples. Reference materials cover the range of elements in the sample and bracket the range of concentrations of those elements. The unknown sample is then directly compared to the calibration curve to provide the concentration. The accuracy can be very high but it is limited by experimental issues including the quality of the standards used, sample

preparation, similarity between the matrices of the standards and samples, and the repeatability and reproducibility of the measurements. This method can be an expensive choice and may require special standards to be manufactured. Concentrations can be reported as ppm, mg/cm2 or wt. % depending on how the calibration curve is fit.

Most manufactures use fundamental parameters or Compton scattering, or a combination of both for their quantification methods. Some manufacturers allow the user to create empirical calibrations. There has been recent interest in developing theoretical calibrations, like the Monte Carlo model, for archaeological materials. This model is currently being used to perform analyses of heterogeneous materials and investigations of complex photon interactions within a sample. Fundamentally it is an FP method but it applies statistical models of photon interaction rather than determining concentration strictly through algorithms and equations.

Several of the methods described here, including fundamental parameters, can be run without using standards or reference materials, but these methods are improved with the addition of reference materials that better reflect the unknowns being investigated. There are strict guidelines suggested for producing reference materials for XRF and there are many companies that specialize in their production. The literature provides much additional information to users who seek the best use of these quantification methods, a better understanding of the algorithms used and more clarity on what can be expected from these methods (*25*, *31*, *32*, *34*, *35*).

Factors Affecting Quantification

For all quantification methods there are several assumed conditions that must be met for them to function as intended and to provide accurate results. Samples must be homogenous, uniform with respect to their structure and the distribution of elements. Samples should have similar small particle size. Samples should have flat smooth surfaces to insure proper geometric interaction with the incident beam. Samples should have densities similar to one another and to the reference materials used for calibration, because density has an effect on photon scattering. Samples must be what can be thought of as 'infinitely thick,' meaning that if another layer of sample was added, there would be no change in the resulting spectrum. Samples must be large enough to cover the entire X-ray beam; smaller samples will cause scatter and alter the resulting spectrum. Samples must be dry, because water scatters X-ray photons, as will be discussed later in this chapter. Samples cannot be porous.

Reading through this list, one can begin to see that archaeological samples offer a serious challenge for acquiring accurate quantification. In fact, the claims made by manufacturers for obtaining accurate results without sample preparation should be considered absolutely false. Unless samples meet the above requirements, reported concentrations cannot be accurate.

The physics that is used to create the quantification algorithms relies on the criteria above. This is well understood. Maybe Jenkins ((*25*), p.141) said it most clearly, "In practice, however, there are two major constraints that may prevent this

ideal circumstance [for quantification] from being achieved, these being sample size and sample heterogeneity". Samples prepared from heterogeneous materials require significant pre-treatments prior to analysis and this is a serious problem for many archaeological artifacts since the pre-treatment involves physical interaction and/or destruction (*25*, *32*, *36*, *37*).

Attenuation of Photons

The main problem with non-homogenous materials is attenuation of X-ray photons. As characteristic photons are emitted by the elements present in the sample, they are attenuated by the material through which they travel. With heterogeneous materials, this attenuation can be even more pronounced, reducing the area under peak for elements that lie further from the surface, and increasing the area under peak for those elements closer to the surface (Figure 3).
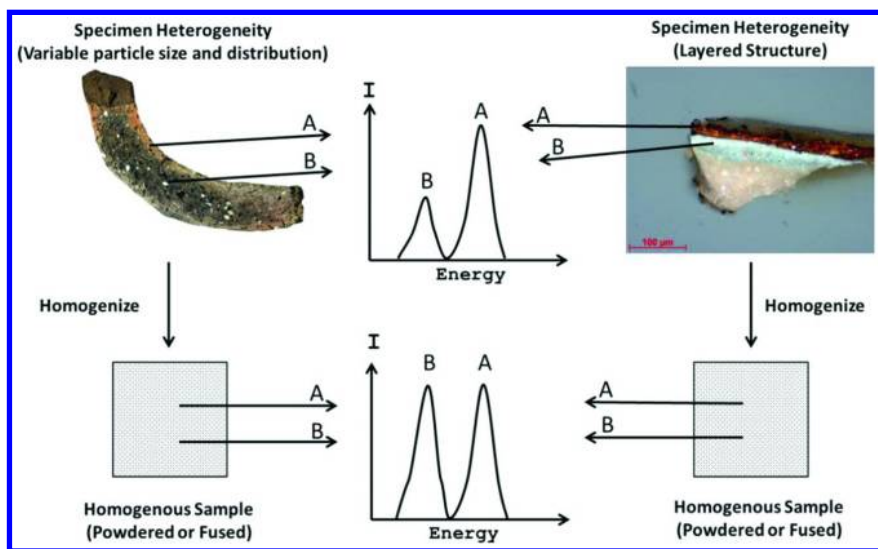
Figure 3. The effects of specimen heterogeneity (particle size, distribution and layering) on relative X-ray intensity in a spectrum (after Jenkins, Figure 9.2, Ref. (25)).

Attenuation is well understood and occurs in all materials whether heterogeneous or not. It is accounted for in all of the quantification methodologies and is described by the exponential attenuation law.

$$(1) \qquad I = I_O \, exp((-\mu/\rho)x)$$

where I is the beam intensity after attenuation, I_o is the beam intensity prior to attenuation, x is the mass thickness defined as sample thickness times density, and μ/ρ is the mass attenuation coefficient for a given material at a given X-ray energy. The exponential attenuation law can also be used to calculate the effect of attenuation of a known layer. For example, the thickness of the gold layer on a gilt artifact can be measured solely by the attenuation of an element in the base metal measured through the gilding layer. It can also be used to measure the thickness of a coating layer.

Understanding attenuation can be challenging but there are some excellent resources that provide guidance through the mathematical concepts (*38*). The effects of attenuation on some typical archaeological materials is discussed below.

Examples

Here are several examples of the effects that non-homogenous structures have on quantification, in particular the effects of layered structures. The focus here is on three types of archaeological materials that have been analyzed and presented in the literature: metals, ceramics and soils.

Metals

Corrosion

All archaeological metals have some level of corrosion and in many cases the corrosion incorporates the surrounding soil. The type, extent, and variation of corrosion are well documented and have been discussed in great detail, from both archaeological and conservation perspectives. Corrosion thickness can vary from thin oxide layers to complete corrosion of an artifact. Corrosion layers themselves will have very different compositions that can differ greatly from the original metal. This alteration in composition can be the result of preferential leaching of one alloy element over another (similar to a galvanic corrosion process), or it can be the result of elemental uptake from the surrounding soils, or even a combination of these processes. One can also see clear differences in composition after dezincification which tends to occur in marine brasses.

An interesting study done by Ehrhardt and Kaiser demonstrated the extensive effect of a thin burial corrosion layer on an archaeological copper alloy (*39*). They performed area scans using a Bruker Artax XRF over the corroded area and a cleaned area on one piece of metal. The maps showed clear increases in elements associated with the surrounding soil, including Si, Ca, Fe, and Cl. It also showed increases in ground pollution, mainly lead. What was amazing to see was the effect of this thin corrosion layer on the quantified results. In the corroded area, there was a 57% decrease in Zn, a 41% increase in Pb, and a 49% increase in Sn. This is a staggering difference in composition which would have significant effects on the archaeological interpretation of the find. It is likely that the data acquired, since it is considered quantitative, would be used to compare this find to other samples analyzed using alternative techniques, performed on the raw metal itself.

The effect of surface contamination on quantification was witnessed by Notis et al. when looking at Tyrian silver shekels (*40*). Slight soil contamination on a few coins increased the reported iron content from 0.05% to over 11% in some cases. When the soil was cleaned off the surface, the values dropped back to within a normal range.

Surface Enrichment

Alteration in surface chemistry or complex microstructures can also have an effect on quantification. Whenever investigating metals, one should have an idea of the general composition and review a phase diagram to see if there is a potential for multiphase structures that may complicate accurate quantification. A prime example of this was presented by Beck et al. in discussing the limitation in the analysis of ancient silver coins by surface techniques (*41*). They reported two very different bulk chemistries on the Cu-Ag phase diagram. One sample had a bulk composition of 80% Ag and 20% Cu and the second sample had a bulk composition of 30% Ag and 70% Cu. With similar manufacturing and cooling rates something very interesting happens at the surface of these alloys. Both samples have copper oxide films that form on the surface. Below that, sample 1 (80-20 Ag-Cu) has an alpha phase coating with a composition of 92% Ag – 8% Cu which is in alignment with the maximum solubility of Cu in Ag at the isothermic temperature of 779 °C. Sample 2 (30-70 Ag-Cu) formed a layer of eutectic, which had a composition of 71% Ag – 29% Cu. In both these cases, the quantities measured using XRF would have been vastly different from that of the bulk metal composition. I strongly recommend that XRF analysis of metals be combined with traditional metallographic investigation of at least one comparable sample to ensure that the data derived from quantification are as accurate as possible.

Ceramics

Images portraying PXRF analysis directly on archaeological ceramic vessels or sherds are easy to find on the Internet. In some cases, this method of analysis might be appropriate, depending on what is being investigated. But in many cases, where one wants to compare paste chemistry to other analyzed ceramic artifacts, there might be serious problems. Archaeological ceramics are complex. They can be layered with soil, accretions, slip or glazes and many have heterogeneous matrices with organic and inorganic inclusions. Ceramics are also porous. Presented here is one example of the analysis of a ceramic sherd with a slip and a coarse paste (Figure 4: from the study collection in the Art Conservation Department at Buffalo State College).

The analysis of this sample was performed in four ways using the same analytical protocol to investigate the lighter elements from Al to Fe. Analysis was carried out with a Bruker Tracer III-SD (15 kV at 55 µA under vacuum with no filter for 120 sec). First the ceramic was analyzed with the slip present. Second, the slip was scraped away with a steel blade and the analysis repeated. Third, the sherd was crushed using a pestle and mortar and the powder placed in a 2 mil

polyethylene bag, which was then analyzed. Finally, the powder was analyzed in an XRF cup with a 1.5 μm Mylar thin film. The polyethylene bag contaminants include Si, P, and Fe in trace amounts and Ca in minor amounts.

Figure 4. Ceramic sample. Cross section is not to scale.
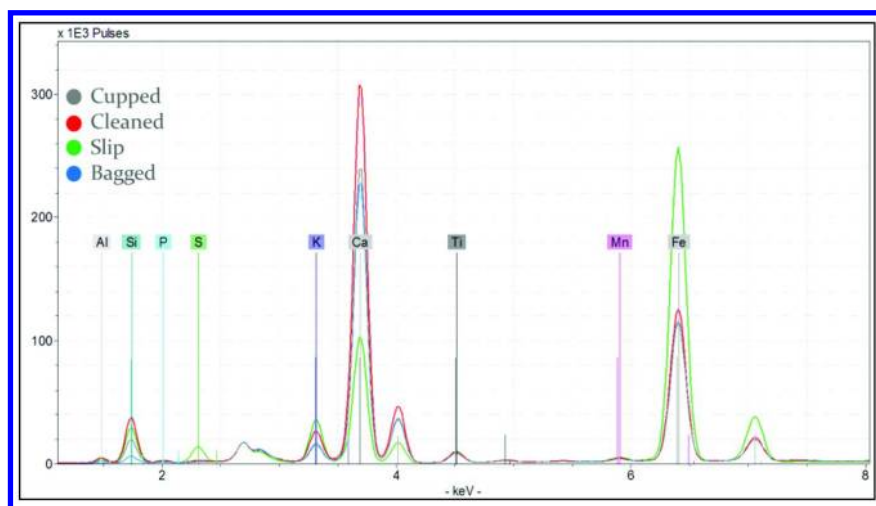
Figure 5. Spectra of the ceramic sample showing the various areas under peak for lighter elements as analyzed by four methods. (The bag contaminates include Si, P, and Fe in trace amounts and Ca in minor amounts.)

What is immediately clear is that there are differences in the resulting spectra with varying degrees of changes in area under peak for all the elements (Figure 5). The red slip is rich in iron and sulfur. Remember that XRF only reports what elements are present and does not give any information concerning the stoichiometry. The level of Ca from the paste is reduced significantly when analyzed through the slip. Removing the slip results in clear increases in Ca and Si while the Fe is reduced and S is not detected. Both crushed samples (either in a bag or in the XRF cup) show variations in elemental concentration as well. Running the spectra through a quantification calibration designed for generic powdered ceramics illustrates the extent of variation in the elemental concentrations determined (Table III). If we refer to the characteristics that affect quantification (listed above), we could infer that this heterogeneous ceramic would require significant pre-treatment prior to being quantified. This would ideally include removal of the slip from the entire sample, crushing the paste to a uniform, even small particle size and either pressing it into a pellet, or fusing it into a glass bead.

Table III. Calculated concentrations for low Z elements in sample 1 using the same calibration. Note the varying compositional data dependent on sample processing

Sample 1	Al	Si	P	K	Ca	Fe
Crushed cupped	1.40	8.30	0.13	1.35	15.78	2.65
Cleaned scraped	3.46	12.85	0.29	2.07	21.05	2.74
Red Slip	2.91	13.43	0.41	3.71	8.10	6.09
Crushed bagged	-0.37	3.51	0.02	1.18	14.18	2.44

When looking at the calculated data (Table III) the variations in reported concentrations are extreme. There is, noticeably, more variation in the lower Z elements. This is due to the higher attenuation of low Z elements. This will be further explored when discussing issues related to the analysis of soils.

Soil

Soil has been analyzed for a variety of purposes related to archaeological pursuits. This would include looking for heavy metals to help indicate the location of metal working and looking for lighter elements like phosphorous to help establish the location of human occupation and activity. Traditional instrumentation used for soil analysis involves wet chemical approaches to obtain quantification of the specific composition of the soil, sometimes with detection limits in the ppb range.

It is common to see PXRF analysis of soils either directly in situ against the ground surface (in some cases neglecting to even clear the ground-covering foliage), or by holding the instrument up against a stratified cross section, or by analyzing the soil while it is contained in a plastic storage bag. For these situations, analysis is performed on heterogeneous materials. In addition, the soil likely has variable moisture content. When investigating lighter Z elements, the attenuation of the layering structures can have an astounding effect on the resulting spectrum. This was demonstrated by the PXRF analysis of soil excavated from Old Fort Niagara (courtesy of Dr. Sue McGuire). The soil was received, as excavated, in a 4 mil polyethylene bag (1 mil = 25.4 μm). It was composed of various sized agglomerates of soil with some smaller inclusions. To exemplify the effects of attenuation, I also placed some of the same soil in a 2 mil polyethylene bag, and I pulverized some additional soil to a uniform homogenous particle size (sum 200 μm) and placed it into an XRF cup with 1.5 μm Mylar film. For the 2 mil bag and the XRF cup, I also ran the samples infused with moisture.

Theoretically, the effects of attenuation can be estimated using the exponential attenuation law. By knowing the original area under peak concentration (**Io**), the thickness of the layer (**ρ**), the density of the polymer in question and the mass attenuation coefficient (**μ/ρ**) for that polymer at various energies of interest, one can back calculate the resultant attenuation (the % value of decrease in area under peak concentration). That plot can be seen in Figure 6 and shows the extent of attenuation for various thicknesses of these polymers for low Z elements, in particular Al, Si, P, K, Ca, Mn and Fe.
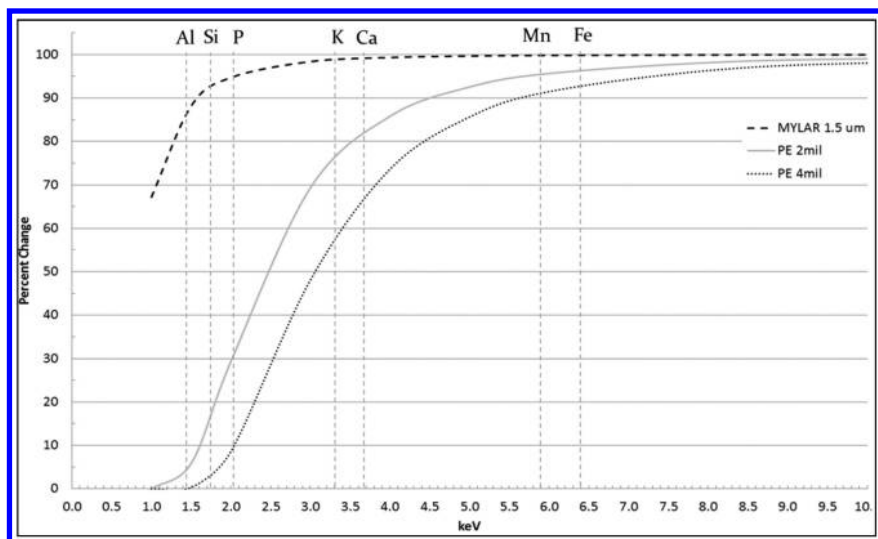
Figure 6. Graph indicating the attenuation by Mylar and polyethylene on low Z elements based on polymer thickness. (Density (g/cm³): Mylar = 1.38, Polyethylene = 0.93).

What should be apparent from this graph is that even the 1.5 μm Mylar film attenuates all elements from approximately 4.5 keV and below. In fact, for Al, it will attenuate the photons by approximately 12%. When using a 2 mil polyethylene bag, that signal is reduced by 96%! With the 4 mil bag the Al is completely attenuated. This means that if a soil sample is analyzed in a 4 mil polyethylene bag no Al will be observed in the spectrum and one could make the assumption that Al is not present in the sample. The resulting calculated concentrations will reflect that error. A similar effect occurs for phosphorous where the 2 mil bag attenuates the signal by 49% and the 4 mil bag attenuates the signal by 90%. When looking for trace level concentrations of these light elements, any attenuation can seriously distort the results.

The spectra for soil in the thick bag, the thin bag and the crushed homogenized soil in an XRF cup with a Mylar film are shown in Figure 7.
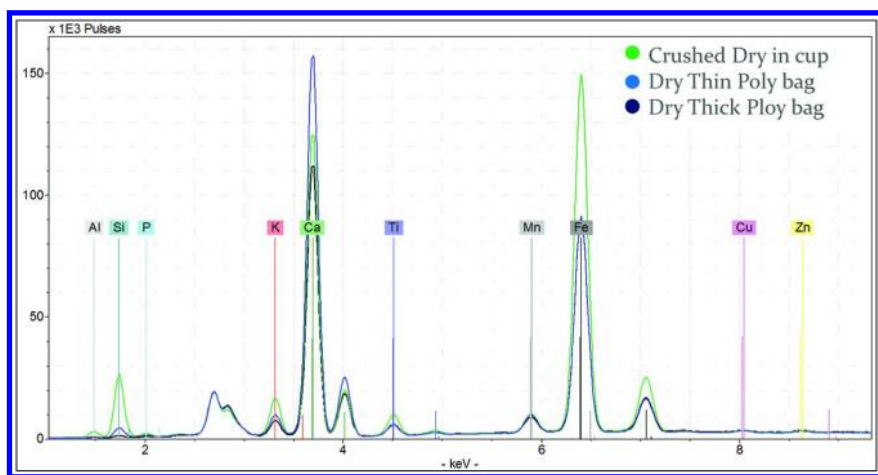
Figure 7. Spectra of soil analysis when taken through a 4 mil and 2 mil polyethylene bag and a 1.5 μm Mylar film. (The bag contaminants include Si, P, and Fe in trace amounts and Ca in minor amounts.)

It should be clear that there is significant difference in the area under peak for Al, Si P and K. The variation in the level of Ca is due to the fact that polyethylene has a minor contamination of Ca. The effect that the Ca concentration in the polyethylene has on the spectrum should not be overlooked as it will alter the overall quantified composition. Running the data through a calibration shows the extent of variation in reported concentrations (see Table IV).

The concentration of Al is completely attenuated by the 2 and 4 mil bags and the concentration of P is all but completely attenuated by the 2 mil bag and entirely attenuated by the 4 mil bag. Using Si as an example allows further exploration of this effect. Based on the attenuation curves calculated and shown in Figure 6, one would expect that the Mylar would attenuate Si ~7% while the 2 mil polyethylene bag would attenuate Si ~ 83% and the 4 mil bag ~ 97 %. This equates to a difference between the Mylar and the 2 mil polymer of 80.7% and 95.7% for the 4 mil polymer. Considering the total area under peak from each spectrum the

actual percent decrease as measured from the Mylar to the other polymers can be calculated. This shows a decrease of 84.6% for the Mylar 2 mil and 96.5% for the Mylar 4 mil bag (Figure 7 show this change visually). These values are likely higher than the calculated ones because the samples were not homogenous and were closely pressed against the bag surface.

Table IV. Calculated concentrations for low Z elements. Note the varying compositional data depending on thickness of polymer. (The bag contaminants include Si, P, and Fe in trace amounts and Ca in minor amounts.)

Soil wt. %	Al	Si	P	K	Ca	Fe
1.5μm Film	1.49	10.62	0.13	1.36	7.38	2.37
2 mil Bag	-0.75	2.83	0.02	0.65	8.61	1.58
4 mil Bag	-0.99	1.68	-0.02	0.45	5.89	1.54

Just imagine that you are interested in calculating the concentration of these lighter elements and you perform your analysis with the samples in bags. Your reported results would be skewed drastically so that your data would have no relevance to other comparable data collected and analyzed properly, nor would you be able to report the trace elements that might be of most interest for your research (such as slight alterations in concentrations of phosphorous). Making matters worse, in many instances, not only was the soil not homogenized and placed in a bag, it was not fully dried and remained moistened.

Effect of Moisture

The effect of moisture on the accuracy of XRF quantification has been explored in detail elsewhere (*11*, *14*, *42*, *43*). However, the soil samples discussed above provide an example of this effect. Previous investigations have suggested that moisture content in soil and sediments of less than 20% has no influence on the accuracy of quantification as compared to dry samples (*42*). More recent research shows a significant effect on calculated concentrations of Mn, Fe, and As with water content well below 20% (*14*). It is surmised that the effect on lower Z elements would be even greater and more significant.

Research investigating moisture content indicates two ways water may interact with soil or sediments. It can interact by forming interstitial fills at open pores and spaces between the structural components or it may be present as water that is considered constitutive, which was trapped during the formation of the minerals present in the soil or sediment. Interstitial replacement is the primary concern with archaeological soils. This replacement of air space with water increases the photoelectric absorption and the scattering of X-ray photons. The physics behind this is based on the fact that water has a higher mass attenuation coefficient than air so that soils enriched in water have a higher overall density. This yields two main results. First, there is a clear alteration to the shape, curve and area under peak for Compton scattering (Figure 8). This is a concern

considering that the quantification method used for soil analysis is typically Compton scattering where the spectra are all normalized to the Compton peak of a known reference material that is typically dry and homogenous. The result would be a loss of accuracy in quantification.
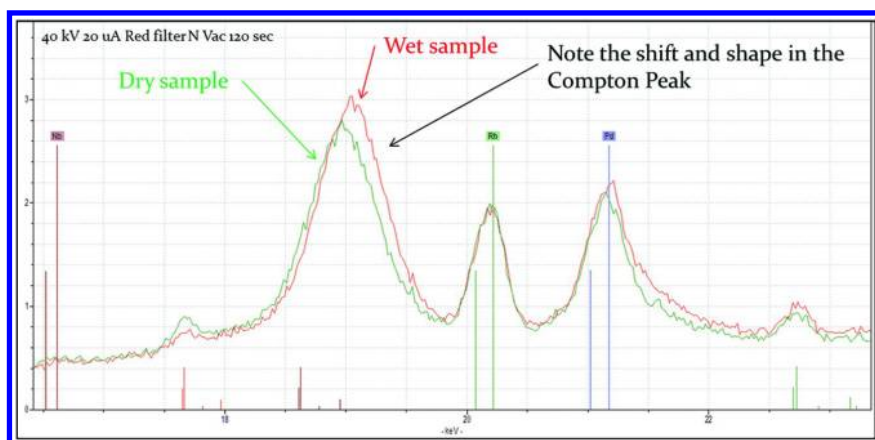
Figure 8. Alteration to the range, shape and area under peak for Compton Scattering when soil is made wet.

Second, there is a reduction of emission peaks for all elements present (Figure 9). Remember, area under peak is directly related to concentration. This effect results in a reduction of the calculated concentration for each element present. The overall decrease measured here was close to 50% for lighter elements and 35% for Mn and Fe (See Table V). It is clear that samples must be dried and homogenized prior to analysis. It is possible to perform a calibration correction for moisture content, but the moisture concentration must be known for accurate results.
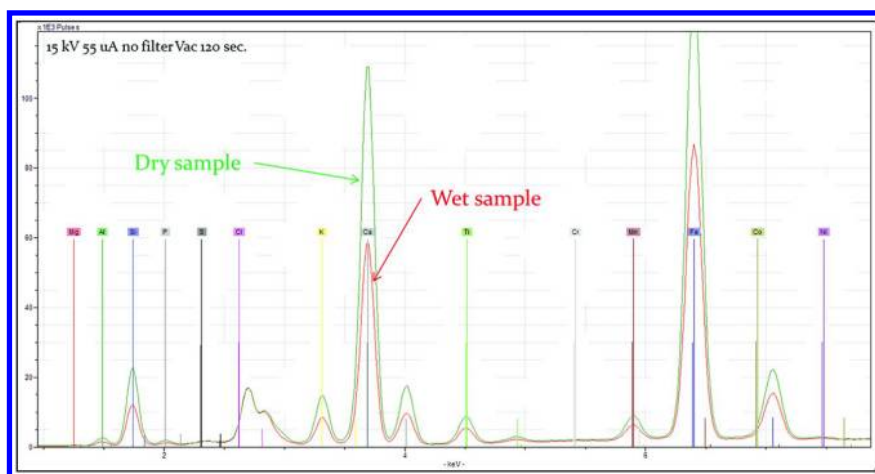
Figure 9. Example of the effect of moisture on soil showing a decreased area under peak for all elements present.

Table V. Percent change in area under peak from a dry soil sample to the same soil sample when wet

	Al	Si	P	K	Ca	Ti	Mn	Fe
Dry/Wet	-52.2	-47.8	-46.6	-46.4	-47.6	-42.8	-36.4	-35.4

Suggestions for Success

One of the important things that you can do when considering performing any analysis of your material is to come to the analysis prepared. Know what your samples are and do the research to investigate any prior analyses and what they uncovered. This is imperative for any analytical technique so that you can best prioritize your analysis and better understand what you are expecting to find. Work with a skilled scientist who has a detailed understanding of the physics behind the instrumentation and of quantification. At a minimum, properly train yourself in the basics of what to expect from the instrument and the analysis under your specific working conditions. Having even a basic understanding of how XRF works will help ensure that you do not proceed down a path of futility.

What might be the most important lesson to learn from the examples discussed in this chapter is that you should be prepared to accept qualitative data. XRF is a powerful instrument and can very successfully provide you with qualitative information about your sample. Qualitative analysis of large datasets can reveal clear groupings in composition without requiring quantitative data as long as your samples are similar to one another. For example, you can survey a large collection of ceramic sherds with the intent of identifying the level of specialization of production. One might look at similarity in design, or in general bulk chemistry. If you qualitatively survey a large number of sherds, you can exclusively look at the area under peak for the elements present to see if they fall into certain categories without determining the actual elemental concentration. This is also the case when looking for increased human activity in soil samples. If properly prepared, as discussed above, you can compare the relative area under peak for phosphorous in ratio with an element that is more stable in the context you are investigating. You can qualitatively look at that ratio to see increases in phosphorous concentrations suggesting increased human activity in those areas. This was successfully done by Neff, Voorhies, and Paredes Umana when looking at sediments from Mesoamerica (*44*).

If you require quantification, know that the manufacturer's quantifications will likely not work for you, even if you are looking at archaeological or historical metals. One might assume that since XRF is used extensively in the scrap metal industry that the pre-installed calibrations will work well. A recent study by Heginbotham et al. looked at comparing inter-laboratory accuracy in quantifying historic metal compositions with staggeringly negative results (*45*). The outcome of the study was that a series of reference materials needed to be produced to replicate the compositions of historic metals to ensure better accuracy with XRF quantification. These reference materials can then be used to create empirical calibrations that better fit the compositions of historic and archaeological metals.

If standard reference materials cannot be manufactured, then a cross analysis calibration can be performed. This entails analyzing a series of unknown samples using a well established technique that can provide a level of quantification better than that which you are hoping to obtain. This has been done for obsidian with great success. To a lesser extent there has been success doing this for ceramic calibrations where the surface of the sherd is scraped clean to reveal a smooth internal surface for analysis (*46*, *47*). If you truly need to get accurate results, you may have to resort to sample preparation that will ensure homogeneity by using techniques like a double dilution method in preparing briquettes or fused beads.

Conclusions

I hope that I have made it clear that while XRF is powerful technology, one still needs to follow sound scientific methodology to achieve desired results. In addition, one cannot, and should not trust manufacturers' claims of accuracy when analyzing archaeological materials. Qualitative data can be valuable in itself. If quantification is needed, much more work will need to be undertaken and a financial burden may have to be overcome. All in all, I recommend that until you gain significant expertise, you work with a scientist who is familiar with X-ray physics and can properly guide you towards successful analysis.

Acknowledgments

References

1. Bosco, G. L. *TrAC, Trends Anal. Chem.* **2013**, *45*, 121.
2. Piorek, S. *Trends Anal. Chem.* **1994**, *13*, 281.
3. Ball, T. K.; Booth, S. J.; Nickless, E. F. P.; Smith, R. T. *J. Geochem. Explor.* **1979**, *11*, 277.
4. Higueras, P.; Oyarzun, R.; Iraizoz, J. M.; Lorenzo, S.; Esbrí, J. M.; Martínez-Coronado, A. *J. Geochem. Explor.* **2012**, *113*, 3.
5. Rhodes, J. R.; Rautala, P. *Int. J. Appl. Radiat. Isot.* **1983**, *34*, 333.
6. El-Taher, A. *Appl. Radiat. Isot.* **2012**, *70*, 350.
7. Lundblad, S. P.; Mills, P. R.; Drake-Raue, A.; Kikiloi, S. K. In *X-Ray Fluorescence Spectrometry (XRF) in Geoarchaeology*; Shackley, M. S., Ed.; Springer: New York, 2011; p 65.
8. Gardner, L. R. *Chem. Geol.* **1990**, *88*, 169.
9. Figueroa-Cisterna, J.; Bagur-González, M. G.; Morales-Ruano, S.; Carrillo-Rosúa, J.; Martín-Peinado, F. *Talanta* **2011**, *85*, 2307.
10. Hołyńska, B.; Lankosz, M.; Ostachowicz, J.; Wolski, K. *Int. J. Appl. Radiat. Isot.* **1985**, *36*, 369.

11. Kalnicky, D. J.; Singhvi, R. *J. Hazard. Mater.* **2001**, *83*, 93.
12. Radu, T.; Diamond, D. *J. Hazard. Mater.* **2009**, *171*, 1168.
13. EPA *Field Portable X-ray Fluorescence Spectrometry for the Determination of Elemental Concentrations in Soil and Sediment*; Method 6200; U.S. Environmental Protection Agency: Washington, DC, 2007.
14. Parsons, C.; Margui Grabulosa, E.; Pili, E.; Floor, G. H.; Roman-Ross, G.; Charlet, L. *J. Hazard. Mater.* **2013**, in press.
15. Zimmer, D.; Kruse, J.; Baum, C.; Borca, C.; Laue, M.; Hause, G.; Meissner, R.; Leinweber, P. *Sci. Total Environ.* **2011**, *409*, 4094.
16. *Physical Techniques in the Study of Art, Archaeology and Cultural Heritage*; Dudley, C., David, B., Eds.; Elsevier: Amsterdam, 2007; Volume 2.
17. *X-Ray Fluorescence Spectrometry (XRF) in Geoarchaeology*; Shackley, M. S., Ed.; Springer: New York, 2011.
18. *Handheld XRF in Art and Archaeology*; Shugar, A., Mass, J., Eds.; Leuven University Press: Leuven, Belgium, 2012.
19. Potts, P. J.; West, M. *Portable X-ray Fluorescence Spectrometry: Capabilities for in Situ Analysis*; Royal Society of Chemistry: Cambridge, U.K., 2008.
20. Frahm, E. *J. Archaeol. Sci.* **2013**, *40*, 1080.
21. Speakman, R. J.; Steven Shackley, M. *J. Archaeol. Sci.* **2013**, *40*, 1435.
22. Frahm, E. *J. Archaeol. Sci.* **2013**, *40*, 1444.
23. Beckhoff, B.; Kanngießer, B.; Langhoff, N.; Wedell, R.; Wolff, H. *Handbook of Practical X-ray Fluorescence Analysis*, 1st ed.; Springer: Berlin, 2006.
24. Bertin, E. P. *Principles and Practice of X-ray Spectrometric Analysis*; Plenum Press: New York, 1970.
25. Jenkins, R. *X-ray Fluorescence Spectrometry*, 2 ed.; John Wiley & Sons, Inc.: New York, 1999.
26. Jenkins, R.; Gould, R. W.; Gedcke, D. *Appl. Spectrosc. Rev.* **2004**, *35*, 129.
27. Potts, P. J.; Webb, P. C. *J. Geochem. Explor.* **1992**, *44*, 251.
28. Shackley, M. S. In *X-Ray Fluorescence Spectrometry (XRF) in Geoarchaeology*; Shackley, M. S., Ed.; Springer: New York, 2011; p 1.
29. Shugar, A. *Western Association for Art Conservation Newsletter* **2009**, *31*, 8.
30. Shugar, A.; Mass, J. In *Handheld XRF in Art and Archaeology*; Shugar, A., Mass, J., Eds.; Leuven University Press: Leuven, Belgium, 2012; p 17.
31. Jenkins, R.; Gould, R. W.; Gedcke, D. *Quantitative X-Ray Spectrometry*, 2nd ed.; Marcel Dekker, Inc: New York, 1995.
32. Mantler, M.; Willis, J.; Lachance, G.; Vrebos, B. A. R.; Mauser, K.-E.; Kawahara, N.; Rousseau, R. M.; Brouwer, P. N. In *Handbook of Practical X-Ray Fluorescence Analysis*; Beckhoff, B., Kanngießer, B., LanghoffN., Wedell, R., Wolff, H., Eds.; Springer-Verlag: Berlin, 2006; p 309.
33. Sitko, R.; Zawisza, B. In *X-Ray Spectroscopy*; Sharma, S. K., Ed.; InTechOpen: New York, 2012; p 137
34. Thomsen, V. *Spectroscopy* **2007**, *22*, 46.
35. Mantler, M.; Naoki, K. *Rigaku Janaru* **2004**, *21*, 17.
36. Jenkins, R.; Vries, J. L. *Practical X-ray Spectrometry*; Springer-Verlag: Berlin, 1973.

37. Liritzis, I.; Zacharias, N. In *X-Ray Fluorescence Spectrometry (XRF) in Geoarchaeology*; Shackley, M. S., Ed.; Springer: New York, 2011, p 109.
38. Hubbell, J. H.; Seltzer, S. M. *Tables of X-Ray Mass Attenuation Coefficients and Mass Energy-Absorption Coefficients from 1 keV to 20 MeV for Elements Z = 1 to 92 and 48 Additional Substances of Dosimetric Interest*; Ionizing Radiation Division, Physics Laboratory, National Institute of Standards and Technology (NIST): Gaithersburg, MD, 1989, 1990, 1996.
39. Ehrhardt, K.; Kaiser, B. *FIRST Newsletter* **2011**, March.
40. Notis, M.; Shugar, A.; Herman, D.; Ariel, D. In *Archaeological Chemistry: Analytical Techniques and Archaeological Interpretation*; Glascock, M., Speakman, R. J., Popelka-Filcoff, R. S., Eds.; ACS Symposium Series 968; American Chemical Society: Washington, DC, 2007; p 258.
41. Beck, L.; Bosonnet, S.; Réveillon, S.; Eliot, D.; Pilon, F. *Nucl. Instrum. Methods Phys. Res., Sect. B* **2004**, *226*, 153.
42. Piorek, S. In *Current Protocols in Field Analystical Chemistry*; Lopez-Avila, V., Barcelo, D., Beckert, W., Goheen, S. C., Jinno, K., Rittenburg, L. H., Eds.; John Wiley & Sons, Inc.: New York, 1998; p 3B.1.1.
43. Markowicz, A. A. In *Portable X-ray Fluorescence Spectrometry: Capabilities for in Situ analysis*; Potts, P. J., West, M., Eds.; Royal Society of Chemistry: Cambridge, U.K., 2008; p 13.
44. Neff, H.; Voorhies, B.; Uman, F. P. In *Handheld XRF in Art and Archaeology*; Shugar, A., Mass, J., Eds.; Leuven University Press: Leuven, Belgium, 2012; p 379.
45. Heginbotham, A.; Bezur, A.; Bouchard, M.; Davis, J. M.; Eremin, K.; Frantz, J. H.; Glinsman, L.; Hayek, L.; Hook, D.; Kantarelou, V.; Karydas, A. G.; Lee, L.; Mass, J.; Matsen, C.; McCarthy, B.; McGath, M.; Shugar, A.; Sirois, J.; Smith, D.; Speakman, R. J. In *Metal 2010: International Conference on Metal Conservation*; Mardikian, P., Chemello, C., Watters, C., Hull, P., Eds.; Clemson University: Clemson, SC, 2011; p 244.
46. Aimers, J. J.; Farthing, D. J.; Shugar, A. N. In *Handheld XRF in Art and Archaeology*; Shugar, A., Mass, J., Eds.; Leuven University Press: Leuven, Belgium, 2012; p 423.
47. Speakman, R. J.; Little, N. C.; Creel, D.; Miller, M. R.; Iñañez, J. G. *J. Archaeol. Sci.* **2011**, *38*, 3483.

Chapter 11

Source Analysis of Prehistoric Obsidian Artifacts in Sicily (Italy) Using pXRF

Robert H. Tykot,[*,1] **Kyle P. Freund,**[2] **and Andrea Vianello**[3]

[1]Department of Anthropology, University of South Florida, Tampa, Florida 33620, U.S.A.
[2]Department of Anthropology, McMaster University, Hamilton, Ontario, Canada LS8 4L8
[3]OUCS, Oxford University, England, Great Britain OX2 6NN
[*]E-mail: rtykot@usf.edu

Obsidian artifacts have been found at many prehistoric sites in Sicily, yet only a few studies have been done to determine the specific geological sources and subsources used. In 2012, nearly 600 artifacts from 25 archaeological sites dating from the Neolithic, Copper, and Bronze Ages (ca. 6th-2nd millennia BC) were analyzed non-destructively using a hand-held portable X-ray fluorescence spectrometer, in museums that would not allow removal of the artifacts. In addition, all of the artifacts were techno-typologically analyzed to understand how obsidian was reduced and used through time. A Bruker III-SD was used to produce data for trace elements Rb, Sr, Y, Zr, and Nb which were calibrated against international obsidian standards, and compared with results obtained with the same instrument on geological sources and subsources in the Mediterranean region. All artifacts tested came either from Lipari or Pantelleria, confirming visually-based predictions but also demonstrating that multiple geological subsources were used on each island. The majority of the obsidian artifacts were blades, while a small percentage were cores. These results are used to assess variation based on site location, time period, and lithic typology, and to inform us about contact, exchange, and socioeconomic aspects of the ancient societies involved and if they changed over time.

Obsidian in Sicily

Extensive studies of obsidian sources, and archaeological sites in mainland Italy, Sardinia, and Corsica have been done over the past 20 years, but few chemical analyses (*1–6*) have been done in Sicily despite its large contribution to archaeological lithic assemblages (Figure 1). The proximity of the island sources of Lipari and Pantelleria to Sicily makes them the most likely used during the Neolithic period, but the realization that different geological subsources on each may have been utilized requires more than visually-based identification (*7*). Chemical analysis would also indicate whether any obsidian from Palmarola, Sardinia (Mt. Arci), or elsewhere made its way to Sicily.

Obsidian Sources

Lipari, one of the Aeolian Islands just north of Sicily, is well known for its high-quality obsidian, black or gray but often highly transparent, and frequently with phenocrysts (Figure 2). Detailed recording, collection, and elemental analysis of source material has revealed two geological subsources near the coast in the northeastern part of Lipari – Gabellotto Gorge and Cannetto Dentro – that had produced obsidian usable for stone tools in prehistoric times (*8*). While Gabellotto has a large number of visible outcrops, Cannetto Dentro is restricted to a very small area, and access and quantity may have been somewhat different prior to historic lava flows which include Forgia Vecchia and Rocche Rosse. Artifacts made of Lipari obsidian have been found throughout peninsular Italy, as far as southern France and the Istrian peninsula of Croatia, and in Malta and Sicily (*9*). Prior to this study, all obsidian artifacts assigned to Lipari were specifically matched to Gabellotto.

Pantelleria, southwest of Sicily, is known for its greenish peralkaline obsidian, while chemical analyses can distinguish between subsources near Lago di Venere in the north, and the three volcanic events at Balata dei Turchi near the south coast (*10*) (Figure 3). Artifacts of Pantellerian obsidian have been found at archaeological sites as far as northern Italy, but mainly in Tunisia, Malta, and southern-western Sicily. In most cases, multiple Pantelleria subsources were being utilized, despite the small quantity and size of the Lago di Venere material.
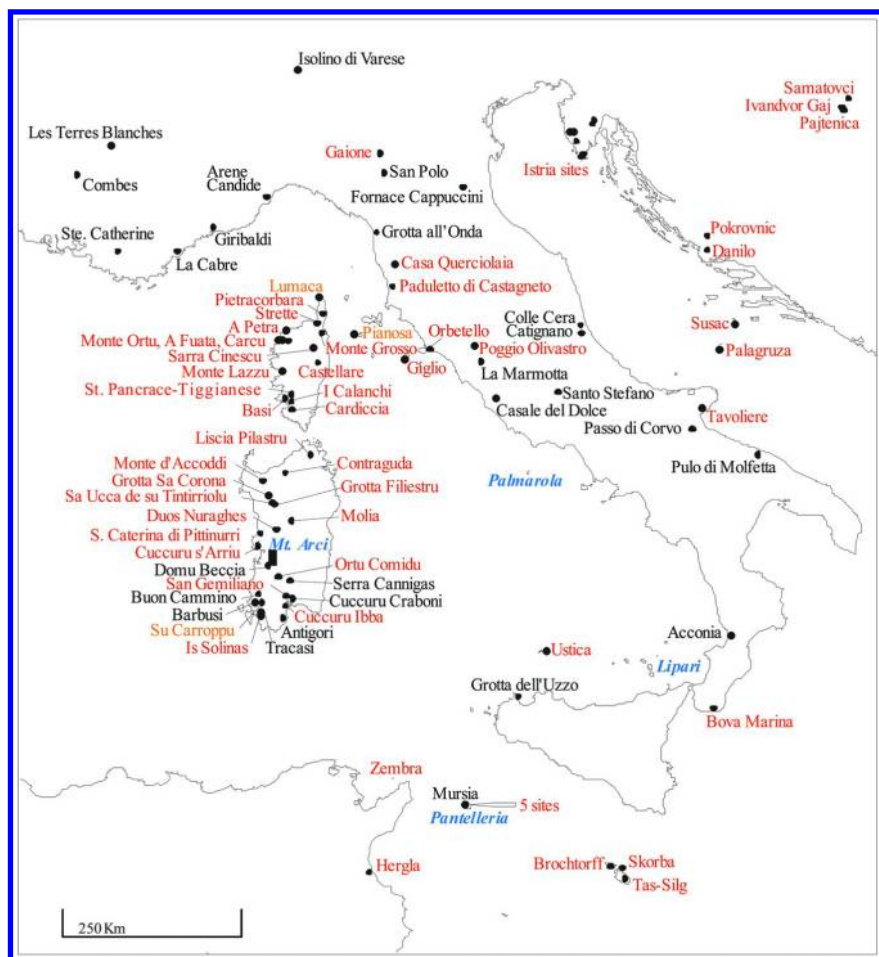
Figure 1. The four Italian island obsidian sources (in all caps), and archaeological sites with 10 or more scientific analyses (sites in bold analyzed by Tykot; in italics by other scholars and Tykot; in plain text by other scholars).
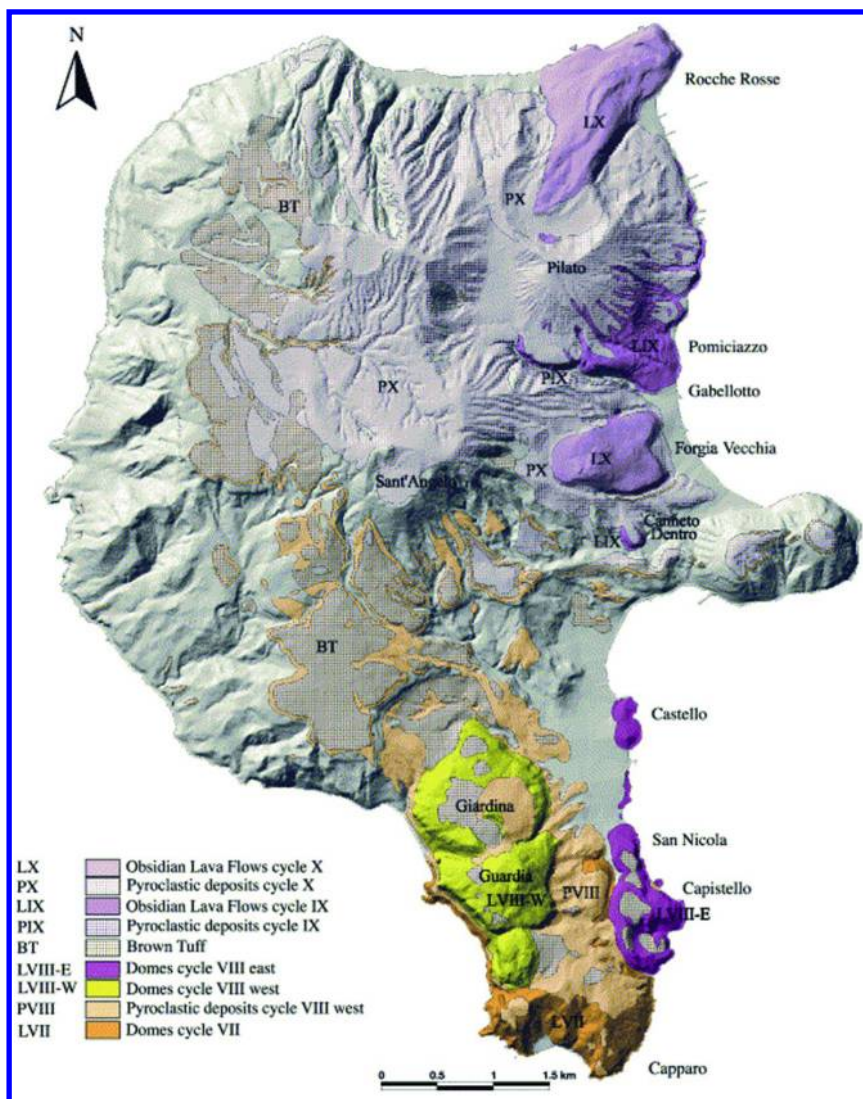
*Figure 2. A geological map of Lipari showing multiple volcanic lava flows.
Gabellotto Gorge and Canneto Dentro obsidian lava flows date to cycle IX.*
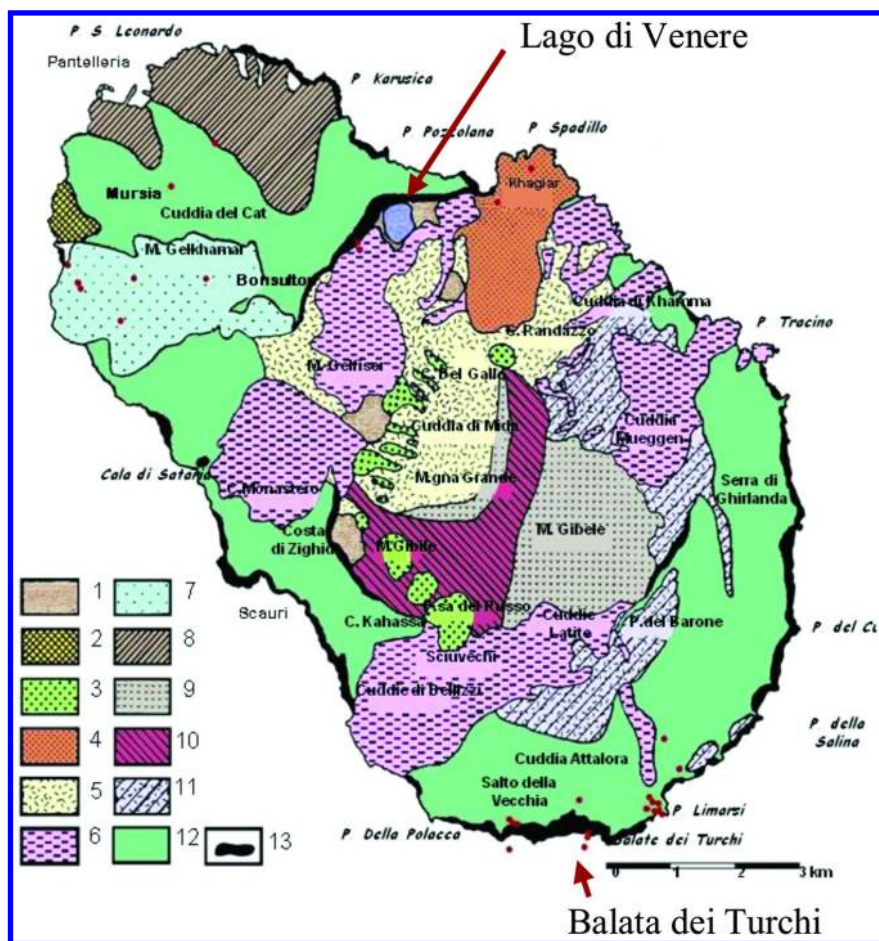
Figure 3. A geological map of Pantelleria showing multiple obsidian outcrops and surface finds.

Obsidian Artifacts Tested in Sicily

In 2012, technological and elemental analyses of obsidian artifacts were done in the Paolo Orsi Archaeological Museum in Siracusa and the Antiquarium "Arturo Petix" in Milena. The obsidian assemblages include blades, cores, and scrapers (Figure 4), and come from 26 sites (Figure 5). The artifacts from some of these sites were not excavated but collected on the surface, while other sites were excavated long ago, with most just assigned to general chronological periods. While the earliest sites tested date to the Middle Neolithic (ca. 5th millennium cal BC), obsidian from Lipari and Pantelleria is known to have been used in the Early Neolithic (6th millennium cal BC), e.g. at Grotta dell'Uzzo (*2*). A summary of our data for nearly 600 obsidian artifacts (individual artifact data available on request) is provided in Table I.

Figure 4. Prehistoric obsidian artifacts from Sicily. Blades and bladelets (left); scraper (upper right); core and other tools (lower right). Courtesy of R.Tykot.
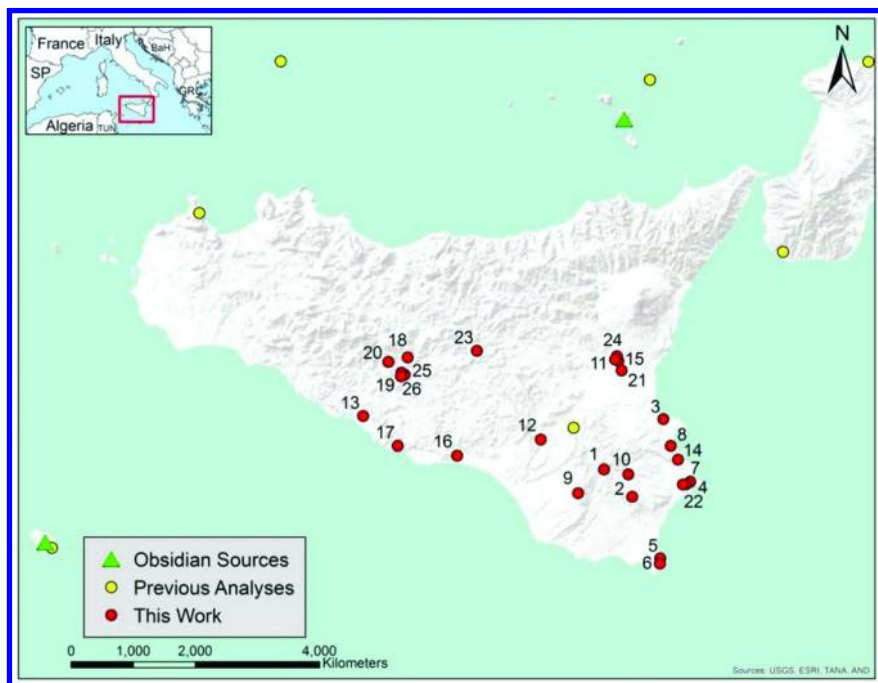
Figure 5. Map showing sites tested in this study (listed in Table I). Dots in yellow represent sites where 10 or more artifacts have been tested before. Sites 17-20, 25-26 also had been analyzed by La Rosa et al. (2).

Elemental Analysis

A portable XRF instrument was used in this study because it is non-destructive, analyses could be performed within the museums and thus without special permissions for export out of Italy, and rapid analysis of statistically robust datasets. A Bruker III-SD was equipped with a filter (12 mm Al, 1 mm Ti, 6 mm Cu) designed to enhance data measurements of mid-Z elements in the spectrum, while settings of 40 kV and 11 µA were selected to maximize trace element analysis. Analyses were done on cleaned obsidian artifacts for 120 seconds. Prior studies by the first author had been done with a Bruker III-V and run for 180 seconds, while this instrument has a silicon-drift detector which is faster and allows for more rapid analyses. The Bruker III-SD also was used to re-analyze many geological samples from all of the European/Mediterranean island sources, showing that each could be discriminated, along with subsources for each (Carpathian, Lipari, Melos, Palmarola, Pantelleria, Sardinia). The resulting data for rubidium (Rb), strontium (Sr), yttrium (Y), zirconium (Zr), and niobium (Nb) were calibrated into ppm values using obsidian standards shared between many laboratories, and compared with the geological database. There was only a small offset in the numeric values produced relative to the previous model. The geological obsidian sources for each island (and Carpathia) are easily discriminated using just a few trace elements, especially as ratios (Figure 6). Nevertheless, for attribution to island sources and specific subsources, results for all elements are examined and evaluated. The four main Sardinian (Mt. Arci) subsources may also be discriminated using Rb, Sr, and Nb, and even subdivided further based on specific geological outcrop locations (*11*). Fe and Rb show significant differences in the Lipari subsource localities (Figure 7), while Zr and Nb separate the Lago di Venere and Balata dei Turchi subsources on Pantelleria (Figure 8).

No.	Site	Dating	Gabellotto Gorge	Cannetto Dentro	Balata dei Turchi	Lago di Venere	Obsidian Samples	Cores	Blades	Flakes	Angular Waste
14	Stentinello	Middle Neolithic	131	2	0	0	133	3	55	67	8
15	Tre Fontane	Middle Neolithic	61	1	0	0	62	1	54	7	0
8	Megara Hyblaea	Middle Neolithic	10	0	0	0	10	1	9	0	0
7	Matrensa	Middle Neolithic	124	0	0	0	124	2	71	46	5
21	Fontana di Pepe	Middle Neolithic	4	0	0	0	4	0	2	2	0
18	Serra del Palco	Middle-Late Neolithic	32	0	8	2	42	0	23	19	0
19	Rocca Aquilia	Middle-Late Neolithic	3	0	0	0	3	0	3	0	0
25	Iannicu	Middle-Late Neolithic	3	0	0	0	3	0	3	0	0
17	Fontanazza Monte Grande Grotta 4	Middle-Late Neolithic	28	2	2	4	36	0	19	17	0

No.	Site	Dating	Gabellotto Gorge	Cannetto Dentro	Balata dei Turchi	Lago di Venere	Obsidian Samples	Cores	Blades	Flakes	Angular Waste
17	Fontanazza Monte Grande Sommita	Middle-Late Neolithic	12	0	2	0	14	1	11	2	0
17	Fontanazza Monte Grande Grotta 2	Middle-Late Neolithic	1	0	0	0	1	1	0	0	0
20	Mizzebbi	Middle-Late Neolithic	5	0	0	0	5	0	3	2	0
10	Palazzola Acreide	Neolithic	4	0	0	0	4	0	4	0	0
6	Grotta Corruggi	Neolithic	2	0	0	0	2	0	2	0	0
11	Poggio Rosso	Neolithic to Copper Age	22	0	0	0	22	0	22	0	0
12	Sant'Ippolito	Neolithic to Copper Age	5	0	0	0	7	2	5	0	0
1	Calaforno	Neolithic to Copper Age	9	0	0	0	9	1	3	5	0

Table I. (Continued). Summary data for each site tested. The location of each site is provided in Figure 5.

No.	Site	Dating	Gabellotto Gorge	Cannetto Dentro	Balata dei Turchi	Lago di Venere	Obsidian Samples	Cores	Blades	Flakes	Angular Waste
22	Grotta del Conzo	Early Copper Age	1	0	0	0	1	0	1	0	0
24	Contrada Orto del Conte	Early Copper Age	70	0	0	0	70	0	67	3	0
5	Grotta Calafarina	Early Copper Age	9	0	0	0	9	0	9	0	0
26	Menta	Middle Copper Age	1	0	2	0	3	0	1	2	0
23	Malpasso	Late Copper Age	4	0	0	0	4	0	4	0	0
13	Serraferlicchio	Copper Age	4	2	0	0	6	0	5	1	0
2	Castelluccio	Early Bronze Age	1	0	0	0	1	0	0	1	0
9	Monte Sallia	Early Bronze Age	1	0	0	0	1	0	0	1	0

No.	Site	Dating	Gabellotto Gorge	Cannetto Dentro	Balata dei Turchi	Lago di Venere	Obsidian Samples	Cores	Blades	Flakes	Angular Waste
16	Gela Manfria	Early Bronze Age	1	0	0	0	1	0	0	0	1
4	Cozzo del Pantano	Early Bronze Age	1	0	0	0	1	0	1	0	0
3	Cava Canabarbara	Early Bronze Age	10	0	0	0	10	0	8	0	2
		Total	559	7	14	6	588	12	385	175	16
		Percent	95.1	1.2	2.4	1.0	100	2.0	65.5	29.8	2.7
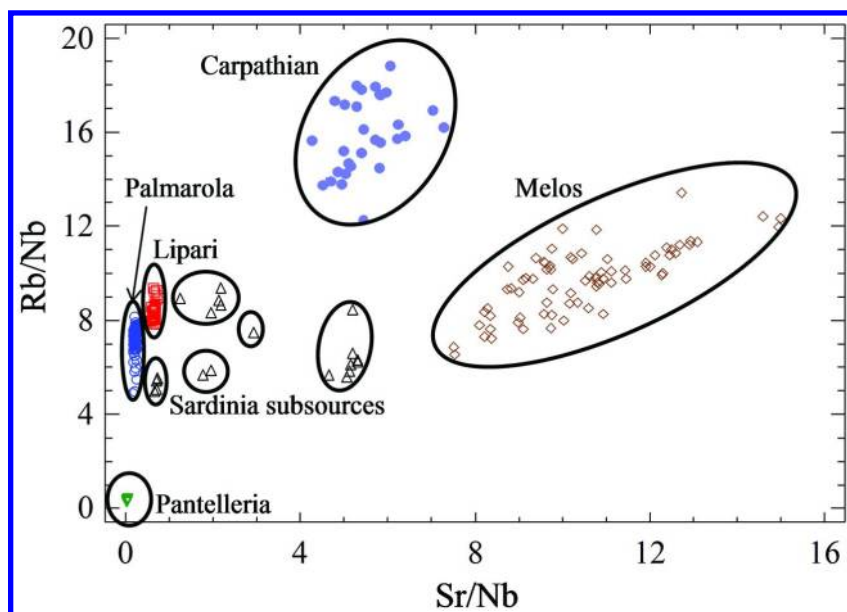
Figure 6. Distinguishing the European/Mediterranean obsidian sources, and Monte Arci (Sardinia) subsources, using geological samples. The ellipses encompass all of the geological samples tested.

Results and Discussion

For the 588 obsidian artifacts analyzed, 96.6% match with Lipari, and just 3.4% with Pantelleria. For no artifact was the source not clearly distinguished from others in the Mediterranean area. The artifacts include 57 at the Antiquarium in Milena which had been analyzed previously by La Rosa et al. (*4*) using a non-commercial, portable XRF, with the reanalysis adding the identification of the specific subsources used at those sites (17-20, 25-26 in Figure 5). The dominance of Lipari obsidian is not a surprise, considering the proximity of the Aeolian Islands to Sicily, and the extensive distribution of Lipari obsidian both to the north (peninsular Italy, Croatia) and south (Sicily, Malta). Obsidian from Cannetto Dentro, however, was identified at several of the sites tested in this study, while previous pXRF analyses for many sites in mainland Italy, Croatia, and Malta were all assigned to Gabellotto Gorge (Figure 7). This has significant implications for our understanding of access and distribution of obsidian from Lipari in the Neolithic and Copper Ages.
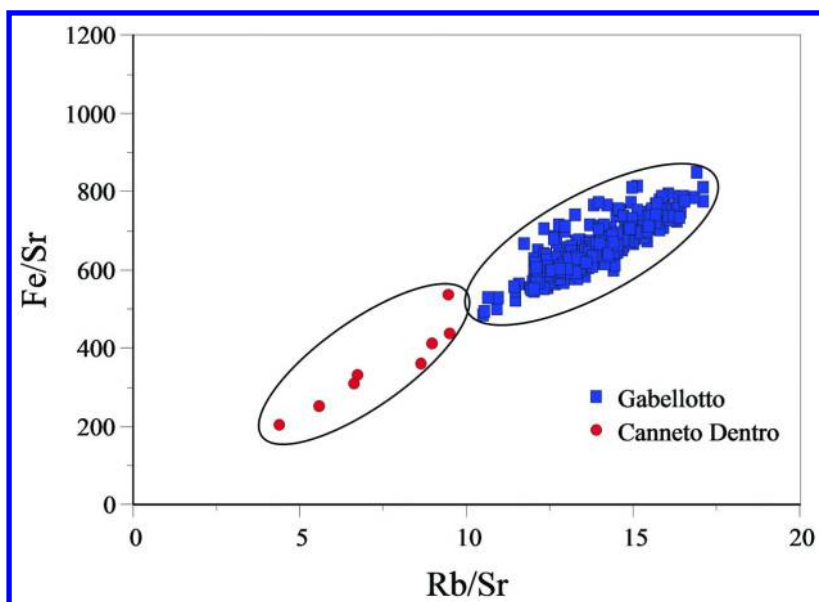
Figure 7. Artifacts assigned to two Lipari subsources represented by ellipses, with 560 assigned to Gabellotto Gorge and 8 to Canneto Dentro.
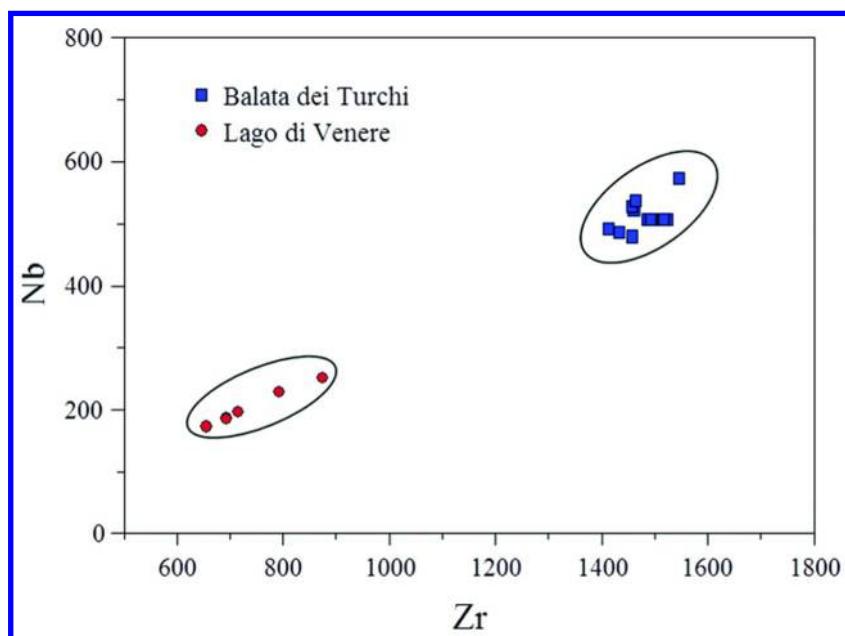
Figure 8. Artifacts assigned to two Pantelleria subsources, as represented by ellipses, with 14 assigned to Balata dei Turchi and 6 to Lago di Venere.

Only three of the twenty-six sites tested have artifacts from Pantelleria, with all three located in central-western Sicily. All but two of the fourteen Pantelleria artifacts come from Middle or Late Neolithic sites. While none were present at six other sites in this area, including two near the southern coast, the number of artifacts found and tested at these sites was very small. For the sites in western Sicily, all those with a significant number of artifacts tested include some from Pantelleria.The absence of Pantelleria obsidian at the sites tested in eastern Sicily supports the visual assessments published by Nicoletti (*7*), and overall is not surprising given the greater distance from the source.

The modest quantity of Pantelleria obsidian making its way to Sicily also is not surprising considering the substantial open-water distance that needed to be crossed, and the limited population living on the small island in the Neolithic (as inferred from field surveys and sporadic finds, e.g. in contrada Buggeber) (*12*). Assigning a fairly large percentage (30%) of the Pantelleria obsidian artifacts to Lago di Venere, which is located inland and for which the quantity and size of the raw material is rather limited, supports a preliminary interpretation that obsidian was irregularly brought to Sicily, after collection and reduction by local residents, rather than visitors from Sicily accessing directly obsidian from the extensive coastal Balata dei Turchi subsources. Nevertheless, more information about the reduction and use of these subsources is needed before more concrete interpretations can be made.

For the artifacts assigned to Pantelleria, five of six from the Lago di Venere subsource were blades while one artifact was a flake. Ten of the seventeen artifacts from Balata dei Turchi were blades and the rest were flakes. The percentages of blades and flakes are quite similar to those from Gabellotto Gorge (n=559; 65% blades, 30% flakes). Canneto Dentro obsidians included three flakes and four blades. Overall, all cores tested (n=12; 2% of total artifacts) came from the Gabellotto subsource.

Despite differences in the procurement of the various raw materials, obsidian from both Lipari and Pantelleria were reduced in a similar manner. Our results clearly show that blades were the primary obsidian artifact type found in Sicily from the Neolithic through Bronze Ages. This long tradition of blade production differs from other regions in the western Mediterranean, such as Sardinia, where obsidian was used for a greater variety of tool types (*13*), and where post-Neolithic reduction strategies were more oriented towards the production of expediently produced flake tools (*14*). The continued usage of obsidian in central and eastern Sicily during the Chalcolithic and Bronze Ages contrasts with elsewhere in the larger western Mediterranean, where obsidian use declined at the end of the Neolithic (ca. 3000 BC).

Conclusion

The use of pXRF is clearly successful in distinguishing not only between the different Mediterranean island sources, but also the important subsources on Lipari and Pantelleria. The ability to rapidly analyze obsidian artifacts non-destructively and within museums was what allowed this research to be done,

and obsidian from many more sites in central and western Sicily, and Calabria, will be tested in the future. This will enable a much greater statistical understanding of the direction and socioeconomic circumstances of obsidian production and distribution in the south-central Mediterranean during the Neolithic through Early Bronze Age periods, and when combined with archaeological evidence for flint and other stone tools, ceramics, and other materials, hypotheses may also be tested regarding chronological change. Direct comparisons may also be made with the more extensive data available for the north-central Mediterranean region.

Acknowledgments

References

1. Hallam, B. R.; Warren, S. E.; Renfrew, C. *Proc. Prehistoric Soc.* **1976**, *42*, 85–110.
2. Francaviglia, V.; Piperno, M. *Rev. d'Archéométrie* **1987**, *11*, 31–39.
3. Tykot, R. H. In Ustica I. The Results of the Excavations of the Regione Siciliana Soprintendenza ai Beni Culturali ed Ambientali Provincia di Palermo in Collaboration with Brown University in 1990 and 1991. Holloway, R. R.; Lukesh, S. S. *Archaeologia Transatlantica*; Providence and Louvain-La-Neuve, 1995; Vol. XIV, pp 87−90.
4. La Rosa, V.; Palio, O.; Pappalardo, G.; Pappalardo, L.; Romano, F. P. *Atti della XXXIX Riunione Scientifica dell'Istituto Italiano di Preistoria e Protostoria: Materie Prime e Scambi nella Preistoria Italiana, Firenze, November 2004*; Instituto Italiano di Preistoria e Protostoria: Firenze, Italy, 2006; pp 499−508.
5. Iovino, M. R.; Maniscalco, L.; Pappalardo, G.; Pappalardo, L.; Puglisi, D.; Rizzo, F.; Romano, F. P. *Archaeometry* **2008**, *50*, 474–494.
6. Iovino, M. R.; Martinelli, M. C.; Skakun, N. N. *Prehistoric Technology 40 years later: Functional Studies and the Russian Legacy*; Longo, L., Ed.; Archaeopress: Oxford, 2008; pp 439−444.
7. Nicoletti, F. In *Prima Sicilia: Alle Origini della Società Siciliana*; Tusa, S., Ed.; Catalogo della Mostra: Palermo, 1997; pp 258−69.
8. Tykot, R. H.; Iovino, M. R.; Martinelli, M. C.; Beyer, L. *Atti del XXXIX Riunione Scientifica dell'Istituto Italiano di Preistoria e Protostoria: Materie Prime e Scambi nella Preistoria Italiana, Firenze, November 2004*; Istituto Italiano di Preistoria e Protostoria: Firenze, Italy, 2006; pp 592−597.

9. Tykot, R. H. In *Exotica in the Prehistoric Mediterranean*; Vianello, A., Ed.; Oxbow Books: Oxford, 2011, pp 33−44.
10. Francaviglia, V. *J. Archaeol. Sci.* **1988**, *15*, 109–122.
11. Tykot, R. H. *Acc. Chem.Res.* **2002**, *35*, 618–627.
12. Cattani M.; Cerasetti B.; Monti A. In *Scoprire. Scavi del Dipartimento di Archeologia, Catalogo della Mostra, Bologna, 18 maggio – 18 giugno 2004*; Guaitoli, M. T., Marchetti, N., Scagliarini, D., Eds.; Bologna, 2004; pp 141−147.
13. Lugliè, C.; Le Bourdonnec, F.-X.; Poupeau, G.; Atzeni, E.; Dubernet, S.; Moretto, P.; Serani, L. *J. Archaeol. Sci.* **2007**, *34*, 428–439.
14. Freund, K. P.; Tykot, R. H. *J. Archaeol. Anthropol. Sci.* **2011**, *3*, 151–164.

Chapter 12

Investigating Obsidian Procurement at Integration Period (ca. AD 700-1500) *Tola* Sites in Highland Northern Ecuador via Portable X-ray Fluorescence (pXRF)

Eric Dyrdahl[*,1] and Robert J. Speakman[2]

[1]Department of Anthropology, The Pennsylvania State University, 409 Carpenter Building, University Park, Pennsylvania 16802
[2]Center for Applied Isotope Studies, The University of Georgia, 120 Riverbend Road, Athens, Georgia 30602
[*]E-mail: erd142@psu.edu

The study of long-distance exchange has long been a focus of research on Ecuadorian prehistory. One of the more prominent archaeological avenues for research on this front has been obsidian sourcing. While much attention has been paid to locating Ecuadorian obsidian sources and documenting their variability, only a few studies have focused on sourcing archaeological artifacts to understand the processes responsible for the distribution of obsidian in prehistory. The results of some of the first chemical characterization analyses of obsidian from Integration Period (ca. AD 700-1500) earthen mound (*tola*) sites in the País Caranqui region of highland northern Ecuador are presented in this chapter. The analyses of obsidian assemblages from two *tola* sites, Huataviro and Puntiachíl, suggest that there was differential access to low Fe Callejones obsidian during the Integration Period. Results also suggest that independent procurement processes most likely are responsible for the obsidian distribution patterns observed in the archaeological record. This initial research demonstrates that Caranquis primarily exploited Callejones and Mullumica obsidian. These sources most likely were utilized because of their proximity and it appears that there was some connection between the expedient flake technology employed

by Caranquis and the lower quality obsidian from these sources. From the standpoint of chemical characterization research, the results of this study demonstrate that the Bruker Tracer III-V+ SD portable X-ray fluorescence (pXRF) instrumentation is capable of producing data that are accurate and precise enough to attribute artifacts to known Ecuadorian obsidian source signatures. The ability to bring portable XRF instrumentation to Ecuador will significantly aid in the further examination of some of the initial findings presented in this chapter.

Introduction

The movement of raw materials and resources in prehistoric Ecuador commonly is viewed as an exception to the non-commercial economies that are believed to have dominated much of the prehistoric Andes. In northern Ecuador, there is ethnohistoric evidence for both long-distance exchange conducted by traders known as *mindaláes* and marketplaces or *tiangueces* in cities such as Quito (*1–7*). Ethnohistoric and archaeological evidence also suggest that the following goods likely were involved in some form of long-distance exchange: coca, capsicum pepper, cinnamon, cotton, salt, pottery, gold, shell, greenstone axes, and obsidian (*1*, *2*, *4*, *8–10*).

Unfortunately for archaeologists, many of these resources either are perishable and do not survive in the archaeological record, or have proven difficult to tie to raw material sources. Some studies have attempted to document the movement of ceramic wares (*3*, *11*) but most of the research conducted on exchange goods has focused on the distribution of obsidian (*2*, *12–24*). A majority of this research has been devoted to documenting the existence of various obsidian sources and their respective geochemical signatures (*12–17*, *19–22*) and only a few researchers have attempted to use geochemical sourcing data to address archaeological questions (*2*, *18*, *23*, *24*).

In this chapter, we examine the nature of long-distance exchange during the Integration Period (ca. AD 700-1500) in the País Caranqui region of highland northern Ecuador. As probable habitation and burial areas for elites, large earthen mounds called *tolas* often display evidence of long-distance exchange (*5*, *25–27*). We present the results of portable X-ray fluorescence (pXRF) analyses on 49 obsidian source specimens as well as 87 obsidian artifacts from excavated contexts at the *tola* sites of Huataviro and Puntiachíl.

From a geochemical perspective, these results demonstrate that the Bruker Tracer III-V+ SD pXRF instrumentation is capable of producing data that are accurate and precise enough to differentiate between Ecuadorian obsidian source areas and assign artifacts to known sources. From an archaeological standpoint, the results suggest that Mullumica and Callejones were the primary obsidian sources utilized by late prehistoric groups living in the northern highlands. Data also suggest differential access to a low Fe variant of Callejones obsidian between *tola* sites and a relationship between the Caranqui's expedient flake technology and the utilization of Mullumica and Callejones obsidian. These findings suggest

that individuals at Huataviro likely had a different mechanism for procuring obsidian than individuals at Puntiachíl. While further analyses from additional *tolas* are planned, these initial results suggest that elites at different *tola* sites procured obsidian via different interaction networks and not through some form of centralized process.

Background

Compared to its Andean counterparts, highland Ecuador has not received much attention in archaeological circles. Much of the recent archaeological research has focused on the Inka's advance into regions of Ecuador and the resulting responses by local populations (*18*, *23*, *28–33*). A notable byproduct of the increasing interest in Inka imperial conquest and consolidation has been a better understanding of the late prehistoric Ecuadorian societies that the Inka encountered. This archaeological research has benefited greatly from ethnohistoric documents that describe local societies (*1*, *34–47*). To orient the reader, the background section is divided into three sub-sections: the Integration Period in the País Caranqui, obsidian research in Ecuador, and information on the two sites examined in this research.

Integration Period in the País Caranqui

The País Caranqui is a small region in the northern highlands of Ecuador bounded by the Mira-Chota River in the north and the Guayllabamba River in the south (*5*, *25*). The eastern and western boundaries are less defined, but Bray (*5*) proposes the continental divide in the east and the Intag River to the west. These proposed boundaries produce a region of roughly 3,600 km² (*5*). A map of the País Caranqui with sites discussed can be found in Figure 1.

País Caranqui society is best characterized as a collection of relatively equivalent chiefdoms with status continually negotiated along multiple dimensions (*5*). The region's inhabitants appear to have had a shared ethnic identity based on a common lingua franca, artistic tradition, level of technological expertise, and style of monumental earthwork (*1*, *5*, *27*, *48*, *49*). The monumental earthworks, or *tolas*, that dot the landscape have been the focus of the majority of archaeological research to date (*8*, *26*, *27*, *50–55*). These *tolas* appear to have been the realm of elite individuals and served as occasional gathering places for ceremonial activities (*5*, *43*, *50*, *52*, *55*, *56*).

Tolas can be divided into two varieties: hemispherical and quadrilateral. Examples of these two varieties can be seen in Figure 2. The two varieties are often found within a single cluster (i.e., they are not mutually exclusive), and the quantity of *tolas* in a cluster typically numbers between 10 and 40 (*5*). Hemispherical *tolas* appear as early as AD 500 and were a well-established feature of the region by AD 700 (*5*, *8*, *26*, *48*). These *tolas* range from 3-6 meters in diameter and 1-2 meters in height to 30 meters in diameter and 5 meters in height (*5*). Smaller hemispherical *tolas* appear to have served as burial mounds whereas larger hemispherical *tolas* were used for both habitation and burials (*5*, *25*).

Quadrilateral *tolas* appear to be a later phenomenon marking a shift in the sociopolitical organization of the region tied to increased population size and agricultural productivity (*5, 25, 48, 57, 58*). The quadrilateral *tolas* were first constructed around AD 1250 and are as large as 90 meters on a single side and up to 20 meters in height (*25, 48*). These larger *tolas* were the foundations for circular habitation structures and occasionally burials (*5, 53*). Arguably the most notable features found on *tolas* are canal-like features with conical stones that are believed to have been hearths for the production of *chicha* (fermented maize alcohol) for special feasts and other rituals (*1, 5, 8, 25, 53*). These features highlight the ability of elites to hold feasts as a likely status indicator (*8*).
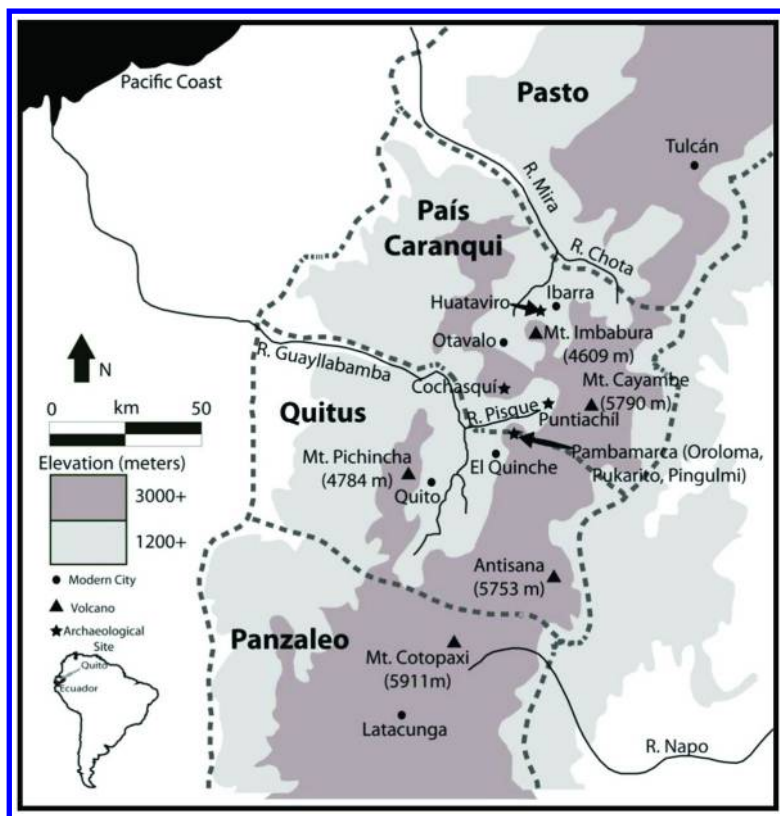
Figure 1. Map of highland northern Ecuador with sites mentioned in chapter. Pambamarca area includes the sites of Oroloma, Pukarito, and Pingulmi mentioned in the discussion.

Evidence from *tola* investigations and ethnohistorical documents suggests that obtaining non-local prestige goods was another major avenue for elites to maintain and demonstrate their status in Caranqui society (*1*). A pair of archaeological contexts exemplify the importance of non-local goods in the late prehistory of this region. Research at sites in the Mira-Chota valley in the northern reaches of the País Caranqui has encountered non-local goods that include obsidian, gold, shell,

In Archaeological Chemistry VIII; Armitage, R., et al.;
ACS Symposium Series; American Chemical Society: Washington, DC, 2013.

greenstone axes, and non-local pottery (*3*, *4*, *54*, *59–63*). Meanwhile, excavations at one of the sites examined in this paper, Huataviro, have uncovered funerary contexts that included goods such as shell beads, a gold mask, gold bracelets, and gold rings (*27*).

Figure 2. Photo at Cochasqui with examples of the two tola varieties. A hemispherical tola is in the right foreground while a pair of quadrilateral tolas can been seen in the left background (Eric Dyrdahl).

Although archaeological research provides evidence for the movement of non-local goods into the País Caranqui, little insight exists regarding the mechanisms utilized to procure non-local goods. Fortunately, ethnohistoric documents highlight a pair of processes that were utilized by Caranquis. Ethnohistoric documents discuss the importance of *mindaláes*, a group of traders that specialized in the trade of low-weight, high-value prestige goods (*1*). Ethnohistorians have debated whether the mindalá were attached or independent specialists (*1*, *46*), and hopefully future archaeological research can address this issue. Regardless of the exact nature of their relationship with elites, the goods transported by *mindaláes* most likely would have been marketed toward elites. Documents from colonial times also suggest that households maintained their own exchange networks to procure non-local goods (*1*, *5*). There is no evidence that non-local resources were obtained solely from *mindaláes* or more informal exchange networks and the reality is most likely varying combinations of the two.

Considering the ethnohistoric evidence for the importance of non-local goods and the archaeological documentation of caches of these goods, it is surprising that artifact assemblages from *tolas* are relatively limited (*5*, *54*). In most instances, there is little evidence for differentiation among groups. It has

been suggested that chiefs, or *caciques*, maintained a residence in their home community as well as at a *tola* cluster (*1*), so minimal evidence for occupation is not necessarily surprising (*5*, *43*). Bray (*5*) suggests that considering the homogeneity and rudimentary nature of the artifact assemblages from occupation contexts, the most likely explanation is that each social unit produced its own crafts and tools. The mortuary contexts found in *tolas* typically have limited assemblages, with few ceramic vessels, including non-local Panzaleo ceramics, and a *mano* or *metate* (*5*). Additionally, the location of the *tolas* themselves normally is limited to the prime maize-growing area of the region and does not appear to suggest any control of special resource zones (*5*, *25*, *55*). Simply put, more research is needed to better understand the discrepancy between the importance placed on long-distance exchange documented in portions of the archaeological and ethnohistorical records and the limited assemblages found in many *tola* excavations.

Obsidian Research in Ecuador

Obsidian is arguably the best non-local resource available to investigate Integration Period procurement strategies. Obsidian tool production is an ideal process to examine in studies on long-distance resource procurement for a pair of reasons. First, the production of sharp cutting edges of obsidian requires the reduction of nodules from raw material sources. The process of obsidian nodule reduction produces both finished tools and waste that can be analyzed to understand the manufacturing techniques employed because of obsidian's predictable conchoidal fracture pattern (*64*). Throughout northern Ecuadorian prehistory, it appears that obsidian was the material of choice for producing expedient flake tools that could be utilized for a variety of tasks (*2*).

The other key aspect of obsidian relevant to studies of procurement strategies is that it is a product of rapidly-cooled lava from volcanic eruptions. This process limits the distribution of obsidian to small numbers of discrete, chemically homogenous flows often located in difficult-to-reach locations at higher elevations (*2*, *12–22*). Twelve obsidian sources have been documented in Ecuador. A map with the location of the 11 obsidian sources located in northern Ecuador can be found in Figure 3. Carboncillo, the 12th obsidian source in Ecuador, is located in the southern highlands in the Loja Province (*20*). Geochemical characterization of archaeological artifacts suggests that only six of these sources were utilized in prehistory (*2*, *18*, *20–24*).

For northern Ecuador, research conducted to date suggests that the most important sources were the Mullumica, Callejones, Yanaurco, and Quiscatola sources along with two La Chimba types whose source areas remain uncertain (*2*, *18*). As depicted in Figure 3, the four documented sources are located in a relatively tight cluster to the south-southeast of the País Caranqui, roughly 35 km east of Quito in the Sierra de Guamaní (*18*, *21*). In contrast, the two La Chimba types, first identified by Asaro et al. (*22*), receive their name from the site with the first documented artifacts with these geochemical signatures (*22*).

Unlike most other regions of the world, chemical characterization studies of Ecuadorian obsidian are somewhat challenging. Two sets of source areas adjacent

to one another, Callejones-Mullumica and Yanaurco-Quiscatola, are chemically indistinguishable and often lumped together (*21*). Additionally, obsidian from both the Callejones and Mullumica source areas have highly variable compositions. It appears that at least one low Fe variant for both Callejones and Mullumica can be differentiated from a high Fe Callejones-Mullumica signature (*17*, *18*). While Ogburn et al. (*18*) present the high Fe Callejones-Mullumica cluster as high Fe Mullumica, recent research has suggested that distinguishing between high Fe Mullumica and Callejones often is not possible (*21*). Therefore, in the discussion section we treat Ogburn et al.'s (*18*) high Fe Mullumica assignments as high Fe Callejones-Mullumica.
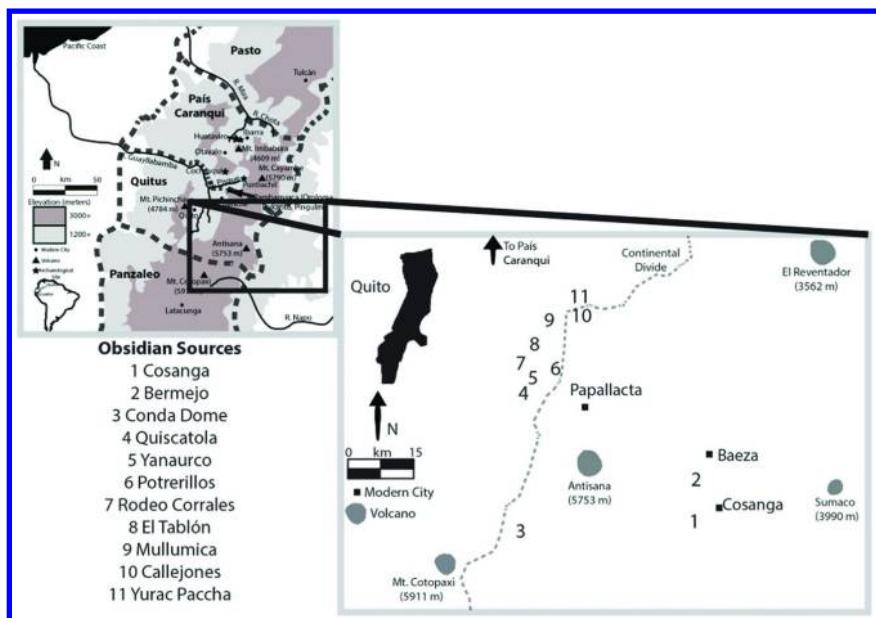
Figure 3. Map of obsidian sources in northern Ecuador.

The recent collection of new geologic samples from these sources documented the potential low Fe variant of Callejones in the eastern reaches of the source area (*17*). This chemical signature matches one of Asaro et al.'s (*22*) La Chimba types (*18*), potentially leaving only one undocumented source area in Ecuador (i.e., the other La Chimba type signature). However, considering the different techniques employed in the relevant studies and the resulting issues of data comparability (see (*65*, *66*)), this conclusion should be treated with caution and highlights the need for further sampling of these complex source areas. Following Ogburn et al. (*18*), we tentatively treat the one La Chimba type signature that appears to have the same chemical signature as a section of the Callejones source area as a "low Fe variant of Callejones." Meanwhile, the remaining La Chimba type signature from a source area of unknown origin is referred to as the "La Chimba type."

Another issue that must be addressed is how representative obsidian procurement is of the procurement processes for the other non-local goods valued

in Caranqui society. The available evidence for obsidian utilization in the País Caranqui indicates obsidian was used almost completely for the production of expedient flake tools (*2*, *4*). This makes obsidian a utilitarian, high-weight, low-value good that stands in stark contrast to the other non-local goods of low weight and high value that were brought into the País Caranqui. This fact makes it likely that obsidian was not a resource within the *mindaláes*' purview (*2*), but it potentially could still have been moved via informal exchange networks.

Site Background

A majority of the obsidian artifacts (n=65) sourced in this study came from the site of Huataviro. This site, first examined during a cultural resource management salvage project, contains a single hemispherical *tola* located in the parish of San Antonio de Ibarra outside of the modern city of Ibarra (Figure 1) (*27*). An investigation of the *tola* was undertaken because a tractor plowing the area uncovered human remains and archaeological artifacts.

This large hemispherical *tola* included evidence of both occupation floors and burials (*27*). For the most part, these contexts alternate in the site's stratigraphy with one stacked on top of another. The excavations focused on documenting the 11 burials within the *tola*. Multiple burials contained goods indicative of long-distance exchange: non-local, fineware ceramics, shell beads, gold rings, gold bracelets, and a gold mask (*27*). Radiocarbon dates of organic materials from burial contexts returned dates ranging from cal. AD 680 to 1300 at two sigma confidence intervals (*27*).

Interestingly, obsidian was not found as a grave good in any of these tombs. Instead, it was routinely found in small quantities in the fill placed between the *cangahua* (hard-packed volcanic mud) blocks used to line the tombs (*27*). The nature of this location makes it difficult to definitively demonstrate which primary context these goods were produced in. Therefore, the results of our geochemical characterization research are treated as merely representative of the site's overall obsidian assemblage and no attempt is made to compare assemblages from various tomb contexts. Despite the lack of clear primary contexts, the obsidian assemblage still is most likely the product of elite activities because the available evidence and our current understanding of Caranqui society suggest there was no permanent non-elite activity at this *tola* site. In total, 97 lithic artifacts were found during excavations at Huataviro, and roughly 80% of the lithic assemblage was obsidian (*27*). An examination of the obsidian found that 65 artifacts were suitable for pXRF analysis. An ideal sample for pXRF analysis is at least 5 mm wide, 8 mm long, and 5 mm thick with at minimum one flat, homogenous surface.

The other set of obsidian artifacts (n=22) analyzed came from the multi-*tola* site of Puntiachíl located in the eastern portion of the modern town of Cayambe. Unlike Huataviro, Puntiachíl was occupied at the time of the Inka's arrival in the region (*8*, *26*). The site is believed to be the center of the Cayambe polity during late prehistory. Notably, Larrain (*67*) suggests that the Cayambe *cacique* Nasacoto Puento was the most powerful *cacique* in the region based on his spearheading the joint resistance to Inka subjugation (*5*).

In the mid-1980's, Buys et al. (*68*) surveyed Puntiachíl and identified seven quadrilateral mounds and nine hemispherical mounds of varying sizes. Due to multiple destructive factors, most of these mounds had been destroyed or were in the process of being ruined at the time of their survey (*8*). As part of her dissertation research, Cordero conducted excavations at the main quadrilateral *tola* at Puntiachíl. Her research documented a significant amount of non-local Panzaleo ceramics that likely came from the eastern lowlands (*3*, *8*, *26*). Organic material pulled from excavations at this mound returned radiocarbon dates ranging from cal. AD 670 to well into historic times (*8*, *26*), suggesting that Puntiachíl was occupied throughout the Integration Period.

All of the obsidian artifacts from Puntiachíl that are analyzed in this study came from various levels of a single *tola*, Tola Peña. Minimal excavations were undertaken at this secondary *tola* and a limited sample of obsidian artifacts was recovered. Although obsidian was obtained from six levels within Tola Peña's stratigraphy, most of it came from a single context. The limited obsidian assemblage available, combined with the lack of absolute dates for Tola Peña, led to the decision to consider the sample as representative of its entire occupation and not to draw inferences about change through time in obsidian procurement. Despite its limitations, the available sample is a useful starting point for understanding the variation in procurement practices and documenting the different obsidian sources utilized by the elite segment of Caranqui society.

Methods

The 87 obsidian artifacts and 49 geologic source specimens were analyzed using a Bruker Tracer III-V+ SD XRF spectrometer equipped with a rhodium target X-ray tube and a silicon drift detector. The silicon drift detector has a resolution of ca. 145 eV FWHM for 5.9 keV X-rays (at 200,000 counts per second) in an area of 10 mm². All samples were measured at 40 kV, 25 µA, with a 12 mil Al, 1 mil Ti, 6 mil Cu filter placed in the X-ray path for a 200-second live-time count. Ten elements were measured: Mn, Fe, Zn, Ga, Th, Rb, Sr, Y, Zr, and Nb. Peak intensities for the Kα peaks of each element were calculated as ratios to the Compton peak of rhodium, and converted to parts-per-million using a calibration based on a set of 40 obsidian standards with known values provided by Bruker. The one exception was Th, for which the Lα peak was used. All analyses were conducted at the Center for Applied Isotope Studies at the University of Georgia in 2012.

Most source specimens (n=40) were loaned to the primary author by the University of Missouri Archaeometry Laboratory. The remaining nine source specimens were collected during a visit to the Mullumica source area in 2011. The geographical coordinates for the two contexts where Mullumica specimens were collected by the primary author can be found in Table I. The 87 obsidian artifacts were loaned to the primary author from the reserve of the Instituto Nacional de Patrimonio Cultural in Quito.

Table I. Information for collection locales at Mullumica source area

Context	Longitude	Latitude	Number of Samples
1	-78.22872	-0.23520	2
2	-78.22489	-0.23230	7

Coordinates are in decimal degrees.

A sample of USGS RGM-1 was analyzed daily over the duration of the analyses in order to check the accuracy and precision of the instrument and calibration. The results of these analyses and the recommended values and values documented by other researchers for this standard can be found in Table II. The data from the Bruker Tracer III-V+ SD instrumentation for RGM-1 are comparable to other published values, demonstrating that the data from our analyses are accurate and precise enough to confidently make source attributions for obsidian artifacts of unknown origin in instances where the relevant sources have discrete chemical signatures.

Table II. Summary statistics for replicate analysis of USGS RGM-1 compared to recommended values and other published values

	This Study (n=6)	USGS Recom.	Shackley (2012)	Skinner (1996)	Hughes (2007)
Mn	282 ± 5	279 ± 50	302 ± 14	291 ± 47	278 ± 10
Fe	12473 ± 223	13010 ± 210	13116 ± 308	13480 ± 745	13079 ± 140
Zn	32 ± 1	32	n.r.	37 ± 7	n.r.
Th	15 ± 1	15 ± 1.3	16 ± 3	n.r.	n.r.
Rb	153 ± 2	150 ± 8	151 ± 3	152 ± 3	143 ± 4
Sr	111 ± 2	110 ± 10	106 ± 3	107 ± 9	105 ± 3
Y	27 ± 1	25	25 ± 2	24 ± 3	23 ± 3
Zr	221 ± 3	220 ± 20	219 ± 5	217 ± 8	214 ± 4
Nb	10 ± 1	8.9 ± 0.6	9 ± 2	11 ± 1	8 ± 3

All concentration values are in parts per million (ppm) and unreported values are designated (n.r.).

Results

Summary statistics for the geologic source samples analyzed can be found in Table III. These data demonstrate that the best way to differentiate between the various source areas and geochemical signatures is a bivariate plot of two ratios: Sr/Zr and Rb/Zr. The data are presented in this format in Figure 4. This manner of presentation is preferable because it allows for the consideration of three

important discriminating elements without having to present a three-dimensional plot on a two-dimensional surface. This bivariate plot demonstrates that with this particular methodology, the Bruker Tracer III-V+ SD instrumentation is able to differentiate among the major sources of Ecuadorian obsidian. The one issue is the small number of source samples available for the minor source of Bermejo. Although not enough samples were analyzed to produce a 95% confidence ellipse, it appears that this signature is discrete when looking solely at the source samples.

When the 87 artifacts are added to the source sample bivariate plot of Sr/Zr and Rb/Zr ratios as seen in Figure 5, a small theoretical Bermejo ellipse overlaps slightly with the low Fe Callejones ellipse. This issue was not apparent in Figure 4 because no source samples with the low Fe Callejones signature were available for inclusion in this research. The signature is only represented in the artifact assemblages. For these two ratios, the Bermejo samples also are quite comparable with the low Fe Mullumica variant as well as the Cosanga B signature. Fortunately, Bermejo and Cosanga B obsidian can be distinguished from low Fe Mullumica and Callejones obsidian because of their distinct Mn concentrations. This can be seen in the Mn vs. Nb bivariate plot in Figure 6 as well as the summary statistics presented in Table III. Once the Mn concentrations are taken into account, it is clear that none of the 87 artifacts analyzed in this research were produced with raw material from the Bermejo or Cosanga source areas.

The summary statistics for the groups of artifacts assigned to various source signatures are provided in Table IV. In addition to the previously mentioned low Fe Callejones variant, two other signatures not documented in the source material were identified. One of these is the La Chimba type whose source area is still unknown (*18*, *22*). This chemical signature is represented by two artifacts. The other new chemical signature is represented by a single artifact. This unassigned artifact has a chemical signature that does not match any known source area in the Andes.

Of the eight source signatures present in our analysis of the source samples, only two are relevant for the artifact assemblages. One of these is the high Fe cluster of Callejones-Mullumica. The other is the low Fe variant of the Mullumica source area. In previous research scholars have suggested that the range of variation in the low Fe Mullumica variant is best treated as one sub-signature (*18*). However, it appears that it might be possible to divide the low Fe Mullumica group in this study into two distinct sub-groups. One of these would cluster nicely with the primary author's source material and have a lower Sr/Zr ratio and higher Rb/Zr ratio than the other sub-group. The other sub-group's signature would vary only slightly and most likely is from the Mullumica source area, but it does not match any documented source material. In another research project, this issue will be examined further. For the purposes of this chapter, this set of artifacts is treated as part of the low Fe Mullumica group.

Source assignments for the archaeological obsidian are provided in Table V. At Huataviro, 79% of the samples analyzed (n=51) were produced with raw material from the high Fe Callejones-Mullumica cluster. Eleven artifacts, or 17% of the assemblage, were assigned to the low Fe Mullumica variant. Two other signatures, the low Fe Callejones variant and La Chimba type, were found in small quantities.

Table III. Summary statistics for Ecuadorian obsidian sources analyzed via pXRF

Element	Bermejo (n=3)	Carboncillo (n=6)	Cosanga A (n=6)	Cosanga B (n=7)
Mn	630 ± 34	502 ± 26	901 ± 36	830 ± 22
Fe	5467 ± 145	9844 ± 328	5169 ± 280	6441 ± 152
Zn	36 ± 4	55 ± 3	52 ± 4	51 ± 3
Ga	19 ± 1	21 ± 1	20 ± 1	20 ± 2
Th	14 ± 2	14 ± 1	10 ± 1	13 ± 1
Rb	135 ± 1	134 ± 5	147 ± 7	132 ± 2
Sr	148 ± 17	85 ± 3	87 ± 5	180 ± 6
Y	17 ± 2	39 ± 2	22 ± 2	18 ± 1
Zr	91 ± 3	120 ± 5	65 ± 3	105 ± 9
Nb	18 ± 1	15 ± 1	21 ± 2	20 ± 1
Sr/Zr	1.63 ± 0.16	0.71 ± 0.02	1.34 ± 0.06	1.72 ± 0.15
Rb/Zr	1.48 ± 0.05	1.12 ± 0.03	2.26 ± 0.06	1.26 ± 0.09

Element	Yanaurco-Quiscatola (n=5)	El Tablón (n=4)	High Fe Callejones-Mullumica (n=9)	Low Fe Mullumica (n=9)
Mn	320 ± 39	436 ± 29	461 ± 32	341 ± 16
Fe	4394 ± 94	6816 ± 646	9733 ± 251	4802 ± 156
Zn	26 ± 3	55 ± 8	46 ± 5	31 ± 3
Ga	17 ± 1	20 ± 1	20 ± 1	18 ± 1
Th	18 ± 1	14 ± 1	16 ± 1	17 ± 2
Rb	165 ± 3	153 ± 14	123 ± 3	137 ± 3
Sr	78 ± 2	14 ± 2	247 ± 10	102 ± 4
Y	16 ± 1	25 ± 3	12 ± 2	13 ± 1
Zr	69 ± 1	118 ± 8	164 ± 4	85 ± 2
Nb	13 ± 1	15 ± 2	14 ± 1	11 ± 1
Sr/Zr	1.14 ± 0.03	0.12 ± 0.02	1.51 ± 0.04	1.20 ± 0.04
Rb/Zr	2.41 ± 0.03	1.30 ± 0.10	0.75 ± 0.02	1.61 ± 0.05

Concentration values for the 10 elements are in parts per million (ppm).
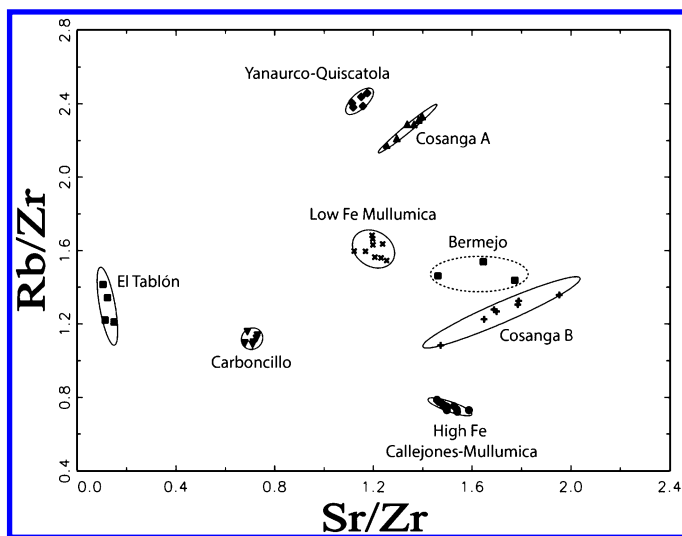
Figure 4. Bivariate plot of Sr/Zr vs. Rb/Zr for the 49 source samples analyzed via pXRF. All solid ellipses represent 95% confidence intervals, while the dotted-line ellipse represents a theoretical range.
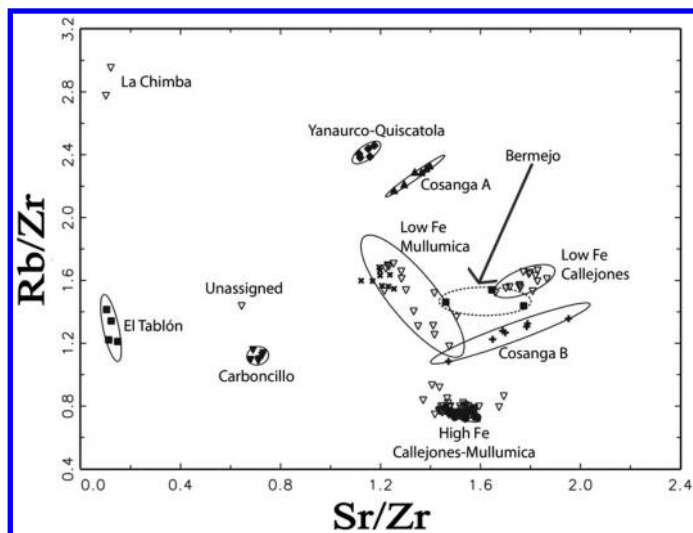
Figure 5. Bivariate plot of Sr/Zr vs. Rb/Zr for the 49 source samples and 87 artifacts analyzed via pXRF. Source samples are in bold and artifacts are presented as unshaded, inverted triangles. All solid ellipses represent 95% confidence intervals, while the dotted-line ellipse represents a theoretical range.
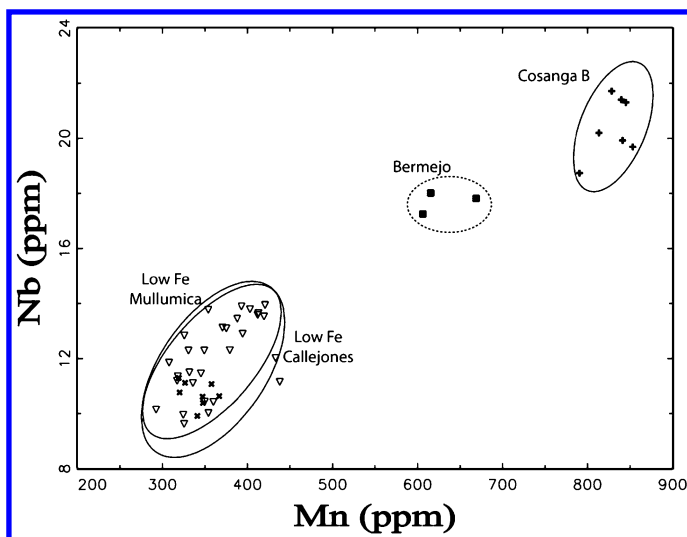
Figure 6. Bivariate plot of Mn vs. Nb for Bermejo, Cosanga B, low Fe Mullumica, and low Fe Callejones material. Source samples are in bold and artifacts are presented as unshaded, inverted triangles. All solid ellipses represent 95% confidence intervals, while the dotted-line ellipse represents a theoretical range. Concentration values are in parts per million (ppm).

Table IV. Summary statistics by source assignment for Ecuadorian obsidian artifacts

	High Fe Cal.-Mul. (n=55)	Low Fe Mullumica (n=15)	Low Fe Callejones (n=14)	La Chimba (n=2)	n.a.
Mn	469 ± 41	368 ± 243	360 ± 39	515 ± 76	316
Fe	10249 ± 829	6009 ± 508	6026 ± 630	6959 ± 163	6864
Zn	45 ± 5	34 ± 4	34 ± 5	42 ± 7	39
Ga	21 ± 2	19 ± 1	20 ± 2	20 ± 1	19
Th	16 ± 1	18 ± 2	20 ± 2	16 ± 1	16
Rb	130 ± 7	150 ± 9	149 ± 14	214 ± 2	141
Sr	253 ± 18	135 ± 22	166 ± 14	8 ± 1	63
Y	13 ± 2	14 ± 2	12 ± 2	39 ± 3	19
Zr	167 ± 7	101 ± 11	93 ± 8	75 ± 2	98
Nb	15 ± 1	13 ± 1	12 ± 1	18 ± 1	12

Table IV. (Continued). Summary statistics by source assignment for Ecuadorian obsidian artifacts

	High Fe Cal.-Mul. (n=55)	Low Fe Mullumica (n=15)	Low Fe Callejones (n=14)	La Chimba (n=2)	n.a.
Sr/Zr	1.52 ± 0.06	1.33 ± 0.10	1.78 ± 0.06	0.11 ± 0.01	0.64
Rb/Zr	0.78 ± 0.04	1.49 ± 0.18	1.60 ± 0.05	2.87 ± 0.13	1.44

Concentration values for the 10 elements are in parts per million (ppm). The final column contains values for the single unassigned artifact in study (n.a.).

Table V. Source assignments for the Huataviro and Puntiachíl assemblages

Source	Huataviro	Puntiachíl	Total
High Fe Callejones-Mullumica	51	4	55
Low Fe Mullumica	11	4	15
Low Fe Callejones	1	13	14
La Chimba type	2	0	2
Unassigned	0	1	1
Total	65	22	87

The Puntiachíl assemblage has a much different composition. Thirteen artifacts, or 59% of the assemblage, were assigned to the low Fe Callejones variant. In ongoing dissertation research being conducted by the primary author, Puntiachíl stands alone as the single site out of 80 whose assemblage consists of more than 10% of the low Fe Callejones variant. Both the high Fe Callejones-Mullumica cluster and the low Fe Mullumica variant constituted 18% of the assemblage. Finally, the single artifact in this study that could not be assigned to a known source area came from Puntiachíl.

Discussion

Although artifacts from two known source areas are present at Huataviro and Puntiachíl, the highly variable nature of these sources provides the opportunity to identify multiple extraction locales in each source area (*18*). The data suggest that Huataviro and Puntiachíl had separate means of procuring obsidian. In fact, the two assemblages are almost the inverse of one another. Huataviro's assemblage consists of primarily high Fe Callejones-Mullumica with smaller quantities of the low Fe variants of Mullumica and Callejones and the La Chimba type. On the other hand, the majority of Puntiachíl's assemblage is low Fe Callejones with small quantities of high Fe Callejones-Mullumica and low Fe Mullumica. The issue of

the contemporaneity of the various intra-site contexts is difficult to address, but based on the available data there is no reason to believe that the artifacts analyzed are not representative of each site's overall assemblage.

The ability to make inferences about the processes responsible for the documented patterns is severely limited by the scope of this initial study. Using geochemical data, archaeologists sometimes are able to differentiate between independent and centralized procurement processes (*69*). In this instance, the data presented in this chapter suggest that *mindaláes* were not responsible for the transport and exchange of obsidian (*2*). If *mindaláes* or some centralized process was responsible, we typically would expect to find more evidence of homogenization in assemblages because a small group of individuals would be responsible for a significant portion of the obsidian distribution in the País Caranqui (*69*).

The small quantities of obsidian found at Integration Period sites provide additional support for informal distribution processes moving obsidian. Although obsidian constitutes the majority of lithics found at Caranqui sites, the quantity of obsidian typically numbers in the hundreds. This pales in comparison to the assemblages from major blade production areas such as central Mexico that often number in the hundreds of thousands (e.g. (*64*, *69*)). Based on the small quantities of lithics present, it would appear that obsidian artifacts either were heavily curated or a large number of perishable tools were employed in lieu of lithics. If merchant-like entities such as *mindaláes* were involved in obsidian distribution, we would expect to find much larger assemblages of obsidian and evidence for more intensive quarrying activity.

The available data suggest that an independent, decentralized process was responsible for the differences in the assemblages. The most likely process would be the household-to-household exchange networks outlined in the ethnohistorical record (*1*). Based on the differences in the two assemblages presented in this chapter, additional research and analysis of obsidian from more *tola* sites is underway. In particular, an effort to obtain more obsidian artifacts from Puntiachíl will be undertaken because of its assemblage's unique composition.

Some of the more interesting findings from this study of obsidian procurement at *tola* sites come from comparisons with the limited set of artifacts previously sourced by other researchers. In the seminal work on Ecuadorian obsidian sourcing, Burger, Asaro and colleagues suggest that Yanaurco, Quiscatola, and Mullumica were the most heavily utilized source areas in Ecuadorian prehistory (*2*). While the Callejones obsidian source only had recently been identified at the time of their publication (*2*), the notable finding of our research is that Yanaurco-Quiscatola obsidian probably was not heavily utilized in the País Caranqui during the Integration Period. This finding supports Ogburn et al.'s (*18*) analyses of material from late Caranqui fortifications that did not include any Yanaurco-Quiscatola material. This also supports the hypothesis that utilization of the Yanaurco and Quiscatola source areas ceased around AD 1000 and was not reinitiated until the Inka arrived in the region (*15*, *18*).

Part of the explanation for the lack of Yanaurco-Quiscatola obsidian in the País Caranqui during the Integration Period might stem from the lithic technology employed. The obsidian assemblage typically includes only small flake fragments

(e.g. (*4*, *18*)) or artifacts that exhibit evidence of bipolar reduction. Therefore, it appears that most obsidian raw material in the País Caranqui was utilized to produce crude expedient flake tools. Based on his research on the Mullumica and Quiscatola source areas, Salazar (*12*, *14*) suggests that the Quiscatola source is much more homogenous than Mullumica and contains higher quality obsidian (*2*). It is probable that in locales where blade production was undertaken, raw material from the higher quality Quiscatola source would have been utilized (*2*).

The lack of Yanaurco-Quiscatola obsidian suggests that individuals might have prioritized limiting procurement costs over obtaining higher quality obsidian. The Mullumica and Callejones source areas are slightly closer to the País Caranqui than Yanaurco and Quiscatola and would have been easier to access based on least-cost path analyses (*23*) (Figure 3). Considering the lithic technology employed in the País Caranqui did not require the highest quality obsidian available, it would have been possible to make the trade-off of lower quality obsidian for lower procurement costs. Alternatively, the lithic technology could have been constrained by package size and the inability to access obsidian of a higher quality than Mullumica or Callejones. At this time, we believe that the former possibility is more likely because there is no available evidence that suggests Caranquis would have been unable to access the Yanaurco or Quiscatola sources that were no more than 25 additional km away (Figure 3). Future research will investigate this issue further.

As part of their study on military procurement strategies, Ogburn et al. (*18*) analyzed 29 obsidian artifacts from the rural habitation site of Oroloma (Figure 1). The inhabitants of this site likely focused on exploiting the mountainous grassland *páramo* ecozone found at elevations above 3200 masl (*18*, *70*). A radiocarbon date and composition analysis of a relevant volcanic ash lens suggest that this site dates to the earlier portion of the Integration Period (cal. AD 690-930) (*70*).

Recently Schreyer (*23*) reanalyzed Ogburn et al.'s (*18*) samples as well as some additional obsidian from Oroloma. She modified some source assignments based on a combination of inductively coupled plasma mass spectrometry and pXRF data. However, considering the issues related to comparing data produced via different chemical characterization techniques (see (*65*, *66*)), we refer only to Ogburn et al.'s (*18*) original source attributions for the Oroloma assemblage. The same practice was applied when considering the obsidian assemblages from the sites of Pukarito and Pingulmi mentioned later in this section.

Fifty-nine percent of the obsidian (n=17) analyzed from Oroloma was attributed to the high Fe Callejones-Mullumica signature. Material with the low Fe Mullumica signature also constituted a healthy portion of the assemblage, representing 28% (n=8) of the samples analyzed. Finally, two artifacts were attributed to both the low Fe Callejones variant and the La Chimba type (*18*).

The composition of the Oroloma assemblage matches the Huataviro assemblage presented in this chapter. In both instances, the high Fe Callejones-Mullumica signature constitutes the majority of the assemblage. Low Fe Mullumica material represents roughly 30-40% of the assemblage and the La Chimba type and low Fe Callejones variant are found in small quantities. This finding suggests that Huataviro and Oroloma utilized similar procurement strategies to obtain obsidian. It also reiterates that the Puntiachíl assemblage is

distinct from the other assemblages analyzed to date. Considering the limited research and the large time spans covered by these sites, it is difficult to determine whether this difference is a product of independent processes or a shift through time in obsidian procurement strategies.

However, additional evidence from Ogburn et al. (*18*) indicates that the Puntiachíl assemblage would be unique even if Tola Peña was only occupied at the end of the Integration Period and was not contemporaneous with Huataviro or Oroloma. As part of their study, Ogburn and colleagues also analyzed obsidian from two late prehistoric Caranqui fortresses: Pukarito and Pingulmi. The obsidian assemblages from these two fortresses had compositions similar to the Huataviro and Oroloma assemblages (*18*). The only notable difference is none of the seven artifacts analyzed from Pukarito were produced from raw material with the low Fe Mullumica signature (*18*). The fact that this type of assemblage composition appears to extend to the end of the Integration Period suggests that a different procurement network is likely responsible for the Puntiachíl assemblage. More research will be done to try to determine which of the possibilities is more likely.

Conclusion

This research produced some interesting findings despite the fact that it represents only an initial examination of obsidian assemblages from Integration Period *tola* sites. The analysis of a combination of source samples and artifacts demonstrates that the Bruker Tracer III-V+ SD is capable of characterizing Ecuadorian obsidian in a manner that is useful to archaeologists. This is important given the portability of pXRF instrumentation and its rapid method of characterization which allows for its use outside traditional laboratory settings (*71*). This is especially significant considering the possibility that the low Fe Mullumica signature can be divided into multiple sub-groups. A much larger assemblage is needed to examine this possibility and the characteristics of pXRF instrumentation will greatly aid in this endeavor.

The most exciting finding of this study from an archaeological perspective is that Puntiachíl has a unique obsidian assemblage compared to other sites in the País Caranqui. This suggests that some form of independent procurement process was responsible for the distribution pattern of obsidian observed in this study. A second important archaeological finding is that Callejones and Mullumica obsidian were more heavily utilized than material from Yanaurco and Quiscatola. This likely is related to the use of a lithic technology in the País Caranqui that could employ obsidian of an adequate yet lower quality. Ultimately, the initial findings of this study demonstrate the need for additional research on Ecuadorian obsidian along a number of fronts.

Conflict of Interest Statement

Acknowledgments

References

1. Salomon, F. *Native Lords of Quito in the Age of the Incas: The Political Economy of North Andean Chiefdoms*; Cambridge University Press: New York, 1986.
2. Burger, R. L.; Asaro, F.; Michel, H. V.; Stross, F. H.; Salazar, E. *Latin Am. Antiquity* **1994**, *5*, 228–255.
3. Bray, T. L. *J. Field Archaeol.* **1995**, *22*, 137–148.
4. Bray, T. L. *J. Field Archaeol.* **2005**, *30*, 119–141.
5. Bray, T. L. In *Handbook of South American Archaeology*; Silverman, H., Isbell, W., Eds.; Kluwer Academic Publishers: New York, 2008; pp 527−543.
6. Topic, J. In *Merchants, markets and exchange in the Pre-Columbian World*; Hirth, K. G., Pillsbury, J., Eds.; Dumbarton Oaks Research Library and Collection: Washington, DC, 2013; pp 335−360.

7. Hirth, K. G.; Pillsbury, J. *Curr. Anthropol.* **2013**, in press.
8. Cordero, M. Ph.D. Thesis, University of Pittsburgh, Pittsburgh, PA, 1998.
9. Martin, A. Ph.D. Thesis, University of Pittsburgh, Pittsburgh, PA, 2009.
10. Oberem, U. In *Native South Americans: Ethnology of the Least Known Continent*; Lyon, P. L., Ed.; Waveland Press: Prospect Heights, IL, 1974; pp 346−357.
11. Yanchar, K., Minc, L. Oregon State University, unpublished.
12. Salazar, E. *Talleres prehistóricos en los altos Andes del Ecuador*; Departamento de Difusión de la Universidad de Cuenca: Cuenca, Ecuador, 1980.
13. Salazar, E. *Miscelánea Antropológica Ecuatoriana* **1985**, *5*, 129–160.
14. Salazar, E. In *Arqueología en América Latina Hoy*; Politis, G., Ed.; Editorial Presencia: Bogotá, Columbia, 1992; pp 116−131.
15. Bigazzi, G.; Coltelli, M.; Hadler, J. C.; Osorio Araya, A. M.; Oddone, M.; Salazar, E. *J. South Am. Earth Sci.* **1992**, *6*, 21–32.
16. Bellot-Gurlet, L.; Poupeau, G.; Dorighel, O.; Calligaro, T.; Dran, J. C.; Salomon, J. *J. Archaeol. Sci.* **1999**, *26*, 855–860.
17. Bellot-Gurlet, L.; Dorighel, O.; Poupeau, G. *J. Archaeol. Sci.* **2008**, *35*, 272–289.
18. Ogburn, D.; Connell, S. V.; Gifford, C. *J. Archaeol. Sci.* **2009**, *36*, 740–751.
19. Santi, P.; Renzulli, A.; Oddone, M. *J. Archaeol. Sci.* **2010**, *37*, 1753–1760.
20. Ogburn, D. *Latin Am. Antiquity* **2011**, *22*, 97–120.
21. Knight, C. L. F.; Cuellar, A. M.; Glascock, M. D.; Hall, M. L.; Mothes, P. A. *J. Archaeol. Sci.* **2011**, *38*, 1069–1079.
22. Asaro, F.; Salazar, E.; Michel, H. V.; Burger, R. L.; Stross, F. H. *Latin Am. Antiquity* **1994**, *5*, 257–277.
23. Schreyer, S. L. MA Thesis, California State University-Fullerton, Fullerton, CA, 2012.
24. Zeidler, J. A., Giauque, R. L., Asaro, F., Stross, F. H. In *Regional Archaeology in Northern Manabí, Ecuador, Volume 1: Environment, Cultural Chronology, and Prehistoric Subsistence in the Jama River Valley*; Zeidler, J. A., Pearsall, D. M., Eds.; Department of Anthropology, University of Pittsburgh: Pittsburgh, PA, 1994; pp 141−144.
25. Athens, S. J. University of Hawaii, unpublished.
26. Cordero, M. *El cacicazgo Cayambi: Trayectoria hacia la complejidad social en los Andes sepentrionales*; Abya-Yala: Quito, Ecuador, 2009.
27. Pazmiño, E., Montalvo, C., Cajas, O. Instituto Nacional del Patrimonio Cultural, Quito, Ecuador, unpublished.
28. Bray, T. L. Ph.D. Thesis, State University of New York-Binghamton, Binghamton, NY, 1991.
29. Ogburn, D. Ph.D. Thesis, University of California-Santa Barbara, Santa Barbara, CA, 2001.
30. Connell, S. V.; Gifford, C. H.; González, A. L.; Carpenter, M. *Antiquity* **2003**, *77*, 295.
31. Fries, E. C. MA Thesis, University of California-Los Angeles, Los Angeles, CA, 2010.

32. Lippi, R. D., Gudiño, A. M. In *Distant Provinces in the Inka Empire: Toward a Deeper Understanding of Inka Imperialism*; Malpass, M. A., Alconini, S., Eds.; University of Iowa Press: Iowa City, IA, 2010; pp 260−278.

33. Sistrunk, H. *Ñawpa Pacha* **2011**, *30*, 189–208.

34. de Aguilar, F. G. In *Relaciones Geográfica de Indias*; Jiménez de la Espada; Tipografia de los Hijos de M. C. Hernández: Madrid, Spain, 1897; Vol. 3, pp 124−127.

35. Borja, P. A. In *Relaciones Geográfica de Indias*; Jiménez de la Espada; Tipografia de los Hijos de M. C. Hernández: Madrid, Spain, 1897; Vol. 3, pp 128−136.

36. Paz Ponce de León, S. In *Relaciones Geográfica de Indias*; Jiménez de la Espada; Tipografia de los Hijos de M. C. Hernández: Madrid, Spain, 1897; Vol. 3, pp 105−120.

37. Cabello Balboa, M. *Miscelánea Antártica:Una Historia del Peru Antiguo*; Instituto de Etnología Seminario, Universidad Nacional Mayor de San Marcos: Lima, Peru, 1951.

38. Cobo, B. *History of the Inca Empire: An account of the Indians' Customs and Their Origin, Together with a Treatise on Inca legends, History, and Social Institutions*; University of Texas Press: Austin, TX, 1979.

39. Espinosa, W. *Bulletin de L'Institut Francais d'Etudes Andines* **1980**, *9*, 89–119.

40. Espinosa, W. *Los Caranquis y Los Cayambes*; Colleción Pendoneros; Instituto Otavaleño de Antropología: Otavalo, Ecuador, 1983.

41. Espinosa, W. *Los Cayambes y Carangues: Siglos XV-XVI: El Testimonio de la Etnohistoria*; Colección Curiñán; Instituto Otavaleño de Antropología: Otavalo, Ecuador, 1988; Volumes 3−4.

42. Caillavet, C. *Revista Andina* **1985**, *3*, 403–423.

43. Caillavet, C. *Etnias del Norte: Etnohistoria e Historia de Ecuador*; Ediciones Abya-Yala: Quito, Ecuador, 2000.

44. de Cieza de León, P. *The Discovery and Conquest of Perú: Chronicles of the New World Encounter*; Cook, A. P., Cook, N. D., Eds.; Duke University Press: Durham, NC, 1998.

45. Salomon, F. *Ethnohistory* **1987**, *34*, 63–77.

46. Ramirez, S. E. In *Ethnicity, Markets, and Migration in the Andes: At the Crossroads of History and Anthropology*; Larson, B., Harris, O., Eds.; Duke University Press: Durham, NC, 1995; pp 135−164.

47. de Gamboa, P. S. *History of the Incas*; Markham, C., Ed.; Cambridge University Press: Cambridge, U.K., 2007.

48. Athens, S. J. In *Resources, Power, and Interregional Interaction*; Schortman, E. M., Urban, P. A., Eds.; Plenum Press: New York, 1992; pp 193−219.

49. Schuller, F. P. *La incursión Inca en el septentrión andino ecuatoriano: antecedentes arqueológicos de la convulsiva situación de contacto cultural: primer informe preliminary*; Instituto Otavaleño de Antropología: Otavalo, Ecuador, 1976.

50. Jijón y Caamaño, J. *Contribución al Conocimiento de los Aborígenes de la Provincia de Imbabura*; Blas y Cía: Madrid, Spain, 1914

51. Jijón y Caamaño, J. *Boletín de la Sociedad Ecuatoriana de Estudios Históricos* **1920**, *4*, 1–120, 183–245.
52. Oberem, U. *Verhandlungen des 38th Internationalen Amerikongresses* **1969**, *1*, 317–322.
53. Oberem, U. *Cochasqui: Estudios Arqueológicos*; Colección Pendoneros; Instituto Otavaleño de Antropología: Otavalo, Ecuador, 1981; Volumes. 3−5.
54. Athens, S. J. *El Proceso Evolutivo en las Sociedades Complejas y la Ocupación del Periodo Tardío-Cara en los Andes Septentrionales*; Colección Pendoneros; Instituto Otavaleño de Antropología: Otavalo, Ecuador, 1980.
55. Gondard, P., Lopez, F. MAG, PRONAREG, ORSTOM, Quito, unpublished.
56. Uhle, M. *Boletín de la Academia Nacional de Historia* **1939**, *18*, 5–14.
57. Currie, E. *Antiquity* **2000**, *74*, 273.
58. Currie, E. *Internet Archaeology* **2001**, *10*.
59. Berenguer, J. *Gaceta Arqueológica Andina* **1984**, *10*, 4–5.
60. Bray, T. L. *Sarance* **1994**, *20*, 135–146.
61. Echeverria, J.; Uribe, M. V. *Sarance* **1981**, *9*, 25–45.
62. Jaramillo, A. *Repertorio Arqueológico Imbaya*; Editorial Cultura: Otavalo, Ecuador, 1968.
63. Rodriguez, E. *Fauna Precolombina de Nariño*; Fundación de Investigaciones Arqueológicas Nacionales; Instituto Colombiano de Antropología: Bogotá, Columbia, 1992.
64. Hirth, K. G. In *Obsidian Craft Production in Ancient Central Mexico: Archaeological Research at Xochicalco*; Hirth, K. G., Ed.; University of Utah Press: Salt Lake City, UT, 2006; pp 3−17.
65. Glascock, M. D. *Int. Assoc. Obsidian Stud. Bull.* **1999**, *23*, 13–25.
66. Hancock, R. G. V.; Carter, T. *J. Archaeol. Sci.* **2010**, *37*, 243–250.
67. Larrain, H. *Demografía y Asentamientos Indígenas en la Sierra Norte del Ecuador en el Siglo XVI: Estudio Etnohistórico de las Fuentes Tempranas (1525−1600)*; Instituto Otavaleño de Antropología: Otavalo, Ecuador, 1980.
68. Buys, J., Manosalvas, O., Camino, B., Benavides, H. Instituto Nacional de Patrimonio Cultural del Ecuador, Quito, unpublished.
69. Hirth, K. G. *Latin Am. Antiquity* **2008**, *19*, 435–457.
70. Gonzalez, A. L. MA Thesis, University of Hawaii, Honolulu, HI, 2010.
71. Craig, N.; Speakman, R. J.; Popelka-Filcoff, R. S.; Glascock, M. D.; Robertson, J. D.; Shackley, M. S.; Aldenderfer, M. S. *J. Archaeol. Sci.* **2007**, *34*, 2012–2024.

Chapter 13

Advantages and Disadvantages of pXRF for Archaeological Ceramic Analysis: Prehistoric Pottery Distribution and Trade in NW Florida

R. H. Tykot,* N. M. White, J. P. Du Vernay, J. S. Freeman, C. T. Hays, M. Koppe, C. N. Hunt, R. A. Weinstein, and D. S. Woodward

Department of Anthropology, University of South Florida, Tampa, Florida 33620, U.S.A.
*E-mail: rtykot@usf.edu

Ceramic artifacts from northwest Florida were tested non-destructively with a portable X-ray fluorescence spectrometer to study production and trade during the Late Archaic, Late Prehistoric, and Protohistoric periods. Analyses using a Bruker III-V were conducted on 500 ceramic samples from 8 archaeological sites, for 180 seconds and using a filter that provides highly precise data for trace elements Rb, Sr, Y, Zr, and Nb. While these ceramics were not painted or glazed, analyses were done on both inside and outside surfaces, and on broken edges. Quantitative values in ppm were produced using widely shared calibration software for these elements, and principal components analysis of the data show that the ceramics fall into distinguishable site groups, with most of the artifacts tested most likely coming from clay sources near each site. Further investigation assesses whether there are patterns based on object type and decoration, and the advantages and disadvantages of using this method.

Introduction

Sherds of pottery and other ceramics are often the most common artifacts found at archaeological sites, and their study is the basis for many interpretations about the pre-modern cultures that created and used them. The major questions addressed by studies of ceramics include (1) the technology used for their formation and firing (use of temper, slip, paint; pits or kilns; temperature and air control); (2) the socioeconomic circumstances in which they were produced (household, village, region, and involvement of specialists); (3) their purpose and actual usage; and (4) their distribution thru trade or exchange, ritual gifting, burial offerings, and other circumstances. In this study we specifically focus on the production and distribution of ceramics from archaeological sites in northwestern Florida by using a portable, non-destructive X-ray fluorescence spectrometer to perform the elemental analyses, while assessing its advantages and disadvantages relative to other instrumentation.

Ceramics Tested

Ceramic production began in the southeastern United States in the Late Archaic period, ca. 3000-1000 BC, and native American production continued at least through the 17th century AD (Table I). The ceramics tested in this study were selected to represent the different time periods involved, and as much as possible to have statistically significant numbers of samples from each archaeological site (Table II).

Assemblages were selected from eight archaeological sites in the panhandle region of Florida, specifically along the Apalachicola River (Figure 1). Some of these sites have been excavated, some surveyed, and some are collections from local residents (*1–3*).

At present, there are no formally published articles on elemental analysis of pottery in Florida, and fairly few in the Southeast overall (*4*). In this study, large numbers of pottery samples were selected from these eight sites for analysis. Most of the ceramics represented are everyday ware, although many have decorations (Figures 2, 3). A number of clay balls, known as Poverty Point Objects (PPO), from the Choctawhatchee Bay area were tested and compared with results obtained in a previous study on Tick Island in northeastern Florida and the actual site of Poverty Point in Louisiana (*5*) (Figures 4, 5).

Table I. Chronology for northwest Florida and the sites tested in this study

Time Period	Culture	Sites
10,000 - 7000 BC	Paleoindian	
7000 - 3000 BC	Early and Middle Archaic	
3000 - 1000 BC	Late Archaic	Choctawhatchee Bay sites, Clark Creek, Louisiana sites Poverty Point and Claiborne
1000 BC - AD 100	Deptford (Early Woodland)	Depot Creek
100 - 700 AD	Swift Creek (Early-Middle Woodland)	Depot Creek; Otis Hare
400 - 700 AD	Early Weeden Island (Middle Woodland)	Otis Hare
700 - 1000 AD	Late Weeden Island (Late Woodland)	Otis Hare
1000 - 1700 AD	Fort Walton (Mississippian to early historic)	Curlee, Dove Point, Richardson's Hammock, Yon Mound
1600? - 1750?	Lamar (early historic Indian)	Dove Point

Table II. Sample selection from eight sites in northern Florida

Site	Site Number	Samples Tested
Choctawhatchee Bay	8Ok51/54/62/other	40
Clark Creek	8Gu60	1
Curlee	8Ja7	167
Depot Creek	8Gu56	41
Dove Point	8Fr79	135
Otis Hare	8Li172	35
Richardson's Hammock	8Gu10	6
Yon Mound	8Li2	83
	Total	508
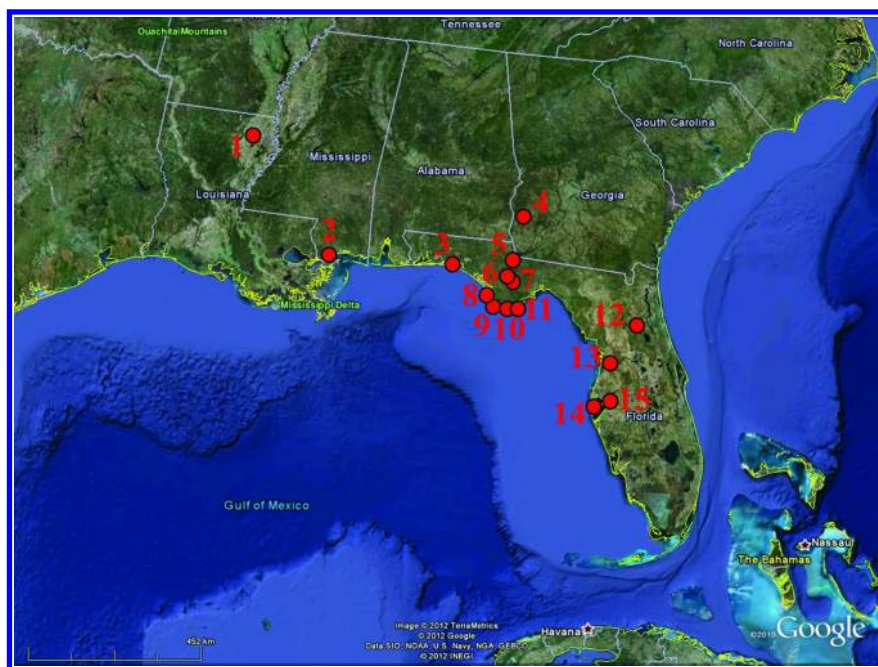
Figure 1. Map of southeastern US showing archaeological sites tested: 1. Poverty Point; 2. Claiborne; 3. Choctawhatchee Bay; 4. Kolomoki; 5. Curlee; 6. Yon Mound; 7. Otis Hare; 8. Clark Creek; 9. Richardson's Hammock; 10. Depot Creek; 11. Dove Point; 12. Tick Island; 13. Crystal River; 14. Bayshore Homes; 15. Jones Mound.
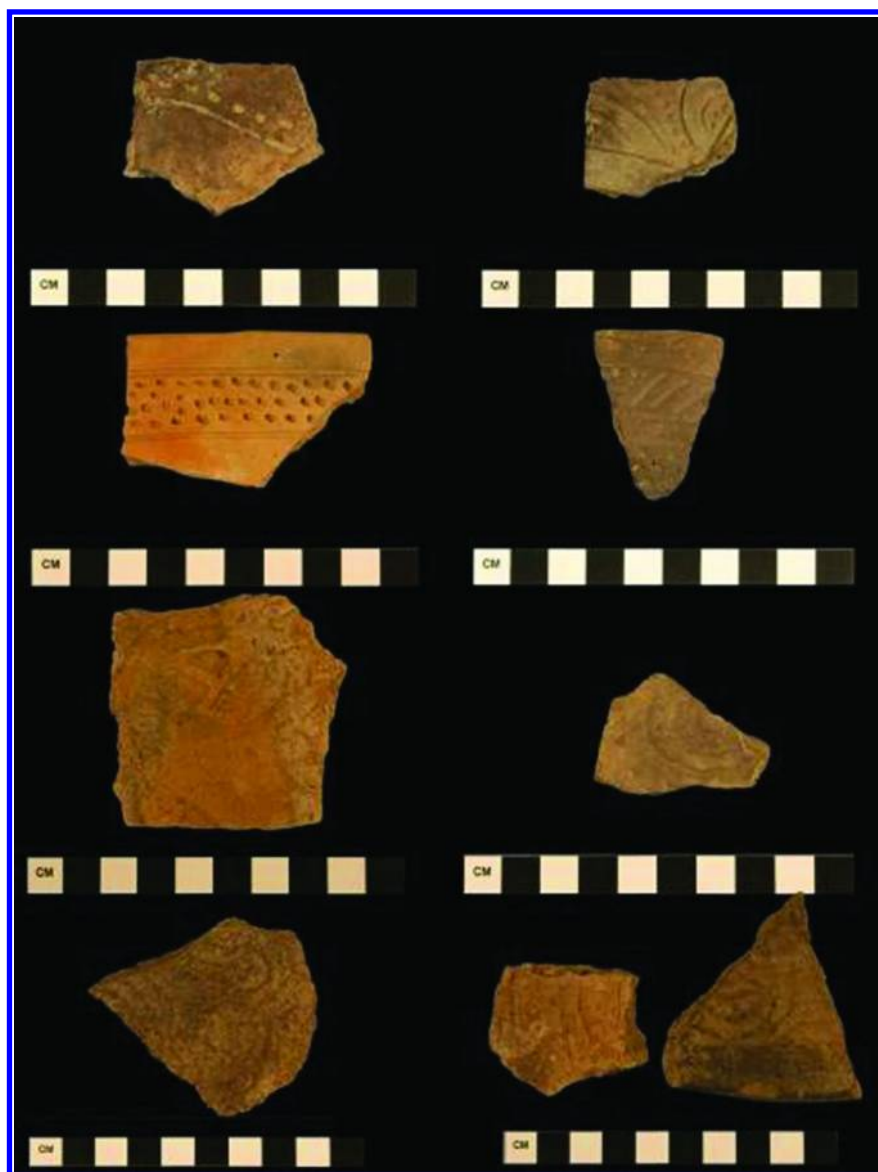
Figure 2. Decorated ceramics from Apalachicola sites in northwest Florida.Top two rows: Fort Walton Incised; bottom two rows: Lamar Complicated-Stamped. Photos courtesy of M. Koppe.

Figure 3. Undecorated (top two rows) and decorated (bottom two rows) pottery sherds from the Curlee site. Photos courtesy of M. Koppe.
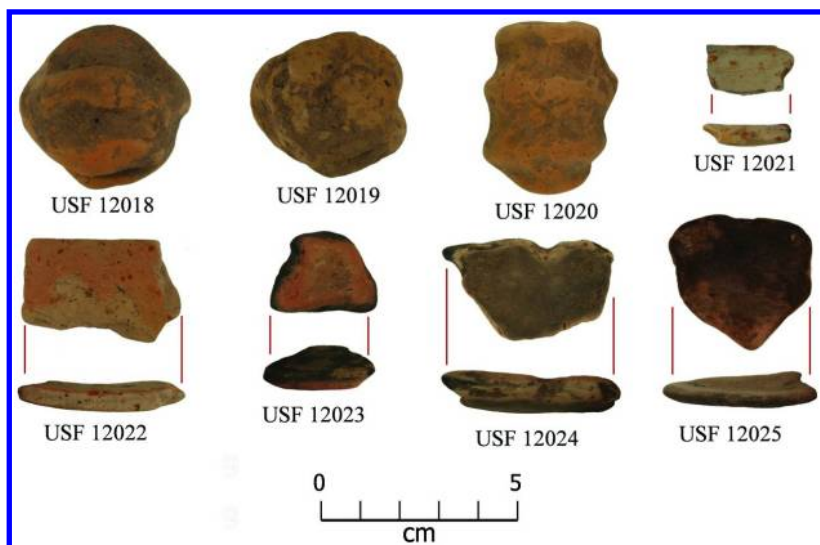
Figure 4. Poverty Point Objects and St. John's pottery sherds from the Archaic site of Poverty Point, Louisiana. Photos courtesy of R. Weinstein.

Figure 5. A selection of the Poverty Point-type baked-clay objects in the Choctawatchee Bay private collection. Photos courtesy of D.S. Woodward.

Elemental Analysis Using pXRF

X-ray fluorescence spectrometry has been applied to archaeological materials for many decades, and the principles of this method will not be discussed here (see (*6*)). The use of portable and especially hand-held X-ray fluorescence spectrometers on archaeological materials, however, was very rare until a decade ago, and now has been widely used on obsidian, which is a homogeneous glassy material (e.g. (*7–9*)). A number of non-destructive studies have also been done on ceramics, with the understanding of their heterogeneity due to clay type and temper added, as well as surface decoration with slip or paint (*10–15*). The advantages of the pXRF include being non-destructive, the ability to conduct analyses in museums and other locations rather than bringing artifacts back to a laboratory, and to rapidly analyze large numbers of objects, and these aspects are well understood. While only analyzing the surface is technically a disadvantage compared to homogenized powder samples, since the depth of most secondary X-rays is less than 1 mm, the X-ray beam area is about 4x6 mm and multiple spots may be selected to average and assess variation. The ceramics in this study are also not painted or slipped, so the surface is likely to represent the clay used for the whole object.

There are several commercially produced hand-held pXRF instruments available. Most of the studies represented here were done using a Bruker III-V model, while one site was analyzed using a more recently acquired Bruker III-SD. The latter has greater sensitivity, and was run at 2048 rather than 1024 channels (thus improving resolution and element identification), and for 120 instead of 180 seconds. Analyses were conducted using two different settings: 40kV/10μA with a filter (6 μm Cu, 1μm Ti, 12 μm Al), providing greater sensitivity and precision for Fe and trace elements Rb, Sr, Y, Zr, and Nb; and 40kV/1.5μA with no filter, for both major element composition of the ceramics (Si, Al, K, Ca, Ti) as well as trace elements, but with less sensitivity and precision for the latter. For better assessment of Si, Al, Mg, K, and Ca, we would have used the latter settings with a vacuum and chosen especially flat surfaces to analyze.

The ceramics were well-cleaned, and analyses conducted on both inner and outer surfaces and occasionally on edges to check for variability in the data produced. The pXRF was positioned upright on a plastic stand with the samples balanced on top. The beam area analyzed is greater than what is typically analyzed by laser ablation ICP-MS, and the combination of spots tested makes this approach similar to INAA and regular XRF studies without being destructive. The calibration software program corrects for analyzing edges that do not cover the entire beam area.

Data Analysis

The raw data were calibrated using software aimed at silicon-based materials and is based on many standards tested by INAA, ED-XRF, and ICP-MS. More than 80 pottery sherds also were tested using both Bruker III-V and III-SD pXRF instruments and a linear equation developed to re-calibrate the data from the older instrument. A direct comparison of the multiple spots tested for each sherd

was made to check for heterogeneity, before taking the average to represent the sample. A preliminary X-Y graph of Zr/Sr vs. Rb/Sr illustrated measurable compositional differences within this one area of northwest Florida, and therefore the capability of analyses with the pXRF to address archaeological questions about ceramic production and trade.

Principal components analysis, using trace element data for Rb, Sr, Y, Zr, and Nb for the PPO-style objects from the Late Archaic sites in Choctawhatchee Bay and at Clark Creek, show that most fall in a separate group from the other sites tested in the Apalachicola River area. The clay-ball sample from Clark Creek, however, is an excellent match with those from Poverty Point, while one from Choctawatchee Bay may have come from that region (Figure 6). Along with the Tick Island artifacts previously tested, these results support the hypothesis of small-scale, long-distance ceramic exchange between northern Florida and Louisiana.

PCA for three of the later period Apalachicola River sites tested (Curlee, Depot Creek, Otis Hare) suggests multiple clay sources near each site were commonly used – hence the range of values for each site's assemblage – but that there were differences in the sources typically used for each site that may be distinguished (Figure 7). Other clay sources were likely located between the archaeological sites so that there was movement of pottery over short distances and/or access to the same source by sites producing pottery. The vast majority of pottery seems to have been produced from local clay sources. Modest variation within a site-based group is best interpreted as the use of multiple clay outcrops in the neighborhood of each archaeological site.
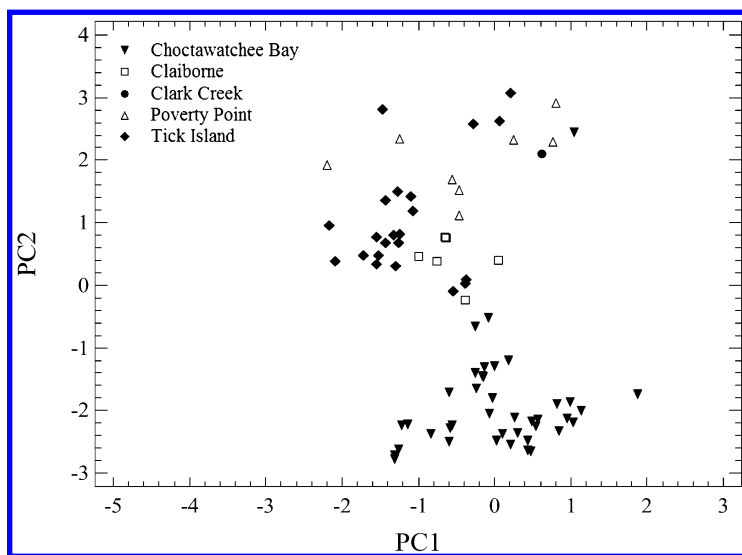
Figure 6. Principle components analysis of trace elements Rb, Sr, Y, Zr, Nb matches a clay ball from Clark Creek (FL) with Poverty Point (LA).

241
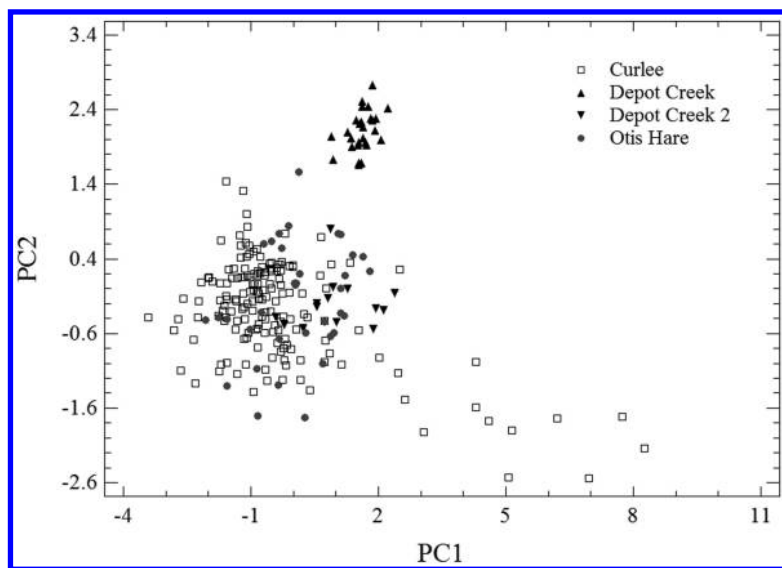
Figure 7. Principle components analysis of trace elements reveals differences in clay composition between sites in the Apalachicola River area.

Discussion and Future Work

Analysis by pXRF of ceramics in northwest Florida and elsewhere is clearly useful for studies of trade and contact. In northwest Florida it appears that there were at least occasional cultural connections with other areas of the southeastern United States, in the Late Archaic period as well as in the Mississippian and early-contact Fort Walton periods (*16*). Ideally, clay sources near the sites of interest should be identified, and samples tested, for much clearer interpretation of the archaeological ceramic analytical data. Analysis of large numbers of selected ceramic artifacts could also be done to assess whether there are patterns based on specific pottery types or decoration.

The ability to conduct such non-destructive and rapid analyses, on both potsherds and full-size vessels, within museums and material depositories, provides large datasets that enable strong hypothesis testing. While only a surface analysis on potentially heterogeneous potsherds, the relatively wide beam size and ability to analyze multiple spots largely removes this issue when compared with powdered homogenized samples from one spot. Of course, surface analysis on painted or glazed ceramics will not reflect the composition of the clay, but edges of a sherd may be analyzed.

Further work is needed however in the development of calibration software for archaeological materials being tested with pXRF spectrometers, especially in order to compare data between laboratories and other kinds of instruments (*17*). For most major elements (Si, Al, K, Mg, Na), their secondary X-rays are largely absorbed in the air, so in order to have even a semi-quantitative measurement it is necessary to use an attachable vacuum and to have a flat surface on the artifact (*18*). Especially when no ceramic thin-sections are taken and studied to identify

the overall clay type, analysis of major elements is necessary. The detection limits of the pXRF spectrometer will not allow measurements of elements in the low ppm or high ppb range that are detected by INAA and other instruments, so that some compositional groups identified using pXRF data may actually represent multiple subgroups, especially if based on just a small number of elements. As with many other scientific methods of analysis, practitioners, collection managers, and data consumers need to be educated as to the advantages and disadvantages of pXRF for archaeological materials.

Acknowledgments

References

1. Du Vernay, J. P. Ph.D. Dissertation, University of South Florida, Tampa, FL, 2011.
2. Koppe, M. M.A. Thesis, Université Michel de Montaigne Bordeaux 3, France, 2010.
3. Woodward, D. S. M.A. Thesis, University of South Florida, Tampa, FL, 2012.
4. Wallis, N. J.; Boulanger, M. T.; Ferguson, J. R.; Glascock, M. *J. Archaeol. Sci.* **2000**, *37*, 2598–2611.
5. Hays, C. T.; Tykot, R. H.; Weinstein, R. A. 66th Annual Meeting of the Southeastern Archaeological Conference, Mobile, AL, November 4−7, 2009.
6. Shackley, M. S. *X-Ray Fluorescence Spectrometry (XRF) in Geoarchaeology*; Springer: New York, 2010.
7. Craig, N.; Speakman, R. J.; Popelka-Filcoff, R. S.; Glascock, M. D.; Robertson, J. D.; Shackley, M. S.; Aldenderfer, M. S. *J. Archaeol. Sci.* **2007**, *34*, 2012–2024.
8. Shackley, M. S. *SAA Archaeol. Record* **2010**, *10* (5), 17–20, 44.
9. Tykot, R. H.; Lai, L.; Tozzi, C. In Proceedings of the 37th International Symposium on Archaeometry, May 13−16, 2008, Siena, Italy; Turbanti-Memmi, I., Ed.; Springer: New York, 2011; pp 321−328.
10. Burley, D. V.; Dickinson, W. R. *J. Archaeol. Sci.* **2010**, *37*, 1020–1026.
11. Goren, Y.; Mommsen, H.; Klinger, J. *J. Archaeol. Sci.* **2011**, *38*, 684–696.
12. Matsunaga, J. M. *Soc. Archaeol. Sci. Bull.* **2009**, *32* (4), 8–12.
13. Morgenstein, M.; Redmount, C. A. *J. Archaeol. Sci.* **2005**, *32*, 1613–23.
14. Speakman, R. J.; Little, N. C.; Creel, D.; Miller, M. R.; Iñañez, J. G. *J. Archaeol. Sci.* **2011**, *38*, 3483–3496.
15. McCormick, D. R. M.A. Thesis, University of South Florida, Tampa, FL, 2013.
16. Marrinan, R. A.; White, N. M. *Southeastern Archaeol.* **2007**, *26*, 292–318.

17. Aimers, J. J.; Farthing, D. J.; Shugar, A. N. In *Handheld XRF for Art and Archaeology*; Shugar, A. N., Mass, J. L., Eds.; Studies in Archaeological Sciences 3; Leuven University Press: Belgium; pp 423−448.

18. Johnson, J. *J. Archaeol. Method Theory* **2012**, October 17, 1–26, DOI: 10.1007/s10816-012-9162-3.

Chapter 14

Interregional Interaction and Dilmun Power in the Bronze Age: A Provenance Study of Ceramics from Bronze Age Sites in Kuwait and Bahrain Using Non-Destructive pXRF Analysis

Hasan J. Ashkanani* and Robert H. Tykot

Department of Anthropology, University of South Florida, Tampa, Florida 33620
*E-mail: hasan@mail.usf.edu

Known as the most interactive period of trade and interregional interaction, Dilmun led and controlled the flow of commodities and the transshipment between Arabian Gulf political entities such as Mesopotamia and far distance ones such as the Indus Valley. This paper presents the first provenance study on 2nd millennium Dilmun pottery in the Arabian Gulf, specifically Kuwait and Bahrain. Our aims are to construct a chemical database of Bronze Age ceramics and to discuss standardization of Dilmun wares using trace elements Nb, Th, Sr, Y, Zr, Rb, and Ba obtained with a non-destructive portable X-ray fluorescence spectrometer. Multiple spots on artifact surfaces were tested to inspect the quantitative precision of the technique and the homogeneity of ceramics was analyzed non-destructively.

Introduction

Dilmun Culture

Dilmun is the name of a political and cultural entity identified by the Sumerians. The Dilmun culture spread from Bahrain circa 2500 BC and some evidence suggests its earliest development began on Tarut Island in the early third millennium (*1*). In general, Dilmun refers to a culture that thrived in modern-day Bahrain, the Eastern Province of Arabia, particularly Tarut Island, Saudi Arabia, and Failaka Island, Kuwait. The Sumerians relied on Dilmun agents to transship

or move raw materials and products back and forth along local waterways and sea routes from southern Mesopotamian ports to their trading partners as far away as Magan in southeastern Arabia and the Indus Valley (see Figure 1). The lack of raw materials in Mesopotamia propelled southern cities to trade with neighbors to acquire metals, wood, onions, shells, ivory, and pearls in exchange for textiles and wool (*2*). Thus, establishing and maintaining trading routes was a major catalyst for the development of Dilmun culture in the Arabian Gulf coastline during the third and second millennia BC. Centrally located in the Arabian Gulf, Dilmun acted as an entrepôt in this long-distance trade linking two large civilizations - Mesopotamia and Harappa.

Dilmun sites are characterized by the presence of 'Dilmun' type seals, chain-ridge pots, red-ridged Barbar ware, and burial mounds. In Bahrain, the Dilmun culture consisted of two major horizons, the Period I or pre-Barbar period (2150-2050 BC) and the Barbar period (2050-1800 BC). Period I is known for the chain-ridged pottery type and a settlement at Qala'at (*3*). Also, the chain-ridge ware type has been identified as Period I or pre-Barbar period in Bahrain, below the early second millennium temple of Saar and from the Eastern Province, on Tarut (*1*). The Period II or Barbar culture has been characterized by the presence of the temple complex, Dilmun/Gulf seals, burial mounds, red-ridged Barbar ware, and settlements at Saar, Diraz, Hamad and Hajar. The Barbar Period, also called the Early Dilmun period, is associated with dramatic expansion within the Dilmun territory and northwards. The presence of the Dilmun culture has been established on Failaka Island, Kuwait from the excavation of different sites, dated to ca. 2000 BC (*1*, *4*).

Figure 1. Map of the Arabian Gulf and adjacent regions showing the major sites and locations mentioned in this text. (Drawing by Hélèn David-Cuny).

Dilmun's Emergence in the Trade Network

Dilmun was favored as the most active entity in the Persian-Arabian Gulf in the early second millennium and transshipped commodities to different regions and dramatically expanded its territory and prosperity (*2*, *5*). Unlike during the 3rd millennium BC, Dilmun would dominate the Mesopotamian trade network in the 2nd millennium BC by expanding to the north, including Failaka Island in Kuwait (Figure 1). During this period, its centers and ports became attractive to traders looking for markets where there was a reliable supply of raw materials and the flow of commodities was secure (*6*). Even though Dilmun's influence in the Gulf region was not prominent until the second millennium BC, it still played a vital role in third millennium trade and exchange. It was a middleman for the copper trade between Mesopotamia and Magan (Oman). Textual evidence from the Early Dynastic mentioned cargos of woods, merchants, and boats shipping from Dilmun (*6*). A textual account from King Sargon (ca. 2334 BC) is one of the most cited references by archaeologists and historians describing the nature of ancient trade in the region. The latter record contained references to the involvement of Dilmun in third millennium trade and its role as one of the smaller entities under the expansion of Akkadian power. Also, it referred to the other neighbors, besides Dilmun, who participated in the extensive trading connection with Mesopotamia as he was proud to receive ships from Meluhha, Magan (Oman), and Tilmun (Dilmun) and moored in front of Akkad (*6*, *7*). This record implied that Akkadian control over the Gulf was extensive, leaving little room for smaller polities to have influence - a loss of 'middlemen' such as the Elamites, the Iranians, and the Dilmun during this period. Several texts from the late third millennium BC, Ur III period, further indicate Dilmun/Magan trade as organized by the temple.

Failaka Island Significance and Research Question

After the collapse of Akkad, Dilmun came to dominate the Arabian Gulf through the control of transshipping different commodities. Ur III and Isin-Larsa tablets and texts (period 2112-1763 BC) testify to the role of Dilmun in the trading activity of merchants and objects going from Dilmun to Ur (*6*, *8*, *9*). It seems Failaka Island was part of Dilmun's administrative strategy to expand its borders and secure a refueling station to its seafarers and the merchants (Figure 2). In the beginning of the second millennium BC, Failaka Island was a Dilmun port and the nearset point on the Arabian Gulf to Mesopotamian. The different trading products to and from Ur, Harappa in the Indus Valley and Oman such as wood, shells, pearl, onions, precious stones and copper (*2*, *8*, *10*) could not be moved without unloading at Dilmun. The architectural features and other Bronze Age and Dilmun materials on Failaka Island support that it shared institutional aspects with the main Dilmun center (*5*, *11*, *12*). It was the heyday of the Dilmun realm because they were able to strengthen their political influence and their economy by controlling the Arabian Gulf trade network. The growth of the Barbar Temple II (ca. 2025 BC) and the Saar settlement on the mainland of Dilmun (Bahrain) in the late third and early second millennium coincided with the rise of Failaka Island's Dilmun settlements (Tell F3, F6 and Al-Khidr). Archaeological evidence

that supports the latter includes ceramic assemblages, Dilmun stamp seals, architectural details, metal tools, and faunal and floral evidence. The presence of Barbar-tradition pottery or ridged red ware and Dilmun seals were very common on Failaka, indicating colonizing of Failaka by Dilmunites.
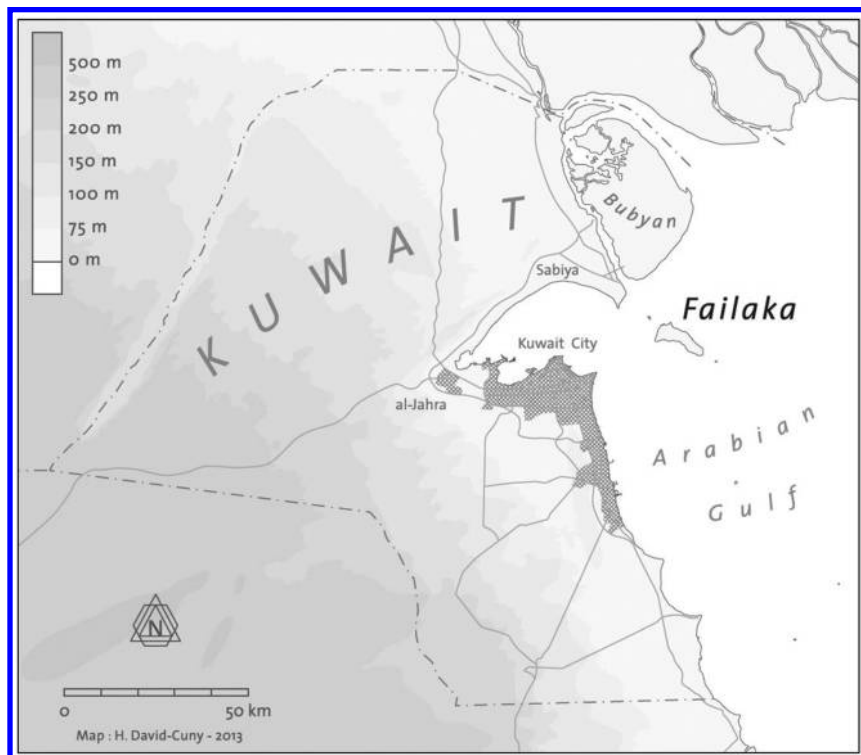
Figure 2. Map of Kuwait and the location of Failaka Island, as the first stop point in the mouth of Shatt al Arab. (Drawing by Hélèn David-Cuny).

Dilmun was seemingly a semi-peripheral entity under the Akkadian empire, but began to emerge as the Akkadians declined. With a lack of discernable military force, it is presumable that Dilmun's emergence and power was expressed culturally. The presence of Dilmun materials can be used to explore how that influence was built. Provenance studies have been used to discuss mechanisms that lend to increased cultural presence, influence, and power of an elite as well as administrative authority. The control of raw materials, craft specialization, standardization of products, and the dissemination of standardized products can be used as indicators of an emerging elite. The need of a new institution, ruler, or governmental personnel was necessary to manage the distribution and production different classes of goods, staple and wealth finance (*13*). In addition to controlling wealth goods, increasing social complexity and emerging elite

and institution could have been in conjunction with staple finance resources. During the Uruk period (ca. 3900-3100 BC), Stein (*14*) noted the control of craft specialists, the standardization of wheel-made pottery, and the wide distribution of utilitarian vessels by temple administrators in ancient Mesopotamia. The staple finance system model was used to discuss how the elite distributed these standardized wares throughout the region. We seek to establish that the mechanism of the rise of a new Dilmun elite in the second millennium was through control of standardized Barbar red-ridge wares. Also, Failaka Island elites or rulers might have sought to enhance their power and prestige through the possession of non-local and far-distance staple and wealth production and through specialized ceramic production.

Dilmun Pottery: Household and Professional Craft Production

The shift of pottery-making in Dilmun from pre-Barbar to the Barbar Period is a crucial key to understand the evolution of ceramic production and Bronze Age craft specialization. Højlund has suggested that pottery-making during the pre-Barbar period in the third millennium at the Qala'at site was exclusively hand-made, with irregularity and unevenness in the rim, nick, and body regions (*3*). The study of remains from the Qala'at site and their development is indeed important as archaeologists consider the site as the capital of Dilmun (*15*). Thus, studying the development of pottery production at Qala'at is one of the crucial windows to understand the scale of labor, specialization and distribution. As mentioned above, the Period I or pre-Barbar period (2150-2050 BC) is known for the chain-ridged pottery type (*16*). Period 1 pottery is tempered with sand and yellowish-white carbonate particles. The color of Period 1 pottery varies from red, light brown to gray, with application of a slip to the outer surface. It is known as Ware Type 1, which is the only ware type found at Qala'at in Period 1. It seems Period 1 pottery was produced at a household level while all of the decorated wares seem to have been imported (*1*, *3*).

During Barbar Period II in the 2nd millennium, use of the wheel technique increases in the Qala'at site and imitation of imported goblets was introduced, indicating the gradual improvements and changes in Dilmun pottery (*3*). The wheel-turntable pottery has a limited number of styles and small luxury production, suggesting craft specialization and standardization in production (*3*). In the Barbar Period (2050-1800 BC), the red-ridged ware, a Barbar type, became widespread in Bahrain and local pottery production had increased compared to a decrease in Mesopotamian pottery and disappearance of southeastern (Umm an-Nar) pottery types (*1*, *3*, *16*). New shapes of pottery were developed in this period and other shapes became much more dominant (*3*). The Barbar Period wares were hand-made, red-brownish, and hard-fired, with yellowish slip covering the outer surface. Painted pottery was introduced in this period, both local and imported, particularly the 'Eastern Tradition' wares from Iran and the Indus Valley (*1*, *3*, *16*). The very distinctive Barbar type wares have been found on Failaka Island, representing a wide range of Barbar ware, including vessels, neck or neckless ridged jars, plates, goblets, bowls, and cooking pots. The Barbar Period II pottery, particularly the IIb phase (ca. 1950 BC), is parallel

to pottery of Barbar Temple Period IIb and Failaka pottery Period 1. The pottery production of this period is continuous with Barbar Period IIa in general with such commonality in wheel-made pottery for the large jars, indicating an improvement in the skills (*3*).

The standardized nature of the pottery strongly suggests that this was mass-produced by professionals, and had shifted gradually from a household level of pottery production (*3*). The shift in ceramic craft production was parallel with increasing social structure and sociopolitical complexity. By the Barbar Period, a fortification wall was achieved in the Qala'at site and an architectural unit of houses at the Saar settlement in Bahrain is also recognized, which shows more in common with the settlement in Tell F3 on Failaka Island (*3*). This period is characterized by the appearance of temples in Bahrain (e.g. Barbar, Saar, Diraz, as-Sujur), and Tell F6 on Failaka Island.

Therefore, we have examined Dilmun ceramics from Failaka Island sites to determine if standardized production recipes were used for Barbar wares. We are suggesting that Dilmun elites controlled the production and distribution of Barbar wares to support their emerging socio-political authority. Specifically, this paper examines the chemical composition of Dilmun ceramic sherds from Failaka Island sites using a non-destructive portable X-ray fluorescence spectrometer (pXRF). Our assumption is that the analytical instrument is able to separate and distinguish ceramic samples within the Tell F6 that comprises the palace-like complex and the Temple. They are the oldest Bronze Age sites on the Island and coincide with the Barbar II period on Bahrain (ca. 2050 BC.). The chemical components can reveal possible standardization of Barbar pottery. Also, the presentation of compositional similarities and differences would also shed light on the extent of Dilmun power over Failaka in terms of craft specialization and distribution. Any chemical separation between the Barbar tradition pottery from Kuwait and Bahrain would suggest that the compositional choice and recipe of each Dilmun center could be differentiated, though there is the standardized appearance (e.g., ridge style).

Toward Archaeometry in the Arabian Gulf

For over thirty years, archaeologists have been studying Dilmun Bronze Age ceramics from Kuwait and Bahrain. Initially, scholars worked to build a chronology for the ceramics in the region by describing and categorizing ceramic types (*5*, *11*, *12*). Later, they would attempt to reconstruct trade networks that could account for the presence of materials from different sites in the Persian-Arabian Gulf region while identifying production centers and distribution routes. Their work would demonstrate the importance of addressing trade and exchange along with social complexity in the Bronze Age (*2*, *5*, *10*, *17*). Employing archaeometric techniques to obtain chemical and mineral composition of ceramics would improve our understanding of trade, exchange and interregional interaction in the Persian-Arabian Gulf in the Bronze Age. Various analytical methods have shown their reliability as tools for geochemical studies and for provenance studies in archaeology (*18–20*). For instance, Kenoyer

and his colleagues used isotopic analyses to suggest the mobility of Harappan individuals to Mesopotamia during the third millennium BC (*21*). The results allowed them to discuss the significance of an individual's mobility in the development of a community despite the large-scale interaction and contact between the two state-level societies. Cross-disciplinary collaboration along with the availability of geological source material, advanced instrumentation, and updated software, ceramics can no longer be considered poor indicators for documenting trade and exchange and interregional interaction. With the chemical characterization of ceramics, archaeologists can use the data generated (i.e., origin, zone of production, and distribution and exchange, etc.) to interpret ceramics as meaningful artifacts.

There are a few studies that have employed archaeometric methods on ceramics in the Persian-Arabian Gulf (*22*, *23*). For instance, Sophie Méry (*24–27*) has used petrographic thin sectioning to characterize ceramics and identify fabric types from fourth and third millennium BC sites in Oman and the United Arab Emirates (UAE). She has demonstrated a connection between the latter by comparing Mesopotamian fabrics from Mesopotamia and the Gulf. The petrographic analyses confirmed the presence of Mesopotamian vessels in Eastern Arabia, implying Gulf participation in the larger trade network that included Iran and the Indus Valley.

Provenance studies of Persian-Arabian Gulf wares using instrumental neutron activation analysis and XRF have yielded interesting results. INAA and petrographic thin section analyses were used to analyze foreign jars recovered from the Oman Peninsula. These techniques established the source of the wares and distinguished between zones of production in the Indus Valley and Iran (*22*, *28–30*). Furthermore, XRF analyses have generated elemental composition data about Bronze Age ceramics from Oman, UAE and Mesopotamia (*31*, *32*). The results pointed to a Southern Mesopotamian origin and were able to distinguish chemical outliers with thin sectioning analysis. In Kuwait, XRF has been used to identify the chemical components of Bronze Age glass and ceramics (*33*). The results have demonstrated that the glazed pottery's alkaline nature makes it particular to the site geologically and temporally.

The significance of this research project is to establish a benchmark using the non-destructive portable X-ray fluorescence (pXRF) technique for the study of Bronze Age ceramics in the Arabian Gulf, particularly Kuwait and Bahrain. Besides constructing a database for the chemical components of Failaka Island and Bahrain ceramics, this study also explores the ancient trade and exchange networks that included Failaka ceramics. The determination of the chemical composition of the second-millennium wares is not only a means of exploring their origin, but also other issues surrounding power and status, such as the accessibility of exotic or prestige items, the expression of status amongst Failaka individuals with such items, and socio-political power and trade. The results obtained are useful for understanding the extent of the Dilmun center's power on pottery production.

Sampling and Analytical Method

Sampling Procedure

The samples analyzed in this study consist of 75 ceramic sherds from various types of early Bronze Age pottery on Failaka Island and Bahrain (Table I). A total of 66 potsherds were taken from Tell F6 in the southwest of Failaka that consists of three sites: the Palace, Trench E, and the Temple (Figure 3). Among 66 sherds, a total of 16 were taken from the palace-like feature known as the Governor's Palace. The samples were taken from the earliest phase known as Failaka Period 1, circa 1950 BC, recovered during the 1960s excavation (*2*). Tell F6, consisting of the Governor's Palace and the Temple, is considered a Dilmun site based on architecture and remnants similar to contemporary Dilmun sites in the Kingdom of Bahrain.

Table I. Summary of sample materials from Kuwait and Bahrain

Site	Structure	Region	Sample Size	Phase
Tell F6	The Palace	Failaka Island, Kuwait	16	Period 1
Tell F6	Trench E	Failaka Island, Kuwait	34	Period 1
Tell F6	Mesopotamian House	Failaka Island, Kuwait	16	Pre-Period 1
Barbar	Barbar Temple	Bahrain	9	Period IIb
			Total 75	

A total of 34 samples were taken from a new trench (Trench E), which lies between the Governor's Palace and the Temple in Tell F6. This trench was excavated during the Kuwaiti-Danish mission of 2009 to determine if there was a connection between the palace and the temple (*34*). All ceramic potsherds selected for this study from Tell F6 are affiliated typologically with the Dilmun tradition and parallel to phase Failaka Period 1 in the Palace, with a few unknown and unusual types found at the site.

During 2008-09 the Kuwaiti-Danish excavation at the Temple in Tell F6, Mesopotamian ceramics were unearthed from a trench. This trench is a stone-built corner of a house embedded in a settlement layer with quantities of animal bones, fragments of bitumen, and Mesopotamian pottery (*34*). Among numerous sherds uncovered, 16 rim and body sherds were selected for this study and marked as a Mesopotamian House collection.

In addition to Failaka Island potsherds, a total of 9 come from the Barbar Temple II in Bahrain (Figure 4). The samples were taken from the IIb phase that is contemporary and parallel with earliest phase in Failaka, Period 1 (1950 BC). The Barbar Temple is located in the village of Barbar in north Bahrain and is the

best preserved of the three Barbar temples. The sacrificial court, shrines and altars suggest that cult ceremonies took place in the temple.
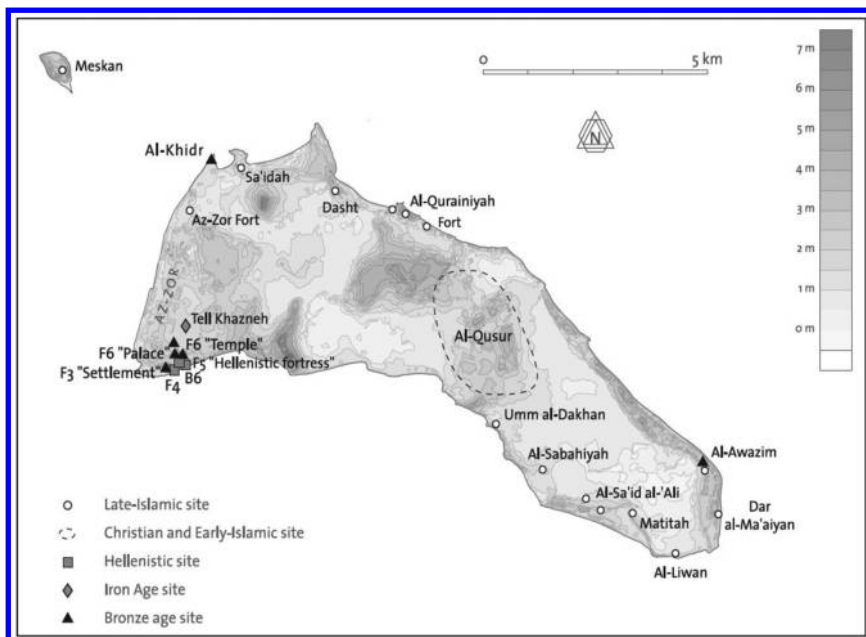
Figure 3. Maps showing various archaeological sites on Failaka Island and the location of tell F6 in southwest of the Island. (Drawing by Hélèn David-Cuny).
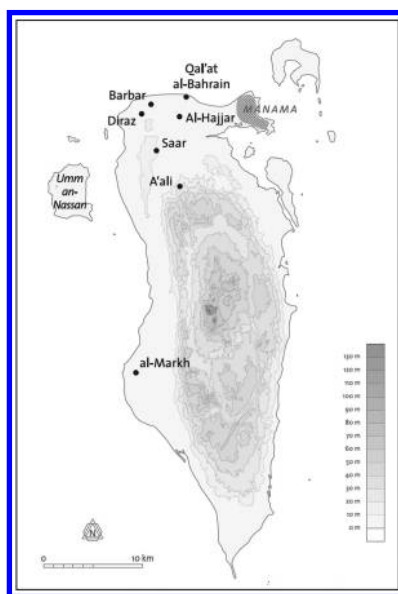
Figure 4. Map of Bronze Age sites in Bahrain and the Barbar village in the north. (Drawing by Hélèn David-Cuny).

Because this paper seeks to possibly fingerprint production centers, we attempt to use well-dated ceramic sherds representing various geographical regions. The goal is to find the possibility of using other ceramic sherds from different regions as a reference for clay and geological features. There is a lack of a database containing information on clay and geochemical data from Bahrain and Kuwait, particularly studies on clay and minerals. In our study, we used Bronze Age ceramic potsherds from Barbar Temple in Bahrain as a reference collection of Bahrain geology and Mesopotamian House potsherds on Failaka Island, Kuwait, as a reference of Iraq clay. Using pottery as a reference has been useful in cases of Aegean archaeology and ceramic studies. The chemical composition of archaeological ceramics of unknown origin is usually compared to ceramics of known origin, or control groups (*35*). The pottery of a control group is established from ceramic materials whose provenance is known or sherds are found in kilns. Arabian Gulf ceramicists are able to identify the provenance of pottery based on typology, temper and sherd fabric, and mass distribution (*3*, *7*, *12*).

Analytical Method

The samples were brushed to remove debris and dirt from excavation and museum storage, and then washed and allowed to dry. After the cleaning of the potsherds, the elemental composition of the surface was analyzed non-destructively using a Bruker Tracer III-SD portable X-ray fluorescence spectrometer. The instrument was set up with a filter (12 mm Al, 1 mm Ti, 6 mm Cu) designed to enhance data measurements of mid-Z elements in the spectrum, while settings of 40 kV and 11 μA were selected to maximize trace element analysis. Only seven trace elements were measured and quantified as they show in our preliminary study their contribution for quantitative analysis including barium (Ba), niobium (Nb), rubidium (Rb), yttrium (Y), strontium (Sr), zirconium (Zr), and thorium (Th). They have been shown in many studies to be successful in determining sources and subsources of ceramic materials (*36–38*). Two major elements, manganese (Mn) and iron (Fe) were excluded due to fluctuation in the measurements, or values below the limits of detection determined in our preliminarily results.

Calibration was conducted on the raw data using a program originally designed for obsidian and other silicate materials. Recently, Speakman and his colleagues (*36*) show that using this calibration for quantifying ceramic data for sherds from the American Southwest worked quite well with potential relative accuracy for calibration. Thus, the data obtained by pXRF in this study is valid for the purpose of the current study, and may be re-calibrated in the future with other software for comparison with other studies.

Each sample was set on the top of the exit window for 120 seconds to obtain elemental composition in parts per million (ppm) concentrations. The ceramic fragments tested are approximately 1-3 cm, and completely cover the beam size of this instrument, which is about 3x5 mm diameter. Because there is some concern about analyzing pottery that does not have a smooth flat surface and thus affecting the actual X-ray angle, the sherd's spot of X-ray exposure has been carefully selected, avoiding a non-flat area and visual temper inclusions. The inner and

outer surfaces of the samples were analyzed and the edges as well for thick samples to overcome the potentially poor representativeness of non-homogenized samples and to ensure that the results are consistent. Our preliminary results showed that the multiple runs on different positions within the whole sample are consistent. Hence, the data value used for each sample is the average of the measurements at different positions.

pXRF Performance

Though it is still considered a new technique in archaeological studies, pXRF has been employed in the last decade for identification and characterization of ancient metals (*39*), gold and silver jewels (*40*), and obsidian tools (*19, 41, 42*). A few studies have employed pXRF on ceramics (*43–45*), while most archaeologists have employed INAA, ICP, and laboratory XRF for clay sourcing to address trade and exchange issues. There has been a reluctance to use this handheld instrument for provenance studies on ceramics because of the inherent complexity of ceramics as well as the sensitivity and precision of the commercial instrument. Because this study is the first of its kind in the Arabian Gulf, we first asked, how effective would the pXRF be for chemical characterization? The heterogeneous nature of ceramics leads archaeologists to use more reliable and accurate analytical instruments that require cutting the ceramics and powdering the sample for dissolution or pelletization procedures. In our case, the potsherd samples had to be returned and the pXRF instrument allowed us to avoid the destruction of the sample that other analyses require.

In our preliminary study, we selected three Bronze Age ceramic potsherd samples from Failaka island to compare chemical compositions obtained from pXRF with the results from one of the most accurate instruments, inductively coupled mass-spectrometry (ICP-MS), at the University of South Florida's Center for Geochemical Research. According to the scatterplot, the database yields from ICP-MS are closely aligned with the composition obtained using pXRF (*46*). They correlate rather well with the exception of Sr that has a partition coefficient larger than 1 in plagioclase and smaller than 1 in clay minerals, so the results yielded from pXRF have to be carefully interpreted for the bulk composition. Overall, the results show the great potential of pXRF for quantitative analyses of ceramic sherds from Failaka Island. The portable XRF application is valuable especially in the study of the Arabian Gulf region because it can be used to establish a chemical database without compromising the integrity of ceramic collections. The instrument has also been shown to be useful in grouping Bronze Age clay cuneiform tablets from Hattuša, Turkey, and el Amarna, Egypt (*47*).

Technically, the pXRF instrument has shown that it is a reliable tool non-destructively, and by using empirical calibration for chemical characterization of ceramics. Speakman et al. (*36*) has demonstrated the value of the pXRF technique on ceramics from the American southwestern region. Additionally, the latter results from the pXRF instrument were comparable to the results obtained from INAA even though INAA is considered more precise (*36*). By generating a dataset that employed both pXRF and ICP-MS for Failaka sherds, this study used

the same approach. The ability of pXRF as a method to measure trace elements effectively and distinguish compositional groups of heterogeneous material is vital to ceramic analysis for the Arabian Gulf region trade network.

Multivariate Statistical Analyses

It is useful to employ multivariate statistics to find which elements can be informative to differentiate ceramic groups. However, we began with simple scatterplots to show variations in chemical composition between samples even if they are not distinguishable visually. A simple scatterplot of trace elements Rb, Sr, and Y shows differentiation between and within sites. The trace elements Rb, Sr and Y suggest a different composition within the Trench E site and the Barbar Temple of Bahrain (Figure 5), and one sample from Barbar Temple of Bahrain and one from Trench E on Failaka are clustered with the Mesopotamian House's samples. Also, one sample from Trench E is clustered alone in the top of the plot as an outlier as well as one from Barbar Temple. The presence of Rb, Sr and Y confirms the variation within and between the four archaeological sites, with a potential small group consisting of a few sherds from the Palace and the Mesopotamian House.
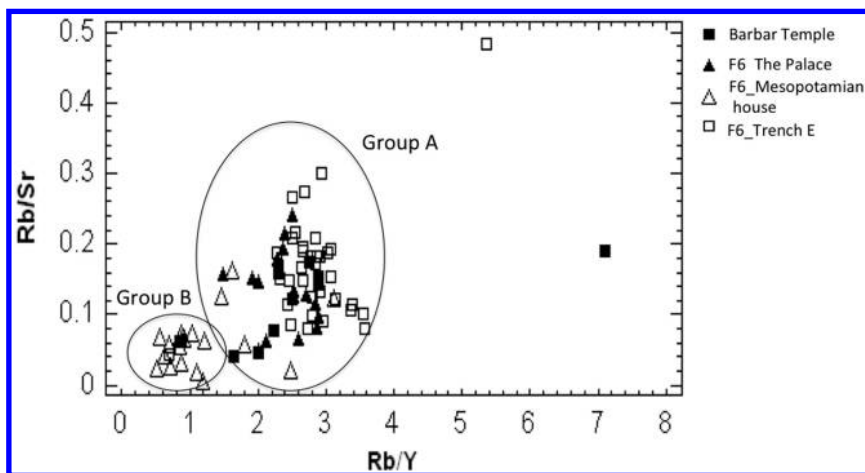
Figure 5. Plot of the Bronze Age ceramics from Kuwait and Bahrain from four sites showing variation within Failaka Island sites, two distinct groups of ceramics (Dilmun sites vs. Mesopotamian House), and a potential separation within the F6 site, showing a few sherds clustering in a small group.

Principal Component Analysis

A variety of statistical applications were employed to evaluate the data collected using SPSS statistical software. Principal component analysis (PCA) is an exploratory method to examine the correlation between chemical elements and suggest which variables or groups of elements are meaningful and can account

for the maximum variance in the data set. Transformation of the dataset into logarithms has been performed to standardize the data. The SPSS component matrix is useful because it contains the loading of each variable onto each factor. The results also show that the values of the first three components explain 79% of the variance.

A scatterplot was performed using PCA scores 2 and 3 that include Nb, Th, Sr, Y, Zr, Rb, and Ba, which previously showed their high contribution in the component matrix. The results show two distinct groups of ceramics (Figure 6), while the Palace, Trench E and Barbar Temple are clustered together (group A). It also shows a distinct group of samples including the Mesopotamian House with a few outliers from the Barbar Temple and Trench E (group B). There are two outliers from the Palace; one is sitting noticeably as an outlier. The PCA results show the separation of sherd samples between and within the archaeological sites.
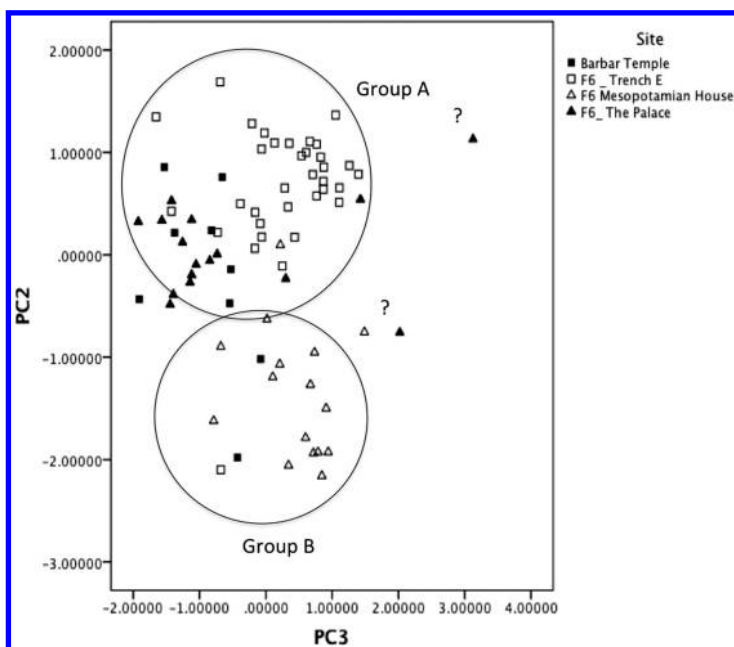
Figure 6. Biplot derived from principal component analysis of 75 sherd samples measured by portable XRF.

Cluster Analysis

The principal component analysis is followed by a cluster analysis using PCA scores, which include all 7 elements (Nb, Th, Sr, Y, Zr, Rb, and Ba), for identifying natural groupings and evaluating PCA results. K-means cluster analysis was utilized for the clustering method because it groups all samples and then finds clusters. K-means cluster analysis is useful to test our research questions about the presence of more than two groups of ceramic sherds, as it

can explore the number of groups. The ANOVA output is the most important aspect in cluster analysis in order to see which factor is great and statistically significant (.000). ANOVA results show that all PCA factor scores are statistically significant, while the PCA scatterplot used in Figure 6 shows how PCA factors are useful for grouping our samples.

Discriminant Function Analysis

Discriminant function analysis (DFA) was employed as a different statistical technique to discriminate between groups and classify our samples into different production centers. We assume that there are four production centers that the samples might have been made at: Dilmun, Mesopotamia, Indus Valley, and Iranian plateau. We used original log data for all seven elements (Nb, Th, Sr, Y, Zr, Rb, and Ba) as variables and site names as a grouping variable. The canonical discriminant function plot shows that the ceramic sherds are separated into two main groups, with a potential small group (Figure 7). It shows a group of Mesopotamian House with two samples overlapping from other sites, and a big cluster includes the Barbar Temple site of Bahrain, the Palace site and the Trench E site on Failaka Island. The Wilk's output shows that the three discriminant functions are statistically significant (p < .000).
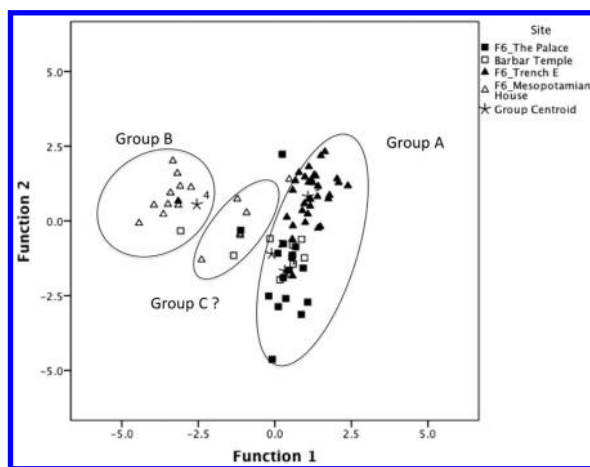
Figure 7. Biplot based on canonical discriminant functions showing two distinct groups (A, B). The small cluster (group C) is a mix from three sites.

Discriminant function analysis also produces a number of scores as PCA factor scores. Thus, a scatterplot was performed using discriminant scores on the discriminant axes (DF1, DF3) as seen in Figure 8. Ceramic potsherds are grouped into two main groups. Those groups that formed the big cluster (group A) come from the Barbar Temple, the Palace, and Trench E, with one overlapping

sample from the Mesopotamian House. Group B consists of samples from the Mesopotamian House on Failaka Island and the overlapping two samples from Trench E and the Barbar Temple of Bahrain. Group C has four outliers from the Palace site and finally group D is clustered in the middle of the scatterplot that consists of mixed specimens from the Barbar temple (No. 13662) and four from the Mesopotamian House on Failaka Island. This group of ceramic sherds obviously appeared in the discriminant analysis more than in the former analyses. Based on statistics, 81.3% of the original grouped cases are correctly classified.
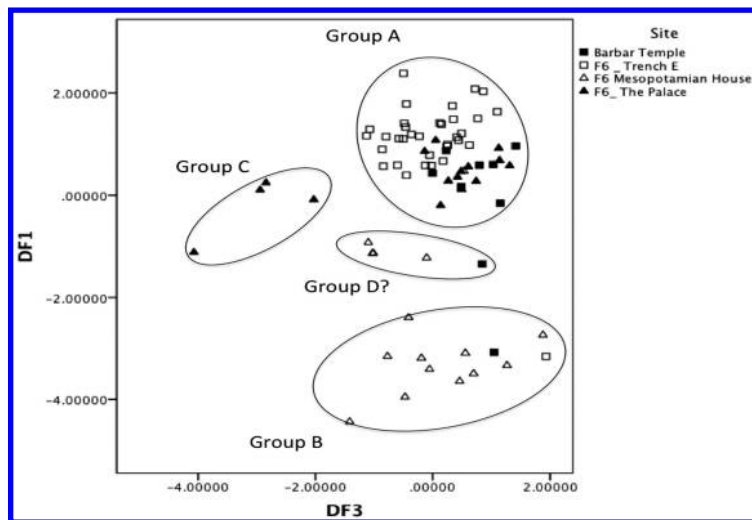
Figure 8. Biplot of discriminant scores on discriminant function 1 and 3 showing a mixed pattern of Dilmun specimens from three sites on Failaka and Bahrain (group A), along with a well-separated group of the Mesopotamian House (group B). Note that a few specimens from the Palace were combined based on discriminant scores (group C).

Results and Discussion

The statistical results performed on Bronze Age ceramics from Kuwait and Bahrain show a pattern of four distinctive groups. Ceramic potsherds from group A are from Barbar Temple of Bahrain, and the Palace and Trench E from the Tell F6 site on Failaka Island (see Figure 9). Group A has a large amount of ceramic artifacts comprised of large red-ridged jars as well as smaller slipped reddish sherds. They have the ridged reddish slipped feature typical for the Bronze Age Dilmun or Barbar pottery type. This type of pottery can be further divided into groups based on color, grain size, and hardness. The Barbar type ceramic artifacts are fired, hand-made, and the colors are homogenous. The first type of this reddish ware is the well-fired ware strongly tempered with sand and white-yellowish lime particles, known as A-ware in the Barbar ware category (*12*). In the center of these particles is a hollow area, seen as irregular rounded spots, which probably arose

from firing lime (*12*). The second type is also well-fired but not harder than the A-ware type. It is medium-tempered with finer particles. The core is yellowish red to reddish brown with a gray or red slip. It is known as the C-ware type in the Barbar ware category (*12*). Within group A, there is a sample (No. 15163) that came from the Mesopotamian House of the Tell F6 site that overlaps with the Barbar ceramic group. Based on its red color, slip, and incised lines, it is diagnostic of Period 3A ceramics on Failaka (Højlund, pers. com.). The Period 3A (1720 –1550 BC) piece could have been deposited later into the Mesopotamian House feature during the rebuilding or restoring of the Temple on top of the Mesopotamian house structure.

Ceramic potsherds of group B were highly tempered with fine material. The sand particles are seldom seen, while the colors range from pale brownish and pale greenish to light gray (see Figure 10). It has a surface of fine texture and smooth clay, while some have straw impressions (G-ware type). The G-ware group was known for being wheel-made, except for the giant storage vessels, and belongs to the Mesopotamian tradition (*12*). They are two- and three-rib rim sherds corresponding to Ur III type 1 vessels. They came from the lowest level of the Temple at F6, which belongs to the Mesopotamian House. It represents the Third Dynasty of Ur or Ur III occupation horizon (2100-2000 BC) that pre-dates the establishment of the Dilmun colony on Failaka Island (*48*).

Within group B, one sample (No. 13661), which came from the Barbar Temple of Bahrain, is overlapping with the Mesopotamian sherds (see Figure 10C). It was assumed to be of the Barbar tradition, but it falls within the Mesopotamian group. Texturally speaking, it is wheel-made and has green to gray color on the outer and inner surfaces. This product might have come to Bahrain during the Isin-Larsa dynasty in Mesopotamian that ruled the south portion from 2000 to 1760 BC. Also, one sample (No. 15137) came from Trench E that represents the early Dilmun occupation level, 2000-1900 BC. It was assumed to be an imported sherd (*49*). Features like its greenish color and inside ridge along with our results support its Mesopotamian tradition (see Figure 10D).

Figure 9. Group A samples consisting of Dilmun sherds comprising large red-slipped and smaller reddish sherds.
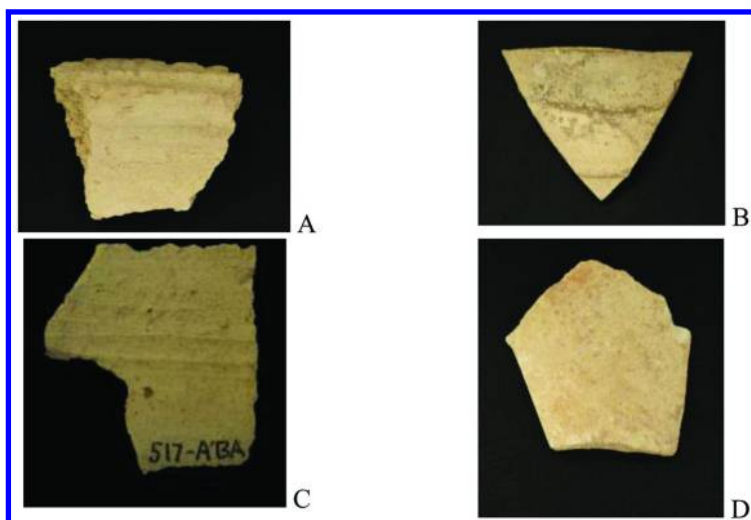
Figure 10. Group B samples consisting of Mesopotamian tradition sherds as their colors range from pale greenish to pale gray found in the Mesopotamian House in the F6 tell (A, B). pXRF and statistical analyses confirming the one sample from Barbar Temple (C) and one specimen from Trench E of Failaka (D) as being of Mesopotamian origin.

Ceramic sherds of group C consist of four samples that came from the Palace of the Tell F6 site on Failaka Island. Three sherds are a reddish color, have a hard clay body, and are wheel-made (see Figure 11) which indicates that they are an Indus Valley type (*49*). It had been assumed that sample No. 13618 is of the Dilmun tradition, but statistically it falls within the Indus sherds group; it has a very smooth surface and is made of hard clay. The other probable explanation is the movement of Indus potters into the Persian/Arabian Gulf who added some Dilmun stylistic elements on the red hard-clay ceramics. One sherd is red ware with whitish slip, covered with yellowish particles as the A-ware type. Pores are clearly seen in the inner surface besides a few whitish-yellowish hollows, but are bigger than A-ware type sherds in group A. It is possible that the outer and inner pores that arose either from lime particles or clay paste due to firing temperature could effectively influence the absorption of X-rays, giving inaccurate results that exclude the sherd from the Barbar wares in group A.

The last potential group of ceramic sherds is group D (see Figure 12), clustered in the middle of discriminant function plot (see Figure 8) and previously mixed with group C in canonical discriminant functions (see Figure 7). They are red-brown in color, have a hard-clay body, smooth outer surface and no visible inclusions. Three of them have been assumed to be Mesopotamian reddish sherds and one as an unknown import. The absence of porosity and the treatment might suggest distinct red-sherd pottery production within the Mesopotamian territory. The one unknown import (15158) might be a sub-group of Mesopotamian pottery. The Eastern Province origin of this sherd also would be a question of interest. Statistically speaking, these Mesopotamia sherds suggest that potters might have

used specific clay and temper, in addition to the well-known greenish-gray and reddish pottery. Therefore, we recommend obtaining more clay or sherd samples from the Eastern Province of Saudi Arabia, Mesopotamia, and the Indus Valley to look for similarities and possibly identify the production center of this group of samples.

Figure 11. Group C consisting of hard reddish and fine clay specimens indicating their Indus Valley type.
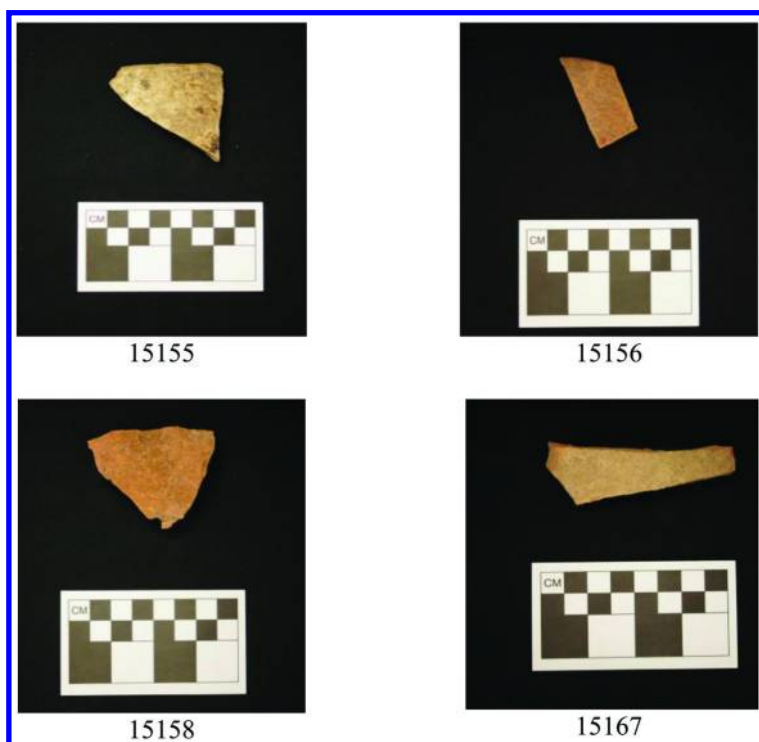
Figure 12. Group D clustering specimens that might have been imported from far-distant region or subgroup of Dilmun or Mesopotamian pottery.

Conclusion

In this paper, we have demonstrated that pXRF can contribute valuable data to construct a database for chemical components of ceramic pottery wares recovered from Failaka Island and Bahrain. Technically, this initial analysis shows the success of pXRF for examining the homogeneity of a sample, identifying unknown samples, and testing previously assumed origins for samples. The pXRF device is a reliable tool to fingerprint or at least create compositional groups for the production center and recognize ceramic centers that stylistic and descriptive methods can confuse. More data is recommended to be selected for more analysis by other analytical instruments, creating empirical calibration for Arabian Gulf ceramics. This would allow other researchers to use the data in the future for comparison.

Statistically, the principal component and cluster analyses successfully differentiated the samples based upon their elemental compositions and were confirmed by discriminant function analysis. The PCA shows a similar chemical compositional profile for Dilmun ceramics from Kuwait and Bahrain, suggesting a centralization of ceramic production and standardized raw materials during the early second millennium BC. The PCA and discriminant analyses show that the Dilmun sherds from the Palace and Trench E in Tell F6 on Failaka Island have the same compositional pattern as those from the Barbar Temple of Bahrain indicating that both ceramics were made of the same raw material. Whatever the treatment of the outer surface for the Dilmun vessels, the choice of using locally available raw materials is noticeable.

Moreover, it is reasonable that Dilmun sites in Bahrain might be the ceramics' production center and the source of ceramics flowing to Failaka Island in Kuwait, considering the archaeological absence of firing kilns for pottery on Failaka Island. Around 2050 BC, Barbar ceramic production grew, indicating a gradual shift from household production to a professional craft production; this shift coincides with the emergence of complex sociocultural elements such as religious monuments, temples at Barbar of Bahrain and the F6 Temple on Failaka Island, fortified stone walls, and local-style stamp seals (*3*, *5*). Thus, it is reasonable by 1950 BC to find more Barbar sherds (period IIb) and these are similar to Failaka Period 1 sherds. The Barbar IIb period is crucial for the Dilmun administration particularly after the collapse of the Ur III dynasty in Mesopotamia. In this period, Dilmun seems to be one of the main suppliers to the Mesopotamian market and to be an active partner with Babylonian merchants (*5*). Thus, the appearance of Mesopotamian sherds in Trench E (earliest Dilmun horizon on Failaka) and at the Barbar Temple is reasonable to reflect this interregional interaction. With more evidence and further study, this dramatic change in Dilmun could push Dilmunites to move to Failaka and create the first social formation to ensure its northern border and enhance the trading relationship with Mesopotamia (*5*). Interestingly, Barbar Temple samples show the usefulness of using the Bahrain collection as a reference group of clay sources and geochemical data, despite the small size of samples selected for this study. However, petrographic thin-section analysis is highly recommended in the future to determine the source of chemical components and mineralogical variation and the influence of behavioral or natural parameters in the composition.

The similarity in chemical composition between one of the samples from Trench E on Failaka and Barbar Temple in Bahrain sherds with greenish sherds from the Mesopotamian House suggests the use of the same raw material; the Mesopotamian House sherds from the Tell F6 site are useful as a group reference for Mesopotamian geology, or at least for Mesopotamian origin. The Mesopotamian house sherds infer the Ur III expansion in the Arabian Gulf. It is documented that under the Ur III rulers, Mesopotamian merchants established a connection with suppliers of copper, particularly with Magan/Oman. The claim of Ur-Namma (2113-2095 BC) referred to the establishment of trade with Magan during his reign, copper in exchange for textiles (*39*). Numbers of Type 1 of Ur III vessels discovered in Dilmun mounds in Bahrain support the long-distance trade and exchange between Ur III and Magan that might have been placed by highly organized institutions (*48*). With this recent discovery of the Mesopotamian structure supported by chemical analysis, Failaka seems under control of the Ur III, as one of those harbors and refueling centers along the trading routes, during the end of the third millennium BC.

The results suggest that not only did Dilmun have standardization of raw materials, but so did other trading polities, such as the Indus Valley and Mesopotamia. The raw materials that lent to the production of Barbar wares are consistent. Also, the hard-clay reddish sample from the Palace is clustered rather well with the appearance of other Indus valley sherds. The presence of Indus valley sherds, particularly from the Palace site, suggests that the residents of the palace or the governor's house of the Tell F6 site on Failaka Island had access to non-local materials, particularly imported ceramics.

Standardization of ceramics can be used to reconstruct interregional interaction, trade and exchange. The control of raw materials available to craft specialists and the imposition of the types of raw materials to be used in production can be traced with the pXRF device. Elites, emerging or established, can exert parameters through close relationships with their native craftsmen to control the types of goods and commodities that circulate within a larger trade network for the good of the larger society (*50*). The presence of Indus valley sherds as exotic items would support our assumption about how elites or rulers controlled the accessibility and distribution of non-local wares, and even their participation in the long-distance, external network to the exclusion of others on the island. The residents of the Palace site on Failaka seemingly sought to take advantage of the prominence of the Dilmun state (mainland center) and its dominance over the Arabian Gulf trade network. Undoubtedly, understating the role of elites or rulers and sociopolitical institutions as well as craft specialization in Dilmun requires more ceramic materials and analyses to shed light on the scale and level of ceramics and other staple finance productions.

This interregional interaction did not start with the establishment of a Dilmun colony on Failaka as we have seen from evidence in the lowest level of Trench E at Tell F6. Even during the pre-Dilmun period, at the Ur III period house on Failaka Island we have seen evidence of an interregional contact. Failaka Island probably seemed a proper transit point or port for the Ur III dynastic authorities because it lies at its southern border. The presence of late third-millennium Mesopotamian sherds, 2nd millennium Dilmun, and Indus type sherds on Failaka

Island support our notions of the power of the political economic institutions. We think these institutions controlled long-distance trade and interregional exchange between different cultural entities on a large scale, and this control and activity increasingly contributed to the emergence of social complexity and economic structure, particularly within the Dilmun entity. The development of sociopolitical power in Dilmun is characterized by the presence of mound burials, Dilmun stamp seals, Barbar ridged ware, and temple complexes as well as establishing a trading port as seen on Failaka Island during the Bronze Age. The craft specialization, particularly pottery production and the control of raw materials, is of interest to understand the practice of sociopolitical and economic power within the Dilmun realm.

Acknowledgments

References

1. Crawford, H. *Dilmun and Its Gulf Neighbours*; Cambridge University Press: Cambridge, U.K., 1998.
2. Weisgerber, G. In *Bahrain through the Ages: The Archaeology*; Al Khalifa, H., Rice, M., Eds.; KPI: London, 1986; pp 135−142.
3. Højlund, F.; Anderson, H. *Qala'at al-Bahrain 1. The Northern City Wall and the Islamic Fortress*; Aarhus University Press: Aarhus, Denmark, 1994.
4. Benedikova, L. *Al-Khidr 2004-2009; Primary Scientific Report on the Activities of the Kuwait-Slovak Archaeological Mission*; NCCAL: Kuwait City, 2010.
5. Højlund, F. *The Burial Mounds of Bahrain: Social complexity in Early Dilmun*; *Jutland* Archaeological Society: Moesgård, Denmark, 2007.
6. Ratnagar, S. *Trading Encounters from Euphrates to the Indus in the Bronze Age*; Oxford University Press: New Delhi, India, 2004.
7. Larsen, C. *Life and Land Use on the Bahrain Islands: The Geoarcheology of an Ancient Society*; The University of Chicago Press: Chicago, IL, 1983.
8. Cleuziou, S. In *Bahrain through the Ages the Archaeology*; Al Khalifa, H., Rice, M., Eds.; KPI: London,1986; pp 143−155.

9. Zarins, J. In *Bahrain through the Ages the Archaeology*; Al Khalifa, H., Rice, M., Eds.; KPI: London,1986; pp 233−250.

10. Potts, D. In *Bahrain through the Ages the Archaeology*; Al Khalifa, H., Rice, M., Eds.; KPI: London,1986; pp 389−398.

11. Højlund, F. In *Bahrain through the Ages the Archaeology*; Al Khalifa, H., Rice, M., Eds.; KPI: London,1986; pp 217−224.

12. Højlund, F., Ed.; *Failaka/Dilmun: The Second Millennium Settlements; Volume 2: The Bronze Age Pottery*; Aarhus University Press: Arhus, Denmark, 1987.

13. Brumfield, E.; Earle, T., Eds.; *Specialization, Exchange, and Complex Societies*; Cambridge University Press: London, 1987; pp 1−9.

14. Stein, G. In *Craft Specialization and Social Evolution*; Wailes, B., Ed.; University Museum Monograph 93; University of Pennsylvania Museum: Philadelphia, 1996; pp 25−38.

15. Højlund F. In *Bahrain: The Civilisation of the Two Seas*; Lombard, P., al-Sindi, K., Eds.; Institute du Monde Arabe: Paris, 1999; pp 73−76

16. Larsen, C. *Life and Land Use on the Bahrain Islands: The Geoarcheology of an Ancient Society*; University of Chicago Press, Chicago, IL, 1983.

17. Edens, C. *Am. Anthrop.* **1992**, *94*, 118–139.

18. Chen, T.; Rapp, G. R.; Jing, Z. C.; He, N. *J. Archaeol. Sci.* **1999**, *26*, 1003–1015.

19. Tykot, R. H. *Acc. Chem. Res.* **2002**, *35*, 618–627.

20. Munita, C. S.; Paiva, R. P.; Alves, M. A.; Oliverira De, P. M.; Momose, E. F. *J. Radioanal. Nucl. Chem.* **2001**, *248*, 93–96.

21. Kenoyer, J. M.; Price, T. D.; Burton, J. H. *J. Archaeol. Sci.* **2013**, *40*, 2286–2297.

22. Blackman, M. J.; Méry, S.; Wright, R. P. *J. Field Archaeol.* **1989**, *16*, 61–77.

23. Mynors, H. S. *Proceedings of the 22nd Symposium of Archaeometry*; Schools of Physics and Archaeological Science, University of Bradford: Bradford, U.K., 1983; pp 377−387.

24. Méry, S. *Paléorient* **1991**, *17*, 51–78.

25. Méry, S. *Annali Istituto Universitario Orientale* **1995**, *55*, 193–206.

26. Méry, S. *Les céramiques d'Oman et l'Asie moyenne: Une archéologie des échanges a' l'Aˆge du Bronze*; CNRS: Paris, 2000.

27. Méry, S. In *The Shadow of the Ancestors: The Prehistoric Foundations of The Early Arabian Civilization in Oman*; Cleuziou, S., Tosi, M., Eds.; Ministry of Heritage and Culture: Oman, 2007; pp 199−201.

28. Méry, S.; Blackman, M. In *Harappan Studies 3*; Lecture, World Archaeology Conference, New Delhi, India; pp 1−32.

29. Méry, S.; Blackman, M. J. *Paléorient* **1999**, *25*, 167–177.

30. Méry, S.; Blackman M. J.; Didier, A. In *Proceedings of the Seminar for Arabia Studies*; Oxford University Press: Oxford, U.K., 2012; Vol. 42, pp 195−204.

31. Méry, S.; Schneider, G. In *Proceedings of the Seminar for Arabia Studies*; Oxford University Press: Oxford, U.K., 1996; Vol. 26, pp 79−95.

32. Méry, S.; Schneider, G. In *Etudes mésopotamiennes. Recueil de textes offert à J.-L. Huot*; Breniquet, C.; Kempinski-Lecomte, C., Eds.; Bibliothèque de la Délégation Archéologique Française en Iraq 9: Paris, 2001; pp 263−275.

33. Pollard, A. M. In *Failaka/Dilmun: The Second Millennium Settlements; Volume 2: The Bronze Age Pottery*; Højlund, F., Ed.; Aarhus University Press: Arhus, Denmark, 1987; pp 185−189.

34. Højlund, F. *Arab. Arch. Epig.* **2012**, 165–173.

35. Day, P.; E. Kiriatzi, A.; Tsolakidou, A.; Kilikoglou, V. *J. Archaeol. Sci.* **1999**, *26*, 1025–1036.

36. Speakman, R. J.; Little, N. C.; Creel, D.; Miller, M. R.; Iñañez, J. G. *J. Archaeol. Sci.* **2011**, *38*, 3483–3496.

37. Goodale, N.; Bailey, D.; Jones, G.; Prescott, C.; Scholz, E.; Stagliano, N.; Lewis, C. *J. Archaeol. Sci.* **2012**, *39*, 875–883.

38. Hoeck, V.; Ionescu, C.; Ghergari, L.; Precup, C. *Geologia* **2009**, *54*, 41–51.

39. Astour, M. In *Eblaitica*; Gordon, C., Rendsburg, G., Eds.; Eisenbrauns: Winona Lake, IN, 2002; pp 57−196.

40. Karydas, A. K.; Kotzamani, D.; Bernard, R.; Barrandon, J. N.; Zarkadas, C. *Nucl. Instrum. Methods B* **2004**, *226*, 15–28.

41. Shackley, S. *Obsidian: Geology and Archaeology in the North American Southwest*; University of Arizona Press; Tucson, AZ, 2005.

42. Craig, N.; Speakman, R. J.; Popelka-Filcoff, R. S.; Glascock, M. D.; Robertson, J. D.; Shackley, M. S.; Aldenderfer, M. *J. Archaeol. Sci.* **2007**, *34*, 2012–2024.

43. Liritzis, I.; Drakonaki, S.; Vafiadou, A.; Sampson, A.; Boutsika, T. In *The Neolithic Settlement at Ftelia, Mykonos*; Sampson, A., Ed.; University of the Aegean: Greece, 2002; pp 251−272.

44. Papadopoulou, D. N.; Zachariadis, G. A.; Anthemidis, A. N.; Tsirliganis, N. C.; Stratis, J. A. *Talanta* **2006**, *68*, 1692–1699.

45. Papagrotgiou, I.; Liritzis, I. *Archaeometry* **2007**, *49*, 795–813.

46. Cirpian, S; Ashkanani, H; Tykot, R. H.; Puscas, M. *Proceedings of the 39th International Symposium for Archaeometry, Leuven*, 2013, in press.

47. Goren, Y.; Mommsen, H.; Klinger, J. *J. Archaeol. Sci.* **2011**, *38*, 684–696.

48. Laursen, S. *Arab. Arch. Epig.* **2011**, *22*, 32–47.

49. Højlund, F. Personal communication; Moesgård Museum, Aarhus, Denmark, 2011.

50. Hirth, K. *J. Archaeol. Res.* **1996**, *4*, 203–2301996.

Chapter 15

pXRF Analysis of Arsenic When Lead Is Present: A Cautionary Tale

Marvin W. Rowe,*,[1,2] Sally J. Cole,[3] and Mohammed Yousuf[1]

[1]Department of Chemistry, Texas A&M University-Qatar, Doha, Qatar
[2]Office of Archaeological Studies and Conservation Laboratory, Museum of New Mexico, Santa Fe, New Mexico 87505
[3]Department of Anthropology, Ft. Lewis College, Durango, Colorado 81301
*E-mail: marvin.rowe@qatar.tamu.edu

Although the InnovX Alpha Series portable X-ray fluorescence device we used to qualitatively analyze ceramics pigments and Lowry Pueblo Kiva white paint repeatedly reported As (in hundreds of measurements) whenever significant amounts of Pb were present, there were in fact no significant amounts of As present in those samples. Obviously, care must be taken when using pXRF, particularly that InnovX device, to determine As when there are significant amounts of Pb present in the samples.

Introduction

Portable X-ray fluorescence spectroscopy (pXRF) is beginning to be used more and more in art, conservation and archaeology (*1–11*) to list a few. We wish to point out a potential difficulty with the use of pXRF when analyzing for arsenic (As) in the presence of significant levels of lead (Pb). In particular, we have faced that situation in two projects we are currently working on: pigment analysis of the decorations of some ceramics from the Colorado Plateau and some white paint on the painted kiva walls at Lowry Pueblo.

Our pXRF analyses indicated that hundreds of the ceramic pigments and some of the kiva wall paint layers contained elevated levels of Pb and As. When significant Pb signals were seen in samples, As was also always detected at elevated levels. As an example of the problem, we will concentrate on one of the Lowry Pueblo Kiva B paint layers here. Paul Martin, the excavating archaeologist, reported Kiva B overall had up to 2 inches of thick plaster with

multiple layers (*12*). Our sample is obviously only a small part of what he saw and had six layers of brown plaster, separated by white paint layers. Our analyses of five of those paint layers indicated that Pb and As were prominent in at least one of them, along with Zn.

Experimental Procedure

For our initial analyses, we used a battery operated InnovX Systems Alpha Series, portable, hand-held, nondestructive pXRF device for measurements of the elemental signal of the white paints used in the Lowry Kiva wall paints and Colorado plateau ceramics. The spectrometer works by irradiating the sample with an X-ray tube that emits primary X-rays that strike the target, in our case the surface pigments associated with individual ceramic design elements and Lowry Pueblo white painted Kiva walls. These primary X-rays sometimes strike an orbital electron in an atom (say Fe) of the sample being analyzed with enough energy to knock out the electron from the inner electron shell of the element. The removal of such an electron from an element is accompanied by the emission of secondary X-rays in the atom's attempt to re-stabilize itself. The energies and numbers of secondary X-ray emissions are measured. The energy of a secondary electron is specific for a given element, and essentially different from all others *with a few exceptions*. Thus, ideally the technique qualitatively detects the atoms that are present in the pigments. Then, with proper calibration and software, the approximate (semi-quantitative) abundances of the elements present can be calculated by measuring the intensities of the radiations of particular energies. Abundances in *uniform*, *homogeneous* samples as low as 10 parts per million (ppm) are possible for some elements. The elemental analysis on the InnovX instrument is displayed on the miniature iPAQ computer as parts per million for a given element. In the situation here, the instrument reported measurable signals from the pigment elements Pb and As (as well as Zn in the kiva wall paint), and Fe, Cu, Mn, Rb, Sr and Zr (present in the ceramics and the plaster that separates the Kiva paint layers). But we emphasize that the method is not even semi-quantitative in the application to ceramic and wall paint pigment analysis. We do not get accurate measures of the *abundance* (ppm, e.g.) of the elements for a number of reasons: (1) the pigment often does not cover the entire area of the target primary X-rays; (2) the paint/pigment is thin, but not of uniform thickness; and (3) the pigment is not necessarily uniform in the paint/pigment layer. These factors combine to render the method *qualitative* with at best a rough indication of the presence at lower vs. higher levels. Nonetheless, we will see that the analyses are useful in spite of these difficulties. We are, at this stage, primarily interested in determining what elements were used as pigments in the paints.

With these difficulties in obtaining quantitative concentrations, one might ask, "Why use pXRF at all?" The advantages are significant. Importantly, *nondestructive* in situ analysis is possible. Second, the device is easy to use – just point and shoot. Third, each analysis is fast – typically just 10 - 30 seconds per analysis will indicate clearly the dominant pigment elements used in a paint, pottery design element; etc. For better statistics in some applications, up to

In Archaeological Chemistry VIII; Armitage, R., et al.;
ACS Symposium Series; American Chemical Society: Washington, DC, 2013.

300 second counts were used. Data reduction takes longer. One can analyze hundreds of samples, so the device is very applicable for survey work. Fourth, the instrument is light enough that it can be carried to remote sites. It is *generally* reliable for *qualitative* analysis, i.e., the presence numerous elements in this study. But extreme caution must be exercised at times, as in the case of the As supposedly detected in this study.

Figure 1 shows one example of a pXRF analysis, one of hundreds of pigmented ceramics where Pb and As were reported on the screen of the InnovX Alpha series handheld X-ray fluorescence spectrometer (pXRF).

Figure 1. A photograph showing analysis of black pigment painted on a white ceramic from the Colorado Plateau. Readout indicated the presence of Pb and As in the pigment. That As was typical of all ceramics where Pb was indicated as a major component of the pigment. That is, in every case when high levels of Pb were recorded, lesser amounts of As were also reported on by the pXRF.

Results and Discussion

Table I shows a table of the average of five determinations from the iPAQ handheld computer readout on the InnovX pXRF device for a typical result yielding high levels of Pb and As (and Zn). The other elements detected are almost certainly due to the underlying plaster layer. In our experience, every time a sizable Pb peak was seen, an elevated As signal was invariably seen as well. Because of the overlap between the Pb L_α and As K_α peaks at 10.6 keV, and that peak is apparently used for both Pb and As determinations in the InnovX

software, we became concerned whether the As results were valid, or were an instrumental software artifact. We therefore consulted the InnovX brochure concerning the peak overlap problem between Pb and As. The Innov-X User Manual Version 2.1, Soil Appendix 14 reads, "Example 1: Lead and Arsenic. Most XRFs are calibrated for lead and arsenic. Lead interferes with arsenic (not vice-versa though). The net effect is a *worsened detection limit for arsenic, and poorer precision. The XRF handles the correction automatically, but the precision is affected. The loss of precision is also reported by the XRF*." The italics were added by us for emphasis. That this is the position held by InnovX was confirmed by a telephone call to them. However, because we invariably "detected" significant As signals whenever we detected substantial indications of Pb, we continued to be wary. High Pb measurements were accompanied by significant As in several hundred ceramics samples (*13*, *14*).

Table I. The table contains an average of five, 300 second determinations from the iPAQ handheld computer readout on the InnovX pXRF device. We bold faced Pb and As, those being the elements of interest here. The pigment here contains principally Zn, Pb and As. Other elements are likely from clay fabric.

Innov-X Results	Kiva B Paint	Innov-X Results	Kiva B Paint
Ti	1002 ± 223	Hg	86 ± 11
Ba	2406 ± 139	**As**	**3329 ± 43**
Cr	172 ± 42	Se	102 ± 7
Mn	120 ± 23	**Pb**	**23496 ± 231**
Fe	8461 ± 111	Rb	84 ± 2
Co	244 ± 22	Sr	88 ± 1
Cu	57 ± 11	Zr	242 ± 4
Zn	57983 ± 570	Cd	78 ± 6

To examine the problem further, we utilized a Bruker Tracer III-V pXRF device at the Conservation Laboratory of the Museum of New Mexico, Santa Fe, NM. With that instrument, unlike our InnovX device, it is easy to display and manipulate the scale for the raw spectra taken. To be fair, spectra from the InnovX can be exported to external software for better visualization of the spectra than is possible on the miniature iPAQ display, but this requires carrying an extra piece of equipment – a laptop – into the field. Figure 2 shows a pXRF spectrum of the sample of Lowry Pueblo Kiva B outer paint layer (shown in Figure 3) taken with the Bruker pXRF device, showing the major peak overlap between Pb and As at the asterisked peak at 10.6 KeV.
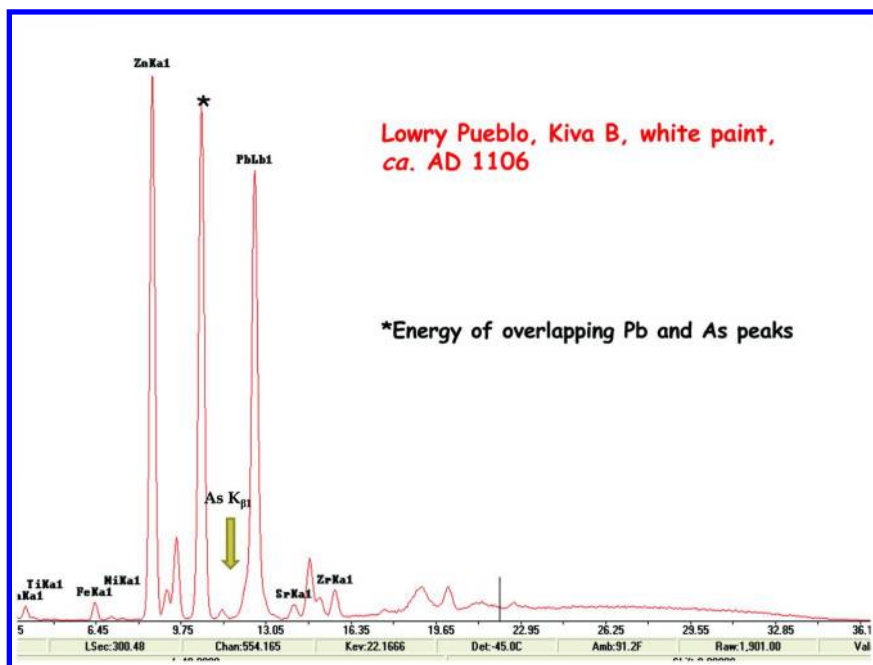
Figure 2. PXRF spectrum of the Lowry Pueblo Kiva B white paint. The asterisk above the peak at ~ 10.6 keV indicates where both the Pb L$_{\alpha 1}$ and As K$_{\alpha 1}$ occur, i.e., overlap, a potential problem. Unfortunately, the algorithm for determining the abundance of As on the InnovX device uses this peak. The yellow arrow points to the position of the As K$_{\beta 1}$ peak of As, a peak that is not interfered with by the Pb.

Figure 3. Photograph of the sample of the outer white paint layer from the Lowry Pueblo Kiva B. Other layers are visible on the edge views.

273

To evaluate this suspected "As" problem more carefully, we examined the $K_{\beta 1}$ peak of As at 11.7 keV, which is not coincident with a Pb peak. That is a more definitive means of seeing whether there is significant As present in a measurement or not. Figure 4 shows the spectrum with the y-axis expanded to investigate the As $K_{\beta 1}$ peak in detail. As can be seen from Figure 4, there is no substantial As observed in the sample. For every case we checked (amounting to many replicate measurements of the Kiva B wall paint, as well as hundreds of measurements on Colorado Plateau ceramics), we did not find evidence for substantial As at the As $K_{\beta 1}$ peak even though As was reported on the iPAQ computer screen of the InnovX pXRF every time in considerable abundance.
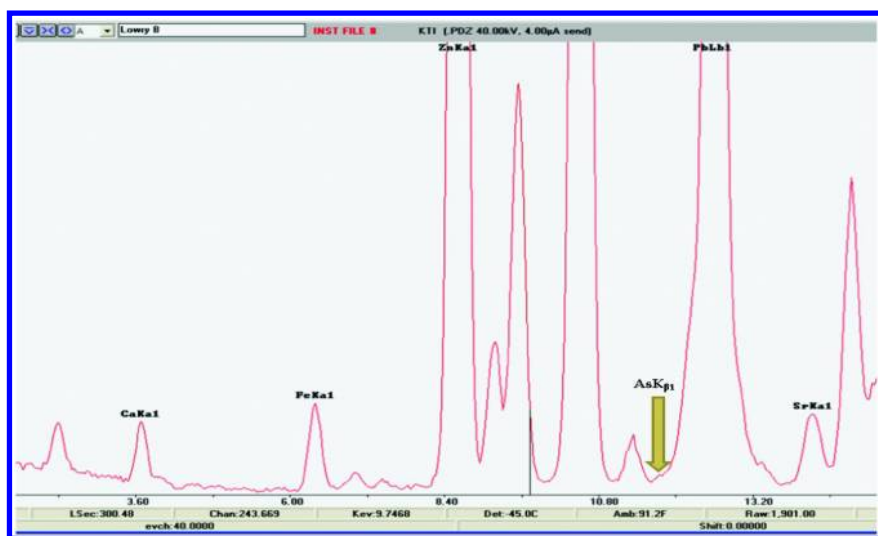
Figure 4. The Figure 2 pXRF spectrum of the Lowry Pueblo Kiva B white paint shown on an expanded scale. The asterisk above the peak at ~ 10.6 keV indicates where both the Pb $L_{\alpha 1}$ and As $K_{\alpha 1}$ occur, i.e., overlap, a potential problem. Unfortunately, the algorithm for determining the abundance of As on the InnovX device uses this peak. The yellow arrow points to the position of the As $K_{\beta 1}$ peak of As, a peak that is not interfered with by the Pb. Even with a strongly expanded scale, there is no evidence seen for more than a very minor shoulder to indicate the presence of As at the As $K_{\beta 1}$ peak.

And finally, to question further whether there was significant As present in the Kiva B white paint sample, we also examined a small sample of the white paint using scanning electron microscopy (SEM) equipped with energy dispersive X-ray analysis (EDX) that yields qualitative chemical information similar to pXRF, with differences in the limits of detection. The device used was a Scanning Electron Microscope Model Quanta 400 by FEI Company (USA), operated at Texas A&M University - Qatar, Doha. The SEM-EDX software distinguishes As from Pb by looking at secondary lines, the 1.28 keV L_{α} for As and the 2.35 keV M_{α} for Pb. Thus, we can tell if there is both As and Pb present by looking at the L_{α}-line for As and the M_{α}-line for Pb. There are also several other Pb L-lines ($L_{\beta 1}$, $L_{\beta 3}$, etc) that

are not overlapping any of the As K-lines, further indicating the presence of Pb. A spectrum of the analysis is shown in Figure 5. Although there is clear indication for Pb and Zn in the paint, as well as C, O, Mg, Si, Ba, and Ca from the plaster layer underlying the thin paint layer, there is no indication of As.
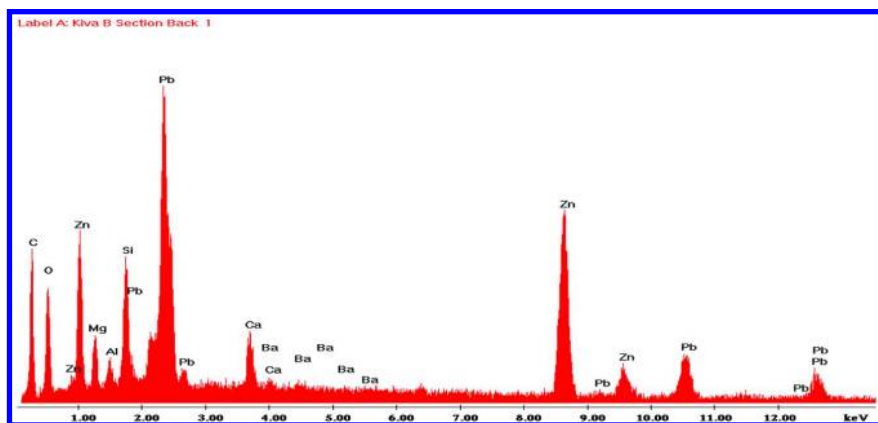
Figure 5. An SEM-EDX spectrum of a small white paint sample from the Lowry Pueblo Kiva B painted wall. Although the pigment obviously contains both Pb and Zn, there is no indication for any As.

Other elements, beyond the scope of this paper, suffer from similar reporting errors. Cadmium may also be incorrectly reported when Pb is high, due to the energies of the two L-lines (10.6 and 12.6 keV, respectively) for Pb yielding a sum peak at 23.2 keV, overlapping with the Kα for Cd. It is important to look for the corresponding higher-energy lines to ensure that the elements identified by the software are confirmed. One can double check this by making a bivariate plot of As and Pb, or Cd and Pb. A strong correlation between these elemental concentrations will indicate the likelihood that artifacts are present in the data. Others (*15*) have noted interferences between barium and titanium as well. Caution should be exercised when evaluating the qualitative analyses for any of these elements.

Conclusion

We conclude from the measurements discussed here that there is no significant As content in any of the hundreds of ceramic pigment designs we examined (this was confirmed in ~100 ceramics samples using the Bruker device described above). Neither is As present in elevated levels in the numerous analyses of paint from the Lowry Pueblo Kiva B sample we examined. Therefore, if Pb is present at significant levels in any sample, it is essential to examine the raw X-ray fluorescence spectrum, or to use another technique (such as scanning electron microscopy used here), in order to be able to ascertain whether or not As is also present. From the raw XRF spectra we examined, one can readily determine the presence or absence of As by examination of the $K_{\beta 1}$ peak of As, a peak

that does not overlap with Pb. Alternatively, SEM-EDX clearly shows whether As is present or not as well. In our experience, the InnovX handheld computer *always* indicates elevated As is present if there is substantial Pb present. Thus, the handheld display of our InnovX device, As results appear to be almost invariably wrong (always in our cases) when measured in the presence of substantial Pb.

Acknowledgments

References

1. Angelini, E; Grassini, S.; Corbellini, S.; Ingo, G. M.; de Caro, T.; Piescia, P.; Riccucci, C.; Blanco, A.; Agnostini, S. *Appl. Phys. A: Mater. Sci. Process.* **2006**, *83*, 643–649.
2. Cecil, L. G.; Moriarty, M. D.; Speakman, R. J.; Glascock, M. D. In *Archaeological Chemistry: Analytical Techniques and Archaeological Interpretation*; Glascock, M. D., Speakman, R. J., Popelka-Filcoff, R. S., Eds.; ACS Symposium Series 968; American Chemical Society: 2007; pp 506−521.
3. Desnica, V.; Škarić, K.; Jimbrih-Simbuerger, D.; Fazin Schreiner, S. *Appl. Phys. A: Mater. Sci. Process.* **2008**, *92*, 19–23.
4. Ferrero, J. L.; Roldán, C.; Ardid, M.; Navarro, E. *Nucl. Instrum. Methods Phys. Res., Sect. A* **1999**, *422*, 868–873.
5. Fonicello, N. A. *ICOM-CC Ethnographic Conservation Newsletter* **2007**, *28*, 4–8.
6. Gianoncelli, A.; Castaing, J.; Bouquillon, A.; Polvoninos, A.; Walter, P. *X-Ray Spectrom.* **2006**, *35*, 365–369.
7. Hayakawa, Y. *Adv. X-Ray Anal.* **2004**, *47*, 36–41.
8. Nazaroff, A. J.; Prufer, K. M.; Drake, B. L. *J. Archaeol. Sci.* **2009**, *36*, 885–895.
9. Padilla, R.; Van Espen, P.; Godo Torres, P. P. *Anal. Chim. Acta* **2006**, *558*, 283–289.
10. Papadopoulou, D. N.; Zachariadis, G. A.; Anthemidis, A. N.; Tsirliganis, N. C.; Stratis, J. A. *Talanta* **2006**, *68*, 1692–1699.
11. Phillips, S.; Colby, S.; Speakman, R. J. *J. Archaeol. Sci.* **2009**, *36*, 1256–1263.
12. Martin, P. S. *Lowry Ruin in Southwestern Colorado*. Field Museum of Natural History, Anthropology Series, 1936, Vol. *23*, no. 1, Chicago, IL.
13. Cole, S. J.; Charles, M. C.; Rowe, M. W. Presentation at the Annual Meeting of the Society of American Archaeology, Vancouver, B.C., Canada, 2008.
14. Rowe, M.; Cole, S. J. Office of Archaeological Studies and Conservation Laboratory, Museum of New Mexico, Santa Fe, NM; Department of Anthropology, Ft. Lewis College, 2012, unpublished data.
15. Potts, P. J.; Tindle, A. G. *X-Ray Spectrom.* **1991**, *20*, 119–129.

Chapter 16

Metal Plate Connectors and Iron Nails on the Tripitaka Koreana Printing Woodblocks

Choon Ho Do,*,1 Chong-Hong Pyun,2 Byung-Yong Yu,2 and Jung Hyun Bae3

1Division of Fisheries System Eng., National Fisheries R&D Institute, 216 Gijanghaean-ro, Kijang-eup, Kijang-gun, Busan 619-705, Korea
2Korea Institute of Science & Technology, Hwarangno 14-gil 5, Seongbuk-gu, Seoul 136-791, Korea
3Joongang Conservation Center for Cultural Heritage, 782-34 Bangbaebon-dong, Seocho-gu, Seoul 137-829, Korea
***E-mail: choondo@sunchon.ac.kr**

The compositions of the metal plate connectors and nails that make up the Korean Buddhist Tripitaka (Canon) Printing Woodblocks, carved between AD 1236 and 1251 were determined using X-ray fluorescence spectroscopy (XRF), electron probe micro-analyzer (EPMA) and scanning electron microscopy. Copper was the main component of the metal plate connectors, as determined by XRF analysis. The composition of the nails used to connect the end pieces and the main printing wooden plate was mainly iron according to EPMA results. The iron nails were made through hand-forging of sponge iron.

Introduction

History

The Korean Buddhist Tripitaka (Canon) printing woodblocks, of which there are more than 81,000, were carved during the Mongolian invasion of Korea in the period AD 1236-1251. 'Tripitaka' is a Sanskrit word meaning three baskets. 'Tripitaka' is used as a term for the Buddhist canons because the Tripitaka contains three categories, sermons, precepts and commentaries. These woodblocks are a second edition. The first ones carved during AD 1011–1087 using the text of Chinese Northern Song (960-1127) burned by another previous

Mongolian invasion in 1231. Today, the woodblocks are stored at the Haein-sa Temple, in Hapchun, Kyungsangnam-do, Korea. These objects are Korean cultural treasures, and the temple where they reside was designated as a UNESCO World Heritage Site in 1995 (*1*) and documentary heritage in 2007 by UNESCO (*2*). The woodblocks are stored in two buildings at the temple site, where they sit on shelves in sequence like books in a library (Figure 1). The text of the second edition was employed as a main text for the Japanese version, the Taishō Tripitaka printed using metal types during 1924-1934.

In this paper, we examined the composition and structures of the metal plate connectors and iron nails used to assemble the woodblocks by optical microscopy, X-ray fluorescence spectroscopy (XRF) and scanning electron microscopy (SEM) with energy dispersive spectroscopy (EDS). The metal plate connectors and nails fixed the main body plate to the end pieces of the woodblocks. We have previously reported studies on the iron nails found in the woodblocks (*3*). Since the metal plate connector sample employed for the elemental analysis in one of our previous studies was a part of a recent repair, our previous study was incorrect, unfortunately.

Because the woodblocks have much significance as part of our shared national and world heritage, there is much interest in the scientific reasons for the excellent state of preservation of these objects. There are several possible reasons for their preservation including (1) the natural environment and climate in which the woodblocks are stored; (2) the remote location and protection during wartime; (3) the dedication of many concerned people, especially the Buddhist monks to whom their care was entrusted; (4) the unique design and preparation of the woodblocks, in particular the Japanese lacquer coatings that are present; and (5) the anti-microbial properties of copper and its compounds. Studies of the surface coatings of these artifacts were presented at the ACS National Meeting in 1996 (*4*), and further reports on that work were featured in *C&E News* later that same year (*5*). We will further elaborate on the anti-microbial properties of copper later in this paper.

Figure 1. (a) Two storage houses for the woodblocks are shown in parallel; (b) The wood blocks stored on shelves in sequence.

Structure of the Canon Woodblocks and the Printing Method Used

The woodblock is composed of three parts (*6*, *7*): two side handles (end pieces) and a main block, as shown in Figure 2. The end pieces are connected to the main block using wooden pegs (holes in Figure 2a), and the four corners are connected using metal plate connectors to reinforce the connections.. The woodblocks are found in two widths, 68 cm and 78 cm. Each is 24 cm high and on average 3 cm thick in the main body. The area on which the carved Buddhist Canon is located is 51 cm x 23 cm.
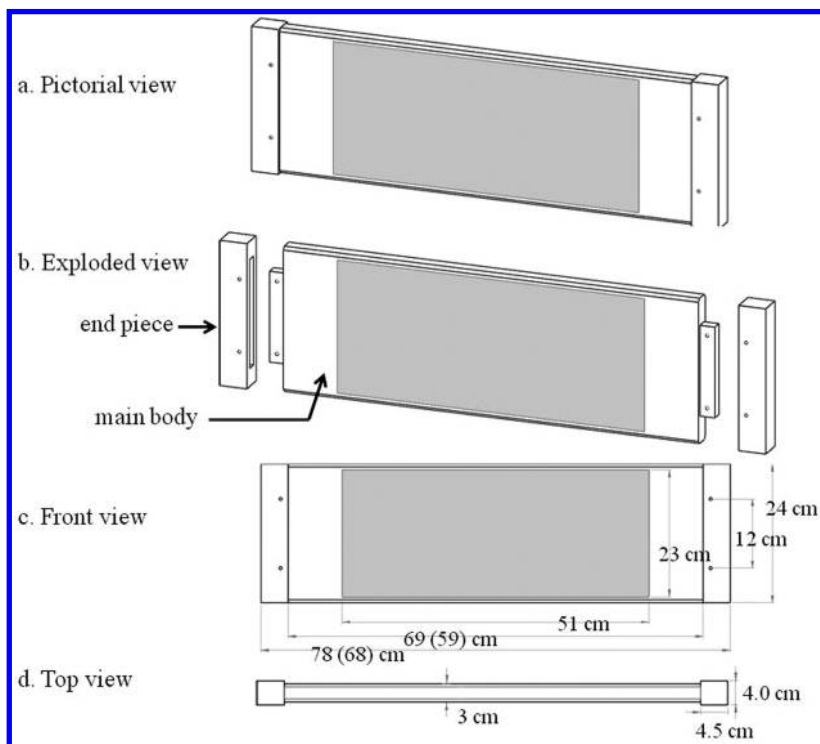
Figure 2. The shape and dimension of a typical Buddhist Cannon printing woodblock.

The method by which the printing blocks were used took four steps. First, the woodblock was placed on the printing table, as shown in Figure 3, and a water-soluble black ink was coated onto the surface of the block. Second, a sheet of rice paper was carefully placed evenly on top of the inked block. Third, the surface of the paper was then gently pressed to transfer the ink to the paper, and finally the paper was removed to yield the final printed page.
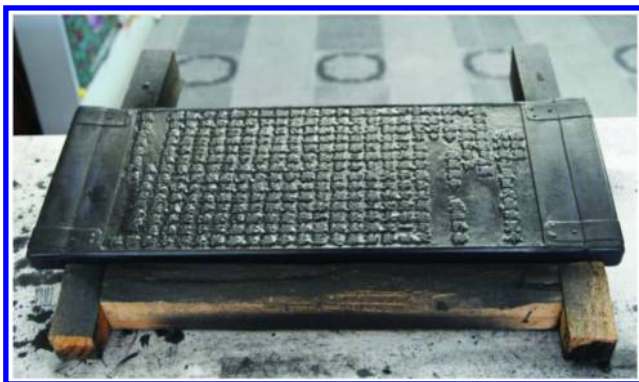
Figure 3. Printing woodblock sitting on a print table.

Description of the Metal Plate Connectors

Metal plates connect the main body and end pieces (or handles) of the woodblocks. Seven different types of these metal connectors have been observed; photos of two of these are shown in detail in Figure 4. Figure 5 shows all of the different connectors and their dimensions. White dots in Figure 5 depict iron nails. The majority of the metal plate connectors are of Types a-e. The number of Type f connectors is small. Type g connectors are made of steel and believed to be recent repairs and occur only rarely. Based on their color, Types a-f appear to be copper. Types a and b are one-piece connectors and type c is composed of two metal strips although their exterior views are very similar each other. The thickness of the connectors is approximately 1 mm. Several different types of the metal connectors indicate that these metal connectors might be fastened at different periods.

Figure 4. Two types of metal plate connectors used four corners to combine end pieces and main body.
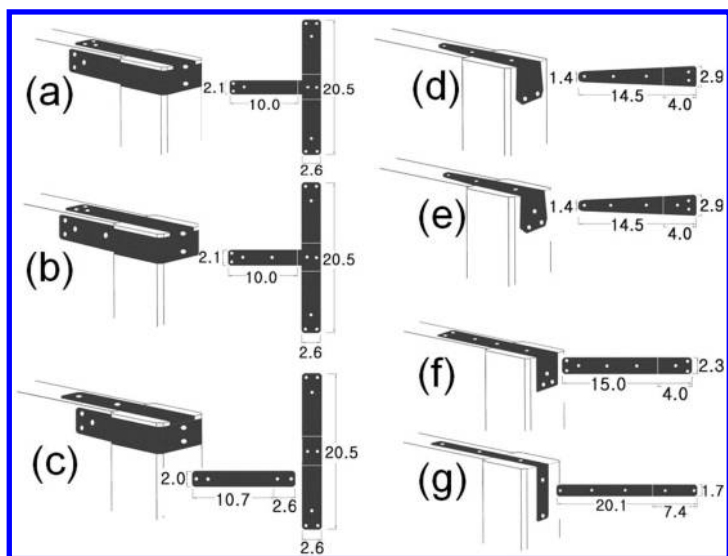
Figure 5. Shapes and dimensions of the metal plate connectors. The dimension of the numbers is centimeter.

Experimental

A piece of the metal plate connector (probably Type d or Type e) was obtained from a staffer of the Conservation Division, the Haein-sa Temple. Modern copper and brass plates were employed for comparison with the woodblock plate connectors. Nails have fallen out of many of the woodblocks due to rusting. Figure 6 shows holes due to missing nails. It also shows the types of the metal plate connectors. These loose nails were collected from the floor of the storage areas using a magnet. Nails were cross-sectioned longitudinally, then cured in epoxy resin prior to polishing for scanning electron microscopy (SEM) and electron probe micro-analyzer (EPMA) analyses. Nital solution, 2% was used for 30 seconds to etch the surface of the nail for surface analysis.

Figure 6. Missing nails – Two holes are shown in the figure.

The metal plate connectors were examined by optical microscopy on a Zeiss Axioscope. Wavelength dispersive XRF analysis was done using a Rigaku model ZSX Primus II. The nails were examined by FEI Corporation SEM (Inspect F50 model) with Ametek EDAX for electron microscopy and EPMA analysis. Because EDAX with Pegasus software performs ZAF correction, it is unnecessary to calibrate the data.

Results and Discussion

Composition of the Metal Plate Connectors

Anyone who is familiar with the blue-green color of an architectural copper-clad dome will recognize the same color in the metal plate connectors. The front and back surfaces of the metal plate connector were examined with WDS-XRF and compared to a modern copper plate (Figure 7). Because we found from Figure 8 that XRF spectrum of the metal plate connector was different from one of known brass plate and didn't contain zinc, we examined the metal plate connector with the known copper plate connector for later study.

The elemental analyses by XRF are listed in Table I. These results show that the metal plate connector is composed of 98% copper. Because neither zinc nor tin are observed, the metal plate connector is not made of either brass or bronze. The metal plate connector contained about 1% silver, indicative that it is not of modern manufacture, as modern copper plate is usually obtained through electrorefining, where noble metals such as silver and gold are separated as anode slime (*8*). The modern copper standard did not show any evidence of silver.

The composition of the surface of the metal plate connector was compared with the oxidation layer intact, and with it removed through polishing, as shown in Figure 9. The oxidized surface shows more silicon and aluminum, as well as several other elements. This indicates that the surface was also contaminated with dust in addition to oxidation.
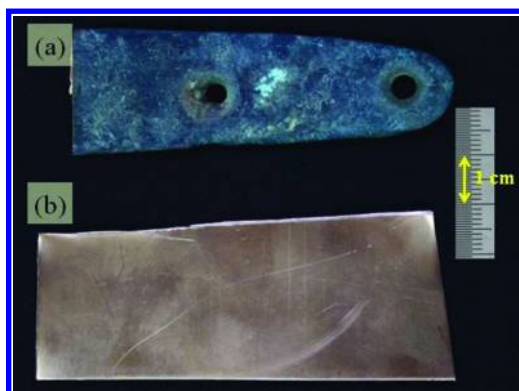
Figure 7. Examined (a) metal plate connector and (b) modern copper plate.

In Archaeological Chemistry VIII; Armitage, R., et al.;
ACS Symposium Series; American Chemical Society: Washington, DC, 2013.
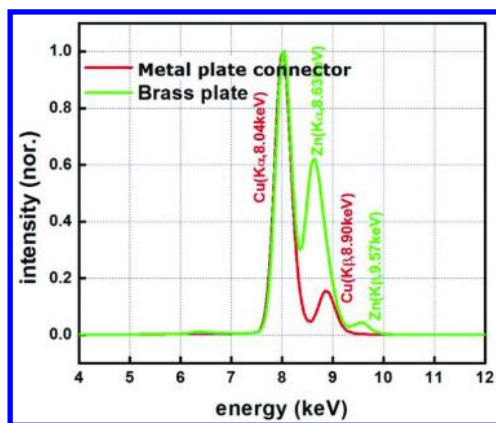
Figure 8. Comparison of XRF spectrum of metal plate connector with brass plate.

Table I. Elemental Analyses of the metal plate connector and modern copper plate (wt%)

	Metal plate connector (inside)	*Metal plate connector (outside)*	*Modern copper plate*
Na		0.908	
Mg		1.1	0.0151
Al	0.0135	6.1	0.0321
Si	0.0708	10.2	0.068
P	0.0223	0.601	0.0586
S	0.0214	0.935	0.0757
Cl	0.475	0.762	0.038
K	-	0.91	0.0107
Ca	-	2.017	0.009
Fe	0.0695	0.867	0.0313
Cu	97.9	74.2	99.4
Ag	0.957	0.699	-
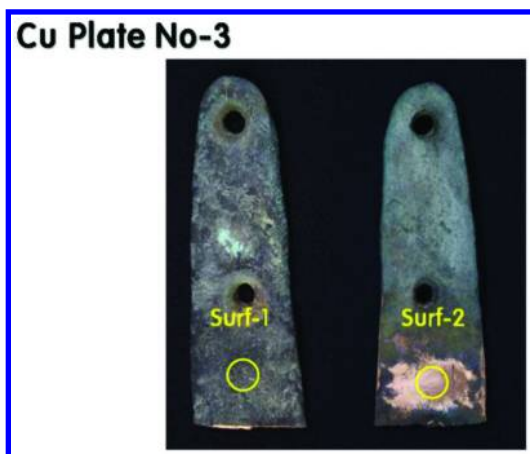
Figure 9. Original oxidized surface and cleaned surface of metal plate connector.

The surface of the metal plate connector was compared to that of the modern copper plate by optical microscopy. Images of the surfaces are shown in Figure 10. The surface of the metal plate connector (Figure 10a) shows a typical "blistered" surface formed during production of copper directly from copper ores. The modern copper plate (Figure 10b) shows streaks formed by rolling the copper flat.
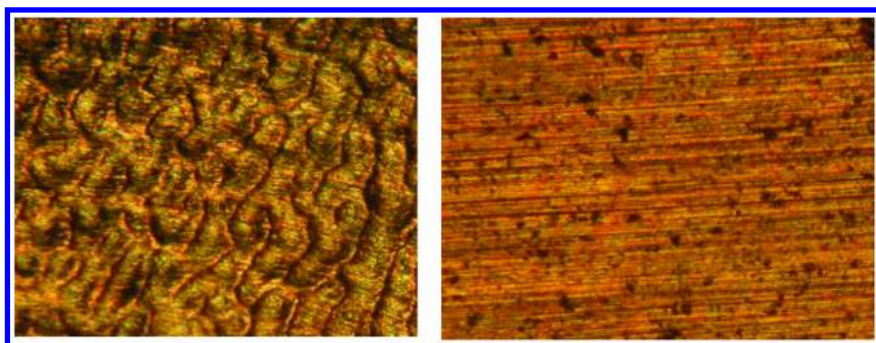
Figure 10. Comparison of the surfaces of (a) metal plate connector and (b) modern copper plate, observed by optical microscope (x50).

Copper is produced by the following method. Copper ore, usually chalcopyrite ($CuFeS_2$) was heated with silica to remove iron as a slag (Equation 1). The resulting copper matte consisting of Cu_2S was then roasted to convert it to copper oxide. Copper oxide is converted to "blister" copper due to the gases evolved during cooling, as shown in Equations 2 and 3.

$$CuFeS_2 + O_2 + silica \longrightarrow Cu_2S + FeSiO_3 \, (silicate\ slag) \quad (1)$$

$$2\,Cu_2S + 3\,O_2 \longrightarrow 2\,Cu_2O + 2\,SO_2 \quad\quad\quad (2)$$

$$2\,Cu_2O \longrightarrow 4Cu + O_2 \quad\quad\quad\quad\quad (3)$$
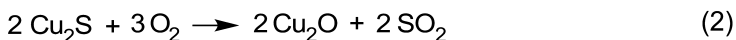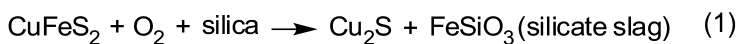
Effects of Copper Metal Plates

The structural role of the metal plate connectors was to connect the main woodblock body to the end pieces and fix them firmly in place. We assume that the metal plate connectors also had a protective role, inhibiting the growth of fungi. Copper and copper compounds are known to have anti-microbial properties (9–11). Because the metal plates are made of nearly pure copper, we believe that this, in combination with the Japanese lacquer coating, has helped to preserve the Koryo Buddhist Cannon Woodblocks from decomposition.

Special Patterns on the Surfaces of the Metal Plate Connectors

A few metal plate connectors have been observed with arabesque patterns depicting lotuses (Figure 11). These patterns appear to have been inscribed manually, as the patterns differ slightly from each other. The metal plate connectors with lotus patterns are rare amongst the collection of woodblocks. We do not yet know why these patterned metal plate connectors are present on some of the woodblocks, but we continue searching for clues, as this may provide additional information about the history of these unique artifacts.
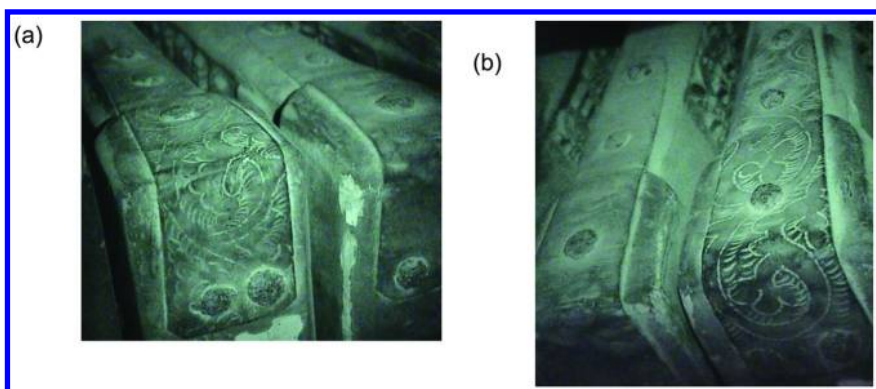
Figure 11. Arabesque patterns of lotus on the some metal connectors are shown.

Composition of the Iron Nails

Iron nails were used to firmly fix the main body of the woodblocks to the end pieces. The nails examined in this study are shown in Figure 12; on average, the nails are approximately 3 cm long. The shapes observed with the naked eye exhibit the typical pattern of nails hand-wrought by hammering. The nails were examined further by SEM-EPMA.

Figure 12. Iron nails used for the woodblocks.

In ancient times, nails were produced form iron ores by the following general process. Iron is produced by reducing iron ore with either charcoal or coal directly, as shown in Equation 4. Because the temperature reached only below 1,000 °C in this process, sponge iron is produced. Sponge iron must then be heated and hammered manually to form the nails. Slag present in the sponge is squeezed out of the porous iron, and in the process of hammering, the iron becomes more dense (*12*, *13*).

$$Fe_2O_3 + 3\,CO \longrightarrow 2\,Fe + 3CO_2 \quad (4)$$
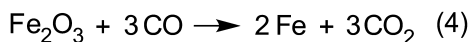
We examined the compositions and structures of the cross-sections and longitudinal-sections of the nails by SEM-EPMA. Nails were cut and the surfaces were polished, as shown in Figure 13. Figure 14 shows the SEM image of the cross-section of nail a from Figure 13. The composition of the flat surface away from the crack (shown in Figure 14a) was approximately 1% carbon and 99% iron, indicative of steel. The roughly "S" shaped crack in Figure 14a indicates that two pieces of metal were folded together in the manufacture of the nail, a sign of forging. These hand-forging (-wrought) iron nails are different from cut nails and modern wire nails (*14*, *15*). The other areas shown in Figure 14b-d were the subject of further SEM-EPMA analysis.

Figure 13. Nails were cut cross section and longitudinal direction.
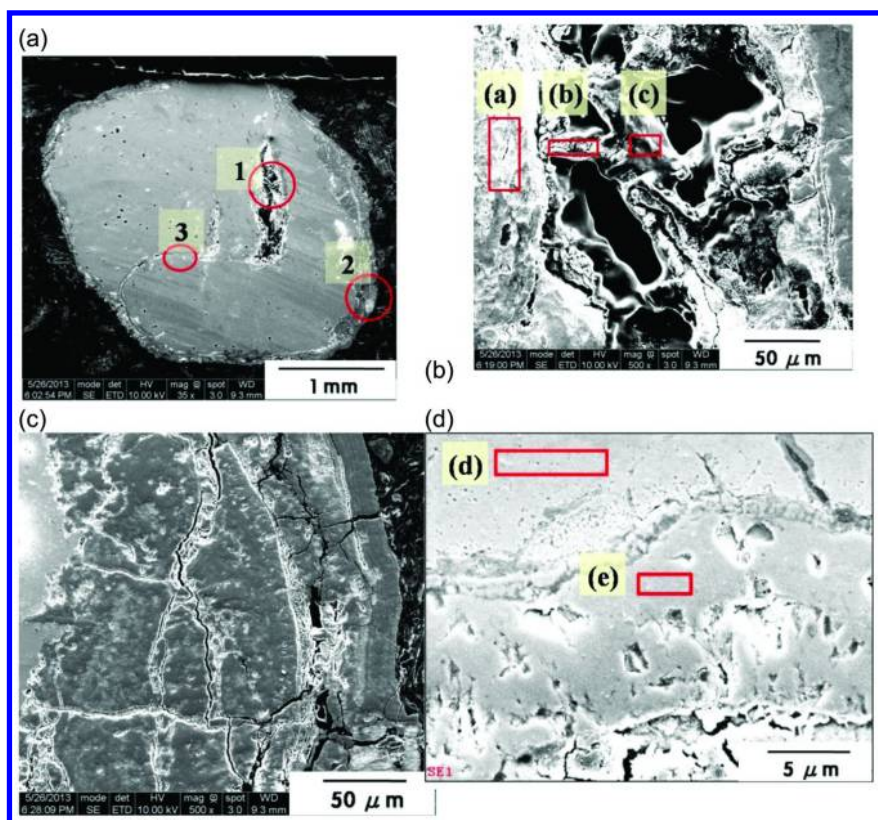
Figure 14. (a) Cross section of nail a in Figure 13; (b) enlarged area 1; (c) enlarged area 2; (d) enlarged area 3.
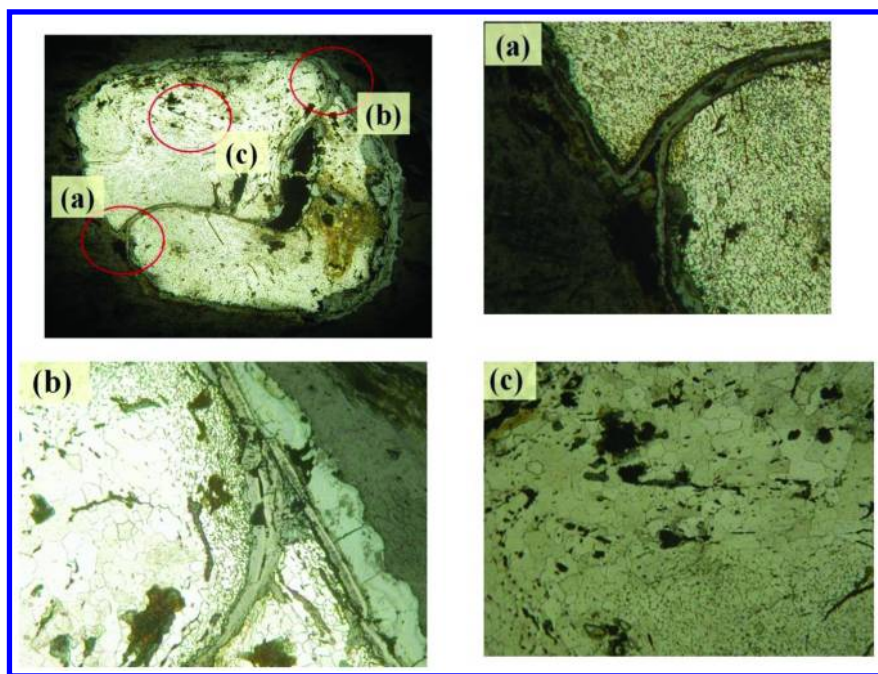
Figure 15. Cross-section of the nail in Figure 14 after acid etching. (a) and (b) show two pieces were folded clearly; (c) grains and their boundaries are observed.

Figure 15 shows the cross-section of the nail in Figure 14 after acid etching using 2% nital. Figures 15a and 15b shows the cross-section of the nail is separated by two and shows that two pieces were folded and forged to form the nail. Figure 15c show the grain boundaries of ferrite, pure iron.

Table II shows the elemental compositions observed for the nail cross-section shown in Figure 14. The crack area (denoted a-c in Table II) contains a high percentage of oxygen, indicative of the presence of oxides in that region. Of note is the large percentage of carbon observed at spot c, which is indicative of the presence of unreduced iron ore, carbon, and slag in that area. In the bulk area, spot d, no oxygen was detected, consistent with the composition of steel. The composition near the surface of the nail shows extensive oxidation, to a depth of 150 micrometers.

Figure 16 shows photomicrographs of the longitudinal sections of a nail. An area near the top of the nail, containing both a crack similar to the one described previously, was enlarged (Figure 16c) and examined with EPMA. The elemental composition of the crack and the bulk of the nail are shown in Table III. The crack in the nail again contains slag, iron silicates, and the bulk composition is again consistent with that of steel. The composition of iron and oxygen elements and the round shapes of area a in Figure 16c indicate the formation of wustite, FeO in the region.

Table II. Elemental analysis of the crack area in Figure 14

4 Element	Wt%				
	(a)	(b)	(c)	(d)	(e)
C	3.54	18.51	58.12	2.51	2.26
O	26.03	50.67	19.50	-	21.77
Fe	58.49	0.29	14.78	90.15	68.54
Na	3.96	0.29	-	-	-
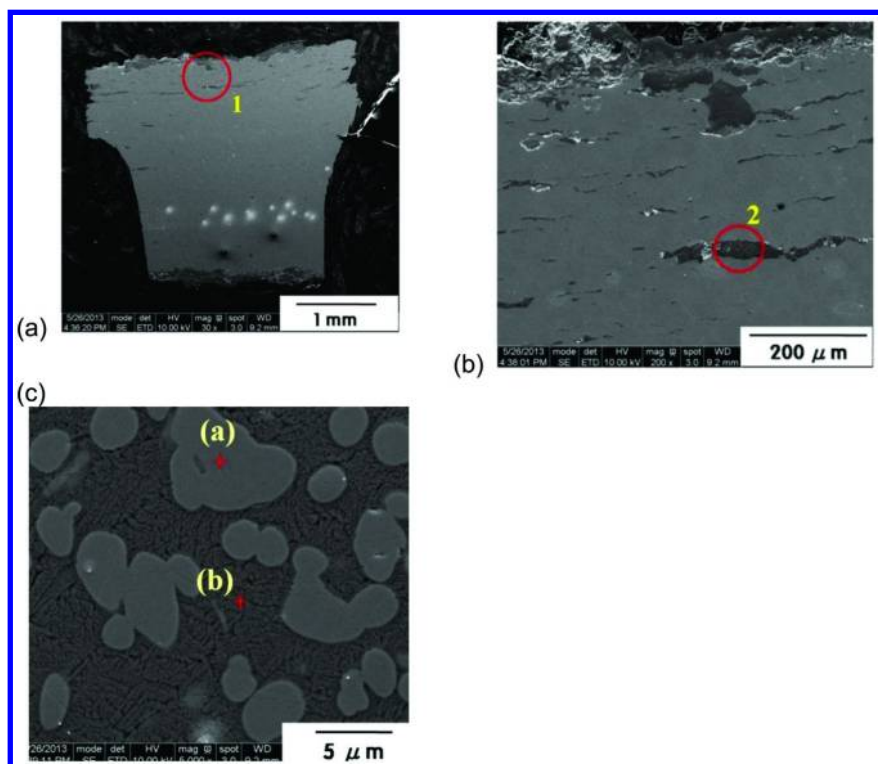
Figure 16. SEM of Longitudinal section of nail and its crack area.

Table III. Elemental analysis of the crack area 2 of Figure 16b

Element	Wt%	
	Area (a)	Area (b)
C	8.45	16.54
O	20.80	25.82
Fe	63.63	36.19
Al	0.47	3.24
Si	-	11.83
P	-	3.78
K	-	1.67
Ca	-	0.93

Conclusions

We confirmed that the metal plate connectors of the Koryo Buddhist canon woodblocks were made from pure copper plate. We believe that the copper plate connectors have played a role in preservation of the woodblocks, acting as an anti-microbial agent in combination with the Japanese lacquer coating. The composition and structure of the iron nails show that they were formed through the hand-forging of sponge iron.

Acknowledgments

References

1. Haeinsa Temple Janggyeong Panjeon, the Depositories for the Tripitaka Koreana Woodblocks. http://whc.unesco.org/en/list/737.
2. Printing Woodblocks of the Tripitaka Koreana and Miscellaneous Buddhist Scriptures. Memory of the World. http://www.unesco.org/new/en/communication-and-information/flagship-project-activities/memory-of-the-world/register/full-list-of-registered-heritage/registered-heritage-page-7/printing-woodblocks-of-the-tripitaka-koreana-and-miscellaneous-buddhist-scriptures/.
3. Do, C. H.; Yi, T. −Y.; Pyun, C.-H.; Seo, J. M.; Kim, H. Lee, D. N.; Chang, S. K. *Programme and Abstracts, 41st IUPAC Congress*, 2007; p 62.
4. Lee, T. Y.; Do, C. H. *Polym. Prepr.* **1996**, *37* (2), 182.
5. Stinson, S. C. *Chem. Eng. News* **1996**, September 9, 34–36.
6. Do, C. H.; Lee, T. Y. *J. Conserv. Sci.* **1999**, *8*, 33–39.

7. Do, C. H.; Lee, T. Y. *J. Conserv. Sci.* **1998**, *7*, 80–85.
8. Copper Extraction Techniques. Wikipedia. http://en.wikipedia.org/wiki/Copper_extraction_techniques.
9. Antimicrobial Properties of Copper. Wikipedia. http://en.wikipedia.org/wiki/Antimicrobial_properties_of_copper.
10. Dollwet, H. H. A.; Sorenson, J. R. J. *Trace Elem. Med.* **1985**, *2* (2), 80–87.
11. Grass, G.; Rensing, C.; Solioz, M. *Appl. Environ. Microbiol.* **2011**, *77* (5), 1541–1547.
12. Park, J. S.; Rehren, T. *J. Archaeol. Sci.* **2011**, *38*, 1180–1190.
13. Scott, D. A. *Metallography and Microstructure of Ancient and Historic Metals*; GCI and J. P. Getty Museum: Los Angeles, 1992.
14. Visser, T. D. Nails: Clues to a Building's History. http://www.uvm.edu/histpres/203/nails.html.
15. Nelson, L. H. Nail Chronology as an Aid to Dating Old Buildings. http://hisp305.umwblogs.org/files/nail_chronology.pdf.

Chapter 17

A Brief Update on Developments in Early Hominin Biogeochemistry

Matt Sponheimer,[*,1] **Julia A. Lee-Thorp,**[2] **and Daryl Codron**[1,3,4]

[1]**Department of Anthropology, 1350 Pleasant St.,**
Hale Sciences 350/233 UCB, University of Colorado-Boulder,
Boulder, Colorado 80309, U.S.A.
[2]**Research Laboratory for Archaeology,**
Oxford University, Oxford OX1 3QY, United Kingdom
[3]**Florisbad Quaternary Research, National Museum, P.O. Box 266,**
Bloemfontein, 9301, South Africa
[4]**Clinic for Zoo Animals, Exotic Pets and Wildlife, Vetsuisse Faculty,**
University of Zurich, 260 Winterthurestrasse, CH-8057, Zurich, Switzerland
[*]**E-mail: msponheimer@gmail.com**

Although two decades have passed since the first biogeochemical studies of early hominin diet were published, the field has only picked up steam in the last few years. There have been major increases in available hominin carbon isotope data which allow exploration of temporal, taxonomic, and biogeographic differences in hominin diet, as well as further investigation of the relationship between diet and masticatory morphology. There have been fewer recent advances in hominin trace element studies (Sr/Ca, Ba/Ca), although evidence of intraindividual dietary variation, including a weaning signal, are likely to spur future research.

Introduction

To a large extent early hominin biogeochemical studies tell a story from two viewpoints (trace elements and stable carbon isotopes) and two regions (eastern Africa and southern Africa). Until recently, almost all such work was done in South Africa (e.g., (*1–3*)), and while new carbon isotope data have become available from eastern Africa (*4–8*), there are still effectively no trace element data from that region (but see (*9*)). This imbalance in coverage has made it difficult to forge a coherent biogeochemical picture of hominin diet, and the imbalance is not likely to be remedied soon given concerns about diagenesis in eastern Africa (*10*, *11*), and the increasing indifference towards trace element approaches to paleodiet among archaeometrists.

Still, there has been progress, especially the massive influx of hominin carbon isotope data over the past few years (see (*12*)). This newfound abundance almost entirely reflects the newfound willingness of curators to allow biogeochemical analysis of fossils in their charge, rather than increased interest or effort on the part of those seeking permission to do such work. The new carbon isotope data are sufficiently intriguing that they have more than justified recent efforts, and point to unanticipated temporal, morphological, regional, and taxonomic differences in $\delta^{13}C$ values (*12*). Nevertheless, most of the story of hominin diet remains to be told, and a major focus will now become what, if anything, can other biogeochemical dietary proxies add to the emerging picture from carbon isotopes?

The purpose of this paper is to provide an update of recent results from carbon isotope and trace element studies of early hominins. No attempt is made to outline the basics of carbon isotopic and trace elemental studies of paleodiet as this has been done recently and at length (*13*). We argue that the general trends from carbon isotopes are fairly clear, and that further work in that area is likely to focus on narrower questions and, in an attempt to better interpret the carbon isotope data, a move away from stable isotopic research per se. We also argue that it is not presently clear how trace element studies will contribute to the dialog about early hominin diets, despite the fact that there appears to be evidence that biogenic patterning can be retained in fossils from some hominin sites (*11*). The biogeochemical data discussed herein are archived at http://figshare.com/authors/Matt_Sponheimer/99071.

Carbon Isotopes

Early studies made it clear that South African australopiths ate at least some foods ^{13}C-enriched foods such as tropical C_4 grasses, C_4 sedges, CAM succulents, or animals eating those plants (*1*, *2*). This contrasts with what has been observed in chimpanzees (*Pan troglodytes*), which consume C_3 vegetation (most trees, bushes, and forbs) even in areas with abundant C_4 grasses (*14*, *15*). Differences between hominin genera (*Australopithecus*, *Paranthropus*, *Homo*) were lacking (*16*), however, despite marked differences in masticatory morphology (*17*). In retrospect, perhaps the most conspicuous result of these early studies was an overall pattern of high intraspecific variability among the hominins (*1–3*, *18*).

The addition of new data from southern Africa, eastern Africa, and central Africa has fleshed out the carbon isotope story (Figure 1) and has allowed new questions to be addressed. Where before the distributions of carbon isotope ratios within all hominin taxa appeared similar, as might be expected for savanna generalists, there is now evidence that hominins spanned the spectrum from almost pure C_3 consumers (*A. anamensis*) to those with that ate few C_3 resources (*P. boisei*), which nearly duplicates the range found among ecologically diverse bovids today (*19*, *20*). Where before there was no evidence of dietary change through time from carbon isotopes, there now exists a strong relationship between $\delta^{13}C$ and time among eastern African australopiths (Figure 2) (*12*). However, the data also intimate that there is a biogeographic tale to be told as the southern and central African data appear to be different from the eastern African data (Figure 1).
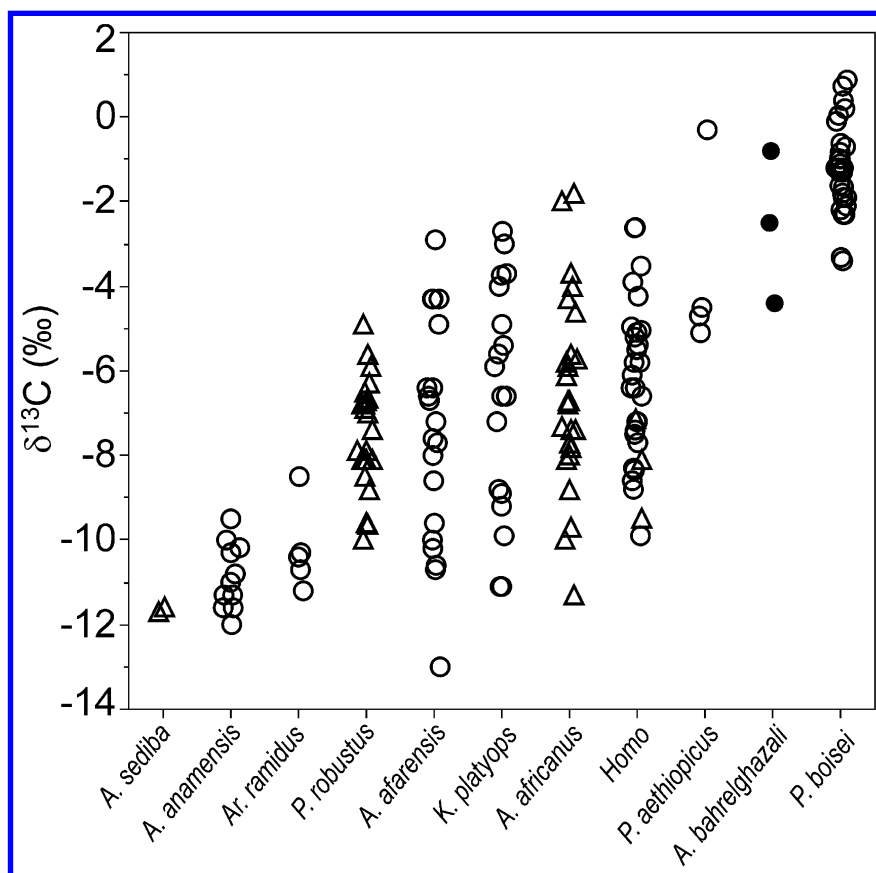
Figure 1. Early hominin taxa from southern Africa (open triangles), eastern Africa (open circles), and central Africa (closed circles) arranged from lowest to highest δ¹³C values.
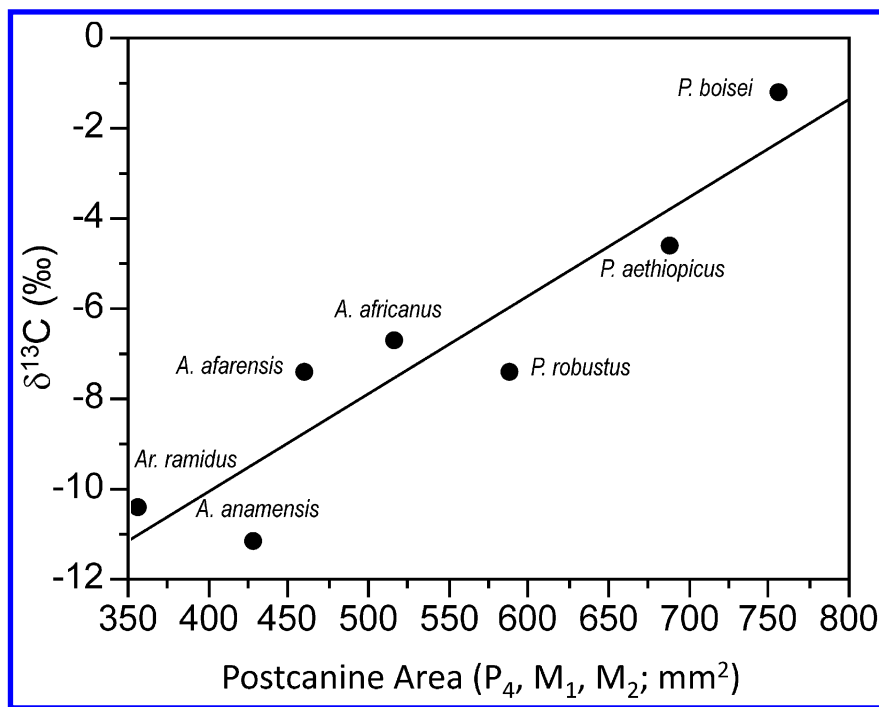
Figure 2. Linear regression shows that australopith postcanine area predicts australopith δ13C values (r²=0.86, t(5)=5.50, P<0.01).

Admittedly, there are few data for *A. bahrelghazali* from central Africa, but what we have indicates high consumption of ^{13}C-enriched foods at an early date (~3.5 Ma) (*21*). This is perhaps the best evidence we possess of a habitat effect on hominin δ^{13}C values. The non-hominin fauna from the site are dominated by C_4 grazers, and it appears there was little else in the area to eat (*21*, *22*), so perhaps the hominin δ^{13}C values should not be too surprising. Regardless, the central tendency of these specimens is distinct from what has been observed in eastern African taxa (*A. afarensis* and *Kenyanthropus platyops*) from the same time period (*7*, *8*). Other than this, there is no clear relationship between hominin δ^{13}C values and environments ((*7*, *8*, *12*); and see below).

Perhaps the most intriguing result made possible by the spate of new data is that some measures of masticatory morphology and δ^{13}C values are correlated. Two metrics that might be expected to be related to diet, postcanine area and mandibular cross-sectional area at M1, in fact strongly predict hominin δ^{13}C values (r^2=0.83 and r^2=0.86 respectively) (*12*)(Figure 2). Given the above discussion of biogeographic differences, it is hardly surprising that these effects are strengthened if only eastern African data are included (r^2=0.90 for both postcanine area and mandibular cross-sectional area).

It might be argued that these relationships are artificially strong due to the fact that morphological and isotopic data are not available for all relevant taxa. For instance, if the dental and mandibular metrics of *A. bahrelghazali* are similar

to those of *A. afarensis* (indeed they may be conspecifics; see (*23*)), the former would have higher δ13C values than expected using linear regression. This is a fair enough concern, although there is little we can do about it until isotopic and morphological datasets become publically available for all taxa. However, it may also be true that such potential outliers will be highly informative in that they may indicate that confounding variables (such as environment) are pulling taxa (or populations) away from the regression line.

Regardless, there has been little time to process the new carbon isotopic data as more specimens have been analyzed and published in the past year than in the previous 15 (Figure 3). We expect that over the next few years researchers will continue to explore along the lines above, with a particular focus on how individual species differ across environments. For instance, are there differences between *A. afarensis* from Hadar and Laetoli, as it has been argued that these hominins experienced different habitats and had slightly variant masticatory morphology (e.g., (*23–25*)).
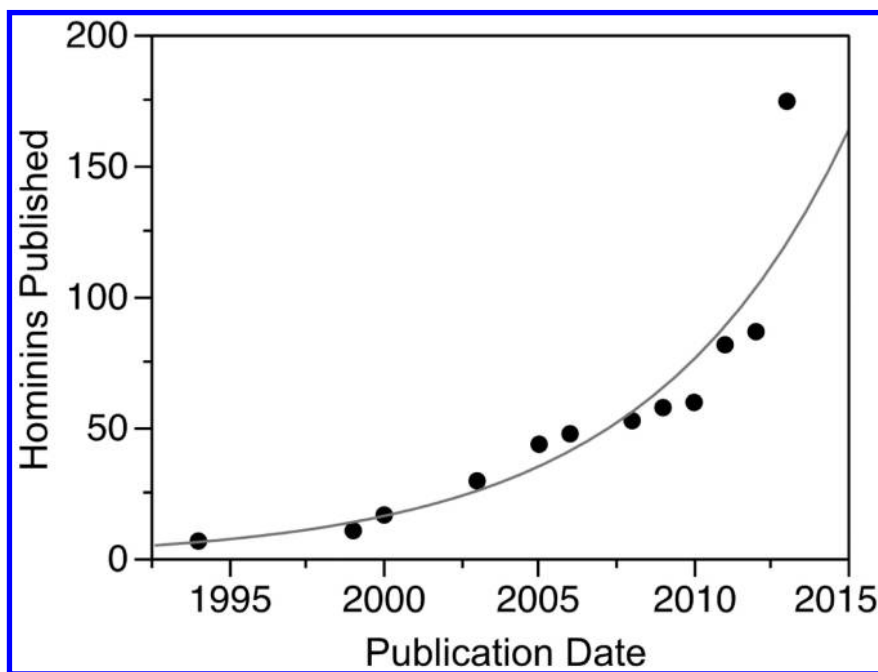
Figure 3. Cumulative number of hominin δ13C values published through time with an exponential fit line. Note the massive increase in available data since 2011 after slow but steady growth over much of two decades.

It is also likely that more attention will be focused on the high variability of some hominin taxa (e.g., *A. afarensis*, *A. africanus*) in the years ahead. It was clear early on that some hominins had highly varied δ13C values that were exceptional among most mammals, but this was not of principle concern given the need to establish that hominin δ13C values were truly distinct from C_3 consumers including

extant chimpanzees (see (*26*)). As a result, there was a focus on central tendency at the expense of variation, but now there are a number of questions to be asked. Why do some hominin taxa have exceptionally variable δ13C values? Does this variability reflect dietary responses to environmental change?

There is little direct evidence that habitat is driving intraspecific δ13C values as they do not covary with %C$_4$ vegetation in the local environment where such environment/diet comparisons are possible (*7*, *8*). This could simply mean that environmentally driven changes in diet were at temporal scales (e.g., precessional or shorter) that we cannot presently resolve in the hominin fossil record (*8*, *27*). It could also indicate that these hominins were generalists that used a variety of microhabitats across landscapes, thus ensuring that dietary variability would be high at any moment in time. It is worth noting, however, that there has been very little theoretical or empirical exploration of how hominin δ13C values should vary with climate/environment, and it is conceivable that fairly large environmental shifts would lead to little change in hominin δ13C values (*12*).

We also expect that there will be continued interest in the carbon isotopic variability manifest *within* individual hominins. At present we know that a number of *A. africanus* and *P. robustus* individuals evinced highly variable hominin δ13C values at intra- and interannual timescales (*28*, *29*), but we have no similar data for other hominin taxa. There are, unfortunately, many methodological barriers to properly interpreting such incremental isotopic data (see (*28*, *30*)), which when coupled with the difficulty of obtaining specimens for this kind of analysis, is likely to make such work with other hominins problematic.

Up to this point we have neglected to talk about what 13C-enriched resources (e.g., C$_4$ grasses, C$_4$ sedges, or animals eating these foods) the various hominins were consuming. Other lines of evidence like masticatory morphology and dental microwear will no doubt provide clues as to their nature (see (*13*, *31*)), but we are still a long way from working out what the carbon isotope data mean in terms of actual foods consumed. This is potentially one area where trace element studies might prove very useful, and to which we now turn.

Trace Elements

Boaz and Hampel (*9*) made an early attempt to use Sr from fossil mammals to examine community trophic structure, including the hominin *P. boisei,* but the cards were stacked against them. For one, they did not have a reasonable idea of how trace elements were distributed in modern African foodwebs (see (*32*)), making it very difficult to interpret trace element data from fossils. They also did not have access to current research on *P. boisei*, which shows it to be very unusual from both a carbon isotope and dental microwear perspective (*4*, *33*), which would have made it much more difficult to distinguish signal from noise, and to know to expect the unexpected. And lastly, they were working with fossils that represented something of a worst case scenario from a diagenetic standpoint. They analyzed material from the Omo, Ethiopia, much of which has experienced fluvial transport and a depositional environment with high Sr concentrations, which likely lead to significant changes in biogenic trace element compositions (*9*).

More promising was the work done by Andrew Sillen (*34*) on *P. robustus* and associated fauna from Swartkrans in South Africa. Sillen developed a solubility profiling protocol which appeared to retrieve biogenic patterning from fossil bone. For instance, he found that herbivores like hyraxes had higher Sr/Ca ratios than carnivores and some folivores, just as is found in modern African ecosystems (*35*). Interestingly, *Paranthropus* also had low Sr/Ca ratios, and since its flat teeth seemed unsuited for folivory (*36*), it was argued that this most likely reflected consumption of animal foods, and that *P. robustus* was less herbivorous than previously thought (*34*). Further work with enamel (to try to minimize concerns about diagenesis) observed biogenic patterning among fossil grazers, browsers, and carnivores from the area; however, this work also hinted that hominins were not distinct from baboons (which rarely include large proportions of animal matter in their diets), making it hard to sustain arguments for significant animal food consumption (*11*, *13*, *37*).

More recently, Balter et al. (*38*) published new data for 13 individual hominins from the taxa *A. africanus*, *P. robustus*, and early *Homo*. Although the data were too few to make robust statistical comparisons (nominally 1, 4, and 3 previously unpublished specimens for those taxa respectively, but see below), in combination with previously published data they should allow us to take a deeper look at hominin trace element distributions. We take such a look below using multivariate statistics in the hope of generating questions for future testing. We admit from the outset that we doubt that existing trace element data, no matter the approach, are sufficient to do much beyond this.

Discriminant function analysis (DFA) of fossil grazer, browser, and carnivore log Sr/Ca and log Ba/Ca data shows the groups to be quite distinct (Figure 4; including old and new datasets). Indeed, grazers, browsers, and carnivores from the training dataset are correctly classified from log Sr/Ca and log Ba/Ca data in all instances, and the 100% classification success is retained using a jackknifed ("leave one out cross validation") dataset. When the hominin data are dropped into the DFA they are classified primarily with carnivores, although some *Paranthropus* and *Homo* specimens are classified as browsing herbivores. The same can be said for contemporaneous baboons, however, as three are classified as carnivores and one is classified as a browser.

To further explore potential trace element structure among the primates we performed a DFA of the hominins and papionins alone. This revealed little clustering (Figure 5; see caption on how the dataset was generated), a 50% misclassification rate, and even poorer performance after jackknifing (0% successful classification for some taxa). The overall pattern is that the hominin and papionin trace element composition data are indistinct, although there is a tendency for *A. africanus* to have higher Sr/Ca ratios. This impression is confirmed by univariate pairwise comparisons as *Australopithecus africanus* has somewhat higher log Sr/Ca ratios than other taxa ($P<0.05$ in all cases; Wilcoxon), while there are no statistically significant differences in the log Ba/Ca ratios of these primates.

It is worth noting that for the above analyses we assigned KB 5223 to the genus *Homo* following Balter et al. (*38*). Most authorities, however, assign this specimen to *P. robustus* (*39*, *40*). Whatever the taxonomic affinities of this specimen, it is

difficult to support an argument that *Homo* engaged in more carnivorous behavior than other hominins, or in fact baboons, from existing data. That is, we do not think a statistical case can be made at present. The small sample of *Homo* enamel (two or perhaps three) is particularly problematic in this region where so much baseline variation is observed in plant trace element concentrations across the landscape. For instance, moving from dolomites to granites, a distance of less than 10 kilometers, results in an increase in plant Sr by an order of magnitude (from about 40 ppm to nearly 400 ppm). Thus, animals moving a relatively short distance could have Sr/Ca compositions that diverge for reasons that have nothing to do with diet (see (*41*)). And even in areas that are less geologically heterogeneous, and in fact in animals on experimental diets, there is high variation in Sr/Ca ratios (*32*). The simplest way to deal with the resultant variability is to analyze many specimens, but this is not always possible when working with paleontological material. Strontium isotope analysis can also help to determine if enamel was formed on a different geological substrate, but this is not sufficient to distinguish plants (and therefore mammals) from some geological substrates in the region (*42*).
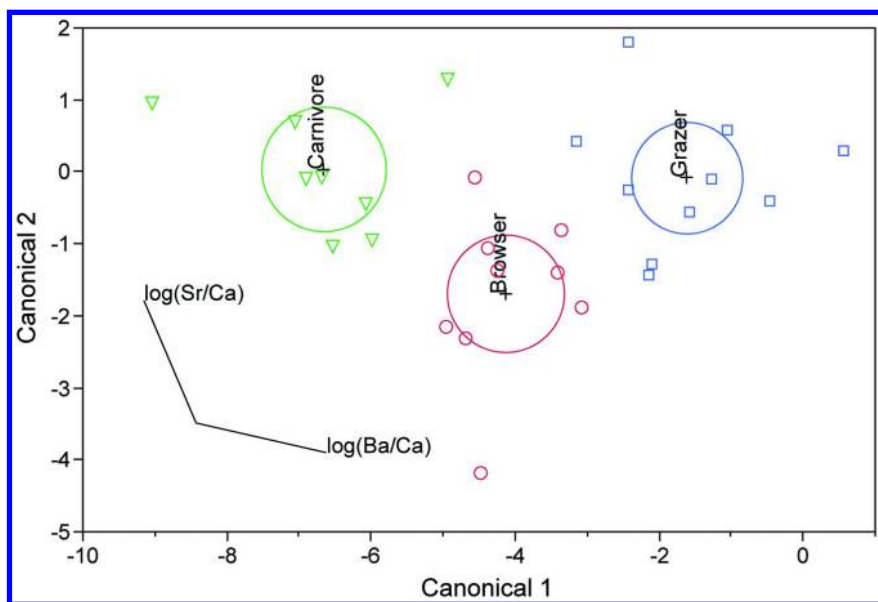
Figure 4. Canonical plot with 95% confidence ellipses for fossil browsers (circles), grazers (squares), and carnivores (triangles) using log Sr/Ca and log Ba/Ca data. The strong partitioning between the ecological groups results in a 100% correct classification rate after leave one out cross validation.

The new Balter et al. (*38*) study represents a significant addition to the existing hominin trace element dataset. Nevertheless, the available sample for *Homo* is insufficient to be anything more than suggestive, and furthermore, our understanding of mammalian trace element distributions remains too poor to allow facile interpretation of the hominin trace element data. The most intriguing

result from this study is that the within tooth variability of *A. africanus* appears to be higher than that of other hominins (*38*), which accords well with its inter- and intraindividual variability in δ¹³C values (*18, 29*).
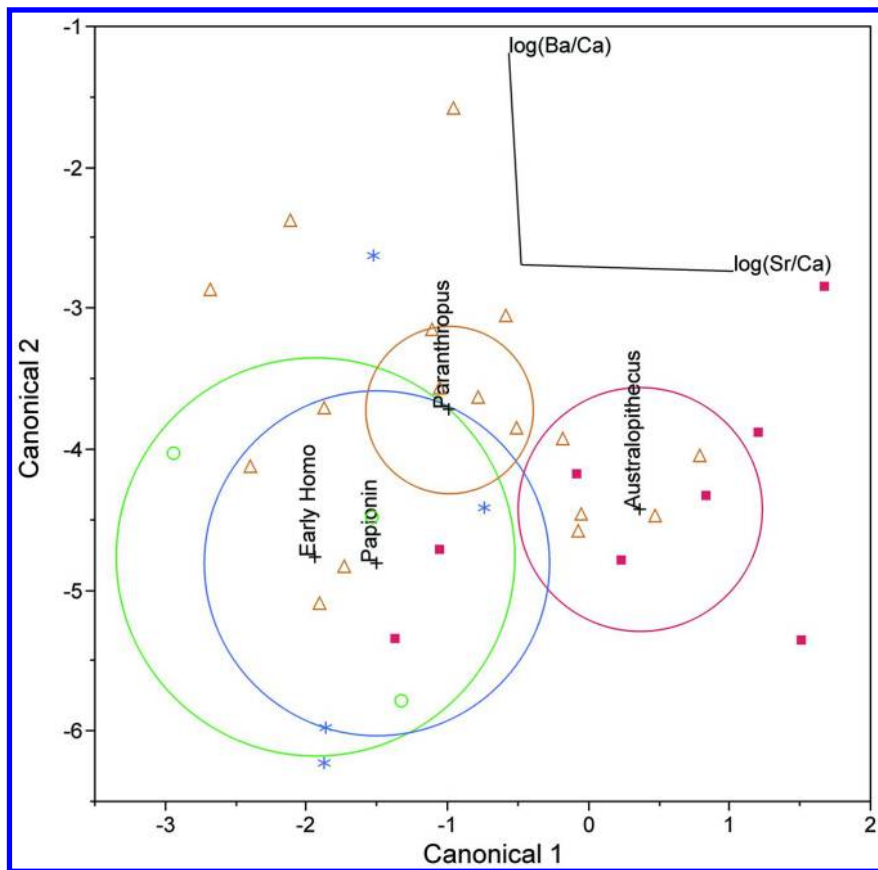
Figure 5. Canonical plot with 95% confidence ellipses for fossil primates (Australopithecus = squares; Paranthropus = triangles; early Homo = circles; papionins = stars) using log Sr/Ca and log Ba/Ca data. The lack of clear partitioning between groups results in poor classificatory success. Mean specimen values were generated from data in Balter et al. (38) to avoid pseudoreplication, and where data were available from two sources (11, 38), we used the mean of those values.

Perhaps the most tantalizing new application for trace element paleodietary analysis is in the area of weaning studies, which are of great interest given the importance of weaning in terms of development and reproductive rate, and the increasing interest in primate life-history generally (*43*). Humphrey et al. (*44*) developed a model suggesting that enamel formed after birth, at the onset of breastfeeding, should have relatively low Sr/Ca ratios, and that Sr/Ca ratios should increase with the introduction of complementary foods. More recently,

however, a study of humans and macaques demonstrated a large increase in Ba/Ca ratios with the onset of breastfeeding (as was expected because milk has higher Ba levels than umbilical cord sera), and a subsequent reduction to prenatal levels after weaning (*45*). They also found a similar, but attenuated pattern, in Sr/Ca ratios.

This is a potentially exciting development as they were able to retrodict weaning dates with uncanny accuracy in at least some cases. For instance, for one macaque, which was weaned at 166 days, they estimated weaning from Ba/Ca at 151-183 days. Austin et al. (*45*) then applied this method to a Neanderthal M1 from Scladina, and estimated an abrupt cessation of breastfeeding at 1.2 years, which would be very early by modern hunter-gatherer standards. The application itself is of less import than the method development, and certainly will engender further discussions of diagenesis, enamel mineralization, and the statistical basis for determining breastfeeding and weaning transitions. Nevertheless, there will certainly be interest in this method for recent human populations where diagenesis is less of a concern, and there will be temptation to apply it to even older material.

Conclusions

The last few years have been very active for early hominin biogeochemical research. The carbon isotope story has been fleshed out considerably, so that there is now evidence of temporal, regional, taxonomic, and morphological differences in $\delta^{13}C$ values. While there is more to do, the broad brush strokes described above are unlikely to change much, and as a result carbon isotope research is likely to be of somewhat lower priority in the years ahead. Carbon isotope studies of hominins will likely focus on narrower questions, such as how taxa vary across environmental gradients. Another focus will be on what ^{13}C-enriched foods were consumed, although this question is not likely to be answered using carbon isotope data on their own.

There has been less movement on the trace element front. There has been an increase in available hominin trace element data (*38*), but all of that has come from specimens in southern Africa. And unlike what we have witnessed in the last few years with carbon isotopes, where many new taxa from across Africa have been sampled, the trace element picture is unlikely to be augmented soon. Much of this reluctance stems from concerns about enamel diagenesis in many eastern African depositional environments (*10*).

However, arguably a bigger difficulty is that even if diagenesis were not a concern, it is not clear that we could meaningfully interpret hominin trace element data in ecological terms. In principle, we should be able to address this shortcoming with more work on African plants and mammals, but there has been very little work along these lines for more than 20 years (as in (*32*); see (*46*, *47*) for work in other regions). This relative neglect at least partially stems from the fact that trace element work of this sort is a high-risk, high-reward undertaking, and until now there has been too much to do on other fronts to justify it. Now, though, with so much of the carbon isotope story told, it would be easier to rationalize work along these, and other biogeochemical, lines.

Recent developments for establishing weaning in modern primates using Ba/Ca ratios suggest further lines of inquiry for paleoanthropologically inclined archaeometrists and geochemists (*45*), although diagenesis is likely to be a problem. Along these lines it is perhaps serendipitous that Ba/Ca seems better linked to weaning than Sr/Ca, as Sr has a higher diffusivity than Ba and is likely more seriously altered post-mortem (*48*). There may also be interest in recent attempts to decipher sex from the Fe and Cu isotope compositions of hard tissues (*49*), although diagenesis and the method's accuracy for extinct species are likely to warrant caution.

More than twenty years have passed since biogeochemical studies made an appearance in the paleoanthropological literature (*1*, *34*), and after a luke warm initial reception, such studies now stand on equal footing with more traditional means of dietary retrodiction (see (*50*)). The pace of publication of early hominin biogeochemical applications has increased tremendously in the past few years, which mirrors a broader increase in publications about hominin diets generally (an increase by over an order of magnitude since 1992; search terms "hominin" OR "hominid" AND "diet" using Web of Knowledge). But if hominin biogeochemical studies are to continue to grow in number and influence, the next few years must be marked by a renewed focus on method development, and increased attention to narrow, but important, questions. Given the new studies discussed above, however, it appears the field is off to a promising start.

References

1. Lee-Thorp, J. A.; van der Merwe, N. J.; Brain, C. K. *J. Hum. Evol.* **1994**, *27*, 361–372.
2. Sponheimer, M.; Lee-Thorp, J. A. *Science* **1999**, *283*, 368–370.
3. van der Merwe, N. J.; Thackeray, J. F.; Lee-Thorp, J. A.; Luyt, J. *Hum. Evol.* **2003**, *44*, 581–597.
4. van der Merwe, N. J.; Masao, F. T.; Bamford, M. K. *S. Afr. J. Sci.* **2008**, *104*, 153–155.
5. White, T. D.; Ambrose, S. H.; Suwa, G.; Su, D. F.; DeGusta, D.; Bernor, R. L.; Boisserie, J.-R.; Brunet, M.; Delson, E.; Frost, S.; Garcia, N.; Giaourtsakis, I. X.; Haile-Selassie, Y.; Howell, F. C.; Lehmann, T.; Likius, A.; Pehlevan, C.; Saegusa, H.; Semprebon, G.; Teaford, M.; Vrba, E. *Science* **2009**, *326*, 67–93.
6. Cerling, T. E.; Mbua, E.; Kirera, F. M.; Manthi, F. K.; Grine, F. E.; Leakey, M. G.; Sponheimer, M.; Uno, K. T. *Proc. Natl. Acad. Sci. U.S.A.* **2011**, *108*, 9337–9341.
7. Cerling, T. E.; Manthi, F. K.; Mbua, E. N.; Leakey, L. N.; Leakey, M. G.; Leakey, R. E.; Brown, F. H.; Grine, F. E.; Hart, J. A.; Kaleme, P.; Roche, H.; Uno, K. T.; Wood, B. A. *Proc. Natl. Acad. Sci. U.S.A.* **2013**, *110*, 10501–10506.
8. Wynn, J. G.; Sponheimer, M.; Kimbel, W. H.; Alemseged, Z.; Reed, K.; Bedaso, Z. K.; Wilson, J. N. *Proc. Natl. Acad. Sci. U.S.A.* **2013**, *110*, 10495–10500.

In Archaeological Chemistry VIII; Armitage, R., et al.;
ACS Symposium Series; American Chemical Society: Washington, DC, 2013.

9. Boaz, N. T.; Hampel, J. *J. Paleontol.* **1978**, *52*, 928–933.
10. Kohn, M. J.; Schoeninger, M. J.; Barker, W. W. *Geochim. Cosmochim. Acta* **1999**, *63*, 2737–2747.
11. Sponheimer, M.; Lee-Thorp, J. A. *Geochim. Cosmochim. Acta* **2006**, *70*, 1644–1654.
12. Sponheimer, M.; Alemseged, Z.; Cerling, T. E.; Grine, F. E.; Kimbel, W. H.; Leakey, M. G.; Lee-Thorp, J. A.; Manthi, F. K.; Reed, K. E.; Wood, B. A.; Wynn, J. G. *Proc. Natl. Acad. Sci. U.S.A.* **2013**, *110*, 10513–10518.
13. Lee-Thorp, J.; Sponheimer, M. In *Yearbook of Physical Anthropology*; Wiley-Liss, Inc.: Wilmigton, DE, Vol. 49, 2006; pp 131–148.
14. Schoeninger, M. J.; Moore, J.; Sept, J. M. *Am. J. Primatol.* **1999**, *49*, 297–314.
15. Sponheimer, M.; Loudon, J. E.; Codron, D.; Howells, M. E.; Pruetz, J. D.; Codron, J.; de Ruiter, D. J.; Lee-Thorp, J. A. *J. Hum. Evol.* **2006**, *51*, 128–133.
16. Lee-Thorp, J.; Thackeray, J. F.; van der Merwe, N. *J. Hum. Evol.* **2000**, *39*, 565–576.
17. Robinson, J. T. *Evolution* **1954**, *8*, 324–334.
18. Sponheimer, M.; Lee-Thorp, J.; de Ruiter, D.; Codron, D.; Codron, J.; Baugh, A. T.; Thackeray, F. *J. Hum. Evol.* **2005**, *48*, 301–312.
19. Cerling, T. E.; Harris, J. M.; Passey, B. H. *J. Mammal.* **2003**, *84*, 456–470.
20. Sponheimer, M.; Lee-Thorp, J. A.; DeRuiter, D. J.; Smith, J. M.; Van der Merwe, N. J.; Reed, K.; Grant, C. C.; Ayliffe, L. K.; Robinson, T. F.; Heidelberger, C.; Marcus, W. *J. Mammal.* **2003**, *84*, 471–479.
21. Lee-Thorp, J.; Likius, A.; Mackaye, H. T.; Vignaud, P.; Sponheimer, M.; Brunet, M. *Proc. Natl. Acad. Sci. U.S.A.* **2012**.
22. Zazzo, A.; Bocherens, H.; Brunet, M.; Beauvilain, A.; Billiou, D.; Mackaye, H. T.; Vignaud, P.; Mariotti, A. *Paleobiology* **2000**, *26*, 294–309.
23. Kimbel, W. H.; Delezene, L. K. *Am. J. Phys. Anthropol.* **2009**, *140*, 2–48.
24. Lockwood, C. A.; Kimbel, W. H.; Johanson, D. C. *J. Hum. Evol.* **2000**, *39*, 23–55.
25. Su, D. F.; Harrison, T. *J. Hum. Evol.* **2008**, *55*, 672–681.
26. Schoeninger, M. J.; Bunn, H. T.; Murray, S.; Pickering, T.; Moore, J. In *Meat-Eating & Human Evolution*; Stanford, C. B., Bunn, H. T., Eds.; Oxford University Press: Oxford, U.K., 2001; pp 179–195.
27. Hopley, P. J.; Maslin, M. A. *Paleobiology* **2010**, *36*, 32–50.
28. Sponheimer, M.; Passey, B. H.; de Ruiter, D. J.; Guatelli-Steinberg, D.; Cerling, T. E.; Lee-Thorp, J. A. *Science* **2006**, *314*, 980–982.
29. Lee-Thorp, J. A.; Sponheimer, M.; Passey, B. H.; de Ruiter, D. J.; Cerling, T. E. *Philos. Trans. R. Soc. London, Ser. B* **2010**, *365*, 3389–3396.
30. Passey, B. H.; Cerling, T. E. *Geochim. Cosmochim. Acta* **2002**, *66*, 3225–3234.
31. Ungar, P. S.; Sponheimer, M. *Science* **2011**, *334*, 190–193.
32. Sillen, A. *Am. J. Phys. Anthropol.* **1988**, *76*, 49–60.
33. Ungar, P. S.; Grine, F. E.; Teaford, M. F. *PLoS One* **2008**, *3*, e2044.
34. Sillen, A. *J. Hum. Evol.* **1992**, *23*, 495–516.
35. Sealy, J. C.; Sillen, A. *J. Archaeol. Sci.* **1988**, *15*, 425–438.

36. Kay, R. F. *Annu. Rev. Anthropol.* **1985**, *14*, 315–341.
37. Sponheimer, M.; de Ruiter, D.; Lee-Thorp, J.; Spath, A. *J. Hum. Evol.* **2005**, *48*, 147–156.
38. Balter, V.; Braga, J.; Télouk, P.; Thackeray, J. F. *Nature* **2012**.
39. Lacruz, R. S. *Am. J. Phys. Anthropol.* **2007**, *132*, 175−182.
40. Moggi-Cecchi, J.; Menter, C.; Boccone, S.; Keyser, A. *Hum. Evol.* **2010**, *58*, 374–405.
41. Burton, J. H.; Price, T. D.; Cahue, L.; Wright, L. E. *Int. J. Osteoarchaeol.* **2003**, *13*, 88–95.
42. Copeland, S. R.; Sponheimer, M.; de Ruiter, D. J.; Lee-Thorp, J. A.; Codron, D.; le Roux, P. J.; Grimes, V.; Richards, M. P. *Nature* **2011**, *474*, 76–78.
43. Bogin, B. *The Growth of Humanity*, 1st ed.; Wiley-Liss, Inc.: Wilmington, DE, 2001.
44. Humphrey, L. T.; Dean, M. C.; Jeffries, T. E.; Penn, M. *Proc. Natl. Acad. Sci. U.S.A.* **2008**, 0711513105.
45. Austin, C.; Smith, T. M.; Bradman, A.; Hinde, K.; Joannes-Boyau, R.; Bishop, D.; Hare, D. J.; Doble, P.; Eskenazi, B.; Arora, M. *Nature* **2013**, advance online publication.
46. Runia, L. T. *J. Archaeol. Sci.* **1987**, *14*, 599–608.
47. Burton, J. H.; Price, T. D.; Middleton, W. D. *J. Archaeol. Sci.* **1999**, *26*, 609–616.
48. Kohn, M. J.; Moses, R. J. *Proc. Natl. Acad. Sci. U.S.A.* **2013**, *110*, 419–424.
49. Jaouen, K.; Balter, V.; Herrscher, E.; Lamboux, A.; Telouk, P.; Albarède, F. *Am. J. Phys. Anthropol.* **2012**, *148*, 334–340.
50. Grine, F. E.; Sponheimer, M.; Ungar, P. S.; Lee-Thorp, J.; Teaford, M. F. *Am. J. Phys. Anthropol.* **2012**, *148*, 285–317.

Chapter 18

Seeking the Local ^{87}Sr/^{86}Sr Ratio To Determine Geographic Origins of Humans

James H. Burton* and **T. Douglas Price**

Department of Anthropology, University of Wisconsin−Madison, 1180 Observatory Drive, Madison, Wisconsin 53706, U.S.A.
***E-mail: jhburton@wisc.edu**

Critical to the success of efforts to determine the geographic origins of humans using ^{87}Sr/^{86}Sr is an accurate knowledge of this ratio and its range for local humans. There can be significant inadequacies in trying to estimate this ratio using available proxies, whether geological (rock, soil, water) or biological (modern or ancient faunal proxies). Empirical examination of the human data, as prima facie evidence, coupled with additional proxy data along with any information about dietary catchments, can improve our resolution of the sought-for 'local' human ^{87}Sr/^{86}Sr ratio.

Use of Bone Data To Assess Locality

The first publication of the use of ^{87}Sr/^{86}Sr to study human mobility is by Jonathon Ericson (*1*), who compared ^{87}Sr/^{86}Sr ratios in dental enamel, as a record of residency 'prior to marriage', to that of bone, reflecting 'post-marital residence'. He proposed, one could compare variation in males to that in females and assess regional intermarriage patterns and suggested that the method could also be used to assess more general issues of human mobility and resource procurement as well as animal ecology. This follows from the fact that most dental enamel mineralizes shortly after birth, trapping the strontium present in the diet at that time, while bone chemically remodels throughout life. A difference between bone and tooth ^{87}Sr/^{86}Sr ratios implies that the individual must have moved during their lifetime to a region with a different ^{87}Sr/^{86}Sr from the place of birth.

In fossil samples, however, diagenetic alteration commonly causes bones to yield an indeterminate mix of biological and geological strontium, precluding them from providing accurate biological $^{87}Sr/^{86}Sr$ data.

From our observations of hundreds of such paired measurements, most bone values do appear to have $^{87}Sr/^{86}Sr$ close to the estimated local ratio. For obvious immigrants with quite different enamel ratios, the bone ratios tend to be between enamel and local ratios, but generally much closer to the local ratio than to the enamel. It is unlikely that all these individuals migrated at such an early age that bone would have enough time to biologically alter. It is far more likely that this represents post-depositional alteration. Nelson and others (2) examined bones of modern and fossil marine animals and found that fossil marine animal bones taken from terrestrial contexts had values matching terrestrial $^{87}Sr/^{86}Sr$, not their biological $^{87}Sr/^{86}Sr$ ratio (i.e., that of modern seawater). Sealy and colleagues (3) likewise discovered significant diagenetic alteration of fossil bone $^{87}Sr/^{86}Sr$ ratios.

Such diagenetic alteration toward the local $^{87}Sr/^{86}Sr$ happens because bone has an enormous capacity for diagenetic absorption of strontium through ion exchange with the soil and can pick up local soil strontium, regardless of how long the individual might have been in residence there (4).

Although one can argue the case that diagenetically added strontium is local strontium so that bones are still a proxy for the place of death, soil ratios $^{87}Sr/^{86}Sr$, like rock ratios, as discussed below, can vary greatly, typically more than the range in biological tissues by an order of magnitude or two; any particular diagenetically affected sample could have ratios either higher or lower than the sought for average exhibited by unaltered biological specimens.

There are also methodological problems with this simplistic comparison. Theoretically, the time for bones to chemically remodel is on the order of tens of years (5) so that, even for immigrants coming from isotopically contrasting terrains, bone ratios need not be greatly different from enamel ratios, but should be somewhere in between the enamel ratio and the (unknown) local ratio. Cancellous tissues remodel fairly quickly (up to 25% per year) so that only 10% of the original strontium might be present after 8 years, but cancellous tissue is also the least likely to be preserved and most likely to be seriously contaminated. Cortical tissues on the other hand are somewhat more robust and more likely to be sampled, but remodel at the rate of approximately 2-3%/year (6); even after twenty years in a new location most of the strontium would be from the earlier place(s) of residence.

There are cases in which bone ratios could equal enamel ratios without implying that the individual is local. In studies of sacrificial burials in which the victims are likely captives from other locations, place of death or burial might not be the same as that of last residence, even though bone values might match enamel values; 'bone=tooth=local' would fail to identify these as exotic.

As an example, in our study of burials from the archaeological site of Aztalan, Wisconsin (7), one individual, MTMC 11, a distinctive bundle burial, had essentially identical ratios for two enamel samples and a bone sample. In the simplistic bone=tooth means local heuristic, this individual would be deemed local, but more intensive study revealed that other bone-teeth pairs have ratios that differed from this one, and they equal ratios of other materials believed to

be local to the area. This individual is an outlier whose bones and teeth had not equilibrated to the local ratio. This individual had apparently been transported as a bundle and reburied at Aztalan, explaining the anomaly. Although this case in probably an extraordinary one, it illustrates a hazard of the 'bone=tooth=local' paradigm. As Ericson explicitly acknowledged, the place of 'post-marital' residence need not be the same as the place of death, which need not be the place of burial.

Use of Geological $^{87}Sr/^{86}Sr$ Measurements

A common premise of the use of $^{87}Sr/^{86}Sr$ to determine geographic origins is that there is some pervasive ratio reflecting source material that passes into soil and plants then into the human diet and ultimately into human dental enamel without any change in the $^{87}Sr/^{86}Sr$ ratio, i.e., local geological $^{87}Sr/^{86}Sr$ = dietary $^{87}Sr/^{86}Sr$ = enamel $^{87}Sr/^{86}Sr$. Ericson suggested as a starting point that one estimate from geological maps, based upon the age, location, and rock types - along with any existing isotope data - what the rock ratios might be and what contrast there might be among regions of interest. This underlying premise is conceptually useful as an explanatory heuristic but has little value beyond that because the variation, locally, in geological materials typically exceeds that of biological tissues by orders of magnitude. The main problem is that most rocks are complex, heterogeneous assemblages of minerals with very different $^{87}Sr/^{86}Sr$ ratios such that whole rock ratios vary according to subtle changes in the percentage of each mineral. For example, granites commonly have high-Sr/low-Rb feldspars, with accordingly relatively low $^{87}Sr/^{86}Sr$ ratios $\approx 0.7+$, along with high-Rb/low-Sr micas that can be extremely radiogenic, with $^{87}Sr/^{86}Sr$ >10.0 (*8*). Naylor and others (*9*) measured $^{87}Sr/^{86}Sr$ in minerals of the Louis Lake batholith and found most ratios to be <0.9, but one biotite sample yielded an $^{87}Sr/^{86}Sr$ of 230! Whole rock ratios from fine grained granites in this area varied from 0.7 to 1.2, a range of 0.5. This range within one geologic unit exceeds the $^{87}Sr/^{86}Sr$ variation in human dental enamel for essentially the entire planet by two orders of magnitude: in the comprehensive database of the Laboratory for Archaeological Chemistry of 4885 samples of human dental enamel, spanning six continents, 95% of the enamel $^{87}Sr/^{86}Sr$ ratios fall within a range of 0.7047 to 0.7190, with a sharp mode at 0.7092 (Figure 1). Even though this range is extremely low compared to the range in geological materials, we commonly find, empirically, that local humans and faunal ratios typically vary by less than ±0.0003.

In an early study of $^{87}Sr/^{86}Sr$ to investigate mobility at the thirteenth-century site of Grasshopper in Arizona, Price and others (*10*) measured local geological materials with ratios ranging from 0.7089 to 0.7152, a range greater than that exhibited collectively by the human samples at Grasshopper (0.7111±0.0014), even though the human samples included many immigrants. The geologic variation in the geological samples is also far greater than that of local fauna (0.71000±0.00031), leading us toward the use of fauna to assess local ratios. If one had to use the geological data as a proxy for the local ratio, the technique would fail; local geological variation greatly exceeds regional biological variation.

In Archaeological Chemistry VIII; Armitage, R., et al.;
ACS Symposium Series; American Chemical Society: Washington, DC, 2013.
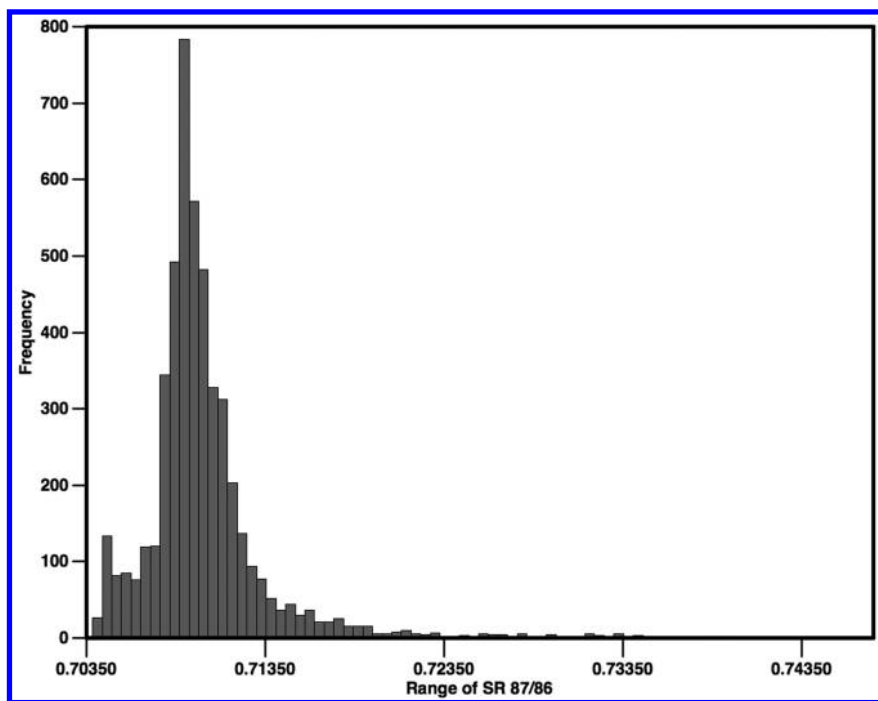
Figure 1. Laboratory for Archaeological Chemistry database histogram of human $^{87}Sr/^{86}Sr$ worldwide, n=4885. 95% of the data fall within 0.7047 to 0.7190.

Even for the case where rocks are presumed to be mineralogically and isotopically homogeneous, as is the case for marine limestones and oceanic basalts, isotopic variation is generally too excessive to be useful. For example, at Chichén Itzá , the bedrock is mapped as the Chichén Itzá Formation, an Eocene limestone. Marine limestones derive their strontium from the seawater and should have $^{87}Sr/^{86}Sr$ representing that of seawater at the time they are deposited, a principle that permits geologists to determine the age of limestones (e.g., (*11*)). For Eocene limestone this value should be 0.7078. Gilli et al. (*12*) measured an average $^{87}Sr/^{86}Sr$ of 0.7081 in rocks and water around Chichén Itzá, but with observed ratios ranging from 0.7078 to 0.7087 within a distance of a few kilometers. Our measurements of $^{87}Sr/^{86}Sr$ in snail shells from the same region, by contrast, have a very narrow range (0.7087±0.0001) and do not match the expected geologic ratio, but are significantly higher.

Likewise, in Iceland, where the geology comprises young basaltic rocks recently derived from the earth's mantle, there has been no time for the accumulation of radiogenic ^{87}Sr, so the rocks have a low $^{87}Sr/^{86}Sr$ of 0.703+, with unusually low variation from 0.7032 to 0.7033 (*13*). Nonetheless, local plants and animals have values slightly above 0.706 (*14*), apparently due to substantial transfer of oceanic strontium, at 0.7093, by sea spray.

Hawaii is another example where geologic values should be in the 0.7030 to 0.7050 range, but soil measurements go as high as 0.7273, which has been

explained by a significant contribution of strontium from wind blown dust of terrestrial origin (*15–17*).

Atmospheric transfer of exogenous strontium appears to be substantial in other areas of the world as well. In the southwestern United States, Capo and Chadwick (*18*) estimate the contribution of wind-blown strontium to soil strontium at 94% to 98%.

The relative contributions of bedrock versus eolian strontium have also been shown to change over time, as do pedogenic processes such as differential weathering of minerals, so that older soils have ratios that differ from younger soils and deeper soils have ratios that differ from more shallow soils (*19–21*). Pedogenic processes can even amplify bedrock variation: Blum and Erel (*22*) found soil ratios on weathered granite yielded 0.7103 to 0.7288; weak extracts to assess available soil Sr ranged from 0.7114 to 0.7947. Water reflected this amplification with local streamwater $^{87}Sr/^{86}Sr$ ranging from 0.7385 to 0.7431, mixing with precipitation ratios of 0.7106 to 0.7144. Although some use water ratios as a proxy for bioavailable $^{87}Sr/^{86}Sr$, groundwaters can differ significantly from both surface and soil waters, and surface waters vary with catchment size, outflow volumes, and seasonally. The assumption that there is a monolithic $^{87}Sr/^{86}Sr$ geologic isotope ratio that moves unchanged from rock to teeth is, for the general case, false.

As a final caveat relating to this fundamental premise, it is commonly stated that biological processes do not fractionate heavy element ratios and that they remain unchanged from those of the diet. This is technically imprecise - the same processes that cause mass-dependent fractionation of light isotopes such as nitrogen and sulfur act on all elements; the effect on strontium is far smaller, and, until the advent of modern multi-collector spectrometers, immeasurable. Nonetheless these slight differences can now be measured. Fractionation has been measured during biological calcification processes (*23*) and soil formation processes (*24*), and there is some evidence trophic level effects that can be detected through $^{88}Sr/^{86}Sr$ measurements (*25*).

Use of Faunal Proxies

Recognizing that the differences in $^{87}Sr/^{86}Sr$ we are trying to distinguish among biological materials is much less than the variation in $^{87}Sr/^{86}Sr$ ratios of geological materials led us to advocate the use of modern faunal to determine 'local' ratios (*26*). Because of the enormous averaging of $^{87}Sr/^{86}Sr$ in the biosphere, biological tissues have much less variation and, presuming they sample the same isotopic catchment of humans, can be used as a better assessment of local ratios. Although we originally considered the use of modern fauna, there are situations in which there have been temporal changes in the isotope ratios in fauna. Changes in geologic conditions, e.g., due to shifting river courses, as is the case in East Asia, anthropogenic effects such as application of fertilizers in agricultural regions, the extensive use of lime in mortar, concrete and cements in urban regions, and the consumption of foods imported by humans are variables that can bias $^{87}Sr/^{86}Sr$ measurements. Today it is common to include archaeological fauna

recovered from the same contexts of the humans, and preferably to use faunal teeth rather than bone to minimize diagenetic effects, as we proposed (*27*).

Nonetheless, problems have emerged here as well. Recent studies of a diverse set of geological and biological materials by Evans and colleagues (*28*) and by Maurer and colleagues (*29*) found considerable discordance between geological and biological ratios and among the biological materials themselves, even among different parts of the same plants and plants sampled at different times.

Snails, though commonly used, have been particularly criticized for being strongly biased to surficial strontium from rainfall and atmospheric dust and even for possibly being exotic (*28*). Although results in these studies might be anomalous due to geological heterogeneity, the critical inference that any given species represents the human $^{87}Sr/^{86}Sr$ catchment can, in cases, be tenuous.

For example, in our isotopic study of the Maya site of Palenque (*30*), analyses of local snail shells matched that of the local limestone, which yielded values of 0.7078, identical to that expected from the geological mapping and seawater $^{87}Sr/^{86}Sr$ for Paleocene (*31*, *32*). The dental enamel of Janaab' Pakal, a ruler of Palenque for most of the seventh century A.D. yielded $^{87}Sr/^{86}Sr$ of 0.0.7086. This is from the third molar, which mineralizes about the time Pacal assumed power at Palenque at the age of 12 (*33*) but is much higher than the geological/faunal estimate of the 'local' ratio. Using the existing fauna = 'local' paradigms, in the absence of contextual evidence that Pacal was local, one would conclude that he is not local. Subsequent fieldwork at Palenque led us to recognize that Palenque is located on steep slopes of Paleocene limestone but agricultural production is best suited on the alluvial floodplains, within kilometers of Palenque, but underlain by Miocene limestones. Miocene seawater $^{87}Sr/^{86}Sr$ ratios range from 0.7083 - 0.7090 (*31*), which fit the 0.7086 value for Pacal as well as our faunal measurements from the village of Palenque, located on the Miocene floodplain, not to be confused with the temple site on the Paleocene slopes. This illustrates where a failure to assess and sample the appropriate isotope catchment could easily yield a contrary interpretation of locality.

In a second example, Lori Wright (*34*), examined 83 individuals from Tikal, with an average value of 0.7080 for the entire set (Figure 2), and a sharp mode at 0.7081. After removing eight obvious outliers, the average for a trimmed set of 75 of 0.7081. Geological measurements, including both limestone and water, within 50 km of Tikal, fall within a wide range of 0.7074 to 0.7081. Shell samples yielded 0.7078 and local faunal bone yielded an average of 0.7079. All of these are lower than the mean of the humans and would imply, non-parsimoniously, that well more than half of the humans were immigrants. Wright speculated that the inclusion of less than six grams/day of sea salt (at 0.7092) in the diet was responsible for elevating the human values above that of the local fauna and geological data.

Likewise, in the above mentioned Iceland study of Price and Gestsdottir (*14*), geological values range narrowly between 0.703 to 0.704, floral and faunal values range from 0.706 to 0.707, while humans were substantially higher, with a mode at 0.7085 (Figure 3). Similar to Wright's inferences, the authors recognized that it was not parsimonious to posit that most of the individuals buried in cemeteries across Iceland were immigrants and speculated that seafood consumption (0.7092) was responsible for the elevated $^{87}Sr/^{86}Sr$.
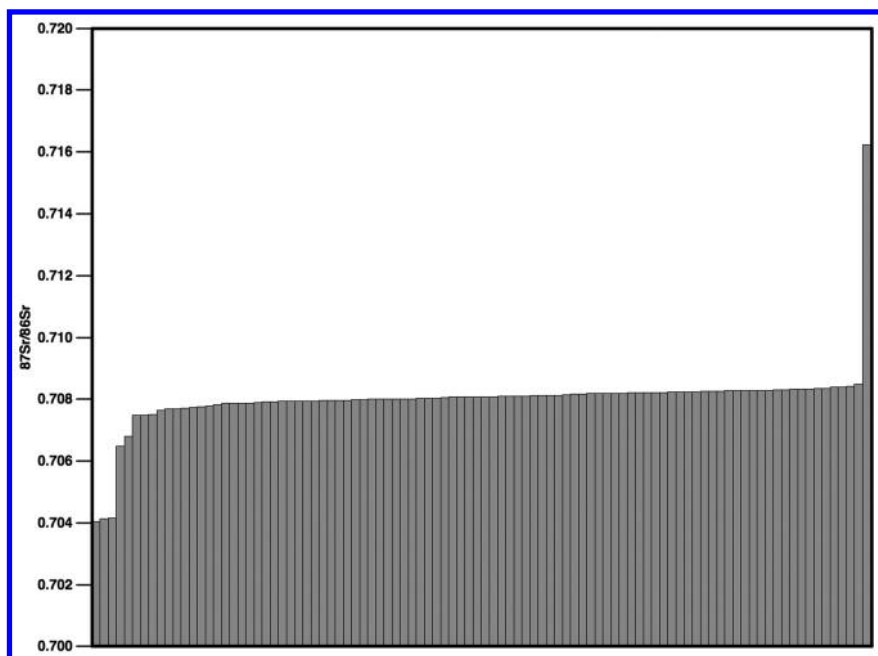
Figure 2. Bar graph of strontium isotope ratios from Tikal burials in rank order. Data from Wright (34). Note pronounced flat 'plateau' at 0.708.
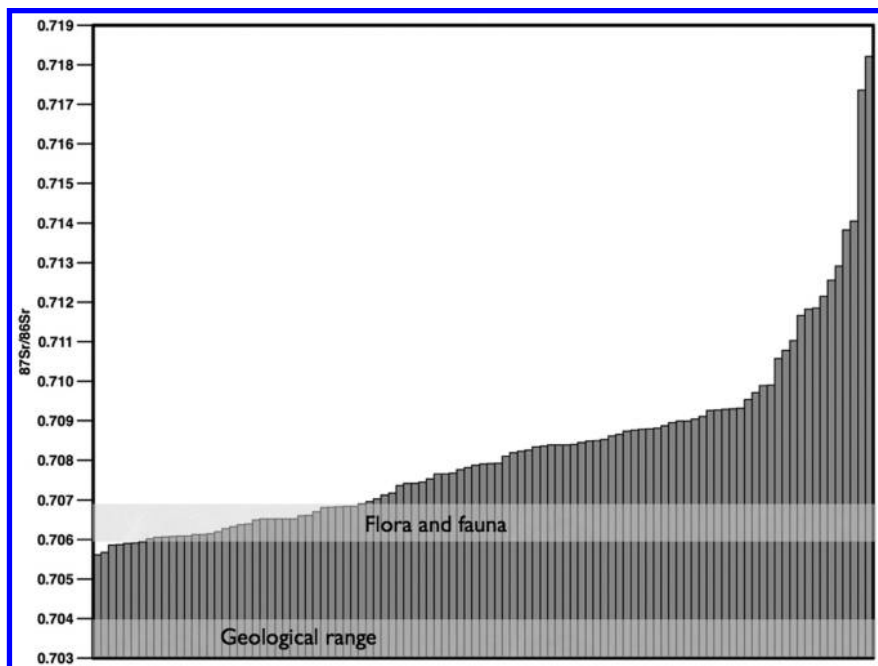
Figure 3. Strontium isotope ratios from Iceland burials in rank order. Data from Price and Gestdóttir (14).

In all three of the above examples, a simplistic use of faunal or floral measurements, with or without geological data, could lead to quite erroneous inferences of mobility. They all required an assessment of the actual dietary catchment and its possible $^{87}Sr/^{86}Sr$ ratio for plausible inferences. It also strengthens the inferences - as in both the Wright and the Price and Gestsdottir studies, as well as the above mentioned study of Maurer and colleagues (*29*), that there is a strong mode in each data set to suggest, empirically, what the 'local' human ratio might be. In many $^{87}Sr/^{86}Sr$ mobility studies faunal data are consistent and probably do approximate that of local humans, but the examples here illustrate that is not always the case.

Modal Analysis

Essentially we need to sample a species that has the same diet and procurement zone as the humans, representing the same isotope pool. The ideal choice would be to sample teeth of humans that we know, or at least strongly believe, are locally born, and contemporary with those whose origins are in question. While there might be extraordinary cases where most or all sampled individuals are not local, typically we will have a sample of local individuals in our data sets. It is possibly ironic that the seminal presentation of Krueger (*35*), contemporary with Ericson's publication, compared $^{87}Sr/^{86}Sr$ in fauna from Copan to those of humans from Copan to determine which fauna were imported.

Although the argument can have some circularity, this use of local humans embedded in the data set is what we actually do when we seek a strong mode in a dataset of individuals of unknown origins.

Commonly, isotope ratios from human enamel, as well as from fauna and other materials, are plotted on a bar graph in rank order - as in Figures 2 and 3 - and the result is examined for a relatively flat portion on the bar graph, representing a set of people with the same ratio, i.e., a mode of the data set. Individual outliers stand out and lesser modes, if they exist, appear as shorter, relatively flat groups separated by slope breaks. In practice, especially when other data are unavailable and there is no evidence for most people being immigrants, it is parsimonious to assume that the flat 'plateau' on such a bar graph reflects the local ratio, the local range being bracketed by the slope breaks.

Kernel Density Estimates

Another representation that has some utility for uncovering such modes in the data is kernel density estimation (KDE), recently advocated by Baxter and Cool (*36*). KDE's are analogous to histograms in seeking modes in data. Histograms have problems with an arbitrary selection of the width of the bins into which measurements are partitioned and, less well appreciated, effects due to the numerical value at which the histogram begins. Too few bins gives an overly smoothed result, hiding possible modes in the data, while too many bins simply approximate the original data (Figure 4).
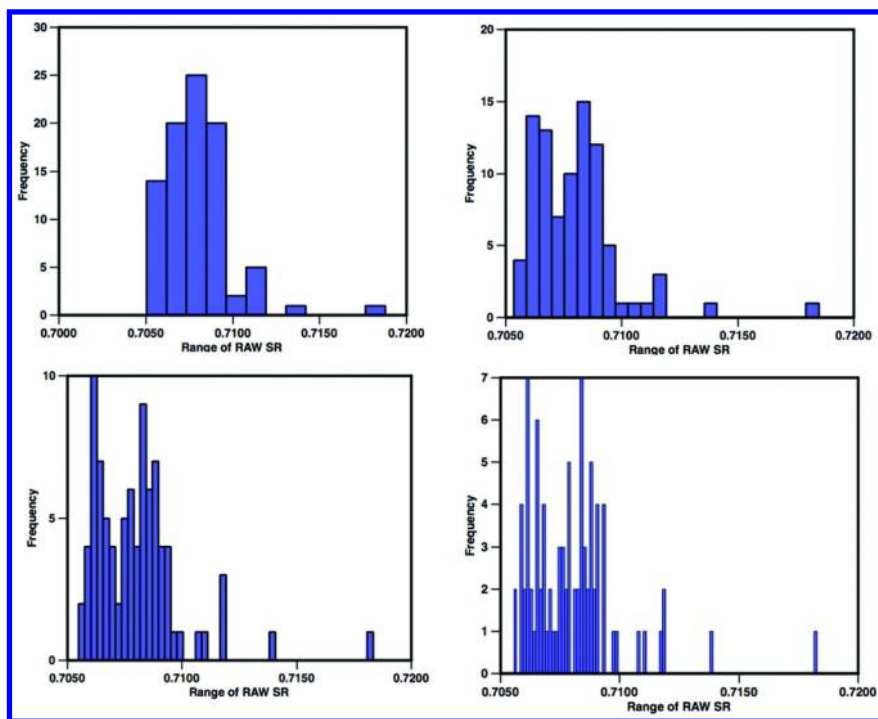
Figure 4. Histograms of Price and Gestdóttir (14) data, using 12, 24, 48 and 96 bins.

KDE's assume that each measurement is a sample from a set with a defined probability distribution (uniform, gaussian, etc.) and a given variance. These distributions are then summed over all measurements to yield an integrated distribution such as shown in Figure 5. KDEs, like histograms, have 'arbitrary' elements in their calculations, i.e., the shape of the underlying distribution and the 'bandwidth' or variance of the distribution. Like the bin width in a histogram, too large a bandwidth results in an overly smoothed profile and too small produces an overly 'spikey' result, but this can be optimized to minimize the error between the calculated result and the underlying structure. For enamel $^{87}Sr/^{86}Sr$ ratios we can posit with confidence that the distribution shape for each measurement is indeed gaussian. Because enamel samples reflect a biological average of dietary inputs, repeated samples (enamel measurements) of the same dietary isotope pool, from the Central Limit Theorem, will have a normal distribution regardless of the distributions of the underlying diet ratios, if they all sample the same dietary catchment. Silverman (*37*) and Baxter (*38*) have shown that one can optimize the 'arbitrary' variance parameter by minimizing the integrated mean standard error for a best-fit KDE. Moreover, from our own assessments of local variation in many studies worldwide, we can state that the standard deviations for local groups are typically on the order of ±0.0003.

In the above Iceland example, a ranked bar graph reveals a gradual slope that is difficult to interpret beyond a broad isotopic range for 'local', along with obvious

outliers above 0.710 that can reasonably be interpreted to be immigrants. It is noteworthy that none of the human samples, nor any faunal or floral ratios are close to the well-established regional geologic ratio (0.703), which would, under any geological $^{87}Sr/^{86}Sr$ = local $^{87}Sr/^{86}Sr$ paradigm, yield seriously erroneous results.

Although histograms (Figure 4) with few bins (<15) reveal outliers above 0.71, it is not clear from the histograms whether the distribution has more than one mode. Increasing the number of bins reveals a deficit of samples in the 0.707 range and suggests more than one mode, possibly many, as the number of bins increases.

An optimized KDE (Figure 5) of the Iceland data of Price and Gestsdottir (*14*), using an optimization algorithm of Shimazaki and Shinomoto (*39*), shows pronounced modes at 0.70638 and 0.70847 as well as minor peaks at higher ratios. The 0.70638 value matches precisely that of the local fauna discussed above, while the 0.70847 mode indicates another population with a different dietary isotope pool, interpreted by Price and Gestsdottir as Icelandic people consuming a mixed diet including sea food (@0.7092). The modes at higher ratios (>0.71) indicate immigrants from Scandinavia.
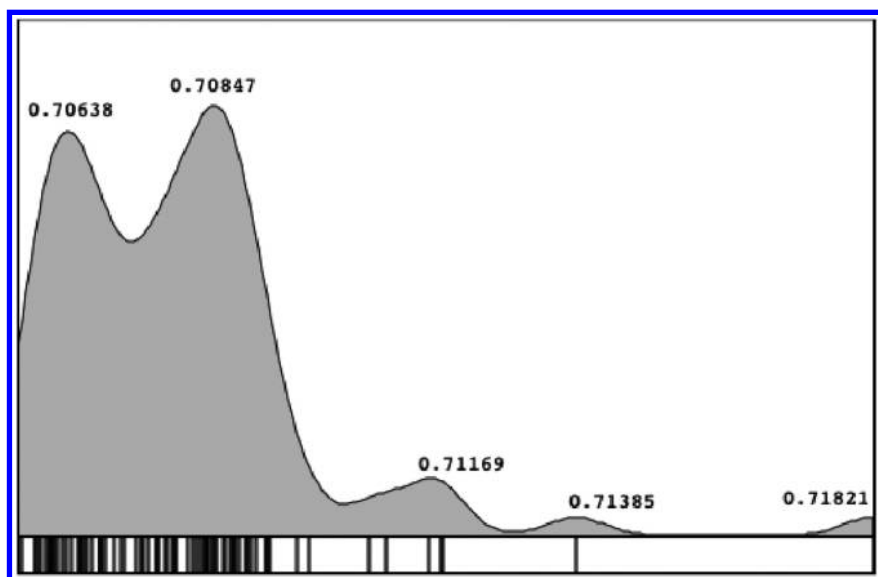
Figure 5. Optimized kernel density estimate for Iceland data, using an optimization algorithm of Shimazaki and Shinomoto (39).

Note that neither kernel density estimates nor histograms nor ranked bar charts imply that any group or sample is immigrant or local, but they do suggest the collective sample set is drawn from populations who had different isotope averages in their diets during early childhood. There could even be more than one locally born isotopic group if they accessed different food sources. By combining this with what is known about the local geology (e.g., that there is no Icelandic source, whether geological or marine >0.709) and the $^{87}Sr/^{86}Sr$ of potential dietary items, we can begin to sort who is who.

While a strong mode in the data - in the absence of large group migration - is a likely candidate for a 'local' ratio, the other lines of evidence discussed above should be compared with the human data, being aware of the possible limitations of each.

Nonetheless, modal data itself will be problematic and probably insufficient when a significant percentage of the population is mobile. Congruence of human data with faunal results adds support to the assessment of a local ratio, while divergence indicates that further scrutiny is required.

Conclusion

Critical to the success of using strontium isotopes to assess human mobility is knowledge of the $^{87}Sr/^{86}Sr$ ratio for local humans. This has been estimated by measuring proxy materials, including geological materials (mineral, rock, soil, ground water, well water, soil and rock leachates) and modern and fossil biological materials, each of which in specific situations can yield inaccurate results for humans. Inspecting the human $^{87}Sr/^{86}Sr$ ratio as *prima facie* evidence, augmented by assessments of the dietary catchment, can improve our confidence that we are identifying local residents.

References

1. Ericson, J. E. *J. Hum. Evol.* **1985**, *24*, 447–466.
2. Nelson, B. K.; DeNiro, M. J.; Schoeninger, M. J .; de Paolo, D. J. *Geochim. Cosmochim. Acta* **1986**, *50*, 1941–1949.
3. Sealy, J. C.; van der Merwe, N. J.; Sillen, A.; Kruger, F. J.; Krueger, H. W. *J. Arch. Sci.* **1991**, *18*, 399–416.
4. Price, T. D.; Blitz, J.; Burton, J. H.; Ezzo, J. *J. Arch. Sci.* **1992**, *19*, 513–529.
5. Watts, N. B. *Clin. Chem.* **1999**, *45*, 1359–1368.
6. Clarke, B. *Clin. J. Am. Soc. Nephrol.* **2008**, *3*, S131–S139.
7. Price, T. D.; Burton, J. H.; Stoltman, J. B. *Am. Antiquity* **2007**, *72*, 524–538.
8. Clauer, N. *Chem. Geol.* **1981**, *31*, 325–334.
9. Naylor, R. S.; Steiger, R. H.; Wasserburg, G. J. *Geochim. Cosmochim. Acta* **1970**, *34*, 1133–1159.
10. Price, T. D.; Johnson, C. M.; Ezzo, J. A.; Ericson, J. E.; Burton, J. H. *J. Arch. Sci.* **1994**, *21*, 315–330.
11. McArthur, J. M.; Howarth, R. J.; Bailey, T. R. *J. Geol.* **2001**, *109*, 155–170.
12. Gilli, A.; Hodell, D. A.; Kamenov, G. D.; Brenner, M. *Geol.* **2009**, *37*, 723–726.
13. O'Nions, R . K.; Grönvold, K. *Earth Planet. Sci. Lett.* **1973**, *19*, 397–409.
14. Price, T. D.; Gestsdottir, H. *Antiquity* **2006**, *80*, 130–144.
15. Dymond, J.; Biscaye, P. E.; Rex, R. W. *Geol. Soc. Am. Bull.* **1974**, *85*, 37–40.
16. Nakai, S.; Halliday, A. N.; Rea, D. K. *Earth Planet. Sci. Lett.* **1993**, *119*, 143–157.

17. Kurtz, A. C.; Derry, L. A.; Chadwick, O. A. *Geochim. Cosmochim. Acta* **2001**, *65*, 1971–1983.
18. Capo, R. C.; Chadwick, O. A. *Earth Planet. Sci. Lett.* **1999**, *170*, 61–72.
19. Stewart, B. W.; Capo, R. C.; Chadwick, O. A. *Geochim. Cosmochim. Acta* **2001**, *65*, 1087–1099.
20. Van der Hoven, S.; Quade, J. *Geoderma* **2002**, *108*, 259–276.
21. Reynolds, A. C.; Quade, J.; Betancourt, J. L. *Geoderma* **2012**, *189-190*, 574–584.
22. Blum, J. D.; Erel, Y. *Geochim. Cosmochim. Acta* **1997**, *61*, 3193–3204.
23. Krabbenhöft, A.; Eisenhauer, A.; Raddatz, J.; Liebetrau, V.; Fietzke, J.; Böhm, F.; Felis, T.; Reynaud, S. *Geophys. Res. Abs.* **2011**, *13*, 6277–6278.
24. Halicz, L.; Segal, I.; Fruchter, N.; Stein, M.; Lazar, B. *Earth Planet. Sci. Lett.* **2008**, *272*, 406–411.
25. Knudson, K. J.; Williams, H. M.; Buikstra, J. E.; Tomczak, P. D.; Gordon, G. W.; Anbar, A. D. *J. Arch. Sci.* **2010**, *37*, 2352–2364.
26. Price, T. D.; Burton, J. H.; Bentley, R. A. *Archaeometry* **2002**, *44*, 117–136.
27. Bentley, R. A.; Price, T. D.; Stephan, E. *J. Arch. Sci.* **2004**, *31*, 365–375.
28. Evans, J. A.; Montgomery, J.; Wildman, G. *J. Geol. Soc.* **2009**, *166*, 617–631.
29. Maurer, A. F.; Galer, S. J.; Knipper, C.; Beierlein, L.; Nunn, E. V.; Peters, D.; Tütken, T.; Alt, K. W.; Schöne, B. R. *Sci. Total Environ.* **2012**, *433*, 216–229.
30. Price, T. D.; Burton, J. H.; Tiesler, V.; Martin, S.; Buikstra, J. E. In *'Janaab' Pakal of Palenque*; Vera Tiesler, V., Cucina, A., Eds.; University of Arizona Press: Tucson, AZ, 2006; pp 91−101.
31. Howarth, R. J.; McArthur, J. M. *J. Geol.* **1997**, *105*, 441–456.
32. Hodell, D. A.; Quinn, R. L.; Brenner, M.; Kamenov, G. *J. Arch. Sci.* **2004**, *31*, 585–601.
33. Tiesler, V.; Cucina, A. In *'Janaab' Pakal of Palenque*; Vera Tiesler, V., Cucina, A., Eds.; University of Arizona Press: Tucson, AZ, 2006; pp 3−20.
34. Wright, L. E. *J. Arch. Sci.* **2005**, *32*, 555–566.
35. Krueger, H. W. Geochron Laboratories, unpublished 1985
36. Baxter, M. J.; Cool, H. E. M. *J. Arch. Sci.* **2010**, *37*, 2379–2385.
37. Silverman, B. W. *Density Estimation for Statistics and Data Analysis*; Chapman and Hall: London, 1986.
38. Baxter, M. J. *Statistics in Archaeology*; Hodder Arnold: London, 2003.
39. Shimazaki, H.; Shinomoto, S. *J. Compu. Neurosci.* **2010**, *29*, 171–182.

Chapter 19

Reconstructing Paleoenvironments in the Western Desert, Egypt: ESR Dating Freshwater Molluscs from Kharga Oasis

Anne R. Skinner,[*,1,2] **Bonnie A. B. Blackwell,**[*,1,2]
Maxine R. Kleindienst,[3] **Jennifer R. Smith,**[4] **Johanna M. Kieniewicz,**[4]
Katherine A. Adelsberger,[4,5] **C. S. "Rufus" Churcher,**[6]
Aislinn E. Deely,[2] **Faizullah Mashriqi,**[2] **Kassandra V. Spiller,**[1]
Joel I. B. Blickstein,[1,2] **Jane J. J. Gong,**[2] **and Rebecca A. Long**[2]

[1]Department of Chemistry, Williams College,
Williamstown, Massachusetts 01267-2692, U.S.A.
[2]RFK Science Research Institute,
Glenwood Landing, New York 11547-0866, U.S.A.
[3]Department of Anthropology, University of Toronto at Mississauga,
Mississauga, ON, L5L 1C6, Canada
[4]Department of Earth & Planetary Sciences, University of Washington at
St. Louis, St. Louis, Missouri 63130-4862, U.S.A.
[5]Present address: Department of Environmental Studies, Knox College,
Galesburg, Illinois 60401-4999, U.S.A.
[6]Departmentof Zoology, University of Toronto,
Toronto, ON, M5S 3G5, Canada
*E-mail: anne.r.skinner@williams.edu (A.R.S.);
bonnie.a.b.blackwell@williams.edu (B.A.B.B).
Phone: 1-516-759-6092. Fax: 1-413-597-4116

Kharga Oasis, in Egypt's hyperarid Western Desert, today lacks naturally occurring surface water. Near Kharga, large tufa deposits ranging from a few hectares to more than 10 km^2 in area dot the edge of the Libyan Plateau. These, and lacustrine sediment, record intervals during the Pleistocene when wetlands, ponds, and small freshwater lakes provided water to enable herbivore and human inhabitation. Along with Pleistocene fossils, archaeological finds in the area include artifacts from Earlier Stone Age, Middle Stone Age, Later Stone Age, and younger cultural materials. ESR analysis was used to date freshwater mollusc shells (*Melanoides tuberculata* and *Gyraulus*) found in tufas and lake silts at Wadi Midauwara, Matana, and Bulaq. In some units, multiple gastropod populations from different times have been preserved as a mixed deposit, while several others appear to only preserve a single population. The mollusc dates suggest that freshwater existed sporadically at Bulaq and Matana during Marine (Oxygen) Isotope Stages (MIS) 2 and 4. At Midauwara, standing freshwater existed during the MIS 7/6 and 6/5e boundaries, and repeatedly in MIS 5-2. Molluscs and water also existed during the earliest Pleistocene, at ∼ 2.4 ± 0.4 Ma, which could have enabled the first hominin migration out of Africa via the Western Desert.

Introduction

While today the hyperarid Western Desert, Egypt, gets ∼ 0.01-0.07 mm/y precipitation, mostly as nocturnal condensation, evaporation rates average > 2 m/y. That, coupled with extensive groundwater pumping for local agriculture, ensures that area now lacks naturally occurring standing water (*1*). In earlier wet climatic phases, however, this area may have received as much as 30 cm/y of net precipitation (*2, 3*).

Kharga Oasis had surface water repeatedly during the Pleistocene, as demonstrated by the Pleistocene lacustrine sediment and tufa deposits that occur in the large carbonate mounds dotting the Libyan Escarpment edge and deposits draping its face. The large mounds, which include Midauwara, Matana, and Bulaq (Figures 1, 2), occur at geological nickpoints for the local groundwater aquifer, where slope breaks occur along the escarpment. When the climate was wet, soil formed on the plateau, dissolution resulted, causing karsting, in which rainfall and CO_2 derived from soil bacteria attacked the bedrock limestone. The dissolved carbonate salts then precipitated as tufa when the water emerged from a spring. Where tufa dams block water flow, small basins form within the tufa deposits. At Kharga, these sedimentary basins ranged in size from 1-5 m^2 up to 1-5 km^2, such as those now exposed at Midauwara's Big Snail Gully, Railway 1, and Johanna's Section. In order for basins to trap, and hence, preserve lacustrine silt or clay deposits, those basins must contain standing water for

In Archaeological Chemistry VIII; Armitage, R., et al.;
ACS Symposium Series; American Chemical Society: Washington, DC, 2013.

several decades to millennia. Freshwater snails, like the *Melanoides tuberculata*, *Gyraulus* sp., *Lymnaea stagnalis*, and *Plantries planorbis* found in all the mounds near Kharga, can only survive and breed when abundant fresh water fills lakes. Moreover, hominids and many ungulate species, also require relatively fresh surface water to drink daily. During higher rainfall events, the water retained in the lakes was likely to be fresher than if solely derived from groundwater (*4*). During wetter phases in the Pleistocene, water was sufficiently abundant to support a large, relatively diverse ecosystem, that included hominins, such as possibly *Homo erectus* as well as early *Homo sapiens*, who left Paleolithic artifacts scattered across the landscape ranging from Oldowan (Earliest Stone Age) choppers to Later Stone Age (LSA) settlements. Later peoples left Neolithic lithic tools, hearths, beads, and stone structures, while the ancient Egyptians and then the Romano-Byzantines left their agricultural deposits, pottery, temples, and waterworks (*5–14*).
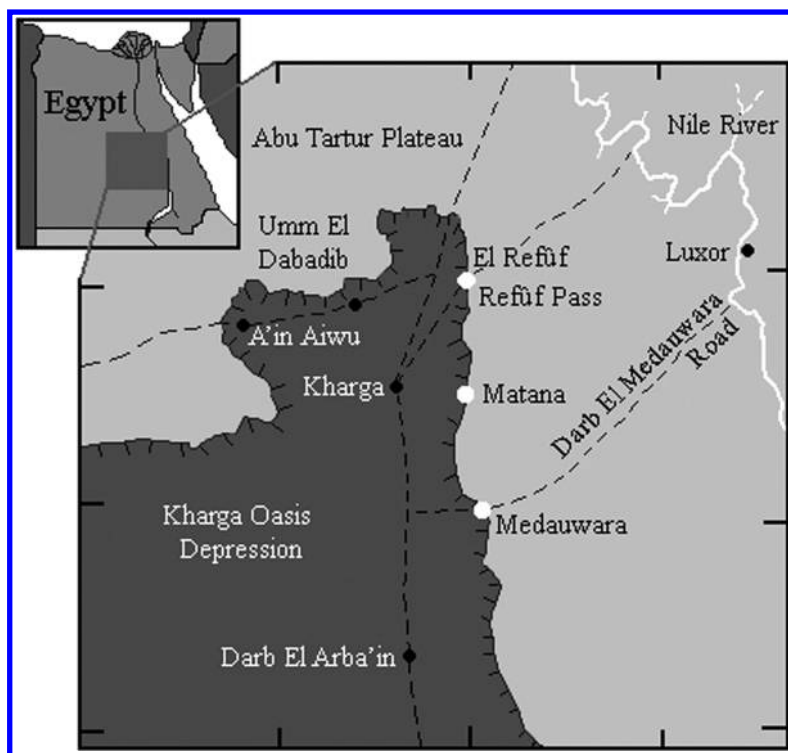
Figure 1. The Kharga Oasis Depression. Near Kharga, large tufa mounds dot the escarpment edge between the Libyan Plateau and the Kharga Oasis Depression. Within Midauwara, lacustrine silts containing freshwater snails were sampled at Midauwara, Bulaq and Matana to assess when water might have been available for hominin and other vertebrates to drink.

While molluscs indicate times when surface water existed, only rarely do the artifacts occur within any sedimentary context that can be correlated with datable materials. Furthermore, intermittent fluvial scouring and the pervasive winds have removed many paleoenvironmental indicators and eroded the context for many fossils and artifacts, leaving them behind in the desert lag that contains mixed debris from several different geological periods. Thus, dating proxy materials becomes imperative.

Unfortunately, datable materials are rare. Although ^{230}Th/^{234}U can sometimes date Kharga's well preserved tufas younger than ~ 400 ka, colluvial and eolian silt and sand with high concentrations of detrital ^{230}Th can contaminate the tufa, thereby complicating or preventing successful ^{230}Th/^{234}U dating (*15*). Commonly, the porous travertines and lake carbonates contain multiple episodes of calcite deposition rimming the pores that preclude accurate dates with any method. Nonetheless, some tufa units from Kharga have been successfully dated, mainly from Midauwara (*1*, *5*, *6*, *11*, *16*) (Table 1). During the wet phases, the same precipitation source that fed the Ethiopian Highlands, the source for the deep Nubian Aquifer, probably also fed the local shallow Libyan Aquifer, surface ponds and lakes in the Western Desert. Likely derived from air masses originating over the Atlantic Ocean, this rainfall produced low δ^{18}O ratios in the tufa and the molluscs, and in deep and shallow groundwater in the Nubian and Libyan Aquifers respectively (*5*). Rainfall also maintained a small recurrent paleolake, and hence, a stable water source at Midauwara. In the early Holocene pluvial period before 8 ka, relatively abundant C^4 species, such as grasses, carpeted the area near the many springs (*3*, *5*, *13*, *17–23*). Vegetation casts preserved in the tufa suggest that varied Pleistocene microenvironments existed within the region (*24*). Faunal remains from Dakhleh Oasis from this period indicate a mid Pleistocene African savanna. Thanks to water from the Nubian Aquifer, the less elevated areas within the oasis (i.e., in the central depression near Kharga City), likely served as refugia for several species (*9*, *25*).

ESR (electron spin resonance) can directly date freshwater molluscs from 5 ka to 2 Ma in age (*26*). No tufa units have yielded sufficiently abundant molluscs for ESR dating, but the lake silts at Kharga (Figures 1, 2) have produced freshwater gastropods for ESR dating. Since these gastropods can only live in fresh or marginally brackish water, dating their shells indicates when hominins and large herbivore herds could inhabit the area (*4*). For example, Blackwell *et al*. (*27*) reported ages for freshwater gastropods from Matana. Here, we report ages for 51 new samples from 16 new sampling localities at Midauwara and Bulaq (Table 2). Potential effects from variable cosmic dose rates, sedimentary dose rates, and evidence for reworked fossils within deposits were also investigated.

Site	Sample Material	Dating Method	Age (ka)	Reference
Kharga	tufa	^{230}Th/^{234}U	157-190; 225-286; 338; > 400	Sultan *et al.* (*50*)
Kharga	tufa	^{230}Th/^{234}U	35; 220-224; 335	Nicholl *et al.* (*16*)
Midauwara	tufa	^{230}Th/^{234}U	120-128	Smith *et al.* (*5*)
Kharga	tufa	^{230}Th/^{234}U	50; 103-128; 136-162; 361; > 400	Smith *et al.* (*5*)
Kharga	carbonates	^{230}Th/^{234}U	75-115; 135; 165; 225-235	Osmond & Dabous (*3*)
Kharga	U ores	^{230}Th/^{234}U	55-75; 115-155	Osmond & Dabous (*3*)
Kharga	Fe ores	^{230}Th/^{234}U	55; 85; 105	Osmond & Dabous (*3*)
Kharga	Po ores	^{230}Th/^{234}U	85-95; 115-125; 195	Osmond & Dabous (*3*)
Matana	tufa	^{230}Th/^{234}U	103 ± 13	Smith *et al.* (*1*)
El Refûf	tufa	^{230}Th/^{234}U	125 ± 2; 240 ± 5	Kleindienst *et al.* (*11*)
Midauwara	tufa	ESR	210-220; 340-360	Abdel-Monem *et al.* (*51*)
Matana	molluscs	ESR	28 ± 2; 65 ± 4	Blackwell *et al.* (*27*)

Table 2. Samples in the Study from Kharga, Egypt

Number	Location				
			GPS Coordinates		
ESR Field	Outcrop	Layer & Split	North	East	Depth (m)
RM14/ KAR30	Lazy Beach 1	weathered from poorly cemented silt	N2761722	E0306027	4/-5
CM46/ KAR116	Johanna's Section 2	gravel between upper and lower sections	24° 56′ 58.7″	31° 5′ 50.0″	6.5/-7
CM44/ KAR117	Johanna's Section 1	upper layer 1: light brown sandy silt	24° 56′ 57.9″	31° 5′ 49.4″	5.5
CM45/ KAR118	Johanna's Section 1	upper layer 2: reddish sandy sed.	24° 56′ 57.9″	31° 5′ 49.4″	5.5
CM42/ KAR115	Johanna's Section 1	lower unit	24° 56′ 58.4″	31° 5′ 50.1″	6
CM47/ KAR108	Snail Trail 1	snail lens	24° 56′ 55.4″	31° 5′ 46.4″	4/-5
CM48/ KAR110	Snail Trail 3	slope surface float	24° 56′ 55.4″	31° 5′ 46.4″	4/-5
CM48a/ KAR110a	Snail Trail 3	slope surface float	24° 56′ 55.4″	31° 5′ 46.4″	4/-5
CM48b/ KAR110b	Snail Trail 3	slope surface float	24° 56′ 55.4″	31° 5′ 46.4″	4/-5

Number			Location			
				GPS Coordinates		
ESR Field	Outcrop	Layer & Split	North	East	Depth (m)	
RM45/ KAR16	Big Snail Gully	massive silt	N2760628/24° 56.929′	E0307807/31° 5.905′	3.5	
FM25/ KAR16a	Big Snail Gully	massive silt	N2760628/24° 56.929′	E0307807/31° 5.905′	3.5	
RM42/ KAR15	Big Snail Gully	snail horizon	N2760628/24° 56.929′	E0307807/31° 5.905′	4	
FM24/ KAR15a	Big Snail Gully	snail horizon	N2760628/24° 56.929′	E0307807/31° 5.905′	4	
RM56/ KAR15b	Big Snail Gully	snail horizon	N2760628/24° 56.929′	E0307807/31° 5.905′	4	
RM47/ KAR17	Big Snail Gully	float	N2760628/24° 56.929′	E0307807/31° 5.905′	0.00/-0.05	
RM53/ KAR17a	Big Snail Gully	largest shells float	N2760628/24° 56.929′	E0307807/31° 5.905′	0.00/-0.05	
RM54/ KAR17b	Big Snail Gully	float	N2760628/24° 56.929′	E0307807/31° 5.905′	0.00/-0.05	
RM51/ KAR17c	Big Snail Gully	float	N2760628/24° 56.929′	E0307807/31° 5.905′	0.00/-0.05	
RM52/ KAR17d	Big Snail Gully	float	N2760628/24° 56.929′	E0307807/31° 5.905′	0.00/-0.05	

Table 2. (Continued). Samples in the Study from Kharga, Egypt

Number					
			Location		
			GPS Coordinates		
ESR Field	Outcrop	Layer & Split	North	East	Depth (m)
RM49/ KAR10	Railway 1, MD16	massive silt above lens	N2761764	E0306709	1.5
RM43/ KAR08	Railway 1, MD16	snail lens	N2761764	E0306709	2
FM8/ KAR08a	Railway 1, MD16	snail lens	N2761764	E0306709	2
RM44/ KAR09	Railway 1, MD16	snail lens	N2761764	E0306709	2
FM7/ KAR09a	Railway 1, MD16	snail lens	N2761764	E0306709	2
RM41/ KAR11	Railway 1, MD16	massive silt below snail lens	N2761764	E0306709	2.5
AM09/ KAR103a	Railway 2	snail lens	24° 57′ 30.4″	31° 5′ 5.4″	2
FM81/ KAR105a	Railway 3	snail lens: dark, smooth, weathered snails	24° 57′ 16.5″	31° 5′ 2.1″	1.0
FM83/ KAR105c	Railway 3	snail lens: light, smooth, weathered snails	24° 57′ 16.5″	31° 5′ 2.1″	1.0

Number	Location				
			GPS Coordinates		
ESR Field	Outcrop	Layer & Split	North	East	Depth (m)
FM82/ KAR105b	Railway 3	snail lens: dark, rugose, unweathered snails	24° 57′ 16.5″	31° 5′ 2.1″	1.0
FM84/ KAR105d	Railway 3	snail lens: light, rugose, unweathered snails	24° 57′ 16.5″	31° 5′ 2.1″	1.0
FM85[2]/ KAR105e	Railway 3	snail lens: light, unweathered snails	24° 57′ 16.5″	31° 5′ 2.1″	1.0
RM26/ KAR31a	Wind Wadi	~ 2 m below cliff top	24° 57′ 18.5″	31° 5′ 56.3″	1.8/-2.0
RM55/ KAR31c	Wind Wadi	~ 2 m below cliff top	24° 57′ 18.5″	31° 5′ 56.3″	1.8/-2.0
RM57/ KAR31d	Wind Wadi	~ 2 m below cliff top	24° 57′ 18.5″	31° 5′ 56.3″	1.8/-2.0
AM05/ KAR114	New Site 2	snail lens, wadi rim	24° 59′ 58.2″	30° 48′ 57″	1.0/-1.5
FM76/ KAR101	Carpark 2	snail horizon	24° 57′ 49.7″	31° 5′ 23.3″	- 1
FM77/ KAR102a	Bonnie Carpark	float and surface central mound: small, light beige, rugose, unweathered	24° 57′ 49.6″	31° 5′ 15.8″	0.00/- 0.05

Table 2. (Continued). Samples in the Study from Kharga, Egypt

330

Number			Location			
				GPS Coordinates		
ESR Field	Outcrop	Layer & Split	North	East	Depth (m)
FM80/ KAR102f	Bonnie Carpark	float and surface central mound: medium-sized, red-stained, rugose, unweathered	24°57′49.6″	31°5′15.8″	0.00/- 0.05
FM78/ KAR102d	Bonnie Carpark	float and surface central mound: medium, light beige, smooth, weathered	24° 57′ 49.6″	31°5′15.8″	0.00/- 0.05
FM79/ KAR102e	Bonnie Carpark	float and surface central mound: medium-size, grey, smooth, weathered	24° 57′ 49.6″	31°5′15.8″	0.00/- 0.05
RM48/ KAR21	central mound Parking Lot Basin	surface *in situ* within central mound	N2762324	E0306918	0.00/- 0.05
FM21/ KAR21a	central mound Parking Lot Basin	surface *in situ* within central mound	N2762324	E0306918	0.00/-0.05
FM28/ KAR21c	central mound Parking Lot Basin	surface *in situ* within central mound	N2762324	E0306918	0.00
RM46/ KAR23a	central mound Parking Lot Basin	25% float 75% surface/atop and in central mound	N2762324	E0306918	0.00/-0.05
RM39/ KAR23b	central mound Parking Lot Basin	60% float 40% surface/atop and in central mound	N2762324	E0306918	0.00/-0.05
RM83/ KAR23b	central mound Parking Lot Basin	60% float 40% surface/atop and in central mound	N2762324	E0306918	0.00/-0.05

Number	Location				
			GPS Coordinates		
ESR Field	Outcrop	Layer & Split	North	East	Depth (m)
RM84/ KAR23b	central mound Parking Lot Basin	60% float 40% surface/atop and in central mound	N2762324	E0306918	0.00/-0.05
RM85/ KAR23b	central mound Parking Lot Basin	60% float 40% surface/atop and in central mound	N2762324	E0306918	0.00/-0.05
FM27/ KAR23b2	central mound Parking Lot Basin	60% float 40% surface/atop and in central mound	N2762324	E0306918	0.00/-0.05
RM59/ KAR25b	NW cliff Parking Lot Basin	snail layer	N2762324	E0306918	3
AM06a/ KAR113a	New Site 1 3 Balls Basin	snail lens	24° 57′ 34.4″	31° 4′ 47.4″	1.0/-1.5
AM08a,b/ KAR106a,d	Matana 2[1]	snail lens	25° 01′ 59.1″	30° 57′ 17.8″	~ 1
AM07a-b/ KAR107a-b	Matana 3[1]	snail lens	25° 01′ 59.0″	30° 57′ 18.3″	~ 1
CM43/ KAR119	Bulaq Bingo	grey silt	24° 56′ 58.7″	31° 5′ 50.0″	~ 1

[1] Data from Blackwell *et al*. (*27*).

[2] All samples *Melanoides tuberculata* save this; *Gyraulus*.

Geology and Archaeology at Midauwara, Kharga Oasis

Kharga Oasis sits roughly 650 km southwest of Cairo at 25°N 30°E and 100 m amsl. Below the Libyan Plateau in Egypt's Western Desert, the Kharga Oasis occupies a depression that extends north-south for ~ 200 km, and east-west for ~ 75 km at ~ 60 m amsl (Figure 1). The depression formed due to wind ablating Cretaceous-Tertiary marine limestone, shale, and sandstone units. The Eocene Thebes Group limestone now rims the depression at ~ 350 m amsl (*5–8*). In 1930-1933, Caton-Thompson and Gardner studied the geology and archaeology in the Kharga depression, on the Libyan Escarpment, and on the surrounding Libyan Plateau (*24*, *28*, *29*). Kleindienst *et al.* (*11*) and Smith *et al.* (*1*) have relocated their artifact sampling localities at Naqb el Refûf, Abu Sighawâl, Bulaq, Matana, and Midauwara on the escarpment rim.

When Kharga experienced heavier rainfall, the large tufa mounds, like Midauwara, and other areas with tufa deposition or deflated basins trapped more water. When the groundwater table is high within the Nubian Aquifer that feeds springs around Kharga, the springs will flow more voluminously, providing more water to fill Midauwara's tufa-bounded basins (*7*). Kharga's Pleistocene ponds and lakes trapped lacustrine silts, which comprise predominantly locally produced carbonate grains and cement mixed with small amounts of detrital clastic sediment and freshwater gastropod fossils, including *Melanoides tuberculata* and *Gyraulus* sp. (*5*). Because the tufa resists aeolian erosion better than the lacustrine or playa sediment, the tufa itself and those lake deposits overlain or rimmed by tufa often preserve the only evidence for the diverse paleoecosystems (*2*).

At Naqb or Wadi el Midauwara, the tufa deposits cover > 10 km² building to a total depth of more than 30 m in places (*7*) (Figures 1, 2). Although Smith *et al.* (*5*, *6*) only recognized three temporally distinct tufa units, more recent analyses suggest a much more complex stratigraphy with intermittent tufa deposition from at least 2 Ma until the late Pleistocene. The limited areal extent for many small lacustrine basins, exacerbated by the extensive erosion that has removed intervening mappable units, complicates efforts to build a detailed stratigraphy for Midauwara. Precipitated directly at spring mouths or as tufa dams that cascade off minor changes in elevation, penecontemporaneous tufas occur at different altitudes on the escarpment, and tufas of different ages can occur at the same elevation (*30*). Erosion plus recent anthropogenic surface modification has left isolated outcrops that contain molluscs, but which cannot be related easily to one another (*31*, *32*). Nowhere in Kharga does a Quaternary section exist with more than a few stacked stratigraphic units. Since the mapped tufa units do not all occur in any one outcrop, but occur as discontinuously distributed, laterally extensive units scattered across the mound surface, correlating between basins has been difficult, and correlation between scattered tufa deposits even more challenging. Only chronostratigraphic dating can indicate penecontemporaneous units. Even where two outcrops sit only < 100 m apart, correlating the units is often impossible.

Certainly, the interglacial-glacial Milanković cycling did affect large swaths of the globe, but the correlation between the desert's wetter periods and the Northern Hemisphere's climate shifts have remained controversial. Based upon

In Archaeological Chemistry VIII; Armitage, R., et al.;
ACS Symposium Series; American Chemical Society: Washington, DC, 2013.

the dates for the tufa units (e.g., Table 1), Smith (*17*), among others, has correlated that the Sahara's wet phases with the Northern Hemisphere's interglacial periods, whereas Abouelmagd *et al.* (*33*) have suggested that the desert's wet phases correlate with glacial periods, thanks to changes in wind patterns. Northern Hemisphere pollen records have shown that, during glacial periods, vegetation belts tended to shift southward, compressed in N-S width, and often acquired new components to produce species mixtures not seen in the interglacial periods, as the climate cooled going into a Northern Hemisphere glacial period, and then to reverse those processes as the climate rewarmed. Since most desert outcrops lack pollen evidence, however, correlating these events with the desert's wetter phases must rely on chronometric dating, like ESR, to test these correlations.
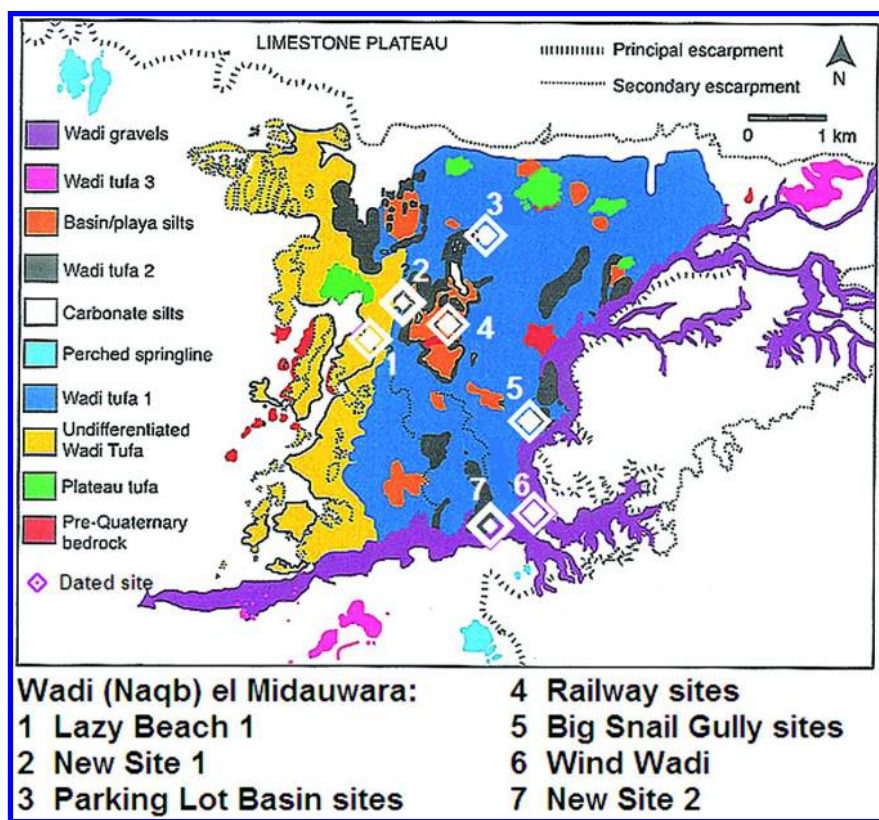
Figure 2. The tufa deposits at Midauwara, Egypt. At least four generations of tufa deposits form the Midauwara mound. The tufa dammed ponds or small lakes which collected carbonate-rich lacustrine silt and freshwater gastropods, such as Melanoides tuberculata and Gyraulus. Gastropods were collected from 16 localities clustered in seven areas. (see color insert)

ESR Dating

Detailed stratigraphic relationships between the outcrops are impossible to verify except through chronological analyses. All samples were collected from within the snail-bearing horizons in areas where snails were found eroding from the underlying sandy silts.

Principles of ESR Dating

Electron spin resonance dating uses radiation damage signals stored in minerals and the radiation dose rate from the sediment and the sample itself to date the molluscs (*26*). For aragonitic molluscs from 5 ka to 2 Ma, ESR can provide absolute dates using the stable signal at $g = 2.0007$ (*34*, *35*) or the signal at $g = 2.0012$ (*36*). Both give comparable results. Equation 1 yields ESR ages (*37*):

$$A_\Sigma = \int_0^t (D_{int}(t) + D_{sed}(t) + D_{cos}(t))\, dt \tag{1}$$

where A_Σ = the total accumulated dose in the sample,

$D_{int}(t)$ = the dose rate from internal sources: U, its daughters, and any other radioisotopes,

$D_{sed}(t)$ = the dose rate from external sources: sedimentary U, Th, and K,

$D_{cos}(t)$ = the dose rate from external sources: cosmic radiation,

t = the sample's age.

Successful dates must consider how reworking and deflation affect the sedimentary and cosmic dose rate calculations.

Molluscs were first separated into species, *Melanoides tuberculata*, *Gyraulus*, or *Bellaphone*, where possible. Hash samples could not be identified to species and were not mixed with other subsamples having identified species. To ensure sufficient sample, where samples permitted, ~ 7 g of shells for each sample were prepared using standard ESR molluscan dating procedures (*34*, *38*). Using a ^{60}CO γ source, all but one aliquot were irradiated at a dose rate of 56-132 Gy/s with added doses ranged from 8 to 1300 Grays (*39*). Molluscs were annealed for 1.0 h at 90°C to remove any unstable interference. At 25°C, aliquots were scanned in a JEOL RE1X spectrometer at 2 mW power under a 100 KHz field modulation, using a 0.3 s time constant. The spectra were scanned over 10 mT, centered at 336 mT with an 8.0 min. sweep time. Gains were set to maximize signal intensity. Peak heights for the g = 2.0007 signal were analyzed (*34*, *38*).

To measure $D_{int}(t)$, U concentrations within the fossils were analyzed geochemically by NAA (see Blackwell (*39*) for analytical details). When coupled dating is not possible for uraniferous materials to determine $D_{int}(t)$, as is the case for most molluscs (see discussion in Blackwell (*15*, *40*)), three uptake models are usually used:

> Early uptake (EU), $p = -1$, assumes that the sample absorbed all its U soon after burial, providing the youngest age given the accumulated dose, A_Σ, and external dose rate, $D_{ext}(t)$. This model only applies to the dentine in very young teeth, quartz sediment, and very old shells (*15*, *26*, *40*, *41*).

Linear uptake (LU), $p = 0$, assumes that the sample absorbs U at a constant rate throughout its burial history, giving a median age. Most studies have found that this model provides the most accurate ages for molluscs, among other materials (*15*, *26*, *40*, *41*).

Recent uptake (RU), $p > 0$, assumes U uptake very late in the sample's burial history, which reduces its internally generated dose, A_{int}, to a minor contribution compared to A_Σ. This gives the maximum possible age. As yet, this model has not been found to apply to molluscs (*15*, *26*, *40*, *41*).

Cosmic dose rates were determined using the dating program Rosy v. 4.2 (*42*). To determine $D_{ext}(t)$, volumetrically averaged sedimentary geochemical analysis was used where sediment samples permitted: Sediment samples from within 30 cm of the dating sample were geochemically analyzed by NAA, for radioactive elements and then volumetrically averaged for each layer around the shells (Table 3). All three model ages do appear in Table 4, but for none of the ages does a significant difference exist between the EU, LU, or RU model ages. Because the LU models ages usually provide the most accurate ages when compared to other chronometric dating results for shells < 1Ma (*27*) and provide a median age for the age variation between the three models, only LU ages will be discussed further. Mean ages were calculated by inversely weighting the ages by their associated standard deviations.

Cosmic Dose Rates

In open air desert sites, cosmic radiation contributes significantly to $D_\Sigma(t)$, the total dose rate, often accounting for 20-35% of $D_\Sigma(t)$, the total dose rate. Due to low sedimentary radioactivity, $D_{sed}(t)$ values for the molluscs constitute ~ 20-50% of $D_\Sigma(t)$, while the internal dose rate, $D_{int}(t)$, seldom represents > 25%. Thus, this requires modelling $D_{cos}(t)$ in order to constrain reliable ESR ages. In order to model the time-averaged cosmic dose rates, $\overline{D}_{cos}(t)$ the fossil's environmental preferences, geological and geomorphological criteria are used to estimate past water or sediment cover depth histories and, thus, the likely minimum and maximum cover thicknesses, as well as the degree of erosion and its relative timing. With ramped box models built with these constraints, the minimum and maximum $\overline{D}_{sed}(t)$ and $\overline{D}_{cos}(t)$ can be calculated, these in turn, can be used to determine the minimum and maximum ages (for a detailed discussion, see Deely *et al*. (*37*)).

Reworking

While the snail-bearing horizons at all 16 localities may or may not represent penecontemporaneous lacustrine units, the presence of visibly different taphonomic characteristics in several makes it necessary to examine the collections for possible reworked samples. To test for reworked molluscs, where sample sizes permitted, several random grab samples from each mollusc-bearing bed were tested for age coherence (Table 4). If the molluscan U concentrations,

accumulated doses, and ages all agree statistically, then the possibility for reworked fossils becomes less likely (*43*) (e.g., Table 4). If reworking does occur, then the age for youngest fossils usually gives the best estimate for the unit's deposition (e.g., Patnaik *et al.* (*44*)). Molluscs from three Midauwara localities demonstrate how reworked fossils affect the ages.

For KAR105 from Railway 3 (Table 4h), the sample had visually distinguishable fossil subpopulations. After separating the sample into five subpopulations, the unweathered *Gyraulus* and *Melanoides* shells that retained their rugose outer surface gave consistently younger ages averaging 25 ± 2 ka. For the strongly weathered *Melanoides*, their ages averaged 34 ± 3 ka. Therefore, at Railway 3, at least two populations appear to be present, an older weathered population, probably dating to late OIS 3 or older, mixed with a younger unweathered population dating to early OIS 2, but possibly younger. This depositional unit must have been deposited at some time ≲ 25 ka.

At Bonnie Carpark in Parking Lot Basin, KAR102 again had visually identifiable subpopulations that were separated before analysis (Table 4l). Their accumulated doses and ages hint that two or more populations may also be temporally mixed here. Shell color did not coincide with weathering patterns, and the size classes do not have uniform color or weathering patterns. The weathered molluscs ranged from 37 to 47 ka, while the unweathered snails ranged from 27 to 36 ka. While somewhat different, the lack of uniformity in the ages, sizes, and weathering patterns suggests that more than two populations may exist here. If only two populations are present, then one population would date to ≲ 27 ka, but could be much younger, and the other layers to ≲ 47 ka, but possibly much older.

Likely, reworking or deflation produced these two sets of mixed shell populations. In a blowout, as the wind winnows away the fine sediment and the blowout deepens, the heavier grains, such as hominin artifacts, gastropod shells, mammalian teeth and bones, drop onto the sediment surface. All other traces for some units may disappear. Thus, deflation can mix coarser grains removed from any stratigraphically higher, but now eroded, units, making it more challenging to date the associated artifacts or fossils. Within the small lakes and ponds, surface wash, small streams, or the wind can transport older shells eroded from nearby stratigraphic units along the basin margins to the pond or lake where they are deposited together with the empty shells from recently dead snails, producing a temporally mixed deposit. Moreover, some basins may dry at times and refill with water much later. Populations from multiple periods can then form a palimpsest. The stratigraphic units in this area should be mapped more extensively to try to locate and date the original units from which these reworked shells could have derived.

At Big Snail Gully (Table 4e), the five surface grab samples from KAR17 all showed little variation in their U concentrations, accumulated doses, or ages. Moreover, all the other snails from this outcrop yielded consistent results (see below). This suggests that the snail lens at Big Snail Gully likely contains only one contemporaneous population of snails.

Table 3. Sedimentary Radioactivity at Medauwara, Kharga

Site Location (analyses)	Concentrations			Dose Rates[1]	
	U (ppm)	Th (ppm)	K (wt%)	$D_{\mathrm{sed},\beta}^{\mathrm{BG}}(t)$[2] (mGy/y)	$D_{\mathrm{sed},\gamma}^{\mathrm{BG}}(t)$[3] (mGy/y)
Lazy Beach (n = 3)	0.82 ± 0.08	0.16 ± 0.10	0.01 ± 0.01	0.078 ± 0.006	0.093 ± 0.009
Johanna's Sections (n = 5)	1.99 ± 0.59	3.04 ± 0.94	0.16 ± 0.13	0.263 ± 0.078	0.376 ± 0.083
Snail Trail (n = 1)	2.15 ± 0.02	2.72 ± 0.19	0.16 ± 0.01	0.271 ± 0.028	0.378 ± 0.025
Big Snail Gully (n = 3)	1.79 ± 0.07	2.37 ± 1.04	0.23 ± 0.07	0.278 ± 0.021	0.339 ± 0.055
Railway 1, MD16 (n = 5)	1.38 ± 0.12	0.88 ± 0.42	0.09 ± 0.07	0.177 ± 0.030	0.203 ± 0.019
Railway 2 (n = 1)	1.68 ± 0.02	0.12 ± 0.02	0.03 ± 0.01	0.161 ± 0.016	0.182 ± 0.011
Railway 3 (n = 1)	2.13 ± 0.02	4.53 ± 0.28	0.48 ± 0.01	0.422 ± 0.039	0.528 ± 0.036
Wind Wadi (n = 1)	2.38 ± 0.02	0.80 ± 0.10	0.10 ± 0.01	0.264 ± 0.027	0.299 ± 0.019
New Site 2 (n = 2)	1.79 ± 0.15	1.50 ± 0.38	0.16 ± 0.03	0.242 ± 0.030	0.297 ± 0.025
Bonnie Carpark (n = 1)	1.89 ± 0.02	4.68 ± 0.03	0.51 ± 0.02	0.452 ± 0.050	0.517 ± 0.035
Parking Lot Basin	1.48 ± 0.22	2.55 ± 0.07	0.30 ± 0.02	0.300 ± 0.011	0.324 ± 0.011
New Site 1 (n = 2)	1.56 ± 0.66	2.99 ± 2.51	0.22 ± 0.21	0.255 ± 0.064	0.368 ± 0.197
Matana 2[4] (n = 1)	1.60 ± 0.02	4.68 ± 0.28	0.54 ± 0.02	0.476 ± 0.050	0.496 ± 0.033

Table 3. (Continued). Sedimentary Radioactivity at Medauwara, Kharga

Site Location (analyses)	Concentrations			Dose Rates[1]	
	U (ppm)	Th (ppm)	K (wt%)	$D_{\text{sed},\beta}^{\text{BG}}(t)$[2] (mGy/y)	$D_{\text{sed},\gamma}^{\text{BG}}(t)$[3] (mGy/y)
Matana 3[4] (n = 1)	1.76 ± 0.02	4.12 ± 0.27	0.44 ± 0.01	0.396 ± 0.043	0.461 ± 0.032
Bulaq Bingo (n = 1)	1.65 ± 0.02	0.56 ± 0.07	0.06 ± 0.01	0.187 ± 0.025	0.181 ± 0.016

[1] Abbreviations: $D_{\text{sed},\beta}^{\text{BG}}(t)$ = bulk sedimentary dose rate from β sources.

$D_{\text{sed},\gamma}^{\text{BG}}(t)$ = bulk sedimentary dose rate from γ sources.

Concentrations and 1 σ errors calculated for closest sample with terrestrial water concentration, $W_{\text{sed}} = 10.0 \pm 5.0$ wt%.

[2] Calculated using mollusc density, $\rho_{\text{mol}} = 2.95 \pm 0.01$ g/cm³;

carbonate sediment density, $\rho_{\text{sed}} = 2.95 \pm 0.01$ g/cm³;

clastic sediment density, $\rho_{\text{sed}} = 2.66 \pm 0.01$ g/cm³.

[3] Calculated using cosmic dose rate, $D_{\text{cos}}(t) = 0.000 \pm 0.000$ mGy/y.

[4] Data from Blackwell et al. (27).

Table 4. ESR ages for Kharga molluscs

Sample		Molluscan U conc'n, $[U]_{mol}$ (ppm)	Accumulated Dose, A_Σ (Grays)	Time-averaged External Dose Rate, $D_{ext}(t)$ ($\mu Gy/a$)	Standard ESR Ages[1]		
					EU (ka)	LU (ka)	RU (ka)
a. Lazy Beach 1							
RM14		0.62	1100.	287	**2290.**	2880.	3630.
KAR30	±	0.02	160.	23	**380.**	460.	590.
b. Johanna's Sections							
CM46		0.75	75.4	629	98.0	**109.**	118.
KAR116	±	0.02	3.7	138	23.1	**28.**	33.
CM45		1.73	82.1	632	87.3	**106.**	124.
KAR118	±	0.02	5.6	138	18.2	**26.**	34.
upper unit			77.7		92.0	**108.**	121.
mean (n = 2)	±		3.1		14.0	**19.**	24

Table 4. (Continued). ESR ages for Kharga molluscs

Sample		Molluscan U conc'n, $[U]_{mol}$ (ppm)	Accumulated Dose, A_Σ (Grays)	Time-averaged External Dose Rate, $D_{ext}(t)$ ($\mu Gy/a$)	Standard ESR Ages[1]		
					EU (ka)	LU (ka)	RU (ka)
CM42		0.75	195.	693	140.	**191.**	247.
KAR115	±	0.02	10.	161	24.	**39.**	62.
c. Snail Trail 1							
CM47		2.29	108.	641	101.	**129.**	158.
KAR108	±	0.02	5.	83	11.	**15.**	20.
d. Snail Trail 3							
CM48		1.63	74.1	609	84.1	**102.**	117.
KAR110	±	0.02	5.4	52	9.2	**11.**	13.
CM48a		2.06	79.3	609	83.3	**104.**	123.
KAR110a	±	0.02	4.2	52	8.3	**10.**	12.
unit			77.5		87.7	**103.**	120.
mean (n = 2)	±		3.3		6.2	**7.**	7.

Sample		Molluscan U conc'n, $[U]_{mol}$ (ppm)	Accumulated Dose, A_Σ (Grays)	Time-averaged External Dose Rate, $D_{ext}(t)$ $(\mu Gy/a)$	Standard ESR Ages[1]		
					EU (ka)	LU (ka)	RU (ka)
e. Big Snail Gully							
RM45		0.65	72.3	584	97.7	**111.**	121.
KAR16	±	0.02	7.3	78	14.5	**17.**	20.
FM25		0.66	63.9	584	87.5	**98.8**	108.
KAR16a	±	0.02	4.8	78	11.9	**14.4**	17.
RM42		0.87	68.1	584	86.9	**101.**	113.
KAR15	±	0.02	0.5	78	9.1	**12.**	15.
FM24		0.74	74.7	584	97.7	**112.**	124.
KAR15a	±	0.02	4.0	78	11.7	**15.**	17.
RM56		0.70	58.6	584	83.3	**92.1**	98.5
KAR15b	±	0.02	2.9	78	10.4	**12.3**	14.5

Table 4. (Continued). ESR ages for Kharga molluscs

Sample		Molluscan U conc'n, $[U]_{mol}$ (ppm)	Accumulated Dose, A_Σ (Grays)	Time-averaged External Dose Rate, $D_{ext}(t)$ ($\mu Gy/a$)	Standard ESR Ages[1]		
					EU (ka)	LU (ka)	RU (ka)
RM47		0.66	62.1	584	84.6	**95.4**	104.
KAR17	±	0.02	6.8	78	13.1	**15.5**	18.
RM54		0.66	58.6	584	83.4	**92.1**	98.5
KAR17b	±	0.02	2.9	78	10.5	12.3	13.8
RM51		0.76	61.0	584	86.6	**95.7**	103.
KAR17c	±	0.02	2.2	78	10.4	**12.4**	14.
RM53		0.66	62.3	584	88.3	**97.7**	105.
KAR17a	±	0.02	3.3	78	11.2	**13.2**	15.
RM52		0.66	68.7	584	96.7	**108.**	115.
KAR17d	±	0.02	2.2	78	11.5	**14.**	16.

Sample		Molluscan U conc'n, $[U]_{mol}$ (ppm)	Accumulated Dose, A_Σ (Grays)	Time-averaged External Dose Rate, $D_{ext}(t)$ ($\mu Gy/a$)	Standard ESR Ages[1]		
					EU (ka)	LU (ka)	RU (ka)
Big Snail Gully		0.70	67.5	584	89.3	**100.**	109.
mean (n = 10)	±	0.07	1.0	78	2.8	**4.**	8.
f. Railway 1, MD16							
RM49		0.35	71.8	492	128.	**136.**	144.
KAR10	±	0.02	3.6	82	21.	**24.**	26.
RM43		0.51	65.9	494	112.	**123.**	131.
KAR08	±	0.02	0.5	82	16.	**19.**	22.
FM8s1		0.05	70.6	492	141.	**142.**	143.
KAR08a	±	0.02	3.7	82	24.	**25.**	25.
FM8s2		0.05	72.7	492	145.	**146.**	148.
KAR08a	±	0.02	4.3	82	25.	**26.**	26.

Table 4. (Continued). ESR ages for Kharga molluscs

Sample		Molluscan U conc'n, $[U]_{mol}$ (ppm)	Accumulated Dose, A_Σ (Grays)	Time-averaged External Dose Rate, $D_{ext}(t)$ ($\mu Gy/a$)	Standard ESR Ages[1]		
					EU (ka)	LU (ka)	RU (ka)
FM8s3		0.06	60.7	492	121.	**122.**	123.
KAR08a	±	0.02	4.2	82	21.	**22.**	22.
FM8s4		0.06	67.7	492	134.	**136.**	137.
KAR08a	±	0.02	2.4	82	22.	**23.**	23.
RM44		0.50	67.5	494	115.	**124.**	134.
KAR09	±	0.02	3.5	82	18.	**20.**	23.
FM7		0.36	76.0	492	135.	**144.**	152.
KAR09a	±	0.02	2.5	82	20.	**23.**	26.
RM41		0.47	70.9	485	123.	**133.**	144.
KAR11	±	0.02	5.4	81	20.	**23.**	26.

Sample		Molluscan U conc'n, $[U]_{mol}$ (ppm)	Accumulated Dose, A_Σ (Grays)	Time-averaged External Dose Rate, $D_{ext}(t)$ ($\mu Gy/a$)	Standard ESR Ages[1]		
					EU (ka)	LU (ka)	RU (ka)
Railway 1					127.	**134.**	140.
mean (n = 9)					7.	**8.**	8.
g. Railway 2							
AM09		0.53	31.6	449	64.8	**70.9**	75.3
KAR103a	±	0.02	1.7	82	10.7	**12.4**	13.9
h. Railway 3							
FM82 (unweathered)		15.34	39.4	812	16.9	**25.1**	40.4
KAR105b	±	0.02	3.9	81	2.5	**3.5**	5.3
FM84 (unweathered)		25.97	52.0	812	15.6	**24.9**	47.2
KAR105d	±	0.02	2.8	81	2.2	**3.0**	4.8
FM85 (unweathered)		7.46	29.5	812	18.9	**25.1**	33.3
KAR105e	±	0.02	1.6	81	2.1	**2.6**	3.5

Table 4. (Continued). ESR ages for Kharga molluscs

Sample		Molluscan U conc'n, $[U]_{mol}$ (ppm)	Accumulated Dose, A_Σ (Grays)	Time-averaged External Dose Rate, $D_{ext}(t)$ ($\mu Gy/a$)	Standard ESR Ages[1]		
					EU (ka)	LU (ka)	RU (ka)
KAR105 (unweathered)					17.5	**25.0**	40.5
mean (n = 3)					1.3	**1.7**	2.6
FM81 (weathered)		11.52	52.8	812	24.8	**36.0**	55.3
KAR105a	±	0.02	3.0	81	3.0	**3.9**	5.8
FM83 (weathered)		26.09	69.1	812	19.8	**31.8**	60.9
KAR105c	±	0.02	3.1	81	2.7	**3.8**	6.0
KAR105 (weathered)					22.6	**34.1**	58.3
mean (n = 2)					2.0	**2.7**	4.3
i. Wind Wadi							
RM26		0.70	89.1	731	103.	**112.**	120.
KAR31a	±	0.02	5.3	60	10.	**11.**	12.

Sample		Molluscan U conc'n, $[U]_{mol}$ (ppm)	Accumulated Dose, A_Σ (Grays)	Time-averaged External Dose Rate, $D_{ext}(t)$ (μGy/a)	Standard ESR Ages[1]		
					EU (ka)	LU (ka)	RU (ka)
RM55		3.25	83.0	731	66.1	**85.1**	106.
KAR31c	±	0.02	3.1	60	6.0	**7.2**	9.
RM57		3.16	57.3	731	49.4	**61.6**	74.1
KAR31d	±	0.02	3.1	60	4.9	**5.7**	7.1
j. New Site 2							
AM05		0.91	44.8	783	49.2	**53.3**	56.4
KAR114	±	0.02	1.9	254	12.9	**15.0**	16.7
k. Carpark 2							
FM76		1.89	69.1	698	69.0	**82.7**	95.0
KAR101	±	0.02	4.0	29	5.7	**6.1**	6.7
l. Bonnie Carpark							
FM80 (unweathered)		0.93	27.6	985	25.4	**26.8**	27.8
KAR102f	±	0.02	2.4	28	2.3	**2.4**	2.5

Table 4. (Continued). ESR ages for Kharga molluscs

Sample		Molluscan U conc'n, $[U]_{mol}$ (ppm)	Accumulated Dose, A_{Σ} (Grays)	Time-averaged External Dose Rate, $D_{ext}(t)$ ($\mu Gy/a$)	Standard ESR Ages[1]		
					EU (ka)	LU (ka)	RU (ka)
FM77 (unweathered)		1.16	38.0	991	33.5	**36.0**	37.9
KAR102a	±	0.02	3.9	28	3.6	**3.8**	4.0
FM79 (weathered)		1.06	39.0	991	34.3	**37.1**	38.9
KAR102e	±	0.02	1.9	28	2.0	**2.1**	2.2
FM78 (weathered)		1.26	50.4	1010	42.9	**46.5**	48.9
KAR102d	±	0.02	4.2	28	3.9	**4.1**	4.3
m. Parking Lot Basin, central mound							
RM48		1.28	9.37	608	12.8	**14.1**	14.5
KAR21	±	0.02	0.52	26	7.2	**7.8**	8.1
FM21		1.29	35.9	697	38.7	**44.6**	49.9
KAR21a	±	0.02	1.9	29	2.7	**3.0**	3.4

Sample		Molluscan U conc'n, $[U]_{mol}$ (ppm)	Accumulated Dose, A_{Σ} (Grays)	Time-averaged External Dose Rate, $D_{ext}(t)$ ($\mu Gy/a$)	Standard ESR Ages[1]		
					EU (ka)	LU (ka)	RU (ka)
RM46[2]		1.52	40.3	705	44.4	**50.6**	55.7
KAR23a	±	0.02	3.4	29	4.4	**4.7**	5.2
RM83a[2]		0.99	24.7	689	29.1	**32.4**	35.2
KAR23b	±	0.02	1.6	28	2.3	**2.5**	2.7
RM84[2]		1.12	26.2	689	29.9	**33.7**	37.1
KAR23b	±	0.02	1.5	28	2.1	**2.4**	2.6
RM85[2]		1.10	27.1	689	31.0	**35.0**	38.4
KAR23b	±	0.02	1.7	28	2.3	**2.5**	2.8
FM27[2]		1.58	27.5	697	28.7	**33.6**	38.1
KAR23b2	±	0.02	2.0	29	2.8	**2.8**	3.1

Table 4. (Continued). ESR ages for Kharga molluscs

Sample		Molluscan U conc'n, $[U]_{mol}$ (ppm)	Accumulated Dose, A_Σ (Grays)	Time-averaged External Dose Rate, $D_{ext}(t)$ ($\mu Gy/a$)	Standard ESR Ages[1]		
					EU (ka)	LU (ka)	RU (ka)
n. Parking Lot Basin, NW cliff							
RM59		1.10	25.5	689	31.4	**34.2**	36.4
KAR25b	±	0.02	0.9	28	1.8	**1.9**	2.0
o. New Site 1							
AM06		0.86	50.1	783	55.1	**59.8**	63.2
KAR113a	±	0.02	3.2	254	14.6	**17.0**	19.0
p. Matana 3[3] Matana 3		0.74	69.0	1036	62.0	**65.1**	67.6
mean (n = 2)	±	0.09	2.0	80	3.8	**4.1**	4.4
q. Matana 2[3] Matana 2		0.55	31.6	1106	27.0	**27.7**	28.3
mean (n = 2)	±	0.06	1.5	80	1.8	**1.9**	2.0

Sample		Molluscan U conc'n, $[U]_{mol}$ (ppm)	Accumulated Dose, A_Σ (Grays)	Time-averaged External Dose Rate, $D_{ext}(t)$ ($\mu Gy/a$)	Standard ESR Ages[1]		
					EU (ka)	LU (ka)	RU (ka)
r. Bulaq Bingo CM43		0.53	13.0	523	22.5	**23.7**	24.6
KAR119	±	0.02	1.3	48	2.9	**3.1**	3.3

[1] Abbreviations: EU = assuming early U uptake, $p = -1$.
LU = assuming linear (continuous) U uptake, $p = 0$.
RU = assuming recent U uptake, $p = 10$. Ages calculated with:
α/γ factor, $\kappa_\alpha = 0.10 \pm 0.01$;
intial U activity ratio, $(^{234}U/^{238}U)_0 = 1.2 \pm 0.20$;
aragonite density, $\rho_{mol} = 2.95 \pm 0.01$ g/cm^3;
radon loss from the shells, $Rn_{mol} = 0.0 \pm 0.0$ vol%,
carbonate sediment density, $\rho_{cal} = 2.96 \pm 0.01$ g/cm^3;
quartz sediment density, $\rho_{qtz} = 2.66 \pm 0.01$ g/cm^3;
sedimentary water concentration, $W_{sed} = 10.0 \pm 5.0$ wt%.
All errors are 1 σ.
[2] Samples were deliberately mixed to produce a mixing line and equation.
[3] Data summarized from Blackwell *et al.* (*27*).

Similarly, the two surface grab samples from Snail Trail 3 were collected to test the effects of reworking on surface collections in that area. Both yielded consistent U concentrations, accumulated doses, and ages (Table 4d), suggesting that the unit weathering out here is likely unmixed.

Therefore, reworking does occur in the Midauwara lacustrine units, but often the molluscan weathering features provide clues that help to identify mixed populations. In units where the snails all look similar for color and weathering, some units do not contain temporally mixed molluscs. While this does not guarantee that any unit that has no obvious visually different shells does not contain multiple subpopulations, it hints that a single date may provide an accurate age where only one date was possible.

Results

Tables 3 and 4 show the results for the 16 sites from Kharga Oasis.

The Early Pleistocene Site: Lazy Beach 1

The Lazy Beach 1 outcrop sits to the northwest of the Railway outcrops on the edge of a large deflated basin edged with steep cliffs. Lazy Beach 1 is separated from Old Jebel by a deflation corridor. At Old Jebel, a stacked sequence of silt units intercalated with old tufas all exceeded the $^{230}Th/^{234}U$ dating limit (usually 400-500 ka (15). Exposed on the southern cliff of the basin, the Lazy Beach 1 site displays a stratified section with a lightly cemented silt, rich in snails, capped by several intercalated silt and tufa units. The snail bearing horizon sits ~ 4 m above the basin floor, overlain by another ~ 5 m of intercalated lacustrine silt and tufa units. A single sample analysis for *Melanoides tuberculata* shells weathered from the snail-bearing horizon here produced an age of 2.3 ± 0.4 Ma (Table 4a). Note the use of the EU age. Studies on U uptake in shell suggest a maximum uptake period of 50-100 ka, making EU the appropriate model for this site. A lack of shell precluded more analyses. Substantially older than any other tufa outcrops found elsewhere and older than any archaeological materials found near that area, this Early Pleistocene age hinted that should artifacts be found within this sequence, they should be Oldowan. During the next field season, when trying to find enough shell for a confirming date, Oldowan artifacts were found, not *in situ* within weathered debris, but in the aeolian sand on the western edge at the base of this outcrop. Although the tufa unit, the cliff face, and the adjacent Old Jebel site were then examined for *in situ* artifacts, none were visible (45). Nor was enough shell found to allow another ESR date. Nonetheless, this association suggests that the units here may indeed be ~ 2.3 Ma in age, which indicates that climates were relatively wet at this time. This age correlates with the Matuyama Chron at MIS 87. At ~ 1.9 Ma, hominins first arrive in Dmanisi, Georgia, in the Caucasus Mts. (46). This wet period dated at Lazy Beach 1 might have enabled early hominins to migrate across North Africa toward Europe and Asia (47).

The Middle-Late Pleistocene Sites

Five younger site clusters occur on the Midauwara mound that yielded molluscs for dating. At several, the size of the exposure only yielded enough snails to permit a single sample analysis. While analyzing multiple samples should occur at every site, the small size of the fossil collections from the deposits at several locations coupled with the current political situation may make further collection and analyses difficult at these sites in the near future.

The Big Snail Gully Outcrops, Midauwara

Near the eastern edge of the Midauwara mound (Figure 2), the Big Snail Gully and Snail Trail sites both sit along the eastern edge of a major tributary valley to the main wadi. Not far away, Johanna's Section 1 and 2 sits furthest downslope to the south. Although the snail lenses can not be tracked down the wadi, the lacustrine units can. Their thickness and areal extent indicate that a relatively large lake occurred here (*18*).

At Johanna's Section (Table 4b), a cliff along the tributary to the wadi exposed a stratified section (*18*). In the upper part of the section, two snail lenses occur at ~ 4-5 m below the cliff top. This site appears to expose deposits from a small lake that partly or completely dried and then refilled. The two ages agreed well, averaging 108 ± 19 ka. Given its proximity to Big Snail Gully, and the similarity in the ages here and at Big Snail Gully (see below), this outcrop likely represents the margin of the same lake that existed in MIS 5d.

At Johanna's Section, a gravel unit comprising fine gravel separates the upper section from the lower section. In the lower unit, another snail lens outcropped about ~ 3 m below. The silt containing the snails overlay a tufa unit, and another, thicker gravel. The molluscs from the snail lens dated to 191 ± 39 ka, which correlates with the MIS 7/6 boundary. Thus, two distinct lacustrine deposits occur in Johanna's Section, with the intervening gravels possibly correlating with MIS 6.

At Snail Trail 1, in a small tributary wadi west of Johanna's Section, the molluscs contained 2.29 ppm U (Table 4c), more than the molluscs from any other site in this part of Midauwara, and they also had a much higher accumulated dose, 108 ± 5 Grays, than those from Big Snail Gully, the upper section at Johanna's Section or Snail Trail 3 (see below). The age for Snail Trail 1's molluscs, 129 ± 14 ka, appears to correlate well with the MIS 6/5e boundary. Given the other dates for snail units in this area, this sampling site falls stratigraphically between the upper and lower units at Johanna's Section.

At Snail Trail 3, which lies just a short walk from Snail Trail 1, a surface collection was made to test if the snails weathering out there represented more than one population. Two grab samples from the molluscs there yielded statistically identical ages, which averaged 103 ± 7 ka (Table 4d). This age, which correlates with MIS 5d, also agrees well with the age for Big Snail Gully (below) and the upper section at Johanna's Section.

At ~ 360 m amsl in the Big Snail Gully site (Table 4e), several units are exposed on the cliffs at a meander in the tributary wadi. About 3 m above the tributary floor and some 4 m below tufa cap on the cliff top, a horizon extremely rich in snails occurs, sandwiched between silts that contain only a few snails. As noted above, all the samples yielded consistent ages, averaging 100 ± 3 ka, which correlates well with MIS 5d. The snail shells here were the largest seen anywhere in the study area. Their size and abundance coupled with the geological evidence hints that the snails lived a nutrient-rich lake that likely persisted for several thousand years, probably with deeper water than the other ponds seen at Midauwara (*9*, *18*, *21*, *22*).

Given the similarity in dates for Big Snail Gully, Snail Trail 3, and the upper section at Johanna's Section, these three sites likely lie on the northern of a large lake that supported a healthy molluscan community and persisted in this area possibly for close to 10 ky during MIS 5d. The southern margins of the lake have not yet been found. This lake in MIS 5d, however, was evidently distinct from two older lakes that occurred in the same area during MIS 6/5e (Snail Trail 1) and MIS 7/6 (Johanna's Section lower unit).

The Railway Outcrops, Midauwara

Several snail-rich layers have been discovered thanks to sections exposed by the railway line. Quarrying for materials to build the railway, which is now not used, excavated several deep sections on both the east and west side of the route, but also destroyed or altered other outcrops. Three outcrops were sampled along the railway. The tufa-capped exposures to the west of the railway represent the type sections for a paleolake described by Smith and Kieniewicz (*18*, *31*, *32*, *48*).

On the west side of the railway, Railway 1 contained several snail lenses separated by massive silts that dipped to the south, where bulldozers or deflation had removed aggregate, probably for construction. Nine samples from three different layers within Railway 1 all had very low U concentrations, ranging from 0.05 to 0.51 ppm. Although RM49 and RM41 were sampled from respectively above and below the snail lens that produced all the other ages, all nine samples yielded very similar accumulated doses (Table 4f). No color differences or differential weathering occurs here to suggest that these three layers have suffered any mixing. Moreover, the whole sequence appears to have been deposited rapidly. Therefore, the snail lens in this outcrop dates to 134 ± 8 ka, which correlates with a warmer blip in late MIS 6 or very early MIS 5. Stratigraphically, this age agrees well with the ^{230}Th/^{234}U age of 126 ± 8 ka for the tufa cap on this outcrop (*6*). Approximately 6-7 m below to the southwest, a tanged point had weathered from a bulldozer cut. These two ages represent the only dates directly associated with any Aterian material in the Eastern Sahara.

On the north face of same sediment remnant, Railway 2 was exposed just to the north of Railway 1. The stratigraphic relationship between the two outcrops has not yet been examined. The only sample analyzed thus far from Railway 2 dated at 71 ± 12 ka (Table 4g). Assuming that the snails here have not been reworked, this site correlates with MIS 4 or possibly, MIS 5a.

To the southeast of Railway 1, Railway 3 was exposed on a small isolated tufa-capped outcrop on the east side of the railway. At Railway 3, as discussed above, the molluscs in the unit probably constitute a temporally mixed sample, with an older more weathered population averaging 34 ± 3 ka, and a younger one, at 25 ± 2 ka (Table 4h). With mixed samples, however, caution urges that the actual ages for the subpopulations can easily be skewed by including a few more or a few less from each shell group. The age similarity argues, however, that the two populations are probably not very different in age, and likely date to MIS 3 and 2 respectively.

The ages here suggest that at least three lakes existed here at different times during the late Pleistocene. The railway may follow a wadi tributary that ran southward through this area for many millennia. If so, the sections may represent a series of cut and fill structures along the route.

The Main Wadi Edge Outcrops, Midauwara

Along the main wadi draining the mound to the east of the main mound, several sites were discovered just 1-2 m below the edge of the tufa mound surface. These include Wind Wadi and New Site 2.

At Wind Wadi, a site located high on the cliffs along the north rim of the main wadi, just as it swings from trending southward toward the west, a snail-bearing tufa was discovered approximately 2 m below the cliff edge. KAR31 collected here was subsampled three times in grab samples (Table 4i). The three accumulated doses are significantly different, as are the ages they produced. The ages range from 112 ± 11 to 63 ± 6 ka, suggesting that at least two populations occur here. The median age of 82 ± 7 ka may result from mixing the two populations, and may not represent a time when water was actually present. Thus, all the samples likely contain a mixture of younger and older shells. Most likely, a thin deposit of snails dating to MIS 5d or 5e, if not older, is overlain by a thin deposit of much younger snails possibly dating to MIS 3 or MIS 4. Given the mixing that seems to occur here, definitively dating this locality requires that the snail lens on the cliff face here be sampled more finely, which unfortunately is unlikely to occur in the near future. Nonetheless, the snails lived in standing water, hinting that water sat here at $\lesssim 112$ ka and $\lesssim 63$ ka.

New Site 2 also sits on the rim of the main wadi, slightly west of Wind Wadi, about 1-1.5 m below the surface of the tufa. Capped by a tufa unit, a snail lens extended along the outcrop for a few metres. One analysis from New Site 2 yielded 53 ± 16 ka (Table 4j), which correlates with early MIS 3. This age also agrees within errors with the possible age for the younger age component at Wind Wadi, which very close to this site.

Thus, along the southeastern rim of the main wadi, the ESR dates suggest that a small lake sat here in early MIS 3 or possibly late MIS 4. At Wind Wadi, the older mollusc community suggests that an older lake was present at least 112 ka, and possibly earlier.

The Parking Lot Basin Outcrops, Midauwara

The Parking Lot Basin outcrops all occurred within or on the edges of a single deflated basin about 150 m across formed by a blowout, just southeast of the main highway and northwest of the railway line and the Railway outcrops. This basin may represent a small lake in which deposition continued intermittently for some time. The basin is rimmed by thick silt units capped by tufas. Exposed by bulldozing, a gravel in the deepest part of the basin contains redeposited Early Stone Age bifaces. Similar bifaces have also been recovered where they eroded from silt units in the basin margins.

Samples were collected *in situ* on the northeastern and northwestern basin margins at several spots and within the basin's centre at outcrops that had been exposed by the blowout. There appear to have been snail layers at several different elevations throughout this basin. Without the intervening units to connect them, however, establishing their interrelationships must rely on their ages. None appear to relate to the oldest units.

At Carpark 2, a single analysis yielded a date of 83 ± 6 ka (Table 4k), which correlates with MIS 5a, or possibly, MIS 5b. This age agrees within errors with that for the snail lens at Railway 2 (see above). Because the Railway 2's silt units appear to trace laterally into Parking Lot Basin, these may represent deposits from the same lake. Given the complexity and modifications to the intervening areas, however, they could be penecontemporaneous deposits from different lakes. Only further analyses of intervening outcrops may solve this question.

At Bonnie Carpark (Table 4l), several samples were collected from a surface outcrop of a unit where snails were weathering out. As noted above, KAR102 was mixed, and suggests that multiple populations exist here all probably dating to the late Pleistocene.

At the central mound in Parking Lot Basin (Table 4m), a layer of snails in a lightly cemented silt outcropped on the surface. A surface scatter of snails appeared to have weathered out from the mound. Samples were collected from the mound itself, and from the surface. Two samples (KAR23a, KAR23b) were collected specifically as mixed samples to test if the ages differed. With 75% *in situ* snails, KAR23a (RM46) gave an age of 51 ± 5 ka, while the four KAR23b samples, which had about 40% *in situ* snails, averaged 34 ± 2 ka. If one assumes that only two populations exist in the mound, one that dates when the deposit formed, and an older population that was reworked into the deposit from an older outcrop eroding in the area, and if the youngest date calculated for the mound, namely that for RM48 (KAR21) at $\sim 14 \pm 8$ ka, really is the youngest possible age for the younger of the two populations at the mound, then one can derive a mathematical equation for the mixing line for these two populations. Solving that equation to derive the age for the older population gives an age of $\sim 64 \pm 8$ ka, which correlates with MIS 4. Of course, the younger population could be younger than 14 ka, which would then mean that the older population would exceed 64 ka. Thus, these ages represent the maximum age for the younger population, and the minimum age for the older population. Therefore, if only two populations occur at the mound, likely its snails date to both MIS 4 and late MIS 2-early MIS 1.

On the NW basin edge in a channel that had been eroded to the west from central basin, a snail layer outcropped about 3 m from the surface. This single sample yielded an age of 34 ± 2 ka (Table 4n). An uncalibrated AMS ^{14}C date for an ostrich egg shell found in float eroding from the middle silt bench dated at 34.1 ± 0.3 ky BP (TO-9970) also suggests that water must have been present in this area at ~ 34 ka in late MIS 3.

Therefore, Parking Lot Basin had small lakes at three or more distinct times in the Late Pleistocene. Whether the lakes that likely date to MIS 4, 3, and 2 were part of a lake that persisted throughout this time, or to several different lakes that reoccupied the basin remains to be determined.

Three Balls Basin

New Site 1 lies on the edge of a small tributary wadi in Three Balls Basin, west of the railroad. A snail lens extended along the outcrop for a few metres, capped by a tufa unit. New Site 1 gave a single age of 60 ± 16 ka (Table 4o), which correlates with the MIS 4/3 boundary. This also agrees within errors with the date for the older age component at the Parking Lot Basin central mound. This hints that water might have existed at the same time in both Parking Lot Basin and Three Ball Basin. More dates are needed to understand the stratigraphy within Three Balls Basin and to confirm these correlations.

The Late Pleistocene: Matana and Bulaq

At both Bulaq and Matana, tufa hugs the Libyan Escarpment rim north of Midauwara. Tufas have built much thinner mounds that cover much less area than Midauwara.

Blackwell *et al.* (*27*) provided a detailed site description for Matana. At both Matana 2 and 3, snails were recovered from snail lenses capped by tufa deposits. At Matana 3, the two samples averaged 65 ± 4 ka (Table 4p), which correlates with mid MIS 4. At Matana 2, however, the two dates averaged 28 ± 2 ka (Table 4q), which correlates with the MIS 3/2 boundary.

Bulaq sits on the escarpment edge between Matana and Midauwara. At the Bingo outcrop, a snail layer > 10 m long, crops out ~ 2 m below the modern surface at an elevation of ~ 160 m amsl. To the east, the silt units are capped by a tufa, but whether the snail bearing deposit was ever capped remains unclear. There might have been a small open pond that formed in a depression eroded into the tufa. This unit may be contemporaneous with settlements of stone-block structures found on the escarpment just to the north by Caton-Thompson (*29*), which were rediscovered in 2011. The age for the snails at 24 ± 3 ka (Table 4r) correlates with a colder time, but not the glacial maximum, within MIS 2. Given this age, this site may also be contemporaneous with the younger spring deposit found at Matana 2 (*27*) and possibly, with the younger snail population occurring in the Parking Lot Basin central mound.

Conclusions

At Kharga, the tufa and lacustrine units clearly show that water has been more abundant in the past than now. Given the snail ages, standing water was available during several periods in the Pleistocene (Figure 3; Table 5). At Lazy Beach 1, in the earliest Pleistocene at ~ 2.4 ka during Marine Isotope Stage (MIS) 87, fresh lake water captured and deposited lacustrine silt. At several times, pulses of lake activity occur in diverse locations. For example, in MIS 5d at 112-100 ka, Big Snail Gully, Johanna's Section, and possibly Wind Wadi all had standing fresh water present during at least part of this time range. During MIS 4 at 65-60 ka, standing fresh water sat at Matana 3, New Site 1, and possibly, at Parking Lot Basin, and Wind Wadi. In MIS 3, at ~ 35-34 ka, another pulse seems to have deposited snails at Matana 2, Bulaq Bingo, and Railway 3. For all the times with multiple penecontemporaneous lakes, global oceanic $\delta^{18}O$ values sat very close to 0. Interestingly, no dates occur for the coldest times throughout MIS 6, a strongly glacial phase, while only two fall within the colder parts of MIS 2, when oceanic $\delta^{18}O$ values are ~ -0.8 and the glaciers were well advanced in the Northern Hemisphere. Instead, the ages appear to agree best with the cusps between major glacial/interglacial swings, such as times when the global climate was warming up toward MIS 5e or was cooling down from MIS 5e. A couple of ESR dates suggest standing water in MIS 5e, but not when oceanic $\delta^{18}O$ values are ~ 1, but rather during slightly colder periods when oceanic $\delta^{18}O$ values approached 0 (Figure 3). That Kharga today sees no rainfall most years, when modern oceanic $\delta^{18}O$ values hover near 0.9, also supports this correlation. For the tufas, some $^{230}Th/^{234}U$ dates by Smith *et al*. (*5*), Kleindienst *et al*. (*11*), and Abdel-Monem *et al*. (*51*) (Table 1) suggest that spring water was flowing during the warmest phases in MIS 5e, 7, and 9 (*1*, *5*, *11*, *16*), but the lack of molluscs in most of these tufas hints that the water may have been a bit too saline or too limited in quantity to allow snails to thrive. Tufas, however, do not need long-term standing freshwater to grow, merely some periodic spring seepage from the aquifer, unlike the molluscs in the lacustrine silt units. Several other tufas gave ages that fall within the same periods as the ESR ages for the snails, namely during MIS 3, 4, and 5a-5d (see references in Table 1).

While these data indicate that standing water occurred at particular times, they cannot distinguish what percentage of that water came directly from local rainfall. Although most of the water probably did come from meteoric precipitation falling at Kharga Oasis, thus keeping the lakes fresh enough for snails to grow, undoubtedly, some water that fed these lakes derived from the local aquifer that drained the Libyan Plateau. Without that aquifer seepage, no tufa could have grown on the Escarpment rim (*1*, *2*, *5–8*). Smith *et al*. (*5*) argued that the MIS 5 tufa likely derived from higher rainfall events. While the local aquifer water comes from rainfall on the plateau, its groundwater residence time could range up to a few thousand years. Hence, a high rainfall event on the Libyan Plateau might not actually appear at the springs that fed the tufa mounds until a few tens of, to a few thousand, years later. That Midauwara and El Refûf continued to have surface springs until the mid-20th century, despite the very low rainfall that currently falls in the area argues that the surface aquifer has residence times of several decades to centuries at least (*49*). For purposes of this discussion, any

uncertainty introduced by this delay is less that most of the quoted uncertainties in Tables 4 and 5 and thus does not materially affect the conclusions. The ESR dates for the silt units here clearly show that standing water occurred more frequently and in more locations during the latter half of MIS 5 and MIS 3. The data also show, however, that water occurred in MIS 4 and the early and late parts of MIS 2, albeit not at the coldest times of the latter.

That water is present in MIS 2 supports the "glacial = pluvial" hypothesis, but the water occurring in MIS 7 and 5 agrees with predictions from the "interglacial = pluvial" hypothesis. Certainly, the size of the snails at Big Snail Gully at 100 ± 4 ka hints at a long-lived deep lake that likely would only be sustained with both frequent rainfall and groundwater flow. From the dates here, the lakes appear to be much more likely to exist extensively when the global climate was neither strongly glacial nor strongly interglacial. ESR dates still to be completed for El Refûf, other locations at Midauwara, at several locations at Dakhleh Oasis and Bir Tarfawi may help to confirm this finding.
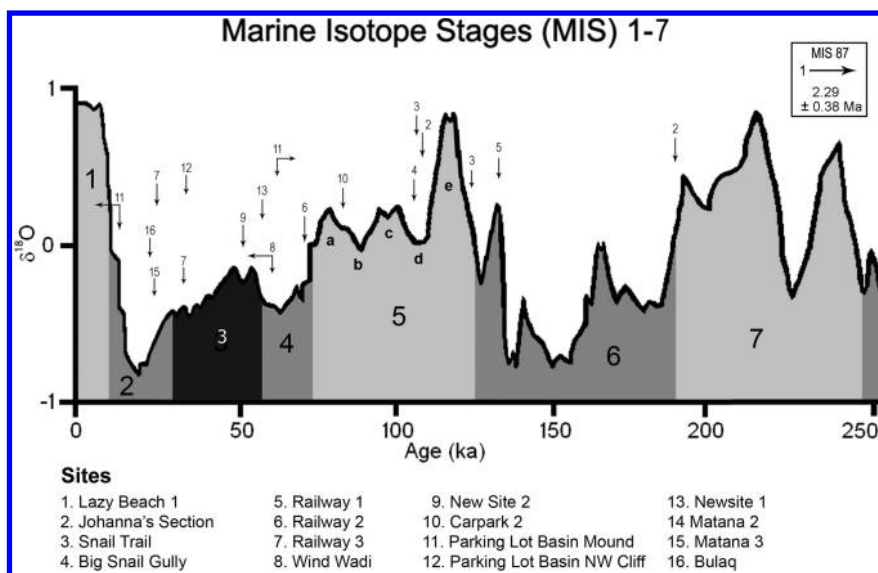
Figure 3. Snail dates and the times for standing water at Kharga Oasis. Snail dates show that standing water was present at Kharga Oasis during Marine Isotope Stage (MIS) 87 in the early Pleistocene. Water was also present at many localities during MIS 5e, 5d, and 5a, as well as during MIS 4, 3, and 2. When multiple penecontemporaneous lakes occurred, global oceanic δ¹⁸O values sat very close to 0. Thus, the lakes appear to have occurred in more locations when the global climate was neither strongly glacial nor strongly interglacial.

Table 5. Age Summary, Kharga Oasis

Sampling Location	ESR Age (ka)	Marine (Oxygen) Isotope Stage[1]
Lazy Beach I	2288 ± 381	87
Lower unit, Johanna's Section	191 ± 39	late 7 (6)
Railway 1	134 ± 8	6 (5e)
Snail Trail	128 ± 15	6/5e
older population Wind Wadi	≲ 113 ± 11	5d (5e) or older?
Upper Unit Johanna's Section	108 ± 19	5d (5e)
Big Snail Gully	104 ± 5	5d
Carpark 2	83 ± 6	5a (5b)
Railway 2	71 ± 12	4 (5a)
Matana 3	65 ± 4	4
older population Parking Lot Basin	≲ 64 ± 8	4 (3) or older?
younger population Wind Wadi	≲ 63 ± 6	4 (3) or younger?
New Site 1	60 ± 16	3/4
New Site 2	53 ± 16	3 (4)
weathered snails, Railway 3	34 ± 3	late 3
NW Cliff Parking Lot Basin	34 ± 2	4 (3) or older?

Table 5. (Continued). Age Summary, Kharga Oasis

Sampling Location	ESR Age (ka)	Marine (Oxygen) Isotope Stage[1]
Matana 2	28 ± 2	3/2
unweathered snails, Railway 3	25 ± 2	2
Bulaq Bingo, Railway 3	24 ± 3	2
younger population Parking Lot Basin	≲ 14 ± 8	2 or younger?

[1] Notation:

a/b: age sits at the Stage *a* and *b* boundary,

d (*c*): *d* = the likely stage,

c = possible stage given the uncertainties

Until the last century, some surface springs, including those at El Refûf and Midauwara on the camel-train routes, did flow in Kharga Oasis, if not as abundantly as in the past. Intensive agricultural activity has now dropped the watertable and the recharge rate significantly, with the watertable dropping at ≥ 0.1-2.2 m/y. The Romans had to abandon the Egyptian Oases when they could no longer reach the water to irrigate (*49*). Predictions suggest that within 2-3 decades, the modern Egyptians will again have to abandon the Oases, when the watertable drops below the pumpable limit.

Acknowledgments

References

1. Smith, J. R.; Hawkins, A. L.; Asmerom, Y.; Polyak, V.; Giegengack, R. *J. Hum. Evol.* **2007**, *52*, 690–701.
2. Hawkins, A. L.; Smith, J. R.; Giegengack, R.; McDonald, M. M. A.; Kleindienst, M. R.; Schwarcz, H. P.; Churcher, C. S.; Wiseman, M. F.; Nicoll, K. *Nyame Akuma* **2001**, *55*, 8–14.
3. Osmond, J. K.; Dabous, A. A. *Quat. Res.* **2004**, *61*, 85–94.

4. Adelsberger, K. A.; Smith, J. R. *Catena* **2010**, *83*, 7–22.

5. Smith, J. R.; Giegengack, R.; Schwarcz, H. P. *Palaeogeogr., Palaeoclimatol., Palaeoecol.* **2004**, *206*, 157–175.

6. Smith, J. R.; Giegengack, R.; Schwarcz, H. P; McDonald, M. M. A.; Kleindienst, M. R.; Hawkins, A. L; Churcher, C. S. *Geoarchaeology* **2004**, *19*, 1–34.

7. Nicoll, K.; Giegengack, R.; Kleindienst, M. R. *Geoarchaeology* **1999**, *14*, 849–863.

8. Nicoll, K.; Giegengack, R.; Kleindienst, M. R. *Geoarchaeology* **2001**, *16*, 47–64.

9. Churcher, C. S.; Kleindienst, M. R.; Schwarcz, H. P. *Palaeogeogr., Palaeoclimatol., Palaeoecol..* **1999**, *154*, 301–312.

10. Mandel, R. D.; Simmons, A. H. *Geoarchaeology* **2001**, *16*, 95–117.

11. Kleindienst, M. R.; Schwarcz, H. P; Nicoll, K.; Churcher, C. S.; Frizano, J.; Giegengack, R.; Wiseman, M. F. In *The Oasis Papers 2: Proceedings of the Second International Conference of the Dakhleh Oasis Project*; Wiseman, M. F., Ed.; Oxbow Books: Oxford, 2008; pp 25−54.

12. Kleindienst, M. R.; Smith, J. R.; Adelsberger, K. A. *Nyame Akuma* **2009**, *71*, 18–30.

13. McDonald, M. M. A. *Afr. Arch. Rev.* **2009**, *26*, 3–43.

14. McDonald, M. M. A. In *Prehistory of Northeastern Africa: New Ideas and Discoveries*; Kabacinski, J., Chlodnicki, M., Kobusiewicz, M., Eds.; Miuzeum Archeologiczne w Poznaniu: Posnan, 2012; pp 307−322.

15. Blackwell, B. A.; Schwarcz, H. P. *Dating Methods for Quaternary Deposits*; *GEOText* 2; Geological Association of Canada: St. John's, NL, Canada, 1995, pp 167−208.

16. Nicoll, K.; Schwarcz, H. P; Kleindienst, M. R.; Wiseman, M. F.; Frizano, J.; Giegengack, R. *GSA Abstracts with Programs* **1997**, *29*, A-319–A-320.

17. Smith, J. R. In *Modern Origins: A North African Perspective*; Hublin, J.-J., McPherron, S. P., Eds.; Springer: Dordrecht, 2012; pp 35−47.

18. Kieniewicz, J. M. Pleistocene Pluvial Lakes of the Western Desert of Egypt: Paleoclimate, Paleohydrology, and Paleolandscape Reconstruction, Ph.D. Thesis, University of Washington of St. Louis, St. Louis, MO, 2007, 271 pp.

19. McDonald, M. M. A. In *The Oasis Papers 3: Proceedings of the Third International Conference of the Dakhleh Oasis Project*; Bowen, G. E., Hope, C. A., Eds.; Oxbow Books: Oxford, 2003; pp 43−69.

20. Neumann, K. *Afr. Arch. Rev.* **1989**, *7*, 97–116.

21. Nicoll, K. Holocene Playas as Sedimentary Evidence for Recent Climate Change in the Presently Hyperarid Western Desert, Egypt, Ph.D Thesis, University of Arizona, Tucson, AZ, 1998, 290 pp.

22. Nicoll, K. *Quat. Sci. Rev.* **2004**, *23*, 561–580.

23. Ritchie, J.-C.; Haynes, C. V. *Nature* **1987**, *330*, 645–647.

24. Gardner, E. W. *Q. J. Geol. Soc. London* **1935**, *91*, 479–518.

25. Churcher, C. S.; Kleindienst, M. R.; Wiseman, M. F.; McDonald, M. M. A. In *The Oasis Papers 2: Proceedings of the Second International Conference of the Dakhleh Oasis Project*; Wiseman, M. F., Ed.; Oxbow Books: Oxford, 2008; pp 1−24.

26. Blackwell, B. A. B. *Acta carsol.* **2006**, *35*, 123–153.

27. Blackwell, B. A. B.; Skinner, A. R.; Mashriqi, F.; Deely, A. E.; Long, R. A.; Gong, J. J. J.; Kleindienst, M. R.; Smith, J. R. *Quat. Geochron.* **2012**, *10*, 430–435.

28. Caton-Thompson, G; Gardner, E. W. *Geogr. J.* **1932**, *LXXX*, 369–406.

29. Caton-Thompson, G. *Kharga Oasis in Prehistory*; Athlone Press: London, 1952; 213 pp.

30. Smith, J. R.; Giegengack, R. In *The Oasis Papers 3: Proceedings of the Third International Conference of the Dakhleh Oasis Project*; Bowen, G. E., Hope, C. A., Eds.; Oxbow Books: Oxford, 2003; pp 103−112.

31. Kieniewicz, J. M.; Smith, J. R. *Quat. Res.* **2007**, *68*, 341–344.

32. Kieniewicz, J. M.; Smith, J. R. *GSA Bull.* **2009**, *121*, 1154–1171.

33. Aboulmagd, A.; Sultan, M.; Milewski, A.; Kehew, A. E.; Sturchio, N. C.; Soliman, F.; Krishnamurthy, R. V.; Cutrim, E. *Palaeogeogr., Palaeoclimatol., Palaeoecol.* **2012**, *329-330*, 137–149.

34. Skinner, A. R. *Quat. Sci. Rev.* **1988**, *7*, 461–464.

35. Blackwell, B. A. B. In *Tracking Environmental Change Using Lake Sediments, Vol. 1: Basin Analysis, Coring, and Chronological Techniques*; Last, W. M., Smol, J. P., Eds.; Kluwer: Dordrecht, 2001; pp 283−369.

36. Molod'kov, A. *Appl. Radiat. Isot.* **1993**, *44*, 145–147.

37. Deely, A. E.; Blackwell, B. A. B.; Mylroie, J. E.; Carew, J. L.; Blickstein, J. I. B.; Skinner, A. R. *Radiat. Meas.* **2011**, *30*, 1–7.

38. Skinner, A. R.; Shawl, C. E. ESR dating of terrestrial Quaternary shells. *Quat. Geochron. (Quat. Sci. Rev.)* **1994**, *13*, 679–684.

39. Blackwell, B. A. *Laboratory Procedures for ESR Dating of Tooth Enamel*; McMaster University Department of Geology Technical Memo 89.2; 1989, 234 pp.

40. Blackwell, B. A. In *Dating Methods for Quaternary Deposits*; GEOText 2; Rutter, N. W., Catto, N. R., Eds.; Geological Association of Canada: St. John's, NL, Canada,1995; pp 209−251.

41. Blackwell, B. A. B.; Skinner, A. R.; Blickstein, J. I. B.; Montoya, A. C.; Florentin, J.; Baboumian, S. M.; Ahmed, I. J.; Deely, A. E. *Annu. Rev. Earth Planet. Sci.* **2013**in review.

42. Brennan, B. J.; Rink, W. J.; McGuirl, E. L.; Schwarcz, H. P. *Radiat. Meas* **1997**, *27*, 307–314.

43. Blackwell, B. A. *Quat. Geochron. (Quat. Sci. Rev.)* **1994**, *13*, 651−660.

44. Patnaik, R.; Chauhan, P. R.; Rao, M. R.; Blackwell, B. A. B.; Skinner, A. R; Sahni, A.; Chauhan, M. S.; Khan, H. S. *J. Hum. Evol.* **2009**, *56*, 114–133.

45. Kleindienst, M. R.; Smith, J. R.; Adelsberger, K. A. *Nyame Akuma* **2009**, *71*, 18–30.

46. Ferring, R.; Oms, O.; Agusti, J.; Berna, F.; Nioradze, M.; Sheila, T.; Tappen, M.; Vekua, A.; Zhvania, D.; Lordkipanidze, D. *Proc. Natl. Acad. Sci. U.S.A.* **2011**, *108*, 10432–10436.

47. Bar-Yosef, O.; Belfer-Cohen, A. *Quat. Int.* **2001**, *75*, 19–28.

48. Smith, J. R. Geoarchaeology, Stable Isotope Chemistry and Geochronology of Fossil Spring Tufas, Western Desert, Egypt, Ph.D. Thesis, University of Pennsylvania, Philadelphia, PA, 2001, 180 pp.

49. *Hydrogeology of Deep Aquifers in the Western Desert and Sinai*; Report No. 10; Water Policy Reform Program, Ministry of Public Works & Water Resources, U.S. Agency for International Development, 1998, 108 pp.

50. Sultan, M.; Manocha, N.; Becker, R.; Sturchio, N. C. In *American Geophysical Union Spring Meeting Abstracts*; 2004, *1*, 03.

51. Abdel-Monem, A. A.; Hassan, G. M.; Elssa, H. M.; El-Sankary, M. M.; Abdel-Razek, Y. A; El-Morsy, M. *Egypt. J. Biophys.* **2006**, *12*, 59–76.

Chapter 20

Laser Ablation–Inductively Coupled Plasma–Mass Spectrometry (LA-ICP-MS) Analysis of Refired Glass Pendants from the North American Upper Great Lakes

Heather Walder[*]

Department of Anthropology, University of Wisconsin−Madison, Madison, Wisconsin 53706
[*]**E-mail: hwalder@wisc.edu**

Indigenous people of the Upper Great Lakes region of North America crushed and refired glass trade beads to produce new adornment forms during the late 17th and 18th centuries. Laser ablation–inductively coupled plasma–mass spectrometry (LA-ICP-MS) was used to assess the chemical composition of refired glass pendants and refired fragments from four archaeological sites, as well as glass beads from these and other sites in the region. The data reflect both glass recipes used in Old World glass manufacturing processes and an individual Native American person's raw material choices for refired glass pendant production. Glass of similar chemical composition recovered from different places may demonstrate trading relationships among archaeological sites. Similarities between beads and pendants from the same archaeological site may indicate that people were producing pendants on-site using available beads as raw material, rather than receiving beads and pendants from separate trade sources.

Problem Orientation

In the North American Upper Great Lakes region during the 17th and early 18th centuries, a complicated network of trade routes and social relationships intertwined Indigenous peoples, displaced Native newcomers, and European explorers, traders, and missionaries. The interactions among these diverse peoples are materially reflected in the exchange of European-made items such as copper and brass kettles, glass trade beads, cloth, firearms, and other commodities. Indigenous people often treated these items as "raw materials" that could be transformed by applying existing and innovative technological practices. For example, copper kettles often were cut apart and reshaped to produce rolled metal beads or other adornment objects. Glass trade beads, produced in European workshops in Amsterdam, Venice, Paris, and elsewhere (*1*), also sometimes served as raw material for ornament production. In previous ethnohistoric and archaeological studies, scholars have suggested Plains peoples, particularly the Arikara who lived along the Missouri River, specialized in a process of powdering, shaping, and refiring glass beads to make trapezoidal blue glass pendants (*2*). These people then traded the finished pendants eastward into the Midwest through down-the-line exchange mechanisms (*3*, *4*).

In this paper, I test this argument by examining evidence for on-site pendant production at locations in Wisconsin and Michigan by 1) identifying specific kinds of blue glass trade beads that could have been used to produce the pendants 2) comparing the chemical composition of refired glass pendants and fragments to intact glass beads from sites in this region and 3) examining archaeological collections for tools or waste from pendant production. I have previously demonstrated that in the Upper Great Lakes region, beads of the same style from the same archaeological site tend to be compositionally more similar to one another than the same style of beads from other sites, possibly indicating that each site's inhabitants had access to different European bead sources or trading partners (*5*). Chemical similarities between beads and refired glass artifacts from the same site, along with glass residue on several metal fragments support the hypothesis that that on-site pendant production took place in the Upper Great Lakes region in at least one location. The data generated from this project will be useful for making comparisons to other regions of North America, with the goal of refining the chronology and trading relationships of archaeological sites where blue beads and pendants are recovered, in addition to clarifying the techniques used to produce ornaments.

Methods

Artifact Selection and Sampling

Glass artifacts selected for LA-ICP-MS constitute one part of a larger dissertation data set developed to refine chronology and migration patterns for Native Americans in the 17th and 18th centuries in the Upper Great Lakes region. This data set consists of 422 samples of blue glass artifacts relevant to this study, including 11 pendants and refired glass fragments recovered from four different

archaeological sites in the research area (Figure 1). Most pendants are opaque, trapezoidal in shape and are either a solid turquoise blue or striped with blue and white bands (Figure 2). While some of these artifacts come from inexact or mixed archaeological proveniences, the blue glass beads selected for analysis represent the best understood archaeological features and contexts at each site, so bead samples may serve as temporal and geographic reference points. To clarify the kind(s) of beads that Native Americans selected as raw material for pendant production, the data set includes beads of several different stylistic types in the Kidd ans Kidd typology (*6*). These are tubular, round, and donut-shaped drawn blue beads of types Ia19, IIa31, IIa36/40, IIa46/47, and IIa55/56/57 (Figure 3). See Mason's Color Pl. 1-4 (*7*) for further type examples.
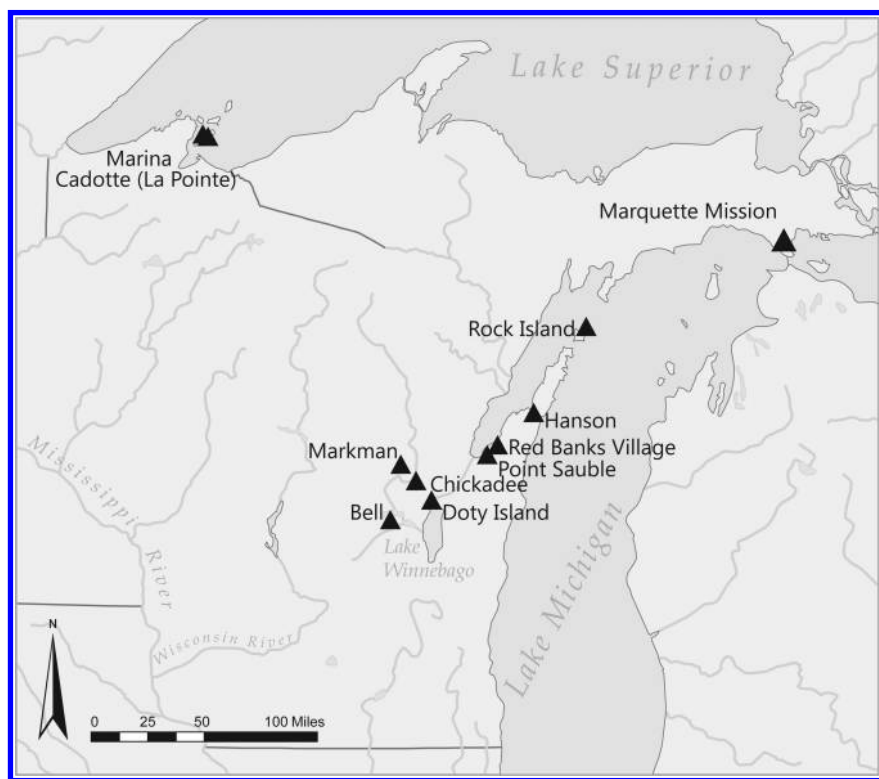
Figure 1. Map of archaeological sites discussed in the text.
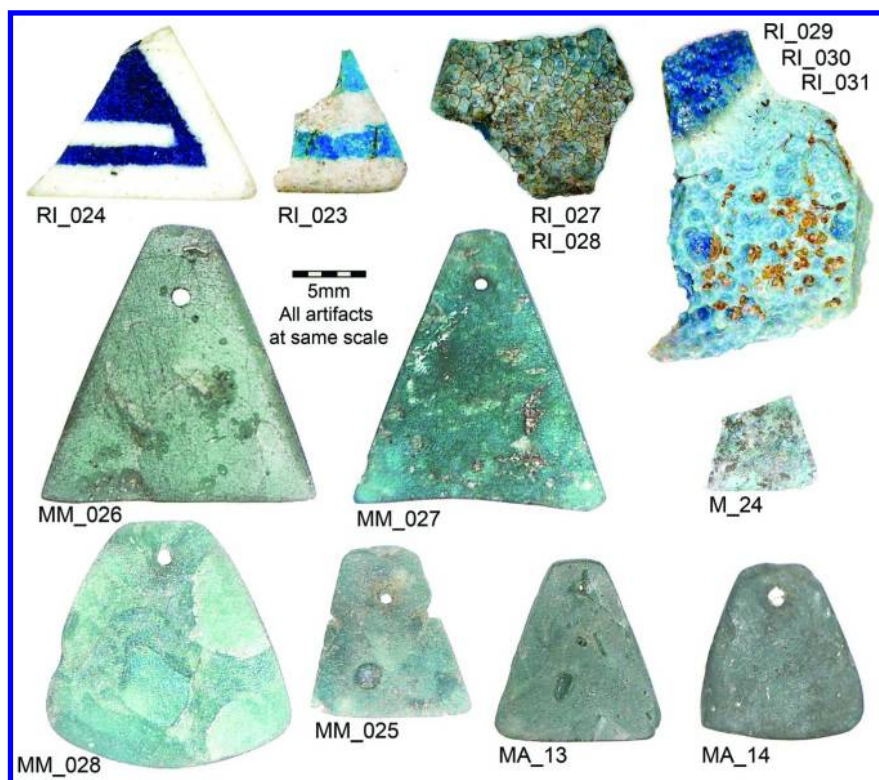
Figure 2. Refired pendants and glass fragments, labeled by Sample ID.

This artifact selection method accounts for the possibility that more than one bead type could have been used as raw material for a single pendant. The ethnohistorically-documented production process requires grinding beads to a powder, re-shaping the powder mixed with water, and heating at temperatures achievable in an open fire until reaching the sintering point of the glass (*2*). Ubelaker and Bass attempted to replicate this process, but only they achieved glass fusion at a temperature of about 1500°C by using a modern kiln. Further experimental replication studies could clarify the process by attempting to sinter the reshaped glass powder using an open-pit fire, capable achieving a maximum temperature of only approximately 1000°C. Whatever the firing temperature, this process would effectively homogenize the original glass recipes of several different European bead types, producing a pendant with a chemical composition that does not exactly match any particular contributing bead.

Refired glass objects examined in the present study were recovered from historic-era contexts on Rock Island, WI (47DR128); Doty Island, WI (47WN30 and 47WN671); surface collections near the Cadotte site on Madeline Island, WI (47AS13), and from the Marquette Mission site near St. Ignace, MI (20MK99). One Rock Island pendant fragment was sampled by selecting two different points on the surface for LA-ICP-MS analysis (RI_027 and RI_028) to determine heterogeneity of the glass. No major differences between the results for the two points are present; therefore, point RI_027 is used as the single representative of this artifact for statistical analysis. Likewise, a partially melted fragment variegated in shades of turquoise and royal blue was sampled in three points in three different color areas in an attempt to provide a chemical explanation for this pattern (RI_029, RI_030, RI_031). This unique artifact is discussed in the high Ca + Fe glass section below.
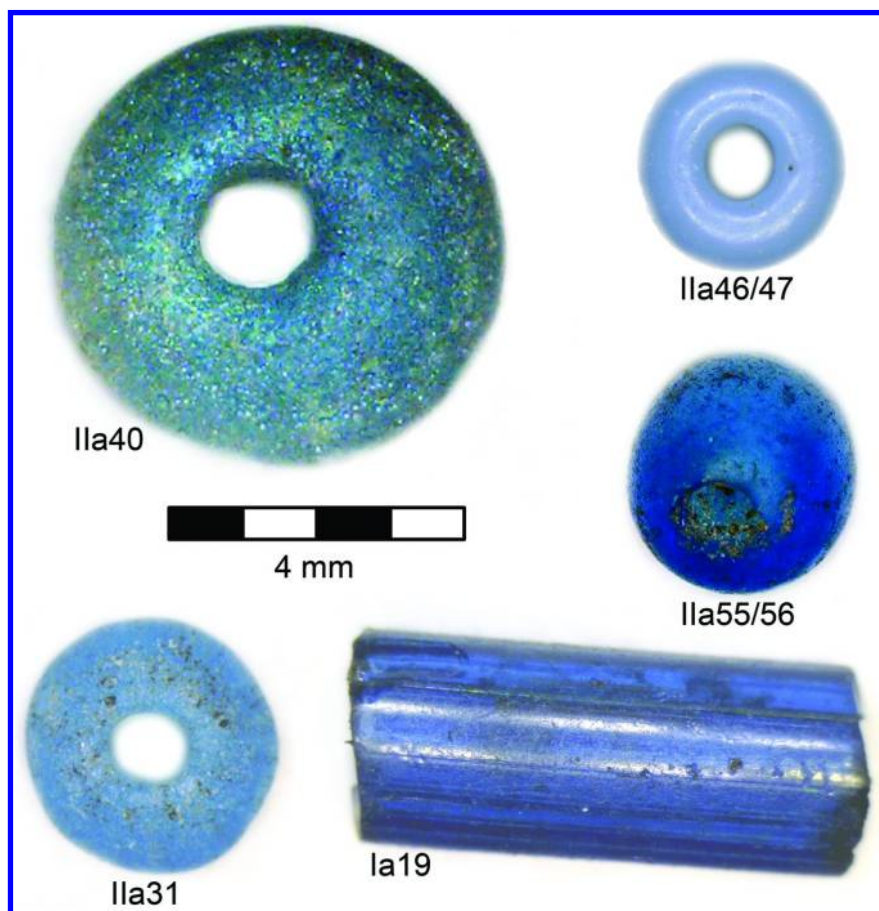
Figure 3. Examples of blue glass trade bead types, labeled according to the Kidd and Kidd classification system.

The comparative glass bead data set includes artifacts from all sites that yielded refired glass, as well as beads from seven additional archaeological sites in Wisconsin: Bell (47WN9), Markman (47WP85), Chickadee (47OU251), Point Sauble (47BR101), Red Banks Village (47BR437), Hanson (47DR185), and Marina (47AS24). All of the study sites date between c. 1640 – c.1770, though some date ranges are approximate. Rock Island is an especially important site because four distinct periods of occupation are stratigraphically defined and can be connected to historically documented activities at that locale (*7*). Table I summarizes the archaeological contexts of the artifacts and reports the number of LA-ICP-MS samples from each site.

Table I. Summary of LA-ICP-MS samples

Site Name	Approx. Dates of Occupation	Refired Glass Samples	Glass Bead Samples	Total LA-ICP-MS Samples
Rock Island Pd. 1	1640s	0	1	1
Rock Island Pd. 2	c.1650	0	6	6
Rock Island Pd. 3	1670 – 1730	0[a]	59	59
Rock Island Pd. 4	1760 – 1770	7[a]	43	50
Doty Island	1680 – 1712	1	74	75
Cadotte (La Pointe)	? – 1670?	2	13	15
Marquette Mission	1671 – 1705	4	115	119
Bell	1680 – 1730	0	34	34
Markman	1660 – 1680?	0	1	1
Chickadee	1600 – 1700?	0	9	9
Point Sauble	1650 – 1700?	0	5	5
Red Banks Village	1630 – 1700s?	0	18	18
Hanson	1640 – 1670	0	18	18
Marina	1665 – 1770	0	12	12
TOTAL		*14*	*409*	*422*

[a] The four refired glass artifacts from Rock Island may date to period 3 or 4; duplicate and triplicate LA-ICP-MS samples were collected for two of these artifacts to assess internal heterogeneity.

Chemical Analysis Methods

The chemical analysis technique applied in this study was laser ablation – inductively coupled plasma – mass spectrometry (LA-ICP-MS), conducted at the Elemental Analysis Facility (EAF) of the Chicago Field Museum, under the supervision of the laboratory manager Dr. Laure Dussubieux. LA-ICP-MS was selected as the analytical method because of its virtually non-destructive analytical procedure and reliable results for glass artifacts. The EAF houses a Varian (now Bruker) inductively coupled plasma - mass spectrometer (ICP-MS) connected to a New Wave UP213 laser for direct introduction of solid samples.

The choice of the parameters of the laser ablation affects the sensitivity of the method and the reproducibility of the measurements, as well as the amount of damage to the sample. To be able to determine elements with concentrations in the range of ppm and below, while minimizing traces on the surface of the sample visible to the naked eye, the EAF protocol uses the single point analysis mode with a laser beam diameter of 55 μm, operating at 70% of the laser energy (0.2 mJ) and at a pulse frequency of 15 Hz. A pre-ablation time of 20 seconds eliminates the transient part of the signal and ensures that possible surface contamination or corrosion does not affect the results of the analysis. For each glass sample, the average of four measurements corrected from the blank is considered for the calculation of concentrations.

To improve reproducibility of measurements, the use of an internal standard is required to correct possible instrumental drifts or changes in the ablation efficiency. The element chosen as the internal standard has to be present in relatively high concentration so its measurement is as accurate as possible. In order to obtain absolute concentrations for the analyzed elements, the concentration of the internal standard has to be known. The isotope silicon-29 was used for internal standardization. Concentrations for major elements, including silicon, are calculated in the oxide form, assuming that the sum of the element oxide concentrations in weight percent is equal to 100% (*8*).

Fully quantitative analyses are possible by using external standards. To prevent matrix effects, the composition of standards has to be as close as possible to that of the samples. Two different series of standards are used to measure major, minor and trace elements. The first series of external standards are standard reference materials (SRM) manufactured by NIST: SRM 610 and SRM 612. Both of these standards are soda-lime-silica glass doped with trace elements in the range of 500 ppm (SRM 610) and 50 ppm (SRM 612). Certified values are available for a very limited number of elements. Concentrations from Pearce et al. (*9*) were used for the other elements. The second series of standards were manufactured by Corning. Glass B and D are glasses that match compositions of ancient glass (*10*). The detection limit ranges from 10 ppb to 1 ppm for most of the elements. Accuracy ranges from 5% to 10% depending on the elements and their concentrations. A more detailed account of the performances of this technique can be found in Dussubieux et al. (*11*).

Data Analysis Methods

The elemental concentration data for 54 elements in each of the 422 glass samples have been examined through the combined use of bivariate scatterplots, cluster analyses (using Ward's method, squared Euclidean distance, cases standardized by Z-scores), and principal component analyses (PCA). Oxide weights of major elements were transformed to elemental ppm by applying the appropriate coefficients, and all data were logged before statistical analyses. PCA proved most useful as a tool to identify elements or groups of elements that had clear differences among glass subtypes in the sample set, which then could sometimes be visualized more simply as bivariate scatter plots. Natural breaks in the data set determine the limits of glass groups identified.

The goal of these analyses was to compare the composition of pendants to that of glass beads, in order to identify the type(s) of beads that may have been used as raw material for pendant production. To determine which beads each pendant most closely resembled, a process of elimination was used to identify and remove non-contributing glass-types from the bead data set. Using PCA and cluster analysis, I identified chemically distinct groups of glass artifacts and the specific glass ingredients that cause these differences, and then progressively eliminated these groups from the bead sample. Identifying these outliers in the data set followed the multi-stage, iterative method recommended by Baxter (*12*), and a combined approach that includes examining bivariate scatter plots along with PCA (*13*, *14*). Specific outcomes of outlier elimination for each pendant glass type are discussed in the next section.

Results

Summary of Results

In the complete set of 422 LA-IC-MS samples, 177 samples were colored with high amounts of Cu, >5000 ppm, while 242 were colored with Co, usually >500 ppm (Figure 4). Three samples from one artifact contained neither colorant, and are discussed in the High Ca + Fe section below.

In general, LA-ICP-MS analysis demonstrates that each pendant sampled has a relatively distinct chemical composition; no two artifacts could be identified as coming from the same "batch" of original bead material. Pendant makers did not select beads for raw material by their chemical composition, but likely by desired color. Chemical differences between beads of the same color and type are not always visible, and so the pendant production process appears to have homogenized beads of different types, producing a chemical signature in pendants that does not match any single bead analyzed. Therefore, the results of this study rely on the process of iteratively removing outlying glass samples until general glass groups emerged, based on relative similarities between bead glass groups and pendants.
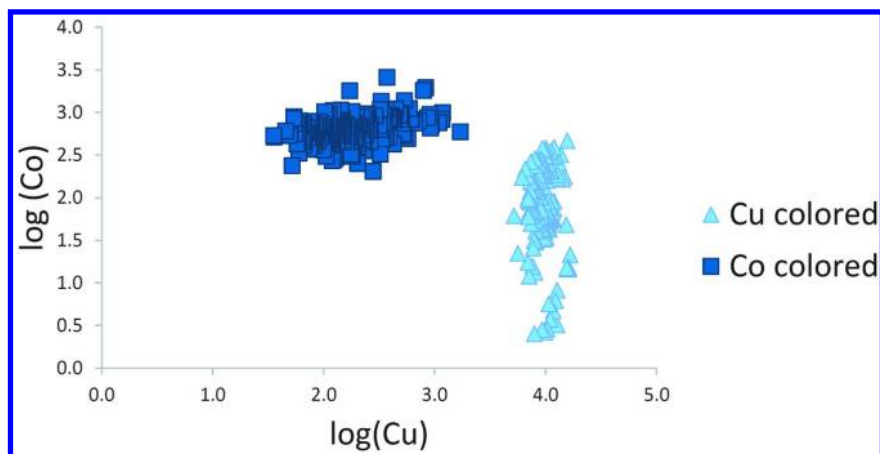
Figure 4. Copper and cobalt bivariate plot of all 422 blue glass samples.

Table II provides a description of each refired artifact as well as the values measured for relevant major, minor, and trace elements. Major elements are presented as weight percent oxides in the upper register while minor elements are presented in parts per million in the lower register. Table III is a summary of identified Co-colored and Cu-colored glass groups, listing the number of beads that fit into these groups and the standard deviation of values within each group. Bead groups are distinguished by one or two elements with concentrations that distinguish them from other beads in the sample (e.g. very high Sb or Zn). The full glass bead data set will be presented in a forthcoming publication.

Table II. Relevant LA-IC-MS results for refired artifacts

Sample ID	Site	Description	SiO₂ %	Na₂O %	MgO %	Al₂O₃ %	P₂O₃ %	K₂O %	CaO %	Fe₂O₃ %	CuO %
M_24	Doty Island	small angular fragment	65.88	13.49	2.95	1.06	0.20	4.28	10.02	0.73	0.90
MA_13	La Pointe (surface)	trapezoidal pendant	64.46	14.71	2.82	1.02	0.48	2.47	10.76	1.01	1.28
MA_14	La Pointe (surface)	trapezoidal pendant	65.20	16.63	2.40	1.23	0.22	2.19	8.87	0.74	1.30
MM_025	Marquette Mission	triangular pendant	66.71	16.61	2.55	1.35	0.26	2.53	6.84	0.37	1.79
MM_026	Marquette Mission	triangular pendant	64.61	10.14	2.96	1.15	0.29	3.62	7.80	0.33	1.36
MM_027	Marquette Mission	trapezoidal pendant	69.60	11.75	2.73	0.98	0.20	5.29	7.01	0.46	1.16
MM_028	Marquette Mission	rounded trapezoidal pendant	66.50	16.83	2.99	1.05	0.24	1.03	9.37	0.43	0.88
RI_023	Rock Island	turquoise section of angular fragment	68.17	14.76	1.25	0.77	0.76	3.76	7.35	0.44	1.46
RI_024	Rock Island	cobalt section of angular fragment	69.01	11.84	1.89	1.22	0.67	3.73	9.72	0.68	0.03
RI_027	Rock Island	Point A of angular fragment	68.74	13.02	1.22	1.33	0.68	4.54	7.73	0.50	1.27

Sample ID	Site	Description	SiO₂ %	Na₂O %	MgO %	Al₂O₃ %	P₂O₃ %	K₂O %	CaO %	Fe₂O₃ %	CuO %
RI_028	Rock Island	Point B of angular fragment	68.49	13.27	1.24	1.17	0.69	4.49	7.62	0.55	1.22
RI_029	Rock Island	partially melted glass, dark blue area	58.99	2.07	4.21	5.10	1.11	2.37	23.01	2.50	0.02
RI_030	Rock Island	partially melted glass, lightest blue	59.86	1.89	4.22	5.05	1.12	2.24	22.65	2.40	0.01
RI_031	Rock Island	partially melted glass, medium blue	59.59	1.89	4.16	5.01	1.11	2.24	22.98	2.43	0.01
Sample ID			Mn (ppm)	Ti (ppm)	Sn (ppm)	Pb (ppm)	Co (ppm)	Zn (ppm)	As (ppm)	Zr (ppm)	Sb (ppm)
M_24			170	222	29	245	89	42	125	18	273
MA_13			343	308	128	1886	68	65	183	10	212
MA_14			639	318	162	858	159	58	185	19	297
MM_025			1465	215	790	676	164	268	489	19	175
MM_026			501	525	13	19372	42	4792	132	80	23759
MM_027			1012	558	7	229	3	3365	0	92	99
MM_028			388	205	225	381	93	46	295	17	221
RI_023			189	118	31	80	57	87	103	11	40

Table II. (Continued). Relevant LA-IC-MS results for refired artifacts

Sample ID			Mn (ppm)	Ti (ppm)	Sn (ppm)	Pb (ppm)	Co (ppm)	Zn (ppm)	As (ppm)	Zr (ppm)	Sb (ppm)
RI_024			776	274	4	1446	642	155	1090	24	712
RI_027			268	154	35	76	34	53	69	18	311
RI_028			276	160	34	82	33	54	57	17	314
RI_029			1718	879	24	425	7	214	15	118	4
RI_030			1697	847	23	381	6	209	17	118	2
RI_031			1747	848	23	391	6	209	14	118	1

Table III. Mean values for identified Co- and Cu-colored glass groups

Group ID	n =	Na$_2$O %	MgO %	Al$_2$O$_3$ %	P$_2$O$_3$ %	K$_2$O %	CaO %	Sn (ppm)	Pb (ppm)	Zn (ppm)	Zr (ppm)	Sb (ppm)
Cobalt colored glass												
High K wood-ash	4	2.26	0.55	1.12	0.36	17.21	12.43	234	514	99	73	237
(+/-)		0.5	0.2	0.3	0.1	1.2	1.1	244	569	32	49	150
high Sb	38	13.07	2.80	1.43	0.56	3.31	9.74	392	2913	83	23	15845
(+/-)		1.3	0.8	0.3	0.4	1.3	0.9	1540	3791	39	9	3723
high Zn (+Co)	2	12.02	1.86	1.03	0.72	4.80	9.12	5	662	763	24	111
(+/-)		1.0	0.1	0.0	0.0	0.1	0.6	2	140	6	2	52
moderate Sn	3	11.89	2.77	1.82	0.25	7.92	8.76	2428	6338	108	49	5
(+/-)		0.7	0.1	0.1	0.0	1.5	0.2	180	1838	27	10	3
moderate Zr	18	13.47	2.76	1.44	0.29	4.26	8.93.	327	1128	148	272	87
(+/-)		1.4	0.3	0.3	0.2	0.8	1.5	306	1906	72	113	242
moderate P	40	11.56	1.74	1.40	1.47	5.31	9.32	10	1924	84	27	427
(+/-)		0.8	0.2	0.3	0.4	0.5	0.7	11	3212	44	9	472
Mg-low-P	71	13.41	3.40	1.68	0.30	2.54	10.60	31	883	67	28	266
(+/-)		1.7	0.4	0.4	0.0	1.0	1.3	88	1798	63	9	269

Continued on next page.

Table III. (Continued). Mean values for identified Co- and Cu-colored glass groups

Group ID	n =	Na₂O %	MgO %	Al₂O₃ %	P₂O₃ %	K₂O %	CaO %	Sn (ppm)	Pb (ppm)	Zn (ppm)	Zr (ppm)	Sb (ppm)
Cobalt colored glass												
P-low-Mg	35	11.85	1.75	1.48	0.68	5.58	9.16	25	2300	91	28	641
(+/-)		1.4	0.2	0.3	0.1	1.3	0.8	28	1821	34	7	575
Copper colored glass												
Pb+Sb+Zn (MM_024)	1	10.76	2.90	1.08	0.25	3.41	7.57	12	13488	4763	75	20239
(no +/-)												
Very high Zn	7	15.80	1.61	1.07	0.18	2.10	5.47	7	390	6503	301	2
(+/-)		0.3	0.0	0.1	0.0	0.0	0.3	2	86	291	7	0
high Zn	2	11.90	2.76	0.91	0.21	5.19	6.98	5	174	4001	86	7
(+/-)		0.0	0.0	0.0	0.0	0.1	0.0	0	5	281	2	0
Sn+Pb+Zn (type IIa40)	10	12.11	2.34	1.17	0.32	7.10	8.54	9405	14571	3349	194	324
(+/-)		1.5	0.2	0.2	0.1	1.7	1.2	3724	11578	827	57	568
low Sn-Pb-Zn (IIa40)	23	16.14	2.26	1.16	0.22	2.88	7.42	284	702	370	32	250
(+/-)		1.6	0.6	0.2	0.1	2.1	1.9	159	1267	886	53	483
P-low-Mg	59	15.07	1.31	0.81	0.78	4.24	7.23	58	337	84	12	178

Copper colored glass												
(+/-)		1.4	0.1	0.1	0.2	0.9	0.5	42	582	48	3	163
Mg-low-P	58	16.29	2.42	1.04	0.22	2.77	7.64	58	437	42	14	171
(+/-)		1.1	0.4	0.2	0.1	0.9	1.1	103	640	20	4	288

High Ca + Fe Refired Fragment

A partially melted glass fragment was recovered from a floor surface context inside a c. 1760 – 1770 Odawa house structure on Rock Island (RI_029, RI_030, RI_031). The refired fragment's surface is pocked by small bubbles, colored in variegated shades of what appears to be turquoise and royal blue. Prior to chemical analysis, archaeologists speculated that the artifact seemed to be a waste product from refired pendant production. However, this artifact does not contain significant amounts of copper (Cu) or cobalt (Co), the two main ingredients used to produce blue color in glass trade beads. It is possible that the relatively high iron (Fe) concentration (2.4% – 2.5% Fe_2O_3) in combination with manganese (MnO 0.2%) produced the blue hues. The high calcium signature of this glass (22.6% - 23.0% CaO) also is unlike any of the blue beads in data set, but a near match was identified in the reference literature (*10*, *15*). The fragment is chemically very similar to an olive green glass wine bottle dated to c. 1750 – 1800 that was analyzed using neutron activation analysis (Brill #502). Table IV presents the mean value for major elements from the three LA-ICP-MS samples from the Rock Island artifact and the Brill #502 bottle glass, demonstrating that all measured oxides common to both samples are similar, within +/- 1.0%. Relative percent difference between the two samples is also presented.

Independent studies of early 17th to mid-19th century wine bottles confirm that high Ca + Fe glass was common for glass containers at this time (*16*, *17*). The refired fragment fits comfortably within Dungworth's chronological "Phase 2" of English high lime-low alkali (HLLA) container glass, dated c. 1700 – 1845 (*18*). HLLA glass has a melting point of approximately 1300° (*16*), which is not generally achievable in an open-pit fire. The partially-melted appearance of the fragment may be result of heating to lower temperatures than necessary to achieve a completely liquid state of the glass. Among the other artifacts recovered from the same mid-18th century Odawa house context are two shards of a blue glass container with bands of color that match the pattern of the refired fragment. The presence of this banding pattern on the refired fragment likely indicates that the container glass was not ground or powdered before heating. Therefore, the refired fragment simply may be a result of trash disposal of broken glass shards in a campfire, rather than an attempt at pendant production. However, likely pendant production waste including glass residue melted onto metal pans was also recovered from this archaeological context, as discussed in the interpretation section below. Further chemical analyses could confirm if the banded blue container shards are also HLLA glass that definitively matches the high Ca + Fe refired fragment.

Table IV. Comparison of high Ca + Fe glass samples to a known glass type

Sample	SiO₂ %	Na₂O %	MgO %	Al₂O₃ %	K₂O %	CaO %	MnO %	Fe₂O₃ %	CuO %
Rock Island High Ca +Fe	59.48	1.95	4.19	5.05	2.28	22.88	0.22	2.44	0.01
Brill #502	59.60	3.28	4.96	4.49	2.54	22.10	0.09	2.36	0.02
+/-	0.1	0.9	0.5	0.4	0.2	0.6	0.1	0.1	0.0
Relative % Difference	-0.2	-40.6	-15.4	12.5	-10.1	3.5	144.1	3.5	-40.7

Co-Rich Soda-Lime Glass

The only refired pendant that was Co-colored is a dark blue and white striped fragment from Rock Island (RI_024). To identify glass types dissimilar to this object, glass beads containing ingredients not found in the pendant in significant quantities have been plotted against each other and in relation to the Co pendant (Figure 5). Mean values for diagnostic elements of glass bead groups are presented in Table III above.

High potassium (K) beads, likely made with wood ash (*19*), were identified (n=4) and removed from the statistical data set (Figure 5a). These beads are slightly large, round beads of type IIa55, recovered from the Cadotte and Point Sauble sites, contained 15.5 to 18.2 K_2O. Co-colored beads of the stylistic type IIa46/47 are opacified with antimony (Sb) at >8000 ppm; beads of this type (n=38) also clearly were not used to produce the pendant (Figure 5b). High Zn is also not present in the Co-colored pendant, and two high Zn samples (Zn > 750 ppm), one from the Marina site and one from Marquette Mission were eliminated as possible pendant contributors.

Once the high K, high Sb, and high Zn groups were eliminated, PCA and cluster analysis of the remaining 195 samples indicated that zircon (Zr) and tin (Sn) were responsible for significant variation in the chemical data set. Because the cobalt-colored pendant contained only 4 ppm of Sn and 24 ppm of Zr, three remaining moderate Sn artifacts (>2000 ppm, not pictured) and eighteen moderate Zr (>60ppm) artifacts were eliminated as candidates for cobalt pendant raw material (Figure 5b). This elimination step removed two beads from the Marquette Mission site and all remaining samples from Hanson and Red Banks, two sites on the Door Peninsula of Wisconsin. These three sites are dated to the mid to late 17th century, some of the earliest dates in the sample. The Co-colored pendant comes from a mid-18th century context at Rock Island, possibly demonstrating that less Zr was used in later beads. Moderate to high Zr levels may warrant further investigation as a possible chronological marker of late 17th century trade in the Upper Great Lakes.

Some of the cobalt-colored beads from the Doty Island site contain higher levels of phosphorus (P) than are present in the Co-colored pendant. The higher-P beads include type Ia19, drawn tubular beads, and IIa55/56, which are small, donut-shaped beads. An additional group of eleven medium to low-P beads of the same types were also eliminated (Figure 5a). After these eliminations, there are 135 possible glass beads that could have served as raw material for the cobalt pendant. The remaining samples values of phosphorus and magnesium were plotted against each other, revealing two final major glass subgroups, as well as more outliers.
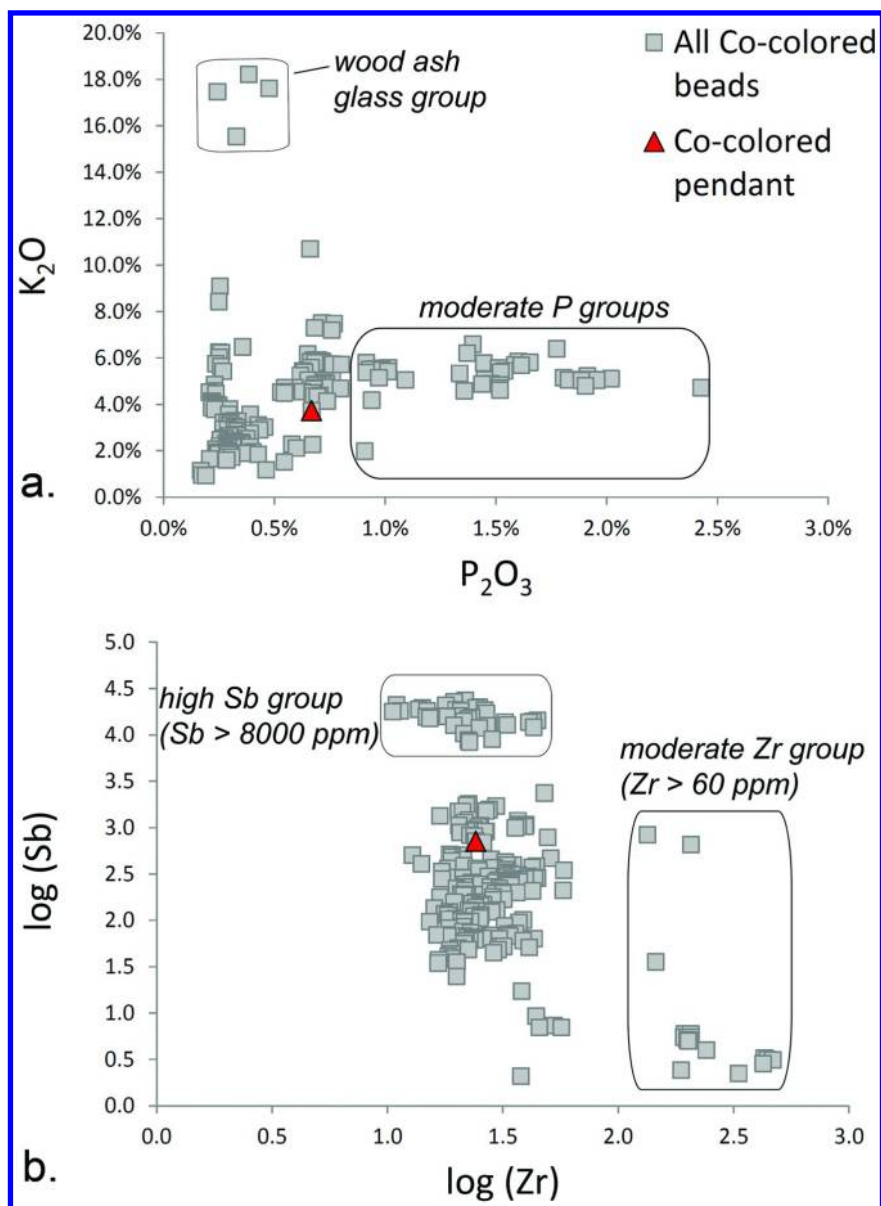
Figure 5. Non-pendant ingredients plotted against each other, demonstrating glass types not used to produce the Co-colored pendant.

In a bivariate plot of P_2O_3 vs MgO, showing all remaining archaeological sites (Figure 6a), the Bell site samples are scattered between the two main groups and do not readily cluster. No refired glass artifacts have been recovered from the Bell site excavations, and the beads from the site are stylistically highly diverse as compared to sites of the same age in this region (*20*). Therefore, the Bell site beads seem to be unlikely contributors to the cobalt pendant from Rock Island. Based on the archaeological contexts, I eliminated the remaining Bell Site samples (n=24), as well as a single bead from Chickadee and five beads from the "village" portion of the Doty Island site. All of these sites have been associated with predominantly Meskwaki habitation activities (*21*, *22*), are all located relatively near one another in the Lake Winnebago region, and may constitute a separate trading network. Removing these sites reveals two distinct glass subgroups, one containing more Mg and less P than the other (Figure 6b). Marquette Mission beads fall only into the Mg-low-P group (n=71). Beads from Rock Island periods 2 – 4 are represented in the Mg-low-P group, while only periods 3 and 4 are present in the P-low-Mg group (n=35). The cobalt blue glass from the Rock Island pendant is more similar to the cobalt blue beads within the P-low-Mg group than beads in any of the other Co-colored bead groups. Most of the beads in the P-low-Mg group are type IIa55/56, though a few Ia19 type beads from Doty Island are represented. Based on the chemical similarity between the beads and pendant fragment, and the archaeological availability of beads, it seems likely that the Rock Island cobalt pendant was produced by remelting the most abundant cobalt blue bead type on Rock Island during Period 4: the type IIa55/56 seed bead (*7*).
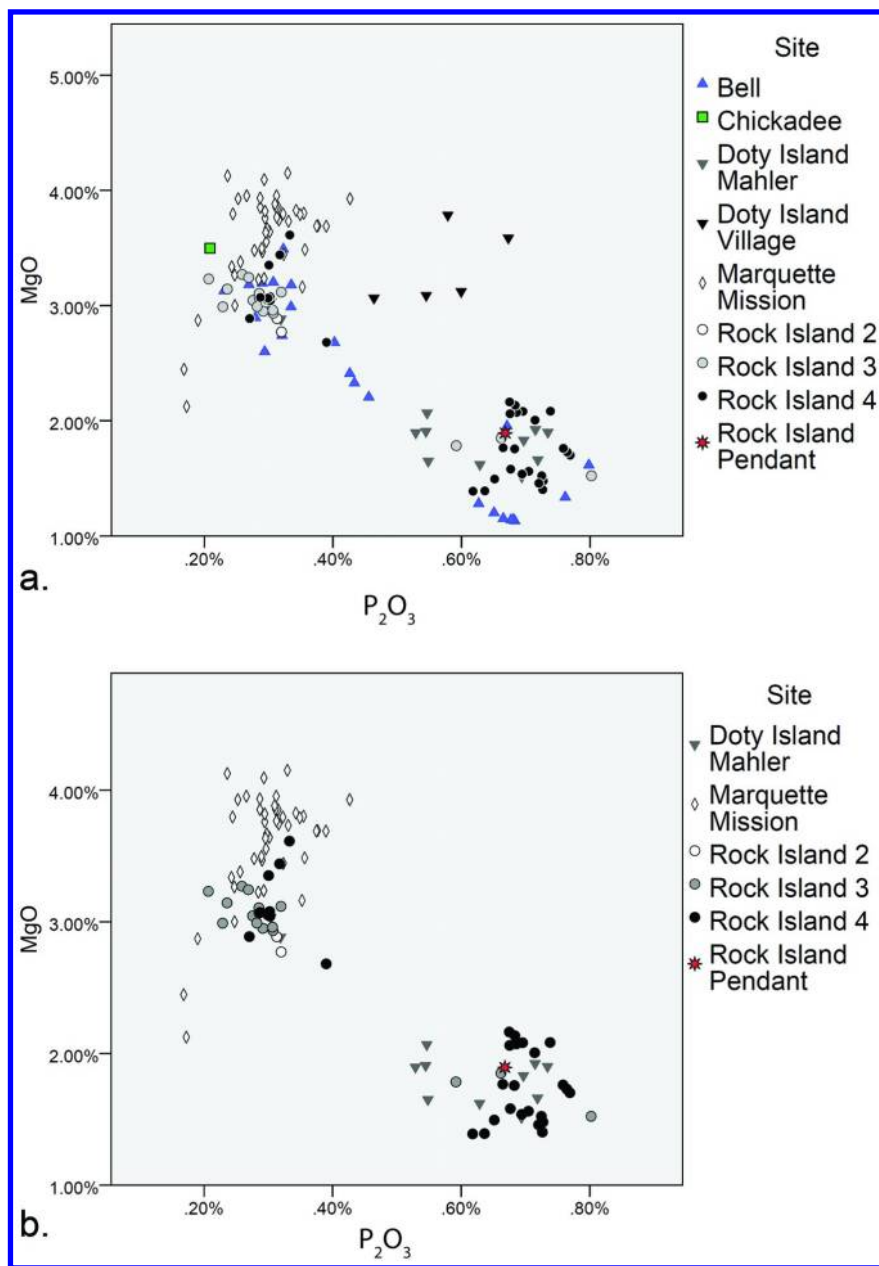
Figure 6. a) MgO vs P₂O₃ demonstrating two major groups, with all sites included and b) MgO vs P₂O₃ with several sites removed, demonstrating the similarity of the Co-colored pendant to beads from Periods 3 and 4 of Rock Island.

Cu-Rich Soda-Lime Glass

Within the data set of 177 Cu-rich samples, there are nine pendants or refired glass fragments recovered from four different archaeological sites. Refer to Table III for the relevant glass data provided for groups discussed in this section.

Zn, Sn, and Pb in Cu-Colored Glass

Within the Cu-colored bead data set, there is a small sub-set of samples that display a positive correlation between Cu and Zn in Zn-rich beads, indicating that a brass alloy likely was used in the glass coloring process (Figure 7a). Two pendants (MM_026 and MM_027) appear to include material from beads of this type. Three high Zn beads were identified in the Marquette Mission assemblage, and one of these three also contains moderate lead (Pb) amounts, like pendant MM_026. Bead MM_024 (presented as its own group in Table III) is the closest bead to pendant MM_026, containing high Zn (4760 ppm), high Pb (13490 ppm), and high Sb (20240 ppm). The high Zn content of MM_026 may derive from including with beads like MM_024 in the powdered pendant raw material.

Two other Marquette Mission beads form another high Zn group, but they do not contain significant Pb, Sn, or Sb, making them very similar to MM_027. Very high Zn beads (n=7) of a similar style were recovered from excavations at the Hanson site in Wisconsin. Both locales are associated with trading activities that extended along a network to the Eastern Great Lakes. The Huron people have been identified as the primary occupants of the Marquette Mission site (*23*), and all LA-ICP-MS bead samples from that site come from features that seem to be either inside or immediately outside of a probable Huron longhouse feature at the site. The Hanson site also is most likely affiliated with an Eastern Great Lakes population, possibly also Huron or a related Petun or Odawa community (*24*). High Zn-beads recovered in Wisconsin and Michigan may indicate that the users of those beads were connected to Eastern Great Lakes trade networks via direct or down-the-line trade.

Visual categories of beads correspond to chemical differences in some cases. The IIa40 beads, a medium to large-sized round or barrel-shaped opaque turquoise bead, are different enough from others in the sample that they stand out as outliers in PCA and cluster analyses, as well as in some bivariate scatterplots. IIa40 beads usually contain some Zn, Sn, and Pb (Figure 7b). The Sn levels present in IIa40 beads are not high as the Sn-rich (5.7% to 15.7% SnO_2) opaque white beads that previous researchers identified as a possible chronological marker for the early-mid 17th century (*25–27*). However, it is possible than the general use of Sn as an opacifier is also temporally diagnostic for Upper Great Lakes opaque blue glass beads.
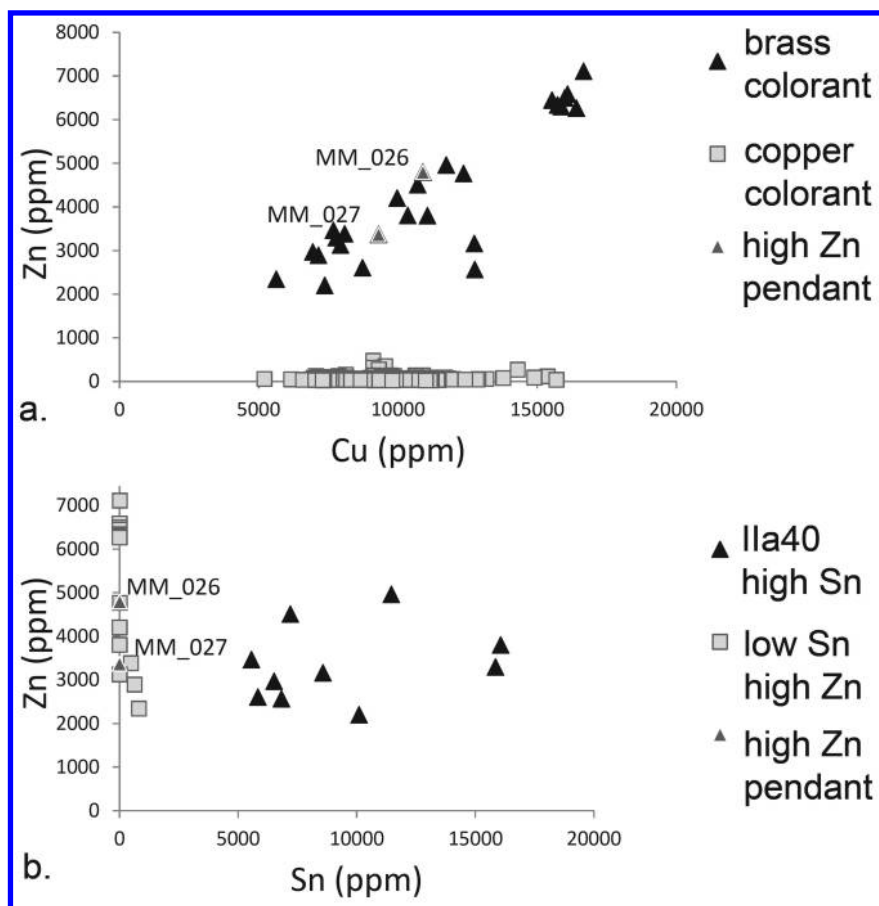
Figure 7. Zn-rich beads and pendants, demonstrating a) positive relationship between Cu and Zn and b) Lack of Sn (type IIa40 beads) in the Zn-rich pendants.

All the moderate Sn + Pb +Zn beads (n=10) are type IIa40, as are a low Sn-Pb-Zn group (n=24). Although pendants MM _025 and MM_028 do not contain enough Sn to be made exclusively from these type IIa40 beads, high Zn beads appear to have contributed to both of these pendants. Beads from the Sn +Pb +Zn group may have been used as raw material along with type IIa31 beads, which constitue the Mg-low-P group discussed below. To understand the possible contribution of IIa40 beads as a visually and chemically distinct group in pendant recipes, cluster analysis was performed using all measured elements for the low Sn-Pb-Zn group of twenty-three IIa40 type beads and all pendants except the high-Zn MM_026 and MM_027 (Figure 8). This figure demonstrates that for Rock Island and Marquette Mission, pendants are most similar to beads from their respective archaeological sites. This likely indicates that some IIa40 beads available at each site partially make up the raw material of pendants recovered there.

Chemical groupings identified among the pendants in cluster analysis also match patterns in the size and shape of these objects. The two pendants that share a similar high-Zn composition, MM_026 and MM_027, are the two largest pendants in the sample, and are nearly identical in size and shape. In the IIa40 cluster analysis, the two main branches separate Marquette Mission and Rock Island, with other sites sorting into one of these two locales. The large, rounded trapezoidal pendant from Marquette Mission (MM_028) is stylistically and chemically distinct from the others in the data set, as are the turquoise-and-white striped Rock Island fragment (RI_023) and the similar turquoise piece (RI_027). The smaller-size pendants from surface collections near La Pointe, WI (MA_13 and MA_14) and the smaller Marquette Mission pendant (MM_025) are grouped together, along with the Doty Island fragment (M_24). These stylistic and chemical differences may reflect different technological traditions of pendant production.

Pendants could have been made from beads of different glass recipes, so leaded beads were also considered as possible contributors to the refired pendants. MM_026 contained 2.24% lead oxide, PbO_2, but no other Cu-rich refired pieces were similarly high in lead. Therefore, after identifying MM_026 as a high Zn pendant from Marquette Mission, several other outliers were eliminated from the Cu-data set: bead RI_0123, which contained a moderate amount of PbO_2 (1.56%), and Doty Island beads DI_050 and DI_051, which contained levels of phosphorus oxide (P_2O_3) that were significantly higher than other Cu-rich beads, but comparable to Co-colored beads from that site. It is unlikely that any of these outliers are similar to the beads used to produce refired pendants.
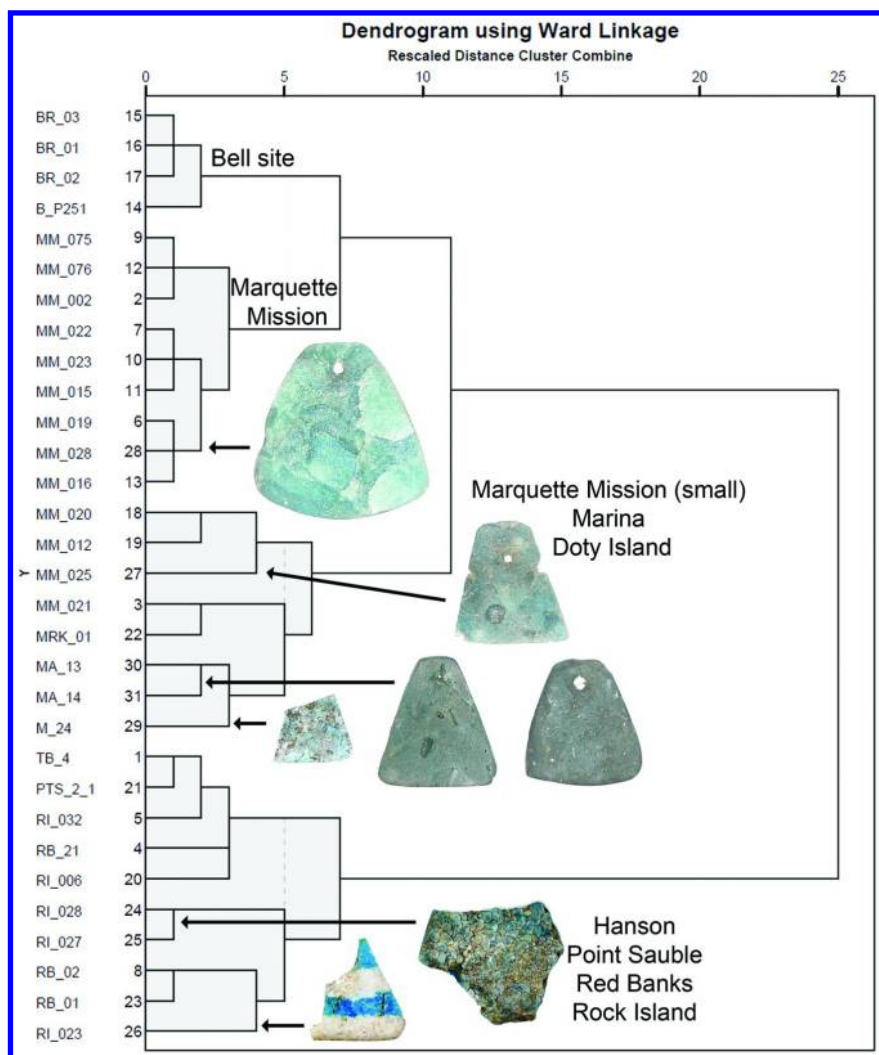
Figure 8. Cluster analysis demonstrating the similarity of pendants and refired fragments to IIa40 beads from the same site.

Mg and P in Cu-Colored Glass

After identifying the contributions of beads containing significant Zn, Pb, and Sn, beads from those groups were removed from the statistical data set. The remaining set of 124 Cu-rich artifacts mainly included type IIa31, a small, turquoise colored opaque donut-shaped bead. A further PCA run using diagnostic elements (Mg, P, Mn, Sr, Ca, K) distinguished the remaining glass subtypes and their relationship to the 7 remaining Cu-colored pendants. Two components with Eigenvalues greater than one were identified, explaining 72.0%% of the variation within the dataset (Figure 9). This figure demonstrates that the two glass subtypes identified in the Co-colored beads, P-low-Mg and Mg-low-P, also are present in the Cu colored pendants and beads. A bivariate scatterplot also illustrates that the Mg and P distinction between Rock Island and Marquette Mission is even more pronounced than in the cobalt-blue glass group (Figure 10). All of the Marquette Mission beads are made of Mg-low-P glass (n=58), while all but two of the Rock Island artifacts are made from the P-low-Mg glass (n=59). In each case, the Rock Island refired fragments are most similar to beads from that archaeological site. The Marquette Mission assemblage is again more diverse, but the two remaining pendants from that site (MM_025 and MM_028) are most similar to beads from that locale. These two sites yielded the largest sample sizes in the data set (Rock Island n=116; Marquette Mission n=119), and interpretations will focus on explaining this main difference.
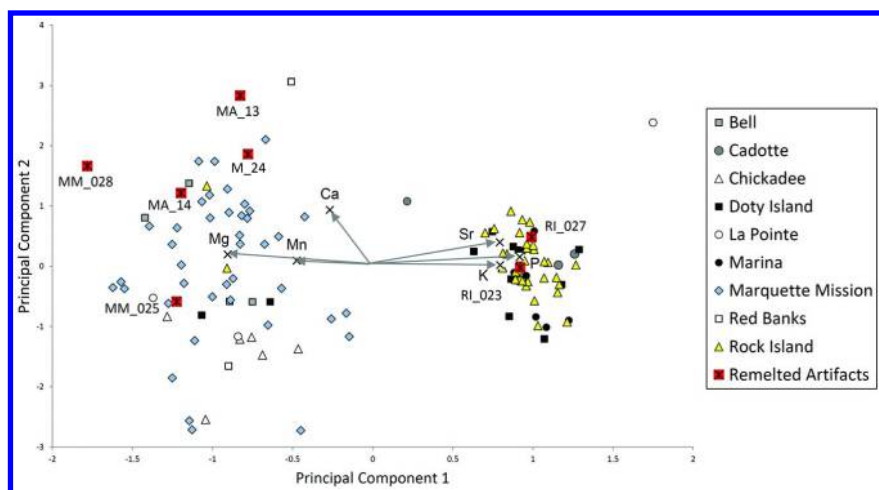
Figure 9. Principal component analysis of 124 Cu-rich beads and refired fragments.
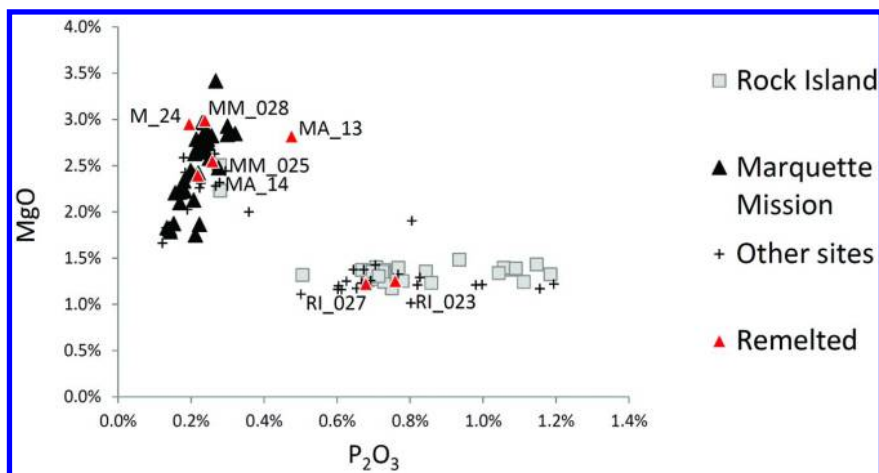
Figure 10. MgO vs P₂O₃ demonstrating the major differences between Rock Island and Marquette Mission site beads and associate refired glass objects.

Interpretations

LA-ICP-MS analysis of glass trade beads and refired glass objects from archaeological sites in Wisconsin and Michigan demonstrates that many of the refired objects are of a similar chemical composition as glass beads recovered from the same location. Crushed seed or "donut"-shaped beads, rather than the larger drawn or wound types were the primary raw material used for pendant production, but there is also circumstantial evidence of a possible failed attempt to remelt bottle glass at the Rock Island site. This study challenges the previous understanding of down-the-line trade, supporting the hypothesis that glass refiring activities may have taken place at locations in the Midwest as well as the Plains. The new data may refute the acculturation-centered notion that "the idea of crushing up European glass trade beads and remelting them into triangular pendants seem [sic] too complex to have been independently invented in several locations" (*28*). The variation among pendant styles and glass bead types used, combined with evidence that Native people likely produced pendants outside the Plains region, demonstrates that this technologically-sophisticated process was used concurrently in at least two different regions. The diffusion of the idea of this novel technological practice combined with independent experimentation may better explain the broad distribution of glass pendants.

Positive evidence of on-site pendant production must include 1) pendants recovered from an archaeological site 2) chemical similarity between beads and refired artifacts, 3) pyrotechnic features such as ash lenses or fire pits, and 4) tools for pendant production including firing pans, clay molds, or bead-grinding stones. The Rock Island Odawa house structure where the high Ca refired fragment was found offers significant evidence of pyrotechnical activity including vitrified sand, ashy lenses, and charcoal scatters. Five cut metal artifacts from this context have adhering blue glass residue that is visually similar in color to refired pendants. One

of these metal scraps (Figure 11) bears a trapezoidal discoloration, the "shadow" of glass being heated on the metal surface (Billeck, personal communication 2013). This artifact is similar to firing pans recovered from the Leavenworth site in South Dakota, a known locale of pendant production (*4*). The Rock Island site therefore meets all four criteria for pendant production. Close chemical similarities between beads and pendants could also indicate that pendants were produced elsewhere and traded as a unit strung with blue glass beads of the same glass type used to produce the pendant. However, when discovered in primary contexts, usually burials, pendants are found singly, as if worn as a hair ornament or sometimes sewn onto a bag or included in a necklace (*4*). Howard does not present any ethnographic evidence for finished items that include pendants and blue beads in large quantities. It seems more likely that if a pendant's glass chemistry is very similar to beads recovered from the same site when compared to other sites in the region, pendant production was occurring at that site.
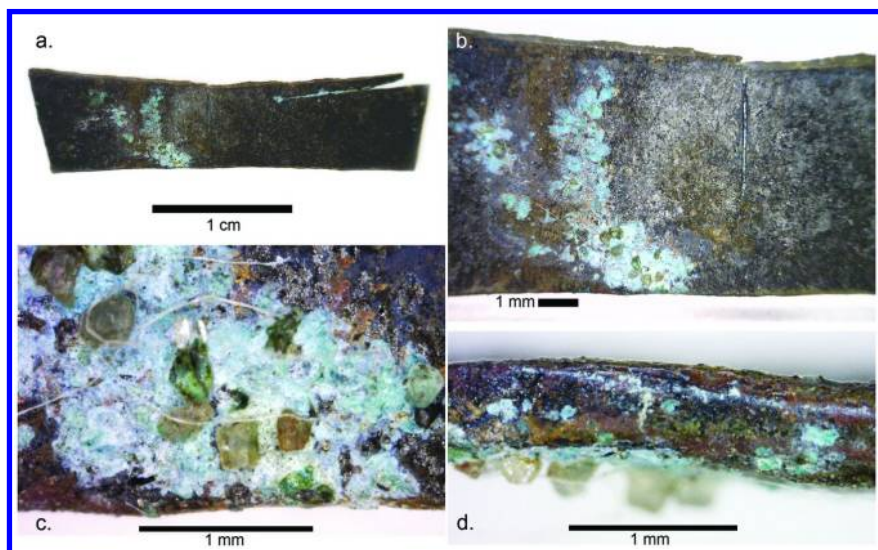
Figure 11. a) Metal artifact with blue glass adhering to the surface, possibly a "firing pan" for pendant production, from Rock Island, WI; b) Trapezoidal discoloration, resulting from glass refiring; c) sand grains, possibly part of the production process, adhering to the glass and d) glass residue on the cut basal edge of the artifact.

There are several other difficulties of interpretation that require discussion. As discussed throughout this paper, refired pendants are composite artifacts, a result of a technological process that blends together beads based on their outward appearance rather than their original glass recipe. As a result, chemical analyses cannot pinpoint particular glass beads used for pendant production; rather, the present research identifies the most likely kinds of beads that were used as raw material for pendant making. Some archaeological sites in the study sample (Red Banks and La Pointe) are represented only by uncontrolled surface collections;

unsurprisingly, the glass recipes detected in those samples are more variable than those of beads from feature contexts. Two pendants, M_13 and M_14, come from surface collections known to have taken place on Madeline Island, likely in the vicinity of the La Pointe area of the island. These two turquoise-colored pendants are chemically and stylistically more similar to those from Marquette Mission than from Rock Island, possibly indicating interaction between the St. Ignace area at the Straits of Mackinac through Lake Superior to Madeline Island. In the present study, there are not enough well-provenienced glass samples from Madeline Island to clarify the timing of such interactions.

Sample size also affects interpretation. Some sites represented by single or a few beads (Chickadee, Point Sauble, and Markman) do not provide enough evidence to discuss them further in this paper. Even within the largest samples from Rock Island and Marquette Mission, some beads do not fit well into the chemical groups most common on those sites, possibly representing unique instances of interpersonal down-the-line trade or individual bead curation. Despite a relatively large LA-ICP-MS sample size (n=75) from two excavations of the Doty Island site's "Village portion" and "Mahler portion" (*29*, *30*), the tiny refired fragment from the Mahler portion (M_24) is most closely related to the Marquette Mission subgroup and less closely related to the two beads recovered from the same feature context or the Doty Island beads in general. This may indicate that the fragment represents a piece of an adornment object that was manufactured elsewhere but was broken and discarded at the site.

Conclusion

Further research will be necessary to identify additional evidence of on-site pendant production and possible trade networks moving finished objects through the Upper Great Lakes region. Some comparative blue glass bead and pendant samples from the Plains region have been analyzed (*31*), and the next step in this research will be to collaborate with researchers working in that region to compare the data sets. Efforts to identify additional production waste, such as metal artifacts with adhering glass residue, will continue during analysis of the Marquette Mission and other metal assemblages. Additional LA-ICP-MS analyses of glass bottle shards from the Rock Island site may clarify if bottle glass could have been used as a raw material in a failed refiring attempt. An expanded regional sample will allow the comparison of the Upper Great Lakes pendants with other locales, in an effort to refine archaeological understandings of pendant production, trade routes, and population mobility during this dynamic period of social and technological change.

Acknowledgments

References

1. Dussubieux, L. *J. Glass Stud.* **2009**, *51*, 95–110.
2. Ubelaker, D. H.; Bass, W. M. *Am. Antiq.* **1970**, *35* (4), 467–475.
3. Brown, M. K. *Am. Antiq.* **1972**, *37* (3), 432–439.
4. Howard, J. H. *Am. Antiq.* **1972**, *37* (1), 93–97.
5. Walder, H. *MCJA* **2013**, *38* (1), 119–142.
6. Kidd, K. E.; Kidd, M. E. *A Classification System for Glass Beads for the Use of Field Archaeologists*; Canadian Historic Sites: Occasional Papers in Archaeology and History, No. 1; Department of Indian Affairs and Northern Development: Ottawa, ON, 1970.
7. Mason, R. J. *Rock Island Historical Indian Archaeology in the Northern Lake Michigan Basin*; MCJA Special Paper No. 6; Kent State University Press: Kent, OH, 1986.
8. Gratuze, B. *J. Archaeol. Sci.* **1999**, *26* (8), 869–881.
9. Pearce, N. J. G.; Perkins, W. T.; Westgate, J. A.; Gorton, M. P.; Jackson, S. E.; Neal, C. R.; Chenery, S. P. *Geostand. Newsl.* **1997**, *21* (1), 115–144.
10. Brill, R. H. *Chemical Analyses of Early Glasses*; Corning Museum of Glass: Corning, NY, 1999; Vol. 2, p 554.
11. Dussubieux, L.; Robertshaw, P.; Glascock, M. D. *Int. J. Mass Spectrom.* **2009**, *284* (1−3), 152–161.
12. Baxter, M. J. *Archaeometry* **1999**, *41* (2), 321–338.
13. Hancock, R. G. V.; Hancock, K. E.; Hancock, J. K. *Archaeometry* **2008**, *50* (4), 710–726.
14. Michelaki, K.; Hancock, R. G. V. *Archaeometry* **2011**, *53* (6), 1259–1279.

15. Brill, R. H. *Chemical Analyses of Early Glasses*; Corning Museum of Glass: Corning, NY, 1999; Vol. 1.
16. Cable, M.; Smedley, J. W. *Glass Technol.* **1987**, *28* (2), 94–98.
17. Stevenson, C. M.; Wheeler, D.; Novak, S. W.; Speakman, R. J.; Glascock, M. D. *Archaeometry* **2007**, *49* (1), 153–177.
18. Dungworth, D. *Ind. Archaeol. Rev.* **2012**, *34* (1), 37–50.
19. Wedepohl, K. H.; Simon, K.; Kronz, A. *Archaeometry* **2011**, *53* (1), 81–102.
20. Lorenzini, M. A. *Diversity Analysis of Glass Trade Beads from Eight Middle Historic Sites*; Reports of Investigations, No. 9; University of Wisconsin-Oshkosh Archaeology Laboratory: Oshkosh, WI, 1999.
21. Behm, J. A. *Wisconsin Archeol.* **2008**, *89* (1−2), 7–85.
22. Reetz, E.; Riggs, R.; Egeland, C.; Kennedy, J.; Meinholz, N. *Life Near the Ledge: Additional Archaeological Investigations of Native American and Euroamerican Sites Located Along S.T.H. 15 Hortonville Bypass in Outagamie County, WI*; Research Reports in Archaeology, No. 212; Museum Archaeology Program: Madison, WI, 2008.
23. Branstner, S. M. In *Calumet and Fleur-De-Lys: Archaeology of Indian and French Contact in the Midcontinent*; Walthall, J. A, Emerson, T. E., Eds.; Smithsonian Institution Press: Washington, DC, 1992; pp 177−201.
24. Rosebrough, A. L.; Broihahn, J. L.; Eisenberg, L.; Walder, H. *On the Edge of History: The Hanson Site (47-Dr-0185), Clay Banks Township, Door County, Wisconsin*; State Archaeology and Maritime Preservation Program Technical Report Series, No.12-001; Wisconsin Historical Society: Madison, WI, 2012.
25. Hancock, R. G. V.; Aufreiter, S.; Kenyon, I. In *Materials Issues in Art and Archaeology V*; Vandiver, P., Druzick, J. R., Merkel, J. F., Stewart, J., Eds.; Symposium Proceedings, Vol 462; Materials Research Society: Pittsburgh, PA, 1997; pp 181−191.
26. Hancock, R. G. V.; McKechnie, J.; Aufreiter, S.; Karklins, K.; Kapches, M.; Sempowski, M.; Moreau, J. F.; Kenyon, I. *J. Radioanal. Nucl. Chem.* **2000**, *244* (3), 567–573.
27. Sempowski, M. L.; Nohe, A. W.; Moreau, J. F.; Kenyon, I.; Karklins, K.; Aufreiter, S.; Hancock, R. G. V. *J. Radioanal. Nucl. Chem.* **2000**, *244* (3), 559–566.
28. Smith, M. T. *Ornament* **1981**, *5* (2), 21–23.
29. Mason, R. P.; Mason, C. L. *Wisconsin Archeol.* **1993**, *74* (1–4), 197–257.
30. Mason, R. P.; Mason, C. L. *Wisconsin Archeol.* **1997**, *79* (1), 208–231.
31. Billeck, B; Dussubieux, L. *Chemical and Chronological Variation of 17th, 18th, and Early 19th Century Blue Glass Beads from the Plains*; Poster presented at the Plains Anthropological Conference, Topeka, KA, 2006.

Chapter 21

Analysis of Samples Excavated from a Royal Tomb in El Zotz: Application of Materials Science Characterization Techniques in Archaeology

Kristina A. Cheung,[*,1] **Nuoya Xie,**[2] **Zhaoying Yao,**[1]
Stephen Houston,[3] **Sarah Newman,**[3]
Edwin René Román-Ramírez,[4] **Thomas Garrison,**[5]
Christian Fischer,[1,6] **Vanessa Muros,**[6] **Sergey Prikhodko,**[1]
and Ioanna Kakoulli[1,6]

[1]**Department of Materials Science and Engineering, University of California Los Angeles, 410 Westwood Plaza, 3111 Engineering V, Los Angeles, California 90095**
[2]**Department of Chemical Engineering, University of California Los Angeles, 5531 Boelter Hall, Los Angeles, California 90095-1592**
[3]**Department of Anthropology, Brown University, 128 Hope Street, Providence, Rhose Island 02912**
[4]**Teresa Lozano Long Institute of Latin American Studies, University of Texas at Austin, 1 University Ave., Austin, Texas 78712**
[5]**Department of Anthropology, University of Southern California, Grace Ford Salvatori Hall, Los Angeles, California 90089**
[6]**UCLA/Getty Conservation Program and Cotsen Institute of Archaeology, University of California Los Angeles, A410 Fowler Building, Los Angeles, California 90095-1510**
[*]**E-mail: kristinacheung@gmail.com**

This project focuses on the characterization of materials from burial offerings and painted decoration in a royal Maya tomb at El Zotz, Guatemala, and their association with mortuary rituals. Archaeological findings included vessels, jade masks, organic materials (wood, cord, and textiles), specular hematite cubes, shells with powdered cinnabar, green (malachite) painted stucco assumed to have decorated the wooden bier where the king was resting, and caches of lip-to-lip Aguila Orange bowls containing human phalanges. In this paper we describe preliminary findings from non-invasive and non-destructive analytical techniques including XRF, VPSEM-EDS, and XRD, emphasizing the potential of these combined technologies in the identification of organic and inorganic markers to infer burial customs. The nature and location of the findings, the evidence of pigment coloration on the bones employing hematite and cinnabar, and the indication of exposure of the bones to high temperatures suggest highly complex, even protracted mortuary practices of Maya elite.

Introduction

Archaeological Context

The royal tomb of a Maya king was discovered below the El Diablo pyramid in El Zotz, located in the San Miguel La Palotada Biotope in the Municipio of San José in the Department El Petén, in the center of the Maya Biosphere Reserve. The exploration of the site was motivated by: 1) its location, with Tikal to the east and El Peru to the west; 2) the connection to the royal family of Yaxchilan in the Usumacinta River; 3) its geopolitical role in the central area of El Petén during the Maya Classic period (AD 250-900), and 4) how the Maya adopted and modified the physical landscape from the Preclassic (1000 BC- AD 250) to the Postclassic (AD 900-early sixteenth century) period (*1–3*). El Zotz contains over 230 buildings with several pyramidal shaped structures (*4*). Among these, on a natural elevation, lies the El Diablo, seemingly built for defensive purposes in Early Classic period (AD 250-550). This complex retains parts of decorated architectural façades, a palace, funerary temples, as well as residential areas (*3*).

While explorations of the site and preliminary excavations were conducted in the 1970s and 80s, systematic survey and excavations at El Zotz only started in 2006. In 2009, excavations along the base of one of the pyramids (structure F8-1) at the El Diablo complex uncovered elaborate stucco decoration, and, in the following season (2010), the archaeological team discovered an undisturbed tomb (Burial 9). It measured 3.12 m long, 1.25 m wide and 1.50 m high and contained the remains of an adult male, along with six child sacrifices (*3*, *5*). This main

burial, is believed to belong to the first king of El Zotz, possibly Chak' "Fish-Dog" Ahk (*3*) venerated by descendants for at least 100 years with funerary ceremonies reflecting how Maya elites perceived their world. The body most likely held an obsidian blade, which may have been used for human sacrifice, as indicated by the signs of bone-cutting on the blade and the discovery of vessels housing the remains of six children, four of them infants, two others a few years older.

Archaeological findings in Burial 9 included vessels and jade masks, shells, and organic materials (wood, cord, and textiles). Also found were 15 specular hematite ingots, shells with powdered cinnabar and green painted stucco assumed to have decorated the wooden bier where the king was resting. In addition, caches of lip-to-lip Aguila Orange bowls were found, some of which contained human remains such as extracted teeth and severed digits (*3*, *5*).

The nature and position of the findings, the evidence of pigment coloration on the bones employing hematite and cinnabar, and the indication of exposure of the bones to high temperatures suggest elaborate and complex mortuary practices of the Maya elite at El Zotz.

Objectives and Scope of Research
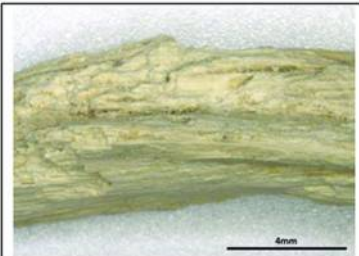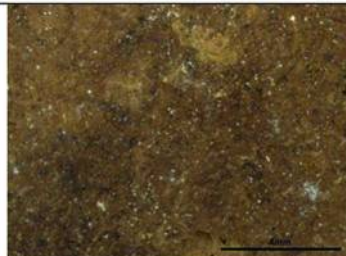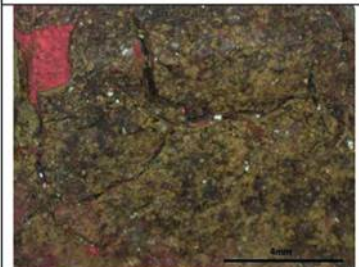
The objective of this research is to apply materials engineering principles and characterization methods to address needs in the study of important archaeological materials that have been affected by weathering and depositional processes. In this arena, the project employs innovative, minimally invasive, non-destructive tools for the characterization of a number of burial offerings and other funerary paraphernalia including wooden and bone artifacts, textiles, and painted stucco found in Burial 9 at El Zotz. Here we report preliminary results to inform the chemistry and properties of the materials and their greater significance to ancient craftsmanship, social organization, and funerary practices of the Maya elite.

Materials and Methods

Archaeological Specimens
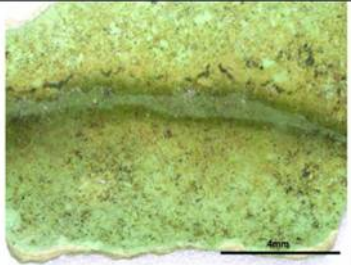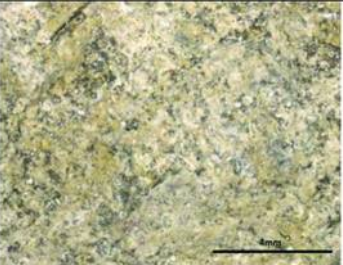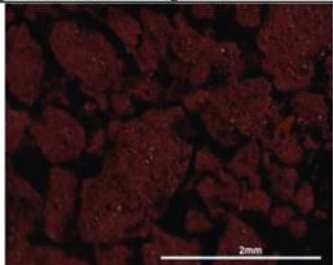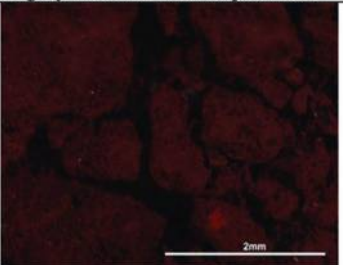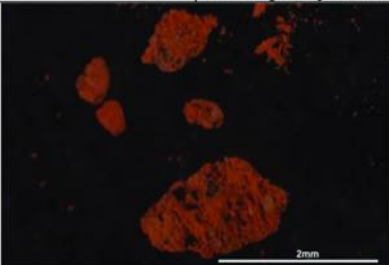
Thirteen archaeological specimens (pieces of original artifacts) were brought to the laboratory for analysis. These included: samples resembling wood, basket, cord, bone, pseudomorphic textiles, clay, hematite pigment (from large hematite blocks found in the tomb), fragments of green painted stucco, and red pigment powders found inside shells. Table I lists all specimens with the archaeologists' initial descriptions of the samples.

Table I. List of sample inventory

Sample 01 Sector C13: "Remains of some kind of basket; possibly cord"	Sample 02 Sector B3: "Possibly bone, but seems to be either coated or mixed with another material"
Sample 03 Sector B6: "Clay and pigment that may have been used to wrap the body"	Sample 04 Sector B9, C9, B10, and C10: "Clay and pigment/painted stucco that may have been below the body"
Sample 05 Sector B5: "Clay and pigment that may have been used to wrap the body"	Sample 06 Sector B9: "Clay matrix"
Sample 07 Sector D5: "Remains of some kind of cordage"	Sample 08 Sector D3: "Remains of some kind of cordage"

Table I. (Continued). List of sample inventory

Sample 09 Sector D6: "Green painted stucco fragments"	Sample 10 Sector A6: "Some kind of grey material with impressions"
Sample P1 Sector E10: "Pigment from cubes"	Sample P2, Sector B7: "Pigment from spondylus shell"

Sample P3: "Unknown pigment associated with shell necklace"

Sample Preparation

Minute quantities of material (in powder or bulk form) were removed from representative areas of the fragmentary archaeological specimens and prepared for analysis using two different types of samples: dispersions and polished cross-sections.

Dispersion Samples

For the preparation of dispersion samples, a few particles were removed (by scraping) from the areas of interest from each specimen, and placed on a clean glass microscope slide. Meltmount™ thermoplastic resin with RI=1.62, was melted (in

double boiler on a hot plate at 50° C) and dropped over the particles. A glass cover slip was positioned on the top and the glass microscope slide was then put on a hot plate to allow the resin to become soft. Using an eraser tip from a standard pencil, mild pressure was exerted over the glass cover slip dispersing the particles in the resin while removing all trapped air. This provided a semi-permanent mount for the particles to be analyzed under polarized light microscopy (PLM).

Polished Cross-Sections

For the preparation of cross-sections, stratigraphic or bulk samples (~2 mm^3) were removed from each archaeological specimen using the point of a scalpel. Owing to the small size of the sample, a special preparation technique was used for embedding (*6*). Buehler EpoxiCure® epoxy resin (mixed with EpoxiCure® Epoxy Hardener as prescribed) was poured into custom-made rubber cubic molds (1.5x1x1cm) to fill half their volume. After hardening of the resin, the sample itself was then placed in the mold with the outer surface (top surface) facing downwards. More resin was then poured over the sample until it was completely covered and put under vacuum using a Buehler Cast n' Vac 1000. Once the resin had set, the samples were cut perpendicular to the outer surface using Buehler silicon carbide grinding papers from 240 to 600 grit. Due to the water-sensitive nature of most of the samples, grinding and polishing could not be done with water-based emulsions. Samples were ground using ethanol and dry polished using Micro-Mesh® polishing pads from 1500 to 8000 grit until a well-polished surface was established. In some cases wet polishing was carried out using the alcohol-based Leco® Ultra Lap Diamond Extender Part No. 812-433 together with Leco® Microid Diamond Compounds Part No. 810-871of 3 microns and Part No. 810-870 of 1 micron. Polishing suspensions were spread on Buehler® MasterTex polishing cloths attached to the Leco® GP-25 polishing turntable.

Characterization Methods

The specimens in Table I were analyzed qualitatively and quantitatively to infer information on their chemistry, microstructure, and properties. All samples displayed some degree of physical and chemical alteration due to the burial environment. To distinguish between products of alteration and original materials, the analysis of the samples involved a multiscale and multianalytical approach from the macro to the molecular length scale, using stereomicroscopy (SM); digital microscopy (DM); field emission gun (FEG) scanning electron microscopy (SEM) at variable pressure (VP) coupled with energy dispersive X-ray spectroscopy (EDS); portable X-ray fluorescence (pXRF); ultraviolet/visible/near infrared reflectance spectroscopy (UV/Vis/NIR), and X-ray diffraction (XRD). The combination of these non-invasive and non-destructive imaging and analytical techniques provided complimentary information and enabled the use of the same sample for multiple analyses with minimal sample preparation and manipulation.

Optical Microscopy (OM): Stereomicroscopy (SM), Digital Microscopy (DM), and Polarized Light Microscopy (PLM)

Initial observations of the unmounted samples were recorded using an Omano stereomicroscope between 7x and 45x magnification and a Canon PowerShot A630 digital camera. These samples were also examined under a KEYENCE VHX-1000 digital microscope at 20x, 50x, 100x, and 200x magnification, focusing on specific areas of interest in each sample, which would be later analyzed using VPSEM-EDS.

Dispersion samples of pigmented areas were analyzed using a Leica DMRM polarized light microscope under plane polarized and cross polarized light. The habit, color, pleochroism, relief, refractive index, birefringence, and extinction angles were used to characterize each particle phase identified in the sample.

Portable X-ray Fluorescence (pXRF) Spectroscopy

For elemental analysis, the Thermo Scientific Niton® XL3t Series GOLDD™ technology handheld portable XRF was used, with a silver anode and silicon drift detector. Readings were taken with an 8mm diameter spot size in both Soil Mode and Mining Mode for 120 seconds for each measurement. In situ study of the samples with this technique gave qualitative and semi-quantitative information regarding the relative concentrations of major, minor, and trace elements found in each sample and complemented other microanalyses.

X-ray Diffraction (XRD)

XRD analysis was performed on the pigment powder samples and on Sample 09, which contained the green painted layer on white stucco. For the analysis, a few particles of the area of interest were mounted on a glass spindle and analyzed using a Rigaku R-Axis Spider X-ray diffractometer. XRD spectra were recorded at 50 kV/40 mA using a Cu-Kα target for 900 seconds. XRD data was processed and matched against reference spectra from the International Center for Diffraction Data (ICDD) files using the JADE, v8.2 software from Materials Data Inc.

Ultraviolet/Visible Light/Near Infrared (UV/Vis/NIR) Reflectance Spectroscopy

UV/Vis/NIR spectroscopy was performed using the FieldSpec3® 3 by Analytical Spectral Devices Inc (ASD), with high spectral resolution (3 nm @ 700 nm and 10 nm @ 1400/ 2100 nm) and wide spectral range between 350-2500 nm. The flexible spot size analyzer for contact analysis facilitated the systematic study of specific areas. The high spectral and spatial resolution of the spectrometer was particularly useful for fingerprint identification of different mineral phases and organic compounds in the samples due to its high sensitivity to both the electron

transitions in the visible part of the spectrum and the overtones from the organic molecules in the near infrared.

Scanning Electron Microscopy (SEM) and Energy Dispersive X-ray Spectroscopy (EDS)

Analysis was performed using an FEI Nova™ NanoSEM 230 scanning electron microscope with field emission gun and variable pressure capabilities, equipped with a Thermo Scientific NORAN System 7 X-ray Energy Dispersive Spectrometer (EDS).

All archaeological specimens were first examined non-invasively (no conductive coating was sputtered over the surface) at low vacuum, so as not to damage, dehydrate, or alter the delicate nature of the specimens. Imaging was provided using secondary electron (SE) detection with the Low Vacuum Detector (LVD) providing topographical details of the samples. For this analysis, each sample was placed on an aluminum foil holder, which was secured to the SEM stub using double-sided carbon tape. In addition, samples were blown with compressed air before being placed inside the SEM chamber to remove any loose surface debris. Chamber pressure for all in situ analyses was held at 50 Pa.

Polished cross-sections were also analyzed with SEM-EDS for spatially resolved inter- and intra-layer visualization and characterization. A gaseous analytical detector (GAD) in variable pressure was used for the detection of backscattered electrons (BSE), providing images with compositional contrast; atoms of heavier elements elastically scatter electrons more strongly compared to those of lighter elements, resulting in higher signal intensity for elements with higher atomic numbers. Thus, areas of the sample that are mostly composed of heavy elements appear brighter than areas composed of light elements in an image obtained using BSE, providing useful information when studying the heterogeneous and multi-layered samples.

Elemental spectra and maps of characteristic X-ray photon emissions were acquired using EDS. The analysis of well-polished surfaces was crucial for more precise quantitative measurements because of the shallow probing depth of electrons interacting with the surface. In addition, flat surfaces minimize the deflection of BSE in different directions, maximizing the collection of electrons by the detector located symmetrically about the incident beam of electrons. EDS spot analysis enabled comparisons of peak intensities, providing data regarding relative concentration of elements found in the specimen, and elemental mapping of certain areas provided a visual of the profile distribution of certain elements.

Preliminary Results and Discussion

Pigment Powder Samples (Raw Pigments)

Red powder, from pigment ingots (Sample P1) and from pigment-containing shells (P2 and P3), was analyzed using PLM, pXRF (Figure 1), and XRD. PLM results of Samples P1 and P2 revealed the presence of specular hematite as

indicated by the occurrence of reddish-brown granular particles identified as hematite associated with tabular flakes with shiny luster and quartz particles. XRD analysis confirmed the presence of hematite and quartz and has also suggested the presence of a calcium-based clay material. The results were further supported by XRF spectroscopy, determining the presence of Fe as the major element and Si and Ca as minor elements. Traces of Ti were also identified that might suggest the presence of a titaniferous mineral associated with hematite. Sample P2 also contained traces of another pigment (most likely an accidental contaminant due to depositional processes) with angular habit, intense red body color and high relief. This red powder was identified as cinnabar, a mercury(II) sulfide compound (α-HgS). Its presence was further validated by XRF with the identification of Hg and S. Sample P3 was identified as pure cinnabar.

The specular hematite ingots (15 of them) found at this archaeological site are the first of this quantity and form to be recorded in the Maya region. The pigment is not indigenous to the area, which confirms that these ingots must have been imported from other parts of the Maya area such as central Mexico (*7*). The scarcity of the pigment ingots is most likely due to their status as valued trade objects. Similarly, cinnabar is a very important and highly priced pigment that has been associated with burials of important Maya rulers and funerary rituals of venerated ancestors (*8–11*).
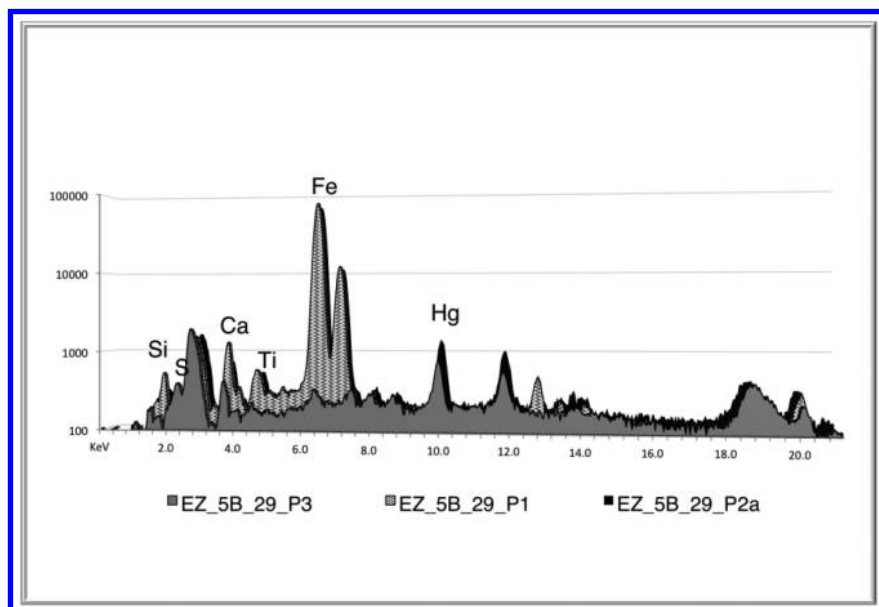
Figure 1. Portable XRF spectra (counts (log) vs. energy in keV) of pigments Samples P1 (light grey patterned spectrum), P2 (solid black spectrum), and P3 (solid grey spectrum). P1 and P2 are almost identical, showing high Fe content and minor Si and Ca. Characteristic X-ray lines for Hg and S in P2 and P3 spectra are attributed to the presence of cinnabar.

Samples with Evident Red Painted Surface

In addition to raw pigment samples, the red color was also evident in painted surfaces of Samples 03, 04, and 05. Samples 03 and 05, described as clay that may have been used to wrap the body of the king, look very similar and were found near the same location in the tomb. Sample 04 (possibly a piece of painted stucco) is pigmented with a lighter red color. UV/Vis/NIR reflectance spectroscopy on all three samples revealed absorptions in the visible range indicative of electronic processes of Fe^{3+}, attributed to the presence of hematite. XRF analysis confirmed the presence of Fe with higher concentrations in Samples 03 and 05. The red pigment in Samples 03 and 05 also appear brighter than the red found in Sample 04. This could be related to the occurrence of cinnabar, since Hg and S were also detected in Samples 03 and 05 using XRF and EDS. UV/Vis/NIR reflectance spectra of these strongly red-tinted layers clearly displayed the characteristic band-gap of S centered at ~610nm, confirming the presence of cinnabar.

Alteration of Cinnabar-Containing Layer

Close examination of Sample 03 demonstrated evidence of degradation with the formation of black spots. These discolored areas in the red cinnabar-rich layer are subrounded in shape with ~50 to 150 μm diameter (Figure 2) Under secondary electron (SE) imaging they appear granular filled with conglomerate microbiological colonies (Figure 3), which are most likely contributing to the formation of the black staining.
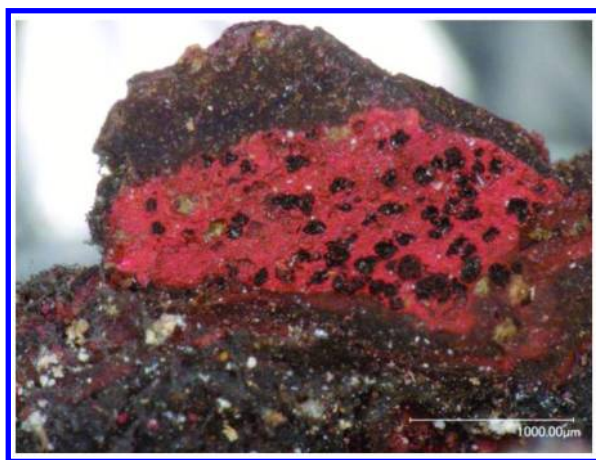
Figure 2. Digital micrograph of Sample 03 at 100x magnification, showing cinnabar alteration with black spots.
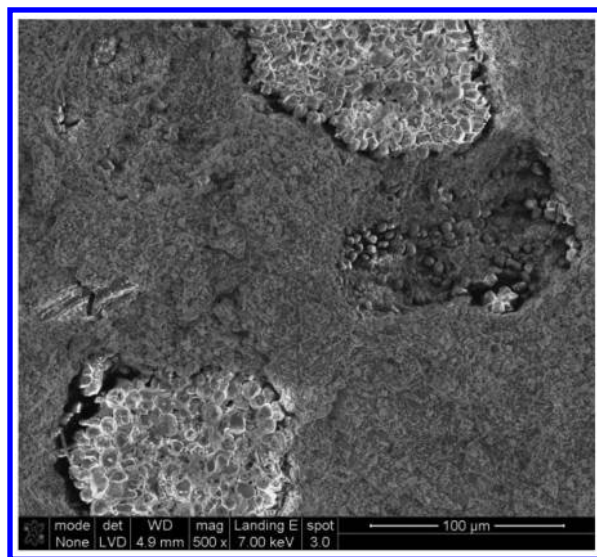
Figure 3. SE image of biological colonies found in black regions of cinnabar on Sample 03.

Qualitative EDS spectra on the surface of the black spots showed significant levels of C, O, and Ca and depletion of S and Hg. BSE images of a polished cross-section of this area (Figure 4) indicated a pit crater in the sample (down to the clay body) with depth of approximately 50 μm and the deposition of microorganisms close to the walls of the crater. EDS spot analysis on the polished sample (Figure 5) confirmed the high levels of C, O, and Ca in the black regions and mainly Al and Si in the clay matrix. While the C and O could be easily attributed to the presence of organic matter and the Al and Si to the clay body, the occurrence of Ca is much less clear. It could potentially be a byproduct of microbiological metabolism in the form of calcium oxalate.

While these are only speculations, we suggest two possible pathways for the formation of the black stains: 1) the presence of microorganisms (bacteria, fungi, or algae, including cyanobacteria) that can cause the breakdown of the sulfide mineral leading to the biotransformation (*11*) or bioleaching (*12–14*) of Hg and 2) the presence of detoxification bacteria that can remove Hg by reduction of Hg^{2+} to Hg^0 and final volatilization of Hg (*15–17*). As the dark areas do not contain much of the original Hg and S, the staining may be of organic origin formed by microorganisms (*18, 19*).
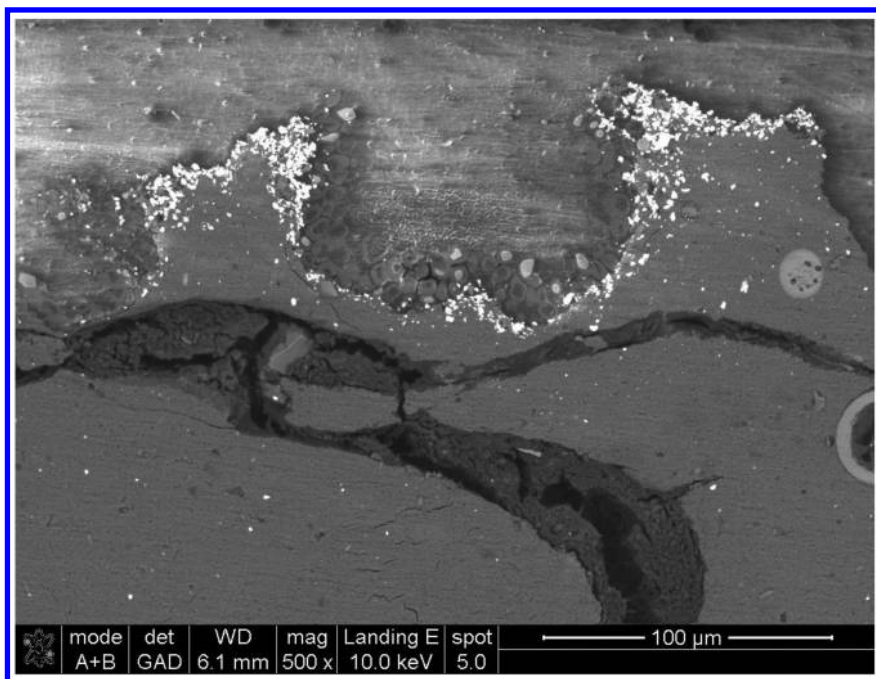
Figure 4. BSE image of a cross sectional view of Sample 03, showing remnants of cinnabar (bright particles) near the pit crater-like formation with microorganisms at the bottom and side walls.

Organic Samples

Sample 02 was described by the archaeologists as possibly bone mixed or coated with another material; however, photographs taken with the digital microscope suggest this sample may actually be a fragment of gourd, which was commonly used to make vessels. The cross-section of this sample looked morphologically similar to wood, with alternating dense and porous areas. The UV/Vis/NIR reflectance spectrum (Figure 6) shows absorptions at 1680, 1730, and 1760 nm corresponding to overtones (higher harmonics) of molecular fundamental vibrations of cellulose-based material, strengthening the hypothesis that this material may be gourd "wood". However, further investigation is necessary to precisely match the organic signature of this material. XRF analysis revealed the presence of some inorganic elements, such as Fe, Ca, P, and Si. Phosphorous is likely present on the sample from the decomposition of the human remains, while Fe, Ca, and Si may be present as a result of the burial soil that has cemented the fibrous material.
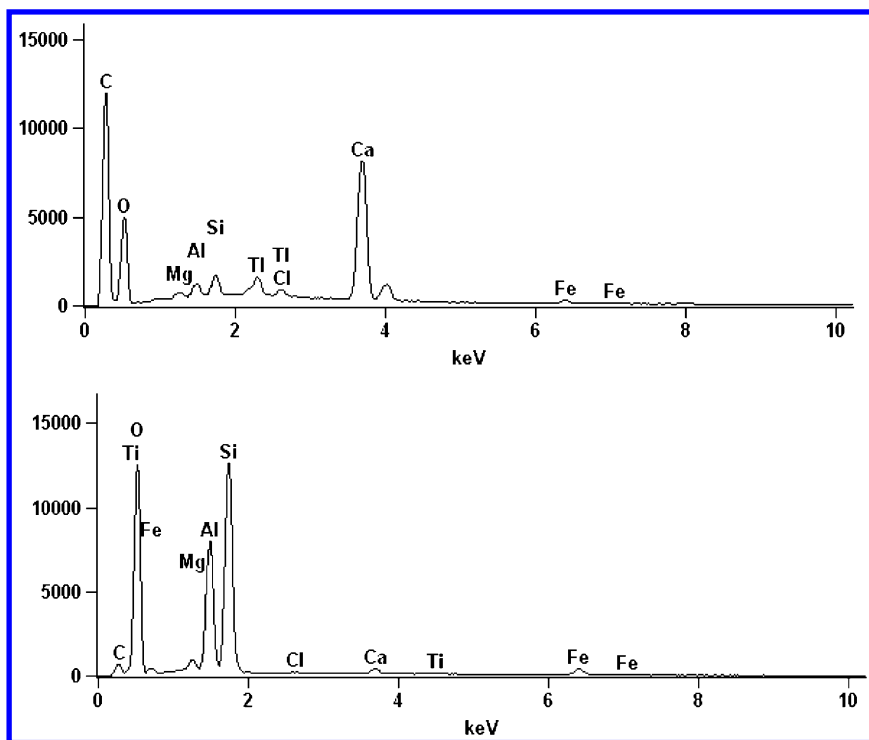
Figure 5. (Top) EDS spectrum of biological black regions in Sample 03, showing intense characteristic X-ray emissions of C, O, and Ca. (Bottom) EDS spectrum of the clay matrix beneath the cinnabar layer with major elements, Al and Si.

Sample with a Lattice-Shaped Structure

Sample 06 (Table I), a dark brown porous sample, was recorded during excavation as a clay-based material. UV/Vis/NIR reflectance spectroscopy suggested the presence of clays and traces of organic materials. XRF analysis of further indicated the presence of Hg.

SEM using SE imaging of a small piece separated from Sample 06 indicated a lattice-shaped (spongy looking) structure with needle-like crystals and spherical particles (50-80 μm in diameter) (Figure 7). EDS analysis of the backbone spongy structure revealed the presence of Si and Al and traces of P, Ca, and Mg, while the spherical particles showed higher concentrations of P and Ca (Figure 7, C) compared to the backbone structure.

The analysis of a polished cross-section indicated the presence of particles (assumed to correspond to the microspheres mentioned above) made of a system of concentric lamellae grouped together in circular arrangements (Figure 8).
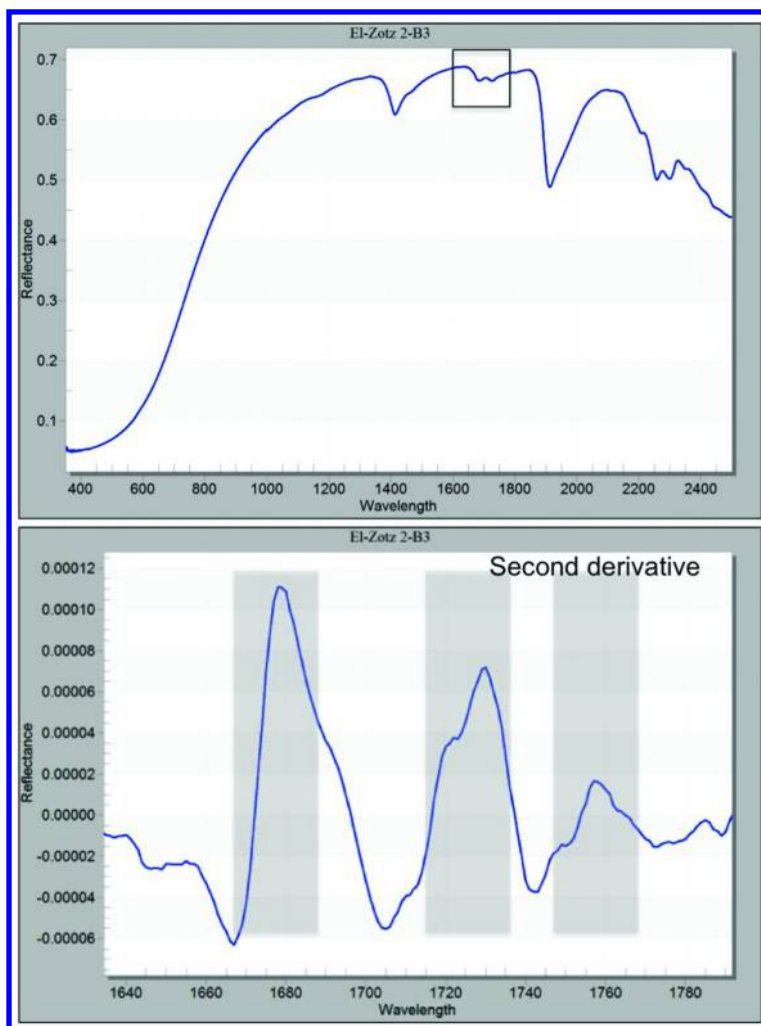
Figure 6. UV/Vis/NIR reflectance spectrum of Sample 06 (top), with the second derivative of boxed region (bottom). Peaks of the second derivative correspond with absorptions in the original spectrum, showing fundamental vibrations of cellulose-based material at 1680, 1730, and 1760 nm.
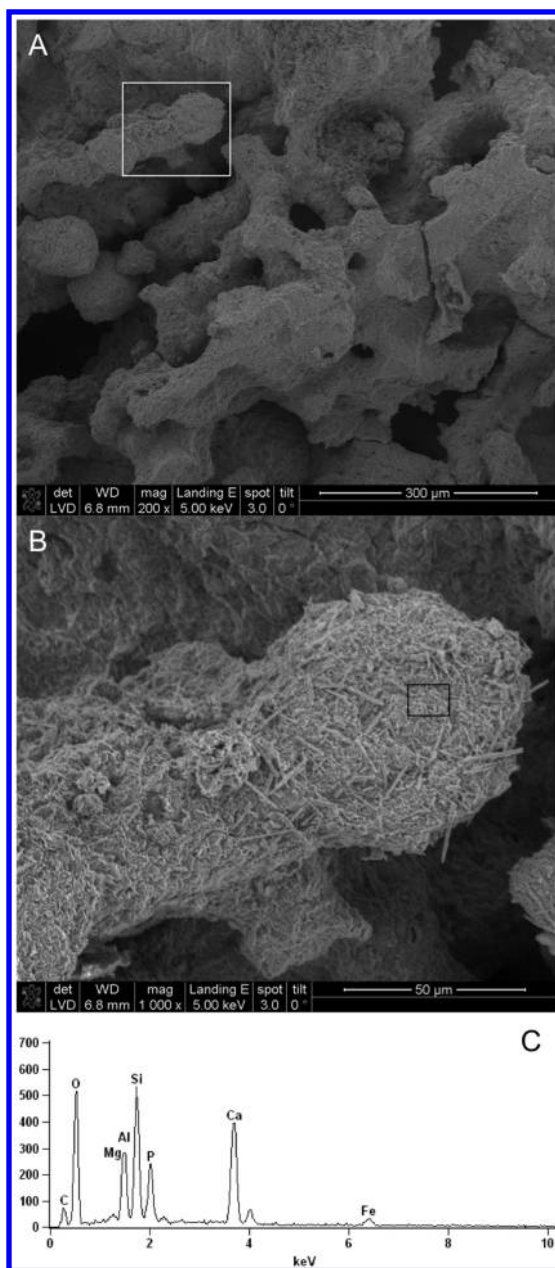
Figure 7. SE micrograph (Image A) of a detail of Sample 06 showing the lattice-shaped (spongy) structure. The white square indicates the area magnified in micrograph B showing the needle-like crystals and one of the spherical-shaped particles. Image C shows a spectrum of the elemental composition of the spherical particle within the area marked with a black square, showing Ca, Si, O, P, and Al as the major elements with C, Mg, and Fe as minor elements.
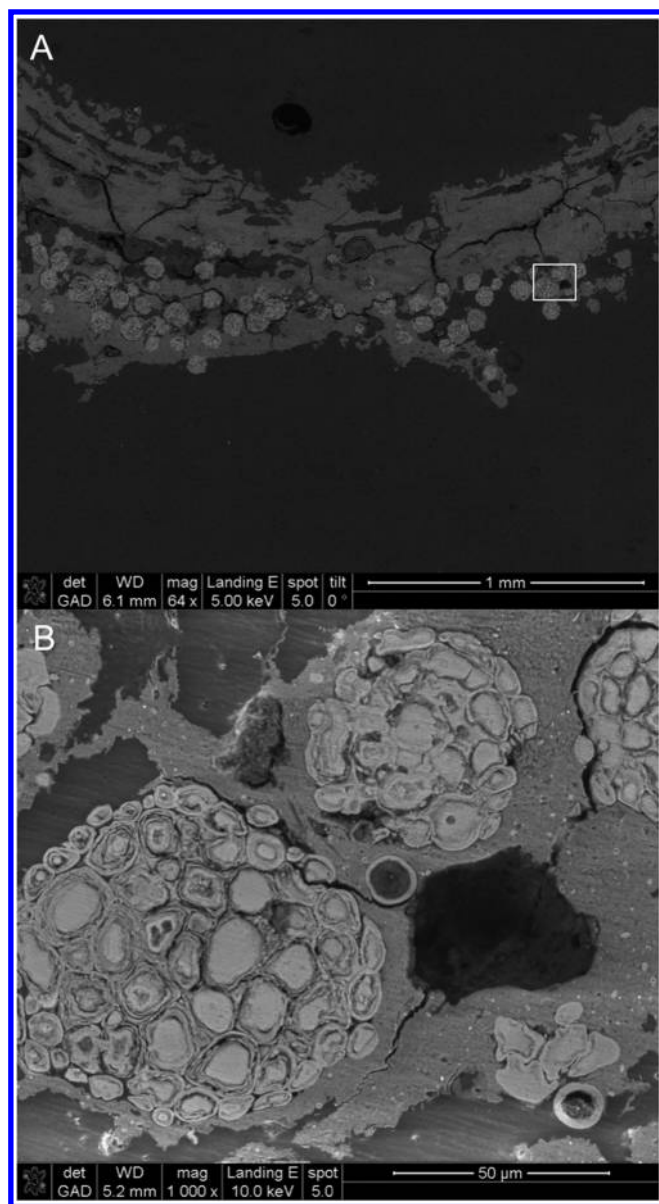
Figure 8. Image A shows the BSE micrograph of a cross-sectional view of a small piece of Sample 06. Image B is a BSE detail view of the white square in Image A, with sphere-shaped clusters and quill-like structures.

Elemental analysis and mapping of these circular features using EDS showed the characteristic X-ray emissions of Ca and P, suggesting the presence of a calcium phosphate phase (Figure 9).

The results so far are preliminary and further analysis of this sample is required to provide more understanding about its precise identity and relationship to its archaeological context.
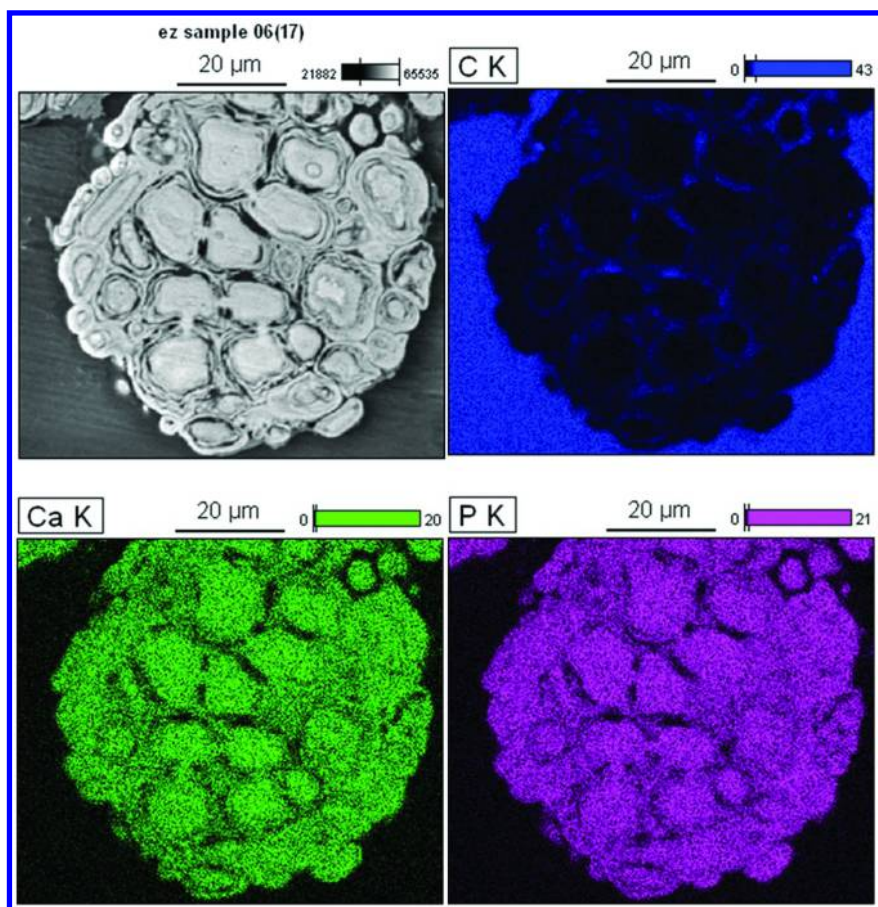
Figure 9. BSE micrograph (top left) and EDS elemental maps on a cross-sectional view of one of the spherical particles, showing the spatial distribution of the predominant elements detected: C, Ca and P. Ca and P are the major elements found in these spherical structures (pointing towards a calcium phosphate mineral) while C corresponds to the voids filled with resin.

Green Painted Stucco Fragment

Sample 09 is a relatively thin sample with a green paint layer (top) of approximately 100 microns and a white layer (substrate) of approximately 0.7 mm. Brown residues beneath the white layer may indicate the presence of a wooden structure that has been lost though further investigation is required for accurate attribution. It is believed to have decorated the bier on which the king

was placed for burial. The sample was first analyzed non-invasively using XRF and UV/Vis/NIR spectroscopy from both sides. XRF results of the top layer (green) indicated the presence of Cu and, to a lesser extent, Ca and P. UV/Vis/NIR reflectance spectra (Figure 10) comparing [1] standard malachite ($CuCO_3(OH)_2$) to [2] the green layer in Sample 09 showed absorptions at ~800 nm and 1300 nm corresponding to electronic transitions of Cu ions and between 2200 and 2400 nm indicative of the CO_3 and OH groups respectively characteristic of malachite. An absorption at ~1920 nm is likely due to the presence of water within the sample. XRF results of the white substrate showed Ca and P with less evident traces of Cu. UV/Vis/NIR reflectance spectroscopy has yielded interesting results in the organic region with small absorptions corresponding to the first overtones of CH stretching, suggesting the presence of organic matter in the white substrate.
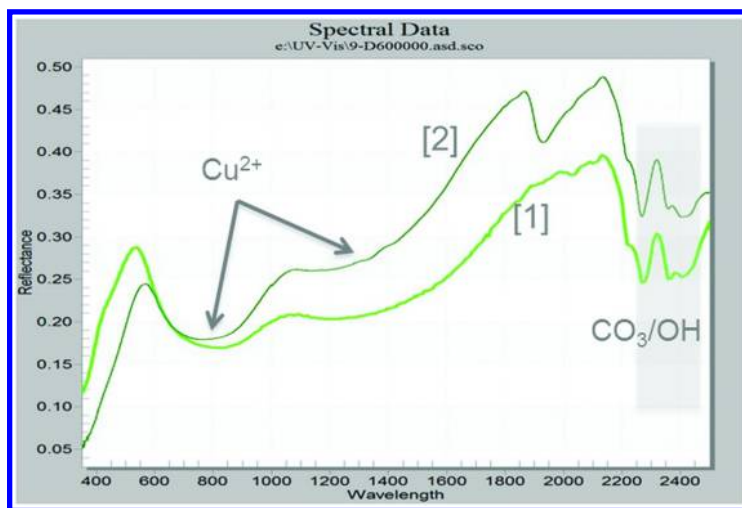
Figure 10. UV/Vis/NIR reflectance spectra comparing [1] standard malachite to [2] the green pigment in Sample 09.

The examination of a polished section of Sample 09 using SEM (Figure 11) clearly revealed the two distinct layers: a green layer (top) appearing brighter under BSE detection and a Ca and P-rich layer (substrate) consisting of angular aggregates in a microcrystalline matrix. EDS analysis of this sample showed the presence of Cu in the green paint layer (Figure 12) and Ca and P in the aggregates of the white substrate (Figure 13). EDS analysis of the microcrystalline matrix revealed a Ca-rich layer with some P (Figure 14). The results from this analysis suggest that the binder might have been calcium hydroxide ($Ca(OH)_2$) (transformed into $CaCO_3$ after carbonation through a chemical reaction with the CO_2 of the atmosphere) mixed with crushed bone (as inert aggregate) to form the white stucco substrate.

In the same burial, some of the lip-to-lip closed vessels contained whitish-grey powder that resembles pulverized bone. This fine grain material has not yet been analyzed and further investigation is required to identify its composition and its

relation to the white stucco substrate. DNA analysis will also be conducted to identify whether the bone fragments in the white stucco layer are either human or animal.
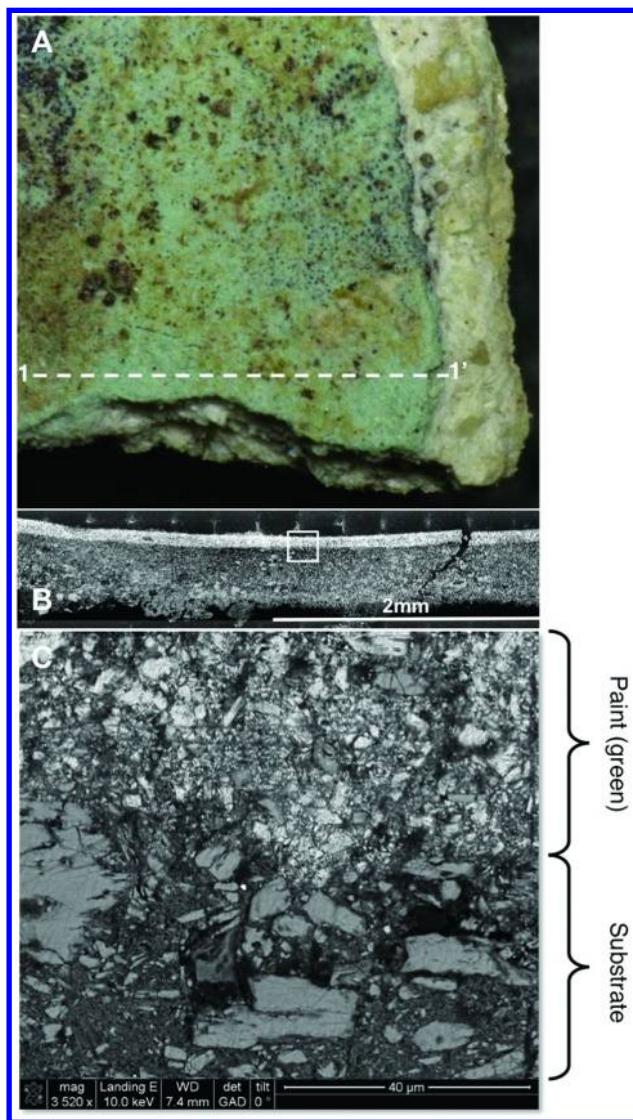
Figure 11. Image A shows a digital photomicrograph of Sample 09 with the green malachite layer (surface) and the white stucco layer (substrate). Dotted line 1-1' indicates the area sectioned for the preparation of a cross section (Image B). BSE micrograph C shows a detail of Image B marked with a white square illustrating the interface between the green layer (paint) and the stucco layer (substrate). The brightness of the green layer indicates its higher density compared to the darker stucco layer beneath.
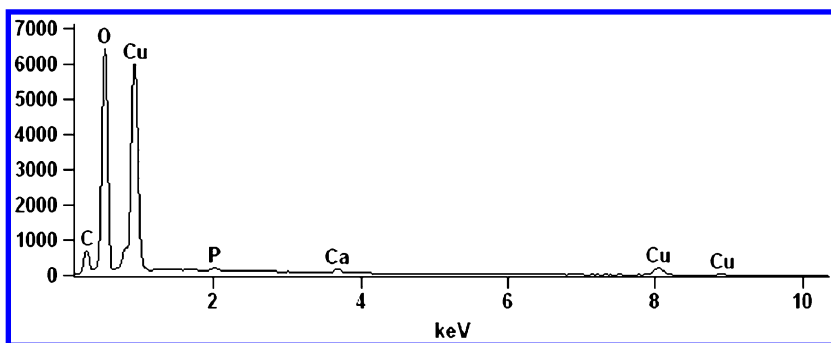
Figure 12. EDS spectrum of green paint layer from Sample 09, showing
characteristic Cu peak at ~8 keV.
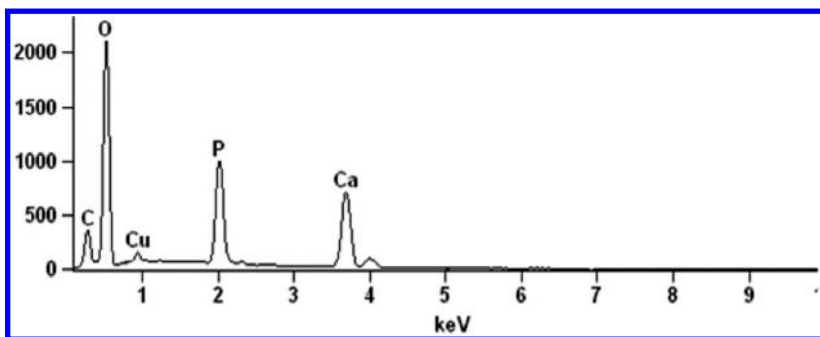
Figure 13. EDS spectrum of aggregates found in white substrate from Sample
09, showing Ca and P present.
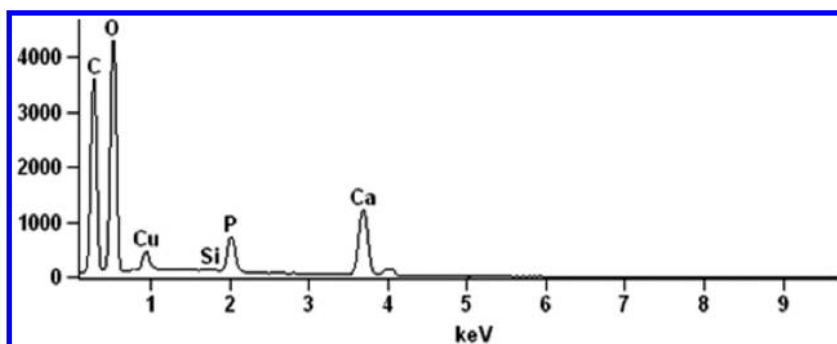
Figure 14. EDS spectrum of the substrate matrix of Sample 09, showing Ca-rich
layer with P present, suggesting a calcium hydroxide (Ca(OH)$_2$) binder which
may have been mixed with crushed bone to form the white stucco.

Summary and Conclusion

The scientific protocol behind this study, based on minimally invasive, non-destructive micro-analytical techniques, was important for the preliminary characterization of fragile archaeological samples. Though most of the work done so far has been primarily qualitative, these initial findings on the morphology, elemental composition, and molecular structure of the excavated samples provide invaluable information on the original materials.

New information on the materials used in funerary decoration and as burial offerings was brought to light, particularly in the use of bone being crushed to form ornamental stucco and the identification of cinnabar and exotic specular hematite unique in form and quantity. The use of cinnabar, specular hematite *spondyllus* shells, suggest a direct association with elite Maya burials and funerary rituals (*3*, *5*, *7*, *20*, *21*). The identification of bone in mortuary decoration is new to the literature. However findings such as child sacrifices, severed digits and blades to saw bone in burial 9 at El Zotz, support the hypothesis of the ritualistic use of bone meal for the decoration of this elite burial.

Further systematic analysis of all samples with microanalytical techniques, will provide more detailed chemical characterization. Other specific points that will receive further detailed study include: the mechanisms and kinetics for cinnabar degradation in Sample 03, provenance investigations to reveal the origin of the specular hematite in Samples P1 and P2, further investigations on the Hg presence in Sample 06 and identification of the lattice-shaped structure and microspheres in the context of the burial and funerary paraphernalia, and aDNA (ancient DNA) testing of the bone fragments found in Sample 09. Conclusive information regarding these specific points and an overall more comprehensive study of all samples will provide the necessary insight into the culture and practices of this ancient civilization.

References

1. Houston, S. Segunda Temporada de Campo en El Zotz: Introducción. In *Proyecto Arqueológico El Zotz, Informe No. 2, Temporada 2007*; Houston, S., Escobedo, H. L., Meléndez, J. C., Eds.; Dirección General del Patrimonio Cultural y Natural de Guatemala, 2007.
2. Houston, S.; Escoberdo, H. L.; Meléndez, J. C. *Proyecto Arqueológico El Zotz: Informe No.2, Temporada 2007*; Houston, S., et al., Eds; Dirección General del Patrimonio Cultural y Natural de Guatemala, 2007.
3. Román-Ramírez, E. R. Living the Sacred Landscape: The Process of Abandonment of the Early Classic Maya Group of El Diablo at El Zotz, Petén, Guatemala. In *Latin American Studies*; University of Texas: Austin, 2011.
4. Houston, S.; Nelson, Z.; Escobedo, H.; Meléndez, J. C.; Arroyave, A. L.; Quiroa, F.; Cambranes, R. *Levantamiento preliminar y actividades de registro en El Zotz, Biotopo San Miguel La Palotada, Petén*; Departamento de Monumentos Prehispánicos y Coloniales, Dirección General del Patrimonio Cultural y Natural de Guatemala, 2006.

5. Houston, S. *In the Shadow of a Giant: Archaeology of El Zotz, Guatemala*; Final Performance Report; National Endowment for the Humanities, 2011.

6. Plesters, J. *Stud. Conserv.* **1956**, *2* (3), 110–157.

7. Moholy-Nagy, H. *J. Field Archaeol.* **1997**, *24*, 293–313.

8. Chelazzi, D.; Poggi, G.; Jaidar, Y.; Toccafondi, N.; Giorgi, R.; Baglioni, P. *J. Colloid Interface Sci.* **2013**, *392*, 42–29.

9. Kelly, D.; Budd, K.; Lefebvre, D. D. *Appl. Environ. Microbiol.* **2006**, *72*, 361–367.

10. Kapridaki, C.; Maravelaki-Kalaitzaki, P. *Prog. Org. Coat.* **2013**, *76*, 400–410.

11. Lefebvre, D. D.; Kelly, D.; Budd, K. *App. Environ. Microbiol.* **2007**, *73*, 243–249.

12. Bosecker, K. *FEMS Microbiol. Rev.* **1997**, *20* (3-4), 591–604.

13. Hansford, G. S.; Vargas, T. *Hydrometallurgy* **2001**, *59* (2), 135–145.

14. Suzuki, I. *Biotechnol. Adv.* **2001**, *19* (2), 119–132.

15. Wagner-Döbler, I. *Appl. Microbiol. Biotechnol.* **2003**, *62* (2-3), 124–133.

16. Mathema, V. B.; Thakuri, B. C.; Sillanpää, M. *Arch. Microbiol.* **2011**, *193* (12), 837–844.

17. Nascimento, A. M.; Chartone-Souza, E. *GMR, Genet. Mol. Res.* **2003**, *2* (1), 92–101.

18. Martin-Sanchez, P. M.; Sanchez-Cortes, S.; Lopez-Tobar, E.; Jurado, V.; Bastian, F.; Alabouvette, C.; Saiz-Jimenez, C. *J. Raman Spectrosc.* **2012**, *43* (3), 464–467.

19. Vasanthakumar, A.; DeAraujo, A.; Mazurek, J.; Schilling, M.; Mitchell, R. *Int. Biodeterior. Biodegrad.* **2013**, *79*, 56–63.

20. Houston, S.; Román, E.; Garrison, T. G.; Garrido, J. L.; Carter, N.; Doyle, J.; Menéndez, E. D.; Newman, S.; Kingsley, M. *En la vista de Pa´Chan: procesos Dinámicos en El Zotz, Petén y sus Cercanías*; 2010.

21. Houston, S.; Román, E.; Garrison, T. G.; Garrido, J. L. Introducción. In *Proyecto Arqueológico El Zotz, Informe 5 Temporada de Campo 2009*; Pérez, G., Román, E., Houston, S., Eds.; Instituto de Antropología e Historia de Guatemala, 2009.

Chapter 22

Preliminary Results on Biomimetic Methods Based on Soluble Ammonium Phosphate Precursors for the Consolidation of Archaeological Wall Paintings

Magdalena Balonis-Sant,*,[1] Xiao Ma,[1] and Ioanna Kakoulli[1,2]

[1]Department of Materials Science and Engineering, University of California Los Angeles, 410 Westwood Plaza, 3111 Engineering V, BOX 159510, Los Angeles, California 90005-1595
[2]UCLA/Getty Conservation Program and Cotsen Institute of Archaeology, University of California Los Angeles, 308 Charles E. Young Drive North, A210 Fowler Building, Box 951510, Los Angeles, California 90095-1510
***E-mail: mbalonis@ucla.edu**

This research develops hydroxyapatite (HAP)-based, inorganic mineral systems for the consolidation of powdery wall paintings of archaeological significance. The scientific approach exploits biomimetic (biologically inspired design) principles to induce in situ the formation of protective HAP crystals by triggering reactions between the calcium carbonate-rich layers in wall paintings and ammonium phosphate precursors. The high solubility and absence of toxicity of ammonium phosphate precursors and the stability of the hydroxyapatite reaction product at varying pH, renders this treatment extremely promising for consolidation and protection of weathered wall paintings. Experimental trials were carried out on wall painting test blocks applying cellulose compresses of 1M and 2M solutions of diammonium hydrogen phosphate for 3 to 6 hours contact time. The consolidating effect was evaluated through microstructurally and compositionally-sensitive analytics including VPSEM-EDS, XRF, water sorption test and scotch tape test. Preliminary results indicated the formation of a porous hydroxyapatite network at the surface and subsurface of the test blocks with improved cohesion, pH-resistivity and

reduced water absorption. These data show the potential of this treatment for the consolidation of powdery wall paintings and their protection from weathering and deterioration induced by natural aging and environmental action-linked effects.

Introduction

Wall paintings provide a testimony of artistic, cultural, and intellectual developments and are often of great archaeological, historical and cultural significance. Physically and chemically, wall paintings are highly complex, heterogeneous composites consisting of a layered structure of at least three phases: binder, aggregate and pigment (*1*).

Owing to their nature and context, wall paintings are faced with imminent threats of deterioration both natural and manmade with broad impact causing chemical, physical and mechanical damage to the constituent materials. These include but are not limited to: moisture, microbiological growth, pollution, seismic activity, vandalism and others. The most common manifestations of weathering on wall paintings include staining of microbiological or chemical origin and color alteration, pitting and severe powdering leading to loss of cohesion within the different layers at the microscopic scale.

Extensive studies have been carried out using a variety of consolidation treatments to improve the condition of surfaces (*2–7*). These studies critically indicate that choosing a proper consolidant for porous materials is challenging. This is specifically related to being able to ensure sufficient penetration beneath the surface, while also providing mechanical strength and abrasion resistance (*2*, *7*, *8*). The definition of a consolidant provided by Warren can be used as a point of reference (*9*):

A consolidant acts at the near-molecular level by fixing or inhibiting the capacity for movement between very small particles, thereby altering the characteristics of the material in terms of its behavior, particularly in the presence of water. It tends to make the material stronger in compression and tension, and may affect inherent characteristics, such as heat and sound transmission and rigidity. (121)

Further, a consolidant should not severely alter the original "nature of the porosity" (*10*), and not be extremely hydrophobic, which could lead to further damage. Ideally, the consolidant should also be photochemically stable to prevent optical changes of the surface of the paint that could affect significantly the saturation of color, gloss and texture (*8*). Also, one of the key factors in the consolidation of wall paintings in particular is retreatability, enabling future treatments, if necessary (*11*).

Polymers, mainly acrylic, vinyl and silicone based, have been widely used as consolidants for cultural heritage objects (*12–17*). However, contrary to expectation, in many cases polymers used for the consolidation of wall paintings have often induced further degradation of the artwork by changing greatly the

physicochemical properties of the plasters and paint layers (*18*). An alternative method to organic polymers is the in situ formation of more compatible inorganic mineral phases re-establishing the loss of cohesion in disintegrated plaster layers (*3, 7, 19–26*). An example is the application of $Ca(OH)_2$-based consolidants that has been practiced extensively (*3, 7, 27, 28*). The consolidation mechanism is based on the transformation of $Ca(OH)_2$ into calcium carbonate ($CaCO_3$) through a carbonation process induced by the CO_2 in the atmosphere through a chemical reaction similar to the setting of the original plaster. However, the low solubility of calcium hydroxide in water (1.73 g/L at 20°C), the low stability of the system and high surface tension of water (as the medium) cause aggregation and phase separation resulting in inefficient penetration, poor consolidation strength and whitening of the surface. Several strategies including "sucrose methods" to increase $Ca(OH)_2$ solubility (*7, 29*) and the synthesis of $Ca(OH)_2$ nanoparticle-alcohol dispersions to prevent agglomeration and improve penetration have been reported (*21*). Yet, in spite of improved working and performance properties, the sensitivity of $CaCO_3$ to a drop in the pH (caused by acid rain and other acid local environments for example) or a phase transformation into gypsum ($CaSO_4 \cdot 2H_2O$) in the presence of sulfate ions (known as 'sulfation') poses limitations in the use of $Ca(OH)_2$-based consolidants. Other inorganic mineralization treatments based on barium or oxalate salts have been questioned due to concerns related to the toxicity of barium (not all nations permit the use of barium in conservation) and the limited penetration of oxalates into a porous medium (*3, 30, 31*).

Recent studies (*31–35*) have demonstrated a considerable potential for developing much improved consolidation methods by bio-mimicking the growth of hydroxyapatite ($Ca_{10}(PO_4)_6(OH)_2$, HAP), the main mineralogical component of teeth and bones on limestone matrices (*31, 32, 34, 36*). In this research, we explore similar principles to induce the in situ formation of protective HAP crystals by triggering reactions between the Ca in the calcium carbonate ($CaCO_3$)-rich plaster layers of wall paintings and ammonium phosphate precursors. Both monoammonium (MAP) and diammonium hydrogen phosphate (DAP) precursors were tested though here only the use of the latter is discussed. Other soluble phosphate-based salts such as potassium/sodium phosphates could also serve as a source of phosphorous. However, in conservation applications it is not advisable to use Na^+ and K^+ cations as upon penetration they may combine with anions present in the system (or deposited from the atmosphere) to form Na and K salts that could be detrimental to the preservation of the wall paintings (*37, 38*).

The theoretical chemical pathway of the HAP formation using DAP as the precursor is presented below (Reaction 1) (*35*) and a schematic diagram of the anticipated consolidation effect in Figure 1.

$$10\ CaCO_3 + 6\ (NH_4)_2HPO_4 \rightarrow \mathbf{Ca_{10}(PO_4)_6(OH)_2} + 10CO_2\uparrow + 12NH_3\uparrow + 8H_2O$$
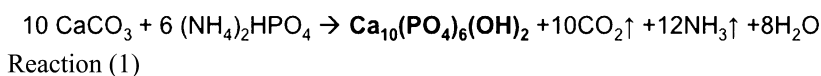
Reaction (1)

In reality, the HAP formed through this reaction may be non-stoichiometric; Ca deficient or HAP containing substituted carbonate species may form (*34, 35, 39, 40*). The HAP precipitation is expected to be preceded by the formation

of intermediate metastable phases, such as amorphous calcium phosphate, monocalcium phosphate monohydrate, dicalcium phosphate dehydrate and/or octacalcium phosphate. These intermediate phases whose formation depends on the reaction conditions (e.g., degree of supersaturation, temperature, pH, presence of foreign ions, etc.), are expected to transform into HAP or its ion-substituted analogues (*34*, *36*, *39*, *41*, *42*). The resulting hydroxyapatite network is expected to improve cohesion between loose particles at the immediate subsurface of wall painting. Since hydroxyapatite is reported to be stable in a wide pH range (between ~pH 4 and 14) (*43*), increased resistivity towards an acid environment is anticipated (*44*).
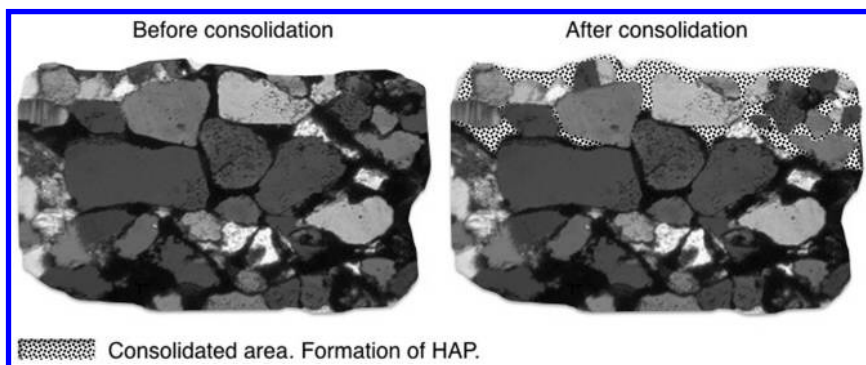
Figure 1. Schematic representation of the in situ consolidation of a wall painting plaster. HAP (black dotted surface) forms on the top of the surface treated, preferentially in areas occupied by microcrystalline $CaCO_3$ (plaster binder). The large grey/whitish particles represent aggregates in the plaster layer. Not in scale.

Experimental Methods

Materials for the Preparation of Wall Painting Test Blocks

Wall painting plaster test blocks were used to test the hydroxyapatite (HAP) consolidation effect. The test blocks were prepared by mixing 1) commercial calcium hydroxide (lime putty) with marble dust (0.2-0.6 mm) and deionized water at 1:4:1 volumetric ratio and 2) commercial lime putty with sand (0.2-0.6 mm) at the same ratio as above. The mixtures at a consistency of a dense paste (mortar) were subsequently placed in custom-made stainless-steel molds (5cm x 5cm x 2cm) and left to dry at 25° C and ~60% RH for one week. Consequently the samples were de-molded and left to set fully for 6 months in order to ensure full conversion of the $Ca(OH)_2$ binder to $CaCO_3$.

The lime putty, marble dust and sand were purchased from Kremer Pigments Inc.

Application and in Situ Formation of HAP

For the application of the reagent, cellulose compresses (poultices) were prepared of 1 and 2 M DAP. Each compress was approximately 1 cm thick. A permeable very thin tissue of compact weave was placed at the interface between the wall painting test block and the cellulose poultice to prevent cellulose fibers from sticking on the surface of blocks (Figure 2). Three and six hours of contact time were tested. Cellophane foil was used to cover the cellulose compress in order to prevent the solution from evaporating too fast. During the reaction, a faint smell of ammonia was detected. After completion of the treatment, the cellulose poultice was removed and the test blocks were left to dry in air.

The DAP solutions were made using deionized water and analytical reagent grade diammonium hydrogen phosphate purchased from Fisher Scientific. Each cellulose compress was prepared by mixing Arbocel cellulose fibers: BC 200 and BWW 40 at a volumetric ratio of 0.4 (BC 200) : 0.6 (BWW 40) : 0.9 (DAP solution). Tengucho tissue purchased from Hiromi Paper, Inc. was used as the intermediate supporting layer.
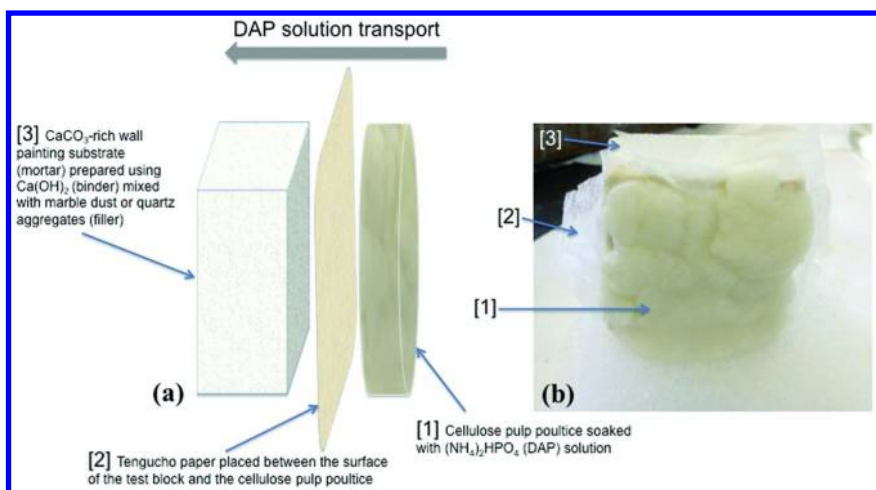
Figure 2. Example of an application of the consolidation treatment on the wall painting test blocks (a: schematic, b: actual).

Determination of Carbonation Level of Simulated Wall Painting Substrate Test Blocks

The calcium carbonate/calcium hydroxide content was determined using thermal analysis (TG/DTG) performed in a nitrogen environment using a Perkin Elmer STA 6000 thermal analyzer. Temperatures were scanned in the range between 35-980°C and heating rate was set for 10°C/min.

Morphological and Physicochemical Characterization of HAP and Assessment of Treatment Efficiency

The effectiveness of the treatment in providing consolidation action and the formation of HAP network was evaluated using scanning electron microscopy (SEM) at variable pressure (VP) coupled with energy dispersive x-ray spectroscopy (EDS); X-ray fluorescence spectroscopy (XRF); water sorption test and scotch tape test.

SEM-EDS

SEM analysis was performed using the FEI Nova™NanoSEM 230. To avoid the necessity of carbon or metal sputtering, a low vacuum mode (variable pressure) was applied during the analysis.

Morphological and topographic characteristics of the surface before and after treatment were recorded using the secondary electron detector (SE). The depth of penetration and spatial localization of the newly phosphate-containing forms was assessed using backscattered electron detector (BSE) and energy dispersive x-ray spectroscopy (EDS) on polished sections. Polished sections were prepared by embedding samples in epoxy resin (Buehler EpoxiCure®) mixed with EpoxiCure® Epoxy Hardener and placed under vacuum using the Buehler Cast n' Vac 1000. Once the resin had set, the samples were cut using Labcut 1010 low speed diamond saw and ground using Buehler silicon carbide grinding papers from 240 to 1200 grit. Samples were subsequently polished on a Leco® GP-25 polishing turntable using water-based diamond suspensions of 6 µm and 1 µm followed by colloidal silica of 0.2 µm spread on Buehler® MasterTex polishing cloths.

XRF

XRF data provided complementary semi-quantitative results on the phosphorous content using the Thermo Scientific Niton® XL3t Series GOLDD™ technology handheld XRF analyzer with a silver anode and silicon drift detector. As all the consolidation trials were performed on the test blocks positioned vertically, it was anticipated that measured P content would be higher for the slices taken from the bottom of the sample due to the gravity, while slightly lower for the slices taken from the top of the wall painting test blocks. To have the most representative and consistent information sections from the center of the samples were chosen for the preliminary XRF analysis. More detailed XRF information on the gravity effect will be conducted in the scope of future analysis.

Water Sorption Test

The water sorption test was conducted following a modified version of the ASTM standard C1585. For this test both untreated and treated test blocks were kept in the atmospheric air at $20 \pm 3°C$ at around 60% RH (relative humidity) for the period of 7 days prior to testing. All sides of each test block (except the surface receiving the treatment) were sealed tightly with duct tape. The surfaces of untreated and treated samples were placed in contact with the water (immersed between 1-3 mm) and the mass of each sample was monitored to the nearest 0.01 g at the intervals specified in the standard.

The absorption, I was calculated according to the equation 1.

$$I = \frac{m_t}{a/d} \qquad\qquad Equation\ (1)$$

where:
I = the absorption
m_t = the change in specimen mass in grams, at the time t
a = the exposed area of the specimen, in mm^2
d = the density of the water in g/mm^3

Scotch Tape Test

The scotch tape test (adhesion test) was performed based on a modified version of the ASTM standard D3359. Strips of scotch tape (4 cm long) were pressed onto the surface of each sample using enough fingertip pressure to remove all visible air bubbles and make good contact between the tape (adhesive side) and the surface. The tape was then peeled off in a single smooth motion. Systematic mass analysis of the tape before and after adhesion with the mortar surface provided an indication of the consolidation treatment performance. The results were evaluated visually and quantitatively based on the amount of material separated from the surface before and after the consolidation treatment.

Results and Discussion

Simulation of Wall Painting Substrate Test Blocks

Thermal analysis (TG/DTG) data revealed that after 6 months in air and at room temperature (~25°C) the surface of the test blocks was completely carbonated whereas the core was carbonated at ~96% (±1%). Example of the TG/DTG evaluation is presented in Figure 3 (a,b) and Table I (a), I (b). Mass losses were determined from the TG curve by the points of deviation for the tangent lines to the curve observed for the weight loss versus temperature. Peak recorded between around 390°C and 550°C corresponds to the dehydration of $Ca(OH)_2$ to CaO and H_2O, while weight loss recorded between 600°C and 950°C comes from the decomposition of $CaCO_3$ to CaO and CO_2.
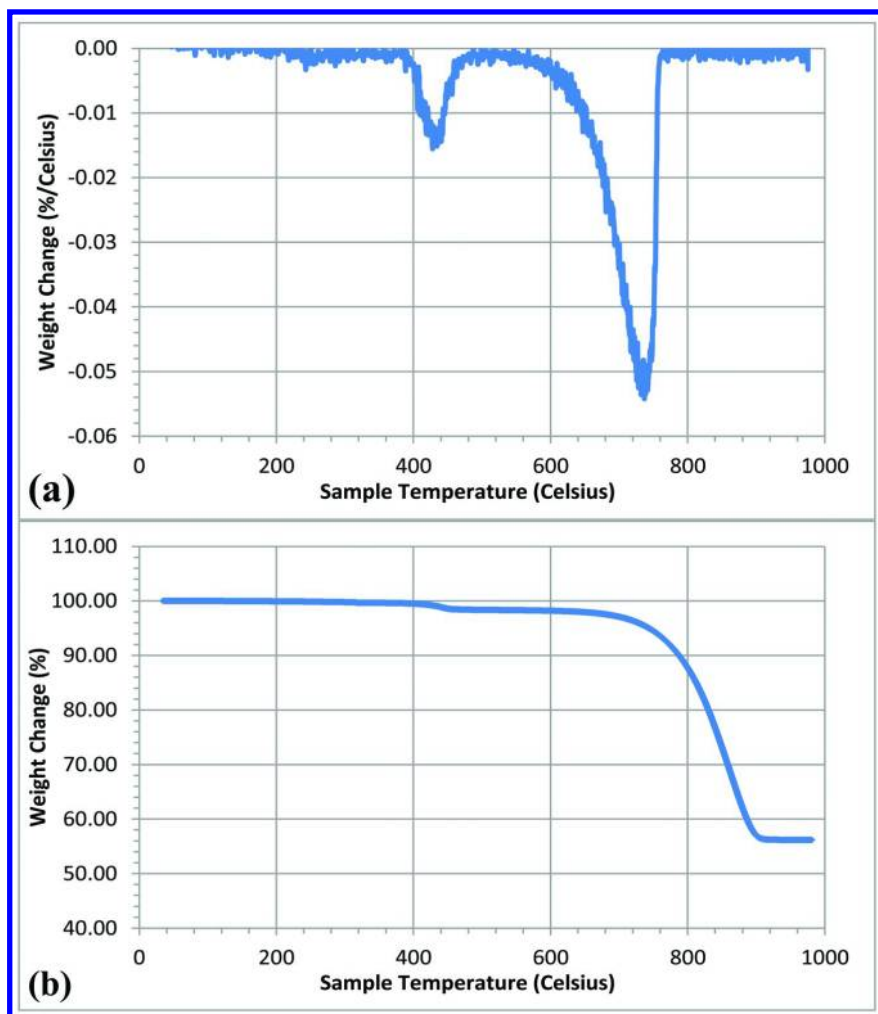
Figure 3. TG/DTG characteristics of test block prepared from marble dust and lime putty after 6 months of carbonation in the air: sample taken from the core; (a) TG (thermogravimetric analysis)- mass loss versus temperature; (b) DTG - derivative of mass loss.

Table I (a). Calculation of Ca(OH)₂ content from the TG/DTG curves (Figure 3)

Temperature (°C)	Sample Mass (mg)	% Mass
390	75.20	99.62
500	74.23	98.35
Ca(OH)₂ Content (%)	5.2 (±1%)	

Table I (b). Calculation of CaCO₃ content from the TG/DTG curves (Figure 3)

Temperature (°C)	Sample Mass (mg)	% Mass
600	74.21	98.32
950	42.39	56.16
CaCO₃ Content (%)	95.8 (±1%)	

Morphological and Physicochemical Characterization before and after Treatment

SEM-EDS

The morphology and topography of the surface of the wall painting test blocks before and after the consolidation treatments was characterized using scanning electron microscopy. Secondary electron micrographs of the control (untreated) samples show large grain-aggregates of marble dust or quartz within a microcrystalline $CaCO_3$ matrix formed through the carbonation of quenched lime (slaked lime, $Ca(OH)_2$) used as the binder (Figure 4 (a,b)).

The treated samples show the formation of calcium phosphate phases (Figures 5 (a,b) and 6 (a,b)) as a result of the in situ reaction between the DAP solution and the Ca mainly from the microcrystalline $CaCO_3$ binder, though the Ca from the larger marble dust particles has also contributed in the formation of calcium phosphate phases.

Elemental analysis using EDS of the Ca-P phases on unmounted samples, though provided semi-quantitative indication on the element wt% content, it enabled some rough evaluations to be made. The P content measured by EDS in phosphorous-rich regions (at spatial resolution of ~1 μm) ranged between ~ 3-6 wt% for 1 M treatments (Table II(a), II(b)) and ~ 2-5 wt% for 2 M treatments (Tables III(a), III(b) and IV(b)). DAP consolidation treatments at 1M concentrations seem to result in precipitation of a much more homogenous network of calcium phosphate crystals (Figure 5 (a,b)) compared to the 2 M DAP treatments (Figure 6 (a,b)). In the test blocks prepared with marble dust

in particular (but also those prepared with quartz aggregate), large crystals of a different Ca-P phase were also present (Figure 7 (a,b)). The P content of this phase ranged between ~9 and 17.5 wt% (Table IV(a), IV(b)). Traces of magnesium (Mg) were also identified.

Though it has not been directly confirmed, it is thought that the newly formed calcium phosphate phase using 1 M DAP is in fact hydroxyapatite. Taking into consideration the experimental conditions (25°C and pH~8 which corresponds to 1M DAP), HAP seems to be thermodynamically the most favored phase to form due to its low solubility and crystallographic compatibility with calcite (the solubility product of HAP at 25 °C being $K_{sp} = 1.6 \cdot 10^{-117}$) (*34*, *39*). The theoretical P content of the ideal hydroxyapatite is approximately 18.5 wt% and the Ca/P molar ratio is close to 1.67. These values significantly differ from what we have observed. However, as already mentioned above, an ideal hydroxyapatite in nature rarely precipitates from the aqueous solutions and therefore it is more common to form hydroxyapatite which is non-stoichiometric and substituted by various ions, such as carbonate ions. Also in this research, the reaction between the DAP and the $CaCO_3$-rich matrices does not involve complete transformations and the overwhelming signal of the unreacted $CaCO_3$ affects the measured Ca to P ratio.

XRD analysis of samples taken from the treated with DAP surfaces (for 3 and 6 hours of reactant treatment time) did not yield a positive identification of Ca-P phases owing to the very strong signal of the dominating $CaCO_3$ and/or SiO_2 particles used as aggregates in the test blocks.

The phosphorous content and profile distribution was also assessed through SEM-EDS on polished cross-sectional areas at the core of the sample. Micrographs and EDS elemental spectra and maps were taken at specific areas along the sample width: a) close to treated surface; b) in the center and c) at the bottom margin (furthest from the surface). Phosphorous (P) maps indicated newly formed calcium phosphate phases located in areas originally occupied by the microcrystalline $CaCO_3$ matrix (Table V(a), V(b), Figures 8 (a,b), 9 (a,b,c) and 10 (a, b,c)). Phosphorus content (measured at 1 μm² of surface area) ranged between 1 and 7 wt% for samples treated with 1 M DAP (Tables VI and VII) and between 1 and 10 wt% for samples treated with 2 M DAP. Traces of chlorine (Cl) were attributed to the epichlorohydrin in the hardener of the epoxy resin used for the preparation of the cross-sections.

The P concentration was found to be higher closer to the surface of the sample which was in contact area with the DAP saturated compresses and in areas surrounded by large pores as more of the DAP solution could enter and fill up nearby pores and react with surrounding $CaCO_3$. As SiO_2 particles are not expected to react with the DAP solution, the formation of calcium phosphate phases for the quartz-based test blocks is considered as the result of the DAP interaction with the microcrystalline $CaCO_3$ binder surrounding the quartz aggregate (Figure 10 (a-d)). Since the marble dust is composed of calcite ($CaCO_3$) it is believed that in the case of the marble dust test blocks, the calcite aggregates also partially react with the DAP solution (Figure 9 (a-c)). The extent of this reaction may be kinetically restrained due to the short contact times (between 3-6 hours) of the proposed consolidation treatments.

In Archaeological Chemistry VIII; Armitage, R., et al.;
ACS Symposium Series; American Chemical Society: Washington, DC, 2013.
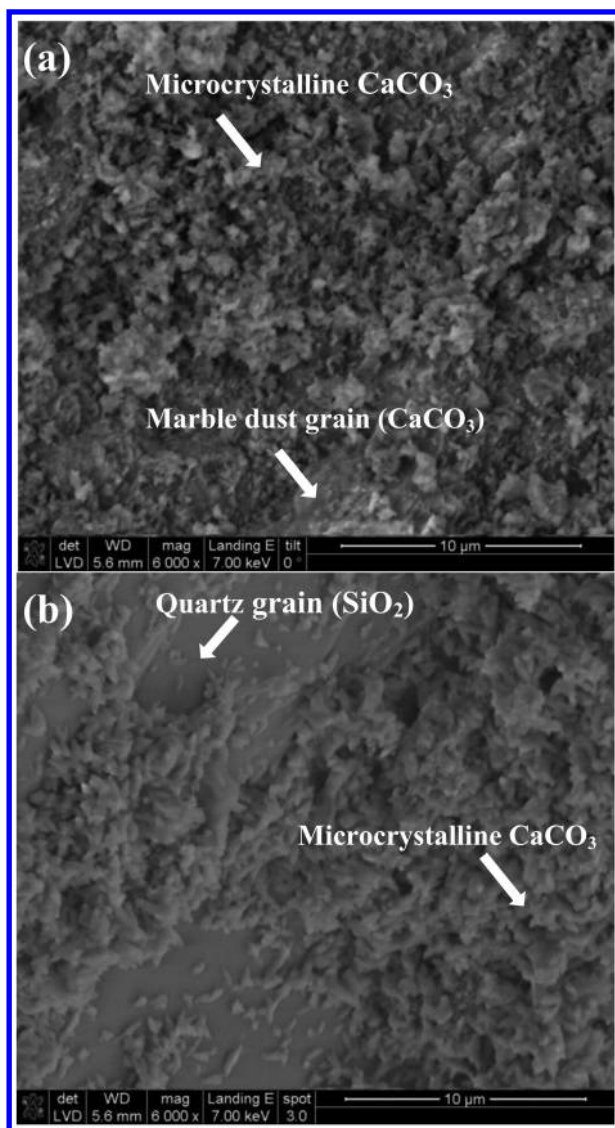
Figure 4. Surfaces of untreated wall painting test blocks prepared from lime putty and aggregates at 1:4 volumetric ratio; (a) marble dust aggregates; (b) quartz aggregates.
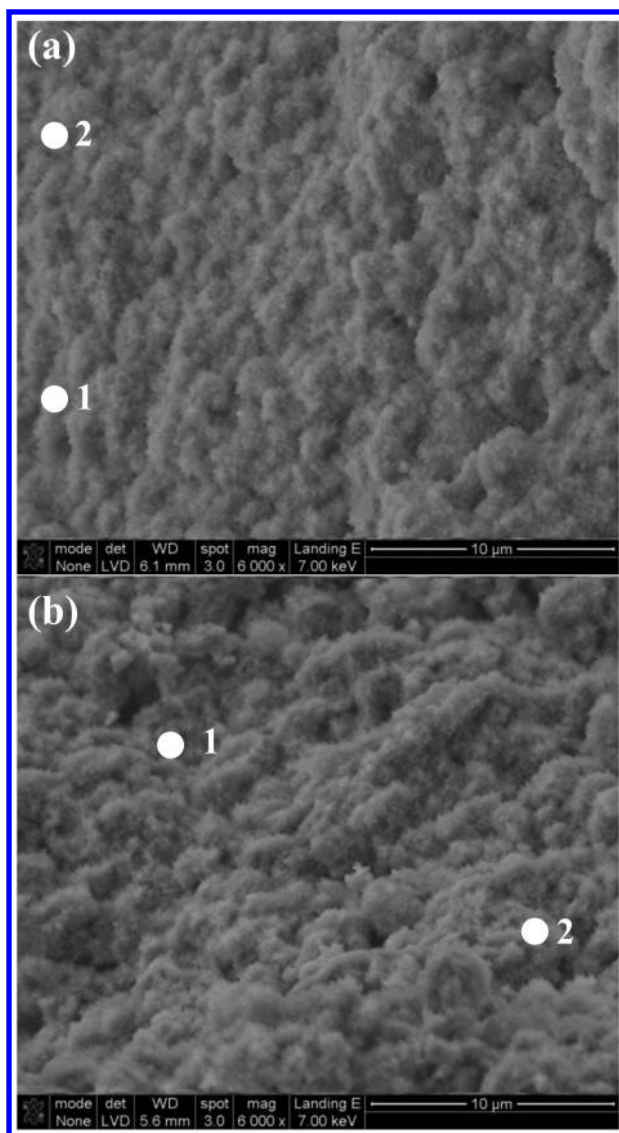
Figure 5. Surfaces of wall painting test blocks prepared from lime putty and aggregates treated with 1M DAP solution for 6 h; (a) samples prepared from marble dust note the formation of calcium phosphate crystals network, points 1 and 2 indicate the areas analyzed using EDS-Table II(a)(a); (b) samples prepared from quartz showing the formation of a calcium phosphate network over the microcrystalline $CaCO_3$ binder in the region where it completely covers SiO_2 grains, points 1 and 2 indicate the areas analyzed using EDS-Table II(b)(b).
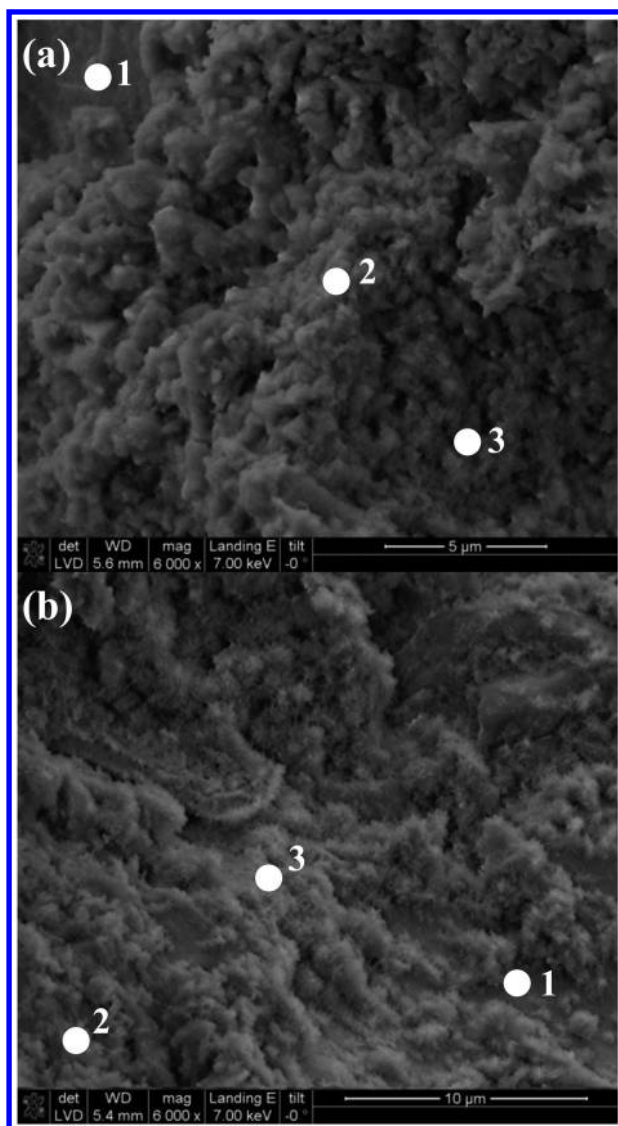
Figure 6. Surfaces of wall painting test blocks prepared from lime putty and aggregates treated with 2M DAP solution for 3 h; (a) samples prepared from marble dust, points 1, 2 and 3 indicate the areas analyzed with EDS-Table III(a)(a); (b) samples prepared from quartz aggregates, points 1, 2 and 3 indicate areas analyzed using EDS-Table III(b)(b).
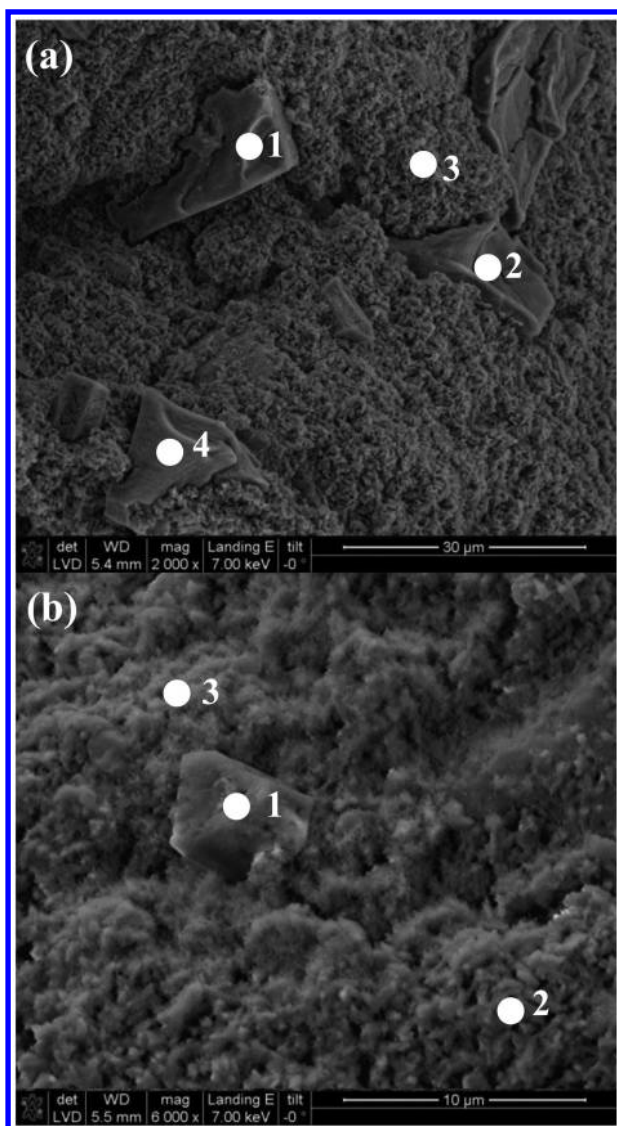
*Figure 7. Surface of wall painting test block prepared from lime putty and
aggregates treated with 2M DAP solution for 3 h showing the formation of
different calcium phosphate phases; (a) samples prepared from marble dust
aggregates, points 1,2 and 4 show large Ca-P crystals of ~150-250 μm², points
1-4 indicate the areas analyzed using EDS-Table IV(a)(a); (b) samples prepared
from quartz aggregates, points 1, 2, and 3 show areas analyzed using EDS-Table
IV(b)(b).*

Table II(a). Weight % of elements measured on the surface of the wall painting test block (prepared using marble dust aggregates and treated with 1M DAP solution for 6 h) in areas 1 and 2 as indicated in Figure 5(a)

Measured point	C content	O content	P content	Ca content
1M marble-1	7.21	37.40	3.75	51.64
1M marble-2	6.94	38.38	5.57	49.10

Table II(b). Weight % of elements measured on the surface of the of the wall painting test block (prepared using quartz aggregates and treated with 1M DAP solution for 6 h) in areas 1 and 2 as indicated in Figure 5(b)

Measured point	C content	O content	Mg content	Si content	P content	Ca content
1M quartz-1	14.72	48.66	0.00	1.00	3.37	32.25
1M quartz-2	14.69	56.06	0.39	1.12	3.15	24.58

Table III(a). Weight % of elements measured on the surface of the wall painting test block in (prepared using marble dust aggregates and treated with 2M DAP solution for 3 h) areas 1, 2 and 3 as indicated in Figure 6(a)

Measured point	C content	O content	P content	Ca content
2M marble-1	11.20	29.29	2.05	57.46
2M marble-2	9.05	31.72	2.54	56.69
2M marble-3	16.62	50.91	2.71	29.76

Table III(b). Weight % of elements measured on the surface of the wall painting test block (prepared using quartz aggregates and treated with 2M DAP solution for 3 h) in areas 1, 2 and 3 as indicated in Figure 6(b)

Measured point	C content	O content	Al content	Si content	P content	C content
2M quartz-1	28.61	50.10	0.63	18.81	0.00	1.85
2M quartz-2	15.94	51.51	0.00	3.30	1.48	27.77
2M quartz-3	17.39	44.99	0.00	8.87	4.03	24.72

Table IV(a). Weight % of elements measured on the surface of the sample (prepared using marble dust, treated with 2M DAP for 3 h) in areas 1-4 as indicated in Figure 7(a). Points 1, 2, and 4 show large crystals of a different calcium phosphate phase.

Measured point	C content	O content	P content	Ca content
2M marble-1	10.32	39.84	17.37	32.46
2M marble-2	9.28	57.66	11.34	21.72
2M marble-3	13.78	48.75	0.76	36.71
2M marble-4	8.76	51.25	15.03	24.95

Table IV(b). Weight % of elements measured on the surface of the sample (prepared using quartz, treated with 2M DAP solution for 3 h) in areas 1, 2 and 3 as indicated in Figure 7(b). Point 1 shows a large crystal of a different calcium phosphate phase.

Measured point	C content	O content	Mg content	Al content	Si content	P content	Ca content
2M quartz-1	14.89	51.28	4.43	0.00	1.63	8.85	18.93
2M quartz-2	19.71	40.59	0.00	0.00	2.93	4.62	32.15
2M quartz-3	21.50	43.67	0.46	1.44	13.86	3.56	15.51

To investigate the formation of calcium phosphate phases on marble dust grains an additional experiment was conducted where loose marble dust particles (diameter 0.2-0.6 mm) were placed in a beaker containing 1M DAP (solid/solution ratio 1:10) and left in the solution for 1 week. Subsequently, the solid was filtered, dried in the air for 3 days and analyzed using SEM. The grains showed a platy morphology with large well defined crystals, typical for the hexagonal hydroxyapatite phase (Figure 11) (*45*) and characteristic for the carbonate substituted hydroxyapatite (*46*).
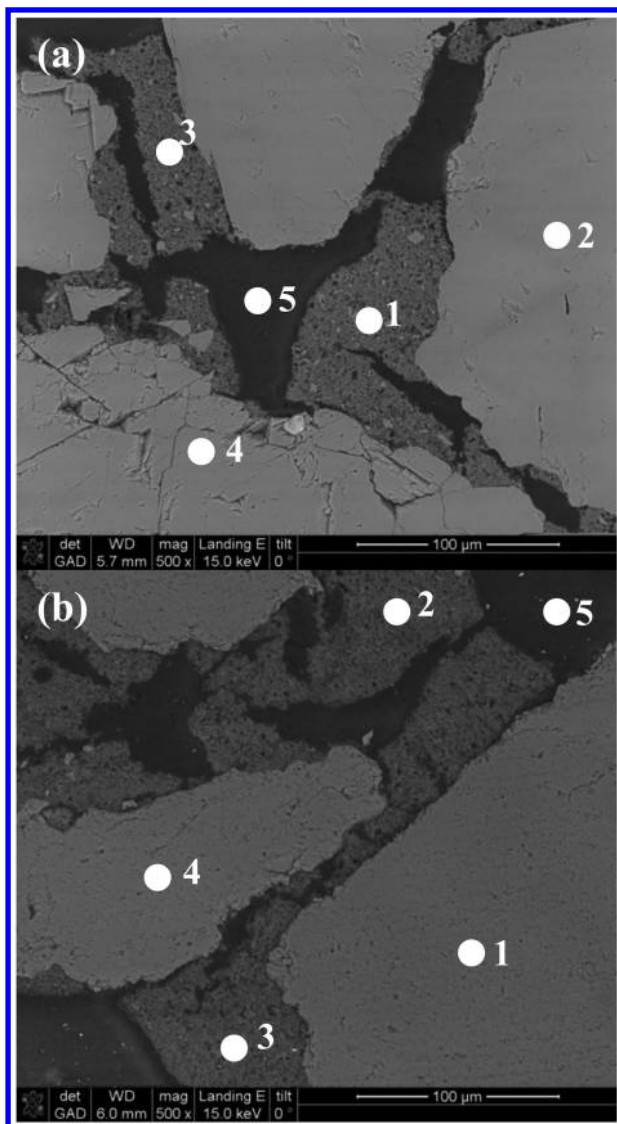
Figure 8. SEM-BSE micrograph of a polished section of the wall painting test block prepared from lime putty and aggregates; (a) marble dust aggregates: untreated, points 1-5 indicate the areas analyzed using EDS-Table V(a)(a); (b) quartz aggregates: untreated, points 1,2 and 3 indicate areas analyzed using EDS-Table V(b)(b).
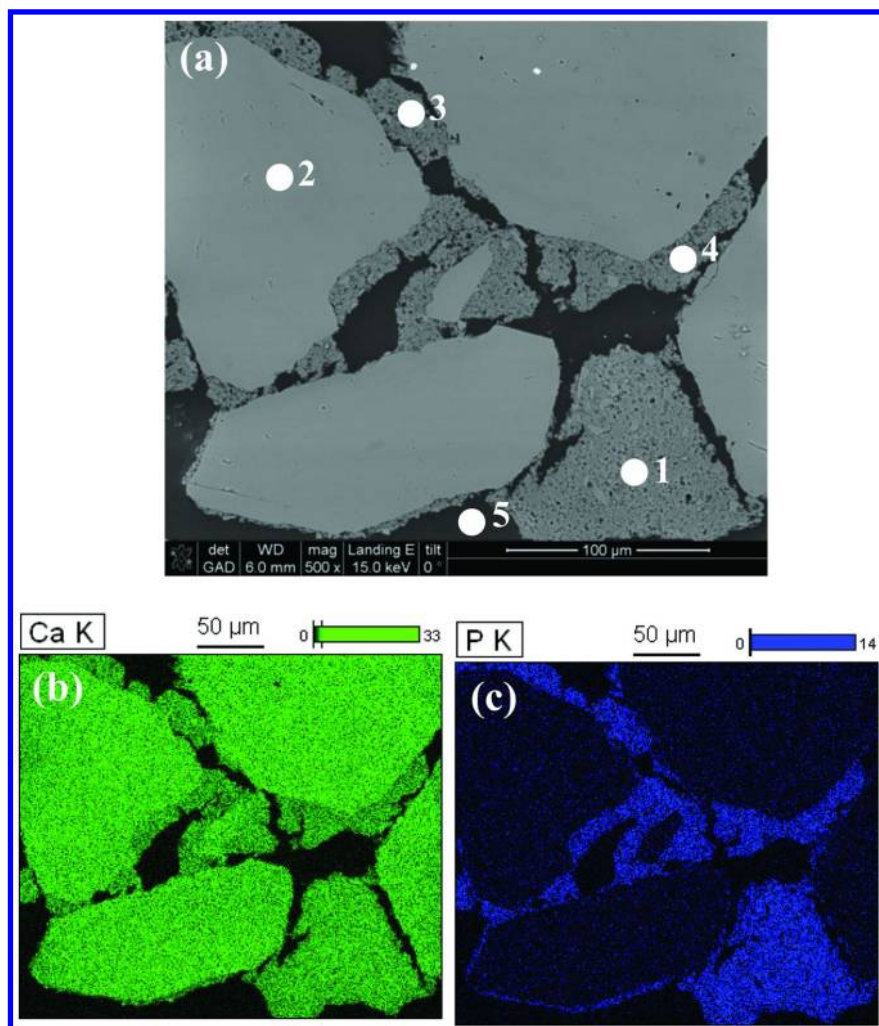
Figure 9. SEM-EDS images of a polished section of a wall painting test block prepared from lime putty and marble dust aggregates and treated for 6 h with 1M DAP solution; (a) points 1-5 indicate areas analyzed using EDS-Table VI; (b) elemental map indicating the spatial distribution of Ca in a cross-sectional view of a test. This image shows that the Ca is located in areas corresponding to the marble dust particles as well as the microcrystalline CaCO₃ binding matrix; (c) elemental map indicating the spatial distribution of P in a cross-sectional view of a test block. This image shows that the P is located in areas corresponding to the microcrystalline CaCO₃ binding matrix and at the boundaries of the large Ca-rich particles.
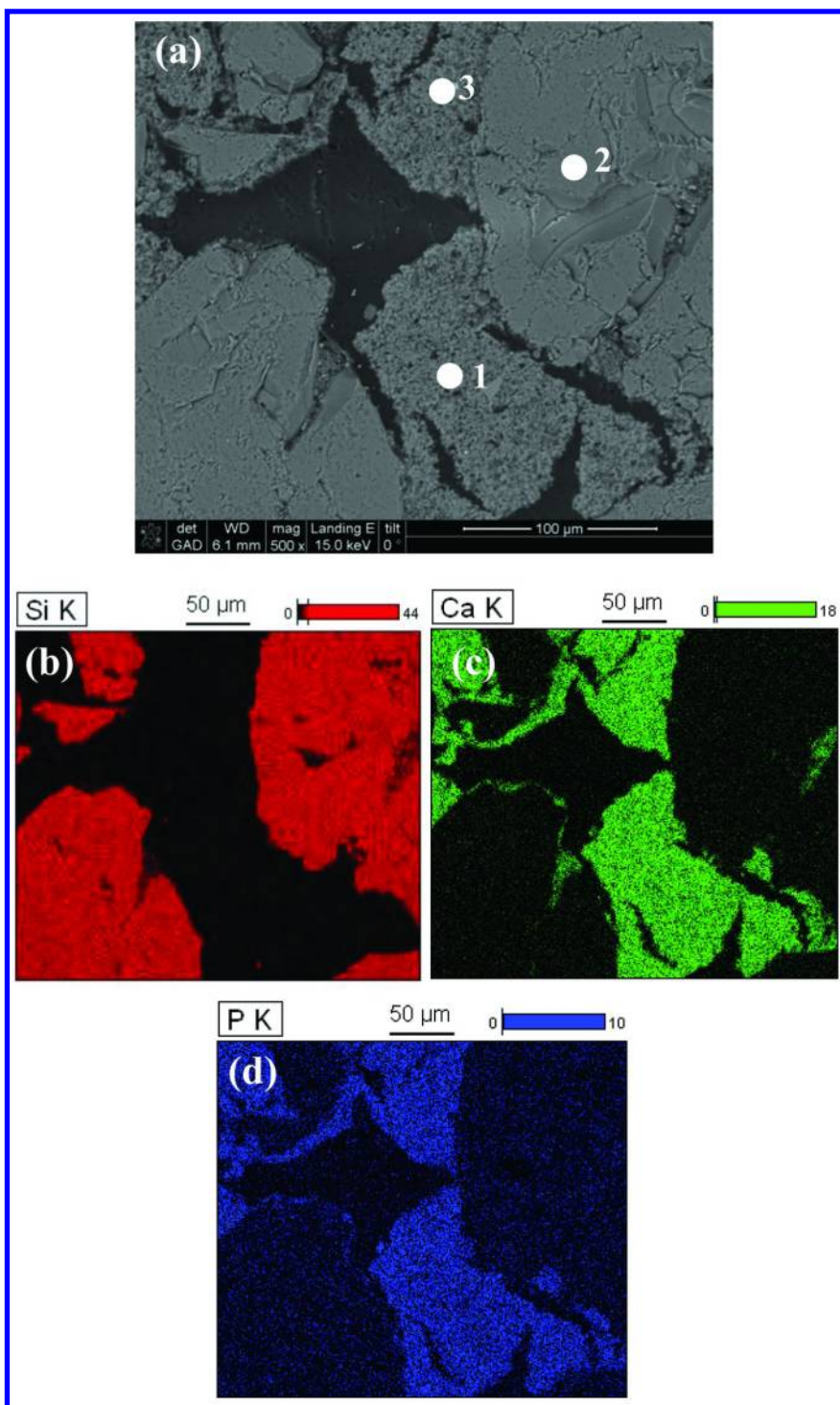
Figure 10. SEM-BSE micrograph of a polished section of a wall painting test block prepared from lime putty and quartz aggregates and treated for 6 h with 1M DAP solution; (a) points 1-3 indicate areas analyzed using EDS-Table VII; (b) elemental map indicating the spatial distribution of Si in a cross-sectional view of a test block. This image shows that the Si is located in areas corresponding to the quartz particles; (c) elemental map indicating the spatial distribution of Ca in a cross-sectional view of a test block. This image shows that the Ca is located in areas corresponding to the microcrystalline $CaCO_3$ binding matrix; (d) elemental map indicating the spatial distribution of P in a cross-sectional view of a test block. This image shows that the P is located in areas corresponding to the microcrystalline $CaCO_3$ binding matrix.

Table V(a). Weight % of elements measured on the surface of the untreated wall painting test block (prepared using marble dust aggregates) in areas 1-5 as indicated in Figure 8(a)

Measured point	C content	O content	Mg content	Cl content	Ca content
Untreated marble-1	25.77	43.89	0.25	0.00	30.09
Untreated marble-2	12.71	43.52	0.58	0.00	43.19
Untreated marble-3	32.45	40.72	0.33	0.00	26.50
Untreated marble-4	13.89	46.27	0.47	0.00	39.38
Untreated marble-5	84.01	8.94	0.00	2.33	4.72

Table V(b). Weight % of elements measured on the surface of the untreated wall painting test block (prepared using lime quartz aggregates), in areas 1 and 2 as indicated in Figure 8(b)

Measured point	C content	O content	Si content	S content	Cl content	Ca content
Untreated quartz-1	3.05	56.02	40.93	0.00	0.00	0.00
Untreated quartz-2	41.42	36.41	1.14	0.20	0.57	20.27
Untreated quartz-3	32.13	40.95	1.30	0.00	0.00	25.63
Untreated quartz-4	3.80	55.07	41.13	0.00	0.00	0.00
Untreated quartz-5	80.17	15.81	1.68	0.00	1.62	0.73

Table VI. Weight % of elements measured on the surface of the wall painting test block (prepared using marble dust aggregates and treated with 1M DAP solution for 6 h) in areas 1-5 as indicated in Figure 9(a)

Measured point	C content	O content	Mg content	P content	Cl content	Ca content
1M marble-1	12.43	37.21	0.14	6.80	0.00	43.42
1M marble-2	11.37	43.20	0.37	0.00	0.00	45.05
1M marble-3	21.16	41.20	0.25	4.83	0.00	32.57
1M marble-4	18.67	39.99	0.00	5.73	0.00	35.61
1M marble-5	84.09	8.84	0.00	0.00	2.80	4.28

Table VII. Weight % of elements measured on the surface of the wall painting test block (prepared using quartz aggregates and treated with 1M DAP solution for 6 h) in areas 1, 2 and 3 as indicated in Figure 10(a)

Measured point	C content	O content	Si content	P content	Ca content
1M quartz-1	30.66	37.13	1.27	3.98	26.96
1M quartz-2	3.69	52.09	44.23	0.00	0.00
1M quartz-3	24.03	41.48	1.06	4.40	29.02

XRF Data (Portable XRF)

XRF analysis was performed on both untreated and treated samples. XRF allowed for semi quantitative measurements of the P at relatively large areas of the sample (spot size ~ 8mm). XRF analysis was carried out on the same cross-sectional areas of the core of the samples analyzed with the EDS. As with the EDS analysis, each of the sections was measured in 3 locations: at the surface, in the center and at the bottom (away from the surface) of each slice (Figure 12).

For each sample an average (mean) of three XRF readings was calculated. It was observed that the P content decreases with increasing distance from the DAP saturated poultice (Figure 13 (a)) while the Ca concentration remained constant throughout the samples (Figure 13 (b)). The results indicated that at the surface (closer to the DAP poultice) the P concentration was the highest. However, even at the bottom of the section (furthest from the surface), phosphorous could be detected. This is an indication that the phosphorous (induced in the DAP solution) was transported for at least 2 cm distance using this application method.

As with the EDS analysis, the Cl detected (~0.3-0.5 wt %) was attributed to one of the components of the embedding resin used. P content of the untreated samples was below the limit of detection.
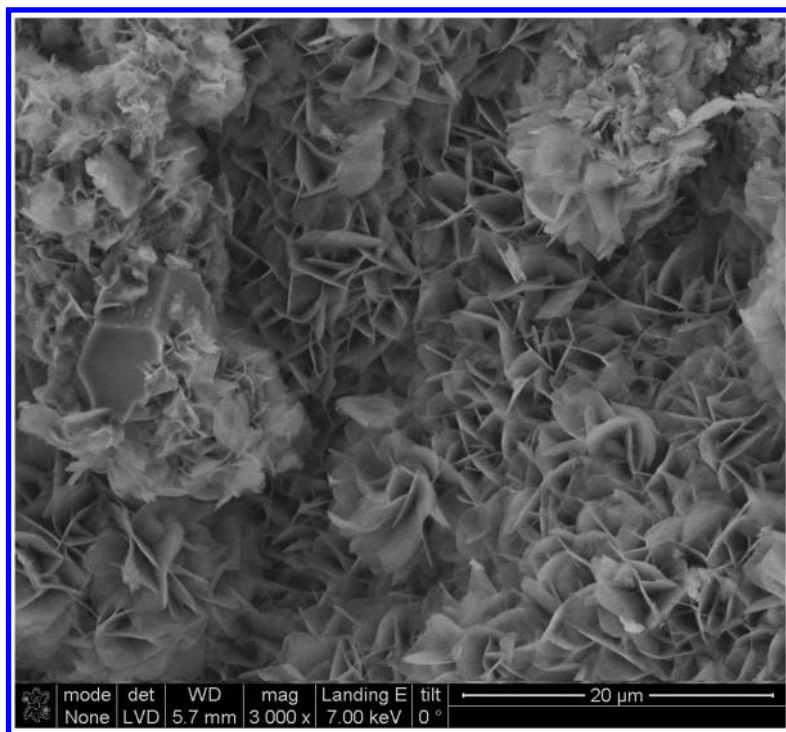
Figure 11. Detail of newly formed Ca-P phases on marble dust particles after immersion in 1M DAP solution for 1 week; note platy morphology typical for carbonate-substituted hydroxyapatite.
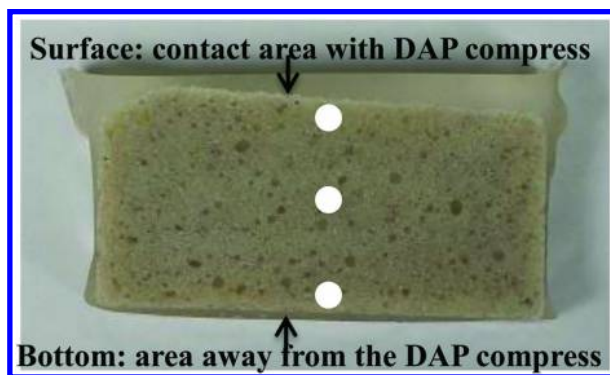
Figure 12. Polished cross-section of the sample analyzed using XRF spectroscopy. Elemental analysis (semi-quantitative) was performed on the surface, in the center and the bottom of the sample; white dots show the locations of the measurements.
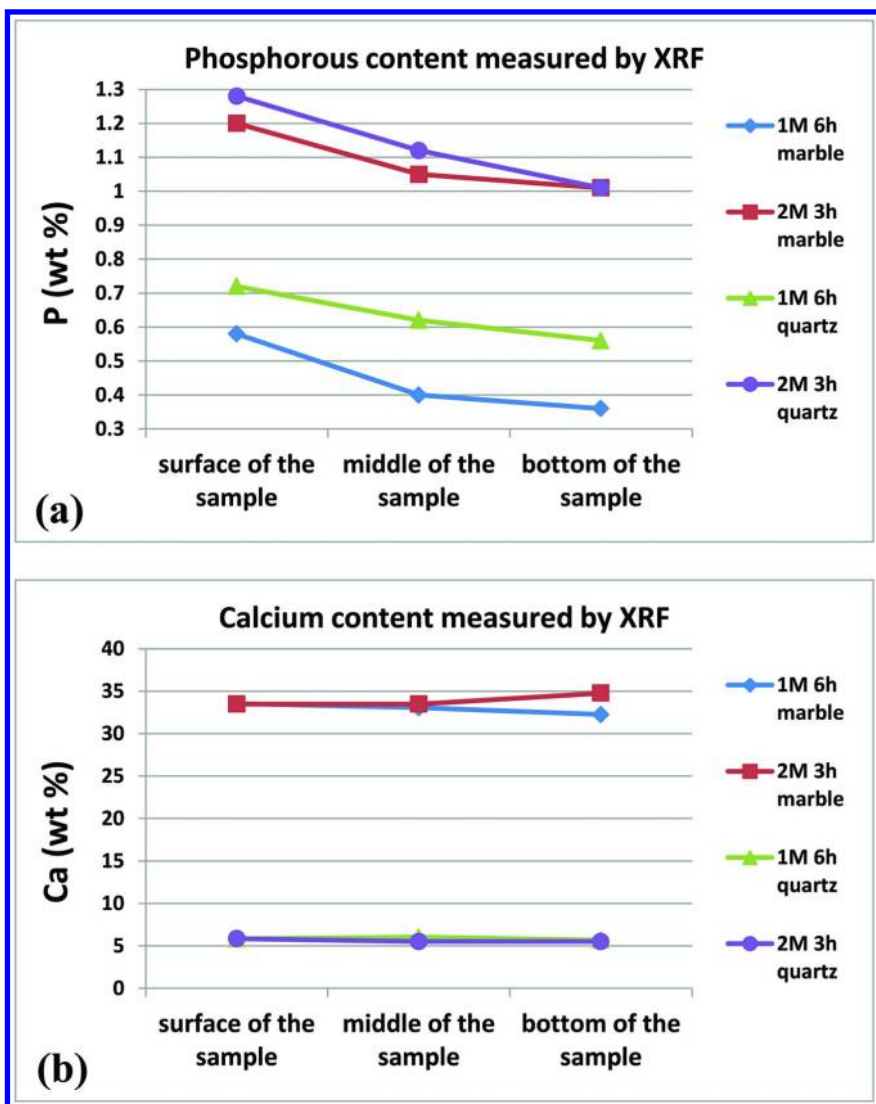
Figure 13. Mean values (n=3) of phosphorus (a) and calcium; (b) contents measured in wt%, at the surface, in the center and at the bottom of the wall painting test blocks at different consolidation treatments.

Water Sorption Test

The water sorption tests between untreated and treated samples show a final reduction in water sorptivity in the range of ~8-11 wt%. The results (Figure 14 (a,b)), show an exponential trend with noticeably reduced initial sorptivity in the DAP treated samples, compared to the untreated ones (time measured up to ~5 min). The delay in the water intake at the beginning of the test for the treated samples suggests potential change (reduction) in porosity, inhibiting water from

entering easily (*34*). In particular, the 2 M DAP-treated sample exhibited an initial sorption rate markedly lower (between ~ 20-32 wt%) than the untreated sample, possibly as a result of the higher pore system modification that occurred on the surface. For the 2 M DAP treatments, excessive whitening and formation of a thin 'crust' on the surface was also detected. This indicated the formation of a much denser layer of calcium phosphates in comparison to the 1 M treatments. However the sorptivity trends > 300 minutes seemed to be similar regardless to the DAP concentration.
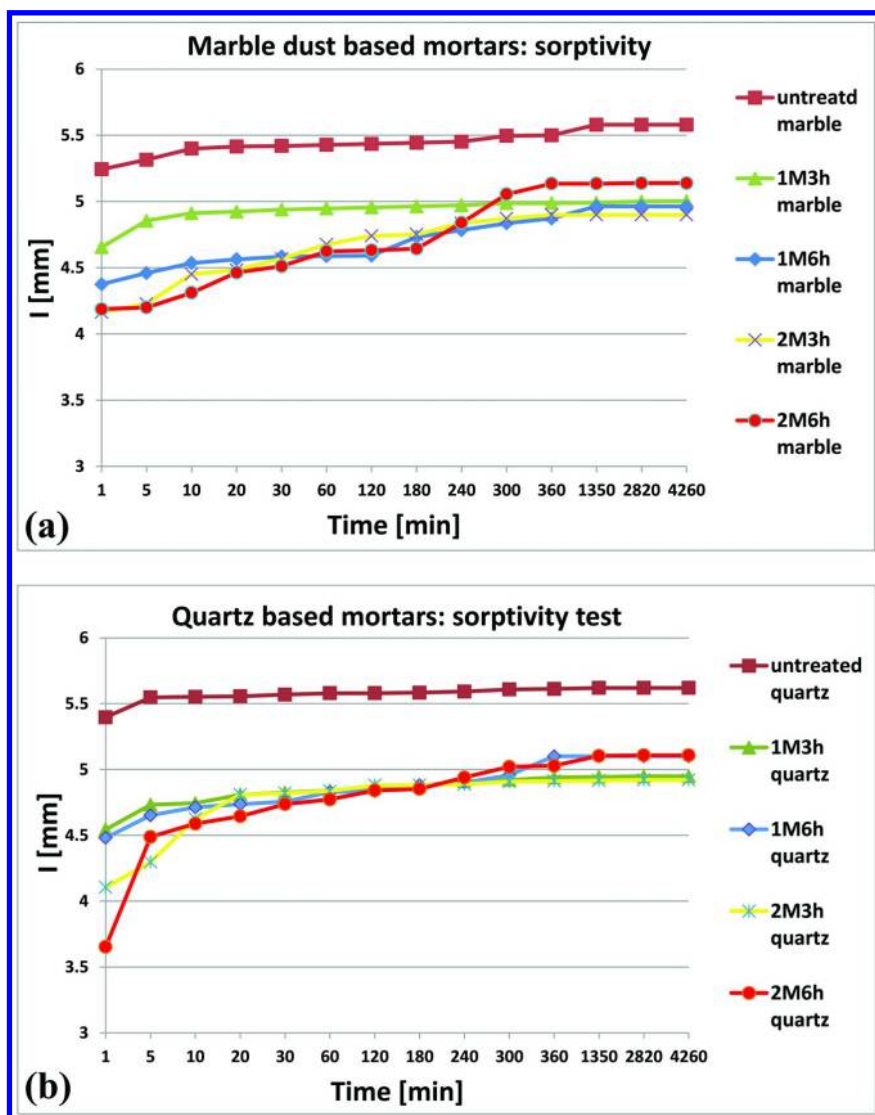
Figure 14. Water sorptivity measured for wall painting test blocks prepared from lime putty and (a) marble dust aggregates; (b) quartz aggregates, which undergone different consolidation treatments.

Scotch Tape (Adhesion) Test

Scotch tape (adhesion) tests were also used to evaluate the performance of the consolidation treatment (Figure 15). The results indicated that fewer particles were separated from the surface for the samples treated with DAP compared to the untreated samples. The mass change results before and after the consolidation are shown in Table VIII(a), VIII(b).
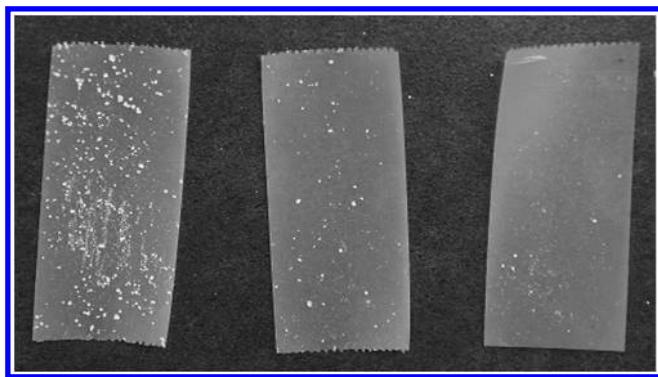
Figure 15. Photograph showing visually the results from the scotch tape test performed on a wall painting test block made with marble dust aggregates: untreated sample (left), 1M DAP treated for 6 h (center) and 2M DAP treated for 6 h (right). The treated samples clearly show a reduction of in the particles adhered to the tape suggesting an effective consolidation treatment.

Table VIII(a). Mass change before and after the consolidation treatment for wall painting test blocks prepared with marble dust aggregates

Treatment conditions	1M DAP 3h	1M DAP 6h	2M DAP 3h	2M DAP 6h
% of mass change before and after the consolidation	84.73%	88.18%	89.66%	98.52%

Table VIII(b). Mass change before and after the consolidation treatment for wall painting test blocks prepared with quartz aggregates

Treatment conditions	1M DAP 3h	1M DAP 6h	2M DAP 3h	2M DAP 6h
% of mass change before and after the consolidation	68.45%	69.90%	67.48%	83.01%

The smaller the percentage is, the better the consolidation effect of the surface. The best consolidation effect was observed for samples treated for 6 hours with 2 M diammonium hydrogen phosphate solution (DAP) e.g. for marble dust-based wall painting test blocks, 98% fewer particles detached in comparison with the untreated samples. However, excessive whitening of the surface was observed. Whitening is not desired as it aesthetically affects wall painting's appearance.

Conclusions

In situ phosphate-based consolidation utilizing ammonium phosphate precursors is a promising treatment to re-establish cohesion of powdery Ca-rich matrices such as wall paintings (like frescoes). Preliminary results indicated the formation of a porous hydroxyapatite network at the surface and subsurface of the wall painting test blocks; reduction of water absorption and insignificant color change. Less 'whitening' of the surface due to the formation of new phases was observed on samples treated with 1 M DAP solutions in comparison with 2 M DAP solutions. It was found that phosphate solution enters deeply into the wall painting test blocks and penetration depth of the proposed consolidation method is at least up to 2 cm.

Due to hydroxyapatite's wide pH stability an improved resistance against low pH (acid rains) is expected. Consolidation treatment seems effective for wall paintings and calcareous stones but is believed to have also potential for archaeological tooth, bone and fossil reconstruction. Investigations on bone consolidation are in progress in the scope of another conservation project.

Future Work

Future work will involve testing of different application methods (controlled spraying) and pre-treatment with nanoparticle calcium hydroxide, peptides and chitosan. Interactions of mineral and organic pigments such as cinnabar, green earth, malachite, orpiment, lead white, hematite, madder lake will be evaluated. Mechanical properties such as measurement of dynamic elastic modulus as well as porosity will be assessed for untreated and treated wall painting test blocks. Different precursors including monoammonium dihydrogen phosphate (MAP) and their consolidation applicability are currently being evaluated. Thermodynamic equilibrium-based modeling to predict and optimize formation

of calcium phosphate phases is in progress. Weathering tests as well as resistance towards acid rains and aggressive salts ingress will be performed in the last stage of the project.

Acknowledgments

References

1. Kickelbick, G. In *Hybrid Materials. Synthesis, Characterization, and Applications*; Wiley-VCH, Verlag GmbH & Co. KGaA: Weinheim, Germany, 2007; pp 1−46.
2. Borgia, G. C.; Camaiti, M.; Cerri, F.; Fantazzini, P.; Piacenti, F. *Stud. Conserv.* **2003**, *48*, 217–226.
3. Baglioni, P.; Giorgi, R. *Soft Matter* **2006**, *2*, 293–303.
4. Miliani, C.; Velo-Simpson, M. L.; Scherrer, G. W *J. Cult. Herit.* **2007**, *8*, 1–6.
5. Dardes, K., Rothe, A., Eds.; *The Structural Conservation of Panel Paintings*; Proceedings of a symposium at The J. Paul Getty Museum, Los Angeles, April 24−28, 1993.
6. Lanterna, G.; Mairani, A.; Matteini, M.; Rizzi, M.; Scuto, S.; Vincenzi, F.; Zannini, P. In *Proceedings of the 9th International Congress on Deterioration and Conservation of Stone*; Fassina, V., Ed.; Elsevier: New York, 2000; pp 387−394.
7. Hansen, E.; Doehne, E.; Fidler, J.; Larson, J.; Matteini, M.; Ridriguez-Navarro, C.; de Tagle, A.; Teutonico, J. M.; Weiss, N. *Rev. Conserv.* **2003**, *4*, 13–25.
8. Laurenzi Tabasso, M. *APT Bull.* **1995**, *26*, 17–21.
9. Warren, J. In *Conservation of Earth Structures*; Butterworth-Heinemann: Oxford, U.K., 1999; p 121.
10. Chiari, G. In *6th International Conference on the Conservation of Earthen Architecture*; Adobe 90 preprints; Las Cruces, New Mexico, October 14−19, 1990; Grimstad; K., Ed.; The Getty Conservation Institute: Los Angeles, 1990; Vol. 273, pp 267−273.
11. Agnew, N.; Preusser, F.; Druzik, J. R. In *5th International Meeting of Experts on the Conservation of Earthen Architecture*; ICCROM: Rome, 1987; pp 75−79.
12. Brus, J.; Kotlik, P. *Stud. Conserv.* **1996**, *41*, 109–119.
13. Karatasios, I.; Theoulakis, P.; Kalagri, A.; Sapalidis, A.; Kilikoglou, V. *Constr. Build. Mater.* **2009**, *23*, 2803–2812.
14. Wheeler, G. *Research in Conservation*; The Getty Conservation Institute: Los Angeles, 2005.
15. Carretti, E.; Dei, L.; Baglioni, P. *Langmuir* **2003**, *19*, 7867–7872.

16. Wayne Smith, C. In *Archaeological Conservation Using Polymers: Practical Applications for Organic Artifact Stabilization*; Texas A&M University Press: College Station, TX, 2003; pp 1−144.

17. Scherrer, G. W.; Wheeler, G. S. *Key Eng. Mater.* **2009**, *391*, 1–25.

18. Giorgi, R.; Baglioni, M.; Berti, D.; Baglioni, P *Acc. Chem. Res.* **2010**, *43*, 695–704.

19. Ambrosi, M.; Baglioni, P.; Dei, L.; Giorgi, R.; Neto, C. *Langmuir* **2001**, *17*, 4251–4255.

20. Baglioni, P.; Giorgi, R. *Soft Matter* **2006**, *2*, 293–303.

21. Baglioni, P.; Giorgi, R.; Dei, L. *C. R. Chim.* **2009**, *12*, 61–69.

22. Elert, K.; Sebastian, E.; Valverde, I.; Rodriguez-Navarro, C. *Appl. Clay Sci.* **2008**, *39*, 122–132.

23. Giorgi, R.; Dei, L.; Baglioni, P. *Stud. Conserv.* **2000**, *45*, 154–161.

24. Matteini, M.; Lanterna, G.; Nepoti, M. R. In *The Oxalate Films in the Conservation of Works of Art*; Proceedings in the II International Symposium; Realini, M., Toniolo, L., Eds.; Milan, Italy, March 25−27, 1996.

25. Matteini, M.; Moles, A.; Giovannoni, S. In *The Conservation of Monuments in the Mediterranean Basin. Stone and Monuments: Methodologies for the Analysis of Weathering and Conservation*; Proceedings of the 3rd International Symposium; Fassina, V., Ott, H., Zezza, F., Eds.; 1994; pp 155−161.

26. Church, A. H. British Patent 220, 1862.

27. Warren, J. In *Conservation of Earth Structures*; Butterworth-Heinemann: Oxford, U.K., 1999.

28. Chelazzi, D.; Poggi, G.; Jaidar, Y.; Toccafondi, N.; Giorgi, R.; Baglioni, P. *J. Colloid Interface Sci.* **2013**, *392*, 42–49.

29. Hansen, E.; Doehne, E.; Fidler, J.; Larson, J.; Martin, B.; Matteini, M.; Rodriguez-Navarro, C.; Pardo, E. S.; Price, C.; Tagle, A.; Teutonico, J. M.; Weiss, N. *Rev. Conserv.* **2003**, 1–13.

30. Matteini, M. In *Conserving the Painted Past: Developing Approaches to Wall Painting Conservation*; Post-prints of a conference organized by English Heritage; Gowing, R., Heritage, A., Eds.; James & James: London, 2003; pp 110−115.

31. Matteini, M. In *Works of Art & Conservation Science Today*; Thessaloniki: Greece, November 26−28, 2010.

32. Yang, F.; Zhang, B.; Liu, Y.; Wei, G.; Zhang, H.; Chen, W.; Xu, Z. *New J. Chem.* **2011**, *35*, 887–892.

33. Liu, Q.; Zhang, B. *J. Mater. Sci. Forum* **2011**, *675-677*, 317–320.

34. Sassoni, E.; Naidu, S.; Scherer, G. W. *J. Cult. Herit.* **2011**, *12*, 346–355.

35. Kamiya, M.; Hatta, J.; Shimida, E.; Ikuma, Y.; Yoshimura, M.; Monma, H. *Mater. Sci. Eng.* **2004**, *B 111*, 226–231.

36. Matteini, M.; Rescic, S.; Fratini, F.; Botticelli, G. *Int. J. Archit. Herit.* **2011**, *5*, 717–736.

37. Steiger, M. *Restor. Build. Monum.* **2005**, *11*, 419–431.

38. Scherer, G. W.; Flatt, R; Wheeler, G. *MRS Bull.* **2001**, *26*, 44–50.

39. Dorozhkin, S. V. *Mater. Struct.* **2009**, *2*, 399–498.

40. Lee, Y.; Hahm, Y. M.; Matsuya, S.; Nakagawa, M.; Ishikawa, K. *J. Mater. Sci.* **2007**, *42*, 7843–7849.
41. Wang, L.; Nancollas, G. H. *Chem. Rev.* **2008**, *108*, 4628–4669.
42. Zhao, J.; Liu, W.; Zhang, H. *Chem. Cent. J.* **2011**, *5*, DOI: 10.1186/1752-153X-5-40.
43. Giere, R.; Stille, P. *Geol. Sci.* **2004**, 451, Special Publication 236.
44. Pan, H.; Darvell, B. W. *Arch. Oral. Biol.* **2007**, *52*, 618–24.
45. Kobayashi, T.; Ono, S.; Hirakura, S.; Oaki, Y.; Imai, H. *Cryst. Eng. Comm.* **2012**, *14*, 1143–1149.
46. Xia, W.; Lin, K.; Gou, Z.; Engqvist, H. In *Hydroxyapatite: Synthesis, Properties and Applications*; Gshalaev, V. S., Demirchan, A. C., Eds.; Nova Science Publishers, Inc.: New York, 2012; pp 243−264.

Chapter 23

"Comin' in on a Wing and a Prayer": Archaeological Chemistry Since 1790

A. M. Pollard*

Research Laboratory for Archaeology and the History of Art, University of Oxford, Dyson Perrins Building, South Parks Road, Oxford OX1 3QY, United Kingdom
*E-mail: mark.pollard@rlaha.ox.ac.uk

This paper reviews briefly the early history of archaeological chemistry, concluding that it is to be traced back to Revolutionary France and the last decade of the 18th century. This period saw a unique combination of the perfection of gravimetric means of chemical analysis and an interest in the contents of the 'cabinets of curiosities' of the day, which included archaeological objects. Particular emphasis is given to tracing the earliest published examples of the chemical analysis of copper alloys (probably Dizé) and of archaeological ceramics (possibly Vauquelin). The position of archaeological chemistry in the academic firmament is compared between 1790 and c. 2010, and it is found to be more marginal now, both to chemistry and archaeology. The reasons for this are explored. It is concluded that good archaeology requires open, respectful, meaningful and iterative dialogue across the many disciplinary boundaries involved.

It is now more than 60 years since Earle Caley began to publish his essays on the history of the relationship between chemistry and archaeology (*1–5*). The advent of the internet and eBooks has made researching the early history of this relationship considerably easier than it was in the 1940s, which only serves to increase the admiration due to Caley in achieving what he did. Caley saw the origins of archaeological chemistry occurring in the middle of the last decade of the 18th Century, and identified Martin Heinrich Klaproth (1743-1817) as one of the

pioneers. Subsequent research (*6*) has pushed back to 1790 the earliest published evidence for the analysis of archaeological metal, with the work of Michel Jean Jérome Dizé (1764-1852) (*7*). It is clear, however, that he was but one of a group of French chemists (including Réamur, Mongez, Fourcroy, and Darcet) interested in the analysis of copper alloys in Revolutionary France, although the main impetus for this appears to have been the need to convert bell metal to cannon (as discussed in (*6*)), rather than a strictly antiquarian interest!

This strand of archaeological chemistry is one which can be seen clearly evolving from two sources – firstly, the developing ability to produce systematic quantitative analyses of insoluble inorganic substances, and secondly, the evolving scientific interest in the 'cabinets of curiosities' of the day. Assaying in the 18th century and the evolution of mineral chemistry has been reviewed by Porter (*8*). The contribution of the 18th century European scientific revolution was to switch from trial by fire to dissolution, precipitation and careful weighing of the products – gravimetric analysis. According to Oldroyd (*9*), the first detailed analytical methodology for the analysis of gemstones is that of Sir Torbern Bergman (1735 – 1784), in his dissertation published in 1788, entitled 'of the Earth of Gems' (*10*). A more detailed and accurate protocol was published by Nicolas-Louis Vauquelin (1763-1829) in 1799 (*11*). Perhaps the most comprehensive analytical protocols of the late 18th century, which were to become the basis of all inorganic analyses until the adoption of instrumental methods in the early 20th century, were those of Klaproth. Caley (*2*) reproduces his method for the analysis of archaeological copper coins, the results of which were first read to the Berlin Academy in 1795 (*12*), and which gave rise to Caley's attribution of Klaproth as one of the pioneers of archaeological chemistry. Klaproth subsequently published (*13*) the analyses of three pieces of coloured Roman glass from the Villa of Tiberius on Capri, which probably constitute the first known analyses of archaeological glass.

The rise of the 'cabinet of curiosities' is a well-documented part of the development of the Renaissance from the 16th century onwards, and can be seen as the beginnings of many of the great museum collections around Europe, such as the Ashmolean in Oxford (*14*) and the British Museum in London. Many of the royal houses of Europe, along with wealthy merchants and travellers, began to collect and display objects drawn from the natural world (minerals, plants and animal remains), from archaeology and ethnography, and curiosities such as, in the case of "Tradescant's Ark" (which became the founding collection of the Ashmolean Museum), a mermaid's hand, a dragon's egg, two feathers of a phoenix's tail, a piece of the True Cross, and a vial of blood that rained in the Isle of Wight (*14*). Further impetus was given to these collections in the late 17th century by the fashion amongst the wealthy to take part in the 'Grand Tour' of Europe to visit the antiquities and natural wonders, and in particular, from 1748 onwards, the newly re-discovered ruins of Pompeii. The height of this passion for 'curiosities' therefore coincided with the ability to produce meaningful chemical analyses of the objects so contained, whether natural or human-made, and so it is not surprising that the last decade of the 18th century marks the beginning of many sciences, such as mineral chemistry, and also of archaeological chemistry.

If the impetus to develop archaeometallurgical analysis can be attributed to the need of Revolutionary France for an ample supply of bronze from which

to produce cannon, which entailed developing methods firstly for analysing bell-metal (a ready and then redundant source of copper, but containing more than 20% tin) and then for reducing tin to the levels required in bronze (c. 8-12%) (*6*), then the origins of the analysis of archaeological ceramics have similar (non-antiquarian) origins (*15*). The arrival of Chinese porcelain into Europe, perhaps first seen in the gift of porcelain vases to Lorenzo de Medici in 1487 via Egypt, was an example of an imported material creating cultural and technological shock waves for many centuries afterwards. Nothing known in Europe could compete with the toughness, and (in some cases) translucency and whiteness of these marvellous products, which were imported in large quantities from the early 17th century onwards, following the foundation in 1600 of the (British) East India Company, and in 1602 of the VOC (Dutch East India Company). The desire to imitate true Chinese porcelain revolutionized ceramic production in Europe for more than two centuries, and resulted, on the way, in the creation of several uniquely European products such as soft-paste porcelain and bone china, but it would appear that much of the work was carried out clandestinely in the various ceramic workshops of Europe, and was certainly not widely published. Starting with the earliest imitations (i.e., not true porcelains) such as the Medici porcelain of the late 16th century, success was finally achieved when the first European hard-paste porcelain was produced in 1709 by Johan Friedrich Böttger (1682-1719) and Ehrenfried Walther von Tschirnhaus (1651-1708), working in the Court of August II, Elector of Saxony and King of Poland, in Dresden.

Almost nothing is known of Böttger's experimental methods – he appears to have published nothing in his lifetime, and is said to have been determined to keep the manufacturing process secret once perfected. It is not known whether he attempted to analyse any Chinese samples to help him in his work, but it is unlikely. Although travellers (including Marco Polo) had brought descriptions of porcelain manufacture, no Chinese raw materials had yet been sent back to Europe, and it is most likely that any specimens of porcelain would have been too precious to submit to assay (which would anyway have been fire assay at the time rather than quantitative gravimetry, and therefore not very informative). It must be assumed, therefore, that Böttger proceeded by trial and error with available raw materials.

In what has been described by some as one of the earliest and most blatant examples of international industrial espionage, detailed descriptions of porcelain production in Jingdezhen (the city famous for production of porcelain, and site of the Ming and Qing Imperial kilns) were provided by Père Francois Xavier d'Entrecolles (1664-1741). He visited Jingdezhen on several occasions, and gathered information on the manufacturing process from personal observation, by discussions with his converts who worked in the manufactories, and from translations of earlier Chinese texts. His two famous letters to Père Orry of the Company of Jesus were dated September 1st 1712 and January 25th 1722, and contain considerable detail about the raw materials used, and the processing, decorating and firing of porcelain (*16*). He also sent back to France (with his second letter of 1722) samples collected in Jingdezhen of the two raw materials needed to make porcelain (*Kao lin* and *Pe tun tse*). These were given to René-Antoine Ferchault de Réaumur (1683-1757) in 1722 (*17*). His analysis of them was by assay rather than by chemical analysis, but he concluded that *Pe tun*

tse was a rock similar to talc, and that *Kao lin* was also a pulverised talc. He states (*17*): "La composition de la Porcelaine de la Chine est donc connuë. il ne nous reste qu'à sçavoir si on a en Europe, et sur-tout dans le Royaume, des mêmes matiéres que celles de la Chine, ou des matiéres equivalents."

It would appear therefore that the art of hard porcelain manufacture was discovered in Europe by trial and error rather than by the analysis of samples of Chinese raw materials, or of examples of Chinese porcelain. Nevertheless, the various manufacturers of European porcelain continued to analyse samples of both European earthenware and European and Chinese porcelain throughout the 19th century, including samples of archaeological pottery and porcelain (*15*), thus giving rise to the archaeological chemistry of ceramics. The most comprehensive set of analyses appear to have been those carried out at the Sèvres factory during the first half of the 19th Century under the guidance of Alexandre Brongniart (1770-1847), and reported by him throughout his two volumes entitled *Traité des Arts Céramiques* (*18*). In the section entitled 'composition des pâtes et glaçures des poteries antiques', Brongniart says, based on a number of analyses, that the paste contains between 55 and 89% silica (the latter in Egyptian 'prétendue porcelaine', i.e., faience), alumina to a maximum of 24%, lime between 4 and 6%, a little magnesia, iron and manganese, the last three totalling between 8 and 24%. He credits this information to Nicolas-Louis Vauquelin, but the original references are not given. Although the correspondence is not precise, it is probably Vauquelin's publication in the *Bulletin des Sciences par la Société Philomathique* (dated Floréal, an 7 de la République, i.e., May 1799), which was subsequently translated into English (*19*). This paper possibly contains the first reported chemical analysis of any ceramic material.

The most systematic analyses of early English porcelains appear to be those of Arthur Herbert Church (1834-1915). Importantly, from the perspective of the analysis of archaeological ceramics, in 1881 he gives the analyses of Bow porcelain 'obtained by means of a careful chemical examination of some fragments of unglazed porcelain of obviously early period, disinterred during draining operations at the works of Messrs. Bell and Black, at Bow' (*20*). On hard paste porcelain, he reproduces (presumably from Brongniart, but not credited) some 'older analyses of Chinese porcelain', which he supplements with some of his own 'of specimens of ancient Chinese porcelain found in a ruined Indian Temple' (a white body, a brown body, and the glaze of the white body).

We may therefore conclude that the chemical analysis of ceramic material was established by the end of the 18th century, and that the analysis of archaeological material (European and Chinese) by the beginning of 19th. It is difficult to pinpoint the 'earliest', since much appears unpublished, or only summarized later in works such as those of Brogniart (*18*) or Church (*20*). It is perhaps because of this that Harbottle (*21*) felt justified in saying that 'one of the earliest analyses of archaeological ceramics' was that published by Theodore William Richards of Harvard in the *American Chemical Journal* of 1895 (*22*), in which he lists the complete composition of a fragment of a vase from Athens in the keeping of the Boston Museum of Fine Arts. Although this is almost certainly the earliest analysis to be conducted outside Europe, and one of the earliest reported on a classical

ceramic, it is unlikely to have been the earliest analysis of any archaeological ceramic, by perhaps as much as 100 years.

It is interesting to draw some observations on the earliest history of archaeological chemistry. Although we must conclude that the impetus to develop the capacity to analyse metals and ceramics came for reasons other than archaeology, we may surmise that the earliest analyses of archaeological examples arose out of pure curiosity, in an atmosphere in which newly-developed analytical skills were being applied to the entire contents of the 'cabinets of curiosities'. Moreover, the greatest chemists of the day were involved in these activities - the likes of Réamur, Dizé, Vauquelin, Fourcroy, Darcet, Mongez, Klaproth, Berthelot, Berzelius, Davy and Faraday. The questions asked were, of necessity, rather simple – primarily 'what is this object made from?' – but it did not take long for chemists to realise that more complex questions could be asked of archaeological material. The subject moved to more systematic and problem-orientated studies in the 19th century with the work of Göbel (*23*) and Wocel (*24*) on copper alloys, Damour (*25*) on stone and Helm (*26*) on amber. These studies shared a number of common aspects – the realization that large numbers of objects needed to be studied in order to draw meaningful conclusions, and a feeling that the objects themselves contained information about their geological source. Collectively, these authors essentially formulated the idea of 'provenance studies'– that some chemical characteristic of the geological raw material(s) provides a 'fingerprint' which can be measured in the finished object, and that if an object from a remote source is identified at a particular place, then it is evidence of some sort of direct or indirect contact and 'trade' between the two places (*27*). For example, in 1865, Damour declared that 'un objet sur lequel la main de l'homme a marqué son travail, et dont la matière est de provenance lointaine ou étrangère à la contrée, on en infère qu'il y a eu transport de l'objet même, ou du moins de la matière don't il est formé' (*25*). This sets out the essential supposition of chemical provenance analysis as applied to prehistoric artefacts such as stone tools, and objects made of metal, ceramic, or glass, and which has underpinned much of archaeological chemistry ever since.

More than 200 years after its origins, what can we now say about the practice of archaeological chemistry? Structurally, it appears to have moved to a more marginal academic position than the other sciences born at around the same time, such as geochemistry, biochemistry, etc. This is true of its relationship to both chemistry and archaeology. Outside of a few established centres, few departments of chemistry have an established subsection devoted solely to archaeological chemistry, although more departments are active in forensic chemistry (which is a somewhat related activity). Mostly archaeological chemistry exists as the personal interest of an individual scholar, often supported by his or her host department (if only for the 'publicity'), but with no guarantee of continuity once that particular scholar has retired or moved on. Conversely, few departments of archaeology or anthropology specialise in archaeological chemistry - it is difficult if not impossible to sustain a high level of chemical research in a department which is primarily funded at humanities or social science levels. Both scenarios therefore provide good examples of research carried out 'on a wing and a prayer'.

It is easy for archaeologists from a scientific background (we should perhaps call them 'laboratory archaeologists') to remonstrate that if only archaeology were properly funded (i.e., as a science), and recognized as a science, then all would be well, thereby echoing the same call made by Gordon Childe more than 70 years ago (*28*). The fact that this is not the case is the reflection of an unpalatable truth – despite the huge strides made in scientific approaches to archaeology since the discovery of radiocarbon dating, the development of geophysical survey techniques, etc., some professional archaeologists (both academic and commercial) still do not regard 'science' as central to the discipline, and certainly not good 'value-for-money' (or, perhaps more accurately, are unwilling or unable to convince their paymasters of this). That this is the case is evidenced, for example, by the choices made when new university positions are filled, and laboratory archaeologists are overlooked in favour of somebody who is 'cheaper to run'. We clearly have still not yet completely countered views of the type expressed in a short but withering book review written twenty years ago by Dunnell (*29*) entitled 'Why archaeologists don't care about archaeometry', which states that 'Many, if not most, archaeologists regard archaeometry as a sometimes interesting, largely irrelevant, and definitely optional endeavour'. More specifically, Ehrenreich wrote in 1995 (*30*) 'Most archaeologists consider archaeometry to be a field populated by physical scientists who are more concerned with the adaptation of scientific methods to the analysis of archaeological material than with the use of analytical instrumentation for the development, clarification, and refinement of archaeological theories', although he does go on to say that 'This may have been true 10 years ago, but the field has changed considerably since then'. We would like to think that, nearly 20 years later, this caricature of archaeological chemistry as being carried out solely by 'parachutists' (typically a physical scientist who specialises in only one sort of instrumentation, and who is determined to apply it come what may to archaeological artefacts, but with no concept of addressing an archaeological question, and no knowledge of the literature on the subject) is even more a thing of the past, but sadly examples can still be found. Papers are still produced where the focus is on an analytical method applied to some particular objects or site (which would be laudable if the method were truly novel, but mostly it is not), and the archaeological outcome can be somewhat unkindly paraphrased as showing that 'things are made of stuff'. It does not, for example, take a synchrotron to demonstrate that pottery is made primarily of clay.

Why does this still occur? There is sometimes a certain arrogance about the natural sciences, which can be encapsulated as 'chemistry is difficult, but I saw a programme on TV about the Bronze Age', with the implication being that archaeology (as a humanity) is something which does not need to be studied rigorously and can therefore be easily assimilated from a few TV programmes. Popular interest, accessibility and media-simplification of archaeology can sometimes be mistaken for a lack of rigour. This position can, of course, be inverted by noting that some non-scientists take positive pride in declaring that they don't understand science, and regard scientists as technicians, capable of producing data but not of interpreting it (and, indeed, such people do exist). In partial defence of the 'parachutist', it has to be said that the enthusiastic physical

scientist cannot be expected at the outset to know what is relevant in archaeology and what is not, and to have read all the relevant literature. Those who do try to engage with truly cutting-edge archaeological issues have several obstacles to overcome. Some archaeological theory is written in a way which appears on the surface to be deliberately obscurantist (although, of course, to a non-chemist the terminology of chemical literature can have the same effect, but we would argue that this is to give precision and clarity, rather than obsurantiscism, and archaeological theoreticians would invoke the same defence). There is also a tendency towards anarchy and myopia in archaeology, which manifests itself as an inability to see priorities over and above those of an individual's own current interest. Ask any group of archaeologists what the current top research priorities are in archaeology, and it is highly unlikely that a single view will emerge. After all, how can further work on the Roman frontier in Scotland be evaluated in priority terms against a better understanding of the decline of the Maya state? It is easy to see, therefore, why those outsiders who do wish to engage in modern archaeological debate find it difficult to get a secure foothold.

Bad science in archaeology, however, is not the sole prerogative of the parachutist. There is a parallel problem but from the opposite direction, which might be termed 'the blind leading the blind'. This is where a technique or tool developed in another field of science is enthusiastically adopted in archaeology by individuals with little or none of the training necessary to truly understand it, but with a high degree of wish fulfilment. This is most common when a piece of equipment is involved which (apparently) produces data in the field at the touch of a button, but it can also apply to situations where data can be bought relatively cheaply from laboratories on a commercial basis. The problem is that the enthusiastic application is most often reported in the archaeological literature (including, regrettably, the scientific archaeological literature), where rigorous reviewing of the scientific assumptions involved can sometimes be difficult to obtain, and therefore simplifications or errors are propagated. The same is true at grant application level, where scientific applications are requested as part of a larger project, but are not always rigorously scientifically reviewed. The end result is an out-of-control bandwagon, with unrealistic or unsustainable claims being made from an inadequate interpretation of scientific data, or a lack of appreciation of the limitations of the method.

Much of the above criticism arises simply because of the difficulties involved in communicating across disciplinary boundaries, especially when Snow's 'Two Cultures' are invoked [resulting in 'a gulf of mutual incomprehension – sometimes (particularly among the young) hostility and dislike, but most of all lack of understanding' (*31*)], and is certainly not unique to archaeology. It must be stated now that there have been and are many examples of excellent integration of science into archaeology. Singling out individual large field projects is somewhat invidious, but recent examples would include Hodder's work at Çatal Höyük, and Barker's at Niah Cave in Borneo and Haua Fteah cave in Libya. In these (and other) cases, the science is of high quality, is relevant (and possibly central) to the overall project aims, and is planned in at the beginning rather than being bolted on later. There are also several recent excellent examples of scientific applications in general and archaeological chemistry in particular which

have genuinely revolutionized the way archaeology is done or interpreted – the Bayesian revolution in radiocarbon dating (e.g., (*32*)), and the investigation of the origins of dairying in the European Neolithic (*33*) spring to mind. The reason these and similar endeavours have been so influential is that, by combining high quality science with significant and relevant archaeological questions, they have made a difference to the archaeological narrative. Although some archaeological science practitioners may still be operating on 'a wing and a prayer', collectively the interaction between science and archaeology has rarely been so extensive, fruitful, and (largely) accepted.

It is tempting, going back to the beginning of this paper, to note that when Citizens Dizé and Vauquelin unwittingly started archaeological chemistry in Revolutionary France in the 1790s, knowledge was such that a single person could expect to be conversant with all aspects of science, in addition to being acquainted with literature and the classics. Regrettably this is now more difficult, and so the essence of good archaeology is open, respectful, meaningful and iterative dialogue across the many disciplinary boundaries involved.

References

1. Caley, E. R. *Ohio J. Sci.* **1948**, *18*, 1–14.
2. Caley, E. R. *J. Chem. Educ.* **1949**, *26*, 242–7, 268.
3. Caley, E. R. *J. Chem. Educ.* **1951**, *28*, 64–66.
4. Caley, E. R. *Analyses of Ancient Glasses 1790−1957: A Comprehensive and Critical Survey*; Corning Museum of Glass: Corning, NY, 1962.
5. Caley, E. R. *Analysis of Ancient Metals*; Pergamon: Oxford, 1964.
6. Pollard, A. M. *Ox. J. Arch.* **2013**, *32*, 333–339.
7. Dizé, M. J. J. *Obs. Phys. Hist. Nat. Arts* **1790**, *36*, 272–276.
8. Porter, T. M. *Ann. Sci.* **1981**, *38*, 543–570.
9. Oldroyd, D. R. *J. Chem. Educ.* **1973**, *50*, 337–340.
10. Bergman, T. *Physical and Chemical Essays Translated from the Original Latin of Sir Torbern Bergman, by Edmund Cullen, M.D*; J. Murray: London, 1788; 2 vols.
11. Vauquelin, N. *Ann. Chim.* **1799**, *30*, 66–106.
12. Klaproth, M. H. *Mém. l'Acad. Roy. Sci. Belles-Lettres. Classe Phil. Exp.* **1792/3**, 97–113, read July 9, 1795.
13. Klaproth, M. H. *Mém. l'Acad. Roy. Sci. Belles-Lettres. Classe Phil. Exp.* **1798**, 3–16.
14. MacGregor, A. *Tradescant's Rarities: Essays on the Foundation of the Ashmolean Museum 1683*; Oxford University Press: Oxford, 1983.
15. Pollard, A. M. *Ambix.*, submitted.
16. Tichane, R. *Ching-te-Chen. Views of a Porcelain City*; New York State Institute for Glaze Research: New York, 1983.
17. de Réaumur, R.-A. F. *Hist. l'Acad. Roy. Sci.* **1727**, 185–203.
18. Brongniart, A. *Traité des Arts Céramiques, ou des Poteries*; Bechet Jeune and Mathias: Paris, 1844; 2 vols.
19. Vauquelin, N. *Phil. Mag.* **1799**, *5*, 288–290.

20. Church, A. H. *Cantor Lectures on Some Points of Contact between the Scientific and Artistic Aspects of Pottery and Porcelain*; Trounce: London, 1881.

21. Harbottle, G. In *Contexts for Prehistoric Exchange*; Ericson, J. E., Earle, T. K., Eds.; Academic Press: New York, 1982; pp 13−51.

22. Richards, T. W. *Am. Chem. J.* **1895**, *XVII*, 152–154.

23. Göbel, F. *Ueber den Einfluss der Chemie auf die Ermittelung der Völker der Vorzeit oder Resultate der chemischen Untersuchung metallischer Alterthümer insbesondere der in den Ostseegouvernements vorkommenden, Behuss der Ermittelung der Völker, van welchen sie abstammen*; Ferdinand Enke: Erlangen, 1842.

24. Wocel, J. *Sitz. Kaiser. Akad. der Wiss. Phil.-Hist. Classe (Wien)* **1854**, *11*, 716–761.

25. Damour, A. *C. R. Hebd. Séances l'Acad. Sci.* **1865**, *61*, 313–321, 357–368.

26. Helm, O. In *Tiryns*; Schliemann, H., Ed.; John Murray: London, 1886; pp 369-372.

27. Wilson, L.; Pollard, A. M. In *Handbook of Archaeological Sciences*; Brothwell, D. R., Pollard, A. M., Eds.; John Wiley and Sons: Chichester, 2001; pp 507−517.

28. Childe, V. G. *Nature* **1943**, *152*, 22–23.

29. Dunnell, R. C. *Archeomaterials* **1993**, *7*, 161–165.

30. Ehrenreich, R. M. *J. Arch. Meth. Theory* **1995**, *2*, 1–6.

31. Snow, C. P. *The Two Cultures and the Scientific Revolution. The Rede Lecture 1959*; Cambridge University Press: Cambridge, 1959.

32. Whittle, A.; Healy, F.; Bayliss, A. *Gathering Time*; Oxbow Books: Oxford, 2011.

33. Salque, M; Bogucki, P. I.; Pyzel, J.; Sobkowiak-Tabaka, I.; Grygiel, R.; Szmyt, M.; Evershed, R. P. *Nature* **2013**, *493*, 522–525.

Subject Index

W